NAME OF AUTHOR...PRADYOT KUMAR CHATTOPADHYAY..

TITLE OF THESIS....RESIDUAL SHEAR STRENGTH OF

......SOME PURE CLAY MINERALS....

....

UNIVERSITY......OF ALBERTA..........................

DEGREE FOR WHICH THESIS WAS PRESENTED.......Ph. D.........

YEAR THIS DEGREE GRANTED........1972......................

Permission is hereby granted to THE NATIONAL LIBRARY

OF CANADA to microfilm this thesis and to lend or sell copies

of the film.

The author reserves other publication rights, and

neither the thesis nor extensive extracts from it may be

printed or otherwise reproduced without the author's

written permission.

(Signed)...PK Chattopadhyay......

PERMANENT ADDRESS:

....Dept. of Civil Engg...

..........Univ. of Alberta

................Edmonton.

DATED...October 30......1972

NL-91 (10-68)

THE UNIVERSITY OF ALBERTA

RESIDUAL SHEAR STRENGTH OF SOME PURE CLAY MINERALS

by

© PRADYOT KUMAR CHATTOPADHYAY

A THESIS

SUBMITTED TO THE FACULTY OF GRADUATE STUDIES AND RESEARCH

IN PARTIAL FULFILMENT OF THE REQUIREMENTS FOR THE DEGREE

OF DOCTOR OF PHILOSOPHY

DEPARTMENT OF CIVIL ENGINEERING

EDMONTON, ALBERTA

FALL, 1972

THE UNIVERSITY OF ALBERTA

FACULTY OF GRADUATE STUDIES AND RESEARCH

The undersigned certify that they have read, and recommend
to the Faculty of Graduate Studies and Research for acceptance, a
thesis entitled "RESIDUAL SHEAR STRENGTH OF SOME PURE CLAY MINERALS"
submitted by Pradyot Kumar Chattopadhyay in partial fulfilment of
the requirements for the degree of Doctor of Philosophy.

....
N.R. Morgenstein, Supervisor

....
Z. Eisenstein

....
S. Thomson

....
S. Pawluk

....
T.C. Kenney, External Examiner

Date ..October 10, 1972....

ii

ABSTRACT

This dissertation deals with the physical basis of the residual shear strength of some pure clay minerals. Reversal direct shear tests have been conducted on kaolinite, Na-attapulgite and Na-montmorillonite at various pore fluid NaCl concentrations to establish the factors that affect the residual shear strength. The arrangements of the mineral particles in the shear zones at large strains have also been studied with a scanning electron microscope in order to investigate the mechanism of strength generation at large strains.

Based on an analysis of the previous studies, it is hypothesized that the residual strength is a frictional characteristic of the clay mineral and it depends on the mode of cleavage and the amount of bonding energy available along the cleavage planes at the interparticle contacts in the shear zone. The Terzaghi-Bowden and Tabor adhesion theory of friction appears to account for the conditions at the interparticle contact.

The residual shear strength (τ_{res}) characteristics of the clay minerals have been studied in terms of the true effective stress (σ_n^*) which is defined as

$$\sigma_n^* = \sigma_n - u_w - (R\text{-}A) = \sigma_n' - (R\text{-}A)$$

where σ_n = total stress,

σ_n' = apparent effective stress,

u_w = pore water pressure,

and (R-A) = the physico-chemical component which may be estimated from the double-layer repulsive stress equation.

A comparison between the residual shear strengths of five saline Na-montmorillonite samples before and after leaching of the saline pore fluids under constant overall volume conditions has proved that the true effective stress (σ_n*) controls the residual shear strength. It is also shown that every mineral possesses a true angle of residual friction (ϕ_r') which is independent of the pore fluid salt content but is dependent on the magnitude of normal effective stress.

Residual friction angles of the clay minerals and some natural soils have been found to be stress dependent below an average normal pressure of 30 psi. Assuming elastic deformations at the interparticle contacts, the dependence of ϕ_r' on σ_n' is believed to be due to the dependence of the area of true contact (A_c) between the shear zone particles on the normal load. Below an average normal pressure of 30 psi, A_c is proportional to $(\text{load})^{2/3}$ and $\tan\phi_r'$ is stress dependent. As normal pressure is increased, A_c becomes proportional to $(\text{load})^{1.0}$ and $\tan\phi_r'$ ceases to be stress dependent.

ACKNOWLEDGEMENTS

TABLE OF CONTENTS

TABLE OF CONTENTS (continued)

LIST OF TABLES

LIST OF FIGURES

LIST OF FIGURES (continued)

CHAPTER I

INTRODUCTION

1.1 Shear Strength

When a soil is subjected to shear, an increasing resistance is built up. For any given applied effective stress and under drained conditions, there is a limit to the resistance that the soil can offer, which is known as the "peak shear strength" of the soil under the given effective stress.

If the shearing is continued after this maximum value of shear strength is mobilised, it is usually found that the resistance of the soil decreases, until ultimately a steady value is reached, this steady value being defined as the "residual shear strength" of the soil. The soil maintains this steady value even when subjected to large displacements. Hence, residual shear strength of a soil may be defined as that shear strength of the soil at large displacements, when all the variable components of strength have been destroyed or overcome. This definition implies that the residual strength is a certain indestructible component of strength for a given soil.

These typical results obtained from a drained shear box test in which the soil is subjected to large displacements are shown in Fig. 1.1. It is seen that at large strains, the strength of the soil remains constant.

1

Further drained shear box tests can be conducted on samples of the same soil but under differing effective stresses. The results previously described would again be obtained, and, from a number of tests, it would be noticed that the peak and residual shear strengths would define envelopes in accordance with the Coulomb-Terzaghi Law (Fig. 1.2). Thus the peak shear strengths (τpeak) can be expressed as:

$$\tau_{peak} = c' + (\sigma_n - u_w) \tan\phi'$$
$$= c' + \sigma_n' \tan\phi' \qquad (1.1)$$

and the residual shear strengths (τ_{res}) can be expressed as:

$$\tau_{res} = c_r' + (\sigma_n - u_w) \tan\phi_r'$$
$$= c_r' + \sigma_n' \tan\phi_r' \qquad (1.2)$$

where c' = cohesion intercept at peak state

c_r' = cohesion intercept at residual state

ϕ' = peak angle of shearing resistance

ϕ_r' = residual angle of shearing resistance

σ_n = total stress

u_w = pressure in the pore water

$\sigma_n' = \sigma_n - u_w$ = effective normal stress.

The difference between peak and residual shear strengths depends on the soil type and stress history, and is most marked for heavily overconsolidated clays and clay-shales.

Results such as shown in Fig. 1.1 are known from the

earliest systematic shear tests by Hvorslev (1936, 1939) and Haefeli
(1938). Heafeli had even suggested the term "residual shear strength"
(Restscherfestigkeit) for the strength of a soil at large strains.
However, it goes to the credit of Skempton (1964) to have reinstated
the concept by demonstrating the relevance of residual strength to
practical problems like slope stability and landslides.

1.2 Relevance of Residual Strength in Stability Problems

There is little doubt that in recent years an appreciation of
the nature and significance of residual strength (Skempton, 1964)
constitutes the most important development in an understanding of the
shear strength of clays. While the concept is relevant to all clays,
it is of particular practical importance for stiff natural clays where
the drop in resistance from peak to residual is often large.

The concept of shear strength being time and displacement
dependent has proved to be extremely successful in explaining long-term
slope failures in overconsolidated clays and clay-shales. If, for any
reason, a clay is forced past the peak value at a particular point within
a slope, the shear strength available at that point will decrease. It
is evident, from simple considerations of statical stability that
additional stress will then be thrown on to the clay at some adjacent
point, and may cause the peak to be passed there as well. Thus a
progressive reduction in shear strength throughout the soil mass can
be initiated.

A more clear-cut example of the significance of residual

strength occurs when considering the stability of slopes which have been subjected to failures at some stages in their history. In all cases where failure has previously occurred, the peak shear strength has evidently been passed and the maximum available strength which can be mobilised on the existing slip surface will be close to the residual value. In passing from the peak to the residual, the cohesion intercept disappears or becomes very small and there is also a reduction in the angle of shearing resistance which varies from soil to soil. The effect of the disappearance of the apparent cohesion term is very marked in over-consolidated clays and clay-shales, particularly since an examination of past failures in these soils reveals that the slip surface is frequently located at a relatively shallow depth below ground level. Consequently, under the low normal pressures then applying, any reduction in the cohesion term in the Coulomb-Terzaghi expression will have a profound significance on the factor of safety. The drop in the angle of shearing resistance from peak to residual states can also be considerable. For example, a dramatic drop from a peak angle of 28° to a residual angle of 2.6°-3.6° (measured from ring shear tests) was observed for Bearpaw shale obtained from the South Saskatchewan dam site (P.F.R.A., 1970). It is interesting to note that a major part of the land area of Western Canada and Western United States is underlain at shallow depths by such highly plastic clay-shales or by soils derived from weathering of these shales which are characterised by significant drops in shear strength from peak to residual.

The relevance of residual strength to the analysis of the

stability of slopes in overconsolidated clays and clay-shales has
been confirmed by a number of examples. Skempton (1964), Petley (1966)
and Eigenbrod and Morgenstern (1971) have conclusively demonstrated that
residual strength, as measured in the laboratory, correlates closely
with the average mobilised strength calculated for a number of field
failures in stiff clays where movement has occurred along existing slip
surfaces. The availability of only residual strength accounts for movements
suffered by the Waco Dam due to sliding in the underlying Pepper shale
(Van Auken, 1963) and the experience in the Bearpaw shale reviewed
by Ringheim (1964). With regard to stability of long natural slopes
in fissured clays with zero residual cohesion and seepage parallel to
the ground surface, the studies carried out in the United Kingdom by
Skempton and De Lory (1957), Hutchinson (1967) and Weeks (1969) have
confirmed that the ultimate angle against land sliding of natural slopes
in fissured clay, as determined in the field, is approximately $\phi_r'/2$.
A number of other case histories supporting the control by residual
strength of the long-term stability of stiff clay slopes exist in the
geotechnical literature.

The magnitude of the residual shear strength is, therefore,
necessary for rational design when dealing with material subject to
previous shear movements. Since the residual strength sets the lower
limit of progressive strength reduction, it also serves as a useful
lower bound for any design. If a design has a factor of safety greater
than unity based on residual strengths (and appropriate pore pressures)
no serious movements are likely. However, analysis on this basis will

often be uneconomical and overconservative.

The residual strength is a parameter not only of practical importance but also of great fundamental value. This is so because it is independent of stress history, original structure and other factors which dominate the path dependent properties of soils.

1.3 Brief Review of Work Done on Residual Strength

Since Skempton's Rankine lecture in 1964, numerous attempts have been made to measure the residual strength of different soils. Some of these results are reported in Table 1.1. All these studies, with the exception of those by Skempton (1964), Borowicka (1965), Kenney (1967), Morgenstern and Tchalenko (1967 a, b) and Tchalenko (1967, 1968 and 1970), had only the purpose of measuring the residual strength as a parameter to be used in a stability analysis. Consequently, very little is known about the fundamental nature of residual strength.

Pioneering research attempts to establish some of the factors that influence the residual strength of a soil were made by Skempton (1964) and Borowicka (1965). Skempton (1964) drew attention to the clear correlation between the percentage of fines and the residual friction angle of the soil (Fig. 1.3). Similar results were also obtained by Borowicka (1965) and from his results he concluded that:

i) As the colloidal content increases, the residual strength decreases (Fig. 1.4),

ii) Beyond a certain percentage of fines (Borowicka established this limit to be 43%), the residual strength is not

affected.

Morgenstern and Tchalenko (1967 a) have also expressed
similar opinions while discussing stable and unstable yielding. Borowicka
also inferred speculatively that the chemical and the mineralogical
composition of the soil should play an important role in the development
of residual strength. While there is agreement, in a general way,
between Skempton's results and those reported by Borowicka, the former's
results leave the impression that there is no upper limit to the
percentage of fines which would be significant to the residual strength.
But Fig. 1.3 also confirms the importance of mineralogical composition
of the clay. Thus, clays of similar grain size composition still show
significantly different residual shear strengths because their
mineralogy is different (See Table 1.1 in conjunction with Fig. 1.3).
Significant also is the position of quartz in Fig. 1.3. The
horizontal line for quartz signifies that irrespective of the fineness
to which quartz is pulverised, its angle of shearing resistance remains
around 32°. It may be added that the general validity of Skempton's
diagram (Fig. 1.3) has been confirmed by subsequent research (Chandler,
1966; Kenney, 1967).

The major steps in the investigation of the nature of residual
strength were taken by Kenney (1967), Morgenstern and Tchalenko (1967 a,
b) and Tchalenko (1967, 1968 and 1970). While Kenney (1967) studied
the frictional characteristics of soil minerals, Morgenstern and
Tchalenko (1967 a, b) and Tchalenko (1967, 1968 and 1970) undertook
microstructural examination of the large displacement shear zones in

soils. The work done by these investigators will be reviewed in detail in appropriate sections of the subsequent chapters. However, a summary of their findings is in order here to justify the need for further investigation into the fundamental nature of residual strength.

Kenney's (1967) work was primarily concerned with pure clay minerals and mixtures of them. He performed drained direct shear tests on pure minerals and mineral mixtures along with several natural soils and demonstrated that residual shear strength is primarily dependent on mineral composition and that it is not related to plasticity or grain-size characteristics nor is it significantly influenced by rate of strain. His tests show that in comparison with layer lattice minerals, massive minerals exhibit higher residual strengths. Kenney (1967) also controlled the composition of pore fluid where possible and concluded that the residual strength properties of the active clay minerals such as hydrous mica and montmorillonite are influenced by system chemistry. To a lesser extent, residual friction angle also depends on the magnitude of normal effective stress. Kenney's results point clearly to the need for a more thorough study of the physico-chemical aspect of residual strength. It may be mentioned here that another comprehensive investigation into the frictional characteristics of minerals was previously undertaken by Horn and Deere (1962). However, they dealt with the friction of few massive and layer lattice minerals and none of the common clay minerals except mica was investigated.

Microstructural examination of the large displacement shear zones in various soils, carried out by Morgenstern and Tchalenko

(1967 a, b) and Tchalenko (1967, 1968 and 1970), revealed that a definite mode of particle arrangement is associated with residual strength. Detailed examination of the development of this shear induced structure in the large displacement shear zones in various soils led them to suggest that the subsequent resistance of a soil will depend upon this shear zone structure and the physical interaction of the soil particles alone. The important contributions made by Morgenstern and Tchalenko (op. cit.) and Tchalenko (op. cit.) provided the first insight into the physical basis of the residual strength of soils and clearly demonstrated the need for a fundamental investigation to further our understanding of the nature of residual strength in soils.

1.4 Scope of the Investigation

Past research has clearly brought out that the residual shear strength is independent of the factors that influence the path dependent properties of soils and hence it is a fundamental and unique soil parameter. A brief review of previous work on residual strength has also indicated a definite need for further investigation into the fundamental nature of residual shear strength and the factors that control the shear strength of soils at large strains.

Since the residual shear strength of a soil is primarily dependent on its mineral composition (Kenney, 1967), a clear understanding of the fundamental factors controlling the residual-strength properties of clay minerals is necessary for understanding of the residual shear strength characteristics of clay soils and clay-shales. A hypothesis for the physical basis of residual shear strength of pure clay minerals

(which, incidentally, are ideal materials for a fundamental study)
is therefore formulated in this thesis. The hypothesis stems
from a critical analysis of the available studies on the large strain
frictional behaviour of various soil minerals and solid lubricants.
Four major aspects of the residual shear strength of clay minerals are
dealt with in the hypothesis and they are:

i) The seat of shear strength at large strains,

ii) The effect of system chemistry on the residual shear
strength,

iii) The stress state variable that controls the residual
shear strength, and

iv) The dependence of the residual friction angle (ϕ_r')
on the magnitude of normal effective stress (σ_n').

Reversal direct shear tests were conducted on three clay
minerals (viz., kaolinite, attapulgite and montmorillonite) at
various pore fluid salt concentrations in order to verify the proposed
hypothesis experimentally.

The available studies on the large frictional
characteristics of soil minerals and solid lubricants were analysed and
the shear induced structures in the large displacement shear zones in
the clay mineral samples were examined in order to establish the physical
basis of the residual strength of clay minerals and the mechanism of
strength generation at large strains.

Examination of the test results obtained from the shear tests

along with the available data on the residual shear strength of various clay minerals in light of the proposed hypothesis revealed the effect of system chemistry on the residual shear strength of pure clay minerals and the stress state variable that controls the residual shear strength.

An explanation for the dependence of the residual friction angle of a clay mineral on the magnitude of normal effective stress has also been presented. This explanation is taken from the available studies on the frictional behaviour of solid lubricants and its validity has been established not only from the shear test results obtained in this investigation but also from the available data on the residual shear strength of several natural soils.

1.5 Organisation of the Thesis

Chapter 2 presents a critical analysis of the available literature concerned with the various aspects of the residual shear strength of clays and clay minerals.

Chapter 3 introduces the hypothesis proposed for the physical basis of the residual shear strength of pure clay minerals.

Chapter 4 outlines the experimental programme that was under-taken for the verification of the proposed hypothesis.

Chapter 5 describes the properties of the clay minerals used, the test equipment, the sample preparation and the testing techniques.

Chapter 6 presents the results obtained from the experimental programme and relates the test results to the hypothesis proposed in

Chapter 3.

Chapter 7 presents the fundamental nature of the residual shear strength of clay minerals as established from the test results obtained in this investigation and also from an analysis of the previous studies.

Chapter 8 summarises the conclusions drawn from this investigation and presents a few suggestions for future research.

Appendix A presents the accuracies and the calibration constants of the instrumentation used in various test equipment.

Appendix B compiles the results of the reversal shear tests conducted on the three clay minerals along with a few typical consolidation test results.

Appendix C describes the double layer repulsion equation.

TABLE 1.1

PHYSICAL PROPERTIES OF MINERALS AND SOILS

	Soil	Reference	Grain Size	Index Properties				Massive Minerals				Clay Minerals				ϕ'_{res}
			Clay Sizes %	Liquid Limit %	Plastic Limit %	Plasticity Index %	Activity	Quartz %	Feldspar %	Calcite %	Others %	Kaolinite %	Illite %	Montmorillonite %	Others %	Deg.
1	Varved Silt (Cod Beck)	Petley (1966)	20-50 / 5	58 / 34	24 / 21	34 / 13										20 / 24
2	Silty Clay (Fiddler's Ferry)	"	30	43	22	21										24
3	London Clay (Guild Ford)	"	55	83	32	51										15
4	Oxford Clay (Peterborough)	"	47	60	27	33										14.5
5	Atherfield (Seven Oaks)	"	58	73	32	41										12-15
6	Walton's Wood	"	69	57	26	31	0.45					60	15		15	13
7	Jari (Mangla)	"	52	58	27	31	0.60					5	65	25	5	14
8	Blue London Clay	"	58	69	26	43	0.74	10								$c'=30$ psi $\phi'=16$
9	Till (Peace River)	-	42	48	17	31	0.74						18	58	12	22.6
10	Keuper Marl	Chandler (1966)	17	34	23	11										27.5
11	Kaolin	Tchalenko (1967)														12

FIG. 1.1   SHEAR STRENGTH VERSUS DISPLACEMENT
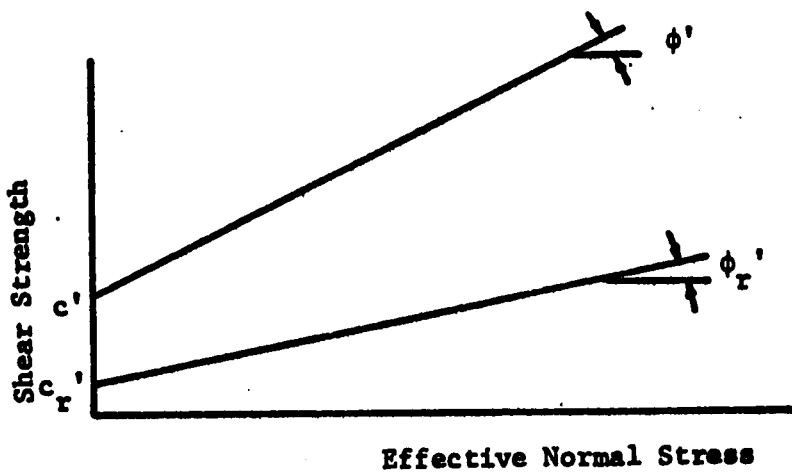
FIG. 1.2   COULOMB-TERZAGHI DIAGRAM
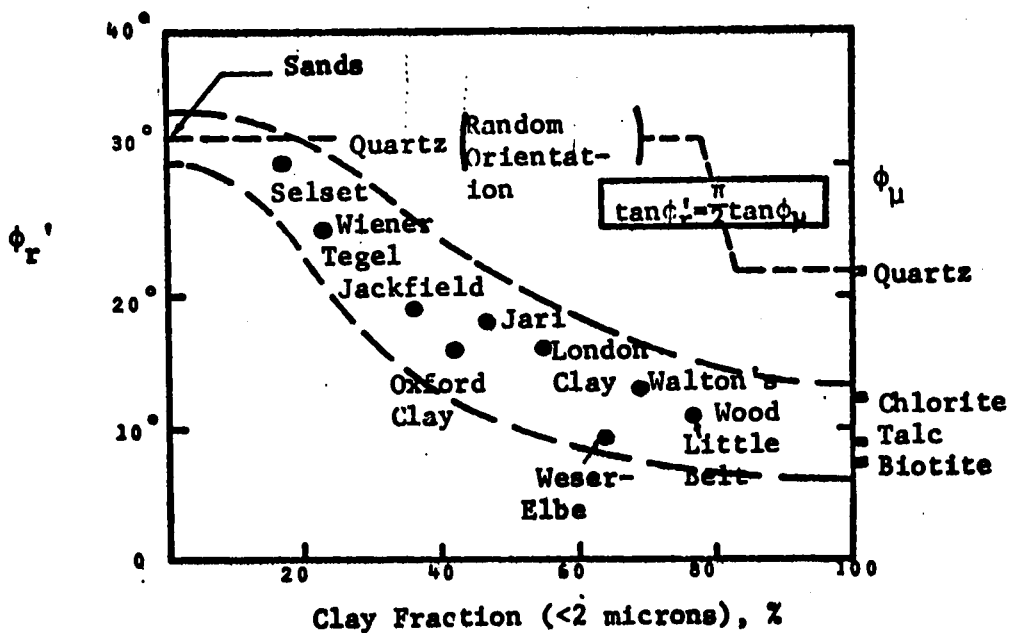
FIG. 1.3   DECREASE IN ϕ_r' WITH INCREASING
CLAY FRACTION (AFTER SKEMPTON, 1964)
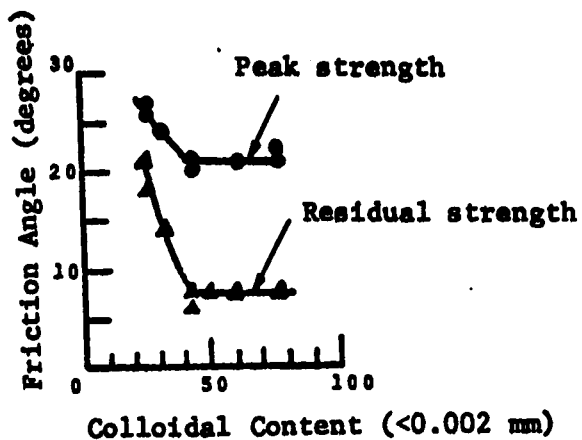
FIG. 1.4   INFLUENCE OF COLLOIDAL CONTENT ON SHEAR
STRENGTH OF SOIL (AFTER BOROWICKA, 1965)

CHAPTER II

REVIEW OF THE AVAILABLE STUDIES ASSOCIATED WITH THE RESIDUAL SHEAR STRENGTH OF CLAYS AND CLAY MINERALS

2.1 Introduction

A great body of evidence is available in the geotechnical literature to demonstrate that the strength, stress-deformation and stress-strain-time behaviour of soils follow organised and often predictable patterns. However, relationships between such observable quantities as strength, compressibility, deformation rate and less easily determined but more fundamental factors such as effective stress, the structure and strength of interparticle bonds, the structure and properties of adsorbed water, true cohesion and friction are still not completely understood. An improved understanding of these factors and their effects on the engineering properties of soils has been developed during the past decade. A detailed account of the past research on all the factors influencing the engineering behaviour of soils is not in order here for obvious reasons. Hence, we will concentrate only on those studies that contribute to the understanding of the fundamental nature of residual shear strength in soils. In particular, we will review the following areas of fundamental research:

      i) Residual shear strength of clay minerals and the factors affecting it,

      ii) Bonding and strength of soils,

iii) Microstructural studies of the large displacement shear zones in clays, and

iv) Frictional behaviour of solid lubricants.

It is hoped that an analysis of the above mentioned studies would lead us to formulate a hypothesis for the physical basis of the residual shear strength of clay minerals.

2.2 Factors Influencing the Residual Shear Strength of Soils

Mitchell (1964) attempted to express shearing resistance of soils, particularly at subfailure stresses, in terms of fundamental soil parameters in order to provide a basis for the study of factors such as strain rate, temperature and soil structure which are known to influence shearing resistance, but which are not adequately accounted for by the Coulomb-Terzaghi Law. On the basis of knowledge of soil behaviour, Mitchell (op. cit.) postulated that strength should be a function of a large number of factors; thus,

$$\text{shearing resistance} = F(e, \phi, c, C', H, T, \epsilon, \dot{\epsilon}, \sigma, u, S) \qquad (2.1)$$

in which, e = void ratio,

ϕ = a parameter expressing the frictional characteristics of the soil,

c = a parameter expressing the interparticle cohesion of the soil,

C' = the soil composition including solid, fluid and gaseous phases,

H = a term equivalent to stress history,

T = the temperature,

ε = the strain,

$\dot{\varepsilon}$ = the strain rate,

σ = the applied stresses,

u = the pore pressures,

and, S = the soil structure.

Not all of these factors are independent variables. For example, the structure of a soil at any instant will reflect the combined influences of C', H, e, σ, u and ε and e is a function of C', H, S, ϕ, c, σ and u. Furthermore, the influences of σ and u may be considered through use of the effective stress, σ_n'. In addition, most of the factors are subject to variation during deformation. If however, a given soil at a given void ratio is considered, then the number of factors influencing the instantaneous value of shearing resistance at any stage of deformation is considerably reduced, and

$$\text{shearing resistance} = F(\phi, e, T, \dot{\varepsilon}, \sigma_n', S) \tag{2.2}$$

This relationship is of slight practical use because the functional term relating the terms are not specified (Mitchell, 1964).

Residual shear strength, however, has been shown to be independent of stress history, original structure, strain rate and other factors which dominate the path dependent properties of soils. Hence, the number of variables is further reduced and we can express residual shear strength as a function of three major factors; thus,

$$\text{residual shear strength} = F(\phi_r', C', \sigma_n') \tag{2.3}$$

The parameter ϕ_r' expresses the frictional characteristics

of a soil at large strains and to establish the seat of this residual strength parameter, one has to investigate the mechanism of strength generation at large strains at the particle level. The factor C' encompasses factors such as the mineral composition and the system chemistry. Residual shear strength is also known to be controlled by the normal effective stress, σ_n'.

2.3 Residual Shear Strength of Soil Minerals and the Factors Affecting it.

As mentioned before, there have been only two comprehensive investigations on the frictional characteristics of the soil minerals, one by Horn and Deere (1962) and the other by Kenney (1967). While the former have in general tried to determine the friction of a few massive and layer-lattice minerals, none of the common clay minerals except mica was investigated. Kenney (op. cit.) has investigated the common clay minerals as well as the massive minerals and the first fundamental insight into the nature of residual strength was obtained from his important contribution. He performed reversal direct shear tests on several natural soils, pure minerals and mineral mixtures at various rates of strain and under different normal loads. Details of mineralogy are reported in his work and where possible the composition of the pore fluid was controlled. Table 2.1 summarises his results. The important conclusions of Kenney are:

i) Residual strength of a clay is governed mainly by the type of mineral in the clay and it is not related to plasticity or grain-size characteristics.

ii) The massive minerals do not show residual strengths appreciably different from their peak strengths. In these cases, any

reduction in strength from the peak could be explained by the interlocking effects of the particles or by dilatancy (see also Borowicka, 1965; Morgenstern and Tchalenko, 1967 a). Residual friction angles for massive minerals are dependent on particle shapes, but are not dependent on particle sizes or on stress magnitudes. Quartz, feldspar and calcite exhibit the same values of $\tan\phi_r'$.

iii) Among the clay minerals, montmorillonite possesses the least strength and strength increases in the order: illite, kaolinite, mica and attapulgite.

iv) Monovalent clay minerals possess less strength than clays with substitutions by divalent ions.

v) System chemistry has a decided influence specially at small stress magnitudes on the residual strength of clay minerals such as Na-hydrous mica and Na-montmorillonite (see Figs. 2.1 and 2.2).

vi) $\tan\phi_r'$ is affected to a lesser extent by the magnitude of normal effective stress (Fig. 2.1). More recently, a variation in ϕ_r' with σ_n' (non-linearity of friction) has also been observed by Bishop et. al (1971) for brown London clay.

vii) Rate of strain has little influence on the residual shear strength (Fig. 2.3).

Although Kenney's (1967) work points out the factors which influence the residual shear strength, it makes no attempt to postulate a mechanism for the generation of shearing resistance at large strains.

Kenney (op. cit.) offered an explanation for the observed effects of system chemistry on the residual strength. In his view,

strength increases are caused by increased ion concentration in the pore fluid and by cations of larger valence and greater polarizability. For both hydrous mica and montmorillonite, the strength increases result from net increases in attraction between individual particles and by the formation of bonds between particles. However, Kenney (op. cit.) did not attempt to measure or estimate the increases in net attraction between individual particles due to increases in the ion concentration of the pore fluid and correlate these increases in net attraction between individual particles with the corresponding increases in the residual shear strength. Furthermore, the samples of any particular mineral he used for demonstrating the increase in the residual strength due to a corresponding increase in the pore fluid ion concentration were not at the same water contents (for example, see the w_{res}^{*} data for Na-montmorillonite and Na-hydrous mica under the pore fluid NaCl concentrations of 0 and 30 g/l in Table 2.1) and different water contents signify different particle spacings and hence varying physico-chemical forces of interaction for the samples. Obviously, this will have significant implications for the physico-chemical interpretation of the effect of system chemistry on the residual shear strength and it would seem that under a particular normal pressure, a direct comparison between the residual shear strengths of a mineral obtained under various pore fluid

---

* w_{res} = Water content of the shear zone at the residual state.

ion concentrations is legitimate only if the mineral samples that are
used for the comparison possess the same failure plane water content
at large strains (w_{res}). Hence, the explanation offered by Kenney (1967)
for the increase in the residual shear strength due to a corresponding
increase in the pore fluid ion concentration is merely speculative
and a definite need for further investigation into the physico-chemical
aspect of residual strength is noted.

With this knowledge in the factors which influence the
residual shear strength of clays and clay minerals, we can now proceed
to explore the mechanism for the generation of shear strength at large
strains. At large strains, the shearing resistance is said to arise
from the physical interaction of the soil particles alone. This
indicates that the most likely mechanism of strength generation at large
strains is a purely frictional one. Moreover, the cohesion component
of shear strength is virtually negligible at large strains. Hence,
in order to study a purely frictional model for the generation of shear
strength at large strains, one has to investigate the nature of inter-
particle contacts. In this context, the treatment of the shearing
resistance of soils as a rate process by Mitchell (1964) and Mitchell,
Singh and Campanella (1969) has made some significant contributions
to the understanding of the nature of interparticle contacts and
bonding between atoms in the surface structure of soil minerals. They
have also used this approach to suggest a mechanism for the generation
of shear strength at subfailure stresses and their work will be
reviewed in the next section.

2.4 Bonding and Strength of Soils

Mitchell and his co-workers (1964, 1969) applied the theory of absolute reaction rates or the rate process theory to the study of time-dependent deformation of soils and determined the nature of bonding energies (which have to be surmounted during shear) some soils possess at their interparticle contacts. They also expressed compressive strength of a soil as a function of the number of bonds at the interparticle contacts. Some significant conclusions about the nature of interparticle contacts were derived from their studies.

Mitchell's work is based on the premise that the deformation of a soil mass involves microscale movements of particles and proceeds at a rate commensurate with the structural state of the soil and the applied stresses. According to the theory of rate process (Glasstone, Laidler and Eyring, 1941), an activation energy is required for the local loosening of the particles or the flow units from their equilibrium positions and displacement to new positions. Sources of this energy are external forces such as shearing forces and the thermal energy contained by the material. The deformation proceeds at a rate dictated by the frequency with which particles can acquire sufficient energy "ΔF" (activation energy) to surmount the energy barriers between equilibrium positions. The magnitude of ΔF provides a measure of bond strengths holding flow units in place. In the unstressed state, particles may be assumed to occupy positions of minimum potential energy.

Using the theory of rate processes as the basis for analysis

of the creep test data, Mitchell et al. (1969) determined the experimental

activation energies for creep of several soils and their results are

reproduced in Table 2.2. Table 2.3 presents the activation energies

for creep of several other materials compiled from literature by the same

authors. For comparison purposes, the theoretical strengths of the

usual bonds in soils are presented in Table 2.4. It is immediately obvious

from Tables 2.2 and 2.3 that the activation energy of soils is in the

range of 30 to 45 kilocalories per mole which is high in comparison with

materials such as plastics and asphalt. Rupture of primary valence bonds

usually requires energies in excess of 20 kilocalories per mole

(Table 2.4). The fact that activation energy for deformation of soil

is well up into this range does not prove that bonding in soils is of

the primary valence type, because simultaneous rupture of several bonds

of a weaker type could yield values of the magnitude observed by

Mitchell et al. (op. cit.). But the fact that the activation energy

for deformation of soils is much greater than for flow of water (Table 2.3),

and that similar values of experimental activation energies were

obtained for wet and dry clays (Table 2.2) led Mitchell et al. (1969)

to conclude that bonding is through solid interparticle contacts.

Water in some form will be adjacent to particle surfaces. The water

structure consists of oxygen held together by hydrogen and is not too

different from the structure of silicate layers in minerals. Thus a

distinct boundary between a particle surface and water may not be

readily discernable as suggested by Trollope (1964). Mitchell

postulates that under these conditions, it might not be unreasonable

to think of a more or less continuous structure which propagates

through interparticle contacts. The observed similarity in magnitude between the activation energies for creep in clays (wet or dried) and in dry sands (Table 2.2) lends further support to the concept of solid-to-solid interatomic bonding.

Mitchell and his co-workers went a step further and determined the number of bonds per unit area in different soils under different conditions. They showed that the number of bonds per unit area is directly proportional to the effective consolidation pressure for normally consolidated soils. Remoulding an undisturbed clay was found to cause a reduction in both the number of bonds and the effective stress; however, the relationship between number of bonds and effective stress remained the same as for the undisturbed clay. They further correlated the number of interparticle bonds to the compressive strength for different soil types and demonstrated that strength is directly proportional to the number of bonds (Fig. 2.4) and is completely independent of whether the soil is undisturbed, remoulded, normally consolidated or over-consolidated. Their tests on sand showed that it behaved in all respects similar to clays which led them to suggest that the strength generating mechanism may be similar for both types of material.

As far as the actual nature of a flow unit is concerned, it could be an atom, a group of atoms or molecules or the entire contact between particles (Mitchell et al., 1969). The experimental activation energy values of 30 to 40 kilocalories per mole are compatible with those measured for solid state diffusion of oxygen in silicate minerals, thus supporting Rosenqvist's concept (quoted by Mitchell et al., 1969)

that creep movement could result from slow diffusion of oxygen ions in and around interparticle contacts. This led Mitchell to suggest that individual oxygen atoms can be considered as flow units.

Although sand and clay appear to behave in a similar fashion as far as interparticle bonding is concerned, Mitchell points out that an equal humber of interparticle contacts in the two materials is unlikely. However, a comparison between dry sand and clays showed that the values of the number of individual bonds were about the same for both the materials. Based on their concept of an interparticle contact containing many bonds between opposing atoms, they postulated from the above observation that because there are fewer contacts to carry effective stress in sand, each contact would contain many bonds; in a clay, the much greater number of contacts would mean fewer bonds per contact. The number of bonds at any contact was shown to depend on the compressive force transmitted at the contact. These findings led Mitchell et al. (1969) to suggest that the Terzaghi-Bowden and Tabor adhesion theory of friction may be applicable to the conditions at the contact. According to this theory in its simplest form, the contact area A_c will be given by

$$A_c = \frac{N}{\sigma_y} \tag{2.4}$$

in which N = the normal force, and σ_y = the yield strength of the material in the contact zone.

From their work on bonding in soils, Mitchell et al. (1969) envisaged the sources of friction and cohesion in soils. According to

them, interparticle bonds may form in response to the interparticle contact
forces generated by either applied stresses, physico-chemical forces
of interaction or both. It should make no difference which of these
generate the contact area in terms of the strength of the contact.
However, the role of physico-chemical forces of interaction is to control
the initial soil fabric and to alter the force transmitted at contact
points from what it would be due to the applied stresses alone.
Thus the total strength along any plane would be proportional to the
number of bonds (and not the number of contacts) which in turn is
controlled by the net contact stresses in that plane. In absence of
significant interparticle physico-chemical forces, contact areas are
formed only due to normal stresses applied to the soil structure and
the strength behaviour would be purely frictional. Any interparticle
bonds existing in the absence of applied contact forces, i.e., $\sigma_n' = 0$,
are responsible for true cohesion. There should be no difference,
however, between friction and cohesion in terms of the shearing process
(Mitchell et al.,1969).

At subfailure stresses, according to Mitchell et al. (op. cit.)
deformation may involve continuous breaking down and making of bonds and
contacts. Complete failure in shear involves simultaneous rupture of
all bonds along the shear plane. Hence, peak shear strength of a soil
may be considered as that applied shear stress which causes a
simultaneous rupture of all the bonds of high activation energy (30-45
kilocalories per mole) along the shear plane.

The concept of shearing strength arising out of shearing

of contacts has also been put forward by Trollope (1961), Newland (1965) and Morgan (1967). The mechanism suggested by Trollope (op. cit.) and Morgan (op. cit.) for the generation of shear strength is that the shear strength of a soil may be related to the summation of the interacting forces at contacts along a plane assuming that the nature of shear strength is similar to the Bowden-Tabor theory of metal friction. Newland (1965), however, postulated somewhat different mechanism than that presented by Mitchell et al. (1969). He proposed that the effective stress is the component of applied stress which is effective in overcoming potential barriers at contact points between particles, thus allowing bonds to be formed. Once formed, however, the resistance to sliding at the contacts is considered to arise solely from the strength of the bond and is independent of the applied stress. The strength of the soil on any plane, according to Newland, is then a function of the number of contacts. No clear distinction is made by Newland between bonds and contacts, although it may be inferred that the term bond is used to indicate the source of the total strength mobilized at a contact. The classical concept of friction is rejected by Newland (op. cit.), because in a frictional system, junctions between particles disappear if the normal force is reduced to zero, and, therefore, the strength becomes zero. Thus, the cohesive nature of clays can not be accounted for by Newland's hypothesis. In Mitchell et al.'s hypothesis, however, this problem is readily overcome by allowing for the existence of interparticle normal forces in clays that originate solely from physico-chemical interactions, e.g., van der Waals forces.

The work of Mitchell et al. (op. cit.) is also open to criticism because they compared the number of bonds determined under subfailure stresses with the failure stress. They, however, argued that the comparison made by them may not be unreasonable in view of some data obtained by Campanella (Mitchell et al., 1969) which apparently showed that the number of bonds does not change significantly with increases in strain. If strength is dictated by the number of bonds along the shear plane, then it can be inferred from Campanella's observation that a steady value of shear strength is attained at large strains because the number of bonds does not change with increases in strain.

Although Mitchell and his co-workers did not postulate a mechanism for the generation of shear strength at large strains on the basis of the total bonding energy available along a shear plane, their study established some important basic aspects of the fundamental nature of shear strength. The important conclusions drawn by Mitchell et al. (1969) from their work may be summarised as follows:

i) Interparticle contacts are effectively solid-to-solid and may contain many bonds between opposing atoms. These contacts are the only significant region between soil grains where effective normal stresses and shear stresses can be transmitted.

ii) While different interparticle contacts may have widely varying strengths because of differing numbers of bonds per contact, individual bonds are of approximately equal strength. Interparticle bonds are strong, perhaps approaching the magnitude of primary valence bonds.

iii) The role of water appears to be to influence the number of bonds that form (through its influence on effective stress) but not to effect significantly the strength of individual bonds.

iv) The number of bonds at any contact depends on the compressive force transmitted at the contact.

v) The Terzaghi-Bowden and Tabor adhesion theory of friction would appear to account for conditions at interparticle contacts.

vi) For normally consolidated clays, the number of bonds developed is directly proportional to the effective consolidation pressure. In clays, reduction of the effective consolidation pressure is not accompanied by a disappearance of all the bonds formed during consolidation, thus accounting for higher strengths in overconsolidated soils.

vii) Strength is directly proportional to the number of bonds and approximately the same proportionality holds for different soil types.

Since shear strength at large strains is said to arise from the physical interaction of mineral particles alone (implying that it is purely a frictional phenomenon), the abovementioned conclusions drawn by Mitchell et al. (1969) from their study of shearing resistance of soils as a rate process form a very important background indeed for establishing a physical basis of residual strength.

2.5 Microstructural Studies of the Large Displacement Shear Zones in Clays

It was briefly mentioned in Chapter I that considerable fundamental insight into the nature of residual strength was obtained

from the microstructural studies of the large displacement shear zones in clays undertaken by Morgenstern and Tchalenko (1967 a, b) and Tchalenko (1967, 1968 and 1970). Their approach was one of correlating the large displacement shear zone structure to the residual strength. From an examination of the development of various structures in the large displacement shear zones in clays, they also suggested a basic mechanism for deformation in the shear induced structures at large strains.

Morgenstern and Tchalenko (1967 a) studied the structures formed at various stages of deformation in the shear box by interrupting tests on initially identical samples of kaolinite at different points of the stress-displacement curve, and by preparing thin sections of the entire sample. The increase in particle parallelism occurring in the shear zones enables the shear induced structures to be distinguished, in polarized light under an optical microscope, from the surrounding material. This is because of the fact that the birefringence ratio in both the shear zone and the ambient material determined from observations on areas of equal size will usually differ. Moreover, the shear zone is characterized by the presence of shear planes. The shear planes are incorporated in a shear matrix which has a texture, extent and orientation of which depend upon the composition of the sediment and its displacement history.

Using the above mentioned technique, Morgenstern and Tchalenko (op. cit.) studied the shear induced structures developed at the following stages of deformation in the shear box test:

a. Pre-peak strength deformation structure,

        b. Peak structure,

        c. Post-peak structure,

        d. Pre-residual structure,

        e. Residual structure.

They interpreted the structures developed at the various stages of shear in terms of the Mohr-Coulomb failure criterion and demonstrated a progressive evolution from simple shear structures at the peak strength state to principal displacement shears at the residual state. However, we need concern ourselves here only with the structural features of the large displacement shear zones. For a more thorough and detailed account of the shear induced structures developed at various stages of deformation in a shear box test, the interested reader is referred to Tchalenko (1967).

From the microstructural examination of the large displacement shear zones, Morgenstern and Tchalenko (1967 a, b) and Tchalenko (1967, 1968 and 1970) noted that a definite mode of particle arrangement is associated with the residual strength. This particle arrangement in the large displacement shear zones is found to be slightly different from the classical concept of a parallel orientation of the shear zone particles aligned in the direction of motion in the shear box. Morgenstern and Tchalenko found that at residual state, the combination of displacement along the first shears, referred to as the "Riedel (R) shears", which appear just before peak shear strength is reached and thrust shears, referred to as the "P shears", which evolve as post peak structures leads to the formation of the principal displacement

shears oriented in the general direction of motion in the shear box. Simultaneously, the active portion of the shear zone decreases in width until movement is concentrated in a very thin zone or on a single slip surface. Morgenstern and Tchalenko (1967 a) also noted that the ultimate structure governing the residual strength is not achieved in one traverse of the shear box. They found that the continuous slip surfaces formed in their kaolinite samples after one traverse of the shear boxes were distinctly wavy and it is fair to assume that further displacement along these planes would have reduced the irregularities.

The residual state shear zone structures formed in the direct shear test, as observed by Morgenstern and Tchalenko (1967 a) and Tchalenko (1968), are illustrated in Figs. 2.5 and 2.6. Generally the particles forming the displacement discontinuity were initially at an angle of 0° to -15° to it. Where these displacement discontinuities evolved further, they were composed of two thin bands of particles at their periphery aligned in the direction of motion, separating a thicker highly oriented band with particles aligned at -40° to -50° (Fig. 2.5). This internal structure was termed "compression texture" by Morgenstern and Tchalenko (1967 a) and compression textures are often found in the shear zones of landslides in clays (Morgenstern and Tchalenko, 1967 b). The basal planes of the particles inside the compression texture are usually found to be approximately normal to the major principal stress (Figs. 2.5 and 2.6).

This ultimate structure governing the residual strength was also produced by the same authors by precutting a horizontal plane in a

kaolinite sample and subsequently shearing it along the precut plane
to the residual state. Tchalenko (1967) studied the ultimate structure formed
in a reversal test specimen (Fig. 2.7) that was subjected to several
travels made in opposite directions. The shearing off of protrusions
at each reversal produced thin horizontal bands (as shown in Fig. 2.7)
which retained to a certain degree the two compression textures produced
by the opposite displacement directions.

Morgenstern and Tchalenko (1967 b) and Tchalenko (1968, 1970)
supplemented their observations on the shear zones from the laboratory
samples with further microstructural observations on the shear zones
from field slips and demonstrated that similar ultimate structures also
characterise the large displacement shear zones in field slips. They
observed well developed compression textures in the shear zones from
slips in Oxford and Atherfield clays (Morgenstern and Tchalenko, 1967 b).
Tchalenko (1968) provided the most impressive example of compression
texture developed in a large displacement shear zone while dealing with a
landslide at Walton's Wood in Staffordshire.

Hence, from their exhaustive study of the microstructural
features of the large displacement shear zones in laboratory samples,
Morgenstern and Tchalenko (op. cit.) and Tchalenko (1968) established
that the principal displacement discontinuities formed at the residual
state in a shear box are comprised of substructures of the thrust type
and compression textures in which the average particle orientation is
approximately normal to the major principal stress (Figs. 2.5 and 2.6).
The major principal stress can be predicted to be at $45°-\phi_r'/2$ to the
direction of the slip surface which is also the general direction of

movement and the microscopic substructure of the shear zones seems to confirm this (Tchalenko, 1970). This is also true for shear zones in the field where deformation approximates direct shear condition at large strains.

In the case of shear box specimens, Morgenstern and Tchalenko (1967 a) and Tchalenko (1967) accounted for all the components of the shear induced structures by some combination of basal-plane gliding producing translation and rotation. The development of displacement discontinuities across a particle did not appear to them to be a possible mode of motion presumably because of the high relative strength of the particles. Hence, imposed irreversible deformations must be accommodated by rigid-body movements of the clay particles. From an examination of the substructures formed in the shear box specimens, Morgenstern and Tchalenko (1967 a) found that kinking is the dominant mode of deformation in the production of the major structures. Paterson and Weiss (1966) emphasized the mechanical instability associated with the kinking process in triaxial tests on phyllite. They demonstrated that when gliding begins locally within the body, the glide plane rotates to orientations more favourable to gliding. The process stops when the shear stress on the glide plane can again be supported by the resistance to gliding. The relaxation and redistribution of stresses around a kink-band* is apparently reflected for these tests on phyllite

---

* Kink-bands are defined as "tabular fold-zones resulting from the operation of a shear couple" (Dewey, 1965). They are structures of a characteristic geometry and are found both in deformed foliated rocks and in single crystals.

in the shape of stress-strain curve. The final orientation of the foliation in each limb of a kink-band has as yet received little attention in the laboratory. The results reported by Tchalenko (1967) suggest that in the shear box configuration, the bedding in the short limb tends towards the normal to the major principal stress direction whereas in the long limb it remains parallel to this direction.

Tchalenko (1968) has shown that the compression textures are usually brought about by the interaction of the microscopic shear discontinuities and kink-bands which form in simple shear deformations taken to large strains. Detailed examination of the development of kink-bands and compression textures led Morgenstern and Tchalenko (1967 a, b) to suggest basal plane slip as the basic mechanism of deformation in the shear induced structures at large strains. Although no detailed explanation for the compression texture was given by Morgenstern and Tchalenko (op. cit.), the closest analogy of this feature is with the observations by Bowden and Tabor (1964) on the attitude of graphite crystals in friction tests. From their observations, Bowden and Tabor (op. cit.) also suggested basal plane slip as the dominant mode of deformation in the compression textures formed in polycrystalline graphite subjected to sliding friction. These friction tests conducted by Bowden and Tabor (op. cit.) on polycrystalline graphite are described in the next section.

These deformation mechanisms postulated from the microstructural examination of the shear zones in laboratory samples were later applied successfully by Tchalenko (1970) to interpret similar

structures in tectonic shear zones in hard rocks. The movement picture
is obviously more complicated in field shear zones than the one postulated
for the laboratory tests because deformation in the field takes place
both on the submicroscopic scale in the compression texture and on the
microscopic scale in the discontinuities.

Hence, if basal plane slip is the dominant mechanism of
deformation in the shear induced structures at large strains, then it
would appear that the physical basis of residual strength may reside
in the solid friction along the mineral basal planes and the shearing
resistance at large strains is due to the frictional property of the
mineral basal planes. A similar view has been expressed by Morgenstern
(1967) who in fact suggested that the physical basis of the low
residual strength exhibited by most clays may reside in basal plane
shear of platy particles. In this respect, the low friction of lamellar
solids such as graphite is suggestive and it may be rewarding to study
recent research in solid lubrication in order to further our under-
standing of the nature of residual strength in clays.

2.6   Frictional Behaviour of Solid Lubricants

The best known solid lubricants which combine anisotropy
with good substrate adhesion are the lamellar solids, graphite and
molybdenum disulphide (MoS_2). Although a large variety of solids is
still being studied, the vast majority of inorganic solid lubricants
in practice contains graphite, MoS_2 or a blend of the two.

The crystal structure of the two materials is similar.

They have a "layer-lattice" structure (similar to some platy clay minerals) in which the atoms in each layer or "basal planes" are located at the corners of regular hexagons. Their hexagonal structures are illustrated in Fig. 2.8. In graphite, the interatomic distance between the carbon atoms within the basal planes is 1.42 $\overset{\circ}{A}$ whereas the basal planes themselves are 3.40 $\overset{\circ}{A}$ apart (Fig. 2.8a). Each layer in MoS_2 consists of three planes - a central molybdenum core sandwiched between sheets of sulphur atoms (Fig. 2.8b). In both graphite and MoS_2, strong covalent bonds exist between the atoms in each layer which are able to withstand high pressures normal to their surface but the bonding between the layers or the basal planes are physical (van der Waal type) rather than chemical and hence comparatively weak. Estimates for graphite indicate that the interlayer bonding energy between adjacent carbon atoms within each plane may range from 1 to 20 kilocalories per mole whereas the bonding energy between the basal planes never exceeds 0.5 to 5 kilocalories per mole (Braithwaite, 1964). Under shear, the lattice therefore separates most easily between the basal planes, although the force required to effect this separation will depend critically upon the manner in which the interlayer bonds are broken. In the case of MoS_2, the lattice also separates easily between the basal planes because the bonding energy between the triple plane sets is weak van der Waal's bonding (0.5 to 5 kilocalories per mole). The force required to shear the graphitic structure along the basal plane is dependent not only upon individual bond strength, but also upon the total number of bonds under shear at any one time. This concept has also been shown to be valid for shearing in soils by

Mitchell et al. (1969) from their extensive study of the relationship between bonding and strength of soils (described previously in section 2.4).

Bowden and Tabor (1964) have favoured molecular adhesion between surfaces as the most possible cause for frictional resistance. Tomlinson postulated the theory of molecular adhesion in 1929 and in its simplest form, the theory states that the load between two sliding surfaces is supported by repulsion between molecules on either side which penetrate beyond one another's field of attraction and that energy lost through penetration followed by separation during sliding manifests itself as friction. A detailed account of the molecular adhesion theory of friction, its limitations and comparison with other postulated theories of friction has been given by Carlisle (1965). While dealing with the Roberts Mountains overthrust in north-central Nevada, Carlisle (op. cit.) demonstrated by crude calculations with the Tabor equations that the low angle (2°-3°) gravity sliding on the eastern 50 miles of the large overthrust can only be accounted for by the coefficient of sliding friction of the wet, undrained clay layer (with abnormally high pore pressures) between the upper and the lower limestone blocks of the thrust sheet and this coefficient of friction of the interface clay layer was estimated from the strengths of materials using a modified adhesion theory of friction developed by McFarlane and Tabor (1950 a, b) for ideal plastic materials. The Terzaghi-Bowden and Tabor adhesion theory of friction has also been favoured by a score of research workers (such as Trollope, 1961; Morgan, 1967 and Mitchell et al., 1969)

as the theory that describes the nature of shear strength in soils.

There are four types of intercrystalline bonding in solid lubricants:

    i)   edge-to-edge,

    ii) edge-to-basal plane,

    iii) multiple junction, and

    iv) basal plane-to-basal plane.

For most solid lubricants, sliding is easy along well defined cleavage planes (Bowden and Tabor, 1964). The low friction of lamellar solids is thus explained by the low force required to shear the cleavages because of weak interlayer bonding. Hence, the recent research in solid lubrication appears to suggest that in the case of a mineral with a well defined basal mode of cleavage, the resistance to shear along the cleavage planes will be low and consequently, the mineral will exhibit low shear strength.

Many measurements have been made of the friction of polycrystalline graphite (Bowden and Tabor, 1964) and the definite mode of structural arrangement of graphite grains observed during these friction tests is remarkably similar to the shear zone particle arrangement associated with the residual strength of clays. For steel on graphite or graphite on graphite, the friction is of the order $\mu \simeq 0.1$. A single crystal of graphite is surprisingly ductile and there is evidence to show that dislocation movement is relatively easy. Hence, as mentioned earlier, separation of one plane from another by cleavage can occur far more rapidly if suitable tensile stresses are

applied. The major deformation mode for polycrystalline graphite subjected to sliding friction is by cleavage from an edge of a grain or defect within the grains rather than by plastic flow. Electron diffraction studies have revealed that after a graphite surface has been subjected to rubbing, some of the grains acquire a preferred orientation as shown in Fig. 2.9. The angle of tilt Θ of the basal planes of these grains is about 5° to the horizontal so that $\tan \Theta \simeq 0.1$. This means that the basal planes are normal to the resultant (R) of the normal load (W) and the frictional force (F) and this has been referred to as a "compressional texture" by Bowden and Tabor (op. cit.). Although the detailed process by which this structure is achieved are not yet known, similar features have been observed during friction and wear studies on a variety of materials (e.g. Alison, Stroud and Wilman, 1965). However, Midgely (quoted by Bowden and Tabor, 1964) has suggested that there may be rotation of individual grains, some basal plane slip and in addition the removal of crystallites in unfavourable orientations. If the direction of sliding is reversed, the friction of graphite is initially increased ($\mu \simeq 0.12$) but soon returns to a lower value ($\mu \simeq 0.1$) and the orientation of the compression texture is reversed in direction. This phenomenon is also observed in shear tests on soils. Hence, the attitude of graphite crystals in these friction tests is the closest analogy from the field of solid lubrication to the ultimate compression textures observed in the large displacement shear zones in clays.

The classical interpretation of the low friction coefficients

of graphite and MoS_2 in terms of weak interlayer bonding has, however, been rejected by some research workers such as Finch (1950) and Spreadborough (1962). Finch (op. cit.) has expressed the opinion that cleavage by simultaneous rupture of bonds in a plane needs very high energy. Spreadborough (op. cit.) has further discredited the idea of "ease of shear" and has proposed that graphite does not shear readily and failures are usually tensile unless a high compression is superimposed. He visualises the friction process in graphite being first an orientation of surface crystallites into a basal plane orientation nearly parallel to the surface. The cleavage fragments then roll up into minute scrolls and Spreadborough (op. cit.) has proposed that the low friction is due to rolling of these scrolls between the surfaces. Although this is an interesting suggestion, there is no quantitative evidence to show that this is so. Most of the evidence is in favour of the view that graphite is strong in compression, so giving a small area of contact, and weak in shear, so giving a low value to the interfacial shear strength (Bowden and Tabor, 1964).

Kenney (1967) has pointed out that the residual friction angle (ϕ_r') of a natural soil or of a clay mineral is dependent on the magnitude of normal effective stress (σ_n'). A variation in ϕ_r' with σ_n' has also been observed for brown London clay by Bishop, Green, Garga, Andresen and Brown (1971). From these results, a significant decrease in residual strength can be found with increasing pressure for clayey materials. This has important implications for the interpretation of large scale geological thrust

and gravity structures. For example, Shouldice (1963) reviews evidence of gravity-induced sliding movements along a thin bentonite seam within the Colorado shale. This seam is inclined at only 2° to the horizontal but is beneath 1,100 feet of sediment. A strength extrapolated from Kenney's (1967) data would account for this feature. A similar example of the reduction of residual friction angle at high normal stresses playing a major role in inducing a low angle (2 to 3°) gravity sliding along a saturated clay seam between the limestone thrust sheets of the Roberts Mountains overthrust is also reported by Carlisle (1965). The practical significance of the variation in ϕ_r' of the brown London clay with σ_n' as applied to slope stability analysis has been discussed by Bishop et al. (1971).

However, no explanation for this observed variation in ϕ_r' with σ_n' has been offered in the geotechnical literature. The coefficients of friction of some solid lubricants (such as graphite and MoS_2) are also found to decrease with increasing normal loads (Fig. 2.10) and an explanation for this non-linearity of friction with stress level is available in the solid lubrication literature. Since it is apparent from reviewing the solid lubrication research so far that the nature of residual strength in clays may be quite similar to that of some common lamellar solids, it may not be entirely unreasonable to presume that the model developed by researchers in solid lubrication to explain the variation in friction of lamellar solids with stress level may also be applicable to explain the variation in ϕ_r' with σ_n' for soils.

The variation in the friction of lamellar solids with

applied stress has been explained in terms of the dependence of the area of real contact between sliding surfaces on the applied load (Bowden and Tabor, 1964). The studies of surface topography using refined profilometer techniques have made it possible to demonstrate that even the most highly polished surfaces have a relief in the order of hundreds or thousands of angstroms and when placed together they are in real contact only at high points. The real contact area increases as the normal load is increased. If frictional resistance is caused by molecular adhesion, then friction might be expected to be related to the area of real or intimate contact rather than the total area of apparent contact. However, according to the classical law of friction proposed by Amonton (1699), coefficient of friction should be independent of the area of the surfaces in contact during sliding. Hence if the friction coefficient decreases as the load is increased (Fig. 2.10), Amonton's law is evidently not being obeyed. This is indeed the case for most lamellar solids and clay minerals which exhibit a marked variation in the coefficient of friction with the applied stress especially in the low pressure range (Figs. 2.10 and 2.1).

Because of the experimental difficulty of determining the true area of contact, a number of theoretical models have been developed in the field of solid lubrication showing how the contact area may be expected to vary with the load. The simplest and most instructive is that due to Archard (1953). He has considered a surface covered with asperities of spherical shape. The two extreme types of deformation are purely plastic and purely elastic. For purely plastic

deformation, the area of contact is directly proportional to the load. If the deformation of asperities is truly elastic, the Hertz theory requires that, for a single asperity pressing against a smooth surface,

$$A_c = k. W^{2/3} \tag{2.5}$$

rather than the direct proportionality of the area of true contact (A_c) and load (W), the constant k being related to the local radius of curvature of the surface and the elastic constants of the materials.

Archard (1953, 1957) has then proposed two possible ways in which elastic deformation can take place.

a. Contact occurs over a fixed number of asperities and the effect of increasing the load is simply to increase the elastic deformation of each asperity. In this case, the area of real contact is proportional to $W^{2/3}$.

b. Contact occurs over a large number of asperities, the average area of each deformed asperity being constant. Increasing the load in this case increases the number of regions of contact proportionately. Clearly the area of real contact is directly proportional to W.

With real surfaces, we may expect an intermediate behaviour. Consequently, for pure elastic deformation the area of real contact will be proportional to W^n, where n lies between 2/3 and 1.0 (Lincoln, 1953; Rubenstein, 1956 and Archard, 1957). If this is the only factor affecting the friction, the friction will also follow a relationship of this sort.

Campbell (1969) has explained the decrease in the coefficient of friction of MoS_2 with increasing normal load (Fig. 2.10) in light of the above model. The model has also been confirmed experimentally, both with polymeric minerals (Archard, 1957) and diamond (Bowden and Tabor, 1964). Diamond is, of course, a very hard material and we should expect the deformation in the contact region to the mainly elastic. Bowden and Tabor (op. cit.) have demonstrated that for diamond on diamond, the geometric area of true contact varies as $W^{2/3}$ (which is in exact agreement with Hertz's solution for purely elastic deformation). Consequently, the coefficient of friction decreases as the load is increased (Fig. 2.11) and follows approximately a law of the type $\mu = k.W^{-1/3}$ in the low normal load range. Archard (1957) and Bowden and Tabor (1964) have further shown that in the high load range where the number of contacts per unit area is large and tends to increase as load is applied, n approaches 1.0 at which limit elastic and plastic junction growth are equivalent. This means that in the high normal load range, the area of true contact is proportional to W and consequently, the coefficient of friction becomes independent of the area of real contact and Amonton's laws are obeyed again.

The abovementioned model may help to explain the variation in ϕ_r' with σ_n' for some clays whose frictional characteristics are remarkably similar to those of the lamellar solids. The concept may be specially applicable to heavily overconsolidated clays which are sheared under low normal stresses because under these circumstances, the deformations at the interparticle contacts may be truly elastic.

An attempt has been made in the next chapter to explain the variation in ϕ_r' with σ_n' for clays in light of the above mentioned model.

In conclusion, it may be stated that there is a striking resemblance between the frictional behaviour of the lamellar solids and some clays and extensive use of the concepts of friction derived from the solid lubrication research has been made in this dissertation to establish a physical basis for the residual strength of pure clay minerals.

TABLE 2.1 PHYSICAL PROPERTIES OF MINERALS AND SOILS (AFTER KENNEY, 1967)

Natural Soil or Mineral (Reference)	Origin	Salinity (1)	Plasticity		Grain Size		Activity	Cation Exchange Capacity m. eqv. per 100 gm	Massive Minerals (% dry weight)					Clay Minerals (% dry weight)					Residual State (2)	
		gm/l	w_L	w_P	Range	<2μ			Quartz	Feldspar	Calcite	Others	Total	Kaolin	Chlorite	Mica, hydrous mica illite	Mixed layers with montmorillonite	Montmorillonite	w_{r-r}	tg φ_r
			%	%	μ	%			%	%	%	%	%	%	%	%	%	%	%	
Natural Soils																				
Selnes, Norway (Kenney, 1967 b)	Very sensitive clays	< 2	23	17	< 60	42	0.16	11	25	10		15	50		5	45			21	0.60
Manglerud III, Norway (Bjerrum and Landva, 1966)		< 2	34	21	< 60	44	0.30	11	15	15	1	5	35		15	45	5		25	0.36
Asrum I, Norway		< 2	37	22	< 60	43	0.34	9	15	15		10	40		15	45			25	0.30
Labrador, Canada (Kenney et al, 1967)		< 2	32	22	< 60	55	0.18	13	10	20			30		15	55			26	0.32
Ottawa (weathered), Canada		< 2	67	31	< 60	70	0.53	20	10	20	1	10	40		5	50	5		30	0.33
Sandnes I, Norway (Bjerrum, 1966)		< 2	31	18	< 200	42	0.30	13	20	10	5	5	40		20	30	10		34	0.33
Sandnes II, Norway (Bjerrum, 1966)		< 2	71	28	< 60	80	0.55	–		10	5	10	25	5	15	40	10	5	52	0.25
Little Belt, Denmark (Hvorslev, 1960)	Clay shales	11	121	40	< 60	58	1.4	45	3		17	5	25	30		10	5	30	40	0.16
Bearpaw, Canada (Peterson, 1958, Bingheim, 1964)		low	117	31	< 60	54	1.6	25	20	5	1		25			15	60		60	0.11
Pierre, USA	↓		148	42	< 20	56	1.8	30	15	5			20			10	←70→		70	0.10
Pepper, USA (Van Auken, 1963)	↓		96	25	< 60	56	1.2	25	15	10	0.3	5	30	45		15	5	5	38	0.10
Cucaracha, Panama	↓		50	33	< 100	(24)	0.7	61	10				10	←90→					42	0.11
Vajont I, Italy	Clay interbeds in limestone strata		106	35	< 75	70	1.0	55	5	5	30	10	50				←50→		–	0.18
Vajont II, Italy			106	40	< 75	68	1.0	70	10		7	3	20			←5→	←75→		48	0.16
Vajont III, Italy Müller, 1964 Kenney, 1967 a)			62	18	< 60	32	0.8	27	5		40		45			←35→	←20→		27	0.28
Minerals (3)																				
Quartz	Crushed				60–2	≈0			100										33	0.60
Quartz	"				< 2	100			100										–	0.70
Feldspar (microcline and albite)	"				60–2	≈0				100									30	0.60
Feldspar (microcline and albite)	"				< 2	100				100									–	0.60
Calcite	"				60–2	≈0					100								22	0.69
Sahara sand (4)	Dune				> 200	0													33	0.58
SiO_2 (amorphous) (5)	Flue dust		33	28	0.5–0.01	100	0.05	2											38	0.56
Attapulgite		≈0	345	106	< 60	74	3.2	22	< 5										166	0.57
Muscovite	Crushed	≈0			60–20	0										100			97	0.36
Muscovite	"	≈0	63	55	< 2	100	0.08	28								100			70	0.43
Na-muscovite	"	30	98	62	< 2	100	0.36	28								100			–	0.34
Na-muscovite	"	≈0			< 2	100		28								100			–	0.31
Na-hydrous mica	Fine fraction of Selnes quick clay	30	99	30	< 2	100	0.60	28		5		5	10		5	85			46	0.43
Na-hydrous mica		≈0	51	33	↓	↓	0.18	↓		↓		↓	↓		↓	↓			30	0.29
K-hydrous mica		30	118	46	↓	↓	0.72	↓		↓		↓	↓		↓	↓			47	0.46
K-hydrous mica		≈0	84	39	↓	↓	0.45	↓		↓		↓	↓		↓	↓			45	0.30
Ca-hydrous mica		15			↓	↓		↓		↓		↓	↓		↓	↓			41	0.47
Ca-hydrous mica		≈0			↓	↓		↓		↓		↓	↓		↓	↓			42	0.44
Na-hydrous mica		30	151	53	< 0.5	100	0.98	28		5		5	10		5	85			51	0.49
Na-hydrous mica		≈0	87	46	< 0.5	100	0.41	28		5		5	10		5	85			–	0.37
Kaolinite		≈0	50	37	< 10	72	0.21	9						95		< 5	< 5		35	0.27
Na-montmorillonite	Fine fraction of KWK bentonite	30	620	45	< 2	100	5.8	115										100	230	0.10
Na-montmorillonite		≈0	1,325	53	< 2	100	12.7	115										100	465	0.07
Na-montmorillonite		30	998	47	< 0.1	100	9.5											100	160	0.13
Na-montmorillonite		≈0	1,995	56	↓	↓	19.4											↓	645	0.07
Ca-montmorillonite		$CaSO_4$ Sat'd	775	47	↓	↓	7.3											↓	116	0.18
Ca-montmorillonite		≈0	795	47	↓	↓	7.4											↓	135	0.17
Treated Soil																				
Na-Grundite, USA		30	130	43	< 2	100	0.85	30								70	30		60	0.18
Na-Grundite, USA		≈0	164	46	↓	↓	1.2	↓								↓	↓		78	0.20
Ca-Grundite, USA		≈0	163	49	↓	↓	1.2	↓								↓	↓		80	0.18

(1) For the natural soils the pore-fluid composition was not determined, and salinity is expressed as the concentration of NaCl that gives equal electric conductivity to that of the pore fluid.

(2) $\sigma'_n \approx 1.0$ kg/cm².

(3) Na-sodium, K-potassium, Ca-calcium. Except where otherwise noted, these homoionic minerals were prepared by using the salts NaCl, KCl and $CaCl_2$ respectively

(4) Mineral mixture.

(5) Non-mineral.

TABLE 2.2

ACTIVATION ENERGIES FOR CREEP OF SEVERAL

SOILS (AFTER MITCHELL ET AL., 1969)

Soil	Experimental activation energy, in kilocalories per mole
Saturated, remolded illite; water contents of 30% to 43%	25 - 40
Dried illite; samples air dried from saturation then evacuated over dessicant	37
Undisturbed San Francisco Bay mud	25 - 32
Dry Sacramento River sand	~25

TABLE 2.3

ACTIVATION ENERGIES FOR CREEP OF SEVERAL MATERIALS

(COMPILED BY MITCHELL ET AL., 1969)

Material	Activation energy, in kilocalories per mole
Water	4 - 5
Plastics	7 - 14
Asphalt	14 - 20
Dilute montmorillonite-Water paste	20 - 26
Soil-asphalt	27
Undisturbed and remolded lake clay	23 - 27
Dry sand	~25
Overconsolidated Osaka clay	29 - 32
Undisturbed San Francisco Bay mud	25 - 32
Saturated illite	23 - 40
Dried illite	37
Concrete	54
Metals	50
Frozen soils	94

TABLE 2.4

THEORETICAL STRENGTHS[*] OF VARIOUS TYPES OF BOND

Type of Bond	Strength in Kilocalories/gm-mole
Primary valence bond	20 - 200
Hydrogen bond	5 - 10
Secondary valence bond	0.5 - 5

[*] Values obtained from the book entitled "Mechanical Behavior of Materials" by McClintock and Argon (1966): Addison-Wesley Publishing Company, Inc., Mass., U.S.A.
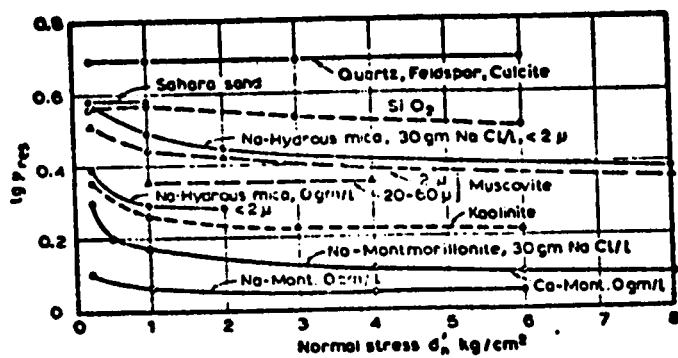
FIG. 2.1   RELATIONSHIPS BETWEEN TANϕ_r' AND
NORMAL STRESS FOR DIFFERENT
MINERALS (AFTER KENNEY, 1967)
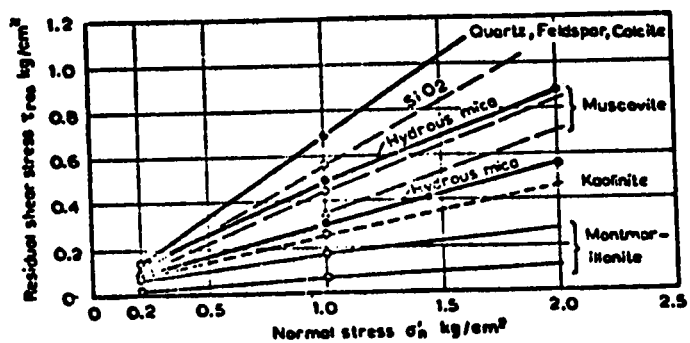
FIG. 2.2   RELATIONSHIPS BETWEEN RESIDUAL
SHEAR STRESS AND NORMAL STRESS
FOR DIFFERENT MINERALS (AFTER
KENNEY, 1967)
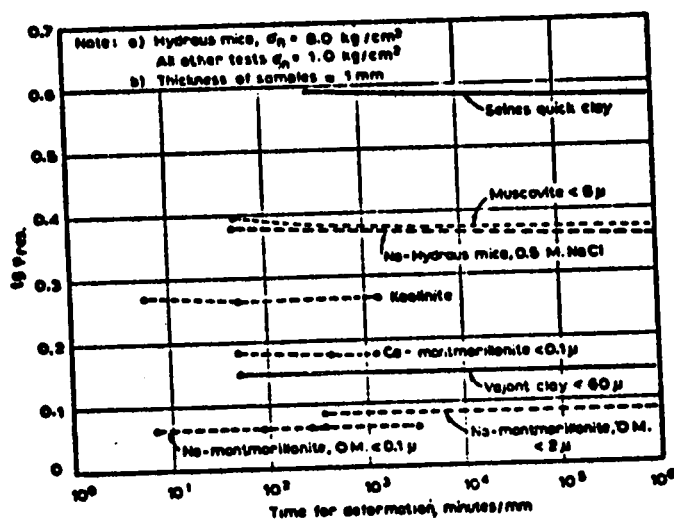
FIG. 2.3 INFLUENCE OF RATE OF STRAIN ON RESIDUAL STRENGTH (AFTER KENNEY, 1967)
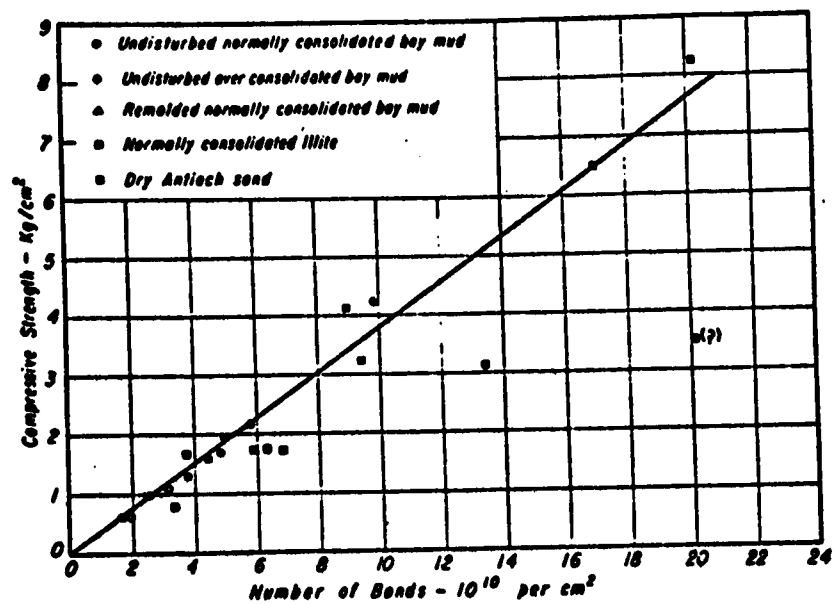
FIG. 2.4   COMPRESSIVE STRENGTH AS FUNCTION OF NUMBER
OF BONDS (AFTER MITCHELL ET AL., 1969)
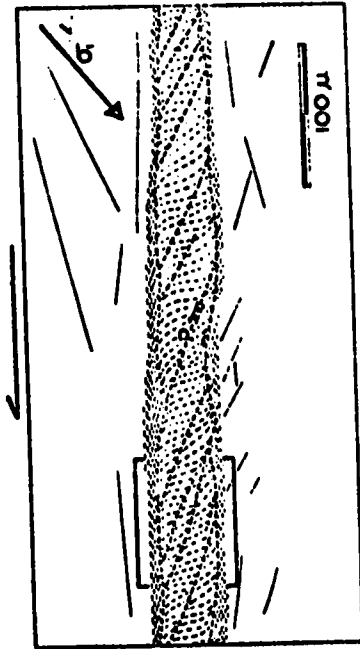
FIG. 2.5   PRINCIPAL DISPLACEMENT SHEARS IN THE DIRECT SHEAR TEST.
P = THRUST SHEARS; σ_1' = MAJOR PRINCIPAL STRESS DIRECTION AT RESIDUAL STRENGTH;
HATCHINGS = PARTICLE ORIENTATION IN THE COMPRESSION TEXTURE; WHITE AREAS =
PARTICLES IN THE INITIAL FABRIC ATTITUDE (AFTER TCHALENKO, 1968)
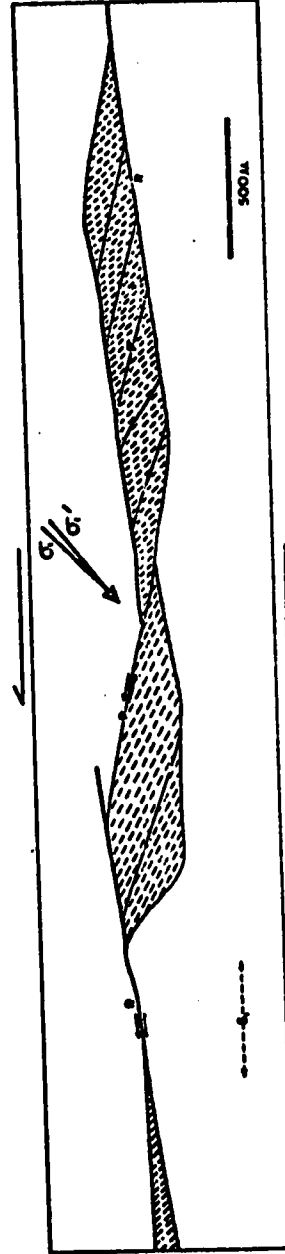
FIG. 2.6   STRUCTURES FORMED IN THE DIRECT SHEAR TEST.
P = THRUST SHEARS; R = RIEDEL SHEARS; S_1 = INITIAL FABRIC ATTITUDE;
σ_1, σ_1' = MAJOR PRINCIPAL STRESS DIRECTIONS AT PEAK AND RESIDUAL STRENGTHS
RESPECTIVELY; HATCHINGS = PARTICLE ORIENTATION IN THE COMPRESSION TEXTURE;
WHITE AREAS = PARTICLES IN THE INITIAL FABRIC ATTITUDE (AFTER TCHALENKO, 1968)

MINERAL: KAOLINITE
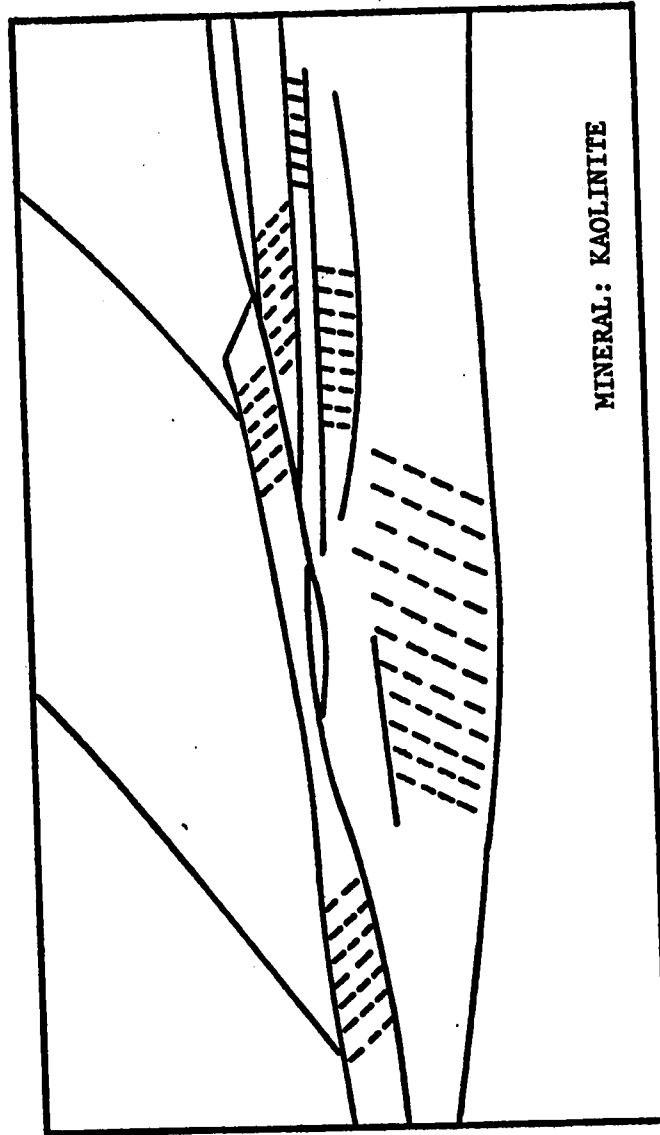
FIG. 2.7   STRUCTURES FORMED IN A REVERSAL TEST SPECIMEN IN THE DIRECT
SHEAR TEST (AFTER TCHALENKO, 1967)

Basal plane →

3.40 Å

1.42 Å

(a) CARBON ATOM ●

a. Graphite

(b) MOLYBDENUM ATOM ○

SULFUR ATOM ◯
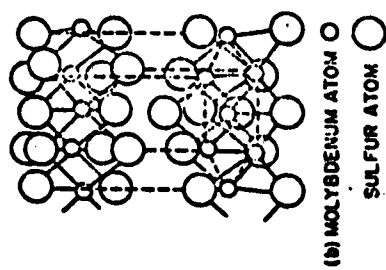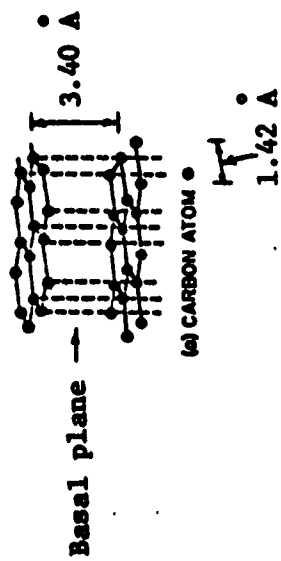
b. Molybdenum disulphide

FIG. 2.8   REPRESENTATION OF CRYSTAL STRUCTURES OF GRAPHITE AND
MOLYBDENUM DISULPHIDE (FROM CAMPBELL, 1969)
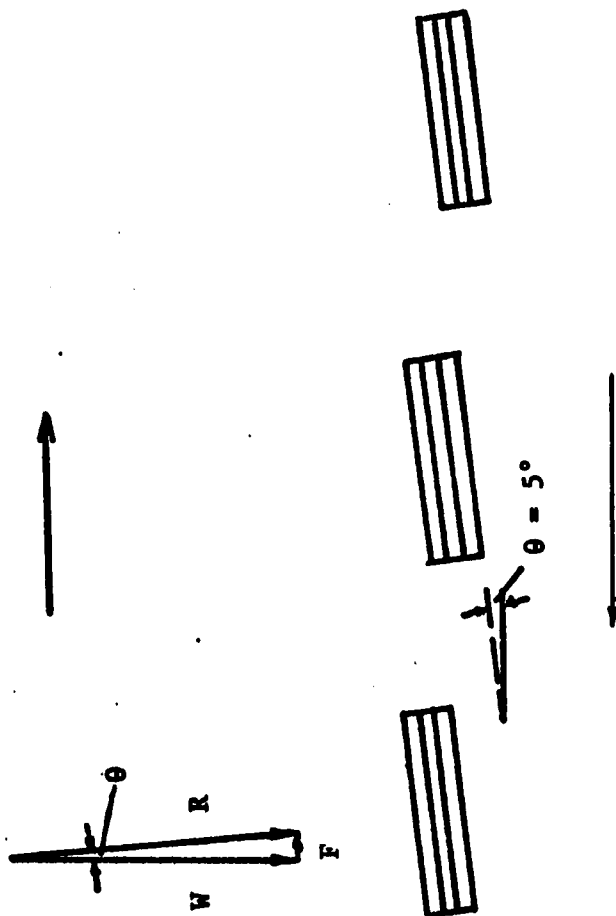
FIG. 2.9 TILTING OF BASAL PLANES OF POLYCRYSTALLINE GRAPHITE AFTER SLIDING (FROM BOWDEN AND TABOR, 1964)
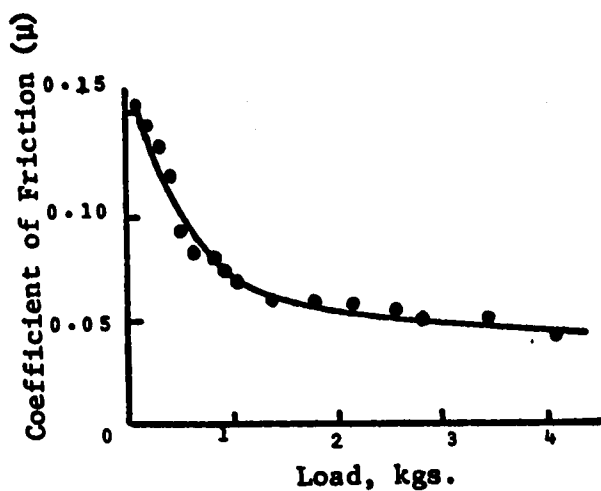
FIG. 2.10 VARIATION OF FRICTION COEFFICIENT WITH LOAD
FOR MoS_2 FILM ON Cr. (AFTER CAMPBELL, 1969)
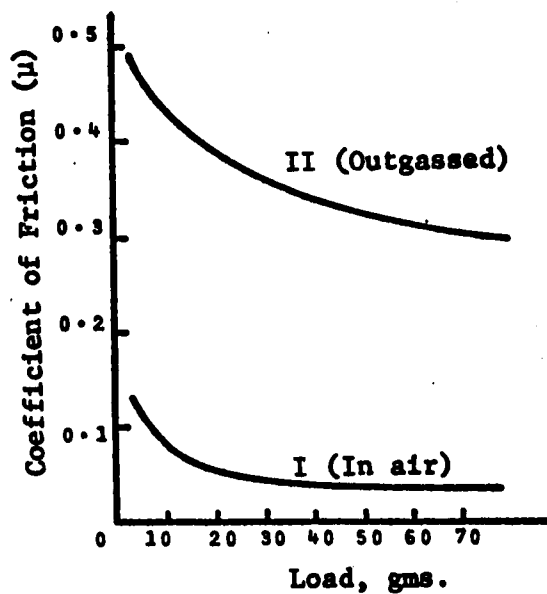
FIG. 2.11 FRICTION OF DIAMOND AS A FUNCTION OF LOAD: THE
COEFFICIENT OF FRICTION INCREASES AS THE LOAD IS
REDUCED AND FOLLOWS APPROXIMATELY A LAW OF THE
TYPE $\mu = kW^{-1/3}$ (AFTER BOWDEN AND TABOR, 1964)

CHAPTER III

A WORKING HYPOTHESIS FOR THE RESIDUAL SHEAR STRENGTH
OF PURE CLAY MINERALS

3.1 Physical Basis of Residual Strength

The residual strength of a soil is governed by the mineral composition of the soil and is independent of factors such as stress history, initial structure and strain rate that affect the path dependent properties of soils. It was stated in the previous chapter that the residual state is reached at large strains when the strength of the soil resides solely in its frictional resistance. Microstructural observations have indicated that the deformation at large strains is mainly accommodated by basal plane slip.

The modes of cleavage and the types of bonding energy available along the cleavage planes for various minerals have been compiled in Table 3.1 and the minerals are listed in Table 3.1 in order of decreasing values of $\tan\phi_r'$. The symbolic structures of the common clay minerals under consideration in this investigation are presented in Fig. 3.1 which also shows the nature and type of cleavage planes in these minerals. Examination of Table 3.1 immediately reveals that most of the minerals that have easy 001 basal cleavage demonstrate relatively low residual angles of friction. In Table 3.1, attapulgite is the only clay mineral with 110 cleavage plane and it exhibits a high residual friction angle compared to the common platy clay minerals with easy 001 basal cleavage. Quartz has no cleavage at all and it possesses the highest friction angle.

Hence, it is postulated that the residual strength of clay minerals depends on the mode of cleavage at large strains. Common platy clay minerals such as kaolinite, illite and montmorillonite which have well defined 001 basal cleavage planes offer low resistance to shear at large strains while a clay mineral such as attapulgite which possesses a staircase-like 110 cleavage plane (Fig. 3.1) offers more resistance to shear at large strains. The meaning of the term "basal cleavage" must be clearly understood at this point. An actual mineral particle does not usually consist of only a few basic layers as suggested by the symbolic structures in Fig. 3.1. Instead, a number of sheets are stacked one on top of another to form a crystal. A normal kaolinite particle may contain about 115 of the basic two-layer units (Lambe and Whiteman, 1969). The linkage between the basic two-layer units in kaolinite consists of hydrogen bonding and weak secondary valence forces (Table 3.1). The planes between the basic two-layer units are called the 001 basal planes along which cleavage is easy. However, this is not to say that at residual state, slippage occurs along the basal planes within a crystal. Slippage within a mineral crystal is conceivable only in the case of montmorillonite for which the c-axis dimension may expand from 9.6 to 18 $\overset{o}{A}$ depending on the availability of water. In the case of kaolinite and minerals of the muscovite group for which the c-axis dimensions do not expand in contact with water, slippage along basal planes will not occur within the mineral crystals. In fact, the work done by Bailey and Courtney-Pratt (1955) and Bailey (1961) on friction and adhesion of clean and contaminated mica surfaces have shown that the force required to shear the junction formed between clean smooth mica surfaces is very high (in the order of 10 kg./mm.^{2}) and a monomolecular layer of soap deposited between the cleavage surfaces of mica reduces the area of mineral-to-mineral contact

considerably and decreases the shear strength to 250 gm./mm.^{2} In view of these findings, it would appear that for minerals of the muscovite group and for kaolinite, slippage at large strains would not occur along the uncontaminated basal planes within the mineral crystals because of the large area of contact (implying high shear strength) along the basal planes within the crystals. Instead, slippage at large strains would be easier along the basal planes in the interparticle contacts (which are fewer in number) in the shear zone. Hence, it is postulated that the resistance of the mineral cleavage planes in the shear zone interparticle contacts against slippage is the source of residual strength and the residual shear strength is due to the frictional property of the mineral along its cleavage planes in the shear zone interparticle contacts.

It now remains to show why minerals having similar modes of cleavage exhibit different residual angles of friction. For example, hydrous mica, kaolinite and montmorillonite have 001 basal cleavages; but among the clay minerals montmorillonite possesses the least strength and the residual strength increases in the order: montmorillonite, kaolinite and hydrous mica. The same trend can be observed for mica and talc (Table 3.1). Both have 001 basal cleavage but mica is stronger than talc in resisting shear. It has been customary so far to explain the difference in strength between common clay minerals on the basis of the thickness of adsorbed water layer. However, the following arguments can be put forth to demonstrate that the nature or the thickness of the adsorbed water layer does not contribute to the residual strength generating mechanism.

    a. Residual shear strength has been found to be independent of the rate of strain (Kenney, 1967). However, if adsorbed water is viscous in nature and if it controls the residual shear strength, then

residual strength should be strain rate dependent. But the very fact that the residual strength is not strain rate dependent implies that the nature of adsorbed water has, if any, very minor effects on the basic strength generating mechanism at large strains.

b. The normal stress across an interparticle contact in the large displacement shear zone would be high enough to extrude any adsorbed water film from between the contact. This means that there is essentially mineral-to-mineral contact at the interparticle contacts. However, at large strains, failure will go through the solid interpraticle contacts and the adsorbed water films between the shear zone particles; but if we accept adsorbed water on clay particles as a two-dimensional fluid whose properties are essentially the same as those of normal liquid water (Martin, 1960), then the contribution of the adsorbed water film in resisting shear at large strains will be negligible. In this context, it is worthwhile to review the intrinsic permeability data reported by Lutz and Kemper (1959) for various clay-water systems. Their data show that increasing the pressure gradient across bentonite and halloysite samples increases the permeability of the samples and they attributed this increase in permeability to a disruption of the water structure around the clay particles by shear force. For Na-clays, the effect was particularly large and an increase in pressure gradient from 2 to 3 psi across a 1 cm. thick specimen resulted in a considerable increase in permeability. This would tend to suggest that the shear strength of adsorbed water films is probably very small. Hence, the primary source of residual strength is postulated to be the frictional resistance offered against slippage by the mineral cleavage planes at the solid interparticle contacts between the shear zone particles.

c. Probably the most convincing argument to illustrate that

physico-chemical explanations are indeed inadequate to establish a physical basis of residual strength was put forth by Morgenstern (1967) in his general report on shear strength of stiff clays to the Oslo conference. While reviewing Kenney's (1967) data, he compared the index properties and the friction angles of needle shaped attapulgite and other common platy clay minerals and made some very interesting observations. The attapulgite used by Kenney (Table 2.1) contained 74% clay size material and had liquid and plastic limits of 345% and 105% respectively. The specific surface (123-190 m.^{2}/gm., Haden, 1963) and cation exchange capacity (22 me./100 gms., Kenney, 1967) of attapulige are comparable to those of illite (80 m.^{2}/gm. and 30 me./100 gms.) and much higher than those of kaolin (10-20 m.^{2}/gm. and 9 me./100 gms.). Thus attapulgite has index properties comparable to montmorillonite or illite but its residual angle of shearing resistance (ϕ_r' = 30°; Kenney, 1967) is well above those found for other clay minerals and it behaves more like a silt or fine sand from the point of view of residual angle of friction. Hence, attapulgite seems to defy all physico-chemical explanations. This prompted Morgenstern (1967) to suggest that investigation into the nature of residual strength of attapulgite would be critical in establishing a physical basis of the residual strength. To explain the high residual friction angle of attapulgite, the following reasons are offered.

1. Attapulgite, as supplied, is always in the form of aggregates - an aggregate being a bunch of many intermeshed crystallites (Haden, 1963). These aggregates have a haystack-like structure in which the individual needles are arranged in a random fashion and are in general incapable of relative motion. The dispersion of attapulgite is said to be extremely difficult. Depending upon the extent of heat treatment of the raw clay during the manufacture of the industrial product, the chances of its

dispersion could be almost negligible (Haden, op. cit.). Borowicka (1965) has expressed the view that massive minerals owe their high strength to their ability to form interlocking grains. The needle shaped aggregates of attapulgite also show a high degree of intermeshing which probably do not segregate even at large strains and this may be one of the reasons for its high residual strength. Haden (op. cit.) has, however, pointed out that attapulgite is dispersible in some organic liquids. Therefore, attapulgite may exhibit lower residual strength in organic dispersing liquids. Tests on this mineral will, therefore, be crucial to the understanding of the nature of residual strength. For the purpose of research envisaged in this study, the special colloidal variety (resulting from controlled heat treatment) should be used.

11. The structure of attapulgite is very different from those of the common clay minerals. In physical shape, attapulgite differs from the more common clay minerals by being fibrous or needle shaped while the others are platy. Attapulgite has an amphibole structure with a double silica chain connected by a magnesium in the octahedral combination (Fig. 3.1). The result is a three layer structure. The three layer strips are joined at the corners by Si-O-Si bonds into a structure resembling a checkerboard in cross section, with free channels about 3.7 $\overset{o}{A}$ by 6.0 $\overset{o}{A}$ running the length of the needles. Since the structure is three dimensional, no montmorillonite type of swelling can occur (Haden, 1963). Also the cleavage of attapulgige is easiest along the Si-O-Si bonds giving it a staircase-like rather than a basal cleavage as in the case of platy clay minerals. The cleavage patterns of attapulgite and montmorillonite are shown schematically in Fig. 3.1. It is easy to conceive that attapulgite with cleavage along 110 plane at the interparticle contacts in the shear zone will exhibit much higher resistance to shear compared

to montmorillonite or any other platy clay mineral with easy 001 basal cleavage.

iii. The composition of attapulgite is an important factor in understanding the residual strength of this material. An interesting comparison can be made between attapulgite and montmorillonite on the one hand and mica and talc on the other.

Attapulgite: $(OH_2)_4$ $(OH)_2 \cdot Mg_5 \cdot Si_8O_{20} \cdot 4H_2O$

Montmorillonite: $(OH)_4 \cdot Al_4 \cdot Si_8O_{20} \cdot nH_2O$

Mica: $(OH)_2 \cdot KAl_2 \cdot (Si_3Al) \cdot O_{10}$

Talc: $(OH)_2 \cdot Mg_3 \cdot (Si_4) \cdot O_{10}$
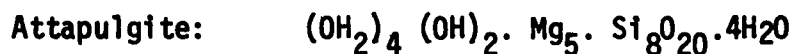
From Table 3.1, it can be seen that while mica has a high frictional resistance (0.3-0.45), talc has a very low frictional resistance (0.1 max.). The difference is due to replacement of one silicon atom in the silica tetrahedra and the total absence of Mg in mica (Bowden and Tabor, 1964). Moreover, one mica sheet is attached to the next by strong potassium bonds while such a bond is totally absent in talc (Brass, 1937). In the case of attapulgite and montmorillonite, the compsoitions are strikingly similar except for the Mg and Al and the greater inter-lamellar water in attapulgite. Preisinger (1963) has shown that this inter-lamellar water is indeed a great stabilising factor in attapulgite. Bradley (1940) has expressed the view that replacement of Mg by Al in attapulgite should yield lower strength for this mineral (see Grim, 1962). However, these changes must occur in the crystal structure and are not to be confused with ion substitutions. Hence they are difficult to achieve.

iv. Since attapulgite has a good cleavage along the 110 plane rather than 001 basal plane, its behaviour is comparable to that of a massive mineral than a layer lattice mineral. In a massive mineral, water sometimes acts as an antilubricant (Horn and Deere, 1962). This together with the fact that attapulgite contains a large amount of stabilising inter-lamellar water indicates that water might also act as an antilubricant for this mineral.

The above discussion on the residual strength of attapulgite tends to confirm one of the postulates made earlier in this section, namely that the residual strength depends on the mode of cleavage at the interparticle contacts between the shear zone particles and physico-chemical explanations are inadequate to explain the difference in residual strength among the common clay minerals. The comparison of frictional behaviour between mica and talc made earlier indicated that the reason for minerals with similar modes of cleavage exhibiting different residual friction angles may residue in the nature and amounts of bonding energy (which must be overcome during shear) available along their cleavage planes. Ample support for this concept can be furnished from Table 3.1 which compiles the avilable data on bonding energies along cleavage planes for various minerals. Let us first compare mica and graphite. Both minerals have good 001 basal cleavage but mica has a higher coefficient of friction (0.3-0.45) than graphite (0.058-0.10). The difference in friction coefficients can be explained by the difference in bonding energies available along their respective basal planes. Along its basal planes, graphite has weak van der Waal's bonding which falls in the category of secondary valence bonds (0.5-5 kilocalories per mole) while mica has strong potassium linkages in addition to

the secondary valance bonding along its basal planes. Hence in comparison with graphite, mica offers a greater resistance to shear. The reason for the difference in the frictional coefficients of mica and talc has already been presented. It is further interesting to compare talc and graphite because both have good 001 cleavage and the bonding along the cleavage planes of both of the minerals is comprised of weak secondary valence bonds. As would be expected, both minerals exhibit approximately the same coefficient of friction (Table 3.1). Turning our attention to the common clay minerals (Table 3.1), we find that all the platy clay minerals such as montmorillonite, hydrous mica and kaolinite have good 001 basal cleavage planes. However, the residual angle of friction increases in the order: montmorillonite, kaolinite and hydrous mica. Like the solid lubricants, the bonding energies available along the cleavage planes of the platy clay minerals can be correlated with their large strain frictional behaviour. The correlation between the bonding energies along the basal planes of the platy clay minerals and their coefficients of residual friction is presented separately in Table 3.2 in which the platy clay minerals are listed in order of decreasing values of $\tan\phi_r'$. Table 3.2 clearly shows that among the platy clay minerals, montmorillonite has the weakest bonding along its basal planes. Furthermore, the d (001) spacing of distilled water montmorillonite can go from 9.6 $\overset{o}{A}$ to 18 $\overset{o}{A}$ depending on water availability (Table 3.1). Consequently, it has the least resistance to shear among the platy clay minerals. The difference in $\tan\phi_r'$ between the distilled water and the saline montmorillonite will be explained in terms of the interparticle forces in the next section. Hydrous mica, on the other hand, has fairly strong

potassium linkages in addition to the secondary valence bonds along its basal planes and as a result, has the highest residual angle of shearing resistance among the common platy clay minerals. Let us now compare kaolinite with montmorillonite and hydrous mica. Comparing the bonding energies from Table 3.2, we find that in addition to the basic secondary valence bonding which is common to all the platy clay minerals, kaolinite has hydrogen bonds (5-10 kilocalories/mole) along its basal planes and this is probably why kaolinite is stronger in shear than montmorillonite. However, these hydrogen bonds along the basal planes of kaolinite particle contacts are probably weaker than the potassium linkages along the basal planes in the hydrous mica particle contacts. As a result, kaolinite is weaker in shear compared to hydrous mica and exhibits a lower ϕ_r' than hydrous mica. Hence, there seems to be a definite correlation between the residual strength coefficients of various minerals with similar cleavage modes and the bonding energies along their respective cleavage planes that have to be overcome at the interparticle contacts during shear at large strains.

Based on the above considerations, a mechanistic pacture of the shearing process at large strains will now be described. Micro-structural examination of the large displacement shear zones in clays has shown that the particles in close proximity to the principal displacement shear generally align themselves approximately perpendicular to the direction of the

major principal stress in the shear box and this shear zone structure
is called the compression texture. It is enclosed by two thin
bands of particles oriented in the direction of shear (Fig. 2.5).
The development of displacement discontinuities across a particle
does not appear to be a possible mode of motion at the residual state
presumably because of the high relative strength of the particles. A
similar view has been expressed by Tchalenko (1967). Hence, most of
the deformation at large strains occurs by basal plane slip in the
compression texture and also in the highly oriented zones enclosing
the compression texture. The resistance offered by the basal planes
of the shear zone particle contacts against slippage at large strains
is the residual shear strength of the mineral. It is also postulated
that the nature of shear strength of a clay mineral at large
strains is similar to the molecular adhesion theory of friction.
Shearing at large strains involves continuous rupturing and making
of bonds along the cleavage planes in the shear zone interparicle
contacts (which are mineral-to-mineral) and the adsorbed water films
between shear zone particles have, if any, very minor effects
on the basic strength generating mechanism at large strains.
The actual nature of these bonds is believed to be essentially
the same as that described by Mitchell et al. (1969) and in their
view, individual oxygen atoms can be considered as bonds or
flow units. An interparticle contact may contain a number of
bonds and a contact in a platy particle (with 001 basal cleavage)
is strong in compression but relatively weak in shear. Hence,
it is postulated that the residual shear strength of a clay mineral

is not only governed by its mode of cleavage but also by the type and number of bonds available along its cleavage planes at the shear zone particle contacts. There will be a direct relationship between the number of bonds along a plane and the effective normal stress on that plane. For the type of large strain shearing process described above, it is imperative to establish that solid-to solid interparticle contacts exist in soils and that they are the only significant region between soil grains where effective normal stresses and shear stresses can be transmitted. This is where the work of Mitchell et al. (1969) make a great contribution because it establishes that interparticle contacts in soils are effectively solid-to-solid.

The above mentioned mechanism of shear at large strains is basically derived from the concepts put forth by Morgenstern and Tchalenko (1967, a, b) and Mitchell et al. (1969). Similar mechanistic pictures of the shearing process have previously been suggested by other researchers (for eg. Rosenqvist, 1959; Trollope, 1961 and Morgan, 1967). However, most of them were concerned with rupturing and making of bonds at subfailure stresses and no attempt was made to postulate a mechanism for shear at large strains. Campanella (quoted by Mitchell et al., 1969) has recently obtained data that show that the number of bonds does not change significantly with increases in strain. This seems to indicate that the reason for observing a stabilised shear strength at large strains resides in the phenomenon that at large strains, a constant number of bonds is always ruptured and the same number of bonds is simultaneously made along the basal planes at the interparticle contacts between the shear zone particles.

3.2.1   General

Kenney (1967) has concluded from his work that system chemistry has a decided influence on the residual strength of Na-hydrous mica and Na-montmorillonite especially at low stress magnitudes (Fig. 2.1). In his view, the strength increases caused by increased ion concentration in the pore fluid result from net increases of attraction between individual particles and by the formation of bonds between particles. Kenney's explanation appears to fall within the reasoning of the conventional double-layer theory. However, if the basis of residual strength resides in the frictional characteristics of the mineral cleavage planes and if residual strength of a mineral is governed by its mode of cleavage, then the double-layer theory of strength should be rejected. It has already been demonstrated that the thickness and nature of adsorbed water have virtually no effect on the residual shear strength because it is independent of stress history, initial structure and rate of strain.

3.2.2   Effective stress in a clay-water system

Since residual shear strength (τ_{res}) is governed by the normal effective stress (σ_n') according to the classical Coulomb-Terzaghi law, it would seem that the effect of system chemistry on residual strength can best be understood by considering the mechanism of effective stress in an active clay-water system.

Fig. 3.2 shows an average interparticle condition for a fully saturated active clay-water system in which besides contact stresses and pore water pressures, electrical forces due to a net charge deficiency within the lattice structure, a high specific surface and the chemical

environment are significant. Following Lambe[*] (1960)and using the model shown in Fig. 3.2, the equation for static equilibrium of normal forces perpendicular to a plane of unit area in the saturated clay-water system may be written as

$$\sigma_n \cdot 1 = \sigma_c \cdot a + u_w(1-a) + (R-A) \cdot (1-a) \qquad (3.1)$$

where

σ_n = the total normal stress acting on the plane under consideration

a = ratio of area of mineral-mineral contact to the unit area (= a_m of Lambe, 1960)

σ_c = the average contact stress acting on the portion of the unit area, a (= $\bar{\sigma}$ of Lambe, op. cit.)

u_w = pore water pressure acting on the portion of the unit area (1-a) where there is water-mineral or water-water contact

and

(R-A) = the net interparticle stress due to the physico-chemical environment that acts over the portion of the unit area, (1-a).

Lambe (op. cit.) considers the physico-chemical component of the stress, (R-A), as acting over the entire area under consideration, whereas here they are considered to be acting only in the interparticle region where there is no mineral to mineral contact. It is also implied

---

[*]The notations used here are different from Lambe's (1960). His equations have been rewritten in terms of conventions and symbols followed in this thesis.

in Equation (3.1) that interparticle contacts are effectively solid to solid which has already been established by Mitchell et al.'s (1969) work. Equation (3.1) can be rearranged as

$$\sigma_n = [\sigma_c - u_w - (R-A)].a + u_w + (R-A) \qquad (3.2)$$

According to Mitchell (1960), $[u_w + (R-A)]$ is the total pore water pressure whereas in all of the equations in this formulation, the pore water pressure u_w is defined as that pressure measured by a piezometer inserted into the soil mass and containing a fluid exactly identical with the fluid that would be squeezed out of the soil mass if additional consolidation stresses are applied to the soil mass (Bailey, 1965). Now, if $(\sigma_n - u_w)$ is called σ_n', Equation (3.2) becomes

$$(\sigma_n - u_w) = \sigma_n' = [\sigma_c - u_w - (R-A)].a + (R-A) \qquad (3.3)$$

Balasubramonian (1972) has shown that $[\sigma_c - u_w - (R-A)]a$ is the effective stress component that controls volume changes in a saturated clay and not σ_n'. Since (R-A) is non-existent in granular soils, the stress that controls volume change behaviour of granular soils is $[\sigma_c - u_w].a$ which is classically stated as the effective stress for these soils. However, for many active clays, the volume change behaviour does not depend on the contact stress (σ_c) or the total pore water pressure $(u_w + R - A)$ or the value of a separately, but rather on the product of $[\sigma_c - u_w - (R-A)]$ and a (Balasubramonian, 1972). Equation (3.2) is now rewritten as

$$\sigma_n = \sigma_n^* + u_w + (R-A) \qquad (3.4)$$

where $\qquad \sigma_n^* = [\sigma_c - u_w - (R-A)].a \qquad (3.5)$

Since this stress component, σ_n^*, has been shown to govern the volume change behaviour of saturated clays involving no change in fabric or particle diminution, it was thought appropriate to call it the "true effective stress" and the conventional effective stress, σ_n' ($= \sigma_n - u_w$), is called the "apparent effective stress". From Equation (3.4), it is possible to express a relationship between the apparent effective stress (σ_n') and the true effective stress (σ_n^*) as follows,

$$\sigma_n' = \sigma_n - u_w = \sigma_n^* + (R-A) \tag{3.6}$$

$$\text{Therefore, } \sigma_n^* = \sigma_n' - (R-A) \tag{3.7}$$

It now remains to investigate whether σ_n^* defined as above (Eqn. 3.7) governs the residual shear strength of clay-water systems or not.

3.2.3 Modified Coulomb-Terzaghi relationships for peak and residual strength

In order to investigate whether true effective stress (σ_n^*) controls the residual strength of a clay-water system or not, it was considered necessary to modify the classical Coulomb-Terzaghi relationship for residual strength in terms of the true effective stress incorporating the mechanism of shearing at large strains proposed in this hypothesis. Since the residual strength parameters are independent of stress history, original structure and other factors which dominate the path dependent properties of soils, it was thought to be more appropriate to relate them to the Hvorslev's peak strength parameters (c_e and ϕ_e) which are also fundamental being independent of stress history. This would not only enable us to obtain an idea of the drop in strength from ϕ_e to ϕ_r' for

a soil but it would also relate this drop in strength to the change in structure from the peak to the residual state. The Coulomb-Terzaghi relationship for peak shear strength can be expressed in terms of the Hvorslev's parameters as

$$\tau_{peak} = c_e + \sigma_n' \tan\phi_e \qquad (3.8)$$

where τ_{peak} = peak shear strength

c_e = Hvorslev's true cohesion = f(water content or void ratio)

ϕ_e = Hvorslev's true angle of internal friction = $f(\sigma_n')$

and σ_n' = externally applied normal stress or the apparent effective stress.

If the shearing process involves continuous rupturing and making of bonds at interparticle contacts as well as along mineral basal planes and if the Bowden and Tabor theory of metal friction (which proposes the concept of asperity contacts giving rise to plastic junctions) applies to the conditions at contact, then an expression for shear strength can be derived independently based on the above mentioned concepts. According to Bowden and Tabor, the frictional force (F) is a product of the total area of the junctions (A_j) and their shear strength (S_j), hence:

$$F = A_j \cdot S_j \qquad (3.9)$$

and they further postulated that the area (A) is given by the normal force (W) divided by the flow pressure (P) so that

$$W = P \cdot A_j \qquad (3.10)$$

and thus coefficient of friction (μ) can be expressed as

$$\mu = \frac{F}{W} \tag{3.11}$$

$$= \frac{S_i}{P_i} \tag{3.12}$$

In the case of soils, $\tan\phi_e$ can be considered to be equivalent to μ and if the normal force transmitted across a junction in a soil be denoted by M, then according to the Bowden and Tabor theory, the frictional force (F_j) required to shear the junction is

$$F_j = \mu M = M.\tan\phi_e \tag{3.13}$$

If there are N number of junctions along a shear plane that must be ruptured simultaneously for achieving a complete shear failure, then the total frictional or shear force (F) is given by

$$F = \sum_{j=1}^{N} F_j = \sum_{j=1}^{N} \mu M = N\mu M \tag{3.14}$$

In the case of soils, Equation (3.14) should read as

$$F = N.\tan\phi_e. M = N.M.\tan\phi_e \tag{3.15}$$

If we postulate at this point that the true effective stress ($\sigma_n{}^*$) at the junctions along the basal planes and at the interparticle contacts in a clay-water system controls the residual shear strength of the clay-water system, then

$$M = [\frac{W}{N} - u_w.a - (R-A)a] \tag{3.16}$$

where $\quad a = \dfrac{\text{Apparent area of contact (A)}}{\text{Number of junctions (N)}}$

It follows then,

$$\text{peak shear strength} = \tau_{peak} = \dfrac{\text{Total frictional or shear force (F)}}{\text{Apparent area (A)}}$$

i.e., $\quad \tau_{peak} = \dfrac{F}{A}$ \hfill (3.17)

Substituting for F from Equation (3.15),

$$\tau_{peak} = \dfrac{N.M.\tan\phi_e}{A} \hfill (3.18)$$

Substituting for M from Equation (3.16),

$$\tau_{peak} = \dfrac{N}{A} \cdot [\dfrac{W}{N} - \dfrac{u_w.A}{N} - (R-A) \dfrac{A}{N}] \cdot \tan\phi_e$$

$$= [\dfrac{W}{A} - u_w - (R-A)] \cdot \tan\phi_e$$

$$= [(\sigma_n - u_w) - (R-A)] \cdot \tan\phi_e$$

$$= [\sigma_n' - (R-A)] \cdot \tan\phi_e$$

Hence, $\quad \tau_{peak} = \sigma_n{}^* \tan\phi_e$ \hfill (3.19)

Equation (3.19) expresses the modified Coulomb-Terzaghi relationship for peak shear strength derived from the concepts outlined in this hypothesis. The relationship between Hvorslev's peak angle of friction and the residual angle of shearing resistance can next be expressed as

$$\tan\phi_e = K'.\tan\phi_r' \hfill (3.20)$$

where K' is the structural factor that designates the drop from the peak to the residual friction angle for a soil in a shear test. The factor K' depends on the structural arrangement, geometry, shape and rugosity of the mineral particles. For example, Caquot (1934) has theoretically derived the K' value for sand to be $\pi/2$ or 1.57 while a value of 2 for K' can be attached to kaolinite from data reported by Gibson (1953). Hence, using the relationship expressed by Equation (3.20), Equation (3.19) can now be written as

$$\tau_{peak} = \sigma_n^* . K' \tan\phi_r' \tag{3.21a}$$

$$= [\sigma_n' - (R-A)] . K' \tan\phi_r' \tag{3.21b}$$

and, $$\tau_{peak} = -(R-A) . K' \tan\phi_r' + \sigma_n' K' \tan\phi_r' \tag{3.21c}$$

In this thesis, the relationship expressed by Equation (3.21) will be referred to as the modified Coulomb-Terzaghi relationship for peak shear strength.

At the residual state, K' is equal to 1.0 by definition and hence,

$$\tau_{residual} = -(R-A) \tan\phi_r' + \sigma_n' \tan\phi_r' \tag{3.22}$$

Equation (3.22) can be further arranged as

$$\tau_{res} = [\sigma_n' - (R-A)] . \tan\phi_r' \tag{3.23a}$$

$$= \sigma_n^* \tan\phi_r' \tag{3.23b}$$

The relationship expressed by Equation (3.23) describes the modified Coulomb-Terzaghi relationship for residual shear strength. We have now derived the modified Coulomb-Terzaghi relationships for both peak and residual conditions in an active clay-water system based on the postulates that the seat of shear strength resides in the frictional characteristics of the mineral cleavage planes and that the residual shear strength is governed by the true effective stress (σ_n^*) on the mineral basal planes.

Comparing Equation (3.8) with Equation (3.22), it seems that

$$c_e = -(R-A) K'\tan\phi_r' \tag{3.24}$$

and,
$$\sigma_n'\tan\phi_e = \sigma_n'K'\tan\phi_r' \tag{3.25}$$

and Equation (3.24) indicates that Hvorslev's true cohesion (c_e) in a clay-water system arises basically out of purely frictional interaction where only the net electrical stress, (R-A), acts as the normal stress governing the frictional behaviour of the clay-water system. Mitchell et al. (1969) seem to offer a somewhat similar mechanistic picture of cohesion. In their view, there should be no difference between friction and cohesion in terms of shearing process. The implications of Equation (3.24) seem to be also in keeping with Hvorslev's concept of true cohesion because as water content is increased, the net (R-A) stress term in Equation (3.24) decreases bringing about a decrease in c_e. We will now proceed to examine the concept of true cohesion so apparently implied by Equation (3.24).

It has recently been demonstrated by Balasubramonian (1972)

that the double-layer repulsive stress equation successfully predicts the net (R-A) stress in a monovalent ion rich swelling soil. This will be discussed in more detail later in this chapter. However, it can be shown from the double-layer repulsive stress equation that for active clay-water systems with very low pore fluid ion concentrations and under nominal externally applied normal stresses, the net (R-A) stresses of interaction are repulsive in nature (for example, see Table 3.3 where the estimated net (R-A) stress for a Na-montmorillonite - 0.0001 moles NaCl system is repulsive in nature). A state of net repulsion in a clay-water system under a nominal normal load implies that the net (R-A) stress term in Equation (3.24) is a positive quantity because R is greater than A. Consequently, the term c_e in Equation (3.24) bears a negative sign implying a negative cohesion intercept which is simply inadmissible.

The classical concept of cohesion has existed in the theory and practice of soil mechanics for a long time. In the author's opinion, the apparent cohesion intercepts usually observed in the Coulomb-Terzaghi envelopes for overconsolidated and even some remoulded active clays (such as Na-bentonite; Gibson, 1953) may arise because of the following reasons:

a. The Coulomb-Terzaghi cohesion intercept arises almost entirely from the variations in dilatancy of specimens tested at varying cell pressures. Rowe, Oates and Skermer (1963) have expressed the same opinion and they have further suggested that the interparticle cohesion term is virtually zero for isotropically overconsolidated specimens not subjected to secondary consolidation. In their view, the cohesion term can show a small value when a clay is subjected to anisotropic consolidation

for periods long enough to allow secondary consolidation. Large strains and rearranging of the particles reduce this term virtually to zero.

b. For most clay-water systems, the Coulomb-Terzaghi envelope is markedly curved in the low normal stress range because of the dependence of friction angle on the magnitude of normal effective stress. However, in most of the investigations reported in the geotechnical literature, very few shear tests have been performed under low normal stresses basically because of the insufficient accuracies of the measuring systems. Consequently, the implications of the marked curvature of the strength envelopes in the low normal stress range have rarely been recognized. Conventionally, a straight line is drawn through the test data obtained under higher pressures and when this straight line is extrapolated back to the τ-axis in the Coulomb-Terzaghi diagram, a geometric intercept is obtained which has so far been called the cohesion intercept. In view of the curvature of the Coulomb-Terzaghi envelope in the low normal stress range, this geometric intercept obtained by extrapolation of the strength envelope to the τ-axis is conceptually not true cohesion and leaves much to be desired. In this context, it is interesting to review the conclusions drawn by Schmertmann (1963, 1971) from his exhaustive study of the Hvorslev's parameters. Schmertmann (1963) has expressed the view that Hvorslev's concept of equal cohesion at equal void ratio can be in error because void ratio is not a sufficient description of soil structure. More recently, Schmertmann (1971) has obtained constant structure Mohr envelopes for several soils (kaolinite, Boston blue clay and other non-swelling clays) which were markedly curved in the low stress

range exhibiting very little cohesion. Based on his recent test results, he has proposed that cohesion is a function of the curvature of the Mohr envelope and is not a function of the water content. Any cohesion exhibited by a soil mass was explained in terms of chemical bonding. Conventionally determined values of Hvorslev's peak cohesion parameter for remoulded and subsequently consolidated samples of kaolinite, illite and Na-bentonite have been reported by Gibson (1953) and Morgan (1967). Their results clearly show that c_e for overconsolidated kaolinite is virtually zero. The relatively larger values of c_e/P_e ($\doteq$ 0.11, 0.11) reported for illite and Na-bentonite (Gibson, 1953) can be questioned in the light of the marked curvature of the Mohr envelopes for these minerals, especially in the low normal stress range.

The ideal approach to the study of cohesion in clays would involve testing specimens in a manner such that the applied effective stresses at failure were zero. Considering this technique of determining cohesion in the light of Equation (3.7) which states

$$\sigma_n^* = \sigma_n' - (R-A) \tag{3.7}$$

we find that when $\sigma_n' = 0$

$$\sigma_n^* = -(R-A) \tag{3.26}$$

The implication of Equation (3.26) is unacceptable if R is greater than A because the existence of a state of net repulsion in a clay-water system under zero applied stress means that the system is unstable and the clay particles will readjust themselves by increasing the distance of separation

between each other until the net (R-A) stress is virtually zero and the system will be in equilibrium. In such a case, σ_n^* will also be equal to zero and since σ_n^* has been postulated to control shear strength, it follows that shear strength under $\sigma_n^* = 0$ condition will also be zero. Conceptually then, no shear strength and hence no cohesion can exist under $\sigma_n^* = 0$ condition. However, it is practically impossible to achieve the $\sigma_n^* = 0$ condition on the failure plane of a sample because even the self weight of the soil above the failure plane will provide a small but definite σ_n' and hence a σ_n^* on the failure plane which will be reponsible for the sample demonstrating a definite shear strength under zero applied stress condition. The source of this shear strength under zero applied stress will, however, be purely frictional.

From the above considerations, it would then seem that a saturated clay-water system cannot exhibit true cohesion if a state of net repulsion exists among the clay particles. It is therefore hypothesized that a clay can exhibit cohesion only if a net attraction exist among the particles. This implies that A is greater than R in the clay-water system. In such a case, the net (R-A) stress term in Equation (3.24) will bear a negative sign which will make c_e a positive quantity and Equation (3.24) can be rewritten as

$$c_e = (A-R)K'\tan\phi_r'$$

(3.24)

The above relationship implies a positive cohesion intercept for the clay-water system. A similar opinion has been expressed by Ladd and Kinner (1967) who also hypothesized that a clay does not possess an

invariant "true cohesion", but rather exhibits a cohesion which is a function of environment and stress. Mitchell et al. (1969) and Schmertmann (1971) have also proposed that under $\sigma_n' = 0$ condition, interparticle bonds arising solely from physico-chemical forces of interaction are responsible for true cohesion. Although they did not specifically point out the nature of these physico-chemical forces of interaction that create the interparticle bonds under $\sigma_n' = 0$ condition, it would appear that the interparticle bonds are created by net forces of attraction.

A basis of true cohesion can now be postulated from the above considerations. True cohesion in a clay-water system arises basically out of purely frictional interaction where only a net attractive stress of interaction acts as the normal stress governing the frictional behaviour of the clay-water system. There should be no difference between friction and cohesion in terms of the shearing process. In nature, net attractive forces among the clay particles are known to exist only in soils with cementation bonds along their particle contacts. Calcium carbonates, aluminium and iron hydroxide precipitates, organic compounds and amorphous magnanese oxide are some of the possible cementation agents. It is therefore suggested that true cohesion can only exist for soils with cementation bonds along their particle contact and the strength of these bonds under $\sigma_n' = 0$ condition should be called the true cohesion of such a soil. However, these bonds occur in field samples on a geological time scale. Hence, it would appear that true cohesion does not fundamentally exist for overconsolidated laboratory specimens of soils

which have no cementation bonds along their particle contacts. However, this is not to say that the use of the conventional cohesion and friction parameters in practical slope stability analyses has been wrong so far because the apparent cohesion intercepts (c' or c_e) and the frictional components ($\sigma_n' \tan\phi'$ or $\sigma_n' \tan\phi_e$) fortuitously add up to the correct shear strengths (under the corresponding normal stresses) which are used for the stability analyses.

Turning our attention to the modified Coulomb-Terzaghi relationship for residual strength (Equation 3.23), it is immediately seen that at the residual state,

$$c_r' = -(R-A) \tan\phi_r'$$
$$= (A-R) \tan\phi_r' \tag{3.27}$$

This is inadmissible because any form of cohesion is classically known to be non-existent at large strains in soils. Hence, the term $(A-R)\tan\phi_r'$ in Equation (3.23) should not be interpreted as being the residual cohesion of a clay-water system. Instead, the modified Coulomb-Terzaghi relationship for residual strength should be interpreted as

$$\tau_{res} = \sigma_n^* \tan\phi_r' \tag{3.23b}$$

which implies that at large strains, friction is the only source of shear strength in a clay-water system.

Somewhat similar forms of modified shear strength equations based on effective stresses derived from mechanistic models of the

interparticle forces in ideal clay-water systems have previously been proposed by several investigators such as Trollope (1960, 1961), Crawford (1963), Morgan (1967) and Mesri (1969). However, most of these previous proposals are either incomplete or incorrect and no attempts were made to verify their validity experimentally.

It now remains to investigate the ability of the modified shear strength equations developed in this hypothesis to describe the shear strength behaviour of various clay-water systems. However, since this investigation is basically concerned with residual strength, we need only concern ourselves with the implications of the modified Coulomb-Terzaghi relationship for residual strength (Equation 3.23) and its ability to further our understanding of the true effect of salinity on the residual strength of clay-water systems.

3.2.4 Effect of pore fluid salt concentration on residual strength

In order to apply the proposed relationship $\tau_{res} = [\sigma_n' - (R-A)]$. $\tan\phi_r' = \sigma_n'^*\tan\phi_r'$ to a set of residual strength results obtained from conventional shear tests on a clay-water system at various pore fluid ion concentrations, one has to know the magnitudes of the net (R-A) stresses of the clay-water system at those pore fluid salinities so that the true effective stress (σ_n^*) of the system at each pore fluid ion concentration can be calculated. The physico-chemical components of interparticle forces are numerous (for eg. see Lee, 1968) and it is not possible to calculate the forces accurately for any clayey soil. The evaluation of (R-A), the physico-chemical component of the interparticle force has been discussed in detail by Bailey (1965) and Lee (1968). The good

correspondence found by Bailey (op. cit.) for Na-montmorillonites with very low salt contents (10^{-4} molar) at low pressures between the (R-A) stress as predicted from the double-layer repulsion theory and the apparent effective stress ($\sigma_n{}'$) led Balasubramonian (1972) to investigate whether the net (R-A) stresses for undisturbed clay-shales could be approximated from the double-layer repulsion theory alone. Balasubramonian (op.cit) has concluded from his study that in the absence of a complete understanding of all the physico-chemical forces between two adjacent clay particles, the net (R-A) stress is best approximated by the double-layer repulsive stress equation especially for swelling soils with sodium as the predominant cation if the effective surface areas of the soils are estimated with reasonable accuracy. In other words,

$$(R-A) = P_y \tag{3.28}$$

where
$$P_y = 2 C_0 R T (\cosh y_c - 1) \tag{3.29}$$

in which. P_y = the double-layer repulsive stress

C_0 = concentration of the bulk solution in the pore fluid

R = gas constant

T = absolute temperature

and, y_c = as shown in Appendix C.

Equation (3.29) is known as the double-layer repulsive stress equation the details of which along with the assumptions involved in the derivation of the equation are outlined in Appendix C. It is sufficient to note here that P_y or the net (R-A) stress for a given soil of known surface

charge density depends on the concentration of the bulk solution (C_o), valency of ions, temperature and the interparticle distance. It is also interesting to note that the success of the $P_y = (R-A)$ approach would only mean that the sum of all other repulsive and attractive forces for a monovalent ion rich swelling soil must be equal to zero.

We are now in a position to analyse Kenney's (1967) data on the residual strength of Na-montmorillonite (which exhibits a considerable increase in the residual strength with a corresponding increase in the pore fluid salinity; Fig. 2.1) in terms of the modified Coulomb-Terzaghi relationship for residual strength (Eqn. 3.23) using the double-layer repulsive stress equation (Eqn. 3.29) for estimation of the net (R-A) stresses. This analysis is performed in Table 3.3 and data given in Table 3.3 clearly demonstrate that under the same apparent effective stress (σ_n'), the influence of a change in salinity of the Na-montmorillonite system was to change the net (R-A) stress in the system thus bringing about a change in the true effective stress (σ_n^*) on the mineral basal planes. If τ_{res} is divided in the conventional manner by the apparent effective stress (σ_n'), different values of the residual friction angle (ϕ_r') are obtained at different pore fluid salinities for the same mineral under the same σ_n' (Table 3.3). However, if one divides the experimentally measured residual shear strengths by the corresponding true effective stresses (σ_n^*) to determine the values of $\tan\phi_r'$, then the same value of ϕ_r' is obtained at different pore fluid salinities for the same mineral under the same σ_n' (Table 3.3). This is significant because it indicates that the residual friction angle (ϕ_r') determined using the modified

residual strength relationship (Eqn. 3.23) is unique for Na-montmorillonite (ϕ_r' = 10°10') and is independent of the pore fluid salinity. Hence it is postulated that for each mineral, there is a unique residual angle of friction which is independent of the pore fluid salinity and the source of shear strength at large strains is purely frictional.

It can also be seen from Table 3.3 that under the same apparent effective stress (σ_n'), the true effective stress (σ_n^*) of the montmorillonite - 0.0001 moles NaCl system was less than the σ_n^* of the montmorillonite - 0.513 moles NaCl system and correspondingly, the τ_{res} of the montmorillonite - 0.0001 moles NaCl system was less than the τ_{res} of the montmorillonite - 0.513 moles NaCl system. This observation together with the fact that there appears to be an unique ϕ_r' for Na-montmorillonite which is independent of the pore fluid salinity tend to indicate that the stress state variable that controls the residual shear strength is the true effective stress (σ_n^*) on the mineral basal planes and not the apparent effective stress (σ_n') because σ_n' was held constant for both the tests in Table 3.3. Hence, when τ_{res} is plotted in a conventional manner against σ_n', two distinct Coulomb-Terzaghi envelopes for residual strength corresponding to two pore fluid salinities (0 and 30 g/l NaCl) are obtained for Na-montmorillonite (Fig. 2.2). However, if the same shear test results are reinterpreted using the modified Coulomb-Terzaghi relationship for residual strength expressed in terms of the true effective stress (σ_n^*) as shown in Table 3.3, the resulting plot of τ_{res} versus σ_n^* will yield a unique residual strength envelope for Na-montmorillonite which

will be independent of the pore fluid salinity. Hence, it is postulated that the effect of changing the pore fluid salinity of an active clay-water system is to change the true effective stress on the mineral basal planes and not the residual angle of friction.

So far, the abovementioned concept of the effect of salinity on the residual strength appears to explain the residual strength behaviour of Na-montmorillonite at various pore fluid ion concentrations. Although Kenney (1967) did not investigate the effect of salinity on the residual strength of kaolinite or attapulgite, his work clearly indicates that the only clay minerals whose residual strength characteristics are significantly influenced by a change in the pore fluid salinity are Na-montmorillonite and Na-hydrous mica (Figs. 2.1 and 2.2) which are both active clay minerals with high surface activity. It is therefore suspected that the residual shear strength of inactive clay minerals such as kaolinite and attapulgite will be almost unaffected by a change in the system chemistry. Both kaolinite and attapulgite have a low cation exchange capacity and a low specific surface (Table 3.1) and consequently,under almost all conditions of salinity and applied stress, the net (R-A) stresses for these minerals are virtually zero. This implies that for these inactive clay minerals, the true effective stress on the mineral basal planes will always be equal to the corresponding apparent effective stress under any environmental or applied stress conditions. As a result, the residual shear strength of these inactive clay minerals will not be affected by a change in the system chemistry.

In the .smectite group, it is also interesting to note
the effect of divalent substitution on the residual shear strength.
It can be seen from Fig. 2.1 that the residual shear strength of the
Ca-montmorillonite - 0 g/l system is the same as the residual shear
strength of the Na-montmorillonite - 30 g/l NaCl. Corresponding to an
apparent effective stress of 1 kg./cm.^{2} and a particle spacing of
27.5 Å, the net (R-A) stress of the Na-montmorillonite - 30 g/l NaCl
system has been shown to be practically zero (Table 3.3). This
implies that under those conditions, σ_n* on the mineral basal planes
of the Na-montmorillonite - 30 g/l NaCl system was equal to the
corresponding apparent effective stress (σ_n') of the sample.
Ca-montmorillonite, on the other hand, has a tendency to form domains.
A domain, as described by Bailey (1965), is a bundle of very closely
packed clay platelets (Fig. 3.3). The platelets in a bundle are
oriented parallel, while the individual bundles themselves might be in
a more or less random arrangement. The interspace between the bundles
is filled with pore fluid which is inert and not adsorbed. An important
feature of domains in Ca-montmorillonite seems to be the irreversible
nature of domain formation. Norrish (1954) and Aylmore and Quirk (1959)
have shown that for Ca-montmorillonite under any environmental condition,
a basal spacing of 19 Å is always found within the domains throughout
most of the pressure ranged of interest to us. Hence, divalent
substitution in a clay-water system has the effect of bringing the
particles closer together. A similar effect can be achieved by
increasing the salt content of the system. According to Bailey (1965),
long range electrical forces vanish for particle spacings of less than

20 Å . Hence, if Ca-montmorillonite systems have domains in which the particle spacing is usually 19 Å irrespective of the applied stress and environmental conditions, then it seems possible that the net (R-A) stresses for Ca-montmorillonite systems are insignificant. This means that for Ca-montmorillonite systems, $\sigma_n{}^*$ is equal to $\sigma_n{}'$ under all conditions of salinity and applied stress. Hence, it appears that for both highly saline Na-montmorillonite and Ca-montmorillonite (with any pore fluid salinity), $\sigma_n{}^*$ is always equal to $\sigma_n{}'$. This is probably why both the systems exhibit same residual shear strength under the same applied stress. From the above considerations, it also seems that the residual shear strength of Ca-montmorillonites will be independent of the pore fluid salinity. Work done by Mesri (1969) on Ca-montmorillonite has already indicated that pore water salt has very little effect on the peaк shear strength of Ca-montmorillonite.

Hydrous micas appear to behave in a similar fashion to montmorillonites as far as the effect of ion substitution on the residual strength is concerned. Kenney's (1967) results (Table 2.1) show that under a normal pressure of 1 kg./cm.^{2}, the $\tan\phi_r{}'$ of the highly saline variety (30 gms./litre NaCl) of Na-hydroua mica is exactly the same as that of the very low salt variety ($\simeq$ 0 gms./litre) of Ca-hydrous mica and the reasons that can be offered to explain this phenomenon are exactly the same as those outlined for montmorillonite.

For Na-systems of the active clay minerals, another approach to bring the particles closer than 20 Å where the net (R-A) stresses become insignificant is to apply sufficiently high normal loads. Under

such loads, since the net (R-A) stresses become insignificant, any
active mineral when tested with distilled water and with other salinities
should yield the same residual strength. Kenney's (1967) results
(Fig. 2.1) show this trend clearly. For instance, the Na-montmorillonite
with distilled water and with sea water (30 g/l NaCl) seem to converge
to the same value of residual strength at high normal stresses ($\simeq$ 250-300 psi)
though at lower normal stresses, the difference is significant.

In conclusion, it can be stated that the modified Coulomb-
Terzaghi relationship for residual strength (Eqn. 3.23) developed in
this hypothesis seems to explain the influence of system chemistry on
the residual shear strength of pure clay minerals. It has been postulated
that the effect of changing salinity in active clay minerals (such as
montmorillonites and hydrous micas) is to change the true effective
stress (σ_n^*) on the mineral basal planes and not the residual friction
angle (ϕ_r'). There seems to be an unique residual friction angle for
every mineral and it depends on the mode of cleavage and frictional
characteristics of the mineral cleavage planes. Residual shear strength
of a clay mineral is governed by the true effective stress on the mineral
basal planes and under constant σ_n', a change in pore fluid salinity
that brings about a change in σ_n^* will cause a change in the residual
strength. Salinity is suspected to have insignificant influence on the
residual strength of inactive clay minerals such as kaolinite and
attapulgite. The source of residual strength in clay minerals is
purely frictional and the nature of shear strength is similar to the
Bowden and Tabor theory of metal friction.

Although it has been postulated in the present hypothesis that there is possibly a unique residual friction angle for every mineral which is independent of the pore fluid salinity, it is already well known that ϕ_r' is markedly dependent on the magnitude of normal effective stress (σ_n') especially in the low pressure range (for eg. see Fig. 2.1; Kenney, 1967). Hence, an attempt is made in the next section to provide an explanation for the dependence of ϕ_r' on σ_n'.

3.3 Dependence of ϕ_r' on the Magnitude of Normal Effective Stress

The explanation for the dependence of the coefficient of friction of lamellar solids on the applied normal stress was outlined in section 2.6 of Chapter II. It was shown that in the field of solid lubrication, the non-linearity of friction with stress level is explained by the dependence of the friction coefficient on the area of true contact between particles which in turn is dependent on the applied load upto a certain normal stress level. The area of true contact for elastic deformation at asperities is proportional to $(\text{load})^n$ where the value of n varies from 2/3 to 1.0 as the normal pressure is increased. The non-linearity of friction is specially marked at low normal pressures. Reference was also made to Bowden and Tabor's (1964) study on diamond which showed that the coefficient of friction of diamond in air rises at light loads and is roughly proportional to $(\text{load})^{-1/3}$ and as load is increased, the area of true contact becomes proportional to $(\text{load})^{1.0}$ and the friction coefficient becomes independent of the contact area. The same concept accounts for the decrease in the coefficient of friction of MoS_2 (which is a lamellar solid) with increasing normal load

(Fig. 2.10; Campbell, 1969). Despite the serious limitations imposed by the assumptions of the Hertz's theory, it was decided to explore the usefulness of the same model in explaining the dependence of ϕ_r' and σ_n' in soils because of the striking resemblance between the frictional behaviour of some lamellar solids and the nature of residual shear strength of clay minerals. However, in order to obtain a direct verification of the applicability of this concept to soils, one has to measure the areas of true contact between mineral particles and their basal planes under various normal pressures (ranging from low to high pressures) and correlate these measured areas of true contact with the coefficients of friction measured under the same normal pressures. This will obviously require highly sophisticated equipment and techniques that are not readily available. Hence we shall seek an analytical relationship between the areas of true contact under various normal pressures and the corresponding residual angles of friction (ϕ_r') in terms of quantities such as σ_n' and τ_{res} that are easily obtained in a conventional shear box test. Let us consider a direct shear test on a clay mineral whose contacts deforms elastically under pressure. The normal load (W) on the sample can be expressed as

$$W = \sigma_n'. A \qquad (3.30)$$

where σ_n' = externally applied normal stress or the apparent effective stress

and,   A = apparent area of contact or the area of the shear box.

The residual shear force (T) measured in the test can be expressed as

$$T = S_j \cdot A_c \qquad (3.31)$$

where $\quad S_j$ = shear strength of a contact

and, $\quad A_c$ = area of true contact.

The residual strength coefficient $(\tan\phi_r')$ can be denoted by

$$\tan\phi_r' = \frac{\tau_{res}}{\sigma_n'} = \frac{T}{W} = \frac{S_j A_c}{W} \qquad (3.32)$$

Now, according to Hertz's theory, the area of true contact in the low normal stress range is proportional to $(load)^{2/3}$, i.e.,

$$A_c \propto W^{2/3}$$

Therefore,

$$A_c = k_1 \cdot W^{2/3} \qquad (3.33)$$

where $\quad k_1$ = the constant of proportionality.

Substituting the value of A_c from Equation (3.33) into Equation (3.32), we obtain

$$\tan\phi_r' = \frac{S_j A_c}{W} = \frac{S_j k_1 W^{2/3}}{W} = \frac{S_j k_1}{W^{1/3}} \qquad (3.34)$$

Substituting for W from Equation (3.30), Equation (3.34) takes the form

$$\tan\phi_r' = \frac{S_j k_1}{(\sigma_n' \cdot A)^{1/3}} = \frac{S_j k_1}{A^{1/3}} \cdot \frac{1}{(\sigma_n')^{1/3}} \qquad (3.35)$$

Since S_j, k_1 and A are all constants for a particular shear test, the term $\frac{S_j k_1}{A^{1/3}}$ in Equation (3.35) can be lumped into one constant which is termed N_k. Therefore, Equation (3.35) may now be written as

$$\tan\phi_r' = N_k \cdot \frac{1}{(\sigma_n')^{1/3}} \qquad (3.36)$$

According to Equation (3.36), $\tan\phi_r'$ in the low normal pressure range is proportional to $(\sigma_n')^{-1/3}$ which is exactly the same as the friction law ($\mu = kW^{-1/3}$) for diamond in the low pressure range. The relationship in Equation (3.36) implies that as σ_n' is decreased, $\tan\phi_r'$ should increase. For an active clay mineral in which the magnitude of the net (R-A) stress can be significant, Equation (3.36) may be rewritten in terms of the true effective stress (σ_n^*) as

$$\tan\phi_r' = N_k \cdot \frac{1}{(\sigma_n^*)^{1/3}} \qquad (3.37)$$

Now, as normal load is increased, the area of true contact becomes proportional to $(load)^{1.0}$. Hence, in the high normal stress range,

$$A_c \propto (W)^{1.0}$$

Therefore,

$$A_c = k_2 \cdot W \qquad (3.38)$$

where k_2 = the constant of proportionality.

The residual strength coefficient $(\tan\phi_r')$ for a clay mineral in the high normal stress range can then be expressed as

$$\tan\phi_r' = \frac{S_j A_c}{W} = \frac{S_j k_2 W}{W} = S_j k_2 = \text{a constant} \qquad (3.39)$$

The relationship in Equation (3.39) implies that in the high normal stress range, $\tan\phi_r'$ is independent of the area of true contact (A_c) and hence of σ_n'.

We have now obtained relationships expressed by Equations (3.36) and (3.39) which describe the dependence of ϕ_r' on σ_n' in both low and high pressure ranges. If these relationships are truly applicable to soils, then a plot on an arithmetic scale between $\tan\phi_r'$ and $(\sigma_n')^{-1/3}$ obtained from a number of shear tests on a soil performed under normal pressures ranging from low to high pressures should be a straight line in the low pressure range exhibiting a linear relationship between $\tan\phi_r'$ and $(\sigma_n')^{-1/3}$ according to the relationship in Equation (3.36). The slope of this line will then be N_k. Above a certain stress level, the same plot of $\tan\phi_r'$ versus $(\sigma_n')^{-1/3}$ should be a horizontal line parallel to the $(\sigma_n')^{-1/3}$ axis in accordance with the relationship expressed by Equation (3.39) indicating that $\tan\phi_r'$ has ceased to be dependent on the area of true contact and hence on σ_n'. Kenney's (1967) results on pure clay minerals and Bishop et al.'s (1971) results on some English clays and a South American shale have been plotted in the form of $\tan\phi_r'$ versus $(\sigma_n')^{-1/3}$ plots in Figs. 3.4 to 3.7 and these plots generally seem to support the explanation offered here for the observed dependence of ϕ_r' of soils on the magnitude of σ_n'. Hence it is postulated that in the low stress range, the residual strength coefficient $(\tan\phi_r')$ of a soil follows a law of the type

$$\tan\phi_r' = N_k \cdot \frac{1}{(\sigma_n')^{1/3}} \qquad (3.36)$$

and as normal pressure is increased beyond a certain level, $\tan\phi_r'$ becomes independent of the area of true contact and hence of σ_n' and follows a relationship described by

$$\tan\phi_r' = S_j k_2 = \text{a constant} \qquad (3.39)$$

It appears from Figs. 3.5 to 3.7 that for stiff natural clays and clay-shales, there is an almost unique threshold normal stress (σ_n') of 20-30 psi above which $\tan\phi_r'$ changes from being stress dependent to stress independent. For pure clay minerals, this threshold σ_n' appears to be around 60-70 psi.

TABLE 3.1

TYPES OF BONDING AVAILABLE ALONG THE CLEAVAGE PLANES AND THE MODES OF CLEAVAGE OF VARIOUS CLAY MINERALS AND SOLID LUBRICANTS

Mineral	Formula	$d(001)$ or c-axis dimension	Mode of cleavage	Types of bonding available along the cleavage planes	$\tan\phi_c$	$\phi_c°$	Specific surface m^2/gm	Cation exchange capacity me./100 grs.	Particle size and shape	General remarks
Quartz	$(OH)_2(OH)_4(OH)_2Mg_5$ $Si_8O_{20}\cdot4H_2O$		No definite cleavage		0.70	35°			Crushed, angular	
Attapulgite		$c_0 = 5.2$ Å	Cleavage along (110) plane	Si-O-Si weak link	0.57	30°	125-190	22	10,000Å long x 100 Å across - fibrous and needle shaped	3 layer and 2-D structure - three layer strips joined at corners by <1-0-Si bonds
Mica	$(OH)_2\cdot K\ Al_2\cdot$ $(Si_3Al)O_{10}$		Good (001) basal cleavage	Secondary valence bonds (0.5-5 k.cal/mole) + K-linkages	0.3-0.45	17°-24°		5-20	Sheet	(2:1) layer clay
Kaolinite	$(OH)_8\cdot Si_4\cdot$ Al_4O_{10}	$d(001) =$ 7.15 Å	(001) basal cleavage	Secondary valence bonds (0.5-5 k.cal/mole) + hydrogen bonds (5-10 k.cal/mole)	0.81	12°	10-20	9	10,000Å x 1,000 Å thick-platy	Typical kaolinite particle consists of at least 115 basic units (1:1) layer clay
Illite	$[(Al,Mg,Fe)(SiAl)_4$ $O_{10}(OH)_2]\ K_2\ (M)$ where, M = exchangeable ions		(001) basal cleavage	Secondary valence bonds (0.5-5 k.cal/mole) + K-linkages	0.18	10.2°	80-100	25	1,000Å x 10 Å thick-platy	(2:1) layer clay
Montmorillonite	$(OH)_4\cdot Al_4\cdot$ $Si_8O_{20}\cdot nH_2O$	$d(001) =$ 9.6 to 18 Å	Excellent (001) basal (001) basal cleavage	Secondary valence bonds (0.5-5 k.cal/mole) + exchangeable ion linkages	0.07-0.10	4°-10.2°	600-1000	100	1,000Å x 10 Å thick-platy	(2:1) layer clay
Talc	$(OH)_2\cdot Mg_3\cdot$ $(Si_4)O_{10}$		(001) basal cleavage	Secondary valence bonds (0.5-5 k.cal/mole)	0.30	6°		1	Platy	
Graphite			(001) basal cleavage	Van der Waal's bonds	0.050-0.10	3°-6°			Sheet	
MoS_2			(001) basal cleavage	Weak interlayer bonds	0.033	4°			Sheet	

TABLE 3.2

CORRELATION BETWEEN THE VALUES OF $\tan\phi_r'$ FOR PLATY CLAY MINERALS AND THE BONDING ENERGIES

AVAILABLE ALONG THEIR (001) BASAL PLANES.

Mineral	Types of bonding along its (001) basal planes	$\tan\phi_r'$
Distilled water montmorillonite	Secondary valence bonds (0.5-5 kilocalories/mole) + some exchangeable ion linkages	0.07
Salt montmorillonite	Secondary valence bonds (0.5-5 kilocalories/mole) + exchangeable ion linkages	0.18
Kaolinite	Secondary valence bonds (0.5-5 kilocalories/mole) + hydrogen bonds (5-10 kilocalories/mole)	0.21 - 0.27
Hydrous mica	Secondary valence bonds (0.05-5 kilocalories/mole) + K-linkages	0.29 - 0.49

TABLE 3.3

INTERPRETATION OF THE RESIDUAL STRENGTH OF Na-MONTMORILLONITE (KENNEY, 1967)

IN TERMS OF THE MODIFIED SHEAR STRENGTH EQUATION

Apparent effective stress, σ_n' (kg/cm²)	Pore fluid NaCl content (moles)	Assumed total specific surface (m²/gm)	Water content at residual state, w_{res} (%)	Particle half spacing (Å)	Experimentally measured residual shear strength τ_{res} (kg/cm²)	Conventional $\tan\phi_r' = \frac{\tau_{res}}{\sigma_n'}$	Corresponding ϕ_r'	Estimated* $P_y - (R\text{-}A)$ (kg/cm²)	True effective stress $\sigma_c' = [\sigma_n' - (R\text{-}A)]$ (kg/cm²)	$\tan\phi_r' = \frac{\tau_{res}}{\sigma_n'}$	Corresponding ϕ_r'
1.0	0.0001	800	465	58.13	0.07	0.07	4°	0.611	0.389	0.18	10°10'
1.0	0.513	800	220	27.50	0.18	0.18	10°10'	≈ 0	1.0	0.18	10°10'

* $P_y = (R\text{-}A)$ is calculated using the double-layer repulsive stress equation which is given by $P_y = 2 C_0 R T (\cosh y_c - 1)$ and a sample calculation is presented in Appendix C.

(001) Basal cleavage plane

a. Kaolinite

(001) Basal cleavage plane

c. Montmorillonite

Cleavage plane

Cleavage planes

55°

a

Amphibole

i. Attapulgite   ii.   Montmorillonite
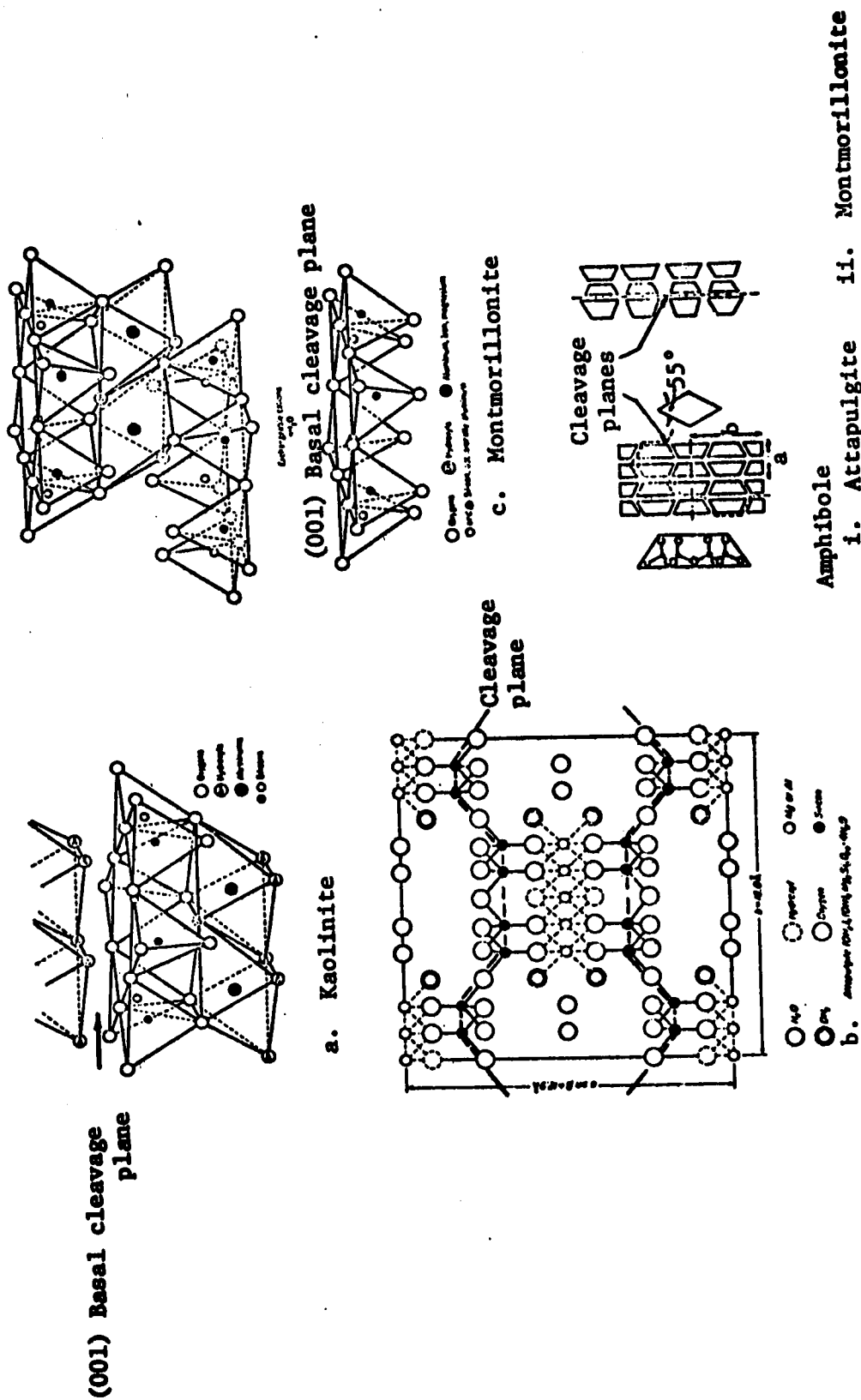
FIG.   3.1   SCHEMATIC REPRESENTATION OF THE STRUCTURES OF COMMON CLAY MINERALS AND THEIR
CLEAVAGE PATTERNS (FROM GRIM, 1968)
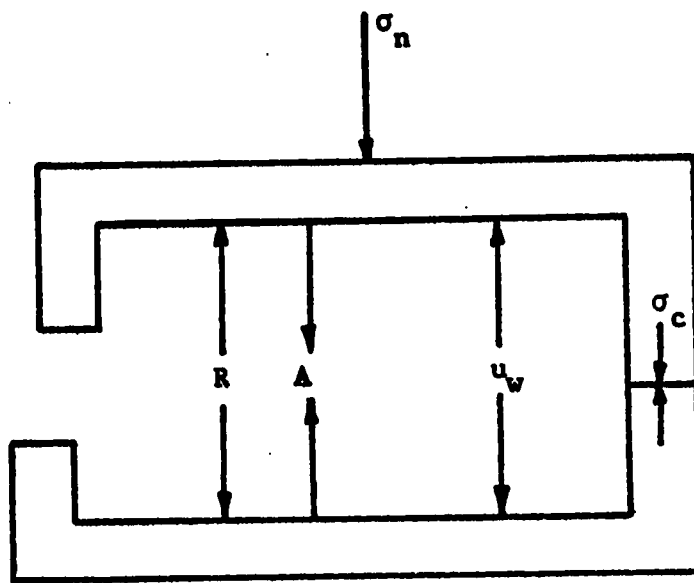
FIG. 3:2 FORCES BETWEEN ADJACENT PARTICLES
IN AN ACTIVE CLAY-WATER SYSTEM

Clay platelets form
closely packed and parallel
oriented packets. The
relative orientation of
the packets could be
random.

Inter-space
water is inert.
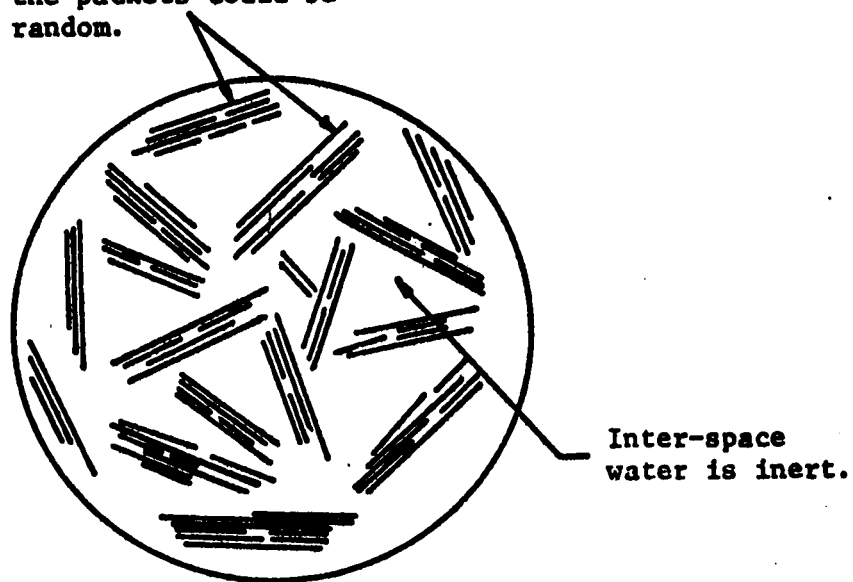
FIG. 3.3 DOMAINS IN DIVALENT CLAYS (AFTER BAILEY, 1965)
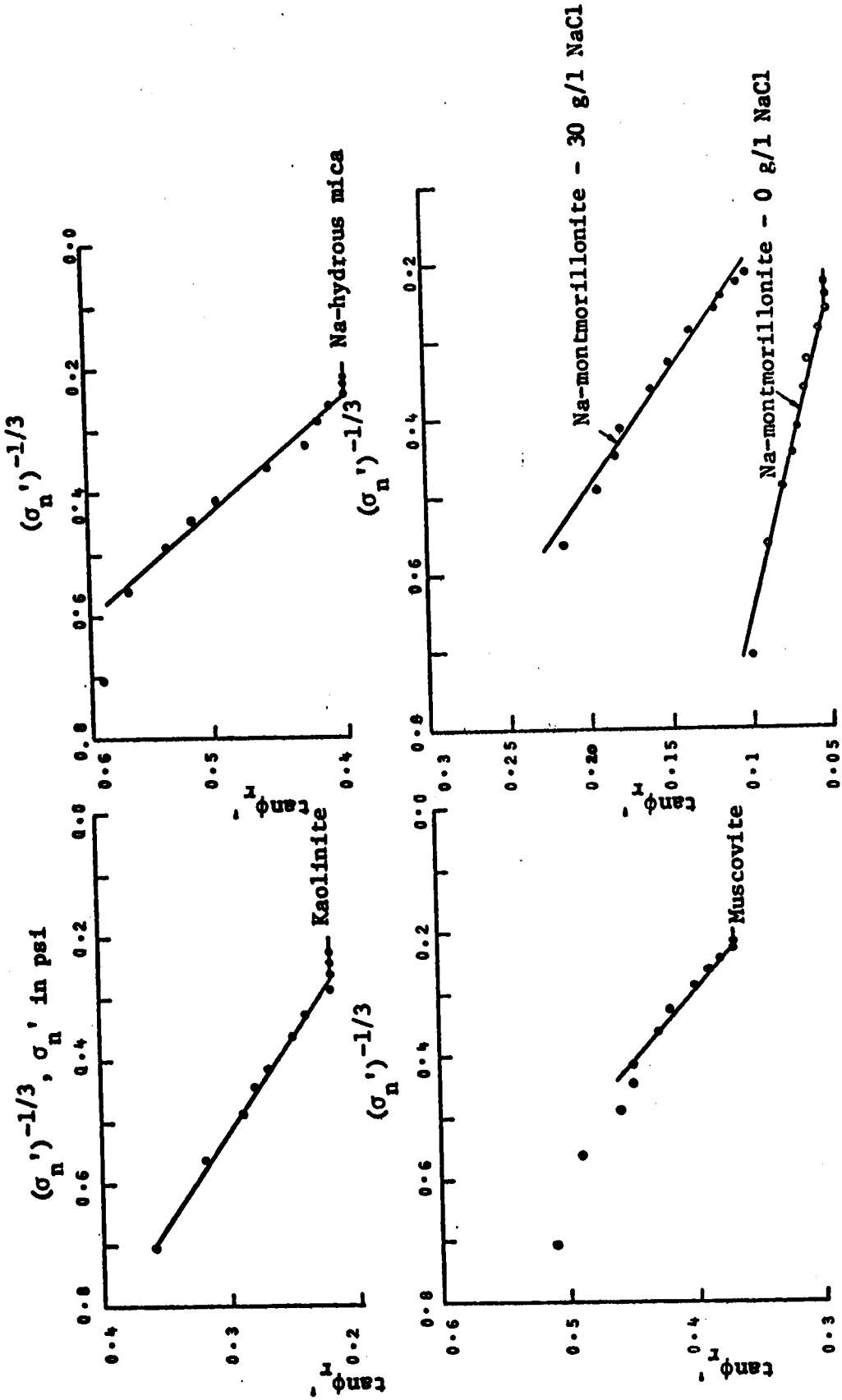
FIG. 3.4 RELATIONSHIPS BETWEEN $\tan\phi_r'$ AND $(\sigma_n')^{-1/3}$ FOR SOME PURE CLAY MINERALS (DATA OBTAINED FROM KENNEY, 1967)
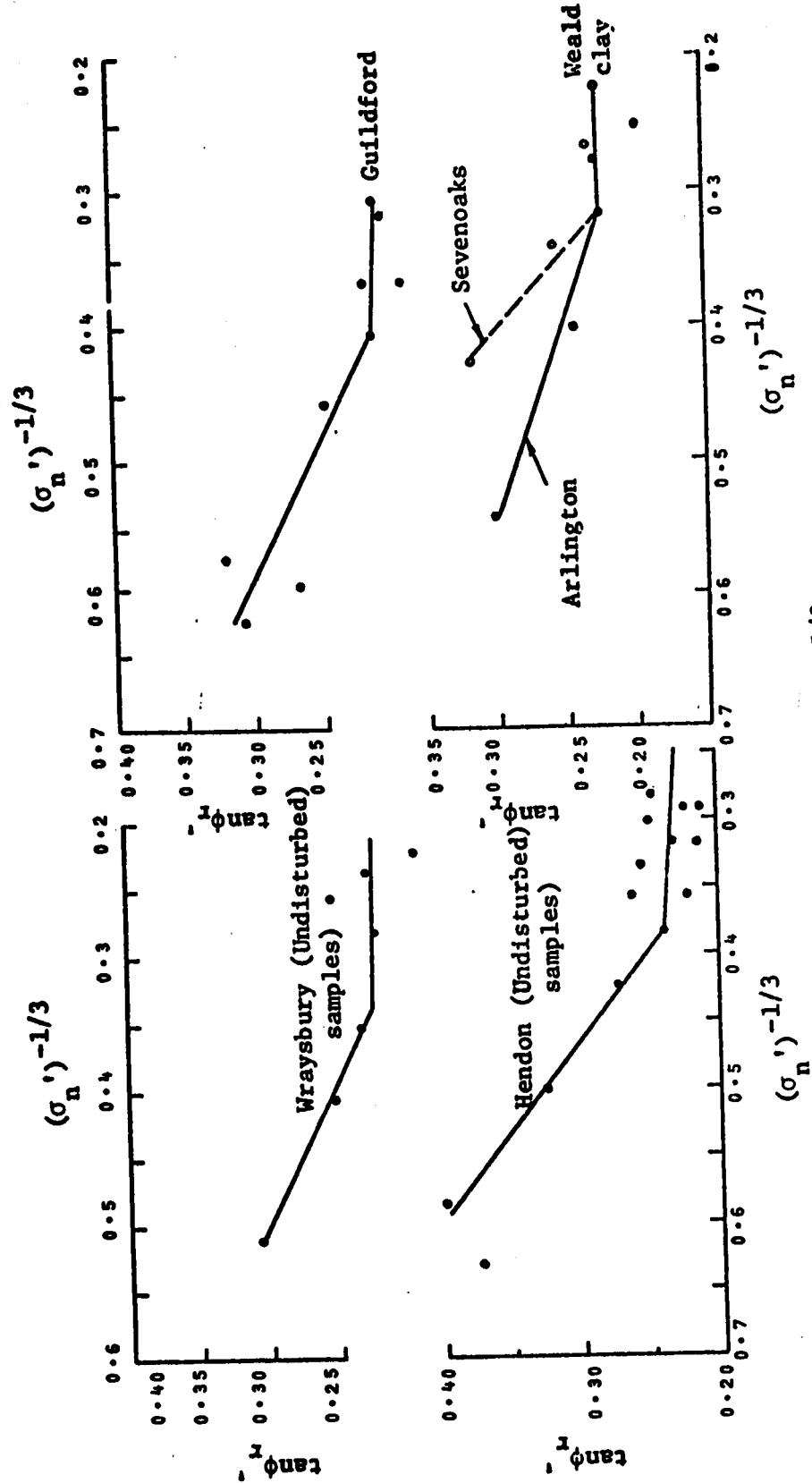
FIG. 3.5 RELATIONSHIPS BETWEEN TANϕ_r' AND $(\sigma_n')^{-1/3}$ FOR SOME ENGLISH CLAYS
(DATA OBTAINED FROM BISHOP ET AL., 1971)
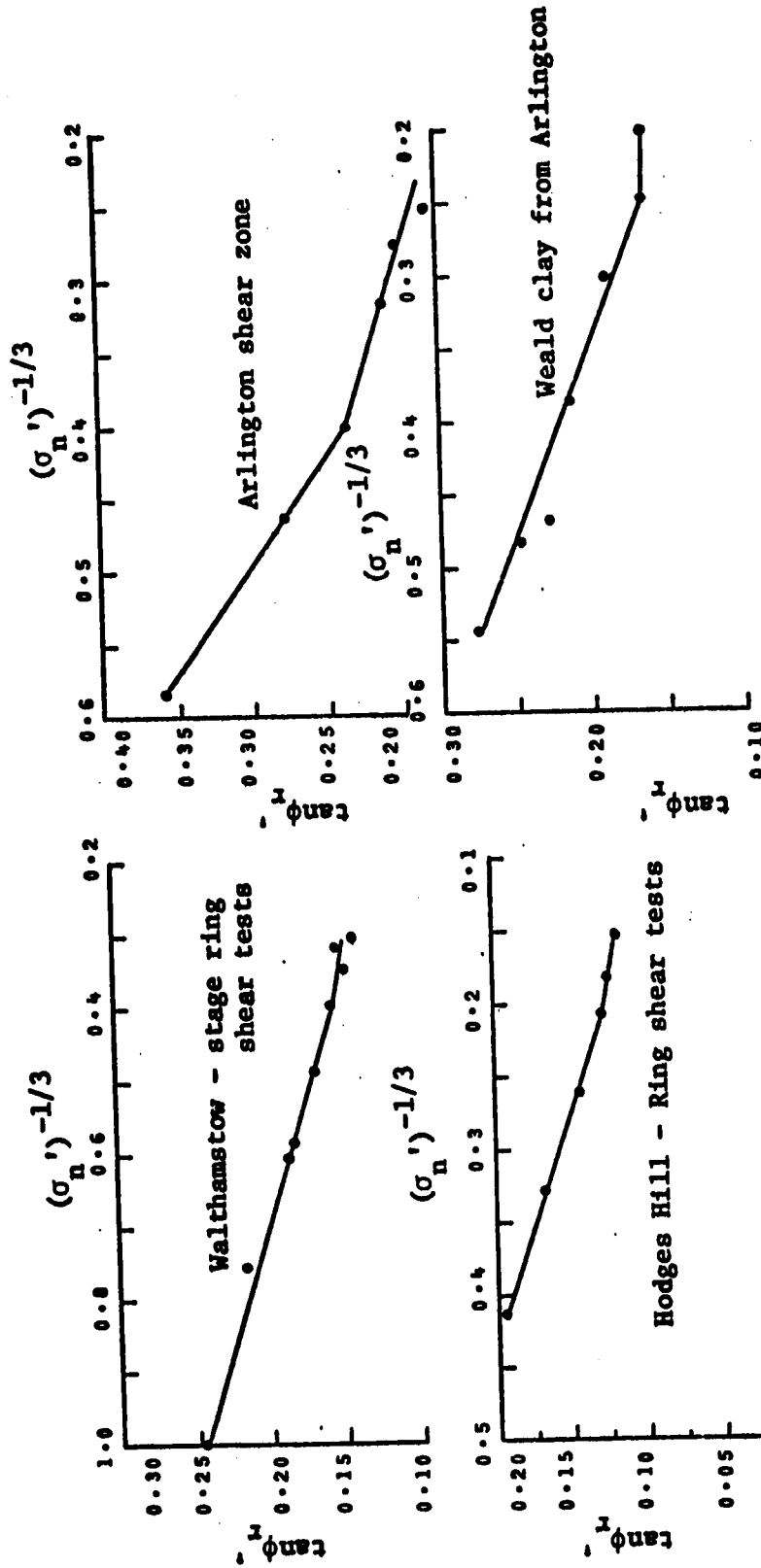
FIG. 3.6 RELATIONSHIPS BETWEEN $\tan\phi_r'$ AND $(\sigma_n')^{-1/3}$ FOR SOME ENGLISH CLAYS (DATA OBTAINED FROM BISHOP ET AL., 1971)
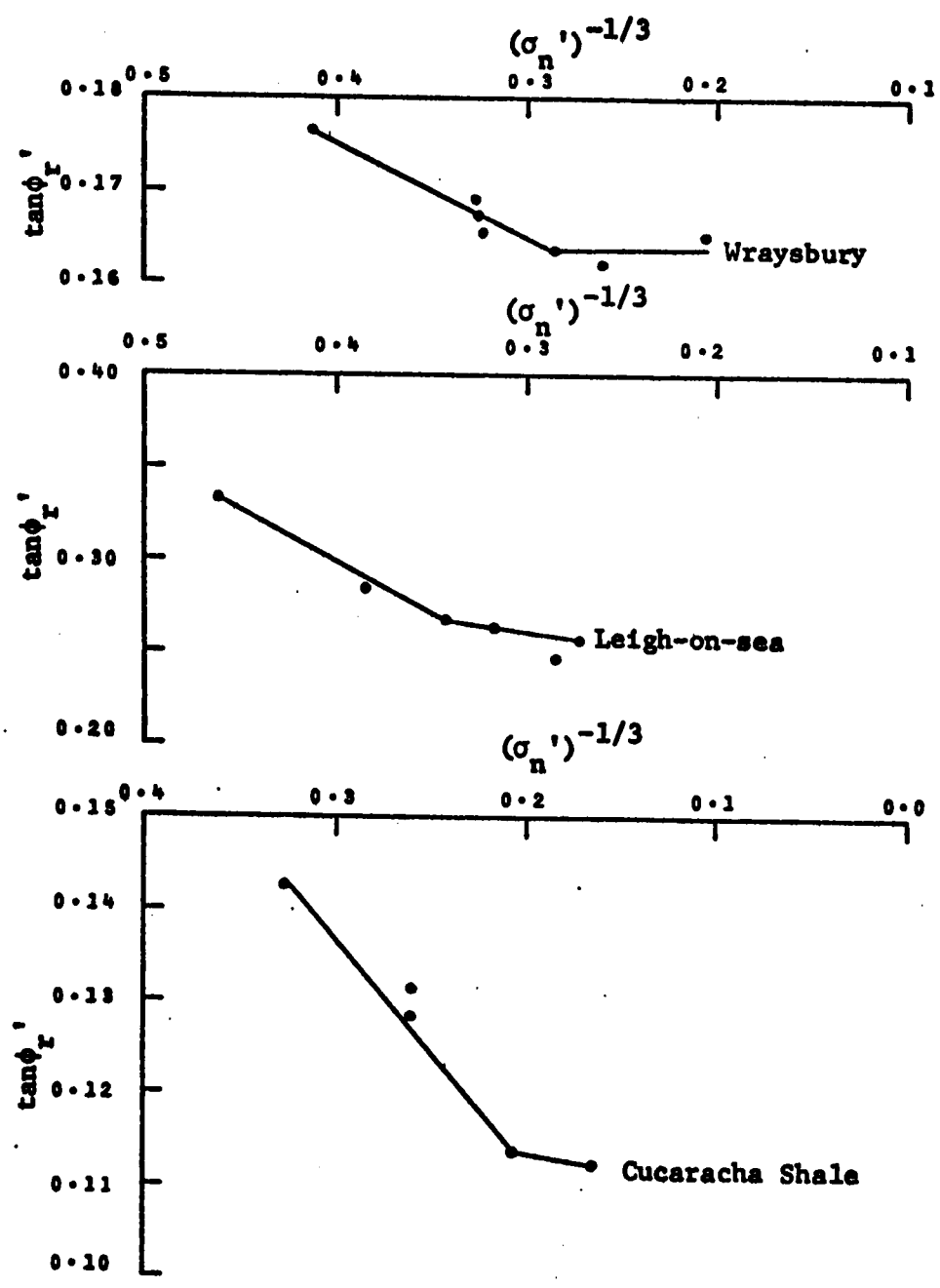
FIG. 3.7 RELATIONSHIPS BETWEEN $TAN\phi_r'$ AND $(\sigma_n')^{-1/3}$ FOR SOME ENGLISH CLAYS AND ONE SOUTH AMERICAN SHALE (DATA OBTAINED FROM BISHOP ET AL., 1971)

CHAPTER IV

EXPERIMENTAL PROGRAMME

4.1 Introduction

In the previous chapter, a working hypothesis for the physical basis of the residual shear strength of pure clay minerals was presented. From an analysis of the previous studies, it was demonstrated that the hypothesis presented here is clearly a reasonable one and has great potential for explaining nearly all the aspects of the nature of shear strength at large strains. However, the previous studies of the residual strength are either insufficient or incomplete to prove the hypothesis conclusively. Hence, a further extensive experimental programme that would include carefully controlled tests specially devised to prove the validity of the hypothesis was considered necessary. This chapter will outline briefly the testing programme that was undertaken to verify the hypothesis.

4.2 Minerals Tested

Since the aim of this study was to investigate the fundamental nature of shear strength at large strains, it was decided to perform the study on pure clay minerals (which are ideal mediums for any theoretical investigation) rather than on natural soils with mixed mineralogical compositions which would have unnecessarily made the interpretations considerably more complex for the purpose of establishing a physical

basis of the residual strength. Moreover, clay minerals are the major
component of clay soils and clay shales and control their engineering
properties, such as compressibility, shear strength and permeability.
Hence, a clear understanding of the fundamental factors controlling the
residual shear strength of pure clay minerals will no doubt further
our understanding of the nature of residual strength in clay soils and
clay shales.

Kaolinite, attapulgite and montmorillonite are the three
clay minerals that were chosen for this investigation. Illite was not
tested because it is difficult to obtain pure illite commercially and
furthermore, the residual strength characteristics of illite appear
to be similar to that of highly saline montmorillonite (as pointed out
in section 3.1 of Chapter III). However, the range of clay minerals
tested here is broad enough to cover most of the common clay minerals
usually found in natural samples.

4.3   Sample Preparation

One of the major objectives of this investigation was to study
the influence of the pore fluid salinity on the residual shear strength.
Therefore, all the clay minerals were tested at three different pore fluid
salt concentrations under a range of normal pressures and the corresponding
residual shear strengths were determined. Since more than one type of
cation in the adsorbed states on the clay mineral surface would unnecessarily
complicate the physico-chemical interpretations of the test results, it was
decided to work with Na-homoionized clay minerals with NaCl as the
principal salt in the pore fluid.

Large batches of these Na-homoionized clay minerals were remoulded at high liquidity indices under the various pore fluid NaCl concentrations. The slurries were then consolidated in large consolidation cells until sufficient undrained shear strengths were imparted to the samples so that they could be treated as undisturbed blocks from which the reversal shear test specimens were obtained. This essentially eliminated possible differences in the initial structures of the shear test specimens of one mineral. Moreover, cores obtained from the large blocks provided shear test specimens with better parallel orientation of particles and less peripheral disturbances. The details of the sample preparation techniques are outlined in the subsequent chapter.

4.4   Type of Shear Test Used in This Investigation

In the last few years, several investigators (e.g. Petley, 1966; Sembenelli and Ramirez, 1969; Lagatta, 1970 and Bishop et al., 1971) have suggested that the true residual strength of a soil can only be measured in a ring shear test. Ring shear tests have the advantage of providing sufficient displacements in one direction in order to attain the residual states and as a result they simulate the field condition more realistically. However, there is so far no direct field evidence to substantiate the applicability of residual strengths measured in ring shear tests. Furthermore, ring shear equipment still fails to satisfy the criteria of simplicity of construction and operation. For purposes other than the measurement of residual strength, it has all the disadvantages of the shear box, such as local concentrations of strains and uncertainty about the directions of the principal stresses as the test proceeds.

Another disadvantage is the variation in strain produced across the sample i.e., for a given angular rotation, the linear displacement is greatest at the outer edge of the sample and a somewhat empirical correction has to be applied. Extreme difficulty is also encountered in preparing specimens for use in the ring shear apparatus, particularly with stiff fissured clays. Above all, the high cost of a ring shear apparatus made its use prohibitive for this study because use of more than one ring shear machine was considered necessary in order to conduct the required number of tests within a reasonable span of time.

The triaxial test has also been used by a number of investigators (Petley, 1966; Chandler, 1966) to determine the residual strength of soils. This method suffers from the serious disadvantage that in many cases the deformation necessary to reach the residual strength state can not be obtained in the triaxial compression apparatus except possibly in the case of very brittle clays. Petley (op. cit.), however, tested samples with precut planes in the triaxial compression apparatus (fitted with rotating bushing) where horizontal movement of the upper half of the specimen above the precut plane was facilitated using two top caps separated by small steel balls. From these tests, he obtained values of ϕ_r' comparable to those obtained from direct shear tests on the same samples. Although Petley's results indicate that comparable values of ϕ_r' are obtained from triaxial and reversal direct shear tests, the simplicity of the shear box test makes it preferable in most cases.

In view of the above considerations, neither the ring shear

nor the triaxial test was used in this investigation. Instead, the next most expedient method which is the reversal direct shear test was chosen for the purpose of measuring residual shear strength in this study. The shear box test has many advantages for residual strength determination, viz.:-

      i) Preparation of samples for use in this test is relatively easy;

      ii) It is a much less involved test to run;

      iii) Large horizontal deformations can be imposed on the samples by continuous reversing of shear direction;

      iv) Specimens can be readily wire cut after consolidation, if desired; and

      v) It is expedient in terms of time involved.

The disadvantages of the direct shear test are that the stress conditions across the sample are complicated and progressive failure occurs. Soil may also be squeezed out between the two halves of the shear box during the later stages of a shear test which may limit the number of reversals in a test. However, more is now known about the nature of shear and the stress conditions in a direct shear test specimen at the peak and residual states from the microstructural studies of Morgenstern and Tchalenko (1967 a). Use of the direct shear testing technique for the measurement of residual strength also permitted comparison of the test results obtained in this study with similar data obtained by others using the same testing technique.

4.5   Residual Shear Tests

      It has been demonstrated by several workers (e.g. Petley,

1966 and Tchalenko, 1967) that shearing along a precut plane is the most suitable method for determining the residual shear strength of a clay. Petley (op. cit.) tested samples containing precut failure planes in the triaxial compression apparatus and found good correlation with the results obtained from tests on actual slip surfaces. Cut plane specimens of kaolinite, tested by Tchalenko (op. cit.), exhibited considerably reduced shearing resistances and from his microstructural studies, Tchalenko concluded that this is consistent with the known influence of particle orientation on the residual strength of clays. Virtually perfect alignment of particles is necessary in a kinematically admissible direction in the shear box in order to obtain the true ϕ_r' and it seems that shearing along a precut plane helps to achieve this in a smaller amount of horizontal displacement. Furthermore, since extrusion of soil during the later stages of a conventional reversal shear test is a problem, the smaller amount of horizontal displacement (and hence less number of reversal cycles) required to attain the residual state in a precut plane test makes it preferable. Hence, precut plane tests were used in this investigation to determine the residual strength parameters of the clay minerals.

Proper choice of sample thickness in a direct shear test is also extremely important for obtaining good residual strength parameters. Kenney (1967) conducted all his shear tests on 2-3 mm. thick samples. It is however believed that if an ultrathin sample is used in a direct shear test, the shear structure soon reaches the boundaries (the carborandum porous stones) and creates a kinematic restraint. Therefore,

the strength measured may not be truly residual but might correspond to one from a restrained structure. This, according to Morgenstern and Tchalenko (1967 a) will be an intermediate value between the peak and residual. Comparison of some of the values reported by Kenney with those of others tend to support this view. For example, Kenney has measured a $\tan\phi_r'$ value of 0.27 for kaolinite, whereas the $\tan\phi_r'$ values for the same mineral measured by Morgenstern and Tchalenko (1967 a) and Cullen and Donald (1971) on samples of larger thicknesses in direct shear tests ranged from 0.18 to 0.21. Moreover, ultrathin samples tend to produce large changes in the shear surfaces between reversals. In thin samples, Cullen and Donald (op. cit.) have observed dual failure surfaces separated by lenses of soil up to 3 mm. thick and this phenomenon, in their opinion, could account for the apparently random variations between the tension and the compression cycle strengths which so often occurs. Hence a sample thickness of about 1 inch or more was chosen for each reversal shear test in this study and the precut plane was made at approximately the mid-height of the specimen.

It was also necessary to choose the rates of deformation that would be suitable for determining the residual strength parameters from the cut plane tests. Since Kenney (1967) has demonstrated that the residual shear strength of the common clay minerals is not significantly influenced by the rate of strain (Fig. 2.3), reasonable rates of displacement (0.0019 and 0.0024 inches per minute) that would be expedient in terms of the time involved for the completion of a test were chosen for all the shear tests on specimens with precut planes.

The rates chosen here for the shear tests on the clay mineral specimens are in keeping generally with the recommendation of Cullen and Donald (op. cit.) who suggested a speed of 0.001 inches per minute for fissured overconsolidated clays. They also demonstrated that beyond a certain rate of strain, erroneous values of residual shear strength are obtained and high speed shearing results in a high strength value. For a test in which the peak shear strength was determined, the rate of deformation that would ensure fully drained conditions during shear was calculated using the Gibson-Henkel (1954) formula.

It was speculated in Chapter III that salinity may not have significant effect on the residual shear strength of kaolinite and attapulgite. Hence, conventional reversal drained direct shear tests were conducted on these two minerals at three different pore fluid NaCl concentrations under various normal pressures in order to study the effect of salt content and the magnitude of normal effective stress on the residual shear strength of these inactive minerals. In the case of montmorillonite (the residual strength properties of which are supposed to be influenced by system chemistry), conventional drained direct shear tests were conducted on samples with pore fluid salinities of 1.15, 15.26, and 33.57 g/l NaCl under a range of normal pressures in order to study the effects of the same factors on the residual shear strength of montmorillonite.

Most of the samples were sheared along precut planes except a number of attapulgite samples which were sheared without precut planes in order to determine the peak shear strength parameters of

attapulgite. The values of ϕ_e for kaolinite and Na-bentonite have already been reported by Gibson (1953) and Morgan (1967). However, no attempt has been made so far to determine the peak friction angle of attapulgite. Hence, a number of attapulgite samples at various pore fluid salinities with no preformed planes in them were sheared under a range of normal pressures not only to determine the peak friction angle but also to obtain an idea of the percentage reduction in shear strength from the peak to the residual state for attapulgite.

4.6 Testing Programme Developed to Verify the Control of True Effective Stress on the Residual Shear Strength

In the working hypothesis for the physical basis of the residual shear strength of pure clay minerals, presented in Chapter III, it was postulated that the residual shear strength of a clay mineral is controlled by the true effective stress (σ_n^*) on the mineral basal planes. It was also demonstrated that the Coulomb-Terzaghi relationship for residual strength (τ_{res}) can be expressed in terms of the true effective stress as,

$$\tau_{res} = [\sigma_n' - (R-A)] \tan\phi_r' = \sigma_n^* \tan\phi_r' \qquad (3.23 \text{ a, b})$$

The available shear strength data on Na-montmorillonite (Kenney, 1967) was reinterpreted in light of the modified Coulomb-Terzaghi relationship and the reinterpreted data (Table 3.3) seem to provide encouraging evidence in favour of the concept of σ_n^* controlling the residual shear strength and the uniqueness of ϕ_r' for a mineral. However, Kenney's tests are of limited value for proving the validity of the modified Coulomb-Terzaghi relationship for residual strength (Eqn. 3.23 a, b).

This is so because in order to study the effect of pore fluid salinity on the residual shear strength of an active clay mineral such as montmorillonite, he sheared separate samples of the same mineral with different pore fluid salinities under the same applied (or apparent effective) stress (σ_n') but his samples had widely different residual state water contents (see Table 3.3). Consequently, the true effective stresses of the samples were different (as shown in Table 3.3) because the net (R-A) stress is greatly dependent on the water content. Hence, in order to verify the control of σ_n^* on τ_{res} experimentally, a better approach would be to replace the saline pore fluid of an active clay mineral sample under constant true effective stress condition and demonstrate that the residual shear strength of the sample is unaffected by the change in the pore fluid salt concentration. With this specific aim in mind, the following testing programme was developed.

1. A number of Na-montmorillonite samples with a high pore fluid NaCl concentration (33.57 g/l NaCl) were consolidated under applied stresses (σ_n') ranging from 2.5 to 15 psi in the direct shear boxes. The testing programme was confined to montmorillonite because this active clay mineral is known to exhibit high net (R-A) stress. However, under a highly saline environment, the apparent effective stress (σ_n') of a sample would be practically equal to its true effective stress (σ_n^*).

2. The saline samples were then sheared along precut planes under the various normal pressures and the

corresponding residual shear strengths were measured.

3. The sheared samples were then leached under constant overall volume conditions with distilled water in order to replace the saline pore fluids. Since leaching is a time consuming process especially in the case of low permeability samples, the tests were confined to the low pressure range so that the samples that were to be leached would not have very low permeabilities. In order to maintain the overall volume of a sample constant during leaching, the true effective stress (σ_n*) of the sample must be held constant because σ_n* is known to control the volume change behaviour of an active clay-water system (Balasubramonian, 1972). Hence, to prevent the swelling of the montmorillonite samples during leaching, the externally applied normal stresses (σ_n') on the samples had to be increased. This means that as the net (R-A) stress of a sample increased due to leaching, the apparent effective stress (σ_n') of the sample was correspondingly increased in such a manner that [σ_n' - (R-A)] or the true effective stress (σ_n*) of the sample was held constant throughout the leaching process.

4. After completion of leaching, the final apparent effective stress (σ_n') of a leached sample would obviously be higher than the initial apparent

effective stress (σ_n') under which the same sample was sheared before leaching. The leached montmorillonite samples were then resheared along the existing precut planes under the new apparent effective stresses (σ_n') after leaching and the residual shear strengths of the leached samples were measured. The residual shear strength of a leached sample was then compared with the corresponding residual shear strength of the saline variety of the same sample measured before leaching and since the true effective stress (σ_n^*) of the sample was held constant throughout the leaching process, such a comparison would conclusively establish the concept of true effective stress controlling the residual strength of a clay mineral.

These key tests did also provide an opportunity to correlate the measured value of the net (R-A) stress developed in a montmorillonite sample due to leaching under constant overall volume condition with the theoretical value of P_y for the same sample estimated from the double-layer repulsive stress equation. A study of the effect of replacing the saline pore fluids on the permeabilities of the montmorillonite samples was also undertaken during these tests.

4.7 Microstructural Studies

It was demonstrated before that a knowledge of the structure at the residual state has been one of the most important contributing

factors towards the development of the physical basis of residual strength. Hence, an investigation of the large displacement shear zone structures in the clay mineral samples was considered essential for this study.

The two techniques which have proven to be particularly useful for microstructural observations in soils are: (i) optical microscopy and (ii) electron microscopy. Since Morgenstern and Tchalenko (1967 a, b) have presented a fairly complete picture of the shear structures in the large displacement shear zones in clays using the technique of optical microscopy, it was decided that the technique of electron microscopy would be used for this study so that the large displacement shear zone structures in the clay mineral samples could be observed at particle level.

There are two methods of electron microscopy and they are: (i) transmission electron microscopy and (ii) scanning electron microscopy. The transmission technique was not used here because this investigation required looking at a larger area of a sample than is possible by transmision electron microscopy. Furthermore, ultra-thin sectioning and surface replication techniques require considerable skill and are also time consuming which make the transmission technique tedious and difficult. Hence, the scanning technique was thought to be more suitable because it allows a larger area to be scanned. The scanning electron microscopy is designed to produce a magnified image of a surface. Some of the main advantages of this instrument are: the large depth of focus at high magnifications, which gives considerable

perspective to the image; the possibility of examining relatively large samples (~ 1 cm. diameter) at low power and at high magnifications when objects of interest have been located; and the relative simplicity of sample preparation. Hence, the scanning electron microscope is an ideal tool for studying the mutual disposition of mineral particles and voids in the micron and the sub-micron size ranges and in this investigation, it was considered to be the most suitable instrument for examining the large displacement shear zone structures in the clay mineral samples.

CHAPTER V

PROPERTIES OF THE MINERALS USED, SAMPLE
PREPARATION AND TESTING TECHNIQUES

This chapter presents the properties of the clay minerals, the procedure for sample preparation, the details of the test equipment and the testing techniques that were used to carry out the experimental programme outlined in Chapter IV.

5.1 Classification Tests on the Clay Minerals

The routine classification tests on the clay minerals (viz., kaolinite, attapulgite and montmorillonite) in their unmodified state were carried out in accordance with the procedures outlined by Lambe (1951). The results of these classification tests are presented in Table 5.1 as well as in Figs. 5.1 to 5.6. The mineralogical compositions of the clay minerals (based on X-ray diffraction analyses) are also reported in Table 5.1. Although a soil known as "Grundite" was originally chosen as a possible source of the clay mineral illite, a subsequent X-ray diffraction analysis indicated that the illite content of this soil was less than 20% and consequently, it was rejected.

The grain size distributions of kaolinite, attapulgite and montmorillonite, presented in Figs. 5.1, 5.2 and 5.3, show that the minerals contained sufficient amounts of less than 2 micron size particles and hence were suitable for this investigation. Figs. 5.4,

5.5 and 5.6 illustrate that while the effect of salinity on the limits of kaolinite and attapulgite is not so significant especially beyond a concentration of 10 gms. NaCl/litre, the Atterberg limits of montmorillonite decrease markedly with increasing NaCl concentration in the pore fluid.

It was mentioned in Chapter IV that since the effect of system chemistry on the residual strength of clay minerals is one of the principal issues in this investigation, all the clay minerals should be homoionized in sodium in order to avoid unnecessary complications in the interpretation of test results due to the presence of more than one type of ion in the adsorbed state on the clay mineral surfaces. Furthermore, sodium varieties of most clay minerals (especially montmorillonite) are ideal mediums for a theoretical investigation of the engineering behaviour of clay minerals. Hence, it was necessary to conduct the following tests in order to determine the chemical properties and the cation impurities of the clay minerals in their unmodified state so that an appropriate method for homoionization of the minerals in sodium could be adopted.

a. Organic content: The organic contents of the clay minerals were determined following the procedure outlined by Akroyd (1957).

b. Carbonate content: The percentages of calcite and dolomite in the clay minerals were determined in a Chittick apparatus following the procedure outlined by Dreimanis (1962) for quantitative gasometric determination of calcite and dolomite in a soil.

c. Cations present in the unmodified clay minerals: The types and concentrations of various cations in the as procured state of a clay mineral were determined by repeatedly leaching the particular mineral with 1N NH_4Ac solution, collecting the leachate and subsequently subjecting the total extract to an analysis for the concentrations of Na^+, Ca^{++}, Mg^{++}, K^+ and H^+ using an atomic absorption spectrophotometer. The unit available in the Soil Science Department of the University of Alberta was used for the purpose. The unit and its working principles have been described elsewhere (Balasubramonian, 1972).

The concentrations of the various cations in the unmodified clay minerals were expressed in milliequivalents per 100 gms. of dry soil and this analysis produced concentrations of the total cation impurities which include all the free and the adsorbed cations in the clay minerals in their as procured state.

d. Cation exchange capacity: The total cation exchange capacities of the clay minerals were determined on the less than 2 micron fraction of the minerals following the procedure outlined in the University of Alberta Soil Science Manual no. 421.

e. Total specific surface: The specific surface of a clay mineral is an extremely important soil parameter used in the estimation of the net (R-A) stress of the mineral from the repulsive stress equation (Eqn. 3.29) because the nagnitude of the net (R-A) stress is quite sensitive to the specific surface. The total specific surface of each clay mineral was determined on the less than 2 micron fraction of the mineral separated by the conventional hydrometer test. The

suspension containing this fine fraction was air-dried to the consistency of a paste and the sample (which contained approximately 10 gms. of the dry mineral) was treated with two 50 ml. batches of 6-10% H_2O_2 for removal of the organic matter. The mixture was continuously stirred on a hot plate at 60°C until no further gas was being generated. The excess H_2O_2 and the burnt product were then removed by repeated leaching of the sample with warm distilled water in a Buchner funnel. A small suction was used to facilitate the leaching process. If the mineral contained carbonates, the sample was treated with 15-20 ml. of 6N HCl followed by distilled water and alcohol wash to remove the carbonates. The procedure for carbonate removal has been outlined in detail by Balasubramonian (1972 a). The sample was next saturated in calcium by repeated leaching (about 5-6 times) with 1N $CaCl_2$ in the same Buchner funnel. This was followed by a number of leachings with distilled water, 50:50 alcohol-water mixture and pure alcohol for removal of excess $CaCl_2$ from the sample. The resulting clay mineral sample was then dried in an oven at 60°F for 24 hours and the sample was subsequently cooled in a dessicator. The total specific surface of the clay mineral sample prepared in the above mentioned manner was then determined by the EGME (Ethylene Glycol Monoethyl Ether) method as outlined in the University of Alberta Soil Science Manual no. 421.

The method adopted here yielded total specific surfaces of the clay minerals. The specific surfaces used in this investigation for the estimation of the net (R-A) stresses were total specific surfaces because the entire study was performed on Na-homoionized samples that

were consolidated from high liquidity index slurries of the clay minerals and hence cluster or domain formation in the samples was not expected.

Although Na-homoionized samples of various minerals were used in this study, the specific surfaces of the minerals were determined on Ca-saturated systems and these specific surfaces were used for the estimation of the net (R-A) stresses in the Na-saturated systems. This may be understood by reviewing the prime requirement in the EGME method for determination of specific surfaces. The EGME method employs a technique of forming a known thickness (usually a monomolecular layer) of EGME on the soil surface and measuring the weight of the EGME absorbed on the soil. This weight divided by the unit weight of EGME times the thickness of the layer on the soil per unit weight of the dry soil yields the required specific surface. Past research has yielded different magnitudes of specific surface values for the same soil with different exchangeable cations (for eg., see Dyal and Hendricks, 1952; Bower and Gschwend, 1952). The formation of a uniform monomolecular layer on the soil surface (which is the prime requirement for successful application of the EGME method) is doubtful with soils saturated with cations like Na^+. Furthermore, it is a known fact that the adsorbed layer of a sodium clay is more extended than a calcium clay and if the specific surface of a Na clay is found to be less than that of a Ca clay, it would only mean that the specific surface measured is not of the clay particle alone, but it is of the clay particle and a part of the adsorbed layer. Until the discovery of a polar liquid which is effective in stripping off the double-layers of the clays completely,

the use of the EGME technique with calcium saturated soils appears to be the only way of determining the true particle specific surface of a soil.

The results of the chemical analyses performed on the clay minerals are reported in Table 5.2 The organic contents of clay minerals were not considerable. Although the supplies of kaolinite and montmorillonite contained very little carbonates in them, the attapulgite stock had abundant carbonate in it. This high carbonate content of attapulgite is also reflected in the high Ca^{++} and Mg^{++} cation concentrations obtained in the analysis of total cation impurities in the mineral (Table 5.2). The data on the total cation impurities in the unmodified minerals, presented in Table 5.2, clearly indicate that except for kaolinite (which possesses a low ion exchange capacity), the as procured states of both attapulgite and montmorillonite minerals were unacceptable in view of the distribution of cations in the adsorbed states. Consequently, both of these minerals had to be purified and homoionized in sodium. The total cation exchange capacities of the clay minerals, reported in Table 5.2, compare favourably well with the values reported in the literature for the same minerals (for eg., see Kenney, 1967; Lambe and Whitman, 1969). Since kaolinite has a low cation exchange capacity, it is usually found in a purer state that required no further treatment. Montmorillonite, on the other hand, has a high exchange capacity and is rarely found in a Na-state because divalent Ca or Mg cations are more easily adsorbed on its surfaces. The total specific surface values, presented in Table 5.2, are also similar to the values reported by other investigators for the same minerals. For

example, Mesri (1969) reported specific surface values of 500 and 680 m.^{2}/gm. for Na and Ca varieties of montmorillonite respectively.

5.2 Sodium Homoionization of the Clay Minerals

A number of techniques such as leaching in a column or use of exchange resins are available for homoionization of a clay mineral. However, use of any one of these standard techniques would have been prohibitively expensive and time consuming for homoionizing the quantities of minerals required for this investigation. Hence, a homoionizing technique that would be relatively inexpensive and expedient in terms of time had to be devised and in this section, the treatment procedures for Na-homoionization of the minerals attapulgite and montmorillonite are outlined.

a. Attapulgite: Large batches (9 to 10 lbs. each) of the mineral attapulgite were mixed thoroughly with distilled water in three polyethylene baths (each containing about 120 lbs. of distilled water) and allowed to settle. The coarse fraction which contained a major portion of calcite and dolomite was removed from each bath by decanting the suspended fines and rejecting the already settled coarse fraction. The sedimentation technique was repeated about 5-6 times for each bath to remove as much of the coarse fraction as possible. Samples were collected from the resulting batches of attapulgite and subjected to carbonate analysis which showed a decrease in the carbonate content from 10.34% to 1.8%.

These three batches of attapulgite were then washed with

1 N NH_4Ac solution in order to replace all the cations in the adsorbed state with a single cation, NH_4, which can easily replace the usual cations in a soil. The dry soil: solution ratio for each bath was maintained at about 10 lbs.: 120 lbs. as before. The mixture in each bath was stirred thoroughly and the soil was allowed to settle for 24 hours after which the supernatant clear liquid was decanted off each bath. This process was repeated about 5-6 times using a fresh supply of 1N NH_4Ac for each wash. The batches were subsequently washed about 9-10 times in a similar manner as the NH_4Ac wash with 35 gms./litre NaCl solution not only to remove the excess NH_4Ac from the batches but also to the replace the adsorbed NH_4 ions with Na ions. The batches were then ready to be washed with solutions of three predetermined NaCl concentrations which were chosen to be the final pore fluid salt contents of the attapulgite samples required for subsequent shear tests. The two extreme pore fluid NaCl contents of 0 and 35 gms./litre were obvious choices. However, the intermediate salt content was chosen after consideration of the liquid and plastic limit data of attapulgite (Fig. 5.5). The limit values of attapulgite are moderately influenced by salinities between 0 and 10 gms./litre but above a threshold NaCl concentration of about 10 gms./litre, salinity seems to have an insignificant effect on the limit values of attapulgite and hence probably does not influence the strength and compressibility either. Hence a NaCl concentration of 2 gms./litre (which is well within the range of 0 to 10 gms./litre where salinity may have some influence on the engineering behaviour of attapulgite) was chosen as the intermediate salt content.

The three batches of attapulgite were then washed a number of times with distilled water, 2 gms./litre and 35 gms./litre NaCl solutions respectively following the same procedure of washing as before and maintaining the same dry soil: solution ratio. The sample in the distilled water environment required more than 24 hours to sediment after every wash whereas in a highly saline environment, clear supernatant liquid on a batch was usually obtained in less than 24 hours. The resistivities of the clear supernatant liquids after every wash were measured with a Beckman RB 3R 104 model solu-bridge with platinum electrodes in glass pipette type conductance cells (calibration curve shown in Fig. A-1 of Appendix A). The washing was continued until the resistivity of the clear supernatant liquid in each bath was equal to the resistivity of the corresponding desired pore fluid salt solution. Approximately 9-10 washes of each batch were required to reach this stage. After decanting the supernatant liquids at the end of the final wash, the water contents of the treated batches were found to range from 380 to 430% which corresponded to liquidity indices of 1.5 to 2.2. The slurried batches were now ready to be consolidated.

b. Montmorillonite: Three batches of montmorillonite were homoionized in soium following nearly the same procedure that was used for attapulgite. The initial sedimentation process was not employed to remove any coarse fraction because the mineral montmorillonite in its unmodified state had very little carbonate in it (Table 5.2). The dry soil: solution ratio in each bath was maintained at about 7 lbs.: 60 lbs. The NaCl concentrations of the final wash solutions for the three batches were selected to be 0, 15 and 35 gms./litre, choosing the intermediate

concentration from the limit data on montmorillonite (Fig. 5.6).

After completion of the washings for Na-homoionization, the 35 gms./litre NaCl slurry of montmorillonite had a water content of approximately 815% (liquidity index ≈ 7.76) and the slurry possessed suitable consistency for immediate deposition in the large cell for consolidation. However, the water contents of the distilled water and the 15 gms./litre NaCl batches were found to be 4600 and 3300% respectively which gave the slurries an unsuitably thin consistency for immediate consolidation because consolidation of such lean slurries would inevitably have caused extrusion around the piston in the consolidation cell. Hence the 0 and 15 gms./litre NaCl slurries were dried down to water contents of about 800 (liquidity index ≈ 1.41) and 850% (liquidity index ≈ 3.66) respectively. The drying of the slurries was facilitated by a draft of warm air into each bath and large mechanical stirrers were used to constantly stir the clay-solution mixture in each bath so that a dried crust would not be formed on the surface of the slurry. The type of polyethylene baths used for homoionizing the clay minerals and the set-up for drying of the mineral slurries to an acceptable consistency for consolidation are shown in Fig. 5.7. After the two batches were dried to water contents of 800-900%, they were ready to be consolidated. The system chemistries of the Na-homoionized attapulgite and montmorillonite slurries were not analysed at this stage but were determined at a later stage from samples of the large blocks that were obtained by consolidating these slurries to desired effective stresses.

The homoionizing technique used here was simple and inexpensive.

The whole process of homoionizing the large batches of the minerals attapulgite and montmorillonite was completed in approximately four months. The effectiveness of the simple procedure adopted here is investigated in the next chapter in terms of the percent homoionization of the batches in sodium accomplished by this technique.

5.3 Sample Preparation Techniques and Associated System Chemistry Analysis

The mineral kaolinite was obtained in a relatively pure state and salinity was not expected to have any significant influence on the residual strength of kaolinite. Consequently, no special modification programme was undertaken for this mineral and instead of preparing large consolidated blocks of kaolinite, the mineral in its air-dry powder state was thoroughly mixed with desired pore fluids (0, 2 and 35 gm./litre NaCl solutions) at liquidity indices of 1-2 and allowed to equilibrate for 24 hours in a moisture room with controlled humidity. For shear tests on kaolinite, these slurries were directly deposited in the shear boxes and allowed to consolidate under desired normal loads.

The Na-homoionized slurries of attapulgite and montmorillonite were consolidated in large circular consolidation cells. Four cells were built for consolidation of the slurries and each cell was comprised of four essential components: (a) an aluminium base plate with a drainage valve, (b) an 11.84" internal diameter , 10.26" high cylindrical aluminium mould which was lined on the inside with teflon to minimize side friction, (c) a 7.5" high aluminium loading piston that fitted smoothly into the mould and (d) a vertical guide for centering of the

piston (or the loading cap) and prevention of undesirable tilting of the piston during the initial stages of consolidation. Leakage between the mould and the base was prevented by an O-ring seal. Polyethylene porous stones (k $\approx$ 1 x 10^{-4} cms./sec.) with filter papers were used on both sides of the samples allowing two-way drainage for the specimens. No side drains were used. The drainage from the top of a sample in a cell was collected in the piston which had a perforated surface in contact with the top porous stone while the drainage from the bottom of the sample was collected in a graduated jar. A pictorial view of the large cell consolidation test set-ups is shown in Fig. 5.8.

Samples for consolidation in the large cells were prepared from the slurries in the following way. The porous stones for a cell were first boiled in a salt solution that was identical in composition and concentration to the pore fluid of the slurry that was going to be consolidated in that particular cell. The mould was then clamped to the base plate and the saturated bottom porous stone with a No. 42 Whatman filter paper (wetted and cut to the size of the stone) was put in place. A quantity of the same NaCl solution was then poured into the cell and the bottom valve was opened to flush out the air bubbles that were trapped in the drainage channels of the base plate. After deairing the base, the 3/16" diameter Eastman tube that carried the drainage from the bottom of the sample to the graduated jar was filled with the same solution and the end of the tube was kept immersed into a small quantity of the same salt solution in the graduated jar so that no air could get back into the drainage channels of the base plate and desaturate the bottom

porous stone. The appropriate slurry was then deposited into the cell in layers. During the entire process of filling up a cell with a particular slurry, the cell was seated on a table vibrator (Soil Test Inc. Model No. CT164) and continuous vibration was applied to the cell to drive out any air entrapped during deposition of the slurry. The usual thickness of the deposited slurry in a cell was maintained at around 7-9 inches so that the loading piston could be seated into the mould upto a depth of at least 2 inches from the surface of the mould. When the desired thickness of the sample in a cell was attained, the consistency of the slurry was such that the vibration applied to the cell produced a perfectly smooth top surface and no further trimming of the top surface was necessary. Saturated porous stones with filter papers were then placed on the top of the samples and the cells were moved to the consolidation bench. The sample thicknesses were measured accurately and the samples were ready to be consolidated.

The first load on each sample was the load of the piston ($\simeq 0.16$ psi). The rods connected to the top of the pistons were guided through the vertical guides (Fig. 5.8) which had practically frictionless teflon bushings in them and the pistons were carefully centred and lowered into the moulds and seated on the samples. Each piston was partially filled with a salt solution that was identical in composition and concentration to the pore fluid of the slurry that was being consolidated in that cell to avoid osmotic diffusion. The settlement readings were obtained from three ½" travel dial gauges that were set on three radial fins attached to the piston in such a way that the

angle subtended between each settlement gauge point was equal to 120°
(Fig. 5.8). As consolidation progressed, the gauges attached to vertical
rods that were clamped to the unyielding base plate of a cell measured
the settlements of the fins. Amount of relative tilting of a piston
during consolidation was determined from the settlement readings
obtained at the three corners of the piston. The procedure for
consolidation was otherwise conventional. A load increment ratio of 1.0
was maintained for all the specimens. The pressure increments were
applied by putting appropriate weights directly on the loading piston
(Fig. 5.8) and just as in a conventional consolidation test, the dial
gauge readings were recorded with time. In each test, a subsequent
load increment was not applied until at least 90% of the primary
consolidation under the previous load increment was over. Furthermore,
as consolidation under the various applied normal stresses was in progress,
the quantity of outflow from each sample was recorded every 24 hours
and a sample from the effluent was also collected every 24 hours for
resistivity measurement.

The final applied normal pressure on all the samples of
attapulgite and montmorillonite with the exception of the 35 g/l NaCl
sample of montmorillonite was 1.27 psi. The 35 g/l NaCl sample of
montmorillonite was subjected to a final consolidation pressure of about
0.32 psi. On average, about 20,000-25,000 c.c. of fluid was expelled
from each attapulgite specimen as the consolidation pressure was
increased from 0 to 1.27 psi whereas about 5,000-12,000 c.c. of fluid
(the amount of fluid expelled increasing with increasing pore fluid salt

concentration) was expelled from each montmorillonite sample. At the
end of the first load increment, each sample was circulated with its
own pore fluid to ensure that the sample acquired the desired pore fluid
salinity. A period of three months was required for consolidating the
three attapulgite samples to a final pressure of 1.27 psi whereas the
consolidation of the montmorillonite samples were carried out for about
nine months. In comparison with the time required for 90% consolidation
of the 0 and 15 g/l NaCl samples of montmorillonite, the 35 g/l NaCl
samples of montmorillonite required less time for consolidation under
the same applied normal stress.

After completion of consolidation, all the fluids were
drained out from both ends of the samples and each sample was carefully
extruded from its consolidation cell. Even under the low applied
pressures the blocks gained enough undrained shear strength so as to
allow easy handling of the soft blocks. After determining the end of
consolidation water contents of the blocks, they were immediately
waxed and stored in a moisture room with controlled humidity. The
final thicknesses of the attapulgite blocks ranged between 5 and 6 inches
whereas the final thicknesses of the 0, 15 and 35 g/l NaCl blocks of
montmorillonite were about 4 inches. The excessive settlement of the
35 g/l NaCl sample of montmorillonite under the applied stress of 0.32 psi
prevented further consolidation of the block in the large cell. All
the block samples obtained in this manner possessed sufficient thick-
nesses   so as to allow the desired number of shear test specimens to
be obtained from them. The consolidation of the slurries into large

blocks thus served the dual purpose of providing the desired
number of shear test specimens with a certain salt content and maintaining
the same initial structure for each shear test specimen obtained from one
block.

The system chemistries of the consolidated blocks were
analysed in order to define the final pore fluid salinities of the samples.
The system chemistry of a mineral sample can be divided into two major
components: (a) the composition and concentrations of various cations
in the pore fluid and (b) the distribution of cations in the adsorbed
state on the clay mineral surfaces. Among the various methods
available for pore water extraction, the most popular methods have been
leaching and saturation extract (in which the water content of a soil
is increased by adding distilled water to such a limit that the water
could be extracted either by filtering or by application of a small
suction). However, both these methods fail to produce a true estimate
of the salinity of pore fluid at natural moisture content because
concentration of the extracted water is not directly proportional to the
inverse of the moisture content of the diluted slurry. This makes it
impossible to calculate the salinity of the pore water at its natural
moisture content from the known salinity at the diluted water content.
It has recently been demonstrated by Balasubramonian (1972) that a high
pressure mechanical squeezer is most suitable for extraction of the true
pore fluids from clays and clay-shales for the correct estimate of the
pore fluid salt contents. This technique involves extraction of pore
fluid from a sample in its natural state and the pressure required

to squeeze out the pore fluid depends on the type of soil. Since the clay mineral blocks were consolidated from slurries, they had high water contents and consequently, the consolidation cells themselves served the purpose of pore fluid squeezers. The fluid expelled out of each sample during the final stages of the last load increment was regarded as the true pore fluid of the sample. The concentrations of Na^+, Ca^{++}, Mg^{++} and K^+ ions in these pore fluid samples were determined using atomic absorption spectrophotometry technique.

To determine the distribution of the adsorbed cations in the blocks, a small sample collected from each block was repeatedly leached with 1N NH_4Ac using fresh supply of 1N NH_4Ac for every leaching. The total leachate was then analysed for concentrations of Na^+, Ca^{++}, Mg^{++} and K^+ and the results of this analysis produced the total cation (i.e. pore fluid + adsorbed) concentrations in the block. The distribution of cations in the adsorbed state for a block was then calculated by subtracting the pore fluid cation concentrations from the total cation concentrations. The distribution of the various cations in the adsorbed state, thus determined, clearly indicated the extent to which the treatment procedure adopted here had been successful in homoionizing the clay minerals in sodium. The results of these analyses are reported in Chapter VI.

5.4 Reversal Drained Direct Shear Tests

5.4.1 Modified direct shear test apparatus

The shear tests were carried out in five direct shear

machines which were modified to suit the requirements of this study. Pictorial views of a modified direct shear apparatus are shown in Fig. 5.9 and 5.10. The total height of each shear box assembly was increased from 2 to 4 inches (Fig. 5.9) in order to accommodate samples of larger thicknesses because the high water content montmorillonite samples were expected to undergo excessive amounts of settlement in the shear box and in a 2" high shear box, this would have resulted in unreasonably thin samples for shear. The inside surfaces of each box were lined with teflon using Scotch-weld 2216 A and B (commercially available from the 3M Company of Canada Ltd.) as the bonding agent and the final cross-sectional area of each shear box was 2.35" x 2.35".

To facilitate the determination of residual strength, the direct shear machines were further modified to allow automatic reversal of the shear boxes. Each machine was fitted with two microswitches at the end of 0.18-0.22 inches travel to either side of the central position (Fig. 5.10). Thus the total displacement between the two microswitches was 0.36-0.44 inches*. Two flat iron pieces attached to both ends of the shear box (Fig. 5.10) activated the microswitches at the end of the

---

*The effect of length of travel of a shear box between reversals on the shape of the load-displacement curve has recently been investigated by Cullen and Donald (1971) and they have concluded from their study that a travel of 0.25 inches between reversals is insufficient to obtain a steady load-displacement curve for some soils. Hence the shear tests conducted in this investigation were all at least 0.36" travel tests.

travel in either direction and the motor was automatically reversed thus reversing the direction of motion. All the tests were started from the central position so that the first reversal came after about 0.18-0.22 inches of horizontal displacement while all subsequent reversals took place after every 0.36-0.44 inches of horizontal displacement. Two additional microswitches, one at each end of travel, were provided in each machine as safety devices (Fig. 5.10). If, for some reason, the reversing microswitches failed to work at the end of a cycle, the box in question was moved further in the same direction till the safety switch was activated which disconnected the power supply and the motor was stopped.

The horizontal and vertical displacements during shear were measured with ½" (model 7DCDT-500) and 1" (model 7DCDT-1000) travel Hewlett-Packard linear voltage differential transducers (Fig. 5.10). Each LVDT had a range of voltage within which a direct proportionality existed between displacement and output voltage. Care was taken to ensure that the displacements (vertical and horizontal) during a shear test were measured within this range. The calibration factors of the LVDT's are presented in Table A.1a of Appendix A.

Load cells (500 lb. capacity) were used in the direct shear machines for the measurement of shear forces. A load cell consisted of four fixed element resistance aluminium strain gauges mounted firmly on a thin hollow aluminium (6063 F Al) cylinder with an internal diameter of 0.25 inches and suitable wall thickness. The wall thickness depends on the desired rigidity of the load cell and the rigidity determines

the utlimate load capacity of the cell. Two of the strain gauges were mounted in such a way that their elements were parallel to the axis of the cylinder while the other two had their elements transverse to the axis. The former were to record the axial deformation of the load cell while the latter compensated for unintended transverse loads or twists. The resistance elements were coated with a water proofing compound to protect the elements from the changes in humidity of the atmosphere and the coating also served as a shock absorber if the load cell was subjected to accidental minor shocks. The ends of the load cells were suitably thickened and flared to suit the fixtures specially made for the shear machines (Fig. 5.10). The ends of each load cell were threaded internally to enable the cell to be mounted in position on the shear machine as shown in Fig. 5.10 so that it can be strained both in compression and tension. The calibration factors of the load cells are presented in Table A.1a of Appendix A. The voltage outputs from the load cells and the LVDTs were scanned, amplified and recorded on a paper strip by an automatic digital voltmeter (Hewlett-Packard Testmobile model 3440A with model 5050B digital recorder).

The side friction in each shear box was reduced by teflon coating and the friction between the two halves of the box was considered to be negligible because the two halves were separated from each other during shear. In order to reduce machine friction, the bushing in the guide through which the extension rod connects the top half of a shear box to the load cell was made out of teflon and an all around gap of 3/1000" was kept between the extension rod and the bushing. This made the machines virtually frictionless. In each

machine, the centre line along which the bottom half of the shear box moves during shear was accurately aligned with the centre line of the load measuring system in order to prevent any undesirable twist that may be exerted on the load cell during shear. The characteristics of the direct shear machines and the associated measuring systems are presented in section A.1 of Appendix A.

5.4.2 Sample preparation

For tests on kaolinite, slurried batches prepared from the air-dried state of the mineral were used to fill up the shear boxes in thin layers until the desired initial thicknesses of the samples were attained. The boxes were continuously tapped during the entire process in order to expel any entrapped air bubbles from the samples. This operation was carried out in a moisture room with controlled humidity. Carborundum porous stones with filter papers saturated in appropriate pore fluid salt solutions were used above and below the slurried samples in the shear boxes. The weight of soil in each box and the water content of the corresponding slurry were determined for calculating the initial void ratio and the degree of saturation of the sample. The shear box assemblies were then moved to the direct shear machines and the samples were subjected to the desired normal loads in conventional steps. A load increment ratio of 1.0 was used in the consolidation phase of each test. The reservoir surrounding each shear box was filled with a salt solution that was identical in composition and concentration to the pore fluid of the sample in the shear box.

In the case of the minerals attapulgite and montmorillonite,

the shear test specimens were obtained from the large consolidated blocks. The peripheral disturbed zone was first removed from each block and smaller blocks (of desired thicknesses) that were of slightly larger dimensions than the internal dimension of a shear box (2.35" x 2.35") were cut out of the central core using a very fine piano wire. An individual small block of desired thickness was then directly set on the top half of a shear box and the four sides of the block were carefully trimmed with a piano wire until the sample fitted into the top half of the box. Water content samples were obtained from the trimmings and the weight of the specimen was determined in order to calculate the initial void ratio and the degree of saturation of the sample. The two halves of the shear box were then assembled with saturated carborundum porous stones and filter papers on both sides of the sample and a gentle pressure on the top porous stone forced the sample into proper location for testing. During sampling, care was taken to ensure that the direction of consolidation for a shear test specimen was kept identical to the direction of consolidation for the large block from which the test specimen was obtained.

The shear box assemblies were then moved from the moisture room to the direct shear machines and the samples were subjected to the same effective normal stress under which the parent block was consolidated. Only after applying this initial normal pressure, each reservoir was filled up with a salt solution that was identical in composition and concentration to the pore fluid of the sample in the shear box. The samples were then subjected to the desired normal

loads in conventional steps using a load increment ratio of 1.0. During each load application on a specimen, the settlement readings from the vertical LVDT were recorded with time.

The shear tests on kaolinite were performed on normally consolidated specimens whereas the tests on attapulgite and montmorillonite were performed on overconsolidated specimens because of the observed tendency of a normally consolidated specimen of any one of these minerals to undergo considerable secondary consolidation during shear. A primary requirement for obtaining a stabilised residual shear strength is to attain minimum volume change condition during shear at large strains.

5.4.3 Shearing technique

If a sample was intended to be sheared along a precut plane after completion of consolidation under the desired normal load, the upper half of the shear box was raised slightly using the two screws provided. A thin piano wire was then slipped into the division between the two halves of the shear box and the wire was wrapped around the sample. The two ends of the wire were then brought out through two holes in the reservoir and a uniform pull was applied on the wire to make a failure plane in the sample. The process was repeated several times using a new piece of wire every time and the wire was always pulled in the same direction. The whole operation of precutting the plane was performed without removing the normal stress on the sample. The sample was then ready to be sheared. The zero reading of the load cell was recorded and the horizontal LVDT was set at proper initial

reading corresponding to the central position of the box. The gears chosen for the desired rate of displacement were then engaged and shearing was commenced. Shear load, horizontal and vertical displacements were recorded as voltage readings by the automatic digital voltmeter. Readings were taken at an interval of 1 minute for the first two cycles after which an interval of 10 minutes was used for the subsequent cycles.

A test was terminated when significant amount of soil was squeezed out of the box which had the apparent effect of increasing the strength. Approximately 3 to 4 inches of total horizontal displacement (representing about 10 reversal cycles) could normally be imposed on a sample before excessive extrusion occurred. Shearing of a cut-plane specimen to the residual state was usually completed in about 24 hours.

A shear test was usually stopped at the centre of the travel and the two halves of the shear box were clamped back together bringing the load cell reading back to zero. The reservoir of the shear box assembly was then drained and the normal load was released. The entire shear box assembly was then lifted out of the reservoir and the sample was carefully extruded from the box by applying a gentle pressure on the bottom porous stone. One half of the sample was used for determining the water content distribution in the sample while the other half was waxed and stored in a moisture room for subsequent microstructural examination.

For a peak strength test, the procedure followed was exactly

the same except no precut plane was made in the sample and the test was run at a speed that was at least ten times slower than the speed employed for a cut-plane test.

5.5 Constant Volume Leaching Tests

5.5.1 General

In order to establish the control of true effective stress (σ_n^*) on residual shear strength (τ_{res}), a special testing scheme was developed. This testing programme was described in Chapter IV and it involved comparing residual shear strengths of Na-montmorillonite samples before and after leaching of the pore fluid salts under constant overall volume conditions. A set of five low pressure $(\sigma_n' = 2.5, 5, 7.5, 10$ and 15 psi) Na-montmorillonite - 33.57 g/l NaCl samples were subjected to constant volume leaching as a part of this test programme and as stated earlier, the tests were confined to the low pressure range so that samples of reasonable permeability could be obtained for leaching.

5.5.2 Shear before leaching

The five overconsolidated saline specimens of Na-montmorillonite were first sheared along precut planes under the low normal pressures using a rate of displacement of 0.0019-0.0024 inches per minute and the residual shear strengths of the samples were determined. These samples were tested in a surrounding cell solution that was identical in composition and concentration to the pore fluid of the samples and the tests were not continued beyond 8-9 reversal cycles because extrusion of soil between the boxes was undesirable before leaching. After

terminating the tests at their centres of travel, the two halves of the shear boxes were clamped back together and the reservoirs were drained. The normal loads were then removed from the samples and the samples were ready to be leached under constant overall volume conditions.

5.5.3   Constant volume leaching of the sheared samples

a.   Leaching test equipment

Special leaching equipment was designed to satisfy the following requirements:

i.   To replace the saline pore fluids of the samples with distilled water by leaching under constant overall volume conditions, and,

ii.   To measure the changes in the apparent effective stresses required to counterbalance the net (R-A) stresses developed due to leaching under constant overall volume conditions.

It was imperative to conduct the leaching tests in the shear boxes because extrusion of the samples into a separate set of leaching cells would have invariably created gross leakage channels around the samples and no leaching of the pore spaces of the samples would have occurred.

Since it was intended to replace the salts from the pore spaces of the samples under constant overall volume conditions, downward leaching technique was not used because of the possibility of further consolidation of the samples due to downward seepage pressures. Hence the samples were leached upward with the idea that upward seepage pressures would tend to reduce the initial effective stresses and thus

induce a tendency of swelling in the samples which would not be very difficult to prevent.

A sectional view of a leaching cell is presented in Fig. 5.11 while Figs. 5.12 and 5.13 illustrate the fully assembled leaching equipment and the close-up of a leaching cell respectively. A leaching test assembly consisted of five essential components: (a) a perspex reservoir, (b) a perspex base plate with valve connections, (c) a leaching cell which was the direct shear box itself, (d) a perspex top cap with a perspex loading piston and (e) a mild steel loading frame with a stiff 500 lb. aluminium load cell. The mechanical details and the dimensions of the first four components are shown in Fig. 5.11.

The perspex reservoir was used as a storage for the leachate and the elevation of the reservoir could be adjusted to produce a desired pressure at the base of the sample for upward leaching. The reservoir was equipped with a 10 c.c. (5/16" I.D.) glass burette for measurement of the quantities of inflow into the sample during leaching.

A 5/16" hole was drilled diametrically through the perspex base (6" diameter x 1½" thick) of the cell and each end of the hole was fitted with a toggle valve. The reservoir was connected to the inlet toggle valve by 1/8" O.D. Eastman tubing and by opening the inlet valve, the trough in the base plate could be filled up with leachate from the reservoir and upward leaching of the sample could be initiated. The outlet toggle valve was basically intended for flushing of the base. Four holes were drilled into the perspex base to accommodate

four 3/16" NC screws that were used for clamping the shear box to the base plate. Once the two were clamped together, a 1/8" diameter O-ring fitted in a square groove in the base plate prevented any possible leakage between the bottom of the shear box and the top of the base plate. The underside of the base plate was provided with a protruding part (4" diameter x 1/4" thick) that fitted into a corresponding groove in the steel base plate of the loading frame so that the entire leaching cell assembly could be located centrally in the loading frame and no lateral movement of the cell would be possible once it is in the loading frame.

As mentioned before, the shear box itself was used as the leaching cell. Consequently, the cadmium coated brass plate that is used below the bottom porous stone in a shear box test was perforated to allow the leachate from the trough to enter freely into the bottom porous stones. Furthermore, for the leaching tests, two carborundum porous stones instead of one were used below each sample so that the shear plane would be closer to the bottom of the sample. This was done in order to ensure that complete leaching of the shear zone would at least be achieved within a reasonable period of time. Only one porous stone was used above the sample and filter papers were used between the stones and the sample. Quick setting General Electric silicone construction sealant was used for plugging the gap between the two halves of the shear box so that no leakage would occur between the halves during leaching and this particular sealant was found to be excellent for the purpose.

The top cap was specially designed to allow only a small
quantity of fluid (70-80 c.c.) to be present above the sample at all
times. This was done with the specific intention of increasing the
accuracy with which the salt content of the effluent could be
measured. The top cap was fitted with a 10 c.c.(5/16" I.D.) glass
burette for measurement of the quantities of outflow from the sample
during leaching. The outflow burette also served the purpose of an inlet
for filling up the space between the underside of the top cap and the top
of the sample with the desired solution. The provision of an inflow
and an outflow burette was intended not only to provide a continuous
check on the maintenance of constant overall volume condition for the
sample during the entire leaching process but also to allow the leaching
test set-up to be simultaneously used as a constant head permeameter
for measurement of the changes in the coefficient of permeability of
the sample during leaching. Four holes were drilled into the top cap
to accommodate four wing nuts that were used to clamp the top cap to the
top of the shear box with a greased rubber gasket in between for
prevention of leakage between the two. The loading piston consisted
of a 3/4" diameter solid perspex cylinder connected to a perforated
square loading platform (2.32" x 2.32"). A central hole in the top cap
accommodated the circular stem. of the loading piston while the perspex
loading platform sat directly on the top porous stone. A rolling o-ring
seal was used in this central hole in order to prevent any leakage
between the top cap and the stem of the piston. A very small clearance
(≈ 0.01") was kept on all sides between the square loading platform
and the inside walls of the shear box.

The loading frame consisted of an aluminium crossbar that could be slided up and down two threaded mild steel rods that were clamped to a steel base plate (Fig. 5.12). The aluminium crossbar could be rigidly fixed at any level along the threaded rods by tightening a pair of nuts (one above and one below the bar) at each end of the crossbar. With the assembled leaching cell in the loading frame, a stiff 500 lb. load cell could be mounted between the top of the loading piston and the underside of the aluminium crossbar using a 1/2" diameter stainless steel ball bearing at each end of the load cell for proper seating. The top ball bearing was housed in a vertical alignment hole that was centrally located in the crossbar while the bottom ball bearing was made to sit in a groove on the top of the loading piston. Stiff 500 lb. load cells were used as load measuring devices in the leaching equipment. Several researchers (Palit 1953; Alpan, 1957) have designed swelling pressure cells where proving rings were used for load measurements. But to measure a load by a proving ring requires some deformation of the proving ring and a corresponding swelling of the soil sample. Since it was intended in this investigation to conduct leaching under constant overall volume conditions, stiff load cells that require negligible deformations to measure loads were used as load measuring devices. A special feature of the loading frame was a carefully centred circular groove (4" diameter x 1/4" deep) in the steel base plate which corresponded to the protruding part on the underside of the perspex base of the leaching cell assembly and once this protruding part of the perspex base was introduced into the groove in the base plate, the vertical centre lines of the piston, the load cell and the aluminium

crossbar were automatically aligned along one vertical line. While setting up the leaching cell assembly in the loading frame, it was imperative to align these three components along one vertical centre line to prevent any bending of the load cell due to eccentricity during subsequent load applications. Hence, with the assembled leaching cell in position in the loading frame and the load cell mounted between the piston and the crossbar, a load could then be applied by simultaneous tightening of the two nuts above the crossbar (keeping the pair below the bar released) by equal amounts which would press the crossbar down on the load cell and the load cell, in turn, would transfer the load to the sample through the loading piston. A spirit level was used to ensure that the crossbar was always kept absolutely horizontal during loading of the sample. Once a desired load was applied to the sample (which was indicated by the load cell reading), the crossbar could be fixed in place and the stiff load cell was then rigidly fixed between the piston and the crossbar. As the sample would tend to swell during subsequent upward leaching with distilled water, the stiff load cell rigidly fixed between the crossbar and the piston would prevent this swelling and measure the resulting load.

Components were built for five leaching tests. However, one of the cells was built for a pilot test and was not equipped with an inflow and an outflow burette. Consequently, no flow or permeability data could be obtained from the test that was conducted in this particular cell.

Since the duration of a leaching test on montmorillonite could be fairly long, the creep of the porous stones, the filter papers

and the perspex loading piston in a cell could be an important factor. In this investigation, however, instead of calibrating the creep of the stones and the pistons, they were all submerged in water and kept loaded under a normal pressure of 80 psi ($\simeq$ anticipated maximum swelling pressure) for at least 15 days before they were used in the tests.

b. Leaching test procedure

After termination of the first time shearing of the five Na-montmorillonite samples in the saline (33.57 g/l NaCl) environment, the shear boxes were removed from the direct shear machines and the boxes were clamped to the perspex bases. The top caps were then introduced into the boxes and the loading pistons were gently seated on the top porous stones. The top caps were subsequently clamped to the shear boxes and the assembled cells were housed in the respective loading frames which sat on a rigid steel I-beam (Fig. 5.12). The 500 lbs. load cells were then mounted between the pistons and the crossbars making absolutely sure that the vertical centre lines of the loading pistons, the load cells and the crossbars in the loading frames were perfectly aligned. The setting up operation was completed in a very short time to prevent any loss of moisture from the samples.

After setting the assembled cells into the respective loading frames, loads corresponding to the initial apparent effective stresses (σ_n' = 2.5, 5, 7.5, 10 and 15 psi) were applied on the samples by pressing the crossbars down on the load cells and after applying the desired loads on the samples, the crossbars were fixed in position.

The gaps between the two halves of the shear boxes were then plugged with the silicone construction sealant. Only after applying the appropriate initial normal loads on the samples, the troughs below the samples and the spaces above the samples were filled up with deaired 33.57 g/1 NaCl solution. Although the flow of solution into a trough was mainly due to the difference in elevation between the reservoir and the base of the cell, complete deairing of the trough during the initial filling (and the subsequent filling of the trough after each flushing of the base) was accomplished by applying a small vacuum at the base through the outlet toggle valve and immediately closing it which was followed by opening of the inlet toggle valve. A hypodermic syringe was used for applying the small vacuum. Care was taken to expel all air bubbles from the spaces above the samples and the quantity of solution required to fill up the space above each sample upto the 1 c.c. mark in the outflow burette was accurately measured. Evaporation was completely eliminated from each system by maintaining a small head of special grade motor oil above the standing solution levels in the inflow and the outflow burette. Hence, with 33.57 g/1 NaCl solution (which is the initial pore fluid of the samples) above and below the samples, the specimens were allowed to reach equilibrium under the reapplied initial effective stresses. Both the inlet and the outlet toggle valves were kept closed during this period.

The samples were then circulated with 33.57 g/1 NaCl solution under heads of 3½' to 9½' (depending on the initial effective stress of the sample) applied at the bases by opening the inlet toggle valves which connected the reservoirs to the troughs below the samples. The

applied heads were so chosen that they also imposed relatively high hydraulic gradients across the samples so that considerable amounts of flow would occur through the samples within a reasonable span of time. Due to these heads applied at the bases, seepage pressures should develop at the top of the samples. These seepage pressures must be subtracted from the constantly changing apparent effective stresses that would be recorded during leaching with distilled water in order to obtain the true changes in σ_n' (or the net (R-A) stresses) due to leaching under constant overall volume conditions. Since it will be impossible to distinguish between the seepage pressures and the net (R-A) stresses developing simultaneously at the top of the samples during leaching with distilled water, it was necessary to determine the seepage pressures independently. Hence, before commencing leaching with distilled water, the seepage pressures (which are independent of salinity) at the top of the samples were independently measured by circulating 33.57 g/l NaCl solution (the initial pore fluid of the samples) through the samples under the same heads ($3\frac{1}{2}'$ - $9\frac{1}{2}'$) that were used for subsequent leaching with distilled water.

As 33.57 g/l NaCl solution was circulated through the samples under the applied heads, seepage pressures developed at the top of the specimens. The rigid load measuring devices fixed against the crossbars prevented any swelling of the samples that could have been caused by the upward seepage and continually increasing loads were registered by the load cells as steady state upward seepage conditions were being established in the samples. These load cell readings representing the sums of the initial apparent effective stresses and the seepage pressures

were recorded with time on the Hewlett-Packard digital recorder.
For four tests, the quantities of inflow and outflow of salt solution
along with the resistivities of the effluents were recorded every
24 hours. The levels of solution in the inflow and the outflow
burettes were also adjusted every 24 hours in order to maintain the head
differences across the samples constant. The circulation of salt
solution through the samples was carried out for about 15 days until
steady state seepage pressure readings were obtained at the top
of the samples.

After measuring the seepage pressures at the top of the
samples, the salt solutions from both sides of the samples were replaced
with deaired distilled water and upward leaching of the samples with
distilled water was commenced. The replacement of the saline (33.57 g/l
NaCl) pore fluids from the samples under constant overall volume
conditions was accomplished not only by an upward flow of distilled
water through the samples but also by diffusion from both ends of the
samples which were now in contact with distilled water. During leaching
with distilled water, the inflow and outflow readings were recorded every
24 hours from the corresponding burettes. The resistivites of the
effluents were also measured at the same time on samples collected by
a hypodermic syringe from the outflow burettes. The distilled water
above and below each sample was flushed out and replaced with a fresh
supply every day. While refilling the troughs below the samples after
each flushing, the same procedure of applying a small vacuum at the
base was used. The levels of water in the inflow and the outflow

burettes were also adjusted every 24 hours in order to maintain constant head differences across the samples for leaching.

As leaching proceeded under constant volume conditions, the load cells registered monotonically increasing load readings with time. The leaching was stopped after stabilised values of the net (R-A) stresses were attained for all the samples. The leaching tests were run for about 120,000-130,000 minutes with the exception of one which was run for about 240,000 minutes.

5.5.4 Reshear after leaching and associated system chemistry analysis

After obtaining the stabilised net (R-A) stresses for the Na-montmorillonite samples which corresponded to the completion of leaching of the samples, all fluids were drained out from both sides of the samples. The leaching test assemblies were quickly dismantled and after removing the silicone sealant from the divisions between the two halves of the shear boxes, the boxes were immediately set into the direct shear machines. Each sample was then subjected to a normal pressure that was equal in magnitude to the final apparent effective stress (σ_n') of the sample at the end of leaching and the reservoirs were filled with distilled water. The volume changes of the leached samples under the new σ_n' values were recorded with time for a week at the end of which the samples were resheared under drained conditions along the existing shear planes in the conventional manner and the residual shear strengths of the leached samples under the new σ_n' values were determined. The same rates of displacement that were used to shear the specimens before leaching were also used for reshearing the specimens after leaching.

Furthermore for these shear tests, if the cycle in which shearing was terminated for a specimen before leaching happened to be a compression cycle, the reshearing of the same specimen after leaching was started also on a compression cycle.

The shearing of these leached Na-montmorillonite samples was continued until excessive extrusion occurred between the boxes. After termination of these shear tests, the samples were extruded from the shear boxes. The water content distribution in each sample was determined from a part of the sample while the rest of the sample was used for pore fluid analysis. A mechanical pore fluid squeezer, the details of which are described elsewhere (Balasubramonian, 1972), was used for extracting the pore fluids from these leached samples. A pressure of about 500 psi was found to be adequate for extraction of about 5 c.c. of pore fluid from each sample in approximately 4 days. These pore fluid samples were then analysed for the concentrations of Na^+, Ca^{++}, Mg^{++} and K^+ using the atomic absorption spectrophotometry technique. The pore fluid ion concentrations, thus determined, demonstrated the extent of leaching that was achieved in the Na-montmorillonite samples and the effectiveness of the flow-diffusion technique that was employed for leaching. These final pore fluid ion concentrations were also used for estimating the net (R-A) stresses of the leached samples from the double-layer repulsive stress equation (Eqn. 3.29).

5.6 Technique Used for Microstructural Study

A number of specimens of each clay mineral sheared along precut planes under various normal pressures to the residual state were

subjected to microstructural examination using the technique of scanning electron microscopy. After termination of shearing, a part of each reversal test specimen that contained the large displacement shear zone and the undeformed area outside the shear zone was waxed and stored in a moisture room with controlled humidity for subsequent preparation of sections for electron microscopy.

It is not possible to analyse the fabric of wet samples by electron optical methods. The water from the samples, therefore, had to be replaced or removed. Three techniques are available for this purpose and they are: (a) air-drying, (b) critical point drying and (c) freeze-drying technique. Gillott (1969, 1970) has described the various methods of drying in detail and has discussed the relative advantages and disadvantages of the various techniques. The air-drying technique obviously produces considerable volume decrease in a sample and fabric is significantly affected by the shrinkage. It is possible to reduce shrinkage caused by surface tension forces and moisture migration by using either critical point drying or freeze-drying technique. In this investigation, the freeze-drying technique was employed to prepare samples for the scanning electron microscope. The technique involved freezing a waxed specimen by immersion in a vessel containing isopentane surrounded by liquid nitrogen at a temperature of about -190°C in an outer container. The wax coating was then removed and the sample was dipped again in isopentane surrounded by liquid N_2 to ensure complete freezing of the sample. The ice was then removed from the sample by sublimation under vacuum in an Edward Pearse tissue drier (model EPD 2).

In the drier, the sample was placed on a plate which was cooled down to a temperature of -80°C so that the sample was not warmed up immediately after freezing. As sublimation proceeded, the temperature of the plate was slowly raised to room temperature. A tray filled with phosphorus pentoxide (P_2O_5) was placed in the drier for absorption of the moisture generated during sublimation so as to keep the vacuum chamber dry. Montmorillonite samples required about 5-6 days for complete drying by the vacuum sublimation process whereas approximately 2-3 days were sufficient for drying of the kaolinite and the attapulgite samples. It was attempted to keep the sample sizes as small as possible so that complete drying of the samples could be achieved in a relatively short time.

After drying, the samples were extremely fragile and had to be handled with utmost care. If a number of samples were prepared in a short time, they were stored in a dessicator after drying and sections were prepared from one specimen at a time. Three types of sections were prepared from each specimen and they are: (a) longitudinal section, (b) transverse section, and (c) a section of the shear plane itself. Fig. 5.14 illustrates the planes of the sections obtained from each reversal test specimen. Since an electron microscope gives information about a surface, it is vitally important that the surface examined in a section be representative of the bulk material. A surface may be exposed by fracture or cutting. In metallurgy, it is a standard procedure to expose surfaces of polycrystalline materials by fracture. Cutting is a shearing action which induces damage, the depth and extent of which depend upon the method of cutting and the nature of material (Kay, 1965).

It has been shown to orient wet clay (Martin, 1966) and hence the arrangement of the particles on a cut surface is unlikely to represent the true fabric of the bulk material. In this study, fresh surfaces which included the shear zones and the undeformed areas outside the shear zones were obtained in the longitudinal and the transverse sections by fracturing and these fractured surfaces were viewed under the scanning electron microscope. For sections of the shear planes themselves, no fracturing was necessary. Instead, the two halves of a sheared specimen were separated and sections of the shear plane were directly viewed under the microscope. The surfaces exposed by fracturing were then cleaned by a spray of freon and the samples were mounted on ½" diameter aluminium stubs using silver iodide paint as the bonding agent. The top surface of each mounted sample was the fractured surface intended for viewing. An average mounted specimen was 0.4" in diameter and 0.1" thick. Usually in each specimen, one more surface perpendicular to the top surface was exposed by fracturing so as to allow microstructural observations to be made on more than one plane per section. The non-conducting specimens mounted on the stubs were next coated with gold-palladium or gold in an Edwards vacuum coating unit (model E 12 E). The gold coating prevents the build up of an electric charge inside the microscope which may cause a serious loss in resolution. The sections were then ready to be viewed under a scanning electron microscope.

A Cambridge stereoscan S4 scanning electron microscope was used in this investigation. The working principles and the details

of this microscope have been described elsewhere (Gillott, 1969).

The Cambridge stereoscan S4 has a magnification range of 14 to 200,000

times and it has also demonstrated a resolution of less than 100 Å

at 100,000 x magnifications. The depth of focus in the stereoscan

S4 model is approximately ½ to 1 micron (5,000-10,000 Å). During

examination, the specimen can be tilted, rotated and moved in the X,

Y and Z directions. Larger specimens can be examined with loss of

movement in some directions.

The structures of the large displacement shear zone and the

undeformed area outside the shear zone in each section were studied under

the stereoscan S4. The specimens were scanned and viewed on a display

screen and pertinent structural features were photographed on

120-plus X roll films. The photomicrographs of the pertinent structural

features are presented and interpreted in the next chapter.

TABLE 5.1

PHYSICAL PROPERTIES OF THE CLAY MINERALS

Clay Mineral	Clay Mineral Composition (%)				Passive Mineral Composition (%)		Grain size		Hygroscopic moisture (%)	Specific gravity of the soil solids (G_s)	Salinity, gms/litre of NaCl	Index Properties			
	Kaolinite	Attapulgite	Montmorillonite	Illite	Quartz	Feldspar	Range	Clay sizes (%)				Liquid Limit (%)	Plastic Limit (%)	Plasticity Index (%)	Activity
E.P. Kaolinite from Alberta Ceramics	97			3			100% less than 6 m.	83	1.23	2.64	0	72	44	28	0.24
											5	68	42	26	0.31
											10	66	40	26	0.31
											15	66	40	26	0.31
											20	67	39	28	0.34
											25	67	39	28	0.34
											30	66	37	29	0.35
											35	66	39	27	0.33
Attapulgite from Dresser Magcobar (Canada) Limited		75-95% depending upon the percentage of quartz			widely varying between 5% and 25%		100% less than 4 m.	75	8.0	2.40	0	311	132	179	2.39
											5	295	133	162	2.16
											10	292	129	153	2.04
											15	282	122	153	2.04
											20	272	122	150	2.03
											25	267	115	148	1.97
											30	252	121	131	1.74
											35	251	116	135	1.81
Commercial bentonite from Dresser Magcobar (Canada) Limited			80	20			100% less than 0.5 m.	90	3.88	2.75	0	591	87	504	5.6
											5	417	75	342	3.8
											10	343	68	275	4.0
											15	279	64	215	3.4
											20	256	59	197	2.2
											25	252	59	193	2.1
											30	189	57	132	1.5
											35	153	55	98	1.1

TABLE 5.2

CHEMICAL PROPERTIES OF THE CLAY MINERALS

Clay Mineral	Organic content (%)	Total specific surface of the calcium variety (m²/gm)	Carbonate Content				Total cation impurities* in the unmodified clay mineral (me/100 gms. of dry soil)					Cation exchange capacity of the -2μ fraction (me/100 gms. of dry soil)	Remarks
			Calcite CaCO₃ (%)	Dolomite CaMg(CO₃)₂ (%)	Calcite Dolomite	Total Carbonate (%)	Na⁺	Ca⁺⁺	Mg⁺⁺	K⁺	H⁺		
Kaolinite	1.68	11.2	0	0	-	0	0.04	6.00	2.31	0.09	1.08	7.22	Further treatment not necessary
Attapulgite	1.4	256.3	5.60	4.74	1.18	10.34	0.24	32.30 (Probably from the carbonates)	56.09	0.74	-	23.22	Definitely needs Na-hcationization
Montmorillonite	2.4	641.0	1.74	0.20	8.7	1.94	34.26	37.27	5.38	0.70	0.50	67.92	Definitely needs Na-h-cationization

*Total cation impurities include the free and the adsorbed cations in the clay minerals in their as procured state.
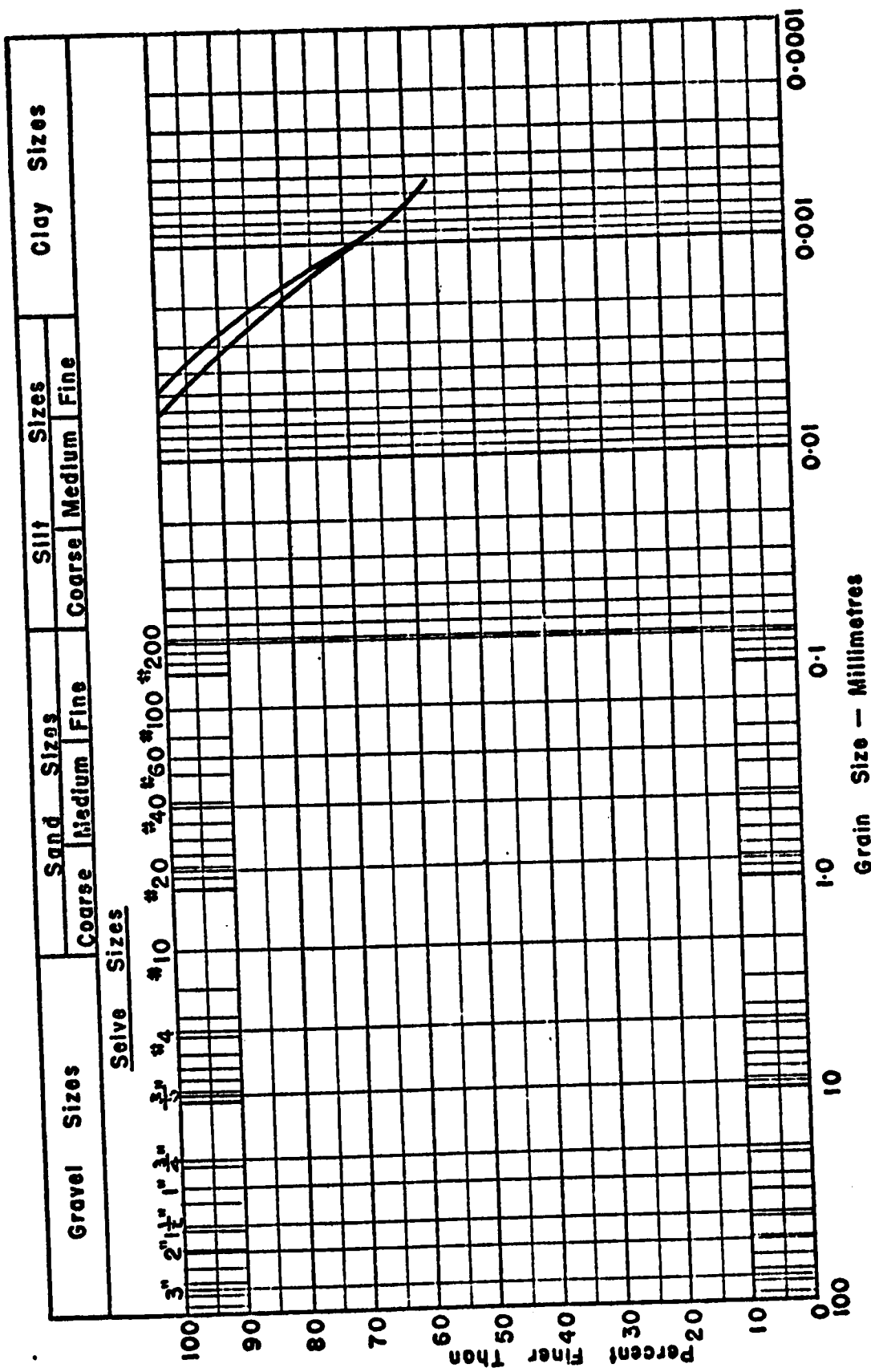
FIG. 5.1   GRAIN SIZE DISTRIBUTION FOR KAOLINITE
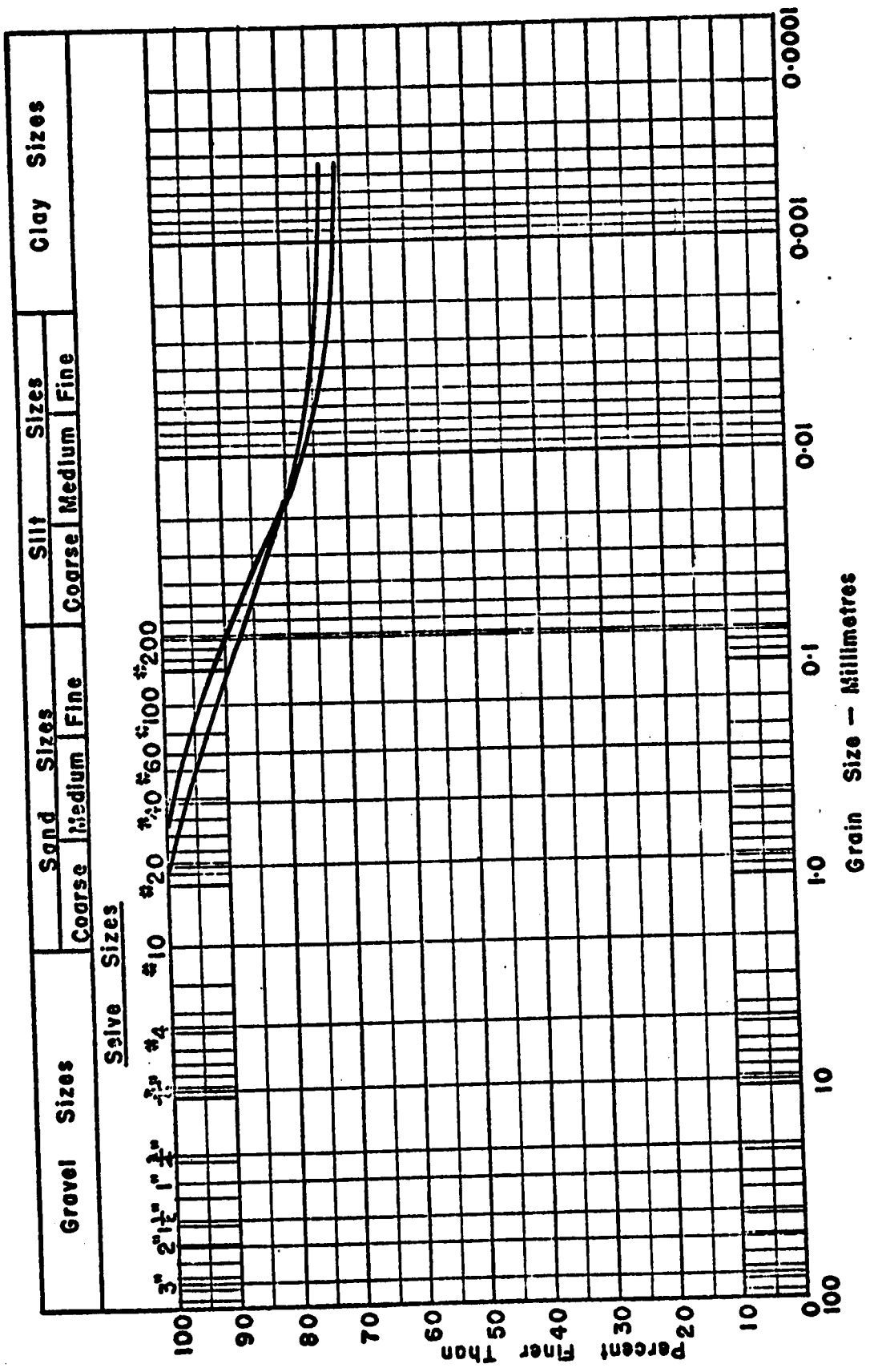
FIG. 5.2 GRAIN SIZE DISTRIBUTION FOR ATTAPULGITE
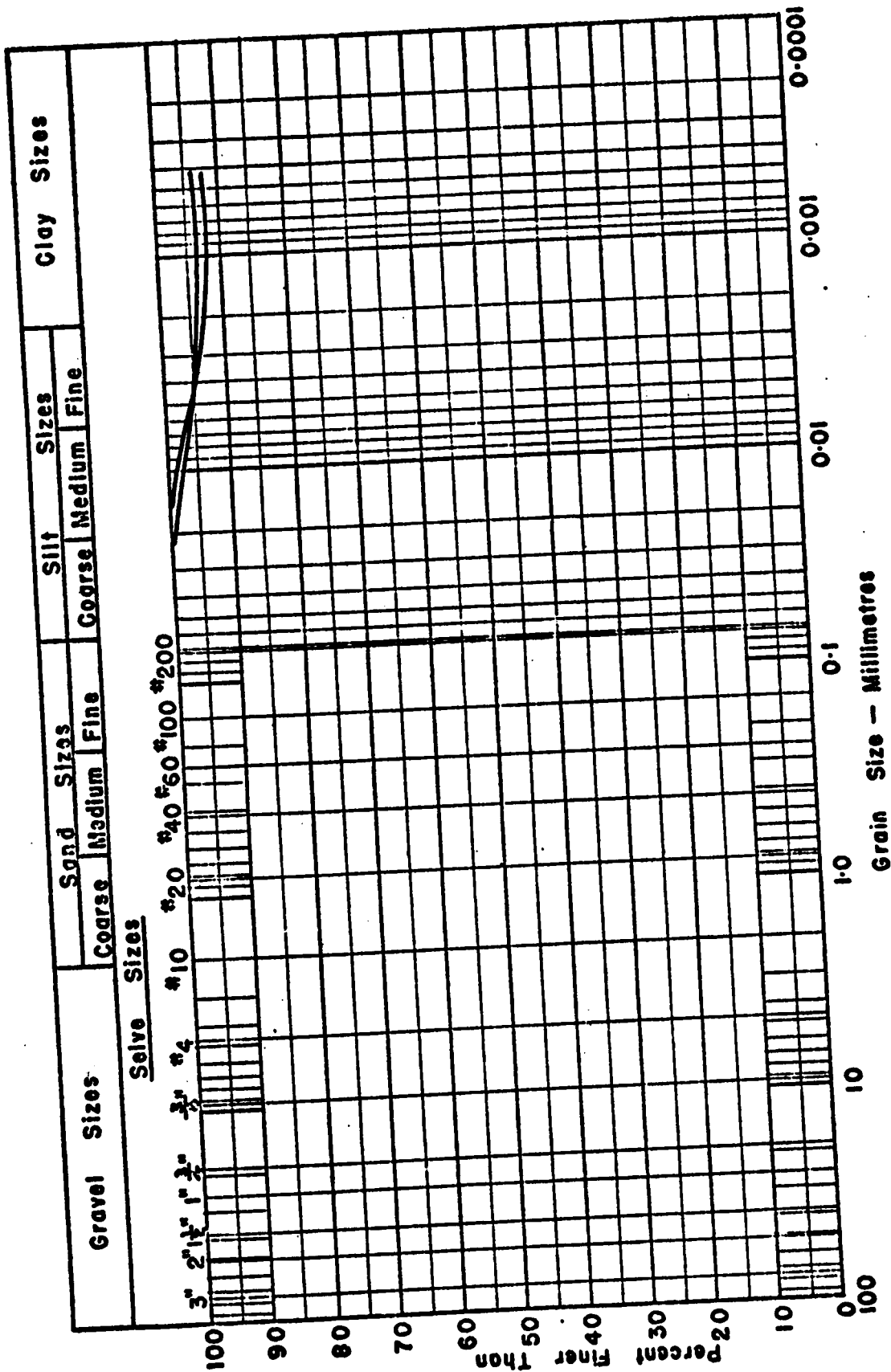
FIG. 5.3 GRAIN SIZE DISTRIBUTION FOR BENTONITE
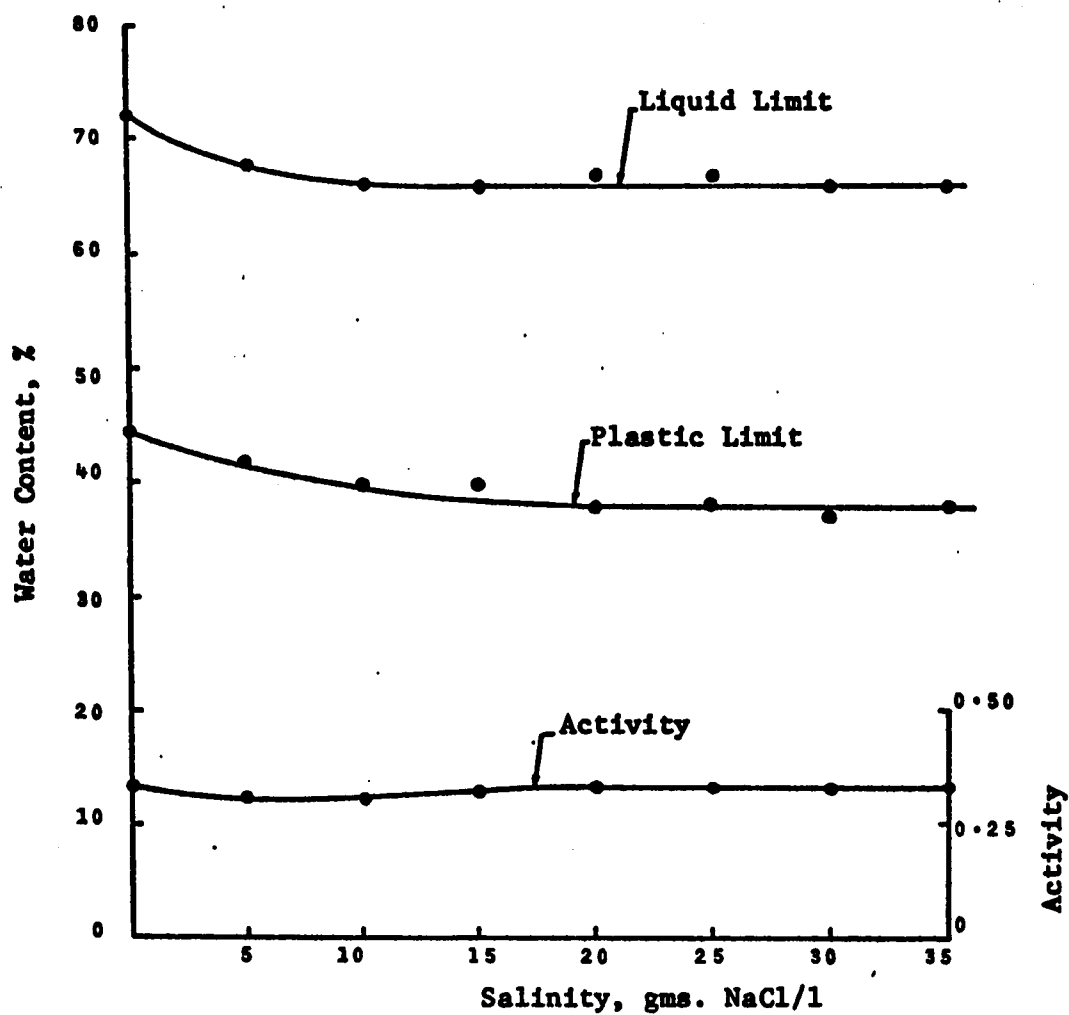
FIG. 5.4 VARIATION OF INDEX PROPERTIES WITH SALINITY
FOR KAOLINITE
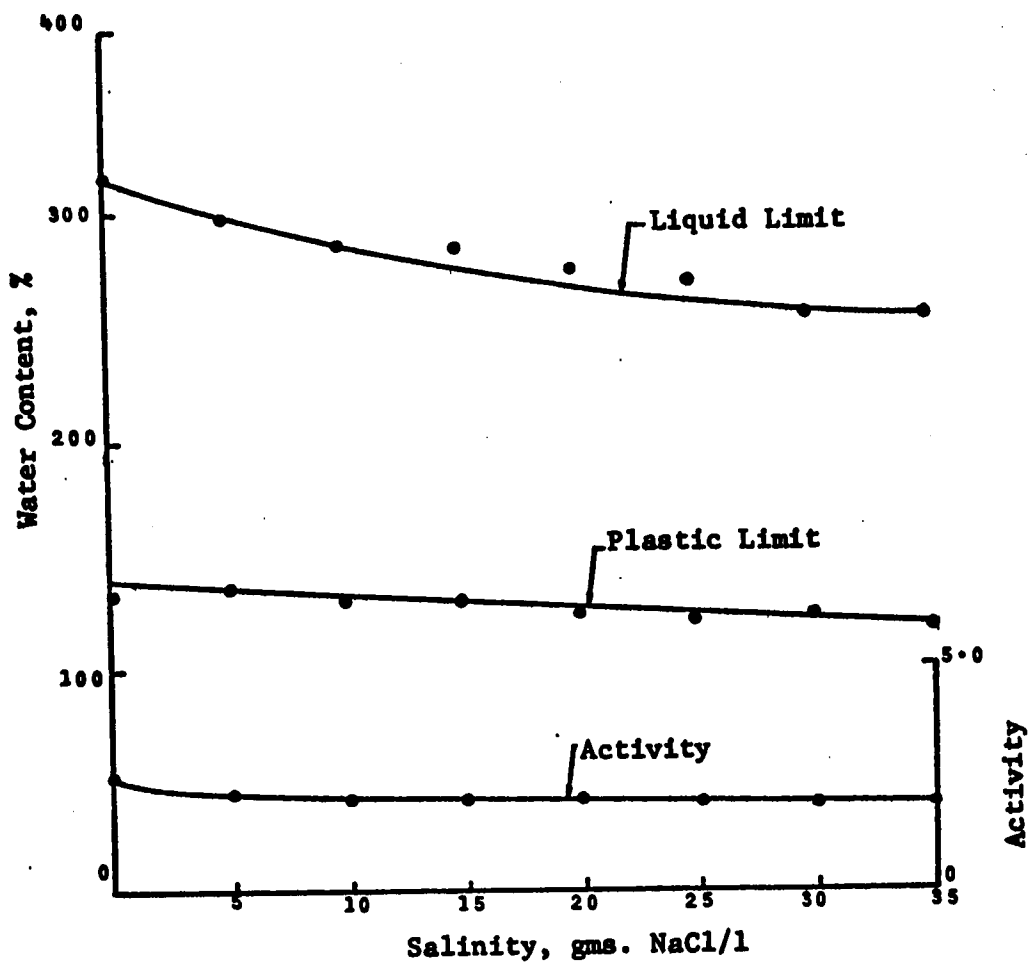
FIG. 5.5 VARIATION OF INDEX PROPERTIES WITH SALINITY
FOR ATTAPULGITE
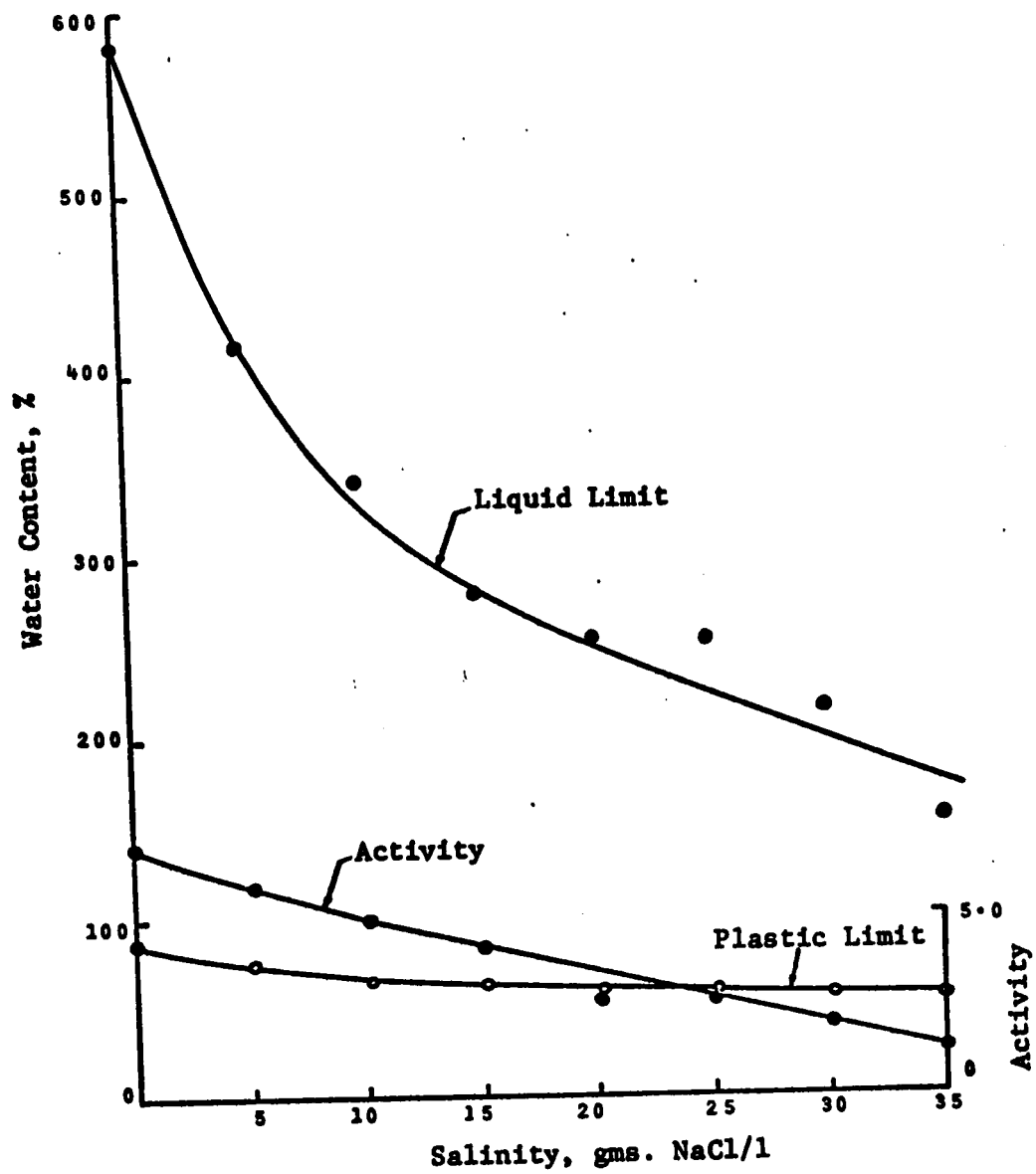
FIG. 5.6. VARIATION OF INDEX PROPERTIES WITH
SALINITY FOR BENTONITE

Fig. 5.7 POLYETHYLENE BATHS USED FOR Na-HOMOIONIZATION OF
THE CLAY MINERALS AND SET-UP FOR DRYING OF
THE SLURRIES

Fig. 5.8 CONSOLIDATION TEST SET-UPS FOR
PREPARATION OF LARGE BLOCK SAMPLES
FROM THE SLURRIES
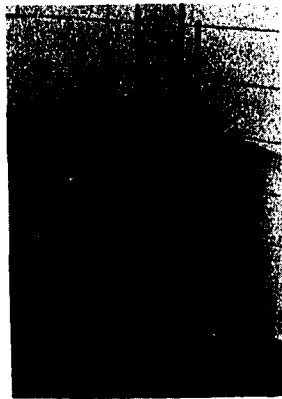
Fig. 5.9 A MODIFIED DIRECT SHEAR APPARATUS

Fig. 5.10 PLAN VIEW OF A DIRECT SHEAR APPARATUS SHOWING THE
INSTRUMENTATION
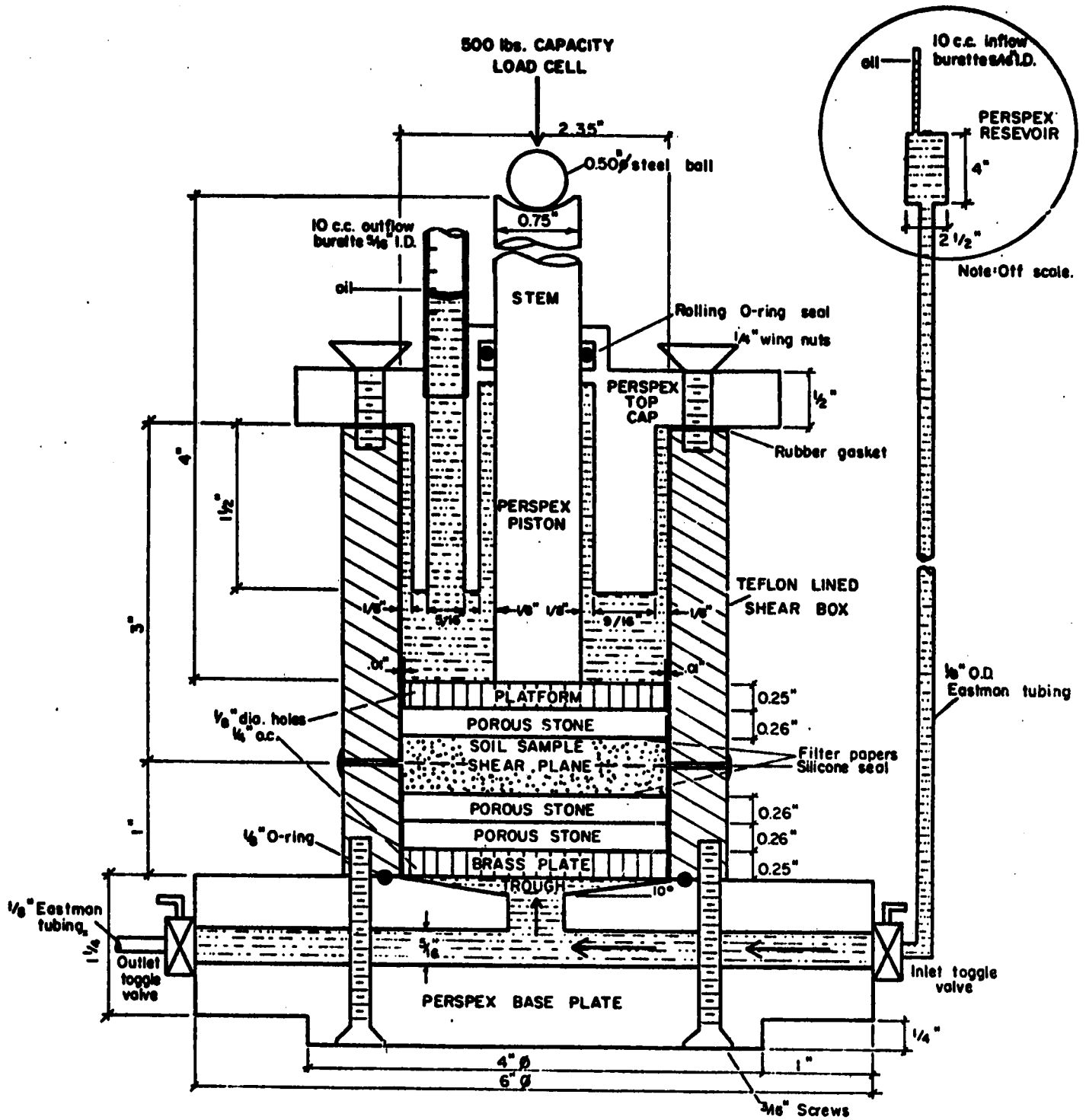
FIG.5.II CROSS-SECTIONAL VIEW OF A LEACHING CELL
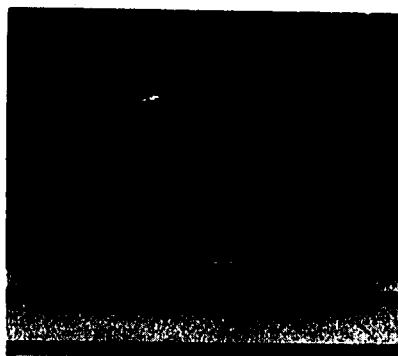
Fig. 5.12 The constant volume leaching test equipment

Fig. 5.13 Close-up of a leaching cell
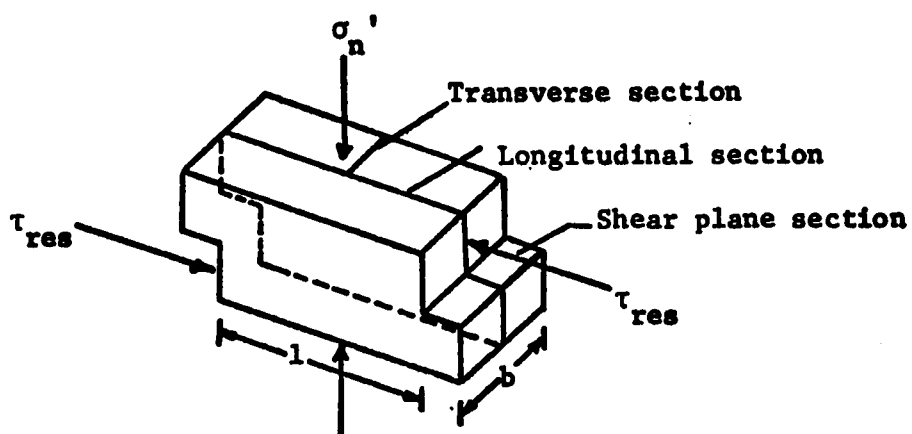
FIG. 5.14 PLANES OF SECTION FOR SCANNING ELECTRON
MICROSCOPE STUDY

CHAPTER VI

PRESENTATION AND INTERPRETATION OF TEST RESULTS

6.1 Analysis of the System Chemistries of the Mineral Block Samples

The distributions of various cations in the pore fluids and the adsorbed cation complexes of the block samples of attapulgite and montmorillonite are presented in Table 6.1. The results of the pore fluid analyses (Table 6.1) confirm that the final pore fluid NaCl concentrations of the mineral block samples were as desired. The final distributions of cations in the adsorbed states on the attapulgite and montmorillonite particles, presented in Table 6.1, clearly indicate that the minerals were about 90% homoionic in sodium which confirms that the simple and inexpensive treatment procedure adopted here was indeed effective in homoionizing rather large quantities (9 to 10 lbs.) of clay minerals in sodium in a relatively short period of time.

6.2 Consolidation Characteristics of the Clay Minerals

The consolidation characteristics of the clay minerals (kaolinite, attapulgite and montmorillonite) were obtained from the large cell consolidation tests that were conducted during preparation of block samples of the clay minerals for subsequent shear tests and also from the consolidation phase in the direct shear boxes while the desired normal pressures were applied to the samples in steps. The consolidation test data were analyzed in the conventional manner using the square

178

root fitting method (Taylor, 1948). The consolidation characteristics of kaolinite, attapulgite and montmorillonite are summarized in Table 6.2.

Among the clay minerals, montmorillonite demonstrated the lowest coefficient of consolidation (c_v) and c_v increased in the order: montmorillonite, attapulgite and kaolinite. The reverse order, however, was found to be true for increasing values of the compression index (C_c) for the clay minerals. Typical settlement versus $\sqrt{time}$ plots for the minerals are presented in Figs. B-1 to B-6 of Appendix B and from Figs. B-5 and B-6, it can be seen that the attapulgite and the montmorillonite specimens exhibited significant secondary compression. The average values for the rate of secondary compression (C_α) of the attapulgite and the montmorillonite samples were about 0.029 and 0.052 respectively (Table 6.2) which are quite comparable to the C_α value of 0.03 reported for highly plastic organic soils by Ladd (1967). Kaolinite, on the other hand, exhibited negligible secondary effects (see Fig. B-3).

An attempt was also made to study the effect of the pore fluid NaCl content on the consolidation behaviour of each clay mineral by comparing the consolidation characteristics of the three batches of each mineral that were remoulded at the same initial water contents but under different pore fluid NaCl concentrations. The comparisons were made for the same consolidation pressures. Such a comparison, presented in Table 6.2, indicates that the pore fluid NaCl content had virtually no effect on the consolidation characteristics of kaolinite and Na-attapulgite whereas the consolidation characteristics of Na-montmorillonite

were significantly influenced by changes in the pore fluid NaCl concentration. In the case of Na-montmorillonite, as the pore fluid NaCl concentration was increased from 1.15 to 33.57 g/l, the compression index (C_c) was found to decrease from 5.85 to 2.7 whereas the coefficient of consolidation (c_v) was found to increase from 0.38 ft.^{2}/year to 3.20 ft.^{2}/year. The data is consistent with the well known effect of varying initial structure (caused by varying depositional environment) on the consolidation characteristics of an active clay-water system. The changes in the consolidation characteristics of Na-montmorillonite due to corresponding changes in the pore fluid NaCl content also seem to be consistent with the observed changes in the liquid and plastic limits of Na-montmorillonite with corresponding changes in the pore fluid salinity (Fig. 5.6).

6.3   Reversal Shear Test Results

6.3.1   General

Approximately 6 to 10 drained direct shear tests were conducted on each clay mineral at each pore fluid NaCl content. The shear tests in each series (except in the case of attapulgite) were carried out under normal pressures ranging from about 2.5 to 80 psi. A numbering system has been adopted here for referencing the shear tests. For example, the first shear test in the series on kaolinite samples with pore fluid NaCl content of 35 gms./litre is numbered K-35-1 in which the abbreviation K stands for the mineral kaolinite and the numbers 35 and 1 stand for the pore fluid NaCl content in gms./litre and the number of the particular test in the series respectively.

No difficulties were encountered in preparing the direct shear test specimens from the consolidated blocks and the technique of sample preparation outlined in Chapter V appeared to be quite satisfactory. The accuracies of the measuring systems used in the direct shear machines are presented in section A.1 of Appendix A which shows that the 500 lb. load cells that were used as load measuring devices in the direct shear machines and the leaching cells were capable of measuring a load as low as 0.3 to 0.4 lbs. The LVDTs, on the other hand, had the accuracy of measuring a deformation as small as 0.00002 inches.

In a direct shear test, the stress-displacement curve shows a maximum shear strength in the first cycle which is followed by a tendency for the shear stress to drop a little at each later reversal until the residual state is reached. However, it is not necessarily sufficient to test a sample until a sensibly constant load value is obtained over a small displacement, but it is generally advisable to test until several consecutive reversals show the same shear stress with negligible volume changes. The practice in this study has been to continue a test until the shear stresses recorded in several consecutive compression and tension cycles are practically the same. The variation between the tension and the compression cycle shear forces at residual state was usually in the order of ± 5% and the lower value has usually been accepted.

6.3.2   Reduction and presentation of the shear test data

The data necessary to compute the shear shresses, the horizontal and the vertical displacements for a shear test consisted

of readings from a load cell and two LVDTS. The load cell readings were corrected for zero drift by subtracting its "no load" reading from its loaded readings. These differences were mutliplied by the appropriate calibration constant (Table A.1a of Appendix A) to obtain the forces measured by a load cell during a shear test. The shear forces obtained in this manner were then divided by the uncorrected area of the shear box to determine the shear stresses. It was not necessary to correct the measured shear forces for machine friction because of certain modifications of the bushings at one particular end of the load cells (described in Chapter V) which made the machines virtually frictionless. To obtain the horizontal and the vertical displacements of a sample during shear, the appropriate initial LVDT readings were subtracted from the subsequent LVDT readings and the differences were mutliplied by the corresponding calibration factors (Table A.1a of Appendix A). The shear stress and the vertical displacements are plotted against the cumulative horizontal displacements on an arithmetic scale for the shear tests on kaolinite whereas a technique of plotting the shear stresses and the vertical displacements against the corresponding cumulative horizontal displacements on a semi-logarithmic scale is used for the shear tests on attapulgite and montmorillonite. The latter technique, suggested by La Gatta (1970) accentuates the slope of the stress displacement curve at large horizontal deformations relative to the slope at small horizontal deformations allowing the stabilised horizontal portion of the stress displacement curve at large strain which represents the residual state to be defined with less ambiguity.

No area corrections were applied while calculating the residual shear stresses (τ_{res}) from the shear test data. Since the effect of reduction in area during a direct shear test equally affects the magnitudes of the normal effective stress σ_n' and the shear stress τ, the ratio τ/σ_n' remains unaffected (Kenney, 1967). Moreover, the τ_{res} values chosen from the shear tests for determining the residual friction angles were calculated from the shear forces at large displacements recorded at the central positions of the boxes during shear which made area corrections unnecessary.

6.3.3 Reversal shear tests on kaolinite

A total of 34 drained direct shear tests divided into three series according to the pore fluid NaCl contents of 0, 2 and 35 gms./litre were carried out on kaolinite. The tests in each series were conducted under normal pressures ranging from 5 to 80 psi and all the specimens were sheared along precut planes. The rate of displacement used for all the tests varied between 0.0019 and 0.0024 inches per minute. The plots of shear stresses and the vertical displacements against the corresponding cumulative horizontal displacements for tests nos. K-0-1 to K-0-14, K-2-1 to K-2-10 and K-35-1 to K-35-10 are presented in Figs. B-7 to B-38 of Appendix B. The τ_{res} and the $\tan\phi_r'$ values measured under each normal stress (σ_n') are recorded on the corresponding plot. Pertinent results from these shear tests are summarised in Tables 6.3a, 6.3b and 6.3c, each table corresponding to results obtained for a particular pore fluid NaCl content.

In the reversal shear tests on kaolinite, pronounced strength peaks were observed after each reversal of shear direction (Figs. B-7 to B-38). This is due to the fact that upon reversal of the direction of shear, the attitude of the slip surface rotates which causes some degree of reorientation of mineral particles. The work required to effect the particle reorientation is believed to be reflected in the strength peaks measured after each reversal of shear direction (Kenney, 1967).

During shearing of the normally consolidated kaolinite specimens, the samples continually decreased in volume throughout the tests although the total settlements observed during shearing were not of considerable magnitude (Figs. B-7 to B-38). For a typical shear test on kaolinite, extrusion of soil usually occurred after about 10 reversal cycles. The total horizontal displacement that could be imposed on a sample before initiation of extrusion appeared to depend on the thickness of the gap between the two halves of the shear box at the commencement of shearing. The larger the gap, the smaller was the total horizontal displacement before extrusion began. Hence before commencement of shearing, it is not advisable to separate the two halves of a standard (6 cms. x 6 cms.) shear box by a gap corresponding to more than a quarter turn of the screws supplied for separating the boxes. However, since each kaolinite sample was sheared along a precut plane, a stabilised value of the residual shear strength was usually attained after about 2 to 3 inches of total horizontal displacement (Tables 6.3a, b and c) which was well before the completion of ten reversal

cycles (representing 4 to 5 inches of total horizontal displacement of the shear box). The volume changes observed at these residual states were minimal (see Figs. B-7 to B-38). For the first 10 reversal cycles during which no extrusion usually occurred, it is interesting to note the sudden increases in the rate of vertical compression of each sample under the reversal peaks and the subsequent reductions in the rate of compression after the reversal peaks (Figs. B-7 to B-38). This may imply a thickening of the shear zone with attendent volume decrease. This may also imply a continuous densification of the shear zone structures at each reversal until the residual state was attained where no such sudden compressions under reversal peaks were noted. The minimal volume changes observed at large strains (Figs. B-7 to B-38) may correspond to possible attainment of dense, low energy packings of kaolinite particles in the shear zones. In this context, it is interesting to examine the after shear water content distributions in the samples from Tables 6.3a, 6.3b and 6.3c. Such an examination reveals that the water contents of the shear zones were always less than the water contents of the undeformed areas outside the shear zones. This lends further support to the possible existence of denser structures in the large displacement shear zones in comparison with the undeformed areas outside the shear zones. A general trend of decreasing intensity of the reversal peak with increasing horizontal displacement can also be observed in some stress-displacement plots (for a typical example, see Fig. B-32), which can be interpreted as a continual decrease in the work necessary to reorient the shear zone particles at each reversal with increasing horizontal deformation. This could be associated with

a displacement induced gradual shift of the initially oriented shear zone structures towards the possible formation of compression textures in which the particles are densely packed with their basal planes oriented approximately normal to the major principal stress in the shear box. At large strains, the existence of dense compression textures in the shear zones in clays have already been demonstrated by Morgenstern and Tchalenko (1967 a, b). Hence during this displacement induced gradual shift of the initially oriented shear zone structures towards the formation of compression textures at large strains, the inclinations between the basal planes of the shear zone particles and the direction of the principal displacement shear must progressively increase until the basal planes of the shear zone particles are oriented normal to the major principal stress. Mechanistically, it can be envisaged that during reversal in a direct shear test, less rotation of particles will be necessary to physically reorient shear zone particles that are steeply inclined to the shear plane in comparison with shear zone particles that are almost horizontally oriented. Based on the above argument, it appears reasonable to postulate that the work necessary to reorient the shear zone particles at each reversal will gradually decrease as the angles between the basal planes of the shear zone particles and the failure plane progressively increases with increasing horizontal displacement and this is probably why the intensities of the reversal peaks gradually decreased with increasing horizontal deformations.

The effectiveness of the method used here for precutting

planes in yielding residual shear strength of kaolinite within reasonably small horizontal displacements can be qualitatively assessed from the results tabulated in Tables 6.3a, 6.3b and 6.3c. Total horizontal displacements ranging from 2 to 4 inches were found necessary to attain the residual states in all the precut plane tests and the corresponding drops from the maximum shear stresses recorded in the first cycles of shear (τ_{max}) to the residual shear stresses (τ_{res}) were found to range from 10 to 40%. The total horizontal displacements required to attain the τ_{max} and the τ_{res} in a precut plane test appeared to decrease with increasing normal pressures (see horizontal displacement data reported in Tables 6.3a, 6.3b and 6.3c).

Individual plots of τ_{res} and $\tan\phi_r'$ (calculated in the conventional manner from the relationship $\tan\phi_r' = \dfrac{\tau_{res}}{\sigma_n'}$) versus σ_n' for the three series are presented in Figs. 6.1a, 6.1b, 6.1c, 6.2a, 6.2b and 6.2c while Figs. 6.1d and 6.2d present the summary plots of τ_{res} and $\tan\phi_r'$ versus σ_n' for the purpose of comparing the residual shear strengths of kaolinite obtained under the three pore fluid NaCl contents. An envelope corresponding to the Hvorslev's angle of true friction for kaolinite ($\phi_e = 20.2°$; Gibson, 1953) is drawn on each τ_{res} versus σ_n' plot (Figs. 6.1a, b, c and d) in order to demonstrate the drop from the peak to the residual friction angle for kaolinite. A check on the strength data is also made by plotting the failure plane water contents for all the three series (tabulated in Tables 6.3a, b and c) against the corresponding residual shear strengths on a semi-logarithmic scale in Fig. 6.3 The straight line relationships in Fig.

6.3 suggest that the strength data is consistent.

Figs. 6.1d and 6.2d indicate that the effect of the pore fluid NaCl content on the residual shear strength and the residual friction angle of kaolinite is insignificant. A residual friction angle (ϕ_r') of about 11° is obtained for kaolinite (Fig. 6.1d) which compares favourably with the ϕ_r' values reported for the same mineral by other researchers (such as Tchalenko, 1967; Kenney, 1967; Morgan, 1967 and Cullen and Donald, 1971). For kaolinite, the value of K' was found to range from 1.86 to 2.32 (Figs. 6.1a, b and c).

It can be seen from Fig. 6.2d that the residual friction angle of kaolinite is normal stress dependent under all conditions of salinity up to a normal stress of about 30 psi beyond which the $\tan\phi_r'$ values become stress independent. This non-linearity of friction with stress level is also reflected in the curvature of the residual strength Mohr envelopes for kaolinite in the low pressure range (Figs. 6.1a, b and c). Based on the theory developed in Chapter III to explain the dependence of ϕ_r' or the magnitude of σ_n', the $\tan\phi_r'$ values from all the shear tests on kaolinite are plotted against the corresponding values of $(\sigma_n')^{-1/3}$ (tabulated in Tables 6.3a, b and c) in Fig. 6.4 which shows linear relationships between $\tan\phi_r'$ and $(\sigma_n')^{-1/3}$ under all conditions of salinity in the low stress range and above an average normal pressure of 30 psi, the relationships become horizontal lines parallel to the $(\sigma_n')^{-1/3}$ axis indicating that the $\tan\phi_r'$ values are no longer stress dependent. This then confirms that the non-linearity of the residual friction angle with stress level for kaolinite is due to the dependence of the area of true contact between the particles in the shear zone on

the applied normal load.

6.3.4 Reversal shear tests on Na-attapulgite

The shear tests on Na-attapulgite were also divided into three series according to the pore fluid NaCl contents of 0.02, 2.42 and 40.95 gms./litre. In each series, about 10 drained direct shear tests were conducted under various normal pressures (ranging from 2.5 to 55 psi) on overconsolidated specimens of attapulgite. Pilot shear tests on normally consolidated specimens of attapulgite exhibited large volume decreases during shear due to the significant secondary consolidation characteristics of the mineral. These volume decreases (which meant a random supply of unsheared particles to the shear zone in every cycle) resulted in random and unacceptable fluctuations of the shear forces in consecutive reversal cycles and stabilised values of residual shear strength could not be obtained at all in these tests. Hence, the samples were overconsolidated to about 2 to 4 times the normal pressures under which they were sheared in order to minimize the volume decreases during shear. As a result, the shear tests on attapulgite could not be performed under normal pressures higher than 50 to 60 psi because beyond these normal pressures undesirably high overconsolidation pressures were needed to impart overconsolidation ratios of 2 to 4 to the samples. Although most of the samples were sheared along precut planes using rates of displacement ranging from 0.0001 to 0.012 inches per minute, at least four samples under each salt content were sheared without precut planes at relatively slow rates of deformation (0.0001 inches per minute) to determine the peak strength parameters. The applied normal stresses (σ_n') for these

peak strength tests were spread out over a wide range of pressures so that a reasonable peak strength envelope could be obtained for each pore fluid NaCl content. The plots of shear stresses and vertical displacements against the logarithms of the corresponding cumulative horizontal displacements for test nos. A-0-1 to A-0-9, A-2-1 to A-2-10 and A-41-1 to A-41-10 are presented in Figs. B-39 to B-67 of Appendix B. The τ_{res} and the $\tan\phi_r'$ values measured under each σ_n' are recorded on the corresponding plot. Specific reference is made in the stress-log (displacement) plot of a test if it was used for determination of peak shear strength and the corresponding τ_{peak} is recorded on the graph. Pertinent results from these shear tests are tabulated in Tables 6.4a, 6.4b and 6.4c devoting each table to the results obtained for each pore fluid NaCl content.

In the shear tests on attapulgite, the reversal strength peaks were not very well defined. It is possible that during reversal in a shear test on attapulgite, very little reorientation of the shear zone particles occurs because of the extremely random nature of orientation of the highly intermeshed needle shaped attapulgite particles. For most of the overconsolidated specimens of attapulgite, the volumes of the samples increased during the first 2 to 4 cycles of shear after which the samples continually decreased in volume (Figs. B-39 to B-67). However, in some shear tests where the overconsolidation ratio was high ($\simeq$ 5 to 11), the samples dilated continually to the residual states (for a typical example, see Fig. B-48). Although overconsolidation of the attapulgite specimens prevented large settlements from occurring

during shear, continual small decreases in sample volumes (probably due to secondary consolidation) were, nevertheless, observed at large strains. Consequently, small variations (in the order of $\pm$ 5%) between the tension and the compression cycle shear forces were observed at the residual states for almost all the tests. The lower value has usually been accepted for calculating the residual shear strength in each test. Extrusion of soil usually occurred after about 8 to 10 reversal cycles in each test.

In the peak strength tests where no precut planes were made in the attapulgite samples, total horizontal displacements ranging from 2 to 3 inches were necessary to attain the residual states. In the precut plane tests, on the other hand, stabilized residual states were generally attained after about 1 to 2 inches of total horizontal displacements (Tables 6.4a, b and c) and the volume changes associated with these residual states were small (Figs. B-39 to B-67). This shows that in comparison with conventional shearing from the peak to the residual state, the horizontal displacements required to attain the residual states are usually smaller if shearing is performed along precut planes. From the horizontal displacement data in Tables 6.4a, 6.4b and 6.4c, it further appears that the horizontal displacement needed to reach the residual state generally decreased with increasing normal pressure. In the peak strength tests,. relatively small reductions ($\simeq$ 5 to 20%) in shear strengths from the peak to the residual states were observed and the horizontal displacements at which the peak shear strengths were mobilised ranged from 0.05 to 0.15

inches. In a cut-plane test, however, the percentage drop from τ_{max} in the first cycle of shear to τ_{res} appeared to depend on a combination of the overconsolidation ratio of the sample and the effective normal pressure under which it was tested. It is immediately seen from Tables 6.4a, 6.4b and 6.4c that the high overconsolidation ratio samples (O.C.R. $\simeq$ 4 to 11) that were tested under low normal pressures ($\simeq$ 2.5 to 15 psi) demonstrated reductions in the order of 25-40% from τ_{max} to τ_{res} whereas the samples with low overconsolidation ratios ($\simeq$ 1 to 4) that were tested under high normal pressures ($\simeq$ 15 to 55 psi) exhibited smaller reductions ($\simeq$ 5 to 15%) from τ_{max} to τ_{res}.

A rate of displacement of 0.0001 inches per minute was used for all the peak strength tests (in which shearing was continued until the residual states were attained) whereas rates ranging from 0.0001 to 0.012 inches per minute were employed for the precut plane tests on attapulgite. Within these limits, no significant influence of the rate of strain on the residual strength coefficient ($\tan\phi_r'$) is discernible from the shear strength results presented in Tables 6.4a, 6.4b and 6.4c. This has already been demonstrated by Kenney (1967).

Examination of the after shear water content distributions in the attapulgite samples (reported in Tables 6.4a, b and c) again reveals that although the samples were overconsolidated, the failure plane water contents were always less than the water contents of the undeformed areas outside the shear zones. This then indicates that like kaolinite, the large strain shear zone structures in the attapulgite

samples were also denser than the structures that prevailed outside the shear zones at large strains.

Shear strengths (τ_{peak} and τ_{res}) and the $\tan\phi_r'$ values (calculated from $\tan\phi_r' = \tau_{res}/\sigma_n'$) for each series are plotted against the corresponding values of σ_n' in Figs. 6.5a, 6.5b, 6.5c, 6.6a, 6.6b and 6.6c whereas Figs. 6.5d and 6.6d present the master plots of shear strength and $\tan\phi_r'$ versus σ_n' for all the three series on attapulgite. The linear relationships on a semi-logarithmic scale between the failure plane water contents and the corresponding residual shear strengths for all the three series, presented in Fig. 6.7, suggest that the strength data is consistent.

Figs. 6.5d and 6.6d clearly indicate that the peak and the residual shear strength parameters of Na-attapulgite are almost independent of the concentration of NaCl in the free pore water. A peak friction angle (ϕ') of 31° and a very high residual friction angle (ϕ_r') of 30° are obtained for attapulgite. The residual friction angle obtained here for attapulgite is in excellent agreement with the value of ϕ_r' (= 29°-30°) reported by Kenney (1967) for the same mineral. Examination of the peak and residual strength envelopes of attapulgite (Fig. 6.5d) also reveals that the drop from the peak to the residual friction angle is rather small (<6%). The peak strength envelopes (Figs. 6.5a, 6.5b and 6.5c) obtained from the shear tests on over-consolidated specimens of attapulgite tend to exhibit apparent cohesion intercepts of 2 to 5 psi if the envelopes are extended back to the shear stress axis. These intercepts are merely extrapolated

geometric intercepts on the shear stress axis and do not represent true cohesion of the mineral because the strength envelopes are believed to be markedly curved in the low stress range. Although peak strength tests were not conducted on attapulgite under low enough normal stresses to demonstrate this curvature, the peak strength envelope for attapulgite - 2.42 g/l NaCl system, presented in Fig. 6.5b, is markedly curved · in the low normal stress range (7.5-15 psi). A part of these apparent cohesion intercepts may also be attributed to the dilatancy of the overconsolidated attapulgite samples observed during the first cycle of shear in the peak strength tests.

Residual friction angle of attapulgite is also found to be dependent on the magnitude of σ_n' up to a normal stress of about 25 psi beyond which ϕ_r' becomes practically independent of σ_n' (Fig. 6.6d). This variation in ϕ_r' with σ_n' is reflected in the curvature of the residual strength envelopes for attapulgite in the low stress range (Figs. 6.5a, b and c). The plots of $\tan\phi_r$' versus $(\sigma_n')^{-1/3}$ for all the three series on attapulgite, presented in Fig. 6.8, indicate that the variation in ϕ_r' with σ_n' for attapulgite is also due to the dependence of the area of true contact between the mineral cleavage planes and the particles in the shear zone on the applied normal load.

6.3.5 Reversal shear tests on Na-montmorillonite

A total of 22 drained direct shear tests divided into three series according to the pore fluid NaCl contents of 1.15, 15.26 and 33.57 gms./litre were carried out on Na-montmorillonite. The tests in each series were conducted under normal pressures ranging from 2.5 to 80 psi.

The tests in the 1.15 g/l NaCl series were performed on normally consolidated samples whereas the samples in the 15.26 g/l and the 33.57 g/l NaCl series were overconsolidated to about 2 to 10 times the normal pressures under which they were sheared in order to inhibit secondary consolidation. All the samples were sheared along precut planes using a rate of displacement of 0.0019 or 0.0024 inches/minute. The shear stress and the vertical displacements for test nos. M-1-1 to M-1-7, M-15-1 to M-15-6 and M-34-1 to M-34-9 are plotted against the corresponding cumulative horizontal displacements on semi-logarithmic scales in Figs. B-68 to B-94 of Appendix B. The τ_{res} and the $\tan\phi_r'$ values obtained from each test are recorded on the corresponding plot. Pertinent results from these shear tests on montmorillonite are tabulated in Tables 6.5a, 6.5b and 6.5c.

In the shear tests on Na-montmorillonite, pronounced strength peaks were measured after each reversal of shear direction (for a typical example, see Fig. B-85). Like kaolinite, the same general trend of a continual decrease in the intensity of the reversal peak with increasing horizontal displacement was also exhibited by some of the shear tests on montmorillonite (for example, see Figs. B-83 to B-85 and B-92 to B-94). This could again be associated with a displacement induced gradual shift of the initial shear zone structures of platy montmorillonite particles twoards the formation of dense, low energy compression textures in the shear zone at large strains. The possibility of a closely packed structure existing in the large displacement shear zones in the montmorillonite samples is

also suggested by the fact that the failure plane water contents were generally less than the corresponding water contents of the undeformed areas outside the shear zones (Tables 6.5a, 6.5b and 6.5c).

During shearing of the normally consolidated montmorillonite - 1.15 g/l NaCl samples and the lightly overconsolidated montmorillonite - 15.26 g/l NaCl samples, the volumes of the specimens decreased throughout the test (Figs. B-68 to B-80), although the rates of decrease in volume usually diminished as the tests proceeded (for a typical example, see Fig. B-70). However in the montmorillonite - 33.57 g/l NaCl series, the volume change behaviour of a sample depended largely on the over-consolidation ratio of the sample and the normal stress (σ_n') under which it was sheared. As expected, the tests performed under high normal pressures on samples with low overconsolidation ratios exhibited continuous decreases in sample volumes throughout the tests (Figs. B-92 to B-94), although these volume changes were very small. On the other hand, the high overconsolidation ratio samples that were sheared under low normal pressures dilated continuously throughout the tests (Figs. B-81 to B-85). Extrusion of soil usually occurred after about 8 to 10 reversal cycles in each test.

Stabilised residual states were usually achieved after about 2 to 4 inches of total horizontal displacement in all the tests on the cut-plane samples of montmorillonite and the volume changes associated with these residual states were rather small. Similar to the volume change characteristics during shear, the reduction from the maximum shear strength recorded in the first cycle of shear to the residual

strength in a cut-plane test also appeared to depend on the over-consolidation ratio of the sample and the normal pressure under which it was sheared. For low pressure, high overconsolidation ratio tests, the strength reductions varied between 25 and 50% whereas strength reductions ranging from 15 to 30% were observed for high pressure, low overconsolidation ratio tests (Tables 6.5a, 6.5b and 6.5c).

Separate plots of the residual shear strengths and the values of $\tan\phi_r'$ (calculated from $\tan\phi_r' = \tau_{res}/\sigma_n'$) against the corresponding values of σ_n' for each series are presented in Figs. 6.9a, 6.9b, 6.9c, 6.10a, 6.10b and 6.10c. The combined pictures of the variations of τ_{res} and $\tan\phi_r'$ with σ_n' for all the three series are presented in Figs. 6.9d and 6.10d. The values of $\tan\phi_r'$ for Na-montmorillonite (0 and 30 gm. NaCl/l) reported by Kenney (1967) are also plotted against σ_n' in Fig. 6.10d.

Figs. 6.9d and 6.10d clearly show the apparent effect of the pore fluid NaCl content on the residual shear strength of Na-montmorillonite. As the pore fluid NaCl content was increased from 1.15 to 33.57 gms./litre, the residual friction angle of Na-montmorillonite increased from 4.8 to 8.5° (Fig. 6.9d). This observed apparent increase in the residual shear strength of Na-montmorillonite due to a corresponding increase in the pore fluid NaCl content will be analysed in the light of the modified Coulomb-Terzaghi relationship defined in terms of the true effective stress in a later section of this chapter. Fig. 6.10d shows an unmistakable trend of the $\tan\phi_r'$ versus σ_n' plots for the 1.15 and 33.57 g/l NaCl series towards convergence at high normal stresses.

This trend is also observed in Kenney's (1967) results on Na-hydrous mica and Na-montmorillonite (Fig. 2.1) and his plots of $\tan\phi_r'$ versus σ_n' for any one of the above mentioned minerals at two different salt contents tend to converge at a normal pressure of about 250-300 psi. It would appear then that any active clay mineral when tested with distilled water and other salinities should yield the same residual friction angle at sufficiently high normal loads. Unfortunately, tests under sufficiently high normal stresses were not performed to be conclusive.

The residual friction angle of montmorillonite is also found to be dependent on the magnitude of σ_n' in the low normal stress range (0-30 psi; Fig. 6.10d). The plots of $\tan\phi_r'$ versus $(\sigma_n')^{-1/3}$ for all the three series on montmorillonite are presented in Fig. 6.11. It would generally seem from Fig. 6.11 that the variation in ϕ_r' with σ_n' for montmorillonite is also due to the dependence of the area of contact between the shear zone particles on the normal load.

6.4 Results of the Constant Volume Leaching Tests on the Na-montmorillonite Samples

6.4.1 General

Five constant volume leaching tests (Test nos. L-1, L-2, L-3, L-4 and L-5) were performed on the low pressure (2.5, 5, 7.5, 10 and 15 psi) Na-montmorillonite - 33.57 g/l NaCl samples in order to replace the saline pore fluids (salt content = 33.57 g/l NaCl) with distilled water under constant true effective stress conditions, so that a comparison of the residual shear strengths of the same samples

before and after leaching could be made. These leaching tests constituted a part of the shear testing programme on montmorillonite specially devised in order to establish that the true effective stress $(\sigma_n{}^*)$ on the mineral basal planes governs the residual shear strength of the mineral.

6.4.2 Results of the shear tests before leaching

The five overconsolidated Na-montmorillonite samples with a pore fluid NaCl content of 33.57 g/l were first sheared along precut planes under normal pressures ranging from 2.5 to 15 psi and the results of these shear tests (Test nos. M-34-1, M-34-2, M-34-3, M-34-4 and M-34-5) are presented in Figs. B-81 to B-85 of Appendix B. These salt rich montmorillonite samples were subjected to only 7 to 8 reversal cycles before leaching so as not to have any extrusion between the two halves of the shear boxes. After termination of the first time shearing under the saline conditions, the five samples were then subjected to constant volume leaching as described in Chapter V. In addition to the measurement of the time rate development of the net (R-A) stresses in the samples due to upward leaching with distilled water under constant overall volume conditions, a systematic study of the various aspects of the leaching process was also undertaken and the results obtained from these leaching tests are presented and discussed in this section.

6.4.3 Seepage pressures developed at the top of the samples due to upward leaching

The seepage pressure developed at the top of each Na-montmorillonite sample due to the corresponding head of distilled water

applied at the base of the sample for upward leaching was determined independently by circulating deaired 33.57 g/l NaCl solution (which is same in composition and concentration as the initial saline pore fluid of the sample) through the sample under the same head.

i) Theoretical analysis

The total, effective and the excess pore water pressure distributions in a sample before application of a head of leachate at the base for upward leaching are as shown in Figs. 6.12a, b and c. Initially, the excess pore fluid pressure throughout the sample is zero (Fig. 6.12b) because the sample was fully consolidated under the corresponding normal pressure and subsequently sheared under fully drained conditions. Hence, the effective stress of the sample before leaching is equal to the total stress of the sample before leaching (Figs. 6.12a and c). Since this analysis is developed for circulation of salt solution through the sample, the true effective stress (σ_n^*) of the sample will be regarded as being equal to its apparent effective stress (σ_n^*) because the magnitude of the net (R-A) stress under a highly saline environment is usually insignificant.

Now, as a head H of salt solution is applied at the base for upward flow, the pore pressure at the base of the sample must immediately rise to a value of $\gamma_w \cdot H$ whereas the excess pore pressure at the top of the sample must always remain at zero because the effluent is being discharged into atmosphere (neglecting the small head of salt solution above the sample). The steady state triangular pore pressure distribution in the sample due to the application of the head H at the

base is shown in Fig. 6.12d. Obviously, this imposed pore pressure is expected to bring about changes in the initial total and effective stresses throughout the sample. However, since the overall volume of the sample will not be allowed to change during leaching, the net area of the apparent (= true) effective stress diagram must remain constant throughout the leaching process. Based on this concept, the total and the effective stress distributions in the sample after establishment of the steady state seepage condition are idealised in Figs. 6.12e and 6.12f. The final effective stress diagram (Fig. 6.12f) suggests that the increase in the total stress (Fig. 6.12e) due to the imposed seepage pressure will be distributed throughout the sample in such a way that there will be a decrease in the area of the effective stress diagram for the bottom half of the sample which will be counterbalanced by an equal increase in the area of the effective stress diagram for the top half of the sample thus maintaining the net area of the effective stress diagram constant at all times during leaching. This is reasonable in view of the fact that since all the Na-montmorillonite samples that were subjected to leaching were overconsolidated, the coefficients of volume compressibility and swelling were probably the same for each sample. Hence according to Fig. 6.12f, the effective stress at the top of the sample must increase by a magnitude of $\gamma_w.H/2$ after the steady state seepage condition under a head H applied at the base of the sample for upward leaching has been established. This increase in effective stress should also be equal in magnitude to the steady state seepage pressure that will develop at the top of the sample due to the same head (H) applied at the base.

ii) <u>Test results</u>

Upward leaching of the samples in test nos. L-1, L-2, L-3, L-4 and L-5 with 33.57 g/1 NaCl solution was carried out for about 15 days in order to establish the steady state seepage conditions. The thicknesses and the initial effective stresses of the samples together with the average hydraulic gradients imposed across the samples for upward leaching are tabulated in Table 6.6. It can be seen from Table 6.6 that although the pressures applied at the bottom of the samples for leaching were always kept less than the initial effective stresses of the samples, these pressures created large average hydraulic gradients (84-199) across the specimens.

The total quantities of outflow from the samples at various elapsed times from the commencement of circulation with the salt solution are plotted against the corresponding total quantities of inflow at the same elapsed times for test nos. L-1, L-3, L-4 and L-5 in Figs. 6.13a, 6.13b, 6.13c and 6.13d and the nearly 45° straight line relationships between the total inflow and the total outflow quantities at various elapsed times indicate that the overall volumes of the samples were held reasonably constant during the entire process of circulation with the salt solution. No flow data was obtained for test no. L-2 because the test was carried out in a particular cell that was not equipped with an inflow and an outflow burette. The initial volumes of fluid in the pore spaces of the samples are also reported in Figs. 6.13a, b, c and d for comparison with the quantities of salt solution that were circulated through the samples. For the same four tests (i.e. Test

nos. L-1, L-3, L-4 and L-5), the averages of the cumulative inflow and outflow quantities at various elapsed times from the beginning of circulation are also plotted against the corresponding elapsed times in Fig. 6.14. These plots exhibit linear relationships between flow and time indicating a constant rate of flow through each sample. They also suggest that under the applied hydraulic gradients of 84-199, the upward flow of salt solution through the samples followed Darcy's law very closely. The flow-time data (Fig. 6.14) further indicate that the large average hydraulic gradients imposed across the specimens caused substantial quantities of flow to take place through the low permeability montmorillonite samples within a reasonable length of time. Hence it would appear that the application of such high hydraulic gradients across the low pressure samples may reduce the length of time required for complete leaching of the specimens with distilled water. The coefficients of permeability (k) of the four samples of montmorillonite were calculated from the flow-time data and they are reported in Fig. 6.14. The coefficients of permeability of the samples under the saline environment ranged from 1.69×10^{-9} to 1.15×10^{-8} cms./sec. depending on the void ratios of the samples (Table 6.6). The permeability values obtained here appear to be reasonable for salt-rich montmorillonite.

The gradual developments of the seepage pressures at the top of the samples to the final steady state values were recorded in the form of monotonically increasing load cell readings which also stabilised eventually as the steady state seepage conditions were established in the samples. The true seepage pressure component at the top of a sample

at any instant was calculated by subtracting the appropriate initial value of σ_n' of the sample from the pressure recorded by the load cell at that instant. The results of the rate of development of seepage pressures for all the five tests are shown in Figs. 6.15a, 6.15b, 6.15c, 6.15d and 6.15e in $\sqrt{time}$ plots. It is interesting to observe from some of the $\sqrt{time}$ plots (Figs. 6.15a and 6.15b) that under constant overall volume conditions, major parts of the final steady state seepage pressures were developed almost instantaneously at the top of the samples. This is specially encouraging in view of the fact that under no volume change conditions, the response at the top of a sample due to any stress change at the bottom should be instantaneous if the measuring system is stiff and the pore fluid is incompressible. Hence the observed developments of the seepage pressures within a very short time (Figs. 6.15a and 6.15b) appear to suggest that the measuring systems (i.e. the load cells and the frames) used in the leaching equipment were reasonably stiff and adequate for the purpose that they were meant for.

Table 6.6 compares the steady state seepage pressures measured at the top of the samples with the corresponding values of seepage pressure predicted from the steady state effective stress conditions in the samples and the agreement is good. This supports the idealization presented in Fig. 6.12.

6.4.4 Results obtained during leaching of the Na-montmorillonite samples with distilled water under constant volume conditions

After determining the seepage pressures at the top of the samples independently by upward seepage of salt solution, the samples

were subsequently leached with deaired distilled water in order to replace the saline pore fluids from the samples and determine the resulting changes in the apparent effective stresses (σ_n') and hence in the net (R-A) stresses of the samples. Since the heads applied for circulation of the salt solution and subsequently the distilled water were kept exactly the same, the seepage pressures at the top of the samples will also be identical in both cases.

i) Flow, salt removal and permeability data

The cumulative quantities of outflow from the samples at various elapsed times from the commencement of leaching with distilled water are plotted against the corresponding cumulative quantities of inflow into the samples for test nos. L-1, L-3, L-4 and L-5 in Figs. 6.16a, 6.16b, 6.16c and 6.16d. The flow, salt removal and permeability data were not obtained for test no. L-2 because it was conducted in the pilot leaching cell which was not equipped with an inflow and an outflow burette. Figs. 6.16a, b, c and d show that at all elapsed times, the total volume of outflow from each of the four samples was always equal to the corresponding total volume of inflow and this confirms the maintenance of constant overall volume conditions for the samples during the entire process of leaching. For the same four tests (i.e. Test nos. L-1, L-3, L-4 and L-5), the averages of the cumulative inflow and outflow volumes at variuos elapsed times are plotted against the corresponding elapsed times in Fig. 6.17. Unlike the linear flow-time relationships obtained for the circulation of salt solution through the samples (Fig. 6.14), the flow-time relationships for the same samples during the initial 40,000-60,000 minutes of

leaching with distilled water were all characterised by non-linearly decreasing rates of flow with progress of leaching. The later stages of leaching (i.e. after 40,000-60,000 minutes) were, however, characterised by linear rates of flow. Examination of the flow-time relationships for the four samples from Fig. 6.17 immediately reveals that the largest total quantity of flow ($\simeq$ 68 c.c.) occurred through the sample with the highest void ratio (e = 6.43; Test no. L-1) although the head applied ($\simeq$ 3.5') for leaching of this sample was the smallest. For the other three tests where identical heads of 9.6' were used for leaching, a general trend of decreasing total quantities of circulation through the samples at any elapsed time with decreasing void ratios is discernible.

The cumulative quantities of NaCl removed from the four samples at various elapsed times from the commencement of leaching are plotted against the corresponding elapsed times in Figs. 6.18, 6.20, 6.21 and 6.22. These plots show that during the initial stages (40,000-60,000 minutes) of leaching, the rates of salt outflow from all the samples decreased markedly with time in a non-linear fashion. However, after 40,000-60,000 minutes of leaching, the rates of salt outflow became almost linear (Figs. 6.18, 6.20, 6.21 and 6.22) and very low concentrations of NaCl were detected in the effluents. The quantities of salt measured in the effluents during the initial stages of leaching contained the salts from the porous stones. Hence, the total quantity of NaCl initially held by the three carborundum porous stones used in each leaching cell was determined (as shown in Table 6.7) and added to the estimated quantity of NaCl initially present in the pore spaces

of each sample in order to define the total quantity of NaCl that was present in each leaching cell assembly before leaching. A comparison between these estimated total quantities of NaCl present in the systems before leaching and the corresponding total quantities of NaCl actually removed from the samples during the entire leaching process is presented in Table 6.7. It can be seen from Table 6.7 that except for Test no. L-5, the total quantity of NaCl leached out of each sample was somewhat more than the corresponding total quantity of NaCl estimated to be initially held by the sample and the porous stones. No satisfactory explanation can be offered for this.

Leaching of the samples was carried out for a total time period of about 130,000 minutes (except for the sample in test no. L-2 which was leached for about 240,000 minutes) until negligible quantities of salt were detected in the effluents over a period of about 10,000 minutes. Figs. 6.18, 6.20, 6.21 and 6.22, however, indicate that major portions of the total NaCl held by the samples and the porous stones before commencement of leaching were removed during the initial 40,000-60,000 minutes of leaching. To illustrate this point clearly, the percentages of the total NaCl removed from the samples at various elasped times are plotted against the corresponding elapsed times on a semi-logarithmic scale in Fig. 6.32b which shows that about 85-95% of the total quantity of NaCl initially held by each sample and the porous stones was removed within 40,000-60,000 minutes from the commencement of leaching. The remaining 5-15% of the total quantity of NaCl in each system was removed during the subsequent 70,000-90,000

minutes of leaching. It also appears from Fig. 6.32b that despite the differences in the void ratios, the sample thicknesses and the heads used for leaching, the percentages of the total NaCl removed from the samples at any elapsed time were virtually identical and complete replacement of the saline pore fluids for all the samples was practically attained at the same elapsed time (which is about 130,000 minutes from the commencement of leaching). In order to provide an explanation for the foregoing observation, let us reexamine the flow-time data obtained from the leaching tests. The quantities of distilled water inflow into the samples at various elapsed times expressed as percentages of the corresponding total volumes of salt solution held by the pore spaces of the samples and the porous stones before leaching are plotted against the corresponding elapsed times on a semi-logarithmic scale in Fig. 6.32a. Fig. 6.32a shows that during the initial 40,000-60,000 minutes of leaching, about 70-75% of the saline pore fluid of the highest void ratio sample (e = 6.43; Test no. L-1) was physically replaced by upward flow alone whereas for the other three samples in test nos. L-3, L-4 and L-5, flow replaced about 30-40% of the saline pore fluids during the initial 40,000-60,000 minutes of leaching. At any elapsed time, the percentages of the saline pore fluids replaced from the samples in test nos. L-3, L-4 and L-5 by upward flow alone were relatively independent of factors such as void ratio and sample thickness (Fig. 6.32a). This observed independence of the percentage replacement of the saline pore fluids (by flow alone) at any elapsed time on void ratio for test nos. L-3, L-4 and L-5 (in which identical heads were used for leaching) is probably due to increasing velocities

of flow through the soil pores with increasing void ratios. Hence a combination of increasing velocities of flow through the pores and increasing total quantities of salt initially held by the samples with increasing void ratios probably resulted in a percentage removal of total salt versus log (time) relationship (Fig. 6.32b) that was relatively independent of factors such as void ratio, sample thickness and the head used for leaching. Furthermore, due to a coincidental combination of void ratios and sample volumes, the total quantities of NaCl held by the samples before leaching were not very different from each other (see Table 6.7). Fig. 6.32a also shows that after 130,000 minutes of leaching, the total quantity of inflow into the highest void ratio sample (e = 6.43; Test no. L-1) was more than 100% of the total volume of the saline pore fluid that was initially present in the system. This signifies a total replacement of the saline pore fluids of the sample in test no. L-1 by upward flow alone although diffusion from both ends of the sample was also facilitating removal of salt from the sample during the entire leaching period. For test nos. L-3, L-4 and L-5, at least 50 to 70% of the saline pore fluids were replaced during the entire leaching period by flow alone (see Table 6.7) and the rest, presumably, were replaced by diffusion from both ends of the samples. The comparison of the inflow data with the volumes of salt solution held by the samples and the porous stones before leaching (Table 6.7) further suggests that during the 120,000-130,000 minutes of leaching, at least the areas around the shear zones (which were close to the base of the samples) were probably completely leached.

The flow-time relationships in Fig. 6.17 were next divided into

small time steps in such a way that the rate of flow in each time step was approximately linear and the average value of the coefficient of permeability (k) was calculated for each time step. The relationship between the average values of k obtained in this manner and the appropriate elapsed times corresponding to the mid points of the time steps for all the four tests (i.e. Test nos. L-1, L-3, L-4 and L-5) are presented on a semi-logarithmic scale in Fig. 6.23. Examination of the time - log (k) relationships from Fig. 6.23 reveals that in accordance with the rate of flow characteristics of the samples during leaching (Fig. 6.17), the permeabilities decreased markedly with time in a non-linear fashion during the initial 40,000-60,000 minutes of leaching after which very little changes in k were observed. The permeability data (Fig. 6.23) is also consistent with the salt outflow data (Figs. 6.18, 6.20, 6.21, 6.22 and 6.32b) which clearly show that the rates of salt outflow also decreased non-linearly with time during the initial 40,000-60,000 minutes of leaching and about 85 to 95% of the total quantity of NaCl in the pore spaces of each sample was removed during this period.

The logarithms of the average coefficients of permeability (k) at various elapsed times from the commencement of leaching are plotted against the corresponding cumulative quantities of NaCl replaced from the samples during these elapsed times in Figs. 6.24a, 6.24b, 6.24c and 6.24d. These plots clearly show that as NaCl was leached out of the samples, the permeability of the samples decreased in a non-linear manner. This falls within the conventional reasoning of

the double-layer theory i.e. as the pore fluid NaCl content of each sample was gradually decreased by leaching, the thicknesses of double-layer water expanded accordingly and consequently,a continual decrease in the permeability of the sample was observed. Figs. 6.24 c and d also show that the decreases in the coefficients of permeability of the samples were rather small until a major portion of the pore fluid salts was removed from each sample by leaching. It must also be remembered that during the initial stages of leaching, major portions of the salts in the effluents were probably derived from the porous stones and not from the samples. It was not until the later stages of leaching when the samples had fairly expanded double-layers (due to low salt contents) and much of the salts measured in the effluents were from the samples (and not from the porous stones) that the permeabilities of the samples became extremely sensitive to further removal of salts and removal of small quantities of NaCl from the pore spaces of the samples induced rather large changes in the coefficients of permeability of the samples (Figs. 6.24a, b, c and d).

The dependence of permeability on void ratio is clearly demonstrated in Fig. 6.23 which shows that at any elapsed time, the sample with the highest void ratio had the highest coefficient of permeability and the permeability of the samples decreased in the order of decreasing void ratio. The void ratios of the samples are plotted against the corresponding coefficients of permeability of the samples measured before and after leaching on a semi-logarithmic scale in Fig. 6.25 in order to illustrate the degress by which the permeabilities

of the four samples decreased due to leaching under constant overall volume conditions. Fig. 6.26 presents a plot between the percentage reductions in the coefficients of permeability of the samples due to constant volume leaching and the corresponding void ratios and a definite relationship between the two emerges from Fig. 6.26. The highest void ratio sample (e = 6.43; Test no. L-1) underwent the largest reduction (≃ 90%) in permeability due to leaching and the percentage reduction in k due to leaching decreased in the order of decreasing void ratio. This is reasonable in view of the fact that in comparison with a low void ratio sample, a high void ratio sample will have larger quantities of water changing from free to double-layer status during constant volume leaching and consequently, the high void ratio sample will suffer a larger reduction in permeability due to leaching.

ii) Development of the net (R-A) stresses due to constant volume leaching

As replacement of the saline pore fluids of the Na-montmorillonite samples progressed with time, the rigid load measuring devices (i.e. the load cells) registered monotonically increasing loads in order to keep the overall volumes (and hence the true effective stresses which control volume changes) of the samples constant during the entire leaching process. As shown earlier, the maintenance of constant overall volume conditions for the samples during leaching is proven by the excellent correspondence between the inflow and the outflow volumes (Figs. 6.16a, b, c and d). The pressures measured at the top of a sample at any instant during the constant volume leaching consisted of three components: (i) the initial

effective stress to which the sample was subjected under the pore fluid NaCl content of 33.57 g/l, (ii) the steady state seepage pressure developed at the top of the sample and (iii) the additional apparent effective stress (σ_n') required to prevent any swelling of the specimen due to leaching. Component (iii) is then directly equal to the net (R-A) stress developed at the top of the sample at that particular instant due to leaching under constant overall volume conditions and it was obtained by subtracting the sum of components (i) and (ii) from the pressure read by the load cell at that instant. The results of the rate of development of the net (R-A) stress during constant volume leaching for test nos. L-1, L-2, L-3, L-4 and L-5 are presented in linear time plots in Figs. 6.18, 6.19, 6.20, 6.21 and 6.22 and they are also presented in log (time) plots in Figs. 6.27, 6.28, 6.29, 6.30 and 6.31. Variations in room temperature had a definite influence on the net (R-A) stresses measured during leaching and this aspect is discussed in section C-5 of Appendix C. The plots presented here (Figs. 6.18-6.22 or Figs. 6.27-6.31) correspond to an ambient temperature of 24.1°C. Figs. 6.27-6.31 clearly show that for all the tests, the net (R-A) stress started to develop after about 1,000 minutes of leaching. This could be due to the fact that during this initial 1,000 minutes of leaching, a major portion of the salts removed was probably from the porous stones and not from the samples themselves. Effective replacement of salt from the samples probably commenced after this initial leaching period of 1,000 minutes and the net (R-A) stresses started to develop. The net (R-A) stresses for all the samples developed at virtually linear rates and the net (R-A) stresses for

test nos. L-1, L-3 and L-4 stabilised after about 120,000-130,000 minutes of leaching (Figs. 6.18, 6.20, 6.21, 6.27, 6.29 and 6.30). Leaching of the lowest void ratio sample (e = 3.01; Test no. L-2) was carried out for about 240,000 minutes and the stabilised state of the net (R-A) stress for this test was attained after about 200,000 minutes of leaching (Figs. 6.19 and 6.28). It can be seen from Fig.6.19 that the net (R-A) stress in test no. L-2 developed at a slow linear rate during the initial 60,000 minutes of leaching after which the rate of development became faster (though not exactly linear) until the stabilised state was reached at 200,000 minutes. In test no. L-5, the lucite piston collapsed after about 35,000 minutes of leaching probably because of eccentrically applied load on the piston (which is possibly if the top surface of the sample is not perfectly horizontal) and although the piston was immediately replaced with a new one, subsequent slow extrusion around the top porous stone prevented further development of the net (R-A) stress (see Figs. 6.22 and 6.31). For each sample, the stabilised final value of the net (R-A) stress which also represent the additional externally applied normal stress (or apparent effective stress, σ_n') that was required to prevent any swelling of the sample during constant volume leaching is recorded on the corresponding plots of (R-A) versus time (Figs. 6.18-6.22) and (R-A) versus log (time) (Figs. 6.27-6.31).

The rate of removal of NaCl from each sample during leaching (except for the sample in test no. L-2) is shown in the corresponding plots of)R-A) versus time (Figs. 6.18, 6.20, 6.21 and 6.22) and (R-A)

versus log (time) (Figs. 6.27, 6.29, 6.30 and 6.31) in order to present a combined picture of the gradual replacement of the saline pore fluid from each sample by constant volume leaching and the resulting development of the net (R-A) stress. It is immediately seen from Figs. 6.18, 6.20, 6.21 and 6.22 that for all the four tests, although the rates of removal of salt from the samples decreased markedly with time in a non-linear fashion during the initial 40,000-60,000 minutes of leaching and subsequently became linear and small, the net (R-A) stresses developed almost linearly with time throughout the entire leaching process until the stabilised values were attained.

A summary plot is presented in Fig. 6.32 in which the quantities of inflow, the quantities of salt removed from the samples and the resulting (R-A) stresses at various elapsed times expressed as percentages of the respective final values are plotted against logarithms of the corresponding elapsed times. This summary plot attempts to show a combined picture of all the interdependent aspects of the leaching tests. Examination of Fig. 6.32 in conjunction with Figs. 6.18, 6.20, 6.21 and 6.22 reveals that during the initial 40,000-60,000 minutes of leaching, although 85-95% of the pore fluid NaCl was removed from the samples in test nos. L-1, L-3 and L-4, the net (R-A) stresses developed at linear rates to values ranging between 45 and 75% (depending on the void ratio of a sample) of the final stabilised values and the remaining 55 to 25% of the final (R-A) stresses developed during the subsequent 60,000-90,000 minutes of leaching. Hence it would appear that when the samples reached low salt environments by leaching, further replacement of small quantities of NaCl from the pore spaces induced larger increases

in the net (R-A) stresses when compared to the initial stages of leaching where replacement of relatively large quantities of salt resulted in smaller increases in the net (R-A) stresses. It is also observed from Fig. 6.32c that at any elapsed time, the lowest void ratio sample developed the highest percentage of the corresponding final (R-A) stress and the stabilised values of the net (R-A) stresses of the samples in test nos. L-1, L-3 and L-4 (with void ratios ranging from 4.2 to 6.4) were all attained approximately at the same elapsed time of 120,000 minutes from the commencement of leaching. This is found to be consistent with the percentage of total salt removed versus log (time) relationships (Fig. 6.32b) which show that at any elapsed time, the percentages of NaCl removed from the samples were virtually identical and practically independent of factors such as void ratio, sample thickness and head used for leaching. Fig. 6.32b further shows that complete leaching of the samples in test nos. L-1, L-3 and L-4 was also attained at the same elapsed time of about 120,000 minutes from the commencement of leaching and this explains why the stablised values of the net (R-A) stresses of the samples, irrespective of the differences in void ratio, were all attained at the same elapsed time.

The water contents and the final pore fluid salt contents of the leached Na-montmorillonite samples are reported in Tables 6.9 and 6.8 respectively. The pore fluid NaCl contents of the leached samples were found to vary between 0.08 and 0.22 gms./litre (Table 6.8) and comparing these final pore fluid salinities with the common initial

salt content ($\simeq$ 33.57 g/l NaCl) of the samples before leaching, it

can be said that the flow-diffusion technique used here for leaching

was indeed effective and successful in replacing the saline pore

fluids from the Na-montmorillonite samples under constant overall

volume conditions.

iii) Comparison between the predicted and the measured values of the net (R-A) stresses

From the measured values of the failure plane water contents

and the final pore fluid salinities of the Na-montmorillonite samples

after leaching (reported in Tables 6.9 and 6.8 respectively), the pore

fluid salt contents of the four samples in test nos. L-1, L-3, L-4 and

L-5 at various elapsed times from the commencement of leaching were

backcalculated and the double-layer repulsive stresses (P_y) corresponding

to these backcalculated salt contents at the various elapsed times were

estimated from the double-layer repulsive stress equation (Eqn. 3.29)

using the specific surface of the calcium variety of the montmorillonite

(641 m.^{2}/gm.; Table 5.2). These estimated double-layer repulsive

stresses are plotted against the corresponding elapsed times in Figs.

6.18, 6.20, 6.21 and 6.22 for comparison with the measured rates of

development of the net (R-A) stresses for the samples. For each sample,

the estimated value of the double-layer repulsive stress (P_y)

corresponding to the completely leached state of the sample is recorded

on the corresponding plots of (R-A) versus time (Figs. 6.18-6.21)

and (R-A) versus log (time) (Figs. 6.27-6.31) and this estimated value

of P_y is compared with the corresponding value of the final net (R-A) stress

that was actually measured at the completely leached state of the sample in Table 6.9. It is immediately seen from Table 6.9 that except for test no. L-5 in which extrusion around the top porous stone was observed, excellent agreement between the estimated value of the double-layer repulsive stress (P_y) and the measured value of the final net (R-A) stress, both corresponding to the completely leached state of each sample, was obtained for each of the four leaching tests (viz. Test nos. L-1, L-2, L-3 and L-4). This excellent agreement is further illustrated by plotting the failure plane water contents of the samples (in Test nos. L-1, L-2, L-3, L-4 and L-5) against the measured final (R-A) stresses and the corresponding estimated values of the double-layer repulsive stresses on a semi-logarithmic scale in Fig. 6.33. The well known trend of increasing net (R-A) stress with decreasing water content (and hence decreasing particle spacing) is clearly exhibited in Fig. 6.33. It is interesting to note at this point that although the measurements of the net electrical forces of interaction were made on the sodium variety of montmorillonite, the measured net (R-A) stresses (corresponding to the completely leached states of the samples) showed agreement only with those double-layer repulsive stresses that were estimated using the specific surface of the calcium variety of montmorillonite. This tends to confirm that the surface that is to be used for successful estimation of the net (R-A) stress for a soil from the double-layer repulsive stress equation (Eqn. 3.29) should be the specific surface of the calcium variety of the soil. The absence of clusters and the probable parallel orientation of clay platelets (due to overconsolidation) in the montmorillonite samples used in the

leaching tests may have been the two most important factors that contributed towards the good agreement obtained between the estimated and the measured values of the final net (R-A) stresses. It can therefore be concluded that for cluster-free active clay-water systems with sodium as the dominant cation, the net (R-A) stresses can be approximated by the double-layer repulsive stresses (calculated from Eqn. 3.29) if the effective surface areas of the clays are determined with reasonable accuracy. However, for natural soils which are not Na-homoionized and which contain clusters, the double-layer repulsive stresses do not always approximate the net (R-A) stresses and an indirect method for prediction of the net (R-A) stresses for natural soils based on the double-layer repulsive stress equation has recently been developed by Balasubramonian (1972).

Agreement between the estimated and the measured rates of development of the net (R-A) stresses (Figs. 6.18, 6.20, 6.21 and 6.22) was, however, not very encouraging. This is probably due to erroneous backcalculated values of the pore fluid salinities (probably caused by erroneous measurement of sample volumes) corresponding to which the net (R-A) stress at various stages of leaching were calculated. The reason for the excellent agreement obtained between the estimated and the measured values of the net (R-A) stresses for the completely leached states of the samples (Fig. 6.33) lies in the fact that the theoretical estimations of the stabilised net (R-A) stresses (corresponding to the completely leached states of the samples) were based on actually determined water contents and final pore fluid NaCl contents of the leached samples.

iv) <u>Change in stresses of the samples due to constant volume leaching</u>

The apparent and the true effective stresses of the Na-montmorillonite samples before and after constant volume leaching are tabulated in Table 6.9 along with the pertinent data obtained from the leaching tests. Since the overall volumes of the samples did not change during leaching (Figs. 6.16a, b, c and d), the true effective stresses (σ_n^*) of the samples were held constant throughout the entire leaching process. However, the apparent effective stresses (σ_n') of the samples in test nos. L-1, L-2, L-3, L-4 and L-5 increased by 400-900% due to complete replacement of the saline pore fluids from the samples under constant overall volume conditions (Table 6.9). The final values of the apparent effective stresses (σ_{n_2}') corresponding to the fully leached states of the montmorillonite samples (reported in Table 6.9) are comprised of the initial effective stresses (σ_{n_1}') under which the samples were sheared before leaching and the additional externally applied stresses that were required to prevent any swelling of the samples during leaching.

6.4.5 Results of the shear tests performed on the leached samples

The shear tests conducted on the five leached samples of Na-montmorillonite are numbered as M-L-1, M-L-2, M-L-3, M-L-4 and M-L-5 choosing the middle letter "L" to indicate that the shear tests were performed on leached samples. These shear tests correspond to continuation of shearing of the montmorillonite samples from test nos. M-34-1, M-34-2, M-34-3, M-34-4 and M-34-5 under the new apparent effective

stresses (reported in Table 6.9) after leaching.

Before shearing the leached samples, the volume changes
of the samples under applied loads corresponding to the appropriate
apparent effective stresses after leaching were studied with time for
a week in the direct shear machines. The vertical displacements of
the leached samples under the applied stresses during this period are
plotted against time in Figs. 6.34a, 6.34b, 6.34c, 6.34d and 6.34e.
The fluctuations in the vertical displacements in Figs. 6.34a, b, c, d
and e are believed to be due to fluctuations in the relative humidity
and the room temperature which affect the LVDT readings. However,
these plots clearly demonstrate that the volume changes of the leached
samples under the applied stresses (σ_{n_2}') that were 400-900% higher than
the initial apparent effective stresses (σ_{n_1}') of the samples before
leaching were between 1 to 2% of the volumes of the samples. In the
case of test nos. M-L-4 and M-L-5, these negligible volume changes
could be partly due to the fact that the samples were heavily
overconsolidated (O.C.R. = 9-10) to start with and in both cases the
apparent effective stresses after leaching were less than the corresponding
maximum preconsolidation pressures by 40 to 65%. However, for test
nos. M-L-1, M-L-2 and M-L-3, although the samples were overconsolidated
(O.C.R. = 3-6), the apparent effective stresses of the samples after
leaching were in all cases more than the corresponding maximum
preconsolidation pressures by 40-120% and the volume changes of the
samples under the applied stresses after leaching were still negligible
(Figs. 6.34a, b and c). These negligible volume changes of the leached
samples in test nos. M-L-1, M-L-2 and M-L-3 under the applied stresses

that were 400-900% higher than the initial effective stresses before leaching tend to confirm that the volume change characteristics of the montmorillonite samples were indeed controlled by the respective true effective stresses (that were held constant during the entire leaching process) and not by the apparent effective stresses (which increased by 400-900% due to constant volume leaching). The volume change data obtained from the leached samples (Figs. 6.34a, b, c, d and e) also indirectly proves that the true effective stresses of the samples were indeed held constant throughout the leaching process.

After studying the volume changes of the leached samples in the direct shear machines for a week, the samples were then resheared along the existing shear planes under the new apparent effective stresses after leaching and the shear stresses and vertical displacements for test nos. M-L-1, M-L-2, M-L-3, M-L-4 and M-L-5 are plotted against the corresponding total horizontal displacements on semi-logarithmic scales in Figs. B-86 to B-90. In test no. M-L-5, since the top half of the shear box was separated from the bottom half by an undesirable amount, excessive extrusion of soil between the two halves commenced after 4 reversal cycles (Fig. B-90) and shearing could not be continued any further. In test nos. M-L-2, M-L-3 and M-L-4, the vertical compressions of the samples during shear were small (Figs. B-87, B-88 and B-89) whereas in test no. M-L-1, the sample expanded monotonically throughout the test (Fig. B-86) even though it was being sheared under an apparent effective stress that was about 800% higher than the initial effective stress of the sample before leaching and 120% higher than the preconsolidation

pressure of the sample. The apparent effective stress (σ_n'), the true effective stress (σ_n*) and the residual shear strength of each leached sample are recorded on the corresponding plot of shear stress versus log (horizontal displacement). The value of $\tan\phi_r'$ for every leached sample was calculated not only in the conventional manner by dividing the τ_{res} by the corresponding σ_n' but also by dividing the τ_{res} by the corresponding σ_n* of the sample and the two different values of $\tan\phi_r'$ thus obtained for the leached sample are also recorded on the corresponding plot of shear stress versus log (horizontal displacement). The results of the shear tests on the unleached (Test nos. M-34-1, M-34-2, M-34-3, M-34-4 and M-34-5) and the subsequently leached (Test nos. M-L-1, M-L-2, M-L-3, M-L-4 and M-L-5) states of the five Na-montmorillonite samples are also combined in Figs. B-81 to B-85 and the values of σ_n', σ_n*, τ_{res} and $\tan\phi_r'$ (calculated with respect to σ_n' and σ_n*) for each sample before and after leaching are presented on the corresponding plot of shear test results. Pertinent residual shear strength results obtained from these shear tests on the leached samples are summarised and compared with the corresponding residual shear strength results obtained from the same samples in their unleached state in Table 6.10. The comparison between the residual shear strengths of the Na-montmorillonite samples before and after leaching from Figs. B-81 to B-85 and Table 6.10 immediately reveals that although the apparent effective stresses of the samples increased by 400-900% due to complete replacement of the saline pore fluids under constant overall volume conditions, the residual shear strengths of the samples did not increase at all after leaching. On the contrary, the residual shear

strengths of the samples decreased by 4 to 13% after leaching (Table 6.10). One exception is in the case of test no. M-L-1 in which the residual shear strength of the sample increased by 5% after leaching. Since the true effective stresses of the montmorillonite samples before and after leaching were the same, these results conclusively demonstrate that it is the true effective stress (σ_n^*) on the mineral basal planes that controls the residual shear strength of a clay mineral. The 4-13% decrease in the residual shear strengths of the montmorillonite samples after leaching could be due to one or both of the following two reasons:

a) At any instant during upward leaching of the samples with distilled water, the pore fluid salt concentrations were definitely not constant with depth and a decreasing salt concentration with increasing depth existed in the samples. This implies that at the same instant, the resulting net (R-A) stresses were not constant with depth either and an increasing (R-A) stress with increasing depth probably prevailed in the samples. But by equilibrium requirements, the externally applied normal stresses (σ_n') at any instant required to prevent any swelling of the samples during leaching were constant with depth. Consequently, a decreasing true effective stress $(\sigma_n^* = \sigma_n' - (R-A))$ with increasing depth prevailed in each sample at any instant during leaching. Since the overall volumes of the samples did not change during leaching (Figs. 6.16a, b, c and d), it can only be speculated that during the entire leaching period, the true effective stress (σ_n^*) distribution with depth in each sample probably readjusted itself continuously in such a way that the net area of the σ_n^* diagram for the

sample was maintained constant at all times so as not to cause any change in the overall volume of the sample during leaching. This means that at all times during leaching, the swelling of the bottom half of each sample was counterbalanced by an equal amount of consolidation of the top half of the sample. This is considered to be quite reasonable because the coefficients of volume compressibility and swelling of the overconsolidated montmorillonite samples were probably the same.

After termination of leaching of the montmorillonite samples, the salt contents of the bottom halves of the samples were probably still less than the salt contents of the top halves implying lower true effective stresses for the bottom halves in comparison with the top halves of the samples. If the precut shear planes were located in the bottom halves of the samples (which is not improbable because the shear planes were in fact reasonably close to the bottom of the samples), then it is possible that the true effective stresses of the shear zones after leaching were less than the desired values and this may have caused the 4-13% decrease in the residual shear strengths of the samples after leaching.

However, the maximum decrease ($\simeq$ 13%) in the residual shear strength after leaching occurred for the sample in test no. M-L-5 (Table 6.10). In this test, the loading piston collapsed after about 35,000 minutes of leaching and although the piston was immediately replaced by a new one, subsequent slow extrusion around the top porous stone probably resulted in some undesirable volume changes in the sample. In test no. M-L-1, the 5% increase in the residual shear

strength after leaching (Table 6.10) could have been caused by a corresponding increase in the true effective stress of the shear zone which was possibly located in the top half of the sample.

b) It is also possible that the true residual shear strengths of the Na-montmorillonite samples were never attained at the end of the first 8 to 9 reversal cycles imposed on them before leaching (for example, see Figs. B-83, B-84 and B-85). Consequently, as the samples were resheared along the existing shear planes after leaching, the shear strengths gradually decreased further until the true residual values were attained. In this context, it is interesting to compare once again the results of the shear tests on the unleached states of the montmorillonite samples (Figs. B-81 to B-85) with the corresponding results of the shear tests on the subsequently leached states of the same samples (Figs. B-86 to B-90) and note that although the shear tests after leaching were started on the same cycles on which the tests were terminated before leaching, each shear test after leaching (except for test no. M-L-5) demonstrated a strength peak in the first cycle that was either 5% lower than or exactly equal to the corresponding shear strength measured in the terminating cycle of shear before leaching and during subsequent shearing of the leached samples, the shear strengths gradually dropped to values that were 4 to 13% lower than the respective shear strengths recorded in the last cycles of shear before leaching.

The residual shear strengths (τ_{res}) of the unleached and the leached states of the Na-montmorillonite samples are plotted

against the appropriate apparent effective stresses (σ_n') in Fig. 6.35 and two distinct envelopes are obtained for the two states. The immediate conclusion from Fig. 6.35 would be that the residual friction angle of the montmorillonite samples before leaching $(\phi_r' = 11.5°)$ was higher than the residual friction angle of the same samples after leaching $(\phi_r' = 3°)$, or in other words, as the pore fluid NaCl content was decreased from 33.57 g/l to 0.08 g/l, the residual friction angle of montmorillonite decreased from 11.5° to 3°. However, if the residual shear strengths of the unleached and leached states of the montmorillonite samples are plotted against the corresponding true effective stresses (σ_n^*) of the samples as shown in Fig. 6.36, the strength envelopes for the unleached and the leached states of the samples virtually coincide signifying a unique residual friction angle for montmorillonite $(\phi_r' = 9.5°-11.5°)$ in the low pressure range which is independent of the pore fluid NaCl content. It is also implied in Fig. 6.36 that the true effective stress of a montmorillonite sample before leaching was equal to its apparent effective stress because the net (R-A) stress of an active clay-water system under a highly saline environment is practically negligible.

If the residual shear strengths (τ_{res}) of the leached montmorillonite samples are divided by the corresponding values of the apparent effective stresses (σ_n') of the samples after leaching, the resulting values of $\tan\phi_r'$ (denoted by closed circles in Fig. 6.37) when plotted against the corresponding values of σ_n' after leaching generates a plot, shown in Fig. 6.37, that virtually coincides with the

relationship between $\tan\phi_r'$ and σ_n' for the montmorillonite - 0 g/l NaCl system reported by Kenney (1967). It can also be seen from Figs. 6.35 and 6.37 that the τ_{res} versus σ_n' plot and the $\tan\phi_r'$ versus σ_n' plot for the leached montmorillonite samples fall below the corresponding plots for the montmorillonite - 1.15 g/l NaCl system because the leached samples had lower pore fluid NaCl contents and this is consistent with the concept of apparent effect of the pore fluid salinity on the residual shear strength of clay minerals. However, if the residual shear strengths of the leached montmorillonite samples are divided by the corresponding true effective stresses (σ_n^*) of the samples, the resulting values of $\tan\phi_r'$ (denoted by open circles in Fig. 6.37) when plotted against the corresponding values of σ_n^* produces a plot, shown in Fig. 6.37, that practically coincides with the relationship between $\tan\phi_r'$ and σ_n' obtained for the same samples before leaching. This again illustrates the independence of the residual friction angle of montmorillonite on the pore fluid salinity. However, the $\tan\phi_r'$ versus σ_n^* plot, presented in Fig. 6.37, shows that this true residual friction angle of montmorillonite is highly dependent on the magnitude of the true effective stress in the low stress range. This variation in the true ϕ_r' (which is independent of the pore fluid salinity) with σ_n^* for montmorillonite is also probably due to the dependence of the area of true contact between the shear zone particles and their basal planes on the true effective stress.

The residual shear strength results obtained from the shear tests on the 1.15 g/l NaCl samples of montmorillonite (reported in

Table 6.5a) was also reinterpreted using the modified Coulomb-Terzaghi relationship for residual strength (Eqn. 3.23 b) written in terms of the true effective stress and the reinterpreted residual strength data for the montmorillonite - 1.15 g/l NaCl system is presented in Table 6.11. This reinterpreted residual strength data (Table 6.11) is also presented in forms of τ_{res} versus σ_n' and σ_n^* plots in Fig. 6.38 and $\tan\phi_r'$ versus σ_n' and σ_n^* plots in Fig. 6.39. Examination of these plots (i.e. Figs. 6.38 and 6.39) lends further credence to the concepts that residual shear strength of a clay mineral is governed by the true effective stress (σ_n^*) on the mineral basal planes and that every mineral possesses a stress dependent angle of friction (ϕ_r') which is independent of the pore fluid salinity. Hence, it can be said that the effect of changing the pore fluid salinity in an active clay-water system under a __constant apparent effective stress__ (σ_n') is to change the net (R-A) stress of the system thus causing a change in the true effective stress which brings about a change in the residual shear strength of the system. On the other hand, if the active clay-water system is held under a __constant true effective stress__ (σ_n^*), a change in the pore fluid salinity will not affect the residual shear strength of the system.

It is also interesting to note that the true residual friction angle of montmorillonite $(\phi_r' = 9.5°-11.5°)$ obtained from the analysis of the residual shear strengths of the montmorillonite samples before and after leaching is same as the ϕ_r' obtained from the conventional shear tests on the montmorillonite - 33.57 g/l NaCl samples (Figs. 6.36 and 6.37). Hence, it can be said that conventional shearing of a

clay mineral under highly saline pore fluid conditions yields the true ϕ_r' of the clay mineral which is independent of the pore fluid salinity but depends on the stress level.

6.5 Microstructural Investigations

Microstructural observations with a scanning electron microscope were made on the shear planes and the longitudinal sections (containing the shear zones) of the cut-plane samples from the following shear tests:

i)   Test No. K-0-14: Kaolinite - Distilled water: σ_n' = 79.14 psi

ii) Test No. M-34-2: Na-montmorillonite - 33.57 g/l NaCl: σ_n' = 5.00 psi

iii) Test No. A-41-2: Na-attapulgite - 40.95 g/l NaCl: σ_n' = 5.09 psi

Photomicrographs of the shear zones and the undeformed areas outside the shear zones in the three clay mineral samples were obtained by viewing perpendicular to the appropriate fractured surfaces and the photomicrographs thus obtained are presented in this section. The magnification is recorded on each photomicrograph. Pertinent structural features of the shear zones and the undeformed areas outside the shear zones are described from the photomicrographs and related to the basic deformation and shear strength generating mechanisms for the three clay minerals at large strains.

6.5.1 Undeformed areas outside the shear zones

The structural features of the undeformed areas outside the

shear zones in the kaolinite and the montmorillonite samples are illustrated in Figs. 6.40, 6.41, 6.48, 6.49 and 6.54. Since these photomicrographs were obtained by viewing perpendicular to the undeformed areas in the longitudinal sections, thicknesses of aggregated platy kaolinite particles are clearly distinguishable in Figs. 6.40 and 6.41.

Figs. 6.40 and 6.41 show that in the kaolinite sample which was prepared from a slurry and consolidated to 79.14 psi under which it was sheared, a near perfect parallel orientation of the platy particles perpendicular to the direction of consolidation was attained. The general structure of the undeformed areas in the kaolinite sample appears to be dispersed and highly oriented which is consistent with the fact that the sample was prepared in a distilled water environment and subsequently consolidated to a high normal effective pressure (79.14 psi) under which it was sheared.

Since the montmorillonite sample had a pore fluid salt content of 33.57 g/l NaCl, the undeformed areas in the montmorillonite sample were, in general, characterised by a porous flocculated structure (Figs. 6.48 and 6.49). In areas outside the shear zone, no general alignment pattern perpendicular to the direction of consolidation is observed in the photomicrographs (Figs. 6.48 and 6.49) of the longitudinal section of the montmorillonite sample which was consolidated to 20 psi and subsequently rebounded back to 5 psi before shear. This seems to suggest that for montmorillonite, a parallel orientation of the small platy particles is not usually achieved under low consolidation pressures.

The undeformed areas outside the shear zone in the attapulgite sample were generally characterised by a high degree of intermeshing of the needle shaped crystallites (Figs. 6.58 and 6.59). It appears from Figs. 6.58 and 6.59 that segregation and subsequent orientation of the intermeshed needles perpendicular to the direction of consolidation are rather difficult to achieve. The hay-stack like structure further suggests that montmorillonite-type swelling probably does not occur in attapulgite. A similar opinion regarding the swelling characteristics of attapulgite has been expressed by Haden (1963).

Figs. 6.50 and 6.51 clearly exhibit the solid contacts between aggregated particles in the kaolinite and the montmorillonite samples. In the case of attapulgite, the high degree of intermeshing of the needle shaped particles (Figs. 6.58 and 6.59) implies innumerable solid particle to particle contacts. These contacts are the only significant regions where effective normal and shear stresses can be transmitted. As stated earlier, this was stressed by Mitchell et al. (1969) and the microstructural evidences obtained here confirm their findings at particle level. Demonstration of this solid particle to particle contacts by microstructural observation establishes a very vital criterion on which the mechanisms of shearing and residual strength generation proposed in this thesis have been based. It must however be mentioned here that the solid contacts illustrated by Figs. 6.50 and 6.51 are probably contacts between aggregates of small particles and not between individual particles. The individual particles of montmorillonite are so small (1,000 Å x 10 Å thick) that they can

not be seen even under a very high magnification of 50,000 x (= 0.2 μm)

and loss of resolution at magnifications of 100,000 x (= 0.1 μm)

or more makes it unusually difficult to discern the structural features

attained by these exceptionally small particles. Aggregates of kaolinite

particles, on the other hand, are easily visible under magnifications

of 10,000-20,000 x (= 1-0.5 μm) because an individual particle of

kaolinite is much larger in size (10,000 Å x 1,000 Å thick). The

relatively large attapulgite needles (10,000 Å long x 100 Å across)

are also visible under magnifications of 10,000-20,000 x (= 1-0.5μm)

6.5.2 Shear zones

The representative structural features of the large displacement

shear zones in the clay mineral samples were obtained not only by viewing

the shear zones in the longitudinal sections but also by looking

straight down on the precut planes themselves under the microscope.

i) Shear plane sections

The shear plane in the kaolinite sample appears to be smooth

and slickensided and evidence of intense shearing is clearly visible

under a magnification of 200 x in Fig. 6.44. The view of the same

general area of the shear plane under a higher magnification of 20,000 x

(Fig. 6.45) reveals an almost horizontal orientation of the platy

kaolinite particles aligned in the direction of motion. The views

of the precut shear plane in the montmorillonite sample, obtained under

various magnifications, are presented in Figs. 6.56 and 6.57 and like

the kaolinite shear plane, the same feature of highly oriented aggregates

of platy particles (some of which may contain some particles of illite)

characterised the shear plane in the montmorillonite sample.

The photomicrographs of the shear plane in the attapulgite sample (Figs. 6.60 and 6.61) clearly illustrate the high degree of intermeshing of the attapulgite needles in the shear plane. The highly interwoven attapulgite needles were not segregated even at large strains. The aggregates show a hay-stack like structure (Fig. 6.61) in which the individual needles are arranged in a random fashion and seem to be incapable of relative motion. A general orientation of the needle shaped crystallites perpendicular to the direction of consolidation can,however,be observed in Fig. 6.61. Some evidence of shearing is discernible in Fig. 6.60.

ii) Longitudinal sections

Figs. 6.41, 6.42, 6.43, 6.52, 6.53 and 6.55 illustrate the shear induced structures in the large displacement shear zones in the kaolinite and the montmorillonite samples while Figs. 6.40 and 6.54 show the corresponding structures of the areas outside the shear zones in the same samples. These photomicrographs were obtained by viewing perpendicular to the shear zones as well as the undeformed areas outside the shear zones in the longitudinal sections.

It is immediately seen from Figs. 6.42 and 6.43 that at large strains, the structure of the shear zone in the kaolinite sample was distinctly characterised by close packing of aggregated kaolinite particles whose 001 basal planes were aligned at 50-55° to the direction of the principal displacement shear. The 001 basal planes

of the kaolinite particles in the densely packed shear zone structure also appear to be normal to the major principal stress in the shear box (Figs. 6.42 and 6.43). This characteristic structural arrangement observed in the residual state shear zone of the kaolinite sample bears a striking resemblance to the compression textures observed by Morgenstern and Tchalenko (1967 a, b) in the large displacement shear zones of landslides and cut-plane specimens of kaolinite sheared in the laboratory.

The structural features of the shear zone in the montmorillonite sample are presented in Figs. 6.52, 6.53 and 6.55. Unlike the kaolinite shear zone, the structural features of the montmorillonite shear zone are not so clearly distinguishable in Figs. 6.52 and 6.53 because of the very small size of the montmorillonite particles and the loss of resolution at high magnifications under which the views were photographed. However, general structural arrangements that resemble the features of compression texture are clearly discernible in the photomicrographs of the montmorillonite shear zone (Figs. 6.52, 6.53 and 6.55).

The oriented particle aggregates observed in the shear plane sections of the kaolinite and the montmorillonite specimens (Figs. 6.45 and 6.56) are believed to be thin bands of highly oriented particles (aligned in the direction of motion in the shear box) that enclose the compression textures in the shear zones. These highly oriented thin bands of particles enclosing the compression texture were also observed by Morgenstern and Tchalenko (1967 a, b) in the

large displacement shear zones of cut-plane specimens of kaolinite
sheared in the direct shear machine.

At the residual state, despite the formation of compression
texture in the shear zone, the original horizontal orientation of the
platy particles was still preserved in the undeformed areas of the
kaolinite sample (Fig. 6.40). The undeformed areas in the montmorillonite
sample also maintained its original loosely flocculated structure at
large strains (Figs. 6.48 and 6.54). Two interesting observations can
be made from a comparison between the structures of the residual state
shear zones and the undeformed areas in the kaolinite and the
montmorillonite samples and these observations tend to support the
displacement induced changes in the shear zone structures that were
speculated earlier from the shear test results. Firstly, in comparison
with the areas outside the shear zones, particles appear to be more
densely packed in the shear zones of the kaolinite and the montmorillonite
samples (for example, compare Fig. 6.40 with Fig. 6.42 and Fig. 6.54
with Fig. 6.53). The possible existence of a more closely packed
structure in the large displacement shear zones of the clay mineral
samples was inferred earlier from the failure plane water contents
which were found to be always less than the water contents of the
corresponding undeformed areas and the microstructural observations
show that this is indeed the case. Secondly, the phenomenon of
decreasing intensities of the reversal peaks with increasing horizontal
displacements in the shear tests on the kaolinite and the montmorillonite
samples (for example, see Figs. B-32 and B-93) was thought to be due
to a displacement induced physical rotation of the shear zone particles

from their "before shear" orientations to some final orientations at large strains where the particles will be steeply inclined to the direction of motion in the shear box. The comparison between the structures of the shear zones and the undeformed areas from Figs. 6.40, 6.42, 6.54 and 6.53 clearly lends credence to this speculation because if the initial structures that prevailed throughout the kaolinite and the montmorillonite samples before commencement of shear resembled the corresponding structures of the undeformed areas of the samples at large strains, then with increasing horizontal displacements during the shear tests the initially oriented platy particles in the shear zones had to rotate physically to attain the residual state structural arrangements (i.e. the compression textures) in which the particles were aligned at 50-55° to the direction of the principal displacement shears.

The observation of compression textures in the large displacement shear zones in the kaolinite and the montmorillonite samples confirms the findings of Morgenstern and Tchalenko (1967 a, b) at particle level. No explanation is yet available for the ultimate compression texture. As stated earlier, the closest analogy of this feature is with the observations by Bowden and Tabor (1964) on the attitude of graphite crystals in friction tests.

It was stated before that detailed examination of the development of compression textures in the large displacement shear zones in clays led Morgenstern and Tchalenko (1967 a, b) to suggest basal plane slip as the dominant mechanism of deformation in shear

induced structures at large strains. The particle level confirmation of the existence of compression textures in the large displacement shear zones in the clay mineral samples lends further support to the above mentioned mechanism of deformation at large strains. It can now be said that the resistance offered by the basal planes of the particle contacts in the compression texture against slippage at large strains indeed forms the basis of residual shear strength, or in other words, residual strength resides in solid friction along the basal planes of the shear zone particle contacts and the shearing resistance at large strains is due to the frictional property of the mineral basal planes.

Compression textures were, however, not observed in the residual state shear zone in the attapulgite sample (Figs. 6.62 and 6.63). It would then seem that compression textures can only develop in the large displacement shear zones in platy clay mineral samples (such as kaolinite, illite and montmorillonite) in which translational and rotational movements of the mineral particles are possible during shear. For a fibrous mineral such as attapulgite, the shear zone structure at large strain was characterised by a rather low angle orientation of the needle shaped particles that remained highly interwoven even at large strains (Figs. 6.62 and 6.63). Hence, besides shearing along stepped 110 cleavage planes at large strains, the intermeshing nature of the attapulgite needles (which were not segregated even at large strains) may be part of the reason for its high residual strength.

The particle reorientation phenomenon upon reversal of

cycles during a shear test was also investigated by microstructural observations on the shear zones in two samples of kaolinite that were both sheared under a normal stress of 70 psi. Both the samples were sheared along precut planes until the residual states were attained and shearing was terminated for the two samples on two opposite cycles i.e. shearing of one of the samples was stopped on a compression cycle while shearing of the other was terminated on the tension cycle. Longitudinal sections containing the shear zones were prepared from both the samples and Fig. 6.46 present the shear zone structure of the sample for which shearing was stopped on a compression cycle while Fig. 6.47 illustrates the shear zone structure of the sample for which shearing was terminated on a tension cycle. Examination of these two photomicrographs (i.e. Figs. 6.46 and 6.47) immediately reveals the physical reorientation of the mineral particles due to rotation of the slip plane upon reversal and it is believed that the work required to effect this physical reorientation of the shear zone particles is reflected in the strength peaks measured after each reversal. Figs. 6.46 and 6.47 also show well developed compression textures.

TABLE 6.1

FINAL SYSTEM CHEMISTRIES OF THE MINERAL BLOCK SAMPLES

Clay Mineral	Block No.	Water Content of the block, %	Pore Fluid Analysis				Na+ (me/100 gms of dry soil)	Adsorbed Cation Complex								
			NaCl (g/l)	CaCl2 (g/l)	MgCl2 (g/l)	KCl (g/l)		Ca++ (me/100 g)	Mg++ (me/100 g)	K+ (me/100 g)	Total (me/100 g.)	% Na	% Ca	% Mg	% K
ATTAPULGITE	1	220.0 to 225.0	0.02	0.004	0.060	-	21.32	1.80	3.08	-	26.20	81.40	6.80	11.80	-
	2	200.0 to 205.0	2.42	0.010	0.140	-	22.55	0.50	2.00	-	25.05	90.00	2.00	8.00	-
	3	210.0 to 215.0	40.95	0.023	0.310	-	24.80	0.0	0.32	-	25.12	98.70	0	1.30	-
MONTMORILLONITE	1	330.0 to 350.0	1.15	0.005	0.004	0.001	72.34	15.32	0.53	0.11	88.30	81.93	17.35	0.60	0.12
	2	430.0 to 450.0	15.26	0.49	0.080	0.001	74.57	12.02	0.85	0.11	87.55	85.18	13.73	0.97	0.12
	3	240.0 to 260.0	33.57	0.31	0.040	0.001	78.72	7.34	0.96	0.11	87.13	90.35	8.42	1.10	0.13

TABLE 6.2

CONSOLIDATION CHARACTERISTICS OF THE PURE CLAY MINERALS

Mineral	Pore fluid NaCl Content (gms./litre)	Average Coefficient of Consolidation, c_v					Average Compression Index $C_c = \frac{de}{d(\log P)}$ (in.²/lb.)	Rate of Secondary Compression[2] $C_t = \frac{\Delta H/H}{\Delta \log_{10} t}$
		From large cell consolidation tests, average pressure range = 0 to 1.25 psf			From consolidation phase in the direct shear tests, average consolidation. Pressure range = 1.25 to 80.00 psi			
		Initial Water Content, (%)	Liquidity Index	c_v (ft.²/yr.)	Range of initial water contents (%)	c_v (ft.²/yr.)		
Kaolinite	0.00	-	-	-	60.0-105.0	25.50	0.40	-
	2.00	-	-	-	60.0-105.0	24.30	0.37	
	35.00	-	-	-	60.0-105.0	26.60	0.37	0.029
Na-Attapulgite	0.01	430.0	1.64	1.37	220.0-225.0	12.03	1.56	
	2.42	383.0	1.52	3.25	200.0-205.0	23.00	1.31	
	40.95	415.0	2.21	7.06	210.0-215.0	25.00	1.24	0.029
Na-Montmorillonite	1.15	830.0	1.41	0.46	330.0-350.0	0.38	5.85	
	15.26	850.0	3.66	3.16	430.0-450.0	1.10	3.0 to 5.1[1]	
	33.57	815.0	7.76	2.17	240.0-280.0	3.20	2.7 to 5.1	0.052

[1] The compression index of montmorillonite is highly dependent on pressure range.

[2] Typical value for rate of secondary compression (C_t) for very plastic and organic soils: 0.03 or higher (Ladd, 1967).

TABLE 6.3a

RESULTS OF REVERSAL SHEAR TESTS ON KAOLINITE-DISTILLED WATER SAMPLES

Test No.	Effective normal pressure (σ_n'), psi	$[\frac{1}{\sigma_n'\gamma}]^{1/3}$	Initial water content, %	Initial void ratio (e_0)	Overconsolidation ratio	Sample thickness before shear, ins.	Type of test	Rate of displacement, inches/minute	Peak shear strength (τ_{peak}), psi	Maximum shear stress recorded in the first cycle of shear in a cut-plane test (τ_{max}), psi	Residual shear strength (τ_{res}), psi	Percentage drop in shear strength from τ_{peak} or τ_{max} to τ_{res}	$\tan\phi_r' = \frac{\tau_{res}}{\sigma_n'}$	Residual friction angle (ϕ_r') in degrees	After shear water content, % Failure plane	After shear water content, % Outside failure plane	Total horizontal displacement, ins. To τ_{peak} or τ_{max}	Total horizontal displacement, ins. To τ_{res}
K-0-1	5.00	0.585	71.90	1.92	1.00	1.48	cut-plane	0.0024	-	2.24	2.04	8.76	0.410	22°20'	48.72	53.69	0.250	2.0
K-0-2	9.95	0.465	71.10	1.91	1.00	1.37	cut-plane	0.0024	-	5.00	4.35	13.00	0.437	23°40'	44.96	49.30	0.430	2.0
K-0-3	10.25	0.461	104.90	2.86	1.00	1.00	cut-plane	0.0019	-	5.14	3.75	26.93	0.366	20°	46.65	51.37	0.093	2.0
K-0-4	10.25	0.461	104.70	2.76	1.00	1.00	cut-plane	0.0019	-	5.01	3.75	25.01	0.366	20°	-	50.90	0.120	2.0
K-0-5	14.97	0.406	81.05	2.17	1.00	1.27	cut-plane	0.0019	-	7.18	4.28	40.39	0.286	16°	42.96	47.64	0.113	5.0
K-0-6	14.97	0.406	81.37	2.13	1.00	1.27	cut-plane	0.0019	-	6.78	4.28	36.89	0.286	16°	42.39	47.50	0.114	4.6
K-0-7	15.24	0.403	63.57	1.66	1.00	1.36	cut-plane	0.0024	-	5.14	4.48	12.84	0.294	16°30'	41.59	45.54	0.193	2.6
K-0-8	20.18	0.367	63.65	1.63	1.00	1.37	cut-plane	0.0024	-	7.74	5.70	26.34	0.283	15°50'	41.35	45.23	0.114	2.8
K-0-9	31.41	0.317	66.61	1.63	1.00	1.22	cut-plane	0.0019	-	12.12	8.37	30.93	0.267	15°	41.70	44.17	0.093	2.7
K-0-10	40.00	0.292	66.06	1.65	1.00	1.19	cut-plane	0.0019	-	12.91	8.39	35.03	0.210	12°	38.95	42.47	0.069	2.7
K-0-11	40.48	0.291	60.85	1.73	1.00	1.21	cut-plane	0.0019	-	13.04	9.86	24.42	0.244	13°40'	40.94	42.36	0.069	2.7
K-0-12	52.94	0.266	61.65	1.91	1.00	1.20	cut-plane	0.0019	-	15.14	12.76	15.70	0.241	13°35'	39.56	41.54	0.054	2.3
K-0-13	56.78	0.260	61.23	1.91	1.00	1.34	cut-plane	0.0024	-	14.55	12.96	10.98	0.228	12°50'	37.85	40.26	0.061	2.8
K-0-14	79.14	0.233	60.67	1.77	1.00	1.26	cut-plane	0.0024	-	22.91	16.85	26.46	0.213	12°	35.92	37.66	0.063	2.6

TABLE 6.3b

RESULTS OF REVERSAL SHEAR TESTS ON KAOLINITE-2 g/l NaCl SAMPLES

Test No.	Effective normal pressure (σ_n'), psi	$\left(\frac{\sigma_n}{\sigma_1}\right)^{1/3}$	Initial water content, %	Initial void ratio (e_o)	Overconsolidation ratio	Sample thickness before shear, ins.	Type of test	Rate of displacement, inches/minute	Peak shear strength (τ_{peak}), psi	Maximum shear stress recorded in the first cycle of shear in a cut-plane test (τ_{max}), psi	Residual shear strength (τ_{res}), psi	Percentage drop in shear strength from τ_{peak} or τ_{max} to τ_{res}	$\tan\phi_r' = \frac{\tau_{res}}{\sigma_n}$	Residual friction angle (ϕ_r') in degrees	After shear water content, % Failure plane	After shear water content, % Outside failure plane	Total Horizontal displacement, ins. To τ_{peak} or τ_{max}	Total Horizontal displacement, ins. To τ_{res}
K-2-1	5.08	0.582	64.01	1.76	1.00	1.36	cut-plane	0.0024	-	2.80	2.55	8.92	0.501	26°40'	44.81	49.24	0.333	3.7
K-2-2	10.06	0.463	64.25	1.78	1.00	1.27	cut-plane	0.0024	-	4.58	4.32	5.72	0.429	23°10'	42.75	46.00	0.166	3.6
K-2-3	14.37	0.411	63.82	1.75	1.00	1.27	cut-plane	0.0019	-	7.62	5.50	27.83	0.383	21°	43.60	45.33	0.145	3.4
K-2-4	20.16	0.367	63.36	1.74	1.00	1.24	cut-plane	0.0019	-	8.46	6.05	28.55	0.300	16°40'	39.82	43.81	0.119	2.9
K-2-5	30.63	0.320	63.80	1.77	1.00	1.19	cut-plane	0.0024	-	12.09	6.21	48.64	0.203	11°30'	38.45	42.44	0.083	3.6
K-2-6	40.12	0.292	63.98	1.78	1.00	1.14	cut-plane	0.0024	-	11.65	8.53	26.78	0.213	12°	37.56	40.58	0.071	2.0
K-2-7	50.48	0.271	63.84	1.78	1.00	1.17	cut-plane	0.0019	-	15.71	14.19	9.71	0.281	15°40'	38.94	42.06	0.074	2.3
K-2-8	60.24	0.255	63.75	1.81	1.00	1.14	cut-plane	0.0019	-	16.86	12.62	25.18	0.210	12°	36.71	39.93	0.064	2.3
K-2-9	70.94	0.242	63.83	1.75	1.00	1.12	cut-plane	0.0019	-	19.08	14.79	22.53	0.208	11°50'	35.31	38.24	0.045	2.5
K-2-10	80.88	0.231	63.46	1.77	1.00	1.11	cut-plane	0.0019	-	28.78	16.85	41.47	0.208	11°50'	35.40	37.91	0.066	2.1

TABLE 6.3c

RESULTS OF REVERSAL SHEAR TESTS ON KAOLINITE-35 g/l NaCl SAMPLES

Test No.	Effective normal pressure (σ_n'), psi	$\frac{1}{(\sigma_n)^{1/3}}$	Initial water content, %	Initial void ratio (e_o)	Overconsolidation ratio	Sample thickness before shear, ins.	Type of test	Rate of displacement, inches/minute	Peak shear strength (τ_{peak}), psi	Maximum shear stress recorded in the first cycle of shear in a cut-plane test (τ_{max}), psi	Residual shear strength (τ_{res}), psi	Percentage drop in shear strength from τ_{peak} or τ_{max} to τ_{res}	$\tan\phi_r' = \frac{\tau_{res}}{\sigma_n}$	Residual friction angle (ϕ_r') in degrees	After shear water content, % Failure plane	After shear water content, % Outside failure plane	Total Horizontal displacement, ins. To τ_{peak} or τ_{max}	Total Horizontal displacement, ins. To τ_{res}
K-35-1	5.06	0.583	61.72	1.74	1.00	1.33	cut-plane	0.0024	-	2.61	2.10	19.52	0.415	22°30'	44.57	47.67	0.224	7.8
K-35-2	10.08	0.463	61.63	1.74	1.00	1.28	cut-plane	0.0024	-	4.76	4.43	6.96	0.439	23°40'	41.95	44.97	0.127	2.7
K-35-3	15.21	0.404	61.32	1.74	1.00	1.23	cut-plane	0.0024	-	5.79	4.84	16.43	0.318	17°40'	-	-	0.125	3.1
K-35-4	20.66	0.364	59.48	1.67	1.00	1.13	cut-plane	0.0024	-	8.59	5.48	36.16	0.265	14°50'	-	-	0.147	2.9
K-35-5	30.42	0.320	61.41	1.73	1.00	1.19	cut-plane	0.0019	-	10.79	6.81	36.88	0.224	12°40'	38.33	40.90	0.100	2.6
K-35-6	40.84	0.290	61.95	1.74	1.00	1.16	cut-plane	0.0019	-	13.67	10.13	25.95	0.248	14°	38.20	40.55	0.078	2.5
K-35-7	51.04	0.270	59.15	1.68	1.00	0.98	cut-plane	0.0024	-	14.43	10.12	29.86	0.198	11°10'	37.52	39.70	0.052	2.4
K-35-8	60.22	0.255	61.52	1.71	1.00	1.01	cut-plane	0.0019	-	16.66	12.62	24.26	0.210	12°	-	-	0.053	2.0
K-35-9	72.63	0.240	59.76	1.74	1.00	0.99	cut-plane	0.0024	-	23.67	16.43	31.14	0.226	12°40'	36.73	38.31	0.072	1.8
K-35-10	80.36	0.232	58.94	1.66	1.00	1.00	cut-plane	0.0019	-	25.16	19.69	21.74	0.245	13°50'	-	-	0.050	2.4

TABLE 6.4a

RESULTS OF REVERSAL SHEAR TESTS ON Ka-ATTAPULGITE-0.02 g/l NaCl SAMPLES

Test No.	Effective normal pressure (σ_n'), psi	$\frac{I}{(\sigma_n'T)^{1/3}}$	Initial water content, %	Initial void ratio (e_0)	Overconsolidation ratio	Sample thickness before shear, ins.	Type of test	Rate of displacement, inches/minute	Peak shear strength (τ_{peak}), psi	Maximum shear stress recorded in the first cycle of shear in a cut-plane test (τ_{max}), psi	Residual shear strength (τ_{res}), psi	Percentage drop in shear strength from τ_{peak} or τ_{max} to τ_{res}	$\tan\phi_r' = \frac{\tau_{res}}{\sigma_n'}$	Residual friction angle (ϕ_r') in degrees	After shear water content, % Failure plane	After shear water content, % Outside failure plane	Total Horizontal displacement, ins. To τ_{peak} or τ_{max}	Total Horizontal displacement, ins. To τ_{res}
A-0-1	5.28	0.574	-	-	3.97	1.85	conventional	0.0001	4.66	-	3.81	18.33	0.722	35°56'	122.06	138.50	0.059	1.2
A-0-2	8.76	0.485	209.60	4.93	4.83	1.80	cut-plane	0.0019	-	6.20	5.78	6.78	0.660	33°30'	-	-	0.104	1.0
A-0-3	10.55	0.456	-	-	4.02	1.55	cut-plane	0.0024	-	6.54	6.17	5.60	0.585	30°20'	110.07	123.10	0.065	0.5
A-0-4	16.70	0.391	209.60	4.93	3.77	1.65	cut-plane	0.00048	-	10.30	10.03	2.70	0.600	31°	100.0	116.58	0.133	3.0
A-0-5	23.24	0.351	211.34	4.99	3.45	1.42	cut-plane	0.012	-	14.70	13.67	7.00	0.588	30°30'	94.23	108.60	0.079	2.5
A-0-6	30.87	0.319	209.6	4.93	3.13	1.36	cut-plane	0.012	-	18.65	17.86	4.23	0.579	30°05'	83.87	98.14	0.085	0.4
A-0-7	40.97	0.290	-	-	2.63	1.56	cut-plane	0.0096	-	25.20	23.78	4.10	0.580	30°10'	87.85	93.18	0.36	1.65
A-0-8	41.93	0.288	209.6	4.93	4.07	1.46	conventional	0.0001	26.68	-	24.45	8.36	0.583	30°20'	65.75	93.25	0.147	2.3
A-0-9	52.22	0.268	209.6	4.93	4.13	1.43	conventional	0.0001	31.75	-	29.94	5.72	0.573	29°50'	-	-	0.174	2.4
A-0-10	15.24	0.403	211.34	4.99	1.00	1.48	cut-plane	0.0003	-	-	8.99	-	0.590	30°30'	-	-	-	1.0
A-0-11	34.77	0.306	209.6	4.93	3.83	1.50	cut-plane	0.00048	-	-	20.16	-	0.580	30°10'	-	97.66	-	1.3
A-0-12	60.83	0.231	211.34	4.99	1.00	1.32	cut-plane	0.0019	-	-	46.39	-	0.574	30°	-	-	-	0.55

Stress-displacement plots for Test Nos. A-0-10, A-0-11 and A-0-12 are not presented in Appendix B.

TABLE 6.4b

RESULTS OF REVERSAL SHEAR TESTS ON Na-ATTAPULGITE-2.42 g/l NaCl SAMPLES

Test No.	Effective normal pressure (σ_n'), psi	$\frac{1}{(\sigma_n'\gamma)^{1/3}}$	Initial water content, %	Initial void ratio (e_o)	Overconsolidation ratio	Sample thickness before shear, ins.	Type of test	Rate of displacement, inches/minute	Peak shear strength (τ_{peak}), psi	Maximum shear stress recorded in the first cycle of shear in a cut-plane test (τ_{max}), psi	Residual shear strength (τ_{res}), psi	Percentage drop in shear strength from τ_{peak} or τ_{max} to τ_{res}	$\tan\phi_r' = \frac{\tau_{res}}{\sigma_n'}$	Residual friction angle (ϕ_r') in degrees	After shear water content, % Failure plane	After shear water content, % Outside failure plane	Total Horizontal displacement, ins. To τ_{peak} or τ_{max}	Total Horizontal displacement, ins. To τ_{res}
A-2-1	3.56	0.655	197.32	4.66	11.59	1.33	cut-plane	0.0019	-	3.83	2.68	30.00	0.753	37°	120.06	127.26	0.025	1.9
A-2-2	5.01	0.584	197.32	4.66	8.18	1.35	cut-plane	0.0024	-	5.73	4.13	27.93	0.824	39°30'	118.96	121.81	0.085	1.75
A-2-3	7.68	0.507	191.45	4.58	8.01	1.28	conventional	0.0001	8.33	-	6.05	27.36	0.787	38°10'	119.96	122.65	0.091	2.0
A-2-4	10.57	0.456	197.32	4.66	3.88	1.38	cut-plane	0.0024	-	7.36	6.87	6.65	0.650	33°	108.73	119.45	0.091	1.25
A-2-5	14.97	0.406	191.45	4.58	4.48	1.27	conventional	0.0001	10.64	-	8.82	17.10	0.589	30°30'	-	109.95	0.055	1.30
A-2-6	20.57	0.365	197.32	4.66	5.93	1.72	conventional	0.0001	14.76	-	12.46	15.60	0.606	31°10'	95.42	103.35	0.049	2.3
A-2-7	25.05	0.342	191.45	4.58	6.53	1.10	conventional	0.0001	17.44	-	14.57	16.46	0.582	30°10'	100.20	100.40	0.046	1.8
A-2-8	30.63	0.320	191.45	4.58	5.62	1.11	cut-plane	0.0024	-	19.40	17.40	10.30	0.568	29°40'	95.98	98.51	0.086	1.6
A-2-9	41.06	0.290	197.32	4.66	4.09	1.60	cut-plane	0.0024	-	25.00	24.07	3.72	0.586	30°20'	83.61	92.76	0.142	1.5
A-2-10	55.22	0.263	191.45	4.58	4.11	1.42	cut-plane	0.0024	-	33.32	32.31	3.04	0.585	30°20'	89.05	92.59	0.087	1.0

TABLE 6.4c

RESULTS OF REVERSAL SHEAR TESTS ON Na-ATTAPULGITE-40.95 g/l NaCl SAMPLES

Test No.	Effective normal pressure (σ_n'), psi	$\frac{1}{(\sigma_n')^{1/3}}$	Initial water content, %	Initial void ratio (e_0)	Overconsolidation ratio	Sample thickness before shear, ins.	Type of test	Rate of displacement, inches/minute	Peak shear strength (τ_{peak}), psi	Maximum shear stress recorded in the first cycle of shear in a cut-plane test (τ_{max}), psi	Residual shear strength (τ_{res}), psi	Percentage drop in shear strength from τ_{peak} or τ_{max} to τ_{res}	$\tan\phi_r' = \frac{\tau_{res}}{\sigma_n'}$	Residual friction angle (ϕ_r') in degrees	After shear water content, % Failure plane	After shear water content, % Outside failure plane	Total Horizontal displacement, ins. To τ_{peak} or τ_{max}	Total Horizontal displacement, ins. To τ_{res}
A-41-1	2.59	0.728	188.78	4.51	7.88	1.42	cut-plane	0.0024	-	3.20	1.80	43.75	0.694	34°50'	121.45	122.43	0.025	2.2
A-41-2	5.09	0.582	166.76	4.51	4.01	1.60	conventional	0.0001	5.45	-	3.32	39.10	0.653	33°10'	114.47	118.74	0.059	2.0
A-41-3	7.51	0.511	188.78	4.51	5.45	1.29	cut-plane	0.0024	-	6.79	4.80	29.36	0.639	32°30'	100.82	108.16	0.081	1.6
A-41-4	10.03	0.464	188.78	4.51	4.07	1.25	cut-plane	0.0019	-	9.18	7.65	16.65	0.763	37°20'	95.49	102.39	0.091	2.0
A-41-5	15.28	0.403	188.78	4.51	3.51	1.18	conventional	0.0001	14.48	-	8.79	39.28	0.576	30°	94.52	95.18	0.172	1.4
A-41-6	20.57	0.365	188.78	4.51	4.90	1.08	cut-plane	0.0019	-	14.05	12.01	14.50	0.584	30°20'	96.35	99.31	0.058	1.9
A-41-7	25.15	0.341	188.78	4.51	4.01	1.03	cut-plane	0.0024	-	18.65	15.02	19.53	0.597	30°50'	84.75	94.15	0.154	0.8
A-41-8	30.02	0.322	188.78	4.51	5.88	1.04	conventional	0.0001	20.48	-	17.42	14.96	0.580	30°10'	87.45	93.59	0.103	2.4
A-41-9	40.13	0.292	188.78	4.51	4.36	1.36	conventional	0.0001	25.51	-	21.89	14.20	0.545	28°40'	85.17	90.11	0.130	3.0
A-41-10	50.12	0.271	188.78	4.51	4.20	1.29	cut-plane	0.0024	-	30.25	29.46	2.62	0.588	30°30'	84.47	87.49	0.169	1.0

TABLE 6.5a

RESULTS OF REVERSAL SHEAR TESTS ON Na-MONTMORILLONITE-1.15 g/1 NaCl SAMPLES

Test No.	Effective normal pressure (σ_n'), psi	$\frac{1}{(\frac{\sigma_n'}{1})^{1/3}}$	Initial water content, %	Initial void ratio (e_0)	Overconsolidation ratio	Sample thickness before shear, ins.	Type of test	Rate of displacement, inches/minute	Peak shear strength (τ_{peak}), psi	Maximum shear stress recorded in the first cycle of shear in a cut-plane test (τ_{max}), psi	Residual shear strength (τ_{res}), psi	Percentage drop in shear strength from τ_{peak} or τ_{max} to τ_{res}	$\tan\phi_r' = \frac{\tau_{res}}{\sigma_n}$	Residual friction angle (ϕ_r') in degrees	After shear water content, % Failure plane	After shear water content, % Outside failure plane	Total horizontal displacement, ins. To τ_{peak} or τ_{max}	Total horizontal displacement, ins. To τ_{res}
M-1-1	2.58	0.730	332.0	9.13	3.94	1.38	cut-plane	0.0024	-	1.17	0.91	22.32	0.354	19°30'	-	-	0.014	2.5
M-1-2	4.99	0.585	334.42	9.20	1.00	1.36	cut-plane	0.0024	-	1.08	0.82	24.31	0.164	9°20'	-	-	0.028	1.7
M-1-3	10.12	0.462	337.28	9.28	1.00	1.42	cut-plane	0.0024	-	1.98	1.18	40.31	0.117	6°40'	270.05	270.77	0.025	2.3
M-1-4	15.12	0.404	332.1	9.13	1.00	1.32	cut-plane	0.0024	-	1.80	1.57	12.80	0.104	6°	240.11	241.12	0.025	1.5
M-1-5	19.99	0.368	342.15	9.41	1.00	0.60	cut-plane	0.0019	-	2.43	2.02	16.85	0.101	5°50'	228.11	230.20	0.074	0.9
M-1-6	40.65	0.291	331.84	9.13	1.00	0.94	cut-plane	0.0019	-	4.69	3.60	23.20	0.089	5°05'	178.40	179.52	0.042	2.2
M-1-7	65.78	0.248	331.20	9.11	1.00	1.07	cut-plane	0.0019	-	6.41	5.60	12.50	0.085	4°50'	150.19	151.41	0.051	2.5

TABLE 6.5b

RESULTS OF REVERSAL TESTS ON Na-MONTMORILLONITE-15.26 g/l NaCl SAMPLES

Test No.	Effective normal pressure (σ_n'), psi	$\frac{1}{3}(\sigma_n')$	Initial water content, %	Initial void ratio (e_0)	Overconsolidation ratio	Sample thickness before shear, ins.	Type of test	Rate of displacement, inches/minute	Peak shear strength (τ_{peak}), psi	Maximum shear stress recorded in the first cycle of shear in a cut-plane test (τ_{max}), psi	Residual shear strength (τ_{res}), psi	Percentage drop in shear strength from τ_{peak} or τ_{max} to τ_{res}	$\tan\phi_r' = \frac{\tau_{res}}{\sigma_n'}$	Residual friction angle (ϕ_r) in degrees	After shear water content, %		Total Horizontal displacement, ins.	
															Failure plane	Outside failure plane	To τ_{peak} or τ_{max}	To τ_{res}
M-15-1	5.08	0.582	422.36	11.61	4.01	1.52	cut-plane	0.0019	-	1.43	1.09	23.78	0.215	12°10'	177.51	133.56	0.026	1.0
M-15-2	14.93	0.406	407.82	11.22	2.75	1.41	cut-plane	0.0024	-	3.57	2.84	20.38	0.190	11°	129.86	135.65	0.065	1.9
M-15-3	25.06	0.342	416.35	11.45	3.25	1.32	cut-plane	0.0019	-	4.77	4.43	7.12	0.177	10°	94.15	103.56	0.059	0.8
M-15-4	30.46	0.320	431.59	11.87	2.63	1.01	cut-plane	0.0024	-	8.32	7.00	15.85	0.230	13°	84.60	78.54	0.036	2.5
M-15-5	50.80	0.270	431.59	11.87	1.60	0.82	cut-plane	0.0019	-	9.60	7.68	20.00	0.151	8°40'	80.05	72.93	0.048	1.5
M-15-6	71.18	0.241	445.51	12.25	2.29	0.71	cut-plane	0.0019	-	14.10	10.90	22.68	0.153	8°40'	70.20	63.94	0.037	1.2

250

TABLE 6.5c

RESULTS OF REVERSAL SHEAR TESTS ON Na-MONTMORILLONITE-33.57 g/l NaCl SAMPLES

Test No.	Effective normal pressure (σ_n'), psi	$(\frac{\sigma_n'}{l})^{1/3}$	Initial water content, %	Initial void ratio (e_o)	Overconsolidation ratio	Sample thickness before shear, ins.	Type of test	Rate of displacement, inches/minute	Peak shear strength (τ_{peak}), psi	Maximum shear stress recorded in the first cycle of shear in a cut-plane test (τ_{max}), psi	Residual shear strength (τ_{res}), psi	Percentage drop in shear strength from τ_{peak} or τ_{max} to τ_{res}	$\tan\phi_r' = \frac{\tau_{res}}{\sigma_n'}$	Residual friction angle (ϕ_r') in degrees	After shear water content, % Failure plane	Outside failure plane	Total Horizontal displacement, ins. To τ_{peak} or τ_{max}	To τ_{res}
M-34-1	2.50	0.737	275.62	7.58	3.50	0.50	cut-plane	0.0019	-	1.58	0.82	47.82	0.330	18°	-	-	0.014	0.5
M-34-2	5.00	0.595	237.58	6.53	6.08	0.59	cut-plane	0.0024	-	2.40	1.60	33.30	0.320	17°40'	-	-	0.015	0.5
M-34-3	7.49	0.511	267.62	7.36	3.33	0.60	cut-plane	0.0019	-	3.11	2.20	29.2	0.290	16°20'	-	-	0.017	>2.0
M-34-4	10.00	0.464	275.06	7.56	9.04	0.62	cut-plane	0.0024	-	4.17	2.54	39.08	0.250	14°15'	-	-	0.012	3.0
M-34-5	15.01	0.405	256.26	7.05	10.23	0.58	cut-plane	0.0024	-	5.31	3.54	33.33	0.240	13°20'	-	-	0.013	>2.8
M-34-6	30.13	0.321	228.58	6.29	5.08	0.77	cut-plane	0.0019	-	8.03	5.90	26.51	0.196	11°05'	60.55	60.98	0.010	1.8
M-34-7	40.53	0.291	228.58	6.29	3.75	0.99	cut-plane	0.0019	-	10.50	7.53	28.29	0.186	10°30'	59.92	60.14	0.012	>3.2
M-34-8	60.70	0.255	228.58	6.29	2.68	0.82	cut-plane	0.0024	-	14.25	10.74	24.65	0.177	10°05'	55.99	57.14	0.020	3.0
M-34-9	79.95	0.232	228.58	6.29	2.06	0.73	cut-plane	0.0024	-	15.80	12.42	21.40	0.155	8°50'	53.49	54.93	0.026	3.0

TABLE 6.6

RESULTS OF THE SEEPAGE PRESSURE STUDY UNDERTAKEN IN THE LEACHING TESTS

Test No.	Sample Thickness l (ins.)	Void Ratio (e)	Initial effective stress of the sample under a pore fluid NaCl content of 33.57 g/l. $\sigma_a' = \sigma_a°$ (psi)	Head of salt solution applied at the bottom of the sample, H (ft.)	Average hydraulic gradient, i = H/l	Pressure imposed at the bottom of the sample due to the head applied at the base, $Y_w H$ (psi)	Steady state seepage pressure predicted at the top of the sample, $Y_w H/2$ (psi)	Steady state seepage pressure measured at the top of the sample (psi)	Coefficient of permeability k (cms./sec.)
L-1	0.50	6.63	2.50	3.50	84	1.52	0.76	1.24	1.15×10^{-8}
L-2	0.54	3.88	5.00	8.80	179	3.82	1.91	1.75	-
L-3	0.60	5.27	7.49	9.63	193	4.18	2.09	2.25	5.45×10^{-9}
L-4	0.62	4.20	10.00	9.63	186	4.18	2.09	2.02	2.17×10^{-9}
L-5	0.58	3.01	15.01	9.63	199	4.18	2.09	2.30	1.69×10^{-9}

TABLE 6.7

DATA ON SALT REMOVAL AND CIRCULATION OF LEACHATE IN THE CONSTANT VOLUME LEACHING TESTS

Leaching test No.	Sample thickness, inches	Cross-sectional area of the sample (in²)	(cm²)	Total volume of the sample (in³)	(cm³)	Average water content of the sample (%)	Void ratio of the sample, e	Porosity of the sample, n = e/(1+e)	(a) Total volume of voids in the sample before leaching, c.c. = volume of salt solution held by the pore spaces of the sample	Concentration of NaCl in the pore fluid of the sample before leaching, gms./litre	(b) Estimated total quantity of NaCl held by the pore spaces of the sample before leaching, gms.	Porosity of the carborundum porous stones used in the leaching cells, %	(c) Total quantity of salt solution initially held by the three porous stones in each leaching cell, c.c.	(d) Corresponding quantity of NaCl initially trapped in the three porous stones, gms.	Estimated total quantity of salt solution to be removed from each system, c.c. = (a) + (c)	(e) Measured quantity of distilled water circulated through the sample during the entire leaching test, c.c.	Percentage of saline pore fluid removed by upward flow alone = (e)/((a)+(c)) x 100 %	Estimated total quantity of NaCl present in each system before leaching, gms. = (b) + (d)	Total quantity of NaCl actually removed from each system, gms.
L-1	0.50	5.543	35.76	2.78	45.62	233.98	6.43	86.55	39.48	33.57	1.325	37.2	25.35	0.851	64.83	67.60	104.58	2.176	3.950
L-2	0.59	5.552	35.82	3.31	54.18	141.06	3.88	79.50	43.07	33.57	1.446	37.2	25.35	0.851	68.42	-	-	2.297	-
L-3	0.60	5.552	35.82	3.36	54.98	191.52	5.27	84.04	46.21	33.57	1.551	37.2	25.35	0.851	71.56	49.75	69.52	2.402	4.042
L-4	0.62	5.543	35.76	3.44	56.34	152.74	4.20	80.77	45.50	33.57	1.528	37.2	25.35	0.851	70.85	37.50	52.93	2.379	3.430
L-5	0.58	5.543	35.76	3.20	52.45	109.37	3.01	75.05	39.36	33.57	1.321	37.2	25.35	0.851	64.71	42.20	65.21	2.172	2.514

TABLE 6.8

CATION ANALYSIS OF SAMPLES OF PORE WATER EXTRACTED FROM THE LEACHED MONTMORILLONITE SAMPLES

Leaching test No.	Concentration of NaCl in the pore water of the sample before leaching, gms./litre	Concentration of various cations in the pore water of the sample after leaching, ppm.				Estimated concentration of the chloride forms of the cations in the pore water of the sample after leaching, gms./litre			
		Na^+	K^+	Ca^{++}	Mg^{++}	NaCl	KCl	$CaCl_2$	$MgCl_2$
L-1	33.57	87.00	0.50	0.00	0.14	0.22	.	.	.
L-2	33.57	33.00	0.37	0.00	0.00	0.08	.	.	.
L-3	33.57	33.00	0.37	0.00	0.00	0.08	.	.	.
L-4	33.57	70.00	0.55	0.00	0.00	0.18	.	.	.
L-5	33.57	33.00	0.33	0.00	0.00	0.08	.	.	.

TABLE 6.9

RESULTS OBTAINED FROM THE CONSTANT VOLUME LEACHING TESTS ON THE Na-MONTMORILLONITE SAMPLES

Leaching test No.	Sample thickness, inches	Apparent effective stress of the sample before leaching, σ_{n_0}, psi	True effective stress of the sample before leaching, σ_{n_0}, psi	Concentration of NaCl in the pore fluid of the sample before leaching, gms./litre	Total specific surface of the mineral, m^2/gm.	Water content distribution in the sample after leaching, %			Pore fluid NaCl content of the sample after leaching, gms./litre	Estimated* $P_y = (R-A)$ kg./cm^2	Measured net (R-A) stress, kg/cm^2	Percentage difference	True effective stress of the sample after leaching, σ_{n_2}, psi	Apparent effective stress of the sample after leaching, σ_{n_2}, psi	Percentage increase in the apparent effective stress of the sample due to leaching under constant overall volume conditions
						Top half of the sample	Failure plane	Bottom half of the sample							
L-1	0.50	2.50	2.50	33.57	641.0	218.92	232.31	250.71	0.22	1.31	1.38	+5.34%	2.50	22.13	785.20%
L-2	0.59	5.00	5.00	33.57	641.0	-	141.06	-	0.08	3.59	3.16	-12.05%	5.00	49.94	898.80%
L-3	0.60	7.49	7.49	33.57	641.0	-	190.52	192.51	0.08	2.07	2.06	-0.48%	7.49	36.77	390.90%
L-4	0.62	10.00	10.00	33.57	641.0	143.79	148.59	165.83	0.18	3.20	3.23	+0.81%	10.00	55.89	458.90%
L-5	0.58	15.01	15.01	33.57	641.0	107.79	110.95	-	0.08	5.46	3.61 ↓ 2.61	Note: Extrusion around the top porous stone	15.01	52.07	246.93%

*$P_y = (R-A)$ is estimated from the double-layer repulsive stress equation which is given by $P_y = 2 C_0 R T (\cosh y_c - 1)$

TABLE 6.10

COMPARISON BETWEEN THE RESIDUAL SHEAR STRENGTHS OF THE Na-MONTMORILLONITE SAMPLES BEFORE AND AFTER CONSTANT VOLUME LEACHING

Shear test No. (After leaching)	Shear test No. (Before leaching)	Apparent effective stress of the sample before leaching, σ_{n_1}, psi	Apparent effective stress of the sample after leaching, σ_{n_2}, psi	Percentage increase in the apparent effective stress of the sample due to constant volume leaching	True effective stress of the sample before leaching, σ_{n_1}, psi	True effective stress of the sample after leaching, σ_{n_2}, psi	Residual shear strength of the sample before leaching, τ_{res_1}, psi	Residual shear strength of the sample after leaching, τ_{res_2}, psi	Percentage change in the residual shear strength of the sample due to constant volume leaching	$\tan\phi_{r_1}'$ before leaching $\left(\frac{\tau_{res_1}}{\sigma_{n_1}} = \frac{\tau_{res_1}}{\sigma_{n_1}}\right)$	Corresponding ϕ_{r_1}' (before leaching)	$\tan\phi_{r_2}'$ after leaching $\left(\text{using }\tan\phi_{r_2}' = \frac{\tau_{res_2}}{\sigma_{n_2}}\right)$	Corresponding ϕ_{r_2}' (after leaching)	$\tan\phi_{r_2}'$ after leaching $\left(\text{using }\tan\phi_{r_2}' = \frac{\tau_{res_2}}{\sigma_{p_{n_2}}}\right)$	Corresponding ϕ_{r_2}' (after leaching)
M-L-1	M-34-1	2.50	22.13	785.20%	2.50	2.2	0.82	0.86	+3.91%	0.330	18°	0.350	19°	0.039	2°15'
M-L-2	M-34-2	5.00	49.94	898.80%	5.00	5.00	1.60	1.40-1.53	-4.38 to -12.56%	0.320	17°40'	0.280-0.310	16°-17°	0.030	2°00'
M-L-3	M-34-3	7.49	36.77	390.90%	7.49	7.49	2.20	2.11	-3.91%	0.290	16°20'	0.280	16°	0.058	3°20'
M-L-4	M-34-4	10.00	55.89	458.90%	10.00	10.00	2.54	2.34	-7.76%	0.250	14°15'	0.230	13°	0.042	2°30'
M-L-5	M-34-5	15.01	52.07	246.93%	15.01	15.01	3.54	3.07	-13.44%	0.240	13°20'	0.200	11°30'	0.059	3°25'

TABLE 6.11

INTERPRETATION OF THE RESIDUAL SHEAR STRENGTH DATA OBTAINED FROM THE Na-MONTMORILLONITE-1.15 g/l NaCl

SERIES IN TERMS OF THE MODIFIED SHEAR STRENGTH EQUATION

Test No.	Apparent effective stress (σ_a'), psi	Pore fluid NaCl content, gms./litre	Total specific surface of the mineral, m²/gm.	Failure plane water content, %	Estimated* net (R-A) stress, psi	True effective stress, $\sigma_a'' = \sigma_a' - (R-A)$, psi	Experimentally measured residual shear strength τ_{res}, psi	$\tan\phi_r' = \dfrac{\tau_{res}}{\sigma_a''}$	$\tan\phi_r' = \dfrac{\tau_{res}}{\sigma_a'}$	Extrapolated value of $\tan\phi_r$ under an environment of 33.57 g/l NaCl at the same true effective stress
N-1-3	10.12	1.15	641.0	270.05	6.45	3.67	1.18	0.117	0.323	0.318
N-1-4	15.12	1.15	641.0	240.11	8.39	6.73	1.57	0.104	0.233	0.287
N-1-5	19.99	1.15	641.0	228.11	10.17	9.82	2.02	0.101	0.206	0.263
N-1-6	40.65	1.15	641.0	178.40	21.82	18.83	3.60	0.089	0.191	0.219
N-1-7	65.78	1.15	641.0	150.19	33.86	31.92	5.60	0.085	0.175	0.193

*$P_y = $ (R-A) is estimated from the double-layer repulsive stress equation which is given by $P_y = 2 C_o R T (\cosh y_c - 1)$
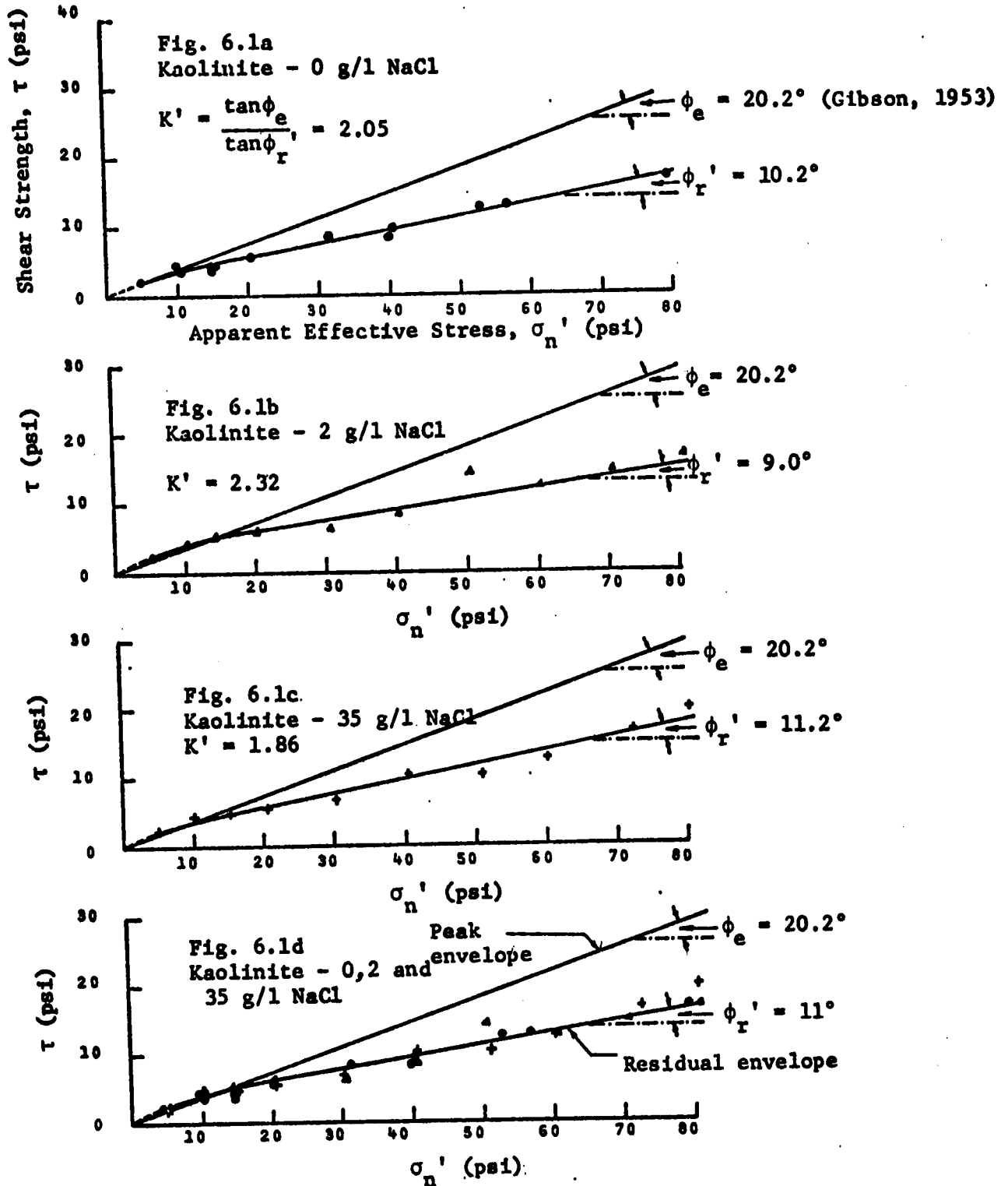
FIG. 6.1 (a, b, c and d) PEAK AND RESIDUAL SHEAR STRENGTH—
APPARENT EFFECTIVE STRESS RELATIONSHIPS FOR KAOLINITE
AT VARIOUS PORE FLUID NaCl CONCENTRATIONS

Fig. 6.2a
Kaolinite - 0 g/l NaCl

Fig. 6.2b
Kaolinite - 2 g/l NaCl

Fig. 6.2c
Kaolinite - 35 g/l NaCl
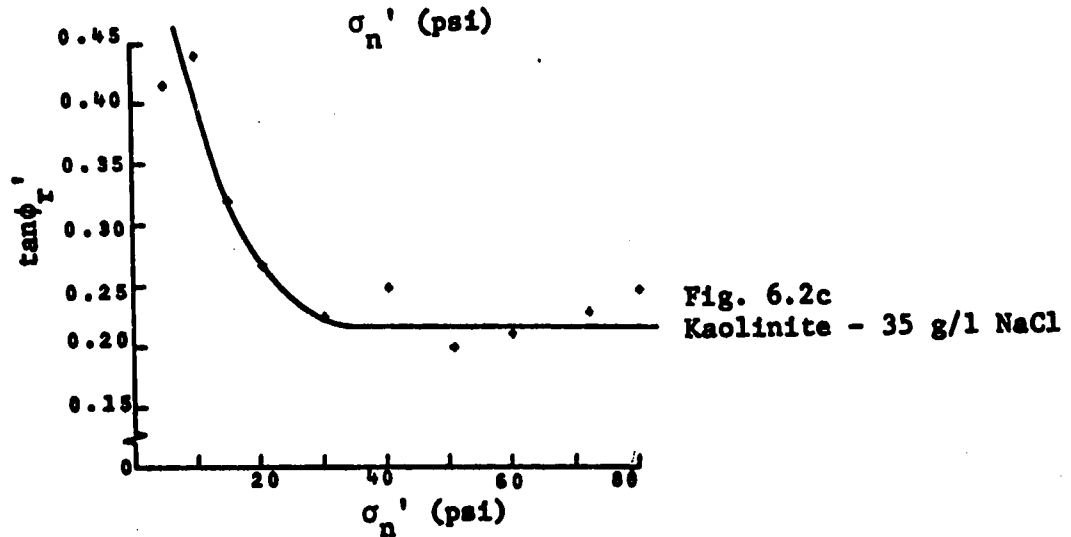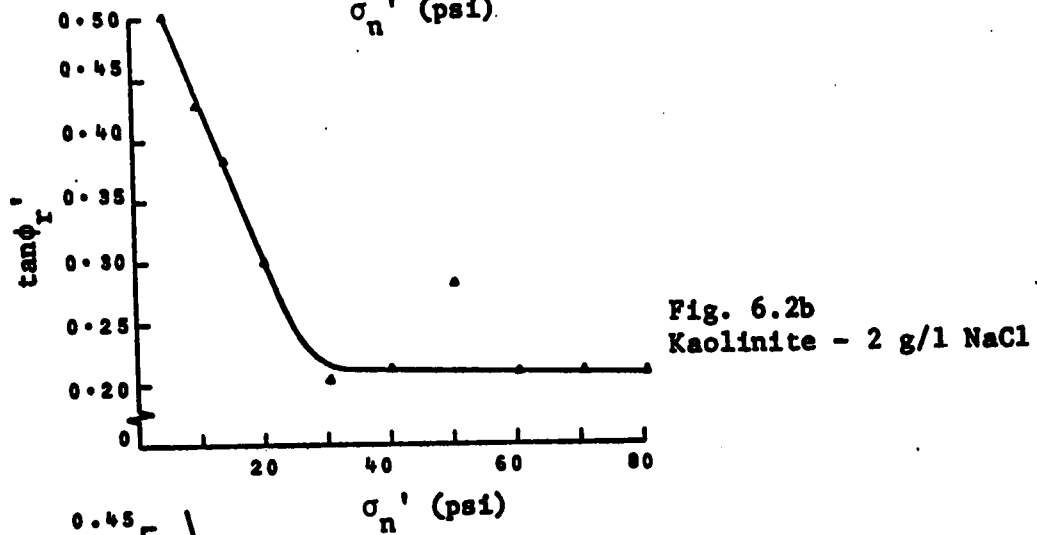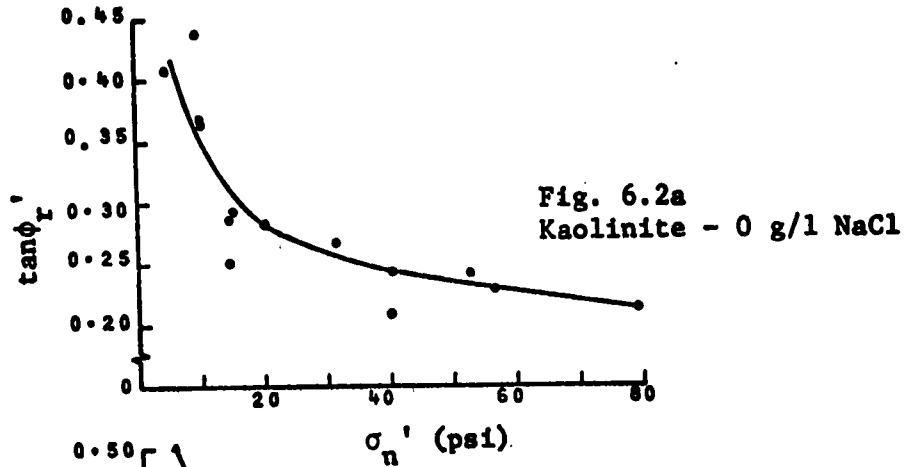
FIG. 6.2 (a, b and c) RELATIONSHIPS BETWEEN TANϕ_r'
AND APPARENT EFFECTIVE STRESS FOR
KAOLINITE AT VARIOUS PORE FLUID NaCl
CONCENTRATIONS
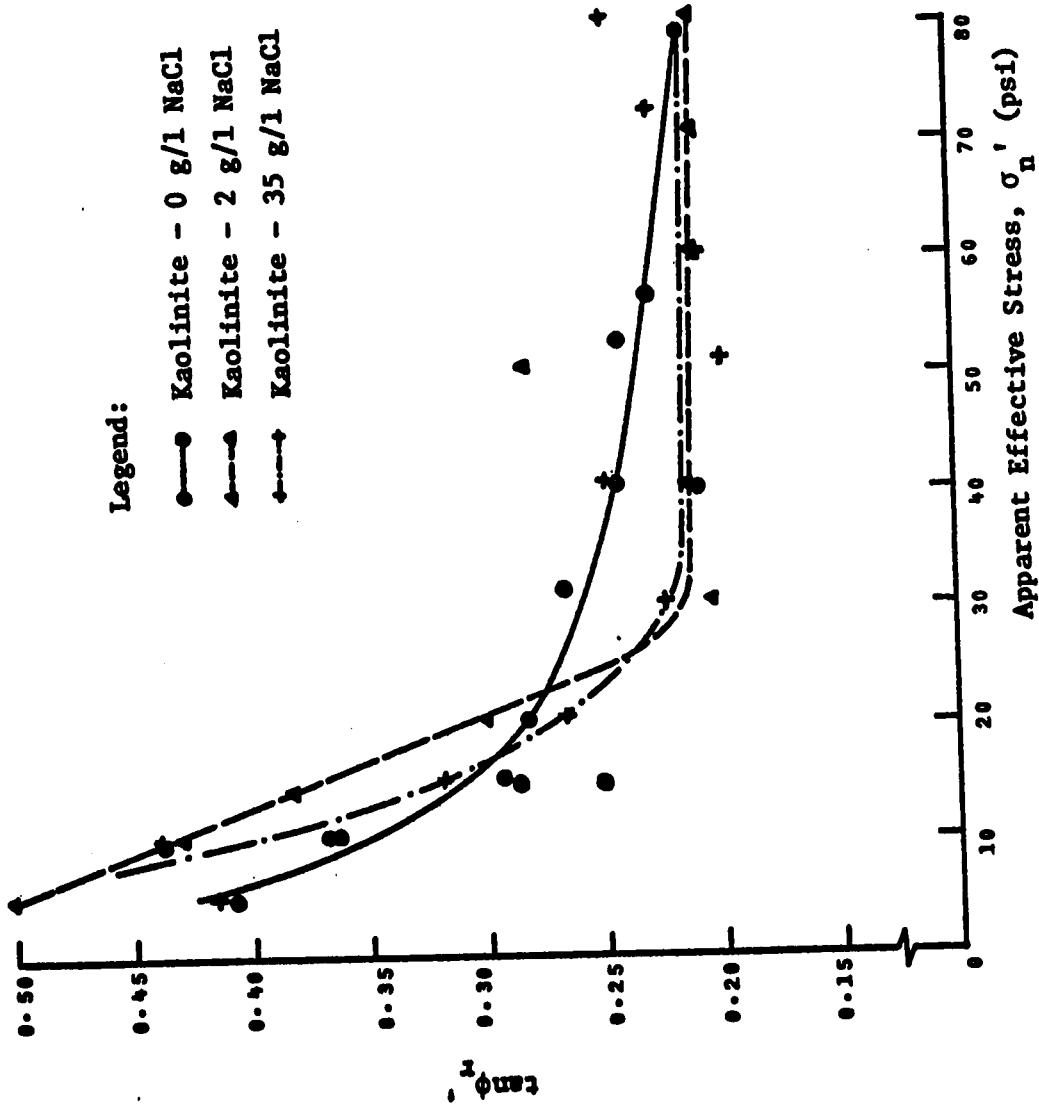
FIG. 6.2d   RELATIONSHIPS BETWEEN TANφ' AND APPARENT EFFECTIVE STRESS
FOR KAOLINITE AT VARIOUS PORE FLUID NaCl CONCENTRATIONS
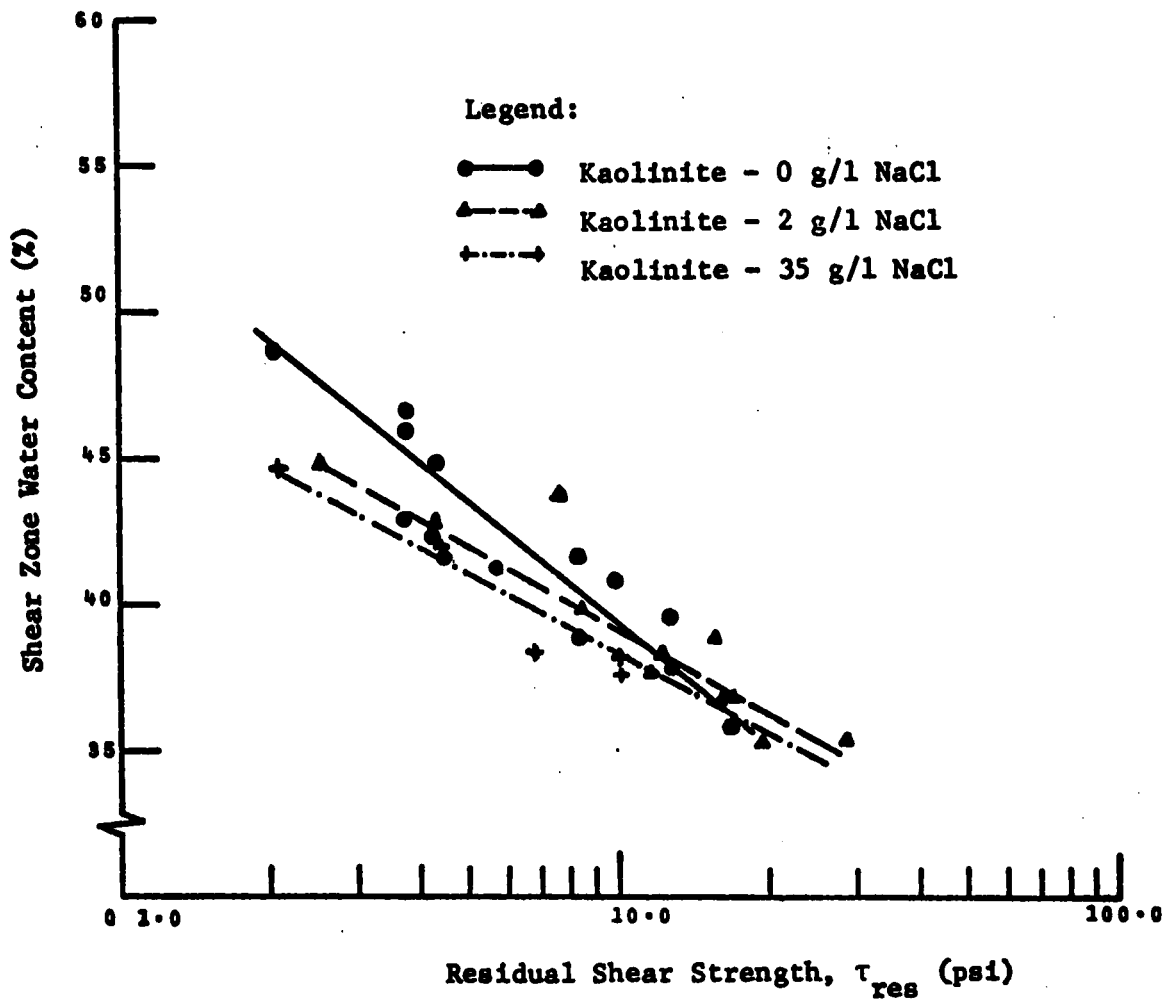
FIG. 6.3   RELATIONSHIPS BETWEEN SHEAR ZONE WATER CONTENT AND
LOGARITHM OF RESIDUAL SHEAR STRENGTH FOR KAOLINITE
AT VARIOUS PORE FLUID NaCl CONCENTRATIONS
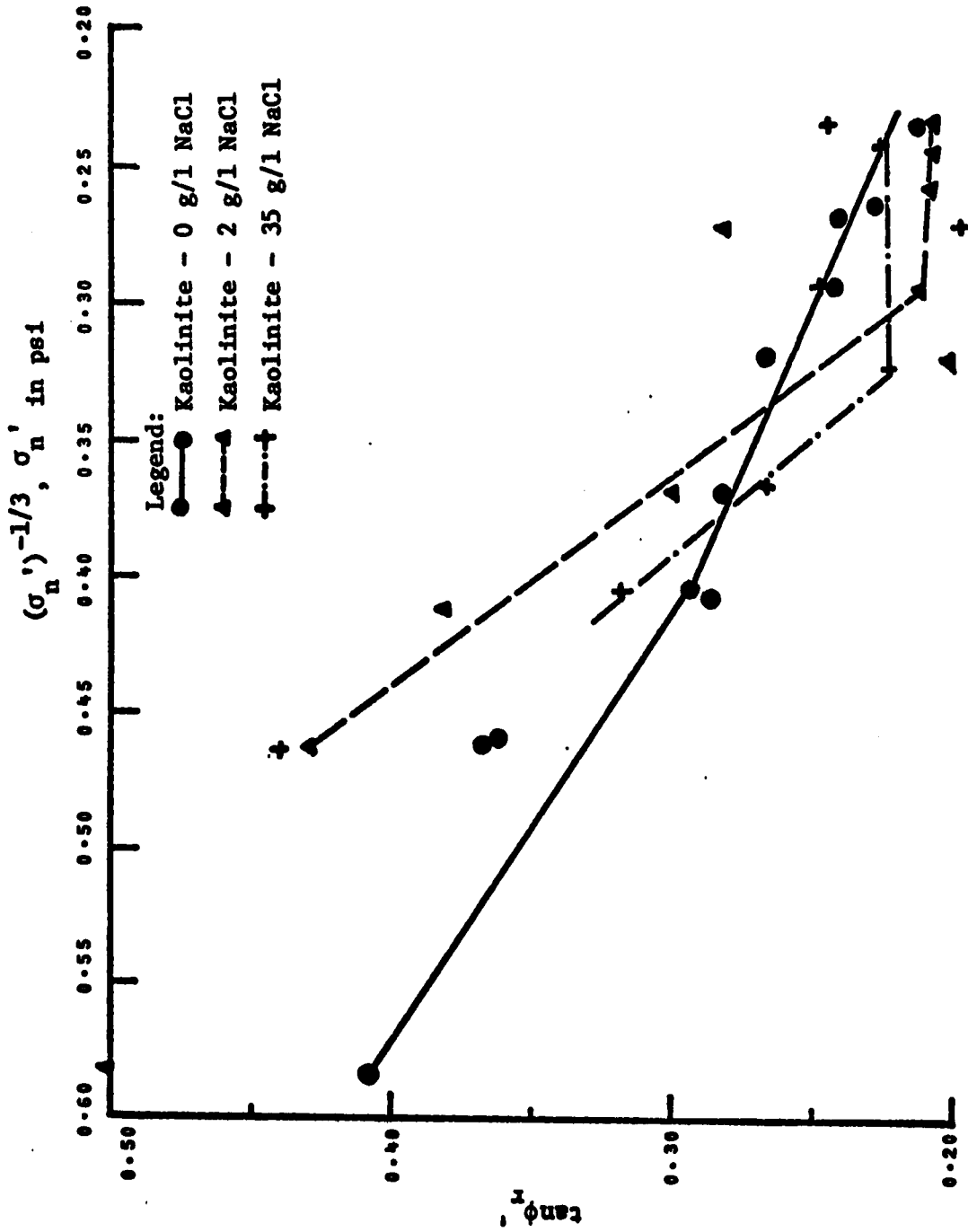
FIG. 6.4 RELATIONSHIPS BETWEEN $\tan\phi_r'$ AND $(\sigma_n')^{-1/3}$ FOR KAOLINITE AT VARIOUS PORE FLUID NaCl CONCENTRATIONS
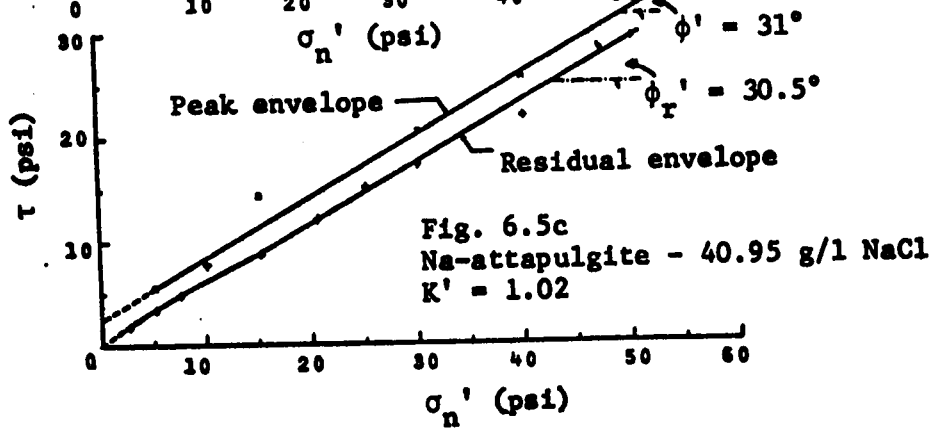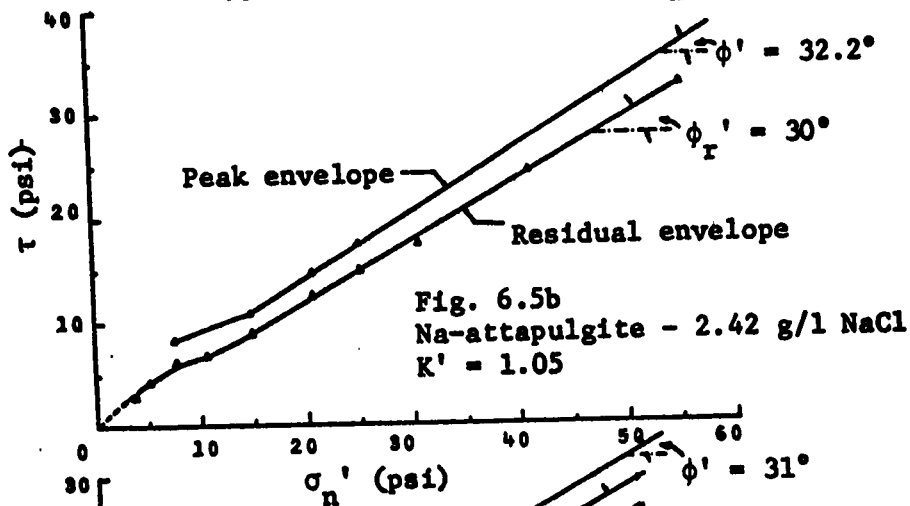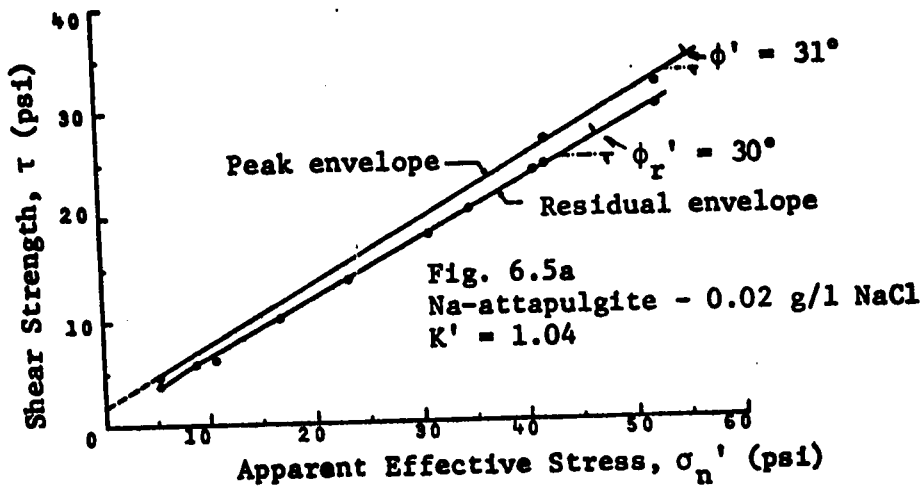
FIG. 6.5 (a, b and c) PEAK AND RESIDUAL SHEAR STRENGTH –
APPARENT EFFECTIVE STRESS RELATIONSHIPS FOR NA-ATTAPULGITE
AT VARIOUS PORE FLUID NaCl CONCENTRATIONS
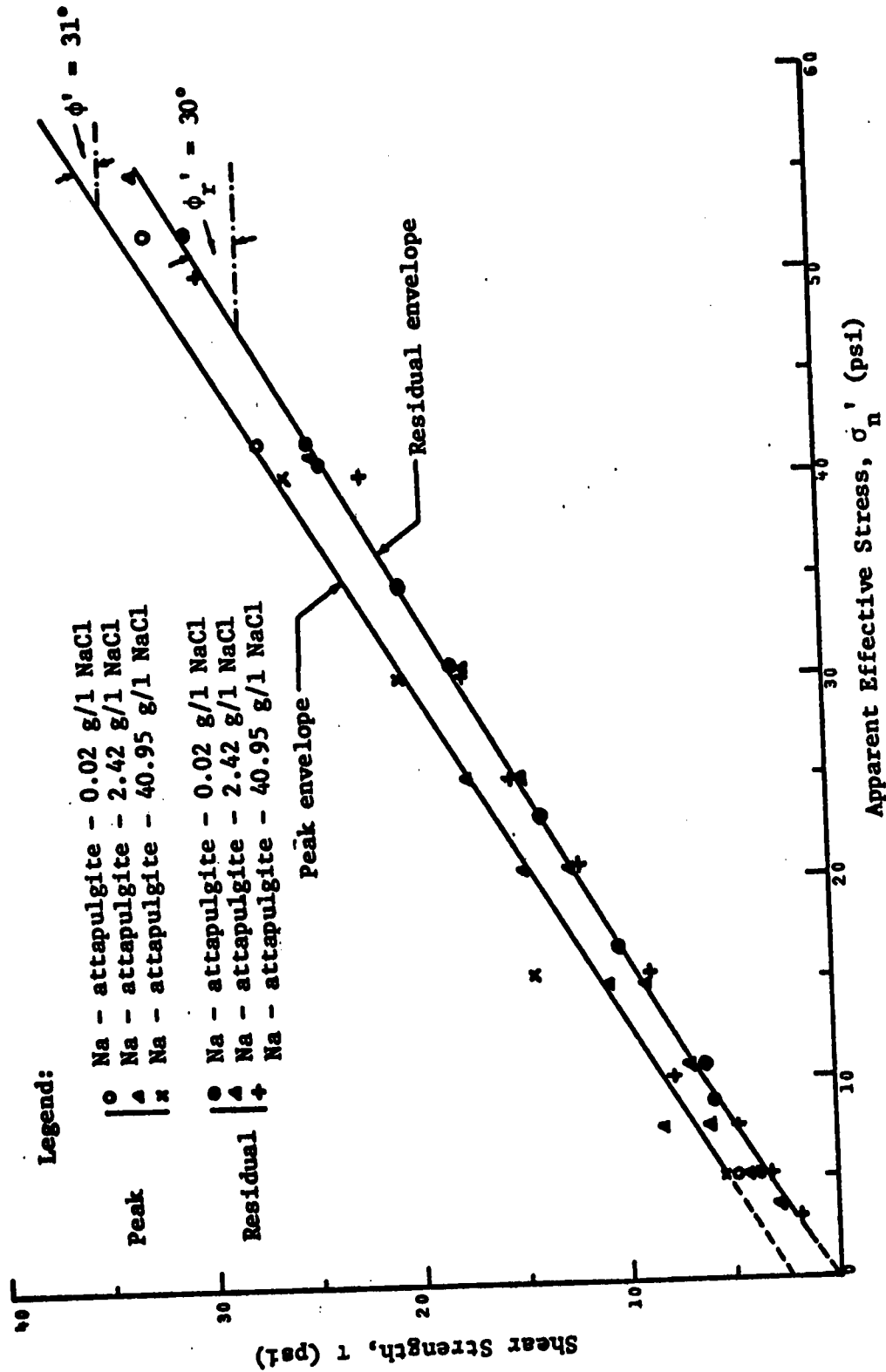
FIG. 6.5d PEAK AND RESIDUAL SHEAR STRENGTH - APPARENT EFFECTIVE STRESS RELATIONSHIPS FOR
Na-ATTAPULGITE AT VARIOUS PORE FLUID NaCl CONCENTRATIONS
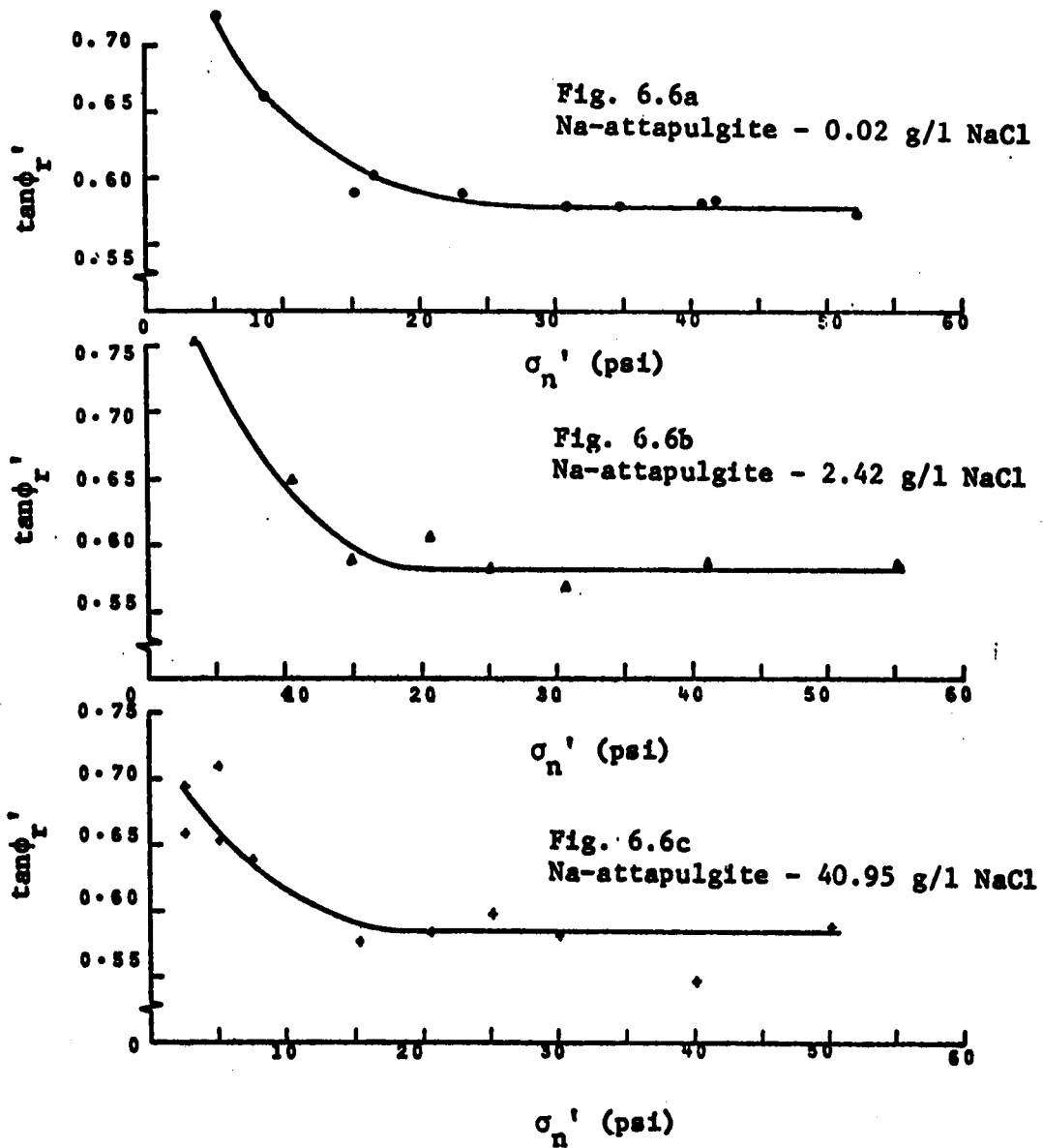
FIG. 6.6 (a, b and c) RELATIONSHIPS BETWEEN TANφ$_r$' AND APPARENT
EFFECTIVE STRESS FOR Na-APPATULGITE AT
VARIOUS PORE FLUID NaCl CONCENTRATIONS

Legend:

● Na-attapulgite - 0.02 g/l NaCl
▲ Na-attapulgite - 2.42 g/l NaCl
+ Na-attapulgite - 40.95 g/l NaCl
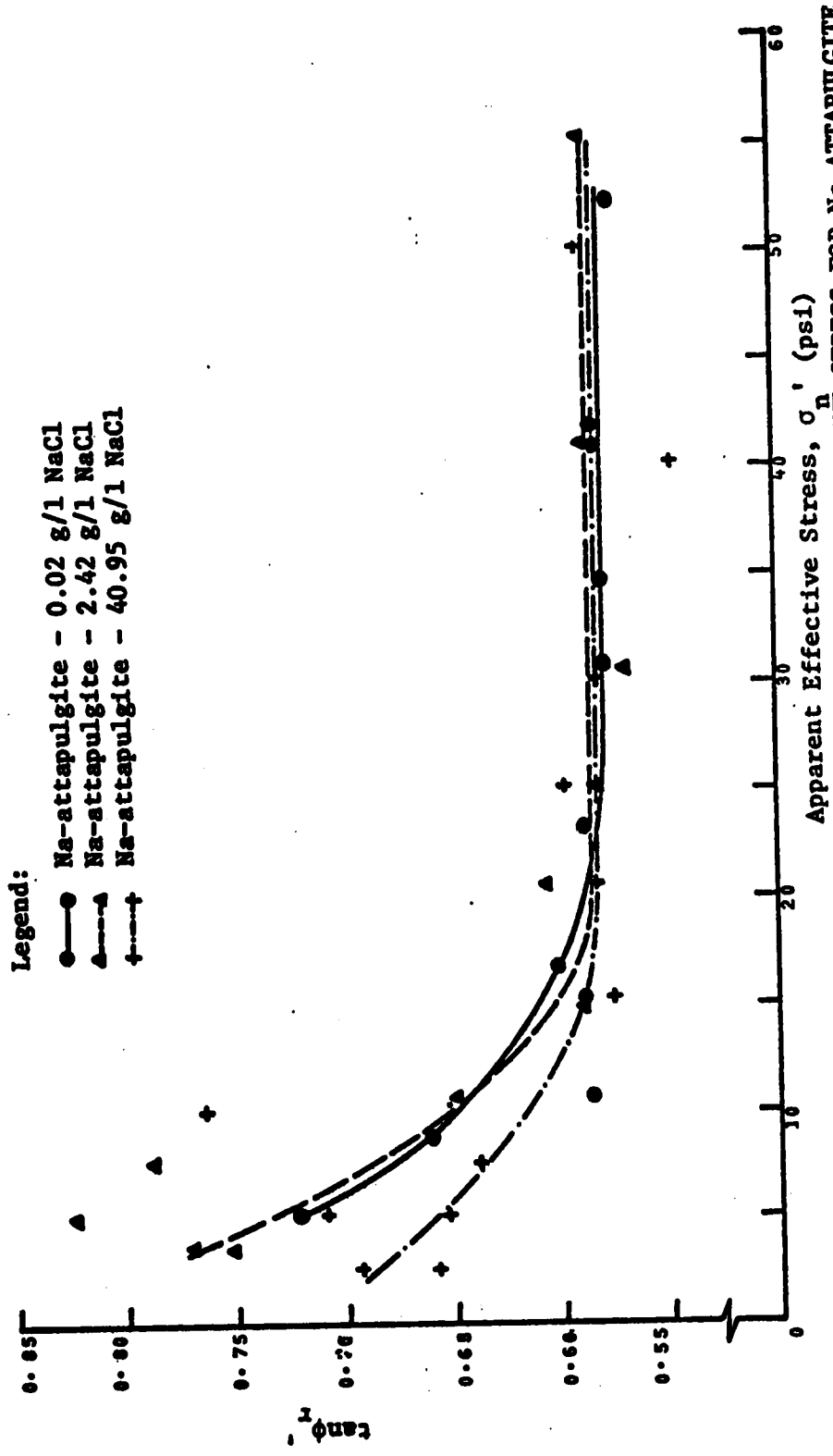
FIG. 6.6d RELATIONSHIPS BETWEEN TANφr' AND APPARENT EFFECTIVE STRESS FOR Na-ATTAPULGITE
AT VARIOUS PORE FLUID NaCl CONCENTRATIONS
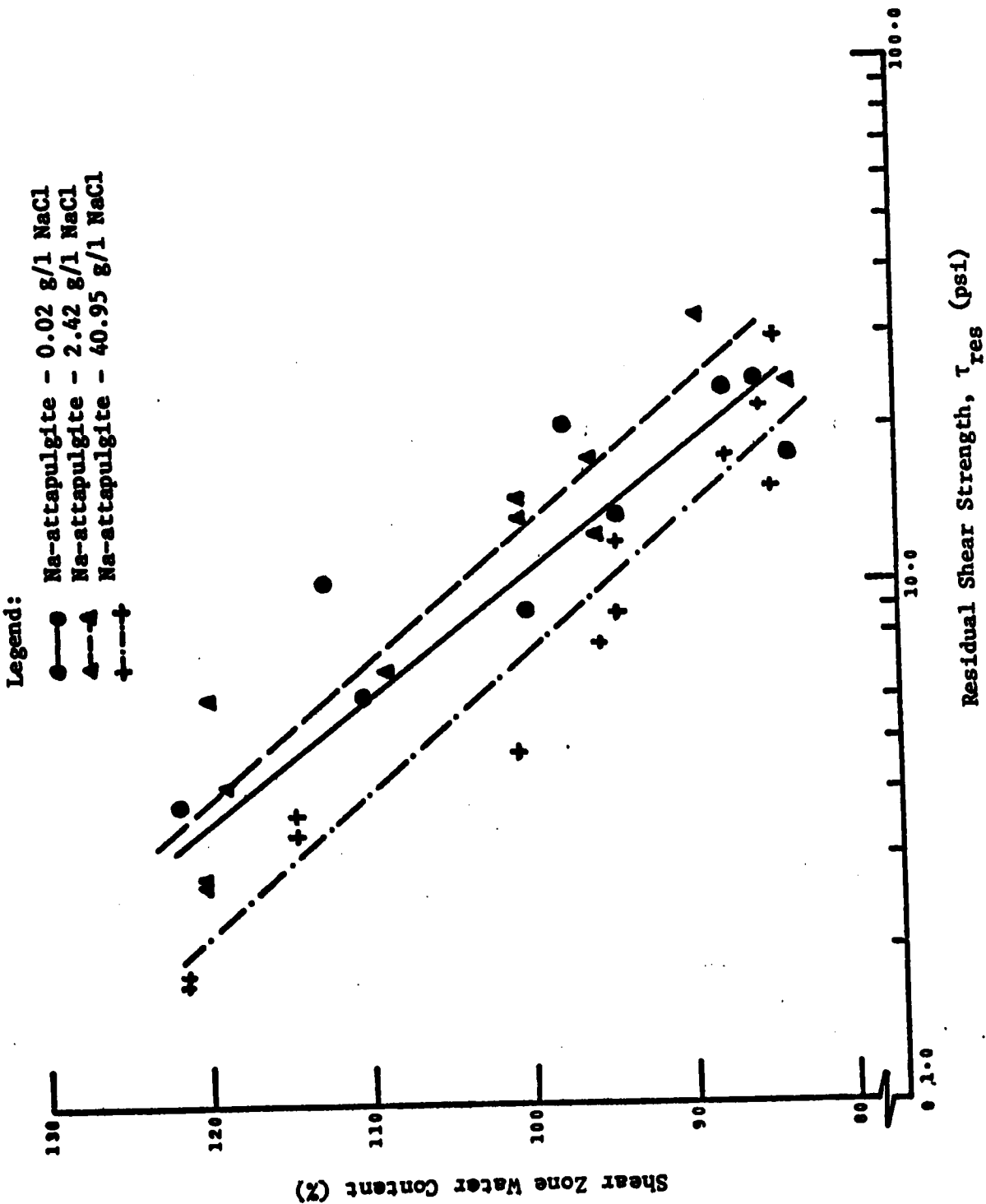
FIG. 6.7 RELATIONSHIPS BETWEEN SHEAR ZONE WATER CONTENT AND LOGARITHM OF RESIDUAL SHEAR STRENGTH FOR Na-ATTAPULGITE AT VARIOUS PORE FLUID NaCl CONCENTRATIONS
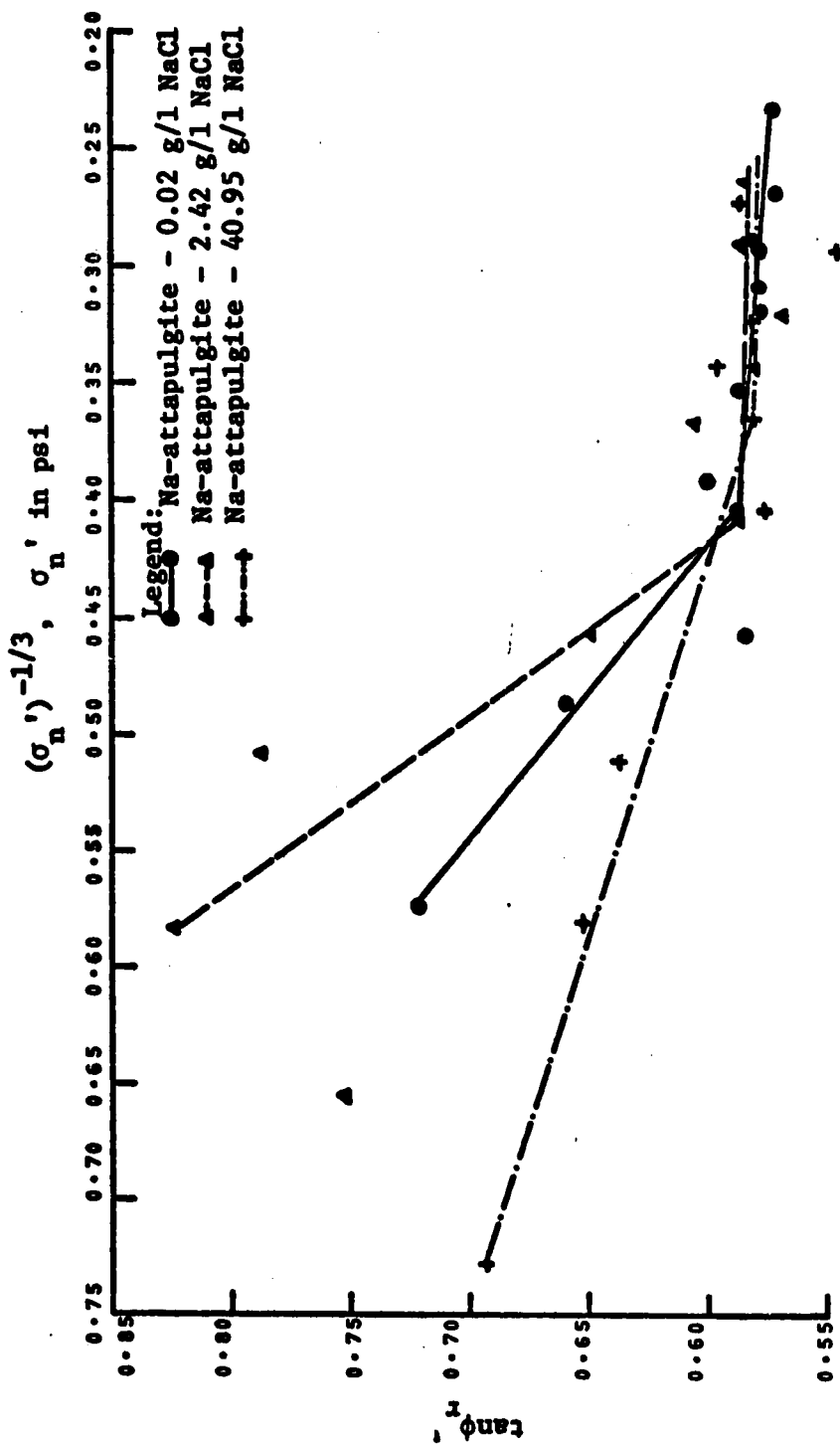
FIG. 6.8   RELATIONSHIPS BETWEEN TANφ$_r$' AND $(\sigma_n')^{-1/3}$ FOR Na-ATTAPULGITE AT VARIOUS
PORE FLUID NaCl CONCENTRATIONS
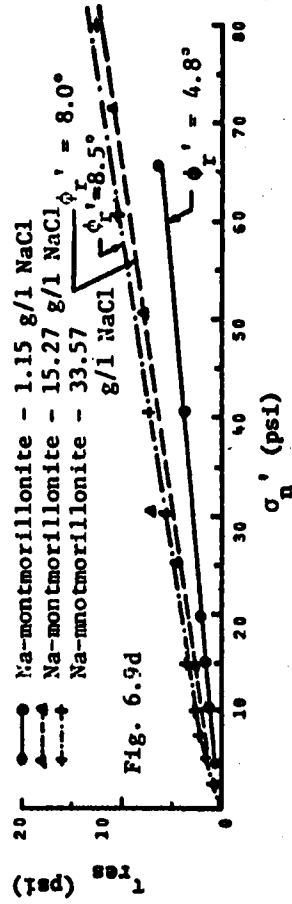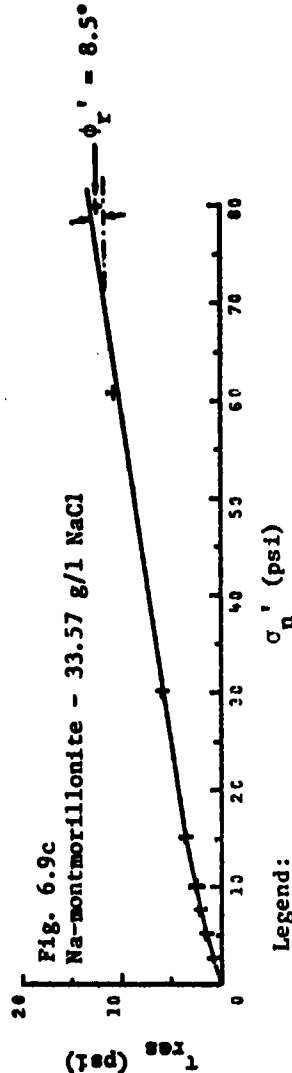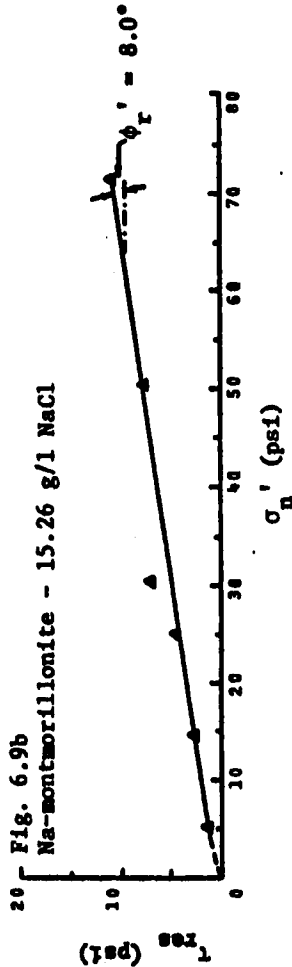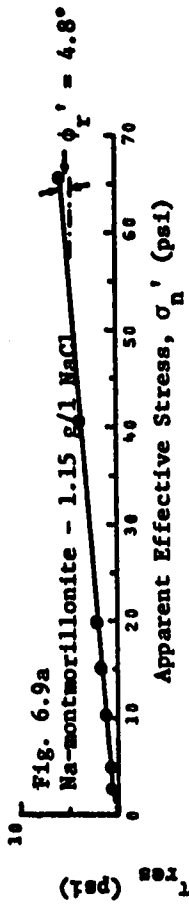
FIG. 6.9 (a, b, c and d) RESIDUAL SHEAR STRENGTH – APPARENT EFFECTIVE STRESS RELATIONSHIPS FOR Na–MONTMORILLONITE AT VARIOUS PORE FLUID NaCl CONCENTRATIONS
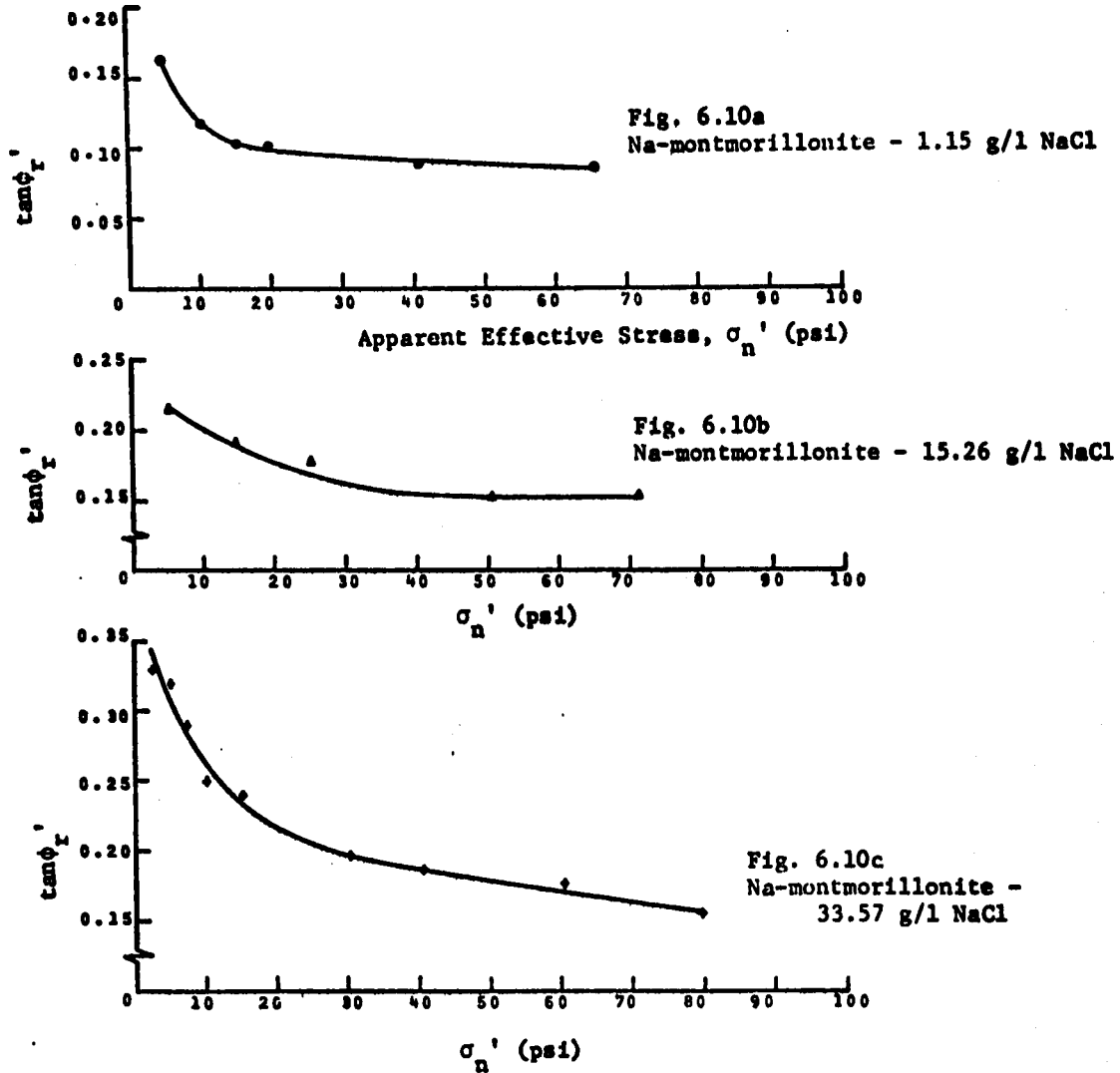
FIG. 6.10 (a, b and c) RELATIONSHIPS BETWEEN TANϕ_r' AND APPARENT EFFECTIVE STRESS FOR Na-MONTMORILLONITE AT VARIOUS PORE FLUID NaCl CONCENTRATIONS
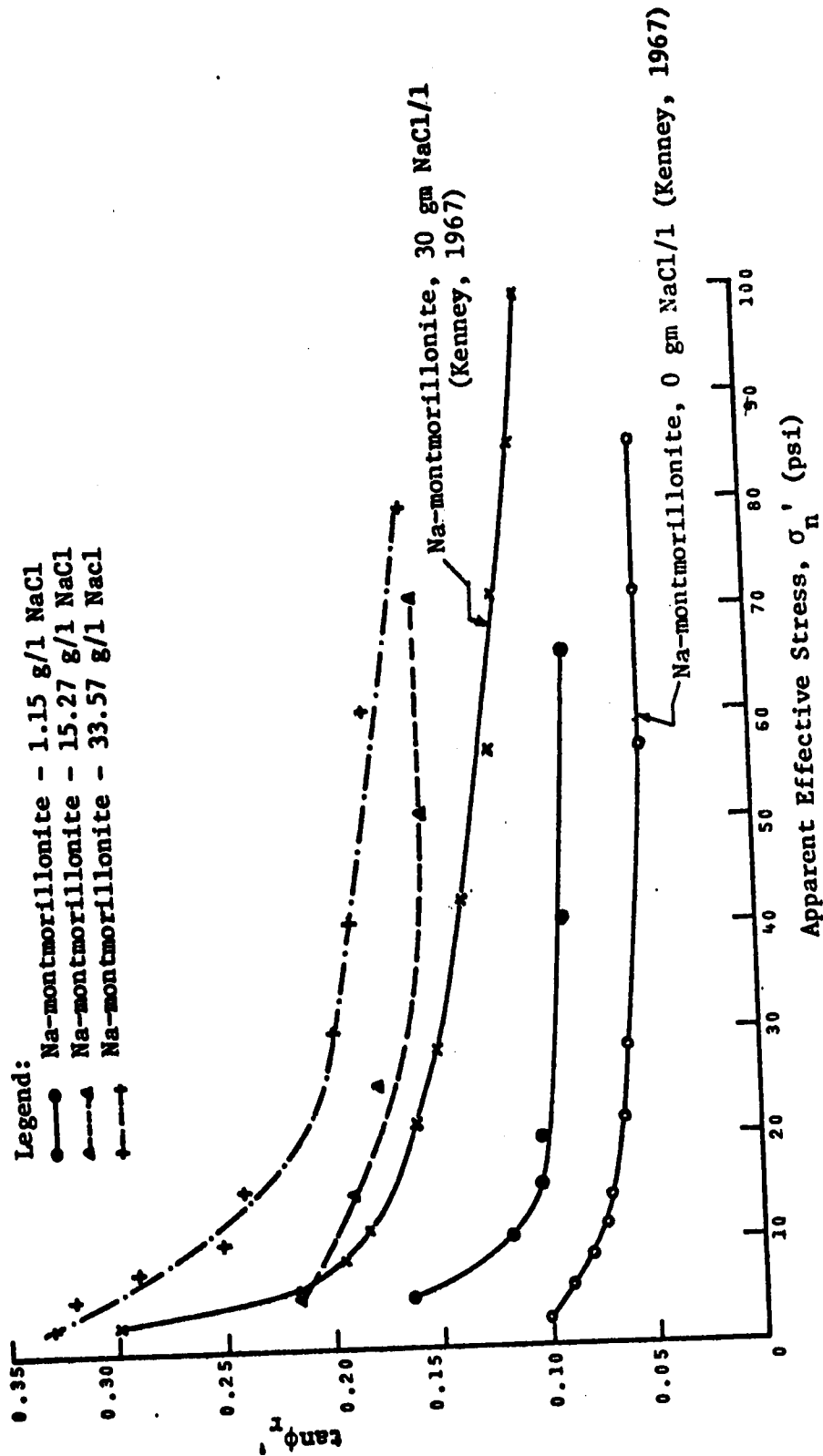
FIG. 6.10d   RELATIONSHIPS BETWEEN TANφ$_r$' AND APPARENT EFFECTIVE STRESS FOR Na-MONTMORILLONITE AT VARIOUS PORE FLUID NaCl CONCENTRATIONS
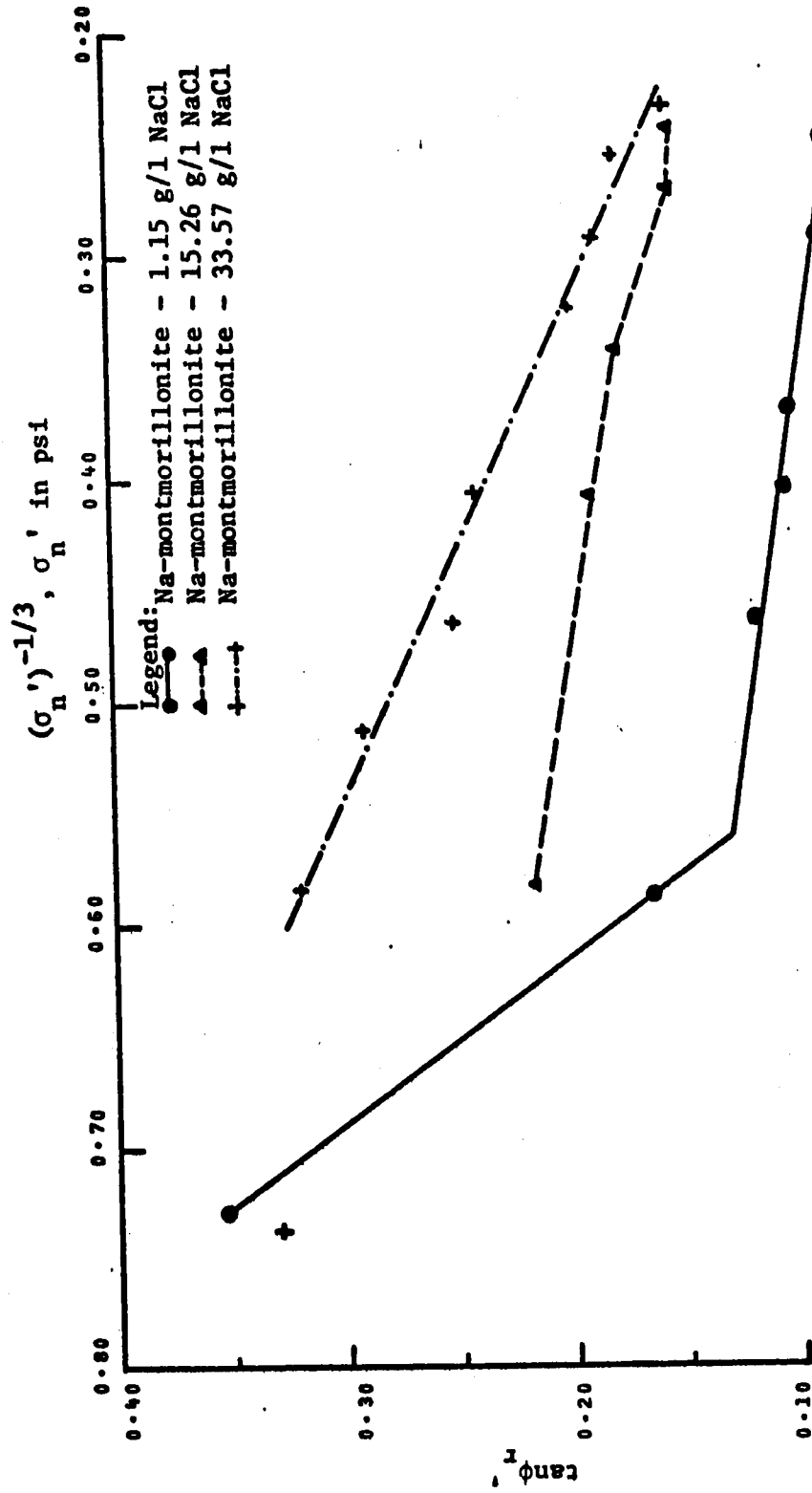
FIG. 6.11   RELATIONSHIPS BETWEEN TANϕ_r' AND $(\sigma_n')^{-1/3}$ FOR Na-MONTMORILLONITE AT VARIOUS PORE FLUID NaCl CONCENTRATIONS
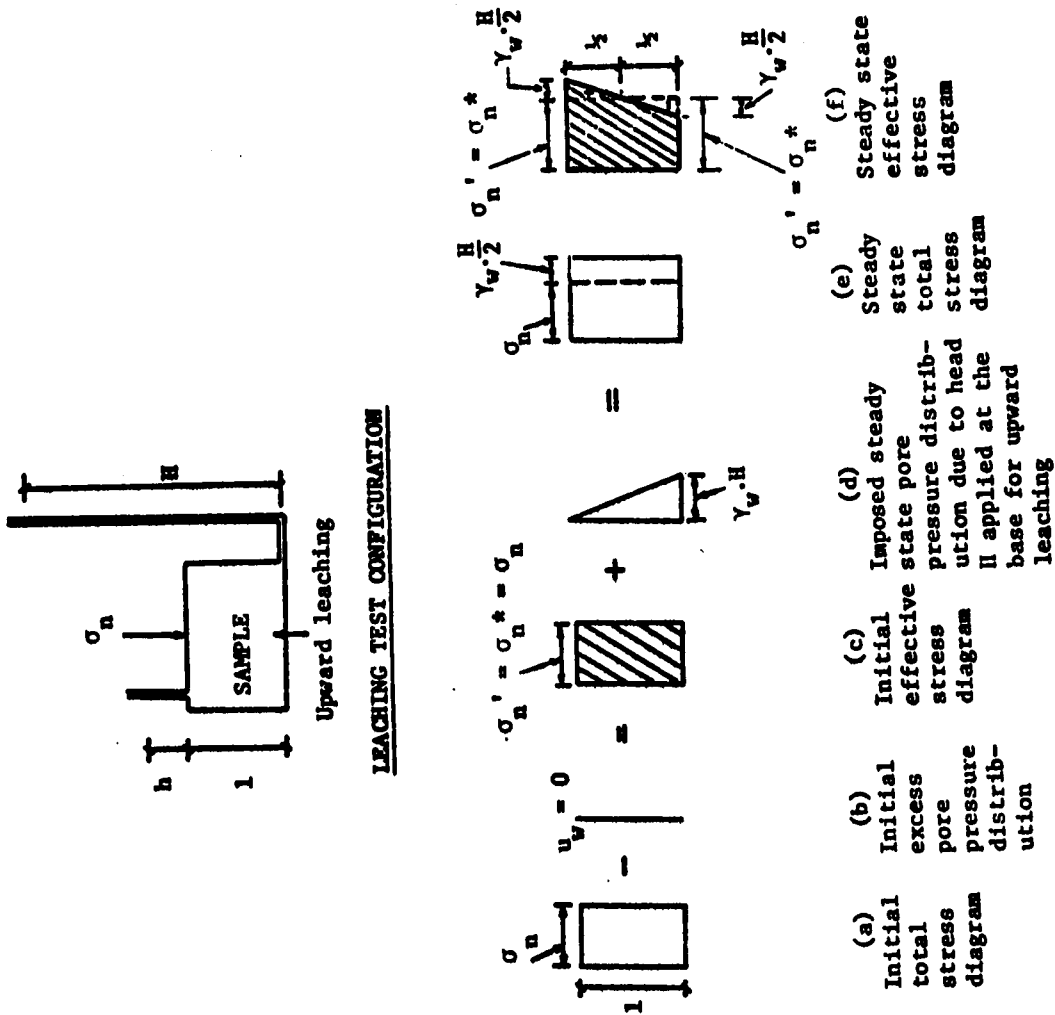
FIG. 6.12 STRESSES IN AN OVERCONSOLIDATED SAMPLE BEFORE AND AFTER APPLICATION OF A HEAD OF SOLUTION AT THE BASE FOR UPWARD LEACHING
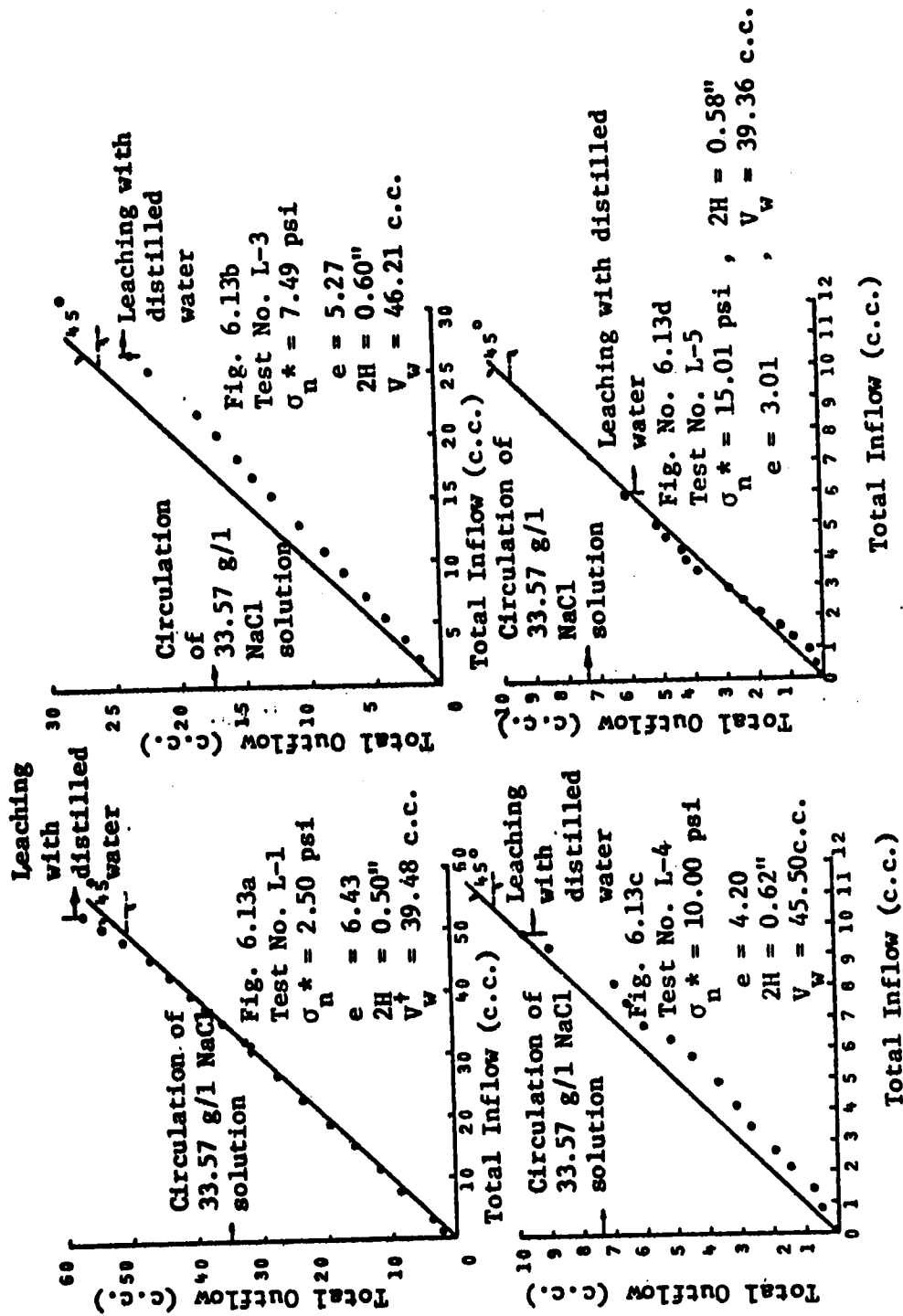
FIG. 6.13 (a, b, c and d) INFLOW-OUTFLOW DATA DURING CIRCULATION OF SALT SOLUTION THROUGH THE Na-MONTMORILLONITE SAMPLES IN THE LEACHING TESTS

† V_w = Estimated volume of salt solution initially held by the pore spaces of the sample.

Legend:

▲	Test No. L-1,	V_w = 39.48 c.c,	*1 i = 84
●	Test No. L-3,	V_w = 46.21 c.c,	i = 193
●	Test No. L-4,	V_w = 45.50 c.c,	i = 186
+	Test No. L-5,	V_w = 39.36 c.c,	i = 199

Circulation of 33.57 g/l NaCl solution

Void ratio (e) = 6.43, 2H = 0.50"

*2 k = 1.15×10^{-8} cms./sec.

e = 5.27, 2H = 0.60"

k = 5.45×10^{-9} cms./sec.

e = 4.20, 2H = 0.62"

e = 3.01, 2H = 0.58"

k = 2.17×10^{-9} cms/sec.

k = 1.69×10^{-9} cms./sec.

k = 1.48×10^{-8} cms./sec.

k = 2.62×10^{-8} cms./sec.

Total $\frac{\text{Inflow + Outflow}}{2}$, c.c.

Time (mins.)
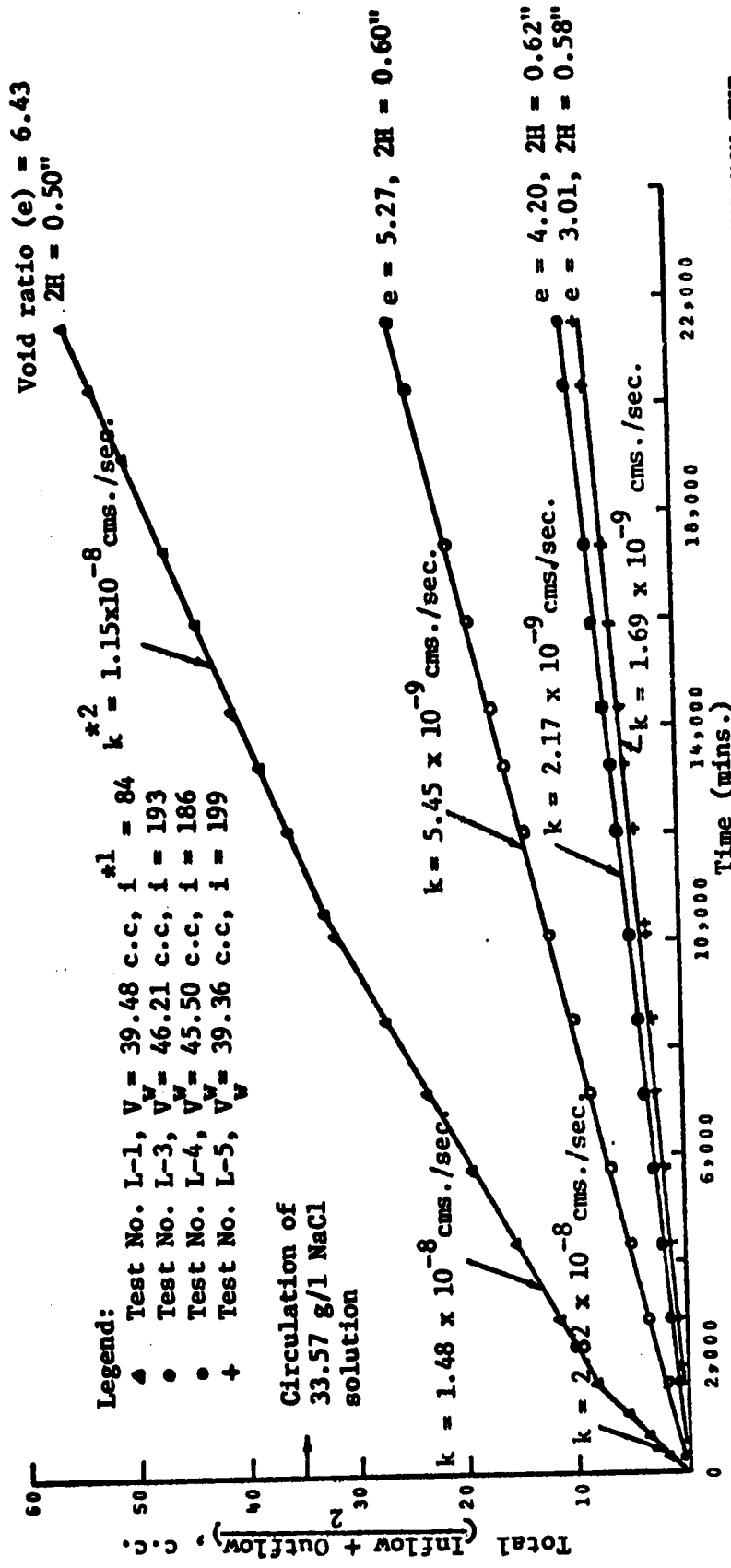
FIG. 6.14   INFLOW, OUTFLOW - TIME RELATIONSHIPS DURING CIRCULATION OF SALT SOLUTION THROUGH THE Na-MONTMORILLONITE SAMPLES IN THE LEACHING TESTS

*1 i = Average hydraulic gradient imposed across the specimen

*2 k = Coefficient of permeability
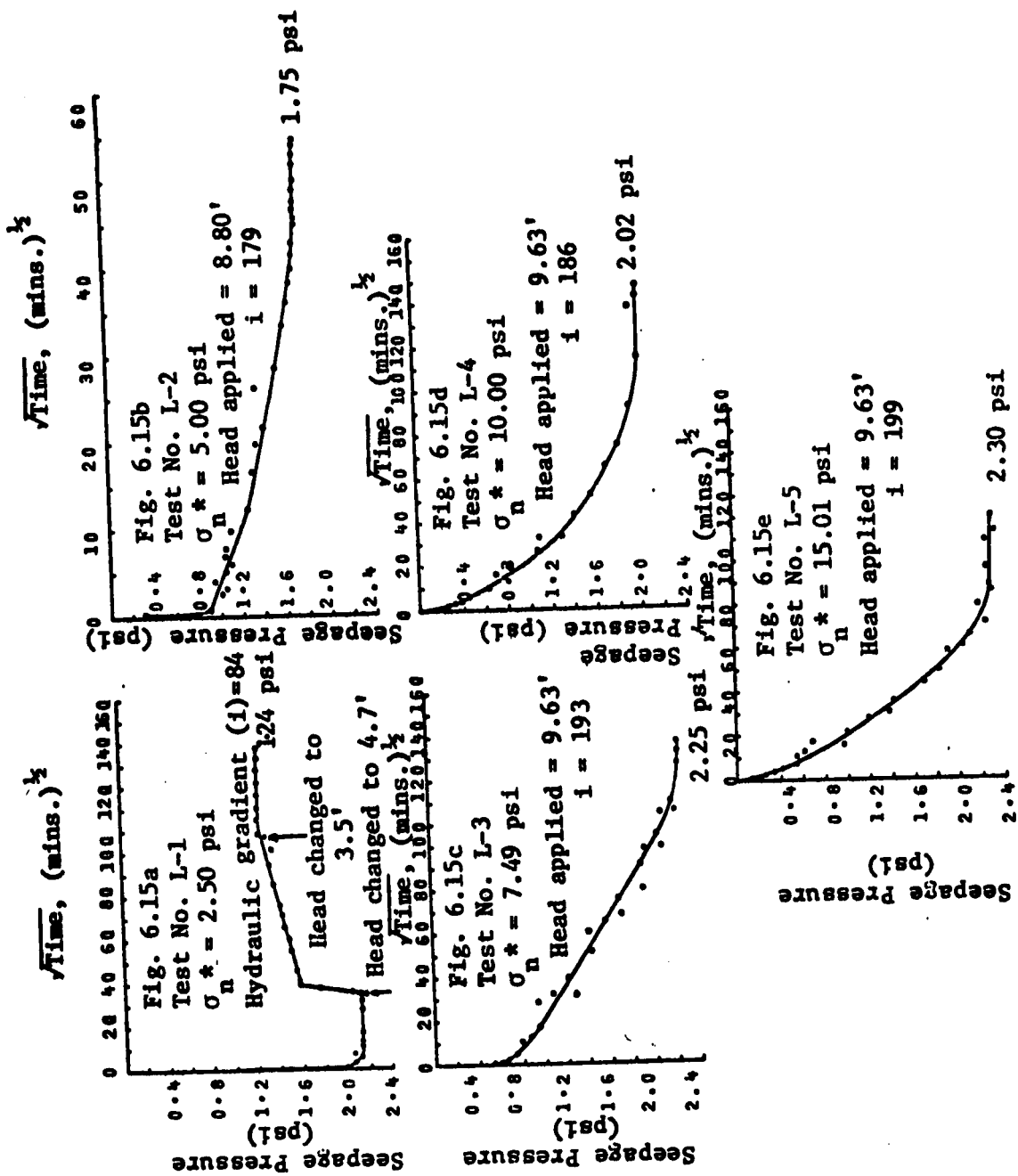
FIG. 6.15 (a, b, c, d and e) DEVELOPMENT OF SEEPAGE PRESSURES WITH TIME IN THE LEACHING TESTS
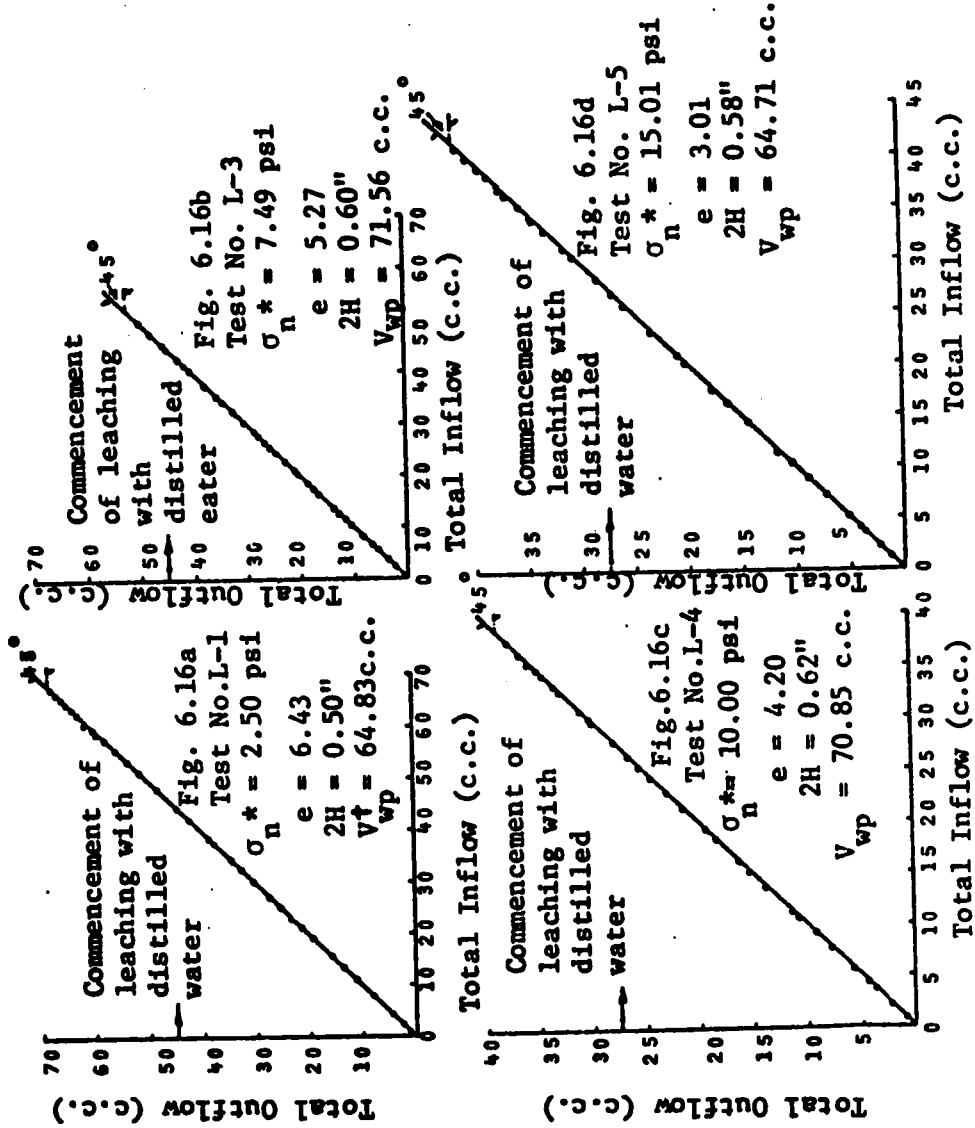
FIG. 6.16 (a, b, c and d) INFLOW-OUTFLOW DATA DURING LEACHING OF THE Na-MONTMORILLONITE SAMPLES WITH DISTILLED WATER IN THE LEACHING TESTS

† V_{wp} = Estimated total volume of salt solution initially held by the sample and the porous stones
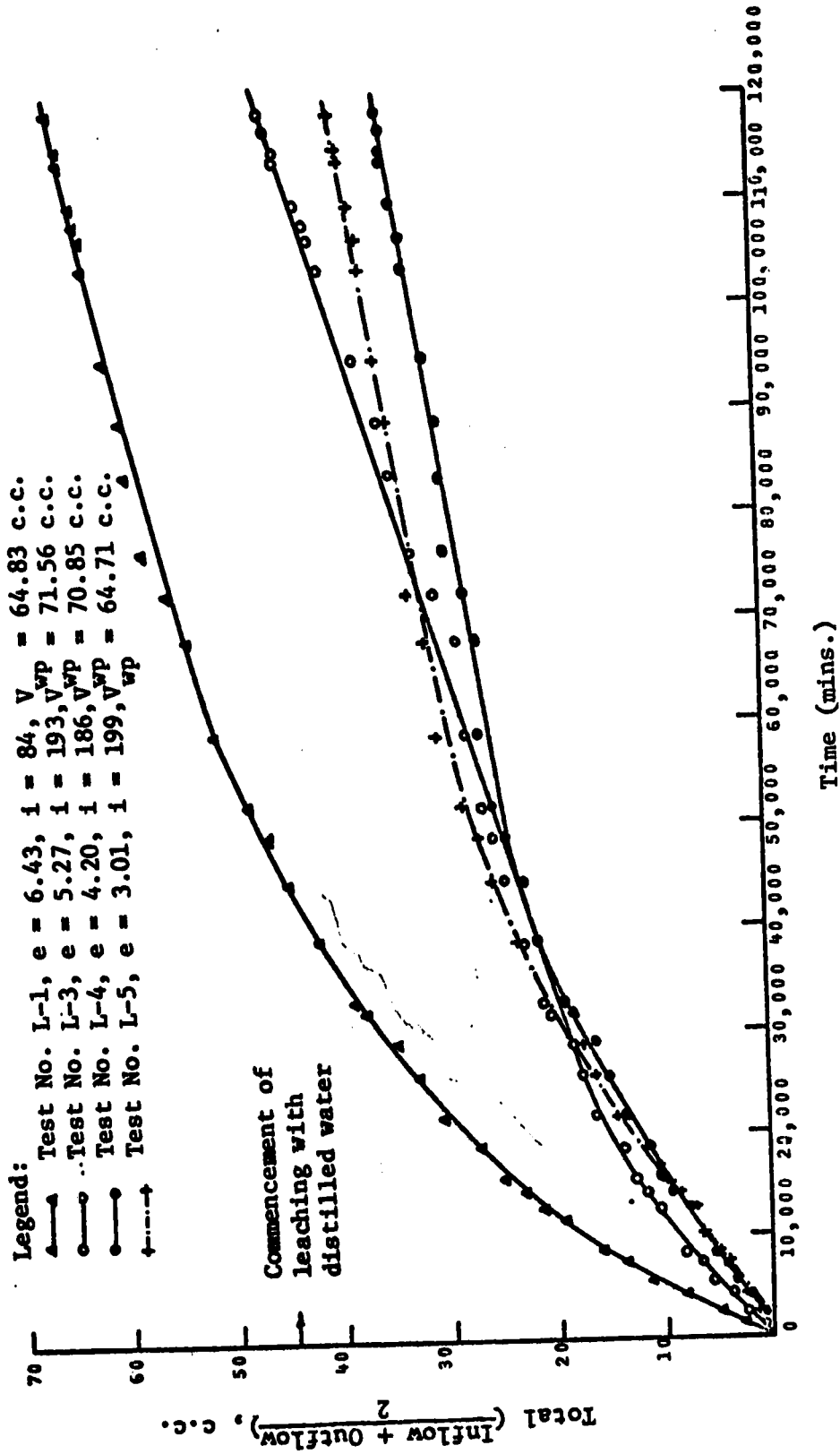
FIG. 6.17 INFLOW, OUTFLOW - TIME RELATIONSHIPS DURING LEACHING OF THE Na-MONTMORILLONITE
SAMPLES WITH DISTILLED WATER IN THE CONSTANT VOLUME LEACHING TESTS
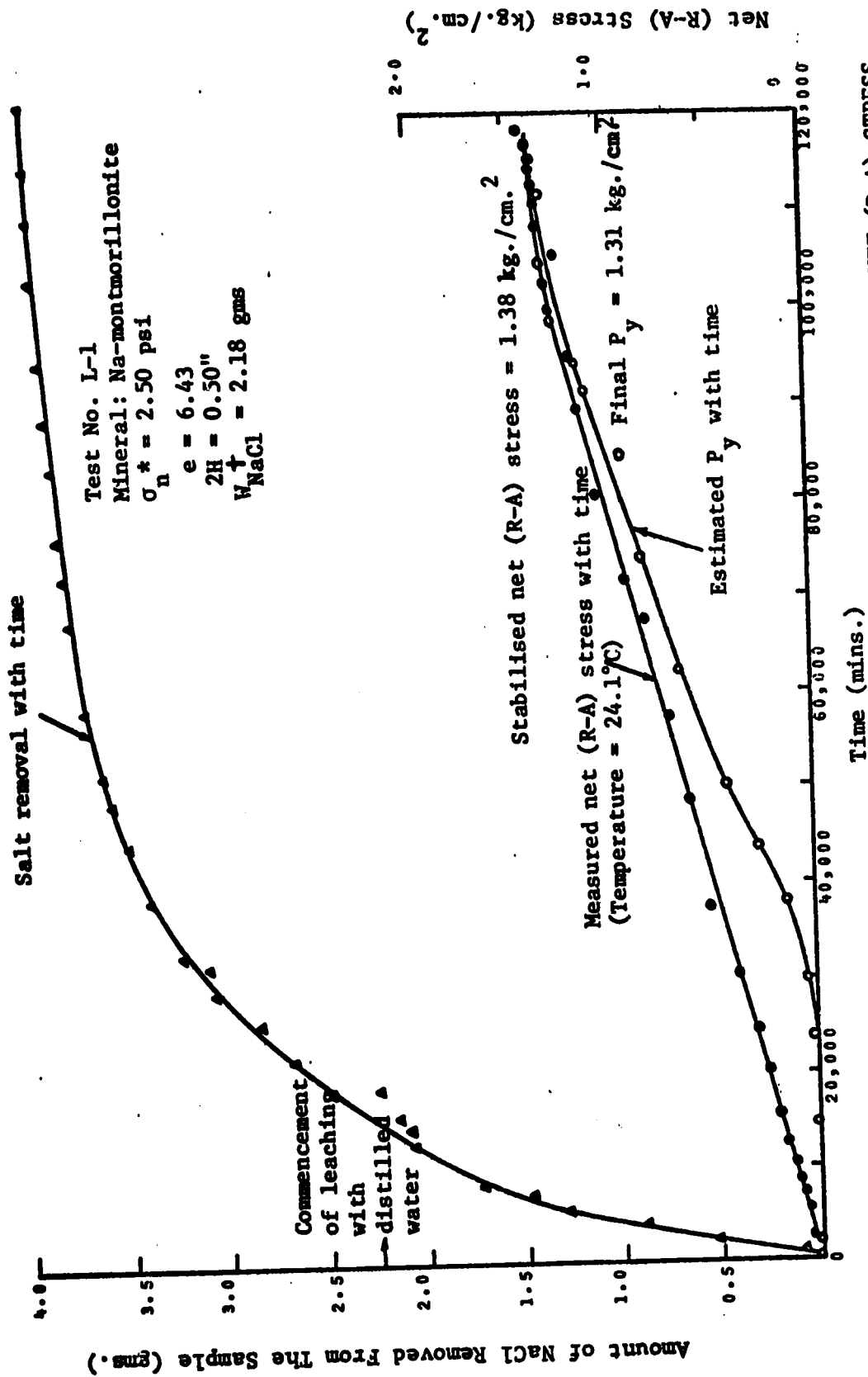
FIG. 6.18 SALT REMOVAL – TIME RELATIONSHIP AND THE CORRESPONDING DEVELOPMENT OF THE NET (R-A) STRESS WITH TIME FOR LEACHING TEST NO. L-1

$\dagger W_{NaCl}$ = Estimated total quantity of NaCl held by the sample and the porous stones before leaching

Stabilised net (R-A) stress = 3.16 kg./cm.^{2}

Estimated final P_y = 3.59 kg./cm.^{2}

Test No. L-2
Mineral: Na-montmorillonite
σ_n^* = 5.00 psi
e = 3.88
2H = 0.59"
W_{NaCl} = 2.30 gms.

Commencement of leaching
with distilled water

Net (R-A) Stress (kg./cm.^{2})

Time (mins.)
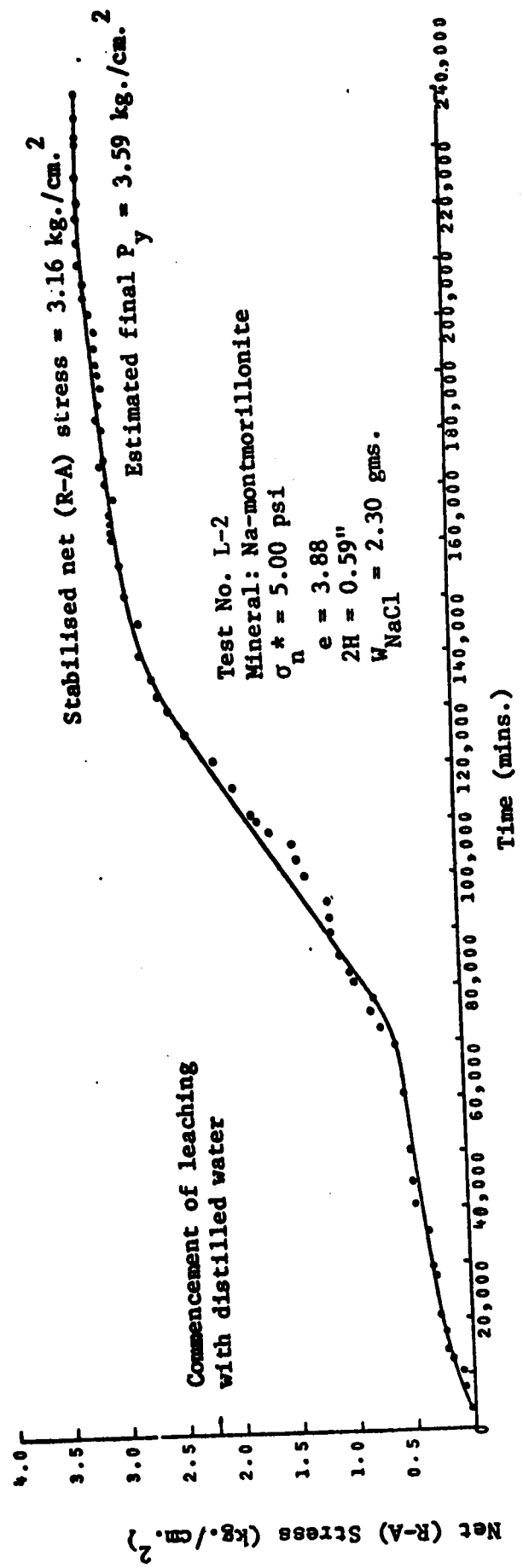
FIG. 6.19   DEVELOPMENT OF THE NET (R-A) STRESS WITH TIME FOR LEACHING TEST NO. L-2
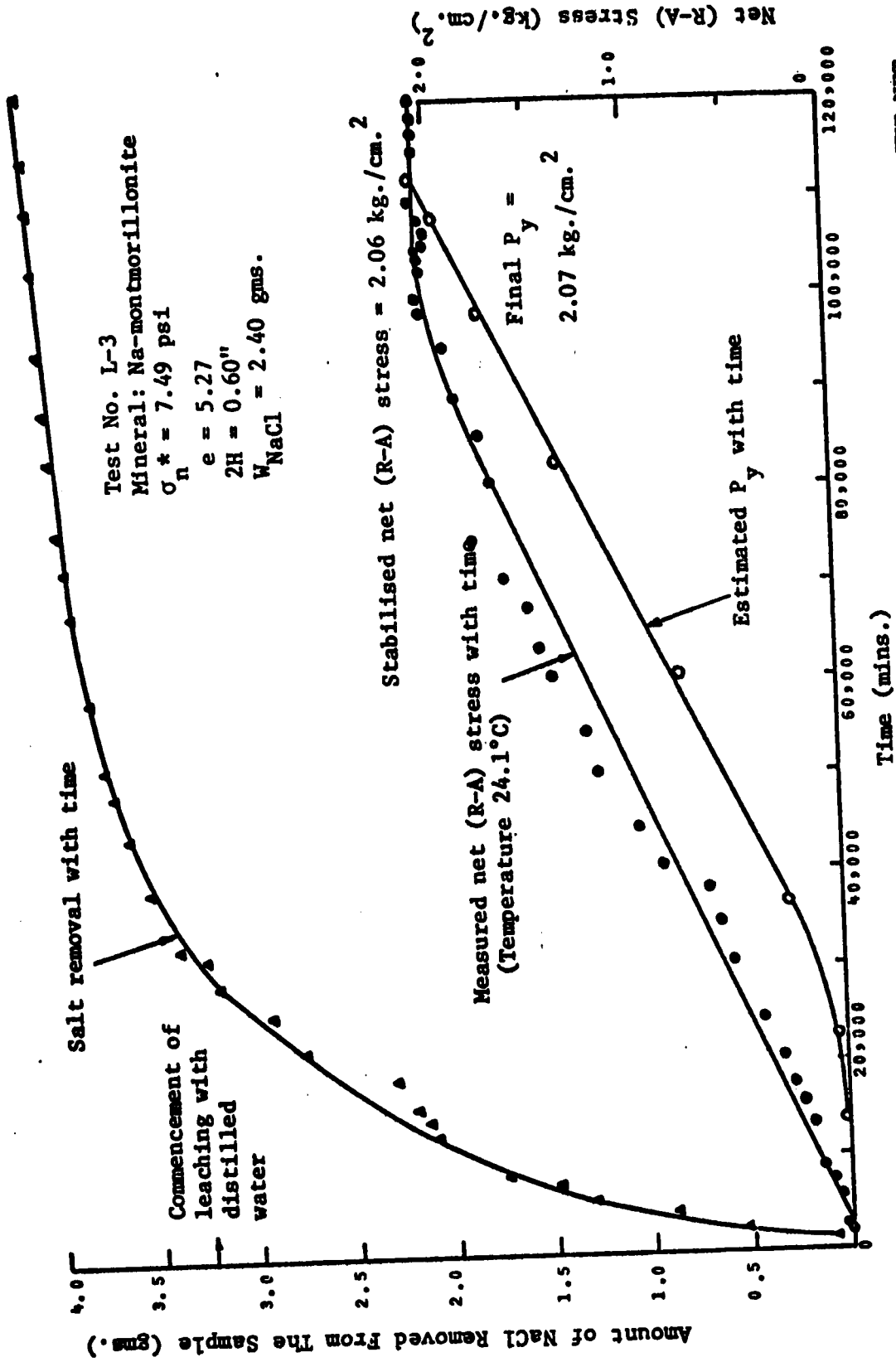
FIG. 6.20   SALT REMOVAL – TIME RELATIONSHIP AND THE CORRESPONDING DEVELOPMENT OF THE NET
(R–A) STRESS WITH TIME FOR LEACHING TEST NO. L–3
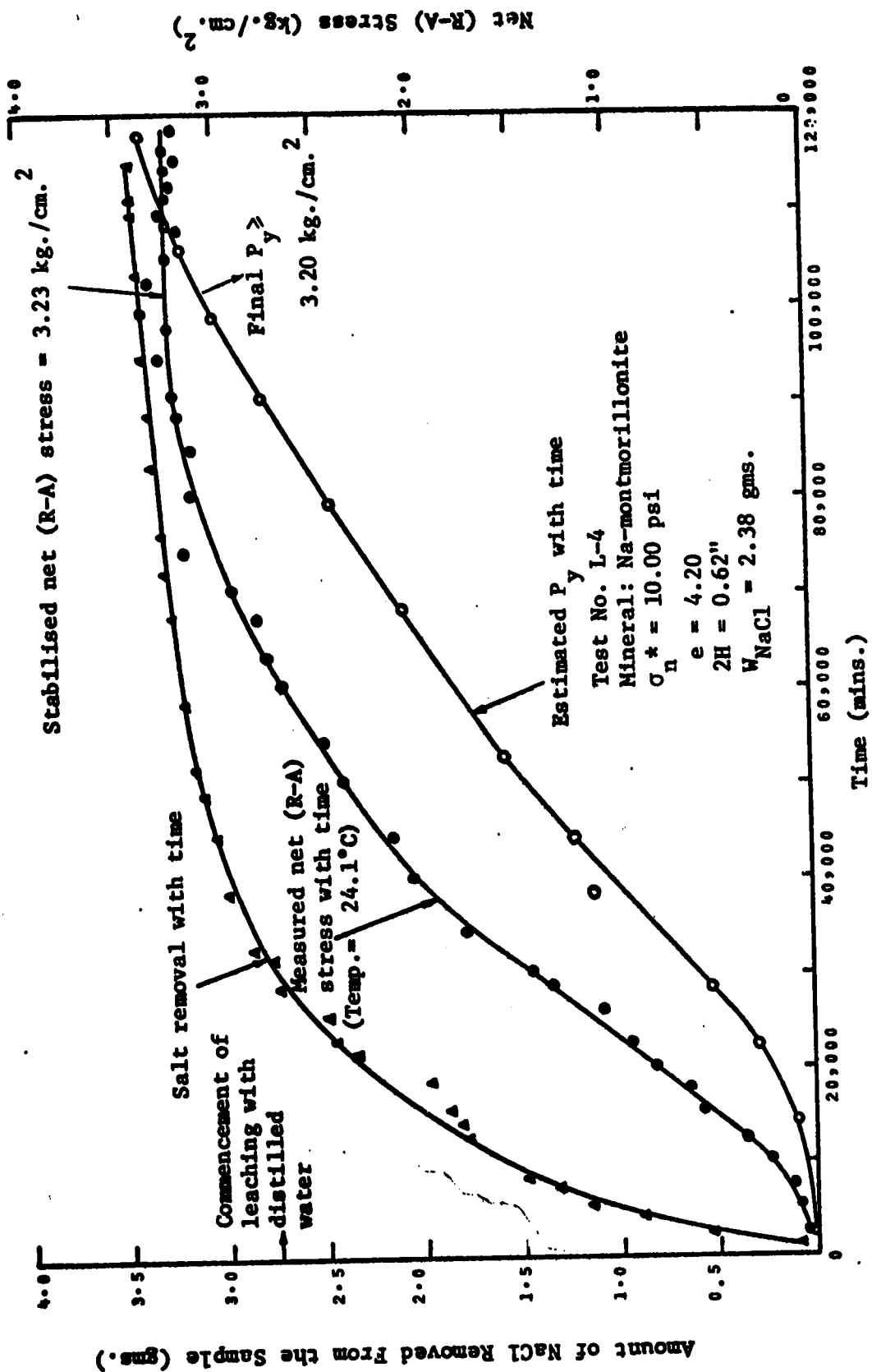
FIG. 6.21 SALT REMOVAL - TIME RELATIONSHIP AND THE CORRESPONDING DEVELOPMENT OF THE NET
(R-A) STRESS WITH TIME FOR LEACHING TEST NO. L-4
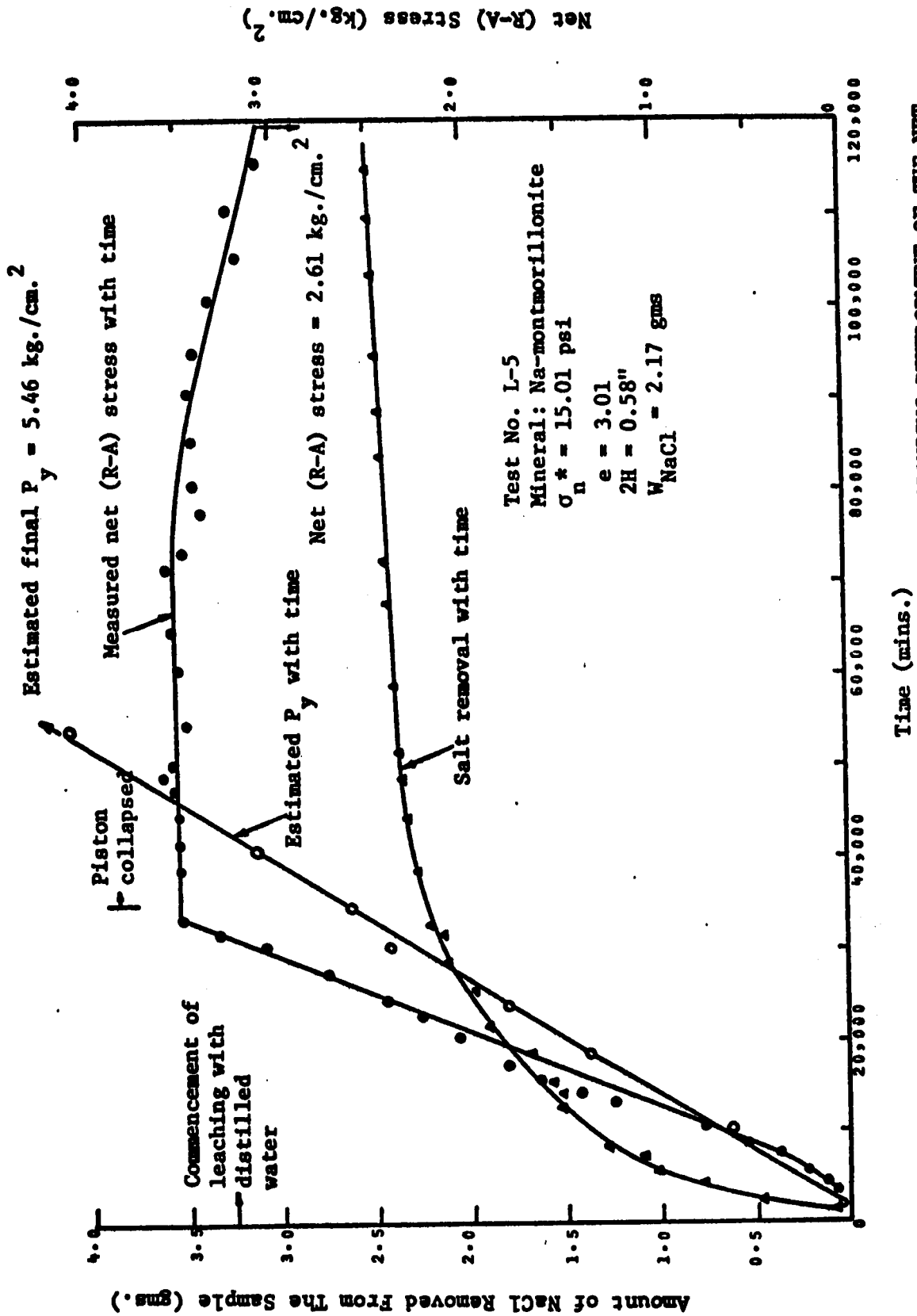
FIG. 6.22 SALT REMOVAL - TIME RELATIONSHIP AND THE CORRESPONDING DEVELOPMENT OF THE NET (R-A) STRESS WITH TIME FOR LEACHING TEST NO. L-5
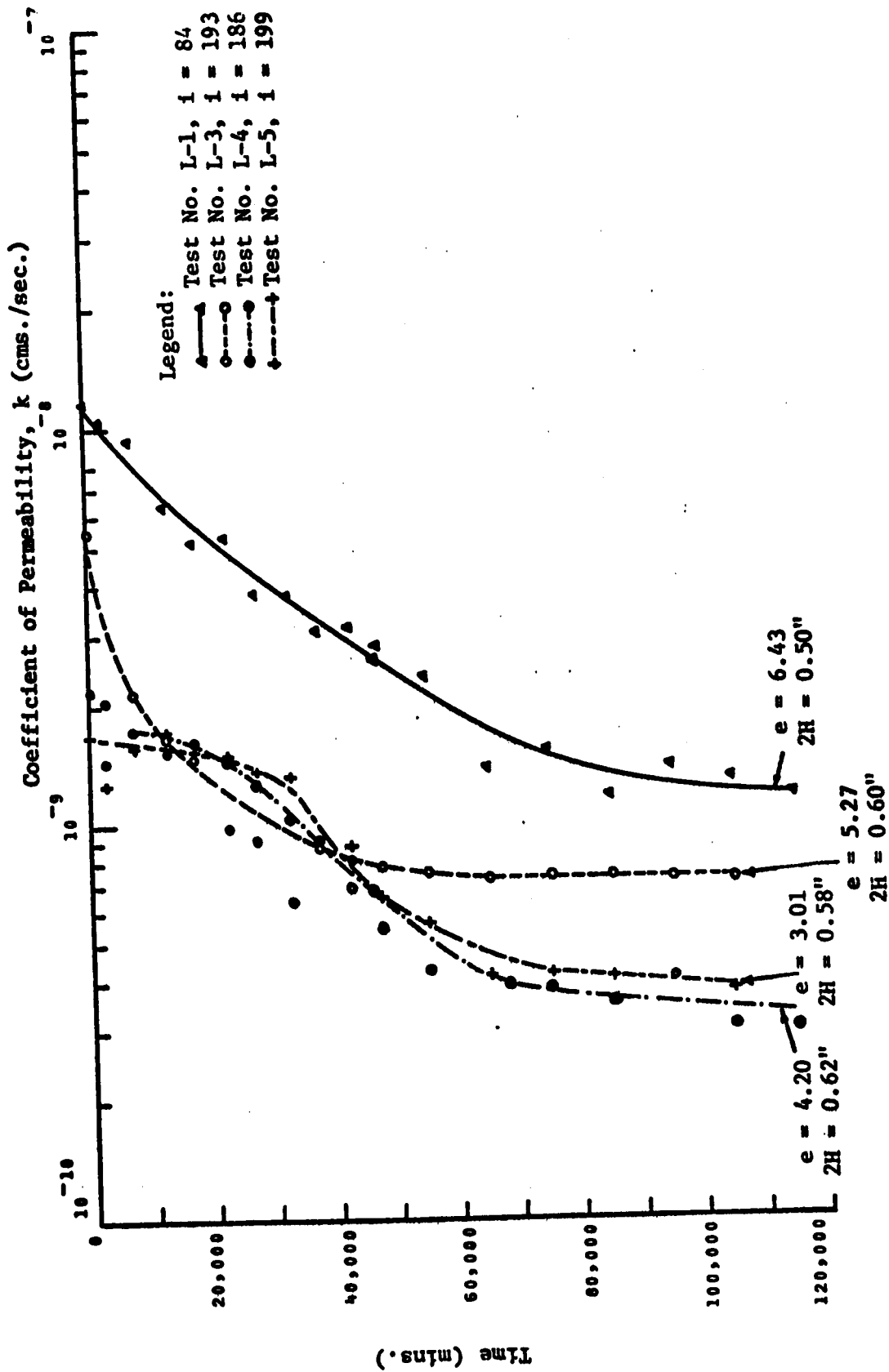
FIG. 6.23 DECREASES IN THE COEFFICIENTS OF PERMEABILITY OF THE Na-MONTMORILLONITE SAMPLES WITH TIME IN THE LEACHING TESTS
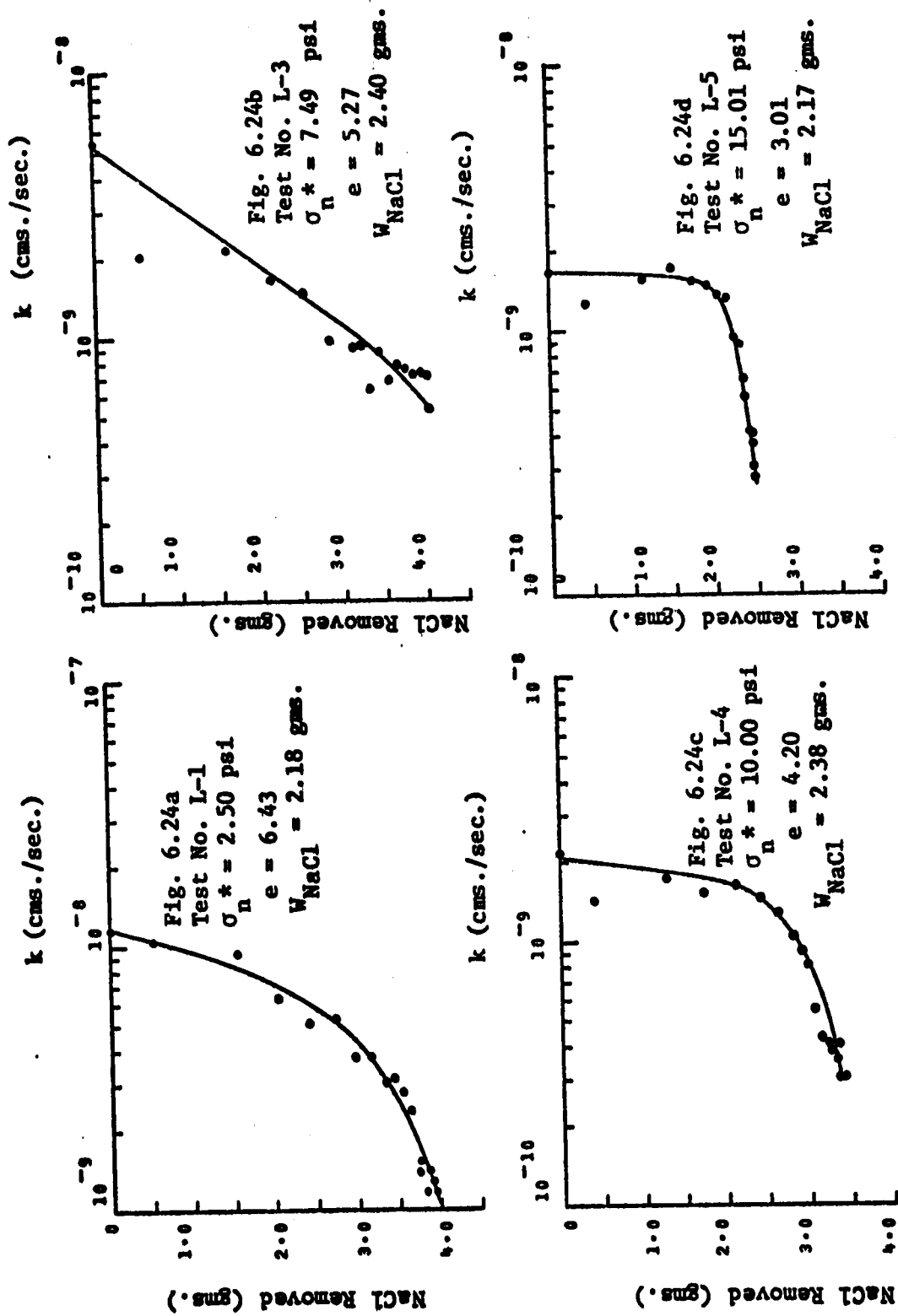
FIG. 6.24 (a, b, c and d) DECREASES IN THE COEFFICIENTS OF PERMEABILITY OF THE Na-MONTMORILLONITE SAMPLES WITH REMOVAL OF SALT IN THE LEACHING TESTS

Fig. 6.24a
Test No. L-1
$\sigma_n^* = 2.50$ psi
$e = 6.43$
$W_{NaCl} = 2.18$ gms.

Fig. 6.24b
Test No. L-3
$\sigma_n^* = 7.49$ psi
$e = 5.27$
$W_{NaCl} = 2.40$ gms.

Fig. 6.24c
Test No. L-4
$\sigma_n^* = 10.00$ psi
$e = 4.20$
$W_{NaCl} = 2.38$ gms.

Fig. 6.24d
Test No. L-5
$\sigma_n^* = 15.01$ psi
$e = 3.01$
$W_{NaCl} = 2.17$ gms.
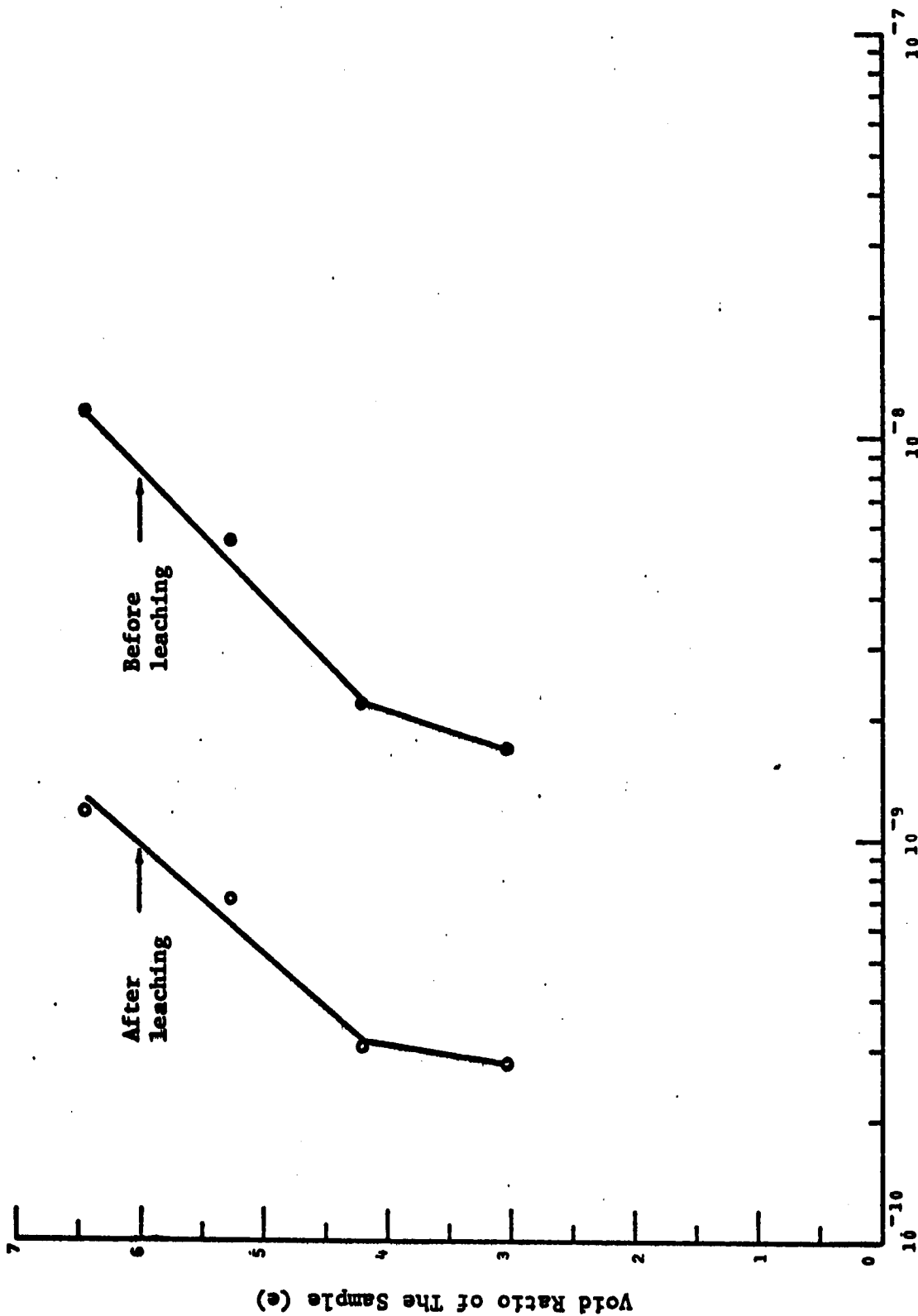
FIG. 6.25 VOID RATIO - LOG (COEFFICIENT OF PERMEABILITY) RELATIONSHIPS FOR THE Na-MONTMORILLONITE SAMPLES BEFORE AND AFTER CONSTANT VOLUME LEACHING
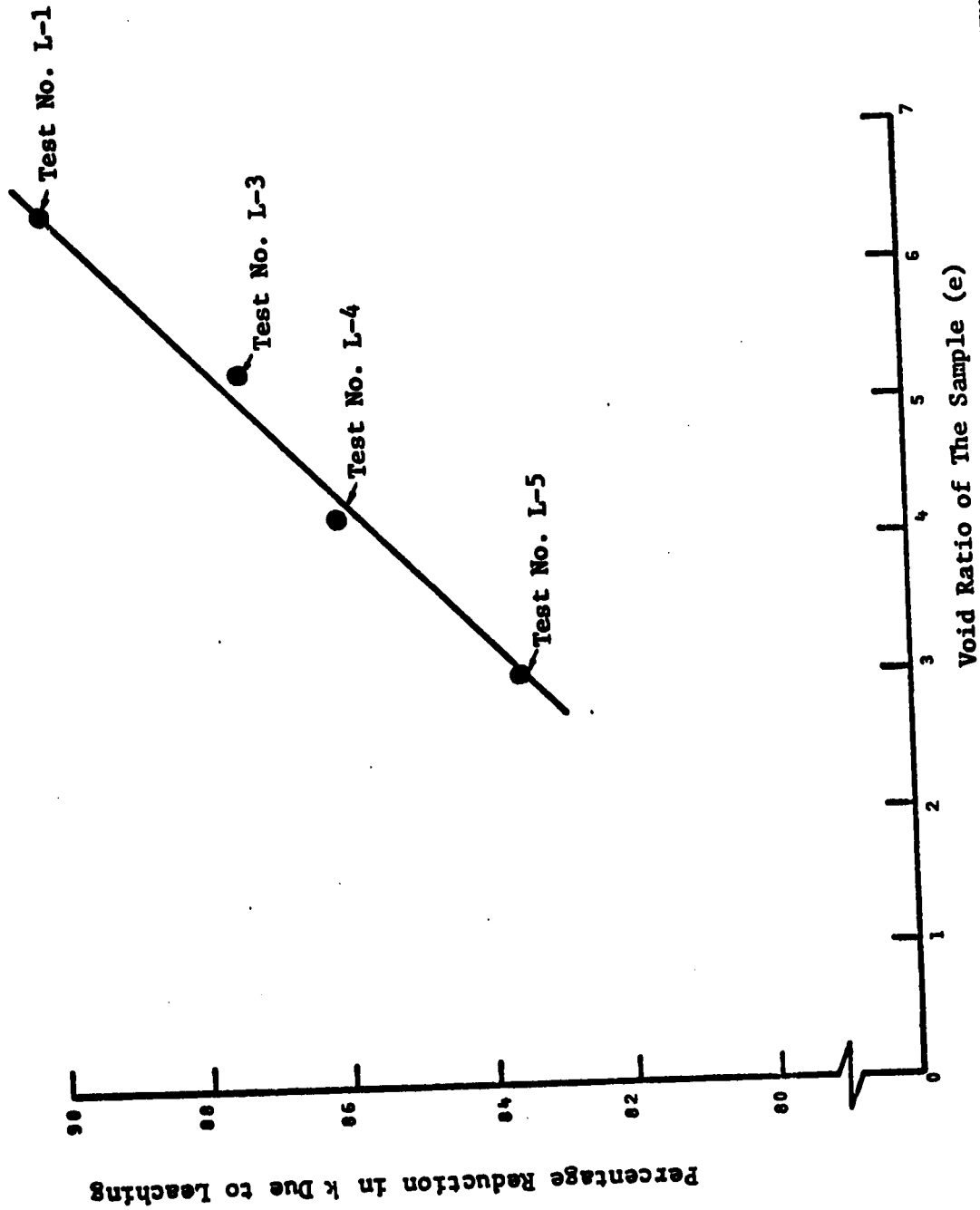
FIG. 6.26   RELATIONSHIP BETWEEN THE PERCENTAGE REDUCTION IN THE COEFFICIENT OF
PERMEABILITY DUE TO LEACHING AND VOID RATIO FOR THE CONSTANT VOLUME
LEACHING TESTS
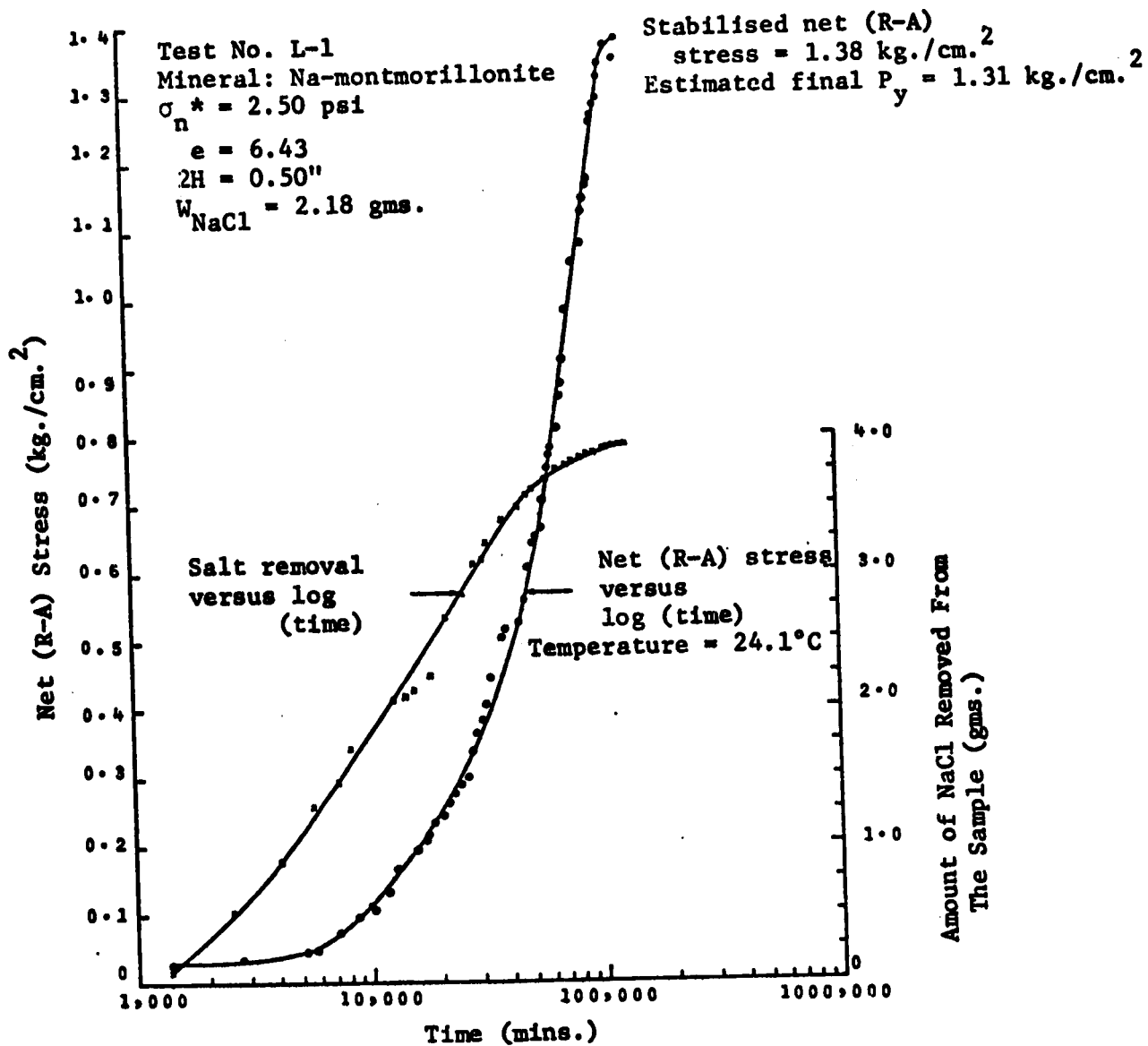
FIG. 6.27   SALT REMOVAL - LOG (TIME) AND THE CORRESPONDING
NET (R-A) STRESS - LOG (TIME) RELATIONSHIPS FOR
LEACHING TEST NO. L-1

Test No. L-2
Mineral: Na-montmorillonite
$\sigma_n^* = 5.00$ psi
 e = 3.88
2H = 0.59"
$W_{NaCl} = 2.30$ gms.

Stabilised net
(R-A) stress = 3.15 kg./cm.^{2}
Estimated final P_y = 3.59 kg./cm.^{2}
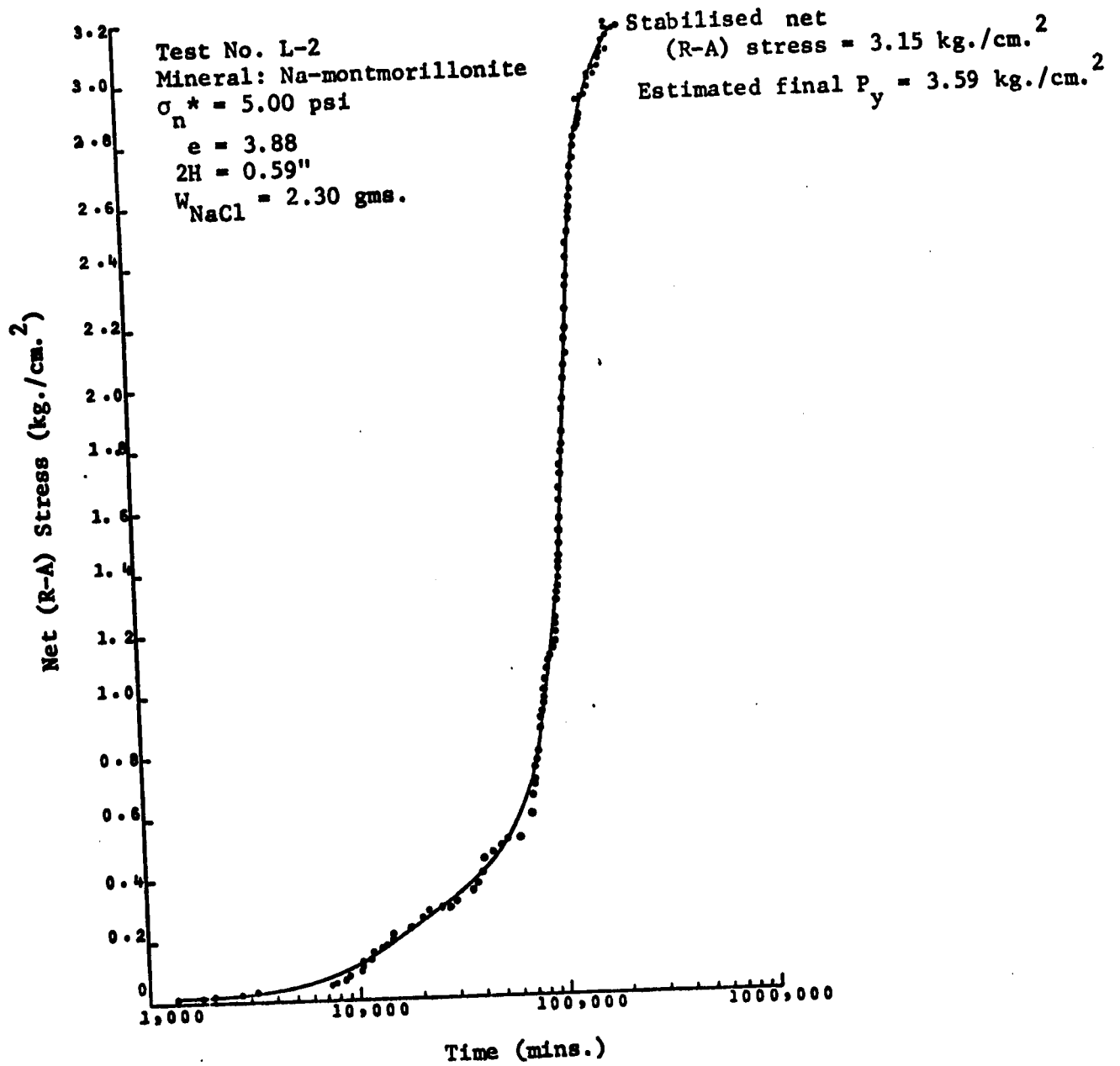
FIG. 6.28   NET (R-A) STRESS — LOG (TIME) RELATIONSHIP
FOR LEACHING TEST NO. L-2

Test No. L-3
Mineral: Na-montmorillonite

$\sigma_n^* = 7.49$ psi

e = 5.27
2H = 0.60"
$W_{NaCl} = 2.40$ gms.

Stabilised net (R-A)
stress = 2.06 kg./cm.^{2}
Estimated $P_y = 2.07$ kg./cm.^{2}

Salt removal
versus
log (time)

Net (R-A) stress
versus log (time)
Temp. = 24.1°C

Net (R-A) Stress (kg./cm.^{2})

Amount of NaCl Removed From The Sample (gms.)

Time (mins.)
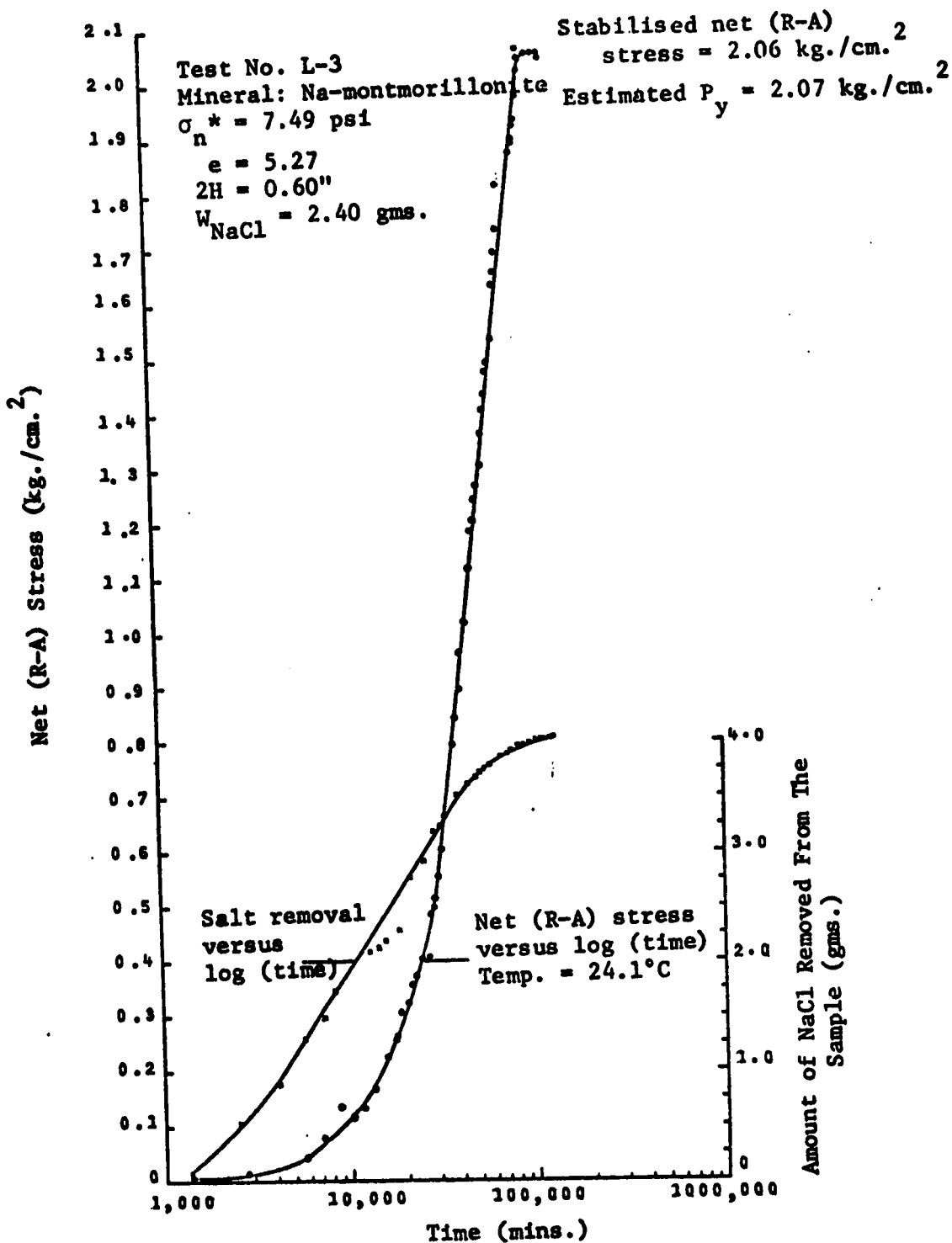
FIG. 6.29 SALT REMOVAL - LOG (TIME) AND THE CORRESPONDING
NET (R-A) STRESS - LOG (TIME) RELATIONSHIPS
FOR LEACHING TEST NO. L-3
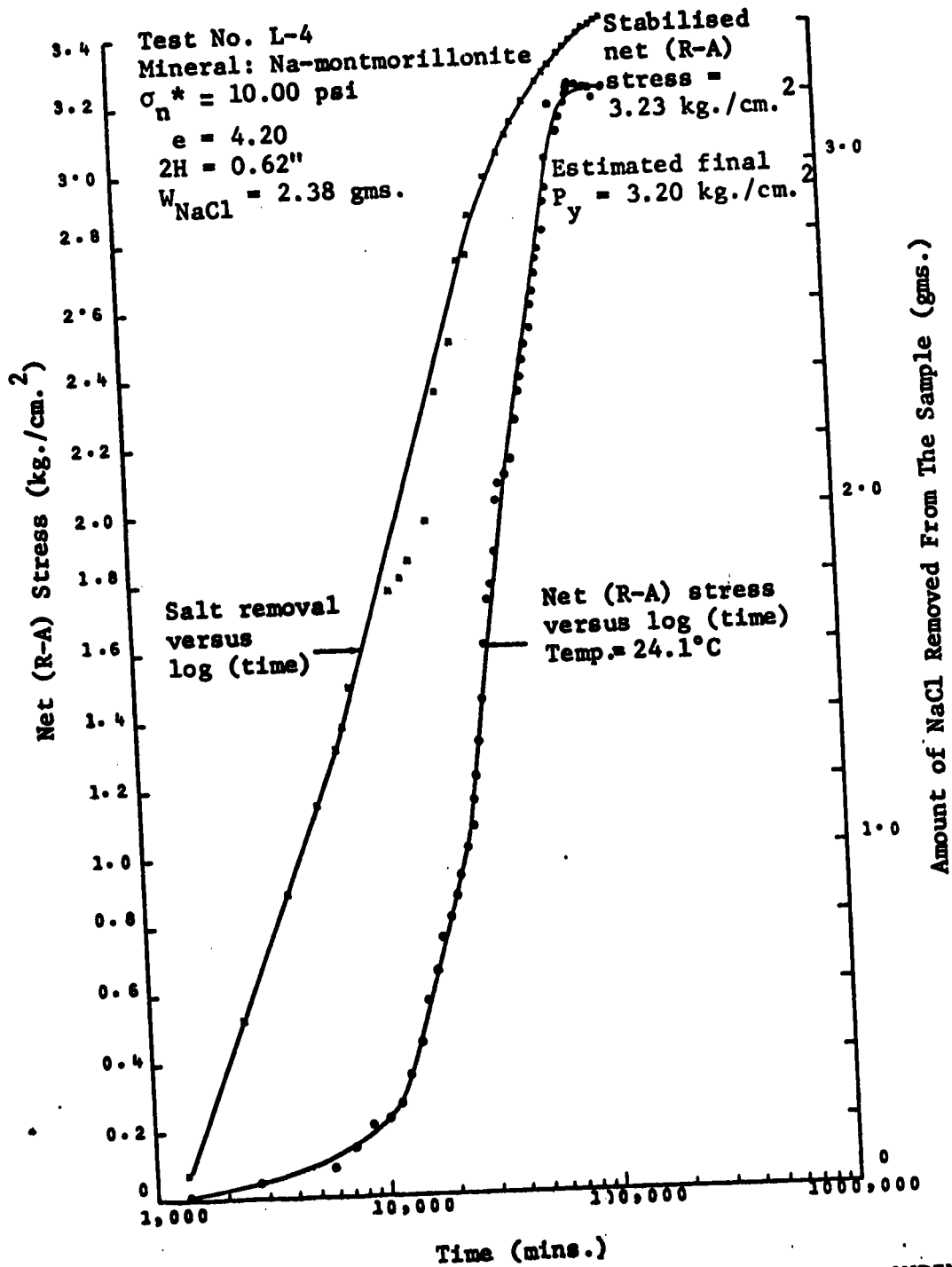
FIG. 6.30 SALT REMOVAL - LOG (TIME) AND THE CORRESPONDING NET (R-A) STRESS - LOG (TIME) RELATIONSHIPS FOR LEACHING TEST NO. L-4
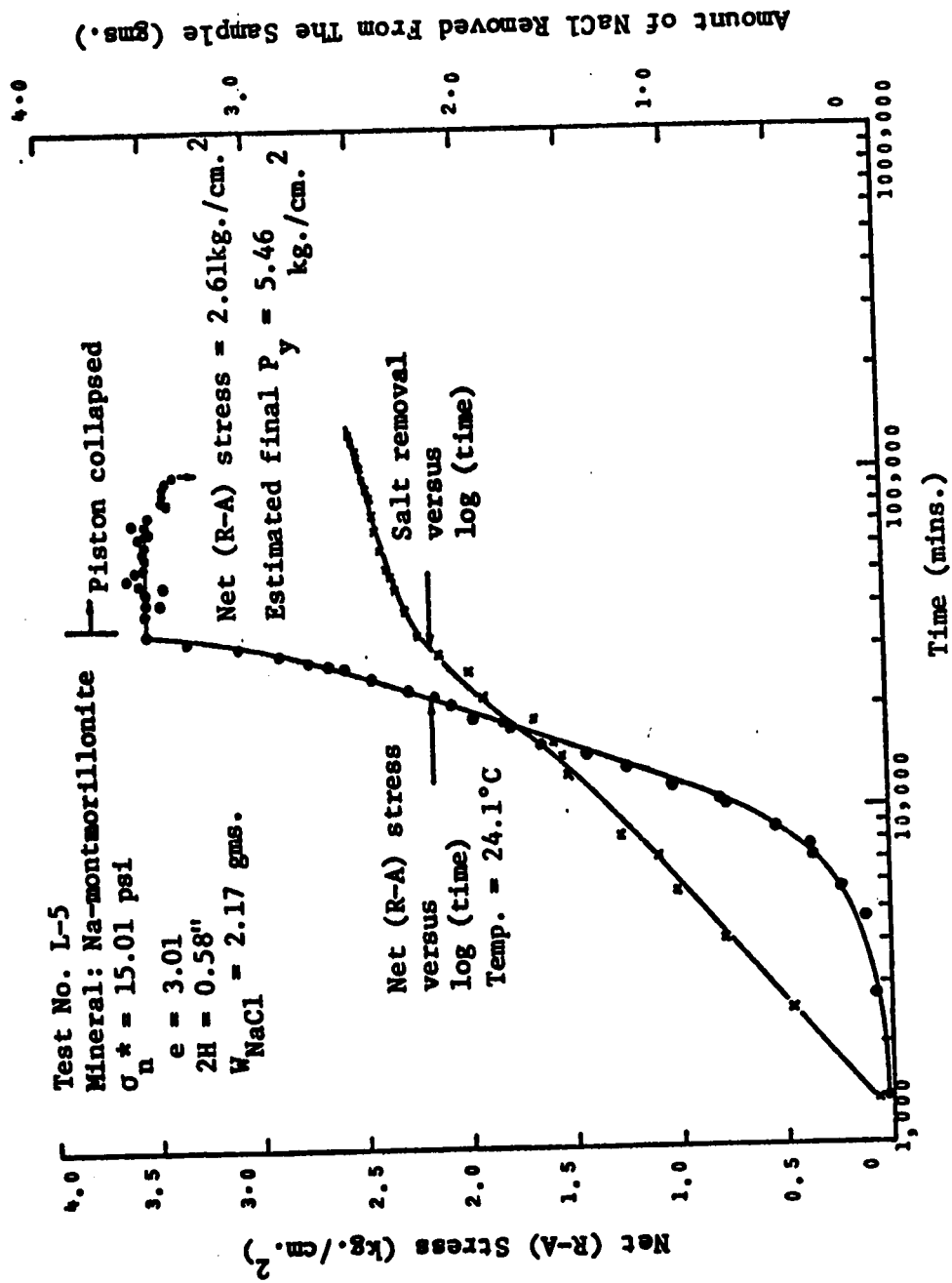
FIG. 6.31   SALT REMOVAL - LOG (TIME) AND THE CORRESPONDING NET (R-A) STRESS
- LOG (TIME) RELATIONSHIPS FOR LEACHING TEST NO. L-5

Inflow As A Percentage Of The Total Volume Of Salt Solution Initially Present In The System

Legend:
Test No. L-1, e = 6.43
Test No. L-2, e = 3.88
Test No. L-3, e = 5.27
Test No. L-4, e = 4.20
Test No. L-5, e = 3.01

Fig. 6.32a

Time (mins.)

Percentage Of The Total NaCl Removed

Fig. 6.32b

Time (mins.)

Percentage Of The Final Net (R-A) Stress

Test No.L-1: $\sigma_n^* = 2.50$ psi
Test No.L-2: $\sigma_n^* = 5.00$ psi
Test No. L-3:$\sigma_n^* = 7.49$ psi
Test No.L-4: $\sigma_n^* =$
10.00 psi
Test No.L-5:
$\sigma_n^* = 15.01$ psi

Fig. 6.32c

Time (mins.)
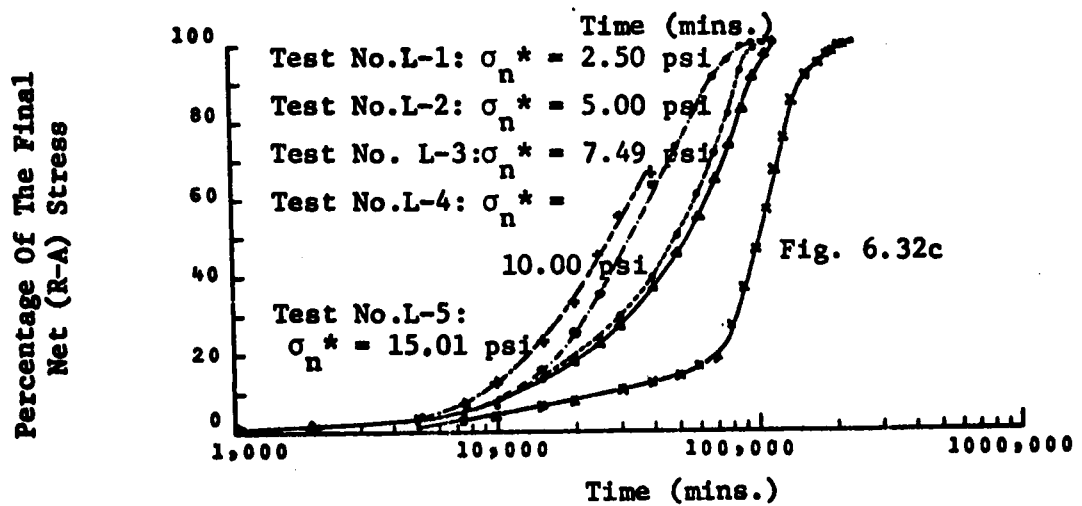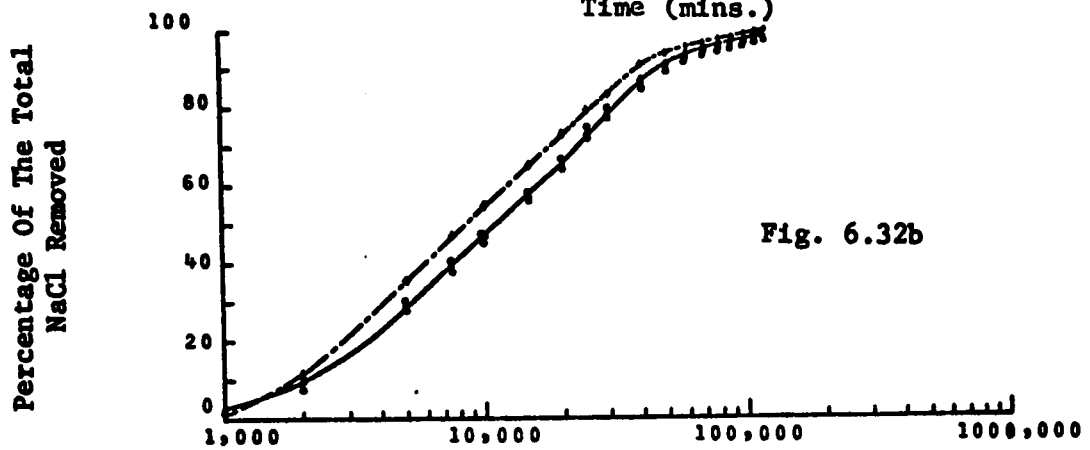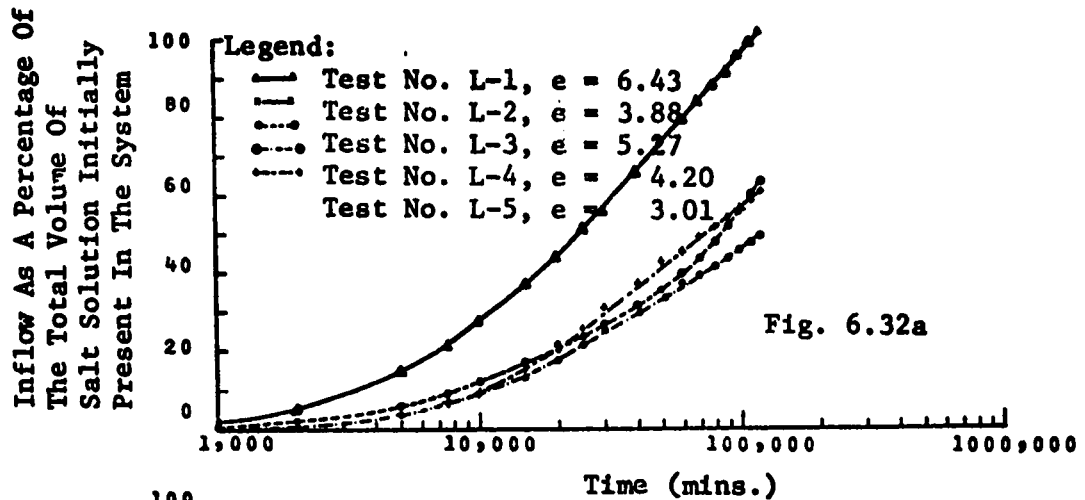
FIG. 6.32 (a, b and c)   SUMMARY OF THE CONSTANT VOLUME
LEACHING TEST RESULTS
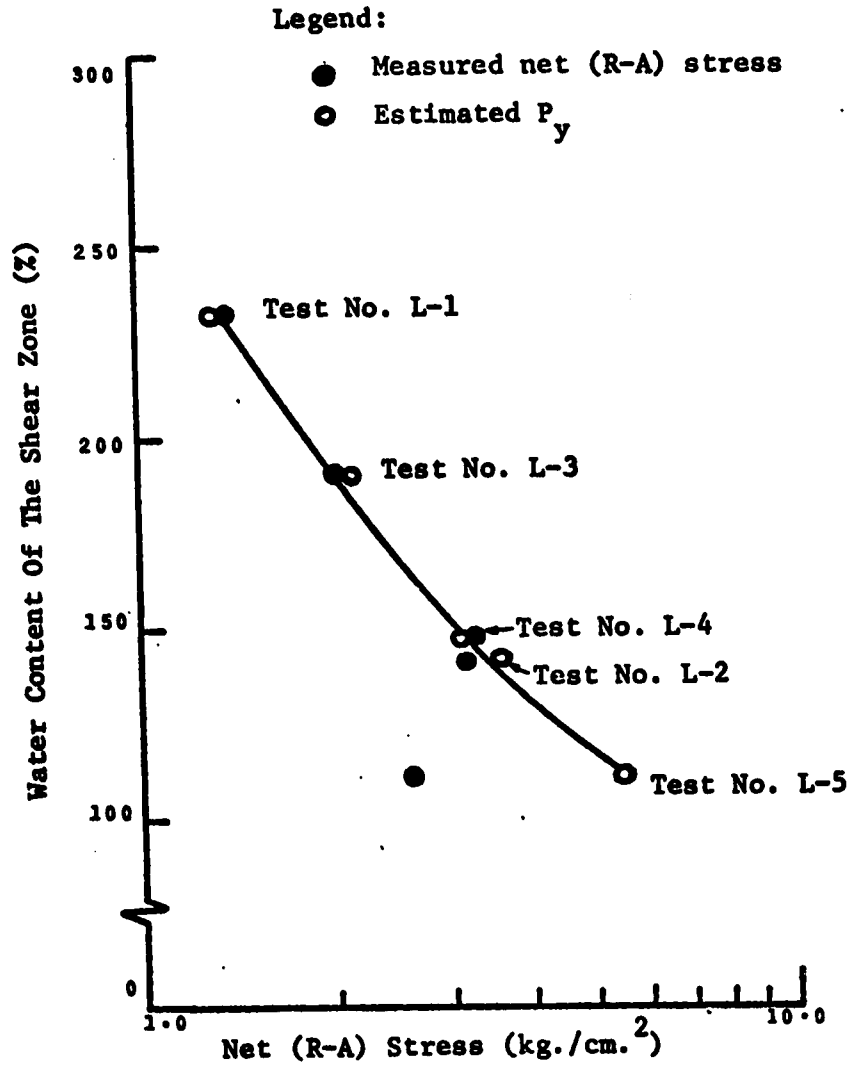
FIG. 6.33   SHEAR ZONE WATER CONTENT - LOG (R-A) STRESS
RELATIONSHIP AND COMPARISON BETWEEN THE
PREDICTED AND THE MEASURED NET (R-A) STRESSES
IN THE CONSTANT VOLUME LEACHING TESTS

Vertical Compression (inches)

+0.01

+0.02

2,000   4,000   6,000

Time (mins.)

$\sigma_n' = 2.50$ to 22.13 psi

$\sigma_n^* = 2.50$ psi

Fig. 6.34a
Test No. L-1
2H = 0.50"
O.C.R. = 3.90

Vertical Compression (inches)

+0.01

+0.02

2,000   4,000   6,000

Time (mins.)

$\sigma_n' = 5.00$ to 49.94 psi

$\sigma_n^* = 5.00$ psi

Fig. 6.34b
Test No. L-2
2H = 0.59"
O.C.R. = 6.08

Vertical Compression (inches)

+0.01

+0.02

2,000   4,000   6,000

Time (mins.)

$\sigma_n' = 7.49$ to 36.77 psi

$\sigma_n^* = 7.49$ psi

Fig. 6.34c
Test No. L-3
2H = 0.60"
O.C.R. = 3.33

Vertical Expan-sion (inches)
Compre-ssion (inches)

-0.001

0

+0.001

2,000   4,000   6,000

Time (mins.)

Fig. 6.34d, Test No. L-4
2H = 0.62", O.C.R. = 9.04

$\sigma_n' = 10.00$ to 55.89 psi

$\sigma_n^* = 10.00$ psi

Vertical Compression (inches)

+0.001

+0.002

2,000   4,000   6,000

Fig. 6.34e
Test No. L-5
2H = 0.58"
O.C.R. = 10.23

$\sigma_n' = 15.01$ to 52.07 psi

$\sigma_n^* = 15.01$ psi

FIG. 6.34 (a, b, c, d and e)   VOLUME CHANGES OF THE LEACHED Na-
MONTMORILLONITE SAMPLES WITH TIME MEASURED IN THE DIRECT
SHEAR MACHINES UNDER THE INCREASED APPARENT EFFECTIVE
STRESSES AFTER LEACHING

τ_{res} vs. σ_n' for the unleached samples ($\phi_r' = 11.5°$)

τ_{res} vs. σ_n' for Na-montmorillonite-1.15 g/l NaCl samples ($\phi_r' = 4.8°$)

τ_{res} vs. σ_n' for the leached samples ($\phi_r' = 3°$)

Apparent Effective Stress, σ_n' (psi)

Residual Shear Strength, τ_{res} (psi)

FIG. 6.35   RESIDUAL SHEAR STRENGTH - APPARENT EFFECTIVE STRESS RELATIONSHIPS FOR THE Na-MONTMORILLONITE SAMPLES BEFORE AND AFTER CONSTANT VOLUME LEACHING

$\phi_r' = 11.5°$

$\phi_r' = 9.5°$

τ_{res} vs. σ_n^* before leaching

τ_{res} vs. σ_n^* after leaching

True Effective Stress, σ_n^* (psi)

τ_{res} (psi)

FIG. 6.36   RESIDUAL SHEAR STRENGTH - TRUE EFFECTIVE STRESS RELATIONSHIPS FOR THE Na-MONTMORILLONITE SAMPLES BEFORE AND AFTER CONSTANT VOLUME LEACHING

FIG. 6.37 TANφ$_r'$ - σ$_n'$ AND TANφ$_r'$ - σ$_n$* RELATIONSHIPS FOR THE Na-MONTMORILLONITE
SAMPLES BEFORE AND AFTER CONSTANT VOLUME LEACHING

FIG. 6.38 $\tau_{res} - \sigma_n'$ AND $\tau_{res} - \sigma_n^*$ RELATIONSHIPS FOR THE Na-MONTMORILLONITE – 1.15 g/1 NaCl SERIES
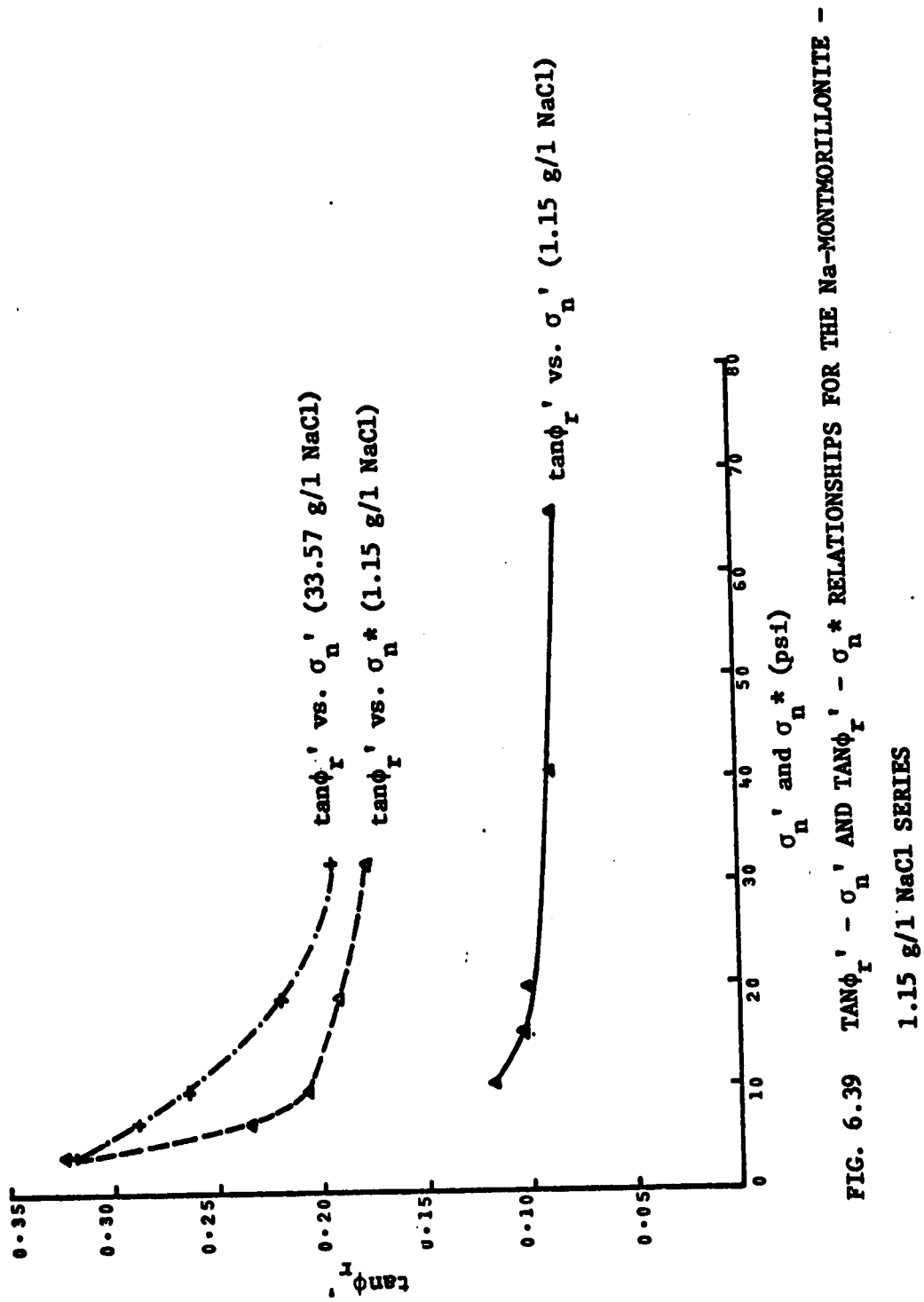
FIG. 6.39   TANϕ_r' - σ_n' AND TANϕ_r' - σ_n^* RELATIONSHIPS FOR THE Na-MONTMORILLONITE -
         1.15 g/1 NaCl SERIES

$\sigma_n' = 79.14$ psi
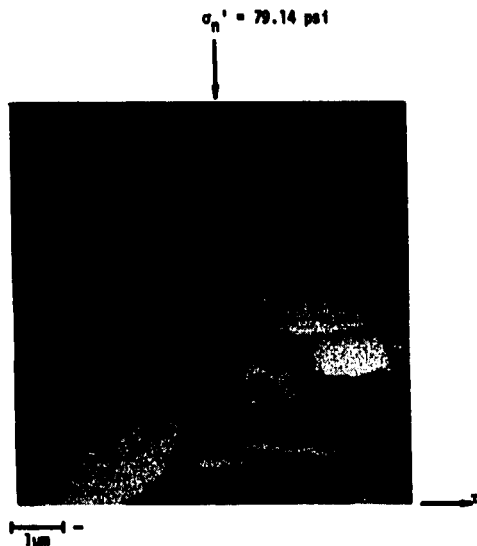
Fig. 6.40 Photomicrograph of the undeformed area outside the shear zone in a kaolinite sample showing aggregates of kaolinite particles oriented normal to the direction of consolidation in the shear box (Longitudinal section, Magnification = 10,000 x)

$\sigma_n' = 79.14$ psi
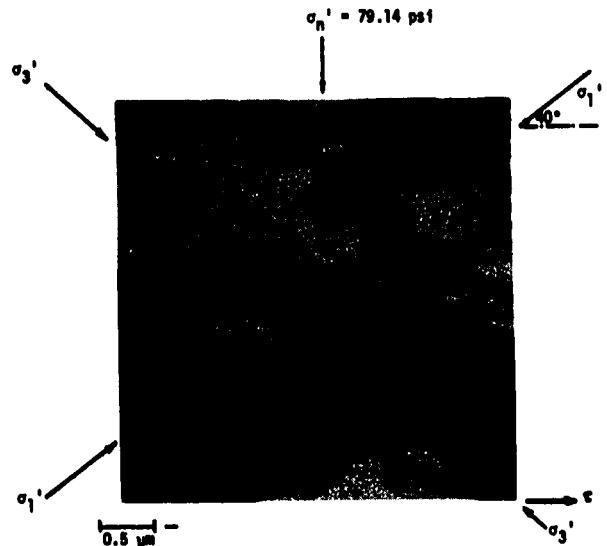
Fig. 6.41 Photomicrograph of the shear zone and the adjoining undeformed area in the kaolinite sample showing a compression texture enclosed by bands of oriented aggregates of kaolinite particles (Longitudinal section, Mag. = 20,000 x)

$\sigma_n' = 79.14$ psi
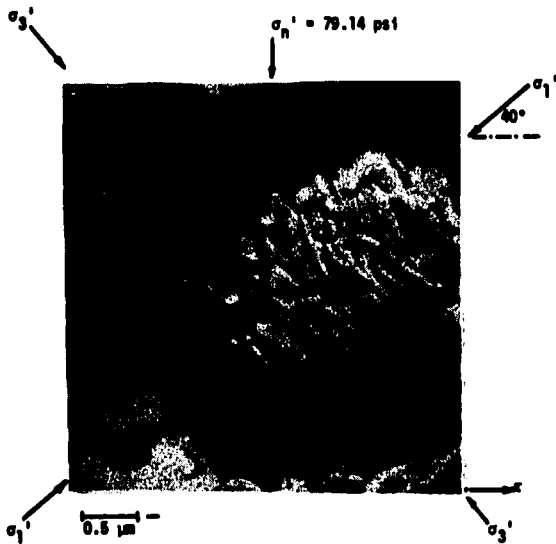
Fig. 6.42 Photomicrograph of the large displacement shear zone in the kaolinite sample showing a well developed compression texture (Longitudinal section, mag. = 20,000 x) σ_1' and σ_3' = Major and minor principal stresses in the shear box.

$\sigma_n' = 79.14$ psi
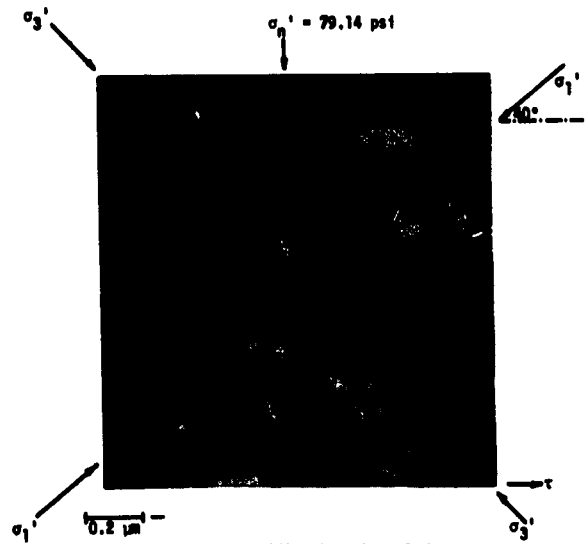
Fig. 6.43 A higher magnification view of the compression texture shown in Fig. 6.42 (Longitudinal section, mag. = 50,000 x)
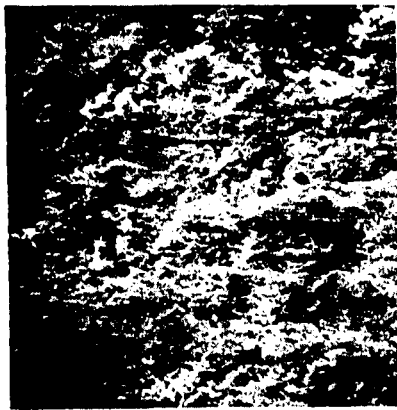
Fig. 6.44 Photomicrograph of the residual state
shear plane in the kaolinite sample
showing evidence of intense shearing
(Shear plane section, mag. = 200 x)
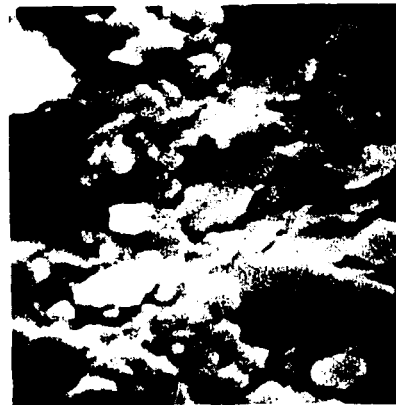
Fig. 6.45 A higher magnification view of the residual
state shear plane in the kaolinite sample showing
oriented aggregates of kaolinite particles
aligned in the direction of motion in the
shear box (Shear plane section,
mag. = 20,000 x)
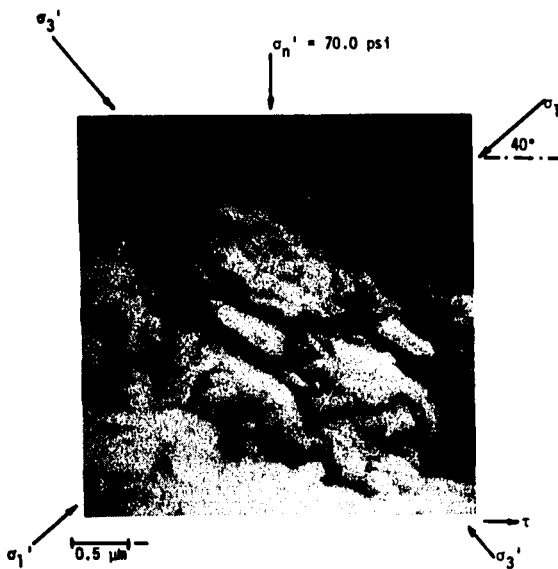
Fig. 6.46 Photomicrograph of the large displacement
shear zone in a kaolinite sample showing the
attitude of kaolinite particles in the
compression texture during a compression
cycle of shear (Longitudinal section,
mag. = 20,000 x)
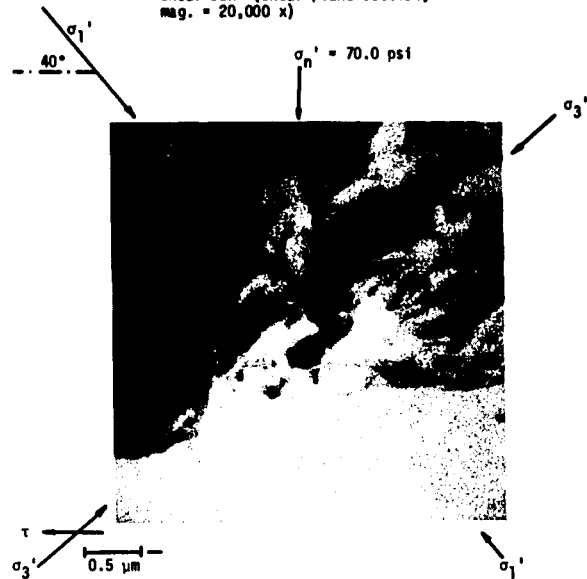
Fig. 6.47 Photomicrograph of the large displacement
shear zone in a kaolinite sample showing the
attitude of kaolinite particles in the
compression texture during a tension cycle
of shear (Longitudinal section, mag. = 20,000 x)
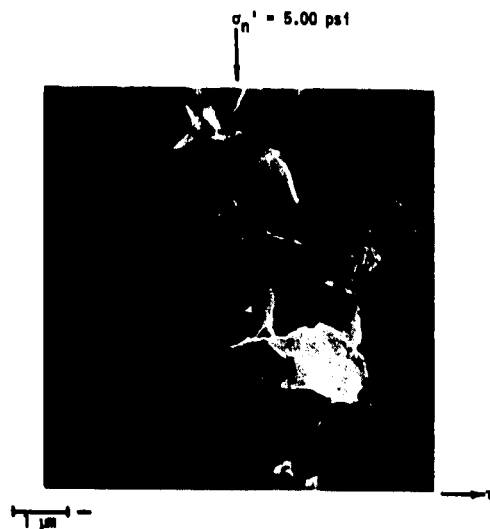
Fig. 6.48 Photomicrograph of the undeformed area outside the shear zone in a montmorillonite sample showing a loosely flocculated arrangement of aggregated montmorillonite particles (Longitudinal section, mag.= 10,000 x)
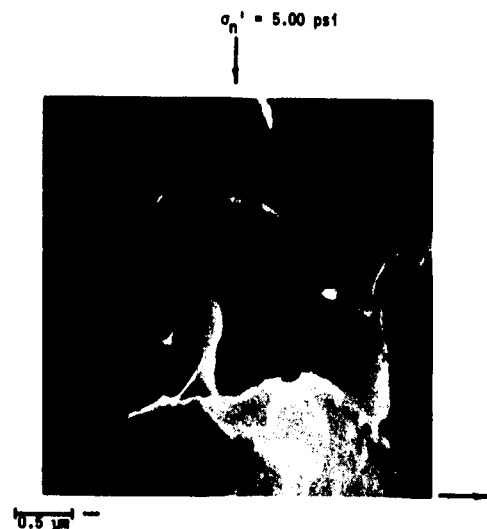
Fig. 6.49 A higher magnification view of the loosely flocculated structure shown in Fig. 6.48 (Longitudinal Section, mag. = 20,000 x)
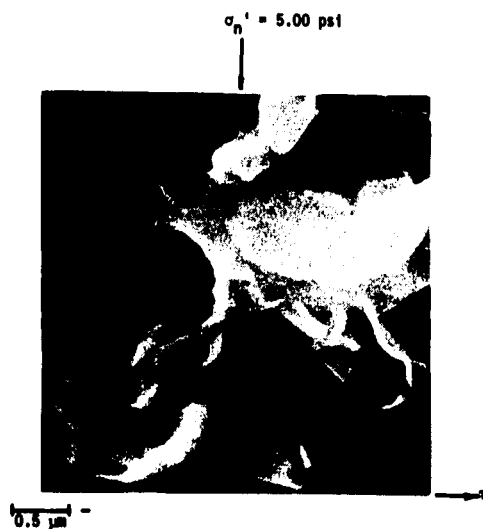
Fig. 6.50 Photomicrograph of the undeformed area in the montmorillonite sample showing a solid interparticle contact (Longitudinal section, mag. = 20,000 x)
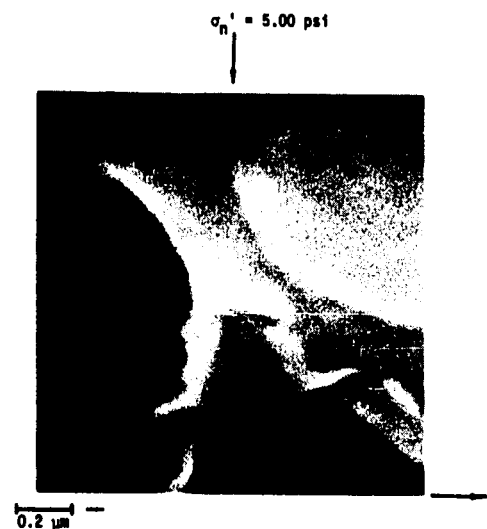
Fig. 6.51 A higher magnification view of the solid interparticle contact shown in Fig. 6.50 (Longitudinal section, mag. = 50,000 x)
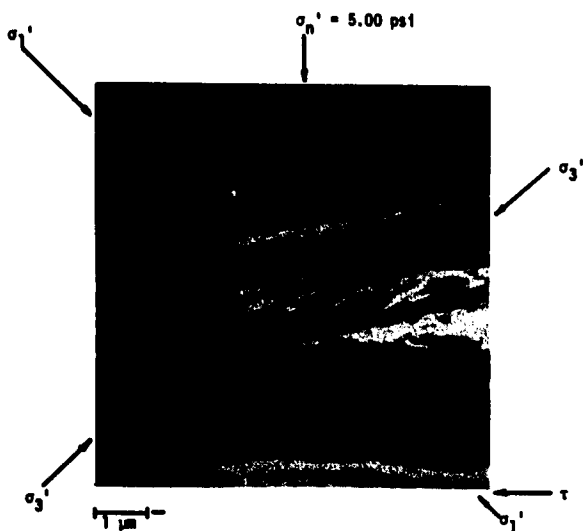
Fig. 6.52 Photomicrograph of the large displacement shear zone in the montmorillonite sample showing a compression texture (Longitudinal section, mag. = 10,000 x)
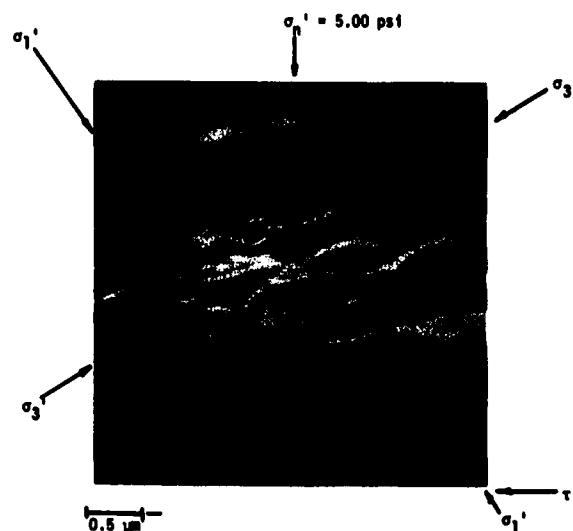
Fig. 6.53 A higher magnification view of the compression texture shown in Fig. 6.52 (Longitudinal section, mag. = 20,000 x)
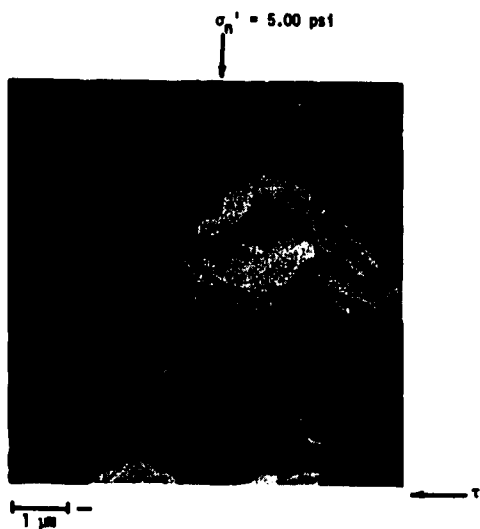
Fig. 6.54 Photomicrograph of the undeformed area just above the compression texture shown in Fig. 6.52 (Longitudinal section, mag. = 10,000 x)
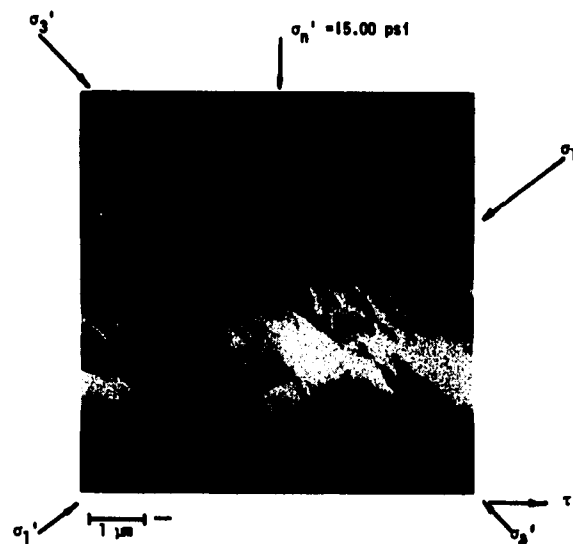
Fig. 6.55 Photomicrograph of the large displacement shear zone in a montmorillonite sample showing more compression texture (Longitudinal section, mag. = 10,000 x)

Fig. 6.56 Photomicrograph of the residual state shear plane in the montmorillonite sample showing oriented aggregates of montmorillonite particles aligned in the direction of motion in the shear box (Shear plane section, mag. = 10,000 x)

Fig. 6.57 A higher magnification view of the residual state shear plane shown in Fig. 6.56 (Shear plane section, mag. = 20,000 x)

$\sigma_n' = 5.09$ psi
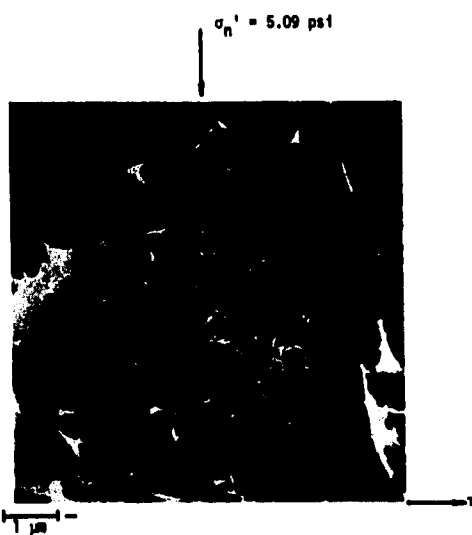
Fig. 6.58 Photomicrograph of the undeformed area outisde the shear zone in an attapulgite sample showing a random and highly intermeshed arrangement of the needle shaped particles (Longitudinal section, mag. = 10,000 x)

$\sigma_n' = 5.09$ psi
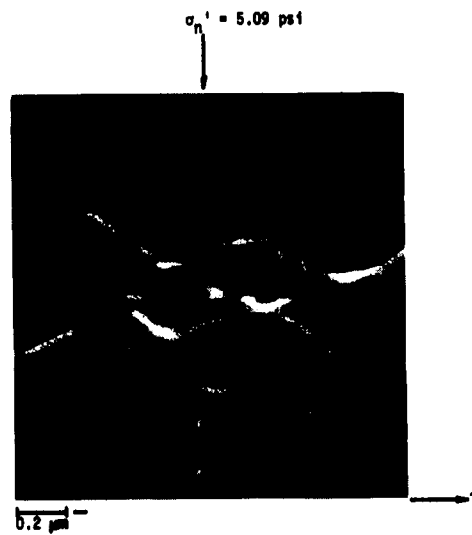
Fig. 6.59 A higher magnification view of the undeformed area shown in Fig. 6.58 (Longitudinal section, mag. = 20,000 x)

Fig. 6.60 Photomicrograph of the residual state
shear plane in the attapulgite sample
showing evidence of shearing
(Shear plane section, mag. = 10,000 x)
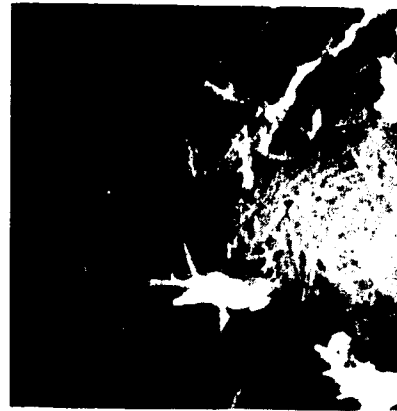
Fig. 6.61 A higher magnification view of the residual
state shear plane in the attapulgite sample
showing the interwoven structural arrangement
of the needle shaped particles in the shear
plane (Longitudinal section, mag. = 20,000 x)

$\sigma_n' = 5.09$ psi
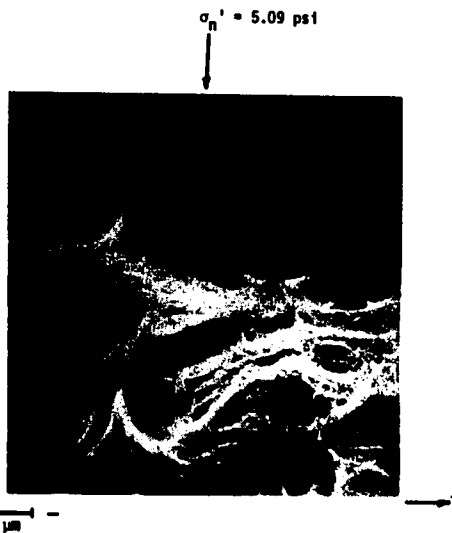
Fig. 6.62 Photomicrograph of the large displacement
shear zone in the attapulgite sample
showing the lath shaped bundles of
attapulgite needles oriented in the
direction of motion in the shear box
(Longitudinal section, mag. = 10,000 x)

$\sigma_n' = 5.09$ psi
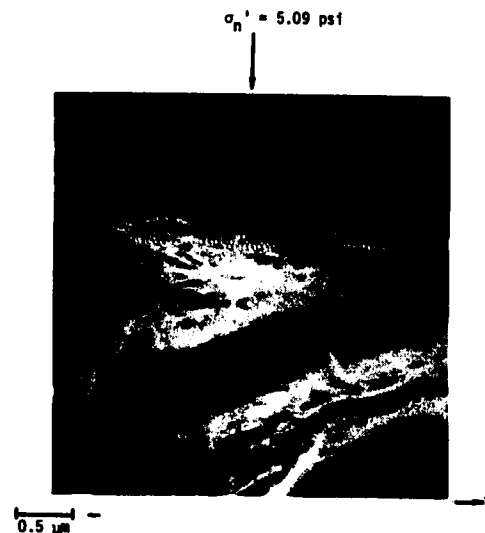
Fig. 6.63 A higher magnification view of the large
displacement shear zone shown in Fig. 6.62
(Longitudinal section, mag. = 20,000 x)

CHAPTER VII

SHEAR STRENGTH OF CLAY MINERALS AT LARGE STRAINS AND THE FACTORS THAT CONTROL THE RESIDUAL SHEAR STRENGTH

7.1 Introduction

Based on the test results obtained in this investigation and an analysis of the associated studies on the bonding in soils, the microstructural features of large displacement shear zones in clays and the frictional behaviour of solid lubricants, a physical basis of the residual shear strength of pure clay minerals and the factors that control the residual shear strength can now be established.

7.2 Residual Shear Strength of Pure Clay Minerals

The residual shear strength of a soil has been shown to depend on its mineral composition (Kenney, 1967). The results of the shear tests conducted on the three clay minerals in this investigation show that among the clay minerals, montmorillonite possesses the least residual shear strength and the residual angle of friction (ϕ_r') increases in the order: montmorillonite $(\phi_r' = 8.5°)$, kaolinite $(\phi_r' = 11°)$ and attapulgite $(\phi_r' = 30°)$. The shear test results (Tables 6.3, 6.4 and 6.5) also show that the residual shear strength of a pure clay mineral is independent of factors such as stress history, initial structure and strain rate which dominate the path dependent properties of soils. The effects of factors such as pore fluid

305

salinity and normal stress level on the residual friction angle of

a clay mineral will be discussed in later sections of this chapter.

The degree by which the shear strength decreases from the

peak to the residual state also varied with the type of clay mineral.

In going from the peak to the residual state, kaolinite demonstrates

a 50% reduction in shear strength whereas a meagre 5 to 6% drop in

shear strength from the peak to the residual state is observed in

the case of attapulgite.

7.3   Physical Basis of the Residual Shear Strength of Pure Clay Minerals

The microstructural examination of the large displacement

shear zones in the platy clay mineral samples (presented in section

6.5 of Chapter VI) has revealed that the large displacement shear zones

are characterised by compression textures in which the particle basal planes

are oriented approximately normal to the major principal stress in the shear

box. Detailed examination of the development of compression textures

leads to the notion of basal plane slip as the basic mechanism of

deformation in the shear induced structures at large strains. A

similar opinion has been expressed by Morgenstern and Tchalenko (1967 a)

from their study of the microscopic structures in kaolinite subjected

to direct shear. Hence, it can be said that the resistance offered by the

cleavage planes at the interparticle contacts in the shear zone against slippage at

large strains forms the physical basis of residual shear strength, or

in other words, residual shear strength resides in the solid friction

along the cleavage planes of the shear zone particle contacts and the

shearing resistance offered by a clay mineral at large

strains is due to the frictional property of the mineral cleavage planes.

From an examination of the available data on the residual friction angles of various clay minerals and solid lubricants along with their modes of cleavage and the types and total amounts of bonding energies available along their cleavage planes (Table 3.1 and 3.2), it was demonstrated earlier that the residual shear strength of a clay mineral depends not only on its mode of cleavage at large strains but also on the types and total amount of bonding energies available along its cleavage planes at the shear zone particle contacts. Platy clay minerals such as kaolinite and montmorillonite that have easy 001 basal cleavage have low resistances to shear at large strains and consequently possess low residual friction angles. On the other hand, a mineral such as attapulgite which has good cleavage along the 110 plane rather than the 001 (basal) plane offers a very high resistance to shear at large strains because at residual state, it has to be sheared along its stair-case like 110 cleavage planes at the interparticle contacts in the shear zone and consequently, attapulgite exhibits a very high residual friction angle $(\phi_r' = 30^{\circ})$. A part of this high residual shear strength of attapulgite might be due to the highly intermeshed nature of the lath shaped bundles of attapulgite needles which can not be segrated even at large strains. However, in the case of minerals with an identical mode of cleavage, the mineral with the lowest amount of bonding energy along its cleavage planes will exhibit the lowest residual shear strength. In this context, it was previously shown from a comparison between the bonding energies available along the 001 basal planes of kaolinite and montmorillonite (Table 3.2) that

although both the platy clay minerals have good cleavage along their
001 (basal) planes, the residual friction angle of kaolinite is higher
that that of montmorillonite because the bonding between the basal
planes of the kaolinite particles is stronger than the bonding between
the basal planes of the montmorillonite particles. In the field of
solid lubrication, the differences between the frictional resistances
of mica, graphite and talc, all having an easy 001 (basal) mode of
cleavage, have also been explained on the basis of the types and total
energies of bonding available along their respective basal planes.
In this respect, the frictional behaviour of clay minerals is strikingly
similar to that of some solid lubricants such as graphite and MoS_2.

The microstructural study undertaken in this investigation
has also confirmed the existence of solid particle to particle
contacts in the clay mineral samples. Based on this observation
and also on the concept that basal plane slip is probably the most
dominant mechanism of defrrmation in the shear induced structures
at large strains (i.e., shearing at large strain occurs predominantly
by slippage along definite mineral cleavage planes at the
solid interparticle contacts in the shear zone), it can now be
postulated with a degree of certainty that the shear process
at large strain involves continuous rupturing and making of bonds
along the solid interparticle contacts in the shear zone.
As stated earlier, a similar mechanistic picture of the
shearing process has also been presented by Mitchell et al. (1969).
The actual nature of these bonds or flow units at the intercleavage

and the interparticle contacts is believed to be the same as that described by Mitchell et al. (op. cit.) and in their view, individual oxygen atoms can be considered as bonds or flow units. The number of bonds at any contact has been shown to depend on the compressive force transmitted at the contact (Mitchell et al., 1969). However, at large strains, the compressive stress transmitted the interparticle contacts will be the appropriate effective stress on the mineral cleavage planes that controls the residual shear strength of a clay mineral. It can be further added that since the mechanisms of shear and generation of strength at large strains for clay minerals appear to be quite similar to those for some solid lubricants, the Terzaghi-Bowden and Tabor adhesion theory of friction, which has been shown to be valid for some solid lubricants and some metals, should also account for the conditions at the intercleavage and the interparticle contacts in the clay minerals. A similar view has also been expressed by Mitchell et al. (op. cit.).

7.4 The Concept of True Effective Stress and the Effect of Pore Fluid Salt Concentration on the Residual Shear Strength of Clay Minerals

i) The Concept of True Effective Stress

In the early 1920's, Terzaghi realised that the shear strength behaviour of soils and their volume change characteristics depend not on the total stress applied to the soil, but on the difference between the total stress and the pressure set-up in the pore fluid. The concept of effective stress for a fully saturated soil, as stated above, really consists of two statements.

1. The effective stress is defined as:

$$\sigma_n' = \sigma_n - u_w \qquad (7.1)$$

where σ_n' = the effective stress,

σ_n = the total stress,

and, u_w = the pore water pressure.

2. The effective stress thus defined controls certain aspects of the behaviour of soils, notably compressibility and shear strength.

Both of these statements are absolutely essential to the principle, for effective stress, defined as above, would be a useless quantity if it were not for its relation to soil behaviour.

It has been known for a fairly long time that the effective stress (σ_n'), defined by equation (7.1), has definite control on the peak and the residual shear strengths of soils and so far, the Coulomb-Terzaghi relationships for the peak and the residual shear strengths have been written in terms of this effective stress (i.e. σ_n') as

Peak shear strength = $\tau_{peak} = c' + \sigma_n' \tan\phi'$ $\qquad (1.1)$

and, Residual shear strength = $\tau_{peak} = c_r' + \sigma_n' \tan\phi_r'$ $\qquad (1.2)$

where, c' and c_r' = the cohesion intercepts at the peak and the residual states,

ϕ' and ϕ_r' = the peak and the residual angle of shearing resistance.

However, the effective stress σ_n', defined by equation (7.1), has been found to be inadequate in explaining the volume change characteristics of some active clays and clay-shales (Balasubramonian, 1972) because it excludes the forces that arise from the peculiar nature of active clays (such as a net charge deficiency within the lattice structure and a high specific surface) and the physico-chemical environment. The magnitude of these forces are so significant in active clay-water systems that they must be considered while dealing with their volume change and shear strength behaviour. Hence, based on the mechanistic picture of forces between adjacent particles in a fully saturated active clay-water system (Fig. 3.2) and from consideration of statical equilibrium of these normal forces perpendicular to a horizontal plane of unit area in the system, a modified effective stress law was derived in Chapter III. According to this relationship,

$$\sigma_n' = \sigma_n - u_w = \sigma_n^* + (R-A) \qquad (3.6)$$

which can be rearranged as,

$$\sigma_n^* = \sigma_n' - (R-A) \qquad (3.7)$$

where σ_n^* is defined as the true effective stress,

σ_n' is defined as the apparent effective stress,

and,   (R-A) is defined as the net interparticle stress due to the physico-chemical environment.

When the excess pore water pressure of an active clay-water system subjected to a certain normal stress is zero, the apparent effective

stress (σ_n') of the system is equal to the externally applied normal stress on the system. However, to obtain the true effective stress (σ_n^*) of the system, the net (R-A) stress of the system must be subtracted from the apparent effective stress (or the externally applied normal stress) of the system and it is evident from Equation 3.7 that the true effective stress of an active clay-water system is not equal to the externally applied normal stress (or the apparent effective stress, σ_n') on the system. But a study of soil behaviour in terms of the true effective stress (σ_n^*) is possible only if the net (R-A) stress can be estimated (or measured) with reasonable accuracy. From the excellent agreement obtained here between the predicted and the measured values of the net (R-A) stresses that developed in the Na-montmorillonite samples due to constant volume leaching (Fig. 6.33), it can be concluded that the net (R-A) stress of an active clay mineral such as montmorillonite (with sodium as the dominant cation) may be approximated by the double-layer repulsive stress (Eqn. 3.29) if the effective surface area of the mineral can be estimated with reasonable accuracy.

The volume change behaviour of soils associated with particle deformation and particle reorientation without a change of fabric have been shown to be governed by the true effective stress, σ_n^* (Balasubramonian, 1972). The results of the constant volume leaching tests on the Na-montmorillonite samples (reported in Chapter VI) provide further support to the concept of σ_n^* controlling the volume change characteristics of active clay-water systems. In these tests, it was found that although the leached samples were subjected to normal

stresses that were 400-900% higher than the initial effective stresses of the samples before leaching, the volume changes under the increased applied stresses after leaching were minimal (Figs. 6.34 a, b, c and d). Since the true effective stress of each sample was held constant throughout the leaching process, the minimal volume changes of the samples under the increased apparent effective stresses after leaching clearly prove that it was the true effective stress $(\sigma_n{}^*)$ that governed the volume change behaviour of the Na-montmorillonite sample.

It was shown earlier that the Coulomb-Terzaghi relationship for the residual shear strength (τ_{res}) of soils can be expressed in terms of the true effective stress as

$$\tau_{res} = [\sigma_n' - (R-A)] \tan\phi_r' \qquad (3.23\ a)$$

$$= \sigma_n{}^* \tan\phi_r' \qquad (3.23\ b)$$

The above relationship for residual shear strength is based on the consideration that the source of shear strength at large strains is purely frictional.

The interpretation of the available data on the residual shear strength of Na-montmorillonite (Kenney, 1967) using the modified Coulomb-Terzaghi relationship for residual strength (presented in Table 3.3) clearly suggests that the residual shear strength of an active clay mineral such as montmorillonite is governed by the true effective stress $(\sigma_n{}^*)$ on the mineral basal planes and not by the apparent effective stress (σ_n'). To establish conclusively that it is

the true effective stress that controls the residual shear strength

of clay minerals, a special testing programme was undertaken in which

the residual shear strengths of saline Na-montmorillonite samples were

compared with the residual shear strengths of the same samples after

replacement of the saline pore fluids under constant true effective

stress (and hence under constant sample volume) conditions. The results

obtained from these special tests have been presented and interpreted

in Chapter VI (section 6.4) and these test results (summarised in

Table 6.10) show that although the apparent effective stresses of the

montmorillonite samples increased by 400-900% due to constant volume

leaching, the residual shear strengths of the samples did not increase

at all. On the contrary, the residual shear strength of a leached sample

under the much higher apparent effective stress was either the same as

or less than the corresponding residual strength of the same sample

under much lower apparent effective stress before leaching. Since

the true effective stresses of the samples were held constant

throughout the leaching process, the observation of no increases in

the residual strengths of the Na-montmorillonite samples conclusively

proves that the residual shear strength of a clay mineral is indeed

governed by the true effective stress on the mineral basal planes.

The residual shear strength data obtained from the montmorillonite -

1.15 g/l NaCl series was also reinterpreted using the modified

Coulomb-Terzaghi relationship for residual strength (Eqn. 3.23 b)

and the reinterpreted strength data, presented in Table 6.11, provide

further support to the fact that it is the true effective stress, and

not the apparent effective stress, that controls the residual shear

strength of clay minerals. This true effective stress on the mineral cleavage planes must then also be the compressive stress transmitted at the intercleavage and the interparticle contacts that governs the number of bonds at any contact.

The effect of pore fluid salt concentration on the residual shear strength of various clay minerals can now be discussed in light of the modified Coulomb-Terzaghi relationship expressed in terms of the true effective stress.

ii) <u>The Effect of Pore Fluid Salt Concentration on the Residual Shear Strength of Clay Minerals</u>

According to the concept of true effective stress, the effect of changing the pore fluid salt concentration of a clay-water system is to change its net (R-A) stress and if the system is held under a constant apparent effective stress (σ_n'), a change in the net (R-A) stress of the system will cause the true effective stress (and hence the volume) of the system to change. Since true effective stress controls residual shear strength, this change in the true effective stress of the system due to a corresponding change in salinity under a constant apparent effective stress will cause the residual shear strength of the system to change. However, instead of holding the apparent effective stress (σ_n') of the system constant, if the true effective stress (σ_n^*) of the system is held constant, a change in the pore fluid salinity will not bring about any change in the residual shear strength of the system as shown by the comparison between the residual shear strengths of Na-montmorillonite samples before and after replacement of the

saline pore fluids under constant true effective stress conditions (Table 6.10).

The residual shear strengths of kaolinite and Na-attapulgite were inappreciably influenced by the pore fluid NaCl concentrations (Figs. 6.1d, 6.2d, 6.5d, 6.6d). Both minerals exhibited unique residual friction angles that were independent of the pore fluid salt contents but dependent on the normal stress level. Since kaolinite and Na-attapulgite have low cation exchange capacities and low specific surfaces (Table 5.2), the net (R-A) stresses in these minerals under almost all conditions of salinity and stress are very small. Moreover, kaolinite is a coarse mineral with a large ratio of edge to face area and this together with the fact that it has a very low specific surface contributes to formation of rather thin adsorbed layers on the kaolinite particles and particles come much closer than about 20 Å. This is substantiated by studies of West (1963) and Smart (1967). The close packing of kaolinite particles observed in the large displacement shear zone in the kaolinite sample (Fig. 6.42) appears to indicate the ability of the shear zone kaolinite particles to reach particle spacings of 20 Å or less at large strains even under low normal stresses. Based on some theoretical considerations, Bailey (1965) has shown that the long range forces in a clay mineral vanish for particle spacings of about 20 Å or less. Hence it would appear that under almost all conditions of pore fluid salinities and applied stresses, the net (R-A) stresses in kaolinite and attapulgite systems are so small that the true effective stresses of these systems are always equal to

the corresponding apparent effective stresses and the only stress governing the residual shear strengths of these inactive clay minerals is the grain to grain contact stress. Therefore, under a constant apparent effective stress, a change in the pore fluid salt content of any one of these inactive clay minerals causes no change in the true effective stress of the system (which, for an inactive clay mineral, is always equal to the corresponding apparent effective stress). Consequently, no change is observed in the residual shear strength of any one of these inactive clay-water systems due to a corresponding change in the pore fluid salinity under a constant apparent effective stress. It can therefore be concluded that the conventional Coulomb-Terzaghi relationship for residual strength, defined by $\tau_{res} = \sigma_n' \tan\phi_r'$, is still adequate to express the residual shear strengths of inactive clay minerals such as kaolinite and attapulgite.

However, in the case of Na-montmorillonite (which demonstrates significantly high net (R-A) stresses because of its high cation exchange capacity and high specific surface), if the residual shear strengths and the $\tan\phi_r'$ values (calculated in a conventional manner using $\tan\phi_r' = \tau_{res}/\sigma_n'$) obtained under various pore fluid salt concentrations are plotted against the corresponding apparent effective stresses (σ_n'), as shown in Figs. 6.9d and 6.10d, a distinct trend of increasing residual friction angle with increasing pore fluid salt concentration is observed. The immediate conclusion from Figs. 6.9d and 6.10d would be that the residual shear strength of montmorillonite increases with increasing ion concentration in the pore fluid. However, if the modified Coulomb-Terzaghi relationship for

residual strength expressed in terms of the true effective (Eqn. 3.23 b)

is used for analysing the residual shear strength data on Na-montmorillonite

obtained under various pore fluid salt contents, the resulting plots

of residual shear strengths and the $\tan\phi_r'$ values (calculated using

$\tan\phi_r' = \tau_{res}/\sigma_n^*$) against the corresponding true effective stresses,

as shown in Figs. 6.38 and 6.39, immediately show that under a certain

true effective stress, montmorillonite also possesses an unique residual

angle of friction that is independent of the pore fluid NaCl concentrations.

This independence of the residual friction angle of montmorillonite on

the pore fluid salt concentration has been demonstrated not only from

the interpretation of the shear strength data on Na-montmorillonite

in terms of the modified Coulomb-Terzaghi relationship for residual

strength (Tables 3.3 and 6.11) but also from the tests in which the

residual shear strengths of saline montmorillonite samples were

compared with the residual shear strengths of the subsequently leached

states of the same samples under constant true effective stress conditions

(see Figs. 6.36 and 6.37 in conjunction with Table 6.10). Hence in the

case of an active clay mineral (which demonstrates high (R-A) stresses

under low pore fluid salt concentrations because of its high surface

activity), if the residual shear strengths measured under various pore

fluid salt contents are divided in the conventional manner by the

corresponding apparent effective stresses to obtain the values of $\tan\phi_r'$,

different values of ϕ_r' will be obtained for different pore fluid

salinities. However, if the same residual shear strengths are divided

by the corresponding true effective stresses, then an unique residual

friction angle that is independent of the pore fluid salt contents but

dependent on the magnitude of true effective stress will be obtained for the mineral. This is the true residual friction angle of the mineral. The relationship between tan (true ϕ_r') and σ_n^* is unique for an active clay mineral and in the case of montmorillonite, it almost coincides with the $\tan\phi_r'$ versus σ_n' plot for the 33.57 g/l NaCl system (Figs. 6.37 and 6.39). This is due to the fact that in highly saline environments, the net (R-A) stresses in montmorillonite are practically negligible (Table 3.3) and the true effective stress of a highly saline montmorillonite system is virtually equal to its apparent effective stress. Hence, the true residual friction angle of an active clay mineral may be determined in a conventional manner from a direct shear test by testing the mineral in a highly saline pore fluid environment. It is also interesting to note that the $\tan\phi_r'$ versus σ_n' plots for montmorillonite (Figs. 6.10d and 6.37) show an unmistakable trend of convergence at very high normal stresses. This means that at sufficiently high normal stresses, the $\tan\phi_r'$ values for montmorillonite, calculated in the conventional manner using $\tan\phi_r' = \tau_{res}/\sigma_n'$, become independent of the pore fluid salt contents and at these high stress levels, the residual friction angle (calculated from $\tau_{res} = \sigma_n' \tan\phi_r'$) obtained under any salt concentration is the true residual friction angle of the mineral. It is possible that under very high normal stresses, the montmorillonite particles in the large displacement shear zone are pushed so close together that the average particle spacing in the shear zone reaches 20 Å or less and the long range forces vanish. Consequently, under a very high normal stress, the true effective stress of a montmorillonite system becomes equal to its apparent effective

stress under all pore fluid salt contents and this is possibly why salinity shows no influence on the residual shear strength of montmorillonite under sufficiently high normal stresses.

7.5 Dependence of the Residual Friction Angles of Clay Minerals on the Normal Stress Level

It has been shown in the last section that every clay mineral possesses a true residual angle of friction (ϕ_r') that is independent of the pore fluid salt concentrations. However, in the low normal stress range (0 - 30 psi), the true ϕ_r' of every clay mineral is found to decrease markedly as the normal stress is increased (Figs. 6.2d, 6.6d and 6.10d) and above a certain normal stress ($\approx$ 30 psi), the true ϕ_r' becomes independent of the normal stress (Figs. 6.2d, 6.6d and 6.10d). Even in the case of a highly active clay mineral such as montmorillonite, the true ϕ_r' is found to decrease markedly with increasing true effective stress in the low stress range (Figs. 6.37 and 6.39).

This variation in ϕ_r' with normal stress is also observed for some solid lubricants and the solid lubrication research attributes this non-linearity of friction to the dependence of the area of true contact between particles on the applied normal load. The area of true contact for elastic deformation of asperities can be expressed as being proportional to $(\text{load})^n$ where the value of n varies from 2/3 to 1.0 as the normal pressure is increased (Archard, 1951; Rubenstein, 1956 and Campbell, 1969). Since the frictional behaviour of clay minerals are strikingly similar to that of some solid lubricants, the above-mentioned model from the field of solid lubrication has been used in

this thesis to derive relationships between $\tan\phi_r'$ and σ_n' for the clay

minerals in the low and the high normal stress ranges. The detailed

derivation of these relationships are presented in section 3.3 of

Chapter III. These relationships suggest that in the low normal stress

range, the $\tan\phi_r'$ of a clay mineral or a natural soil follows a law

of the type, $\tan\phi_r' = \text{constant} \times (\sigma_n')^{-1/3}$, and consequently, ϕ_r' decreases

with increasing σ_n'. As the normal stress is increased beyond a certain

level where the area of true contact between particles is proportional

to $(\text{load})^{1.0}$, ϕ_r' becomes independent of σ_n'.

In order to verify whether the values of $\tan\phi_r'$ for the clay

minerals are truly described as a function of σ_n' by the above

relationships, the $\tan\phi_r'$ values for each clay mineral were plotted

against the corresponding values of $(\sigma_n')^{-1/3}$ on arithmetic scales.

The linear relationships obtained between the measured $\tan\phi_r'$ values

and the corresponding values of $(\sigma_n')^{-1/3}$ in the low stress range for

each clay mineral confirm that the marked decrease in ϕ_r' of clay

minerals with increasing σ_n' in the low stress range is due to the fact

that the area of true contact between the mineral

particles in the large displacement shear zone is proportional to

$(\text{load})^{2/3}$ in the low stress range. Figs. 6.4, 6.8 and 6.11 also show

that beyond a normal stress of about 30 psi, the $\tan\phi_r'$ versus $(\sigma_n')^{-1/3}$

relationships become horizontal lines parallel to the $(\sigma_n')^{-1/3}$ axis

and ϕ_r' becomes independent of σ_n' because the area of true contact

in the shear zone is now proportional to $(\text{load})^{1.0}$.

CHAPTER VIII

CONCLUSIONS AND RECOMMENDATIONS FOR FURTHER RESEARCH

8.1 Conclusions

Based on the results of the present work and an analysis of the previous studies, the following conclusions regarding the physical basis of residual shear strength of pure clay minerals and the various factors affecting it are drawn.

1. The residual shear strength of a soil is known to be dependent on its mineral composition. Among the clay minerals, montmorillonite possesses the lowest residual shear strength and residual strength increases in the order: montmorillonite, kaolinite, hydrous mica and attapulgite.

2. The residual shear strength of a pure clay mineral is independent of factors such as stress history, initial structure and strain rate which dominate the path dependent properties of soils. Hence residual strength is a fundamental soil parameter.

3. The degree by which the shear strength decreases from the peak to the residual state also varies with the type of clay mineral. A factor K' (= $\tan\phi_e/\tan\phi_r'$) relating the two fundamental friction angles ϕ_e (Hvorslev) and ϕ_r' has been

322

defined to indicate the degree of strength drop for a mineral from the peak to the residual state. The average value of K' for kaolinite varies between 1.86 and 2.32 signifying about 50% decrease in shear strength from the peak to the residual state. In the case of attapulgite, K' is about 1.1 indicating a meagre 5 to 6% drop in strength from the peak to the residual state.

4. From microstructural examination of the large displacement shear zones, it has been established that compression textures (in which the basal planes of the platy clay minerals are approximately normal to the major principal stress) are formed in the principal displacement shear at residual state. These compression textures are enclosed between two thin highly oriented bands of particles. The dominant mechanism of deformation in the large displacement shear zone is basal plane slip and this implies that the physical basis of residual shear strength of a clay mineral resides in the solid friction along the cleavage planes at the shear zone particle contacts. The shearing resistance of a clay mineral at large strain is due to the frictional property of the mineral cleavage planes.

5. Microstructural observations have also established that the mineral interparticle contacts are effectively solid-to-solid and these are the only significant regions between soil grains where effective normal stresses and shear

stresses can be transmitted.

6. The residual shear strength of a clay mineral depends on its mode of cleavage at large strain. Platy clay minerals such as kaolinite and montmorillonite which have easy 001 basal cleavage at the interparticle contacts in the shear zone have low resistance to shear and consequently low residual friction angles. On the other hand, a high residual friction angle is demonstrated by the fibrous needle shaped mineral attapulgite because at large strain, it has to be sheared along its staircase like 110 cleavage planes at shear zone particle contacts and consequently, it offers a high resistance to shear.

7. The residual shear strength of a clay mineral also depends on the type and total amount of bonding energy available along its cleavage planes at the interparticle contacts in the shear zone. The types of bond that could exist between the mineral cleavage planes are the secondary valence, the exchangeable ion-linkage and the hydrogen bonds. In the case of two clay minerals with the same mode of cleavage, the mineral with the weaker bonds and the lower bonding energy along its cleavage planes at the interparticle contacts will possess the lower residual shear strength. In this respect, the frictional behaviour of the clay minerals is quite similar to that of some solid lubricants such as graphite and molybdenum di-sulphide (MoS_2).

8. At large strain, shearing occurs predominantly by slippage

along the definite mineral cleavage planes at the solid
interparticle contacts in the shear zone. It involves
continuous rupturing and making of bonds along the
cleavage planes at the solid interparticle contacts in the
shear zone. The number of bonds at any solid contact probably
depends on the true effective stress transmitted at the contact.
The Terzaghi-Bowden and Tabor adhesion theory of friction
would appear to account for the conditions at the intercleavage
and the interparticle contacts in the shear zone.

9. For most clay minerals and some natural soils, the residual
   friction angle is markedly stress dependent below an average
   normal pressure (σ_n') of 20 to 30 psi beyond which ϕ_r' becomes
   almost independent of σ_n'. Provided the deformations
   at the interparticle contacts are truely elastic,
   this non-linearity of ϕ_r' in the low stress range is due to the
   dependence of the area of true contact (A_c) between the mineral
   cleavage planes and the particles on the normal pressure. In
   the low normal stress range (i.e., between 0 and 30 psi), A_c
   is proportional to $(\text{load})^{2/3}$ and the residual friction coefficient
   follows a law of the type, $\tan\phi_r' = \text{constant} \times (\sigma_n')^{-1/3}$.
   Consequently, ϕ_r' decreases with increasing σ_n' in the low
   normal stress range. As the normal stress is increased
   beyond 30 psi, A_c becomes proportional to $(\text{load})^{1.0}$ and
   ϕ_r' becomes independent of σ_n'.

10. The effective stress in a fully saturated clay-water
    system is defined by the equation,

$$\sigma_n' = \sigma_n - u_w = \sigma_n^* + (R-A)$$

where
- σ_n = the total stress
- σ_n' = the apparent effective stress
- σ_n^* = the true effective stress
- u_w = the pressure in the pore water

and
- $(R-A)$ = the net interparticle stress due to the physico-chemical environment.

11. The volume change behaviour of clay minerals associated with particle deformation and particle reorientation without a change of fabric are governed by the true effective stress (σ_n^*).

12. The residual shear strength of a clay mineral is controlled by the true effective stress (σ_n^*) on the mineral cleavage planes. The residual shear strength (τ_{res}) of a clay mineral can be expressed by the modified Coulomb-Terzaghi relationship defined in terms of the true effective stress on the mineral cleavage planes. The relationship is given by the equation,

$$\tau_{res} = [\sigma_n' - (R-A)] \tan\phi_r' = \sigma_n^* \tan\phi_r'$$

13. Every clay mineral possesses a true residual angle of friction that is unique and independent of the pore fluid salt content although the absolute value of the true ϕ_r' is dependent on the magnitude of true effective stress. The values of the true ϕ_r' (obtained from Mohr envelopes beyond a normal pressure of 20 to 30 psi) for the clay minerals tested here are as follows:

Mineral	Mode of Cleavage	Bonding along the Cleavage Planes	ϕ_r'
Montmorillonite	Easy (001) basal cleavage	Secondary valence + exchangeable ion link	8.5°
Kaolinite	Easy (001) basal cleavage	Secondary valence + hydrogen bonding	11°
Attapulgite	Staircase like (110) cleavage	Si - O - Si weak link	30°

The true ϕ_r' of a clay mineral can be obtained conventionally either by testing the mineral under a high salt environment or by testing it under very high normal pressures.

14. The basic residual strength generating mechanism for the clay minerals is purely frictional and the influence of the pore fluid salinity on the residual shear strength of an active clay mineral such as montmorillonite is indirect. In an active clay-water system, the effect of changing the pore fluid salt content under a constant apparent effective stress is to change the net (R-A) stress of the system thus causing the true effective stress on the mineral basal planes to change which then brings about a corresponding change in the residual shear strength of the system. If an active clay-water system is held under a constant true effective stress, a change in the pore fluid salinity will not affect the residual shear strength of the system.

15. In the case of inactive clay minerals such as kaolinite and attapulgite that have low surface activities, the net (R-A) stresses are small under all environmental conditions and as a result the true effective stresses of such systems are always equal to the apparent effective stresses. Consequently, the residual shear strength properties of the inactive clay minerals are virtually unaffected by the pore fluid salinity.

16. The evaluation of the true effective stress for a clay-water system requires an estimate of the net (R-A) stress. For an active clay mineral such as montmorillonite with sodium as the dominant cation, the net (R-A) stress may be approximated by the double-layer repulsive stress if the effective surface area of the mineral can be estimated with reasonable accuracy.

8.2 Recommendations for Further Research

1. The control of the true effective stress on the residual shear strength has been established in this study by tests on pure Na-homoionized montmorillonite. It will be worthwhile to repeat these tests on pure Na-homoionized illite not only to provide additional support to the findings of this investigation but also to extend the study to encompass most of the common clay minerals usually found in natural soils. In comparison with montmorillonite, illite has a lower surface activity and exhibits a higher coefficient of permeability. Hence constant volume leaching of illite samples will probably require less time. Mineral mixtures may also be studied as

part of further research.

2. In this investigation, the modified Coulomb-Terzaghi relationship expressed as

$$\tau_{res} = \sigma_n^*.\tan\phi_e = [\sigma_n' - (R-A)].K'.\tan\phi_r' \qquad (3.21\ b)$$

was originally developed for peak shear strength. The residual shear strength becomes a specialised case of the above relationship by simply substituting a value of 1.0 for K'. It will indeed be worthwhile to investigate the applicability of the proposed modified Coulomb-Terzaghi relationship to express the peak shear strength of a soil. An extensive supplementary investigation to study the factor K' (= $\tan\phi_e/\tan\phi_r'$) for various common clay minerals and possibly some mineral mixtures could also be undertaken.

3. It was proposed in this dissertation that a soil can exhibit a true cohesion if and only if the net electrical stress of interaction of the soil is an attractive one (i.e., if $A > R$). In such a case, the true cohesion can be expressed as

$$c_e = - (R-A).K.\tan\phi_r' = (A-R).\tan\phi_e \qquad (3.24)$$

which proposes that Hvorslev's true cohesion arises basically out of purely frictional interaction where only the net attractive force acts as the normal stress governing the frictional behaviour of the clay-water system. A fundamental

study of the phenomenon of cohesion to investigate the
validity of the hypothesis proposed here may be worthwhile.

LIST OF REFERENCES

Akroyd, T.N.W. 1957. "Laboratory Testing in Soil Engineering",
Geotechnical Monography No. 1, Soil Mechanics Ltd., London.

Alison, P.J., Stroud, M.F., and Wilman, H. 1965. "Abrasion of Metals
and Binary Alloys", Proc. 3rd Conf. Lub. and Wear,
Inst. Mech. Enggs., pp. 50-61.

Alpan, I. 1957. "An Apparatus for Measuring the Swelling Pressure in
Expansive Soils", Proc. 4th Int. Conf. Soil Mech. and Found.
Eng., London, Vol. 1, pp. 3-5.

Amontons, G. 1699. See Encyclopaedia Britannica, 13th Ed., 1926.

Archard, J.F. 1953. "Elastic Deformation and the Contact of Surfaces",
Nature, Vol. 172, pp. 918-919.

Archard, J.F. 1957. "Elastic Deformation and the Laws of Friction",
Royal Soc. Proc., Series A, Vol. 243, pp. 190-205.

Aylmore, L.A.G., and Quirk, J.P. 1959. "Swelling of Clay Water Systems",
Nature, Vol. 183, pp. 1752-1753.

Bailey, A.I., and Courtney-Pratt, J.S., 1955. "The Area of Real Contact
and the Shear Strength of Monomolecular Layers of a Boundary
Lubricant", Royal Soc. Proc., Series A, Vol. 227, pp. 500-515.

Bailey, A.I., 1961. "Friction and Adhesion of Clean and Contaminated Mica
Surfaces", Jour. App. Phys., Vol. 32, no. 8, pp. 1407-1412.

Bailey, W.A. 1965. "The Effects of Salt on the Consolidation Behaviour
of Saturated Remoulded Clays", Phase Report No. 3, USAE
Waterways Experiment Station, Vicksburg, Miss., Contract
Report No. 3-101, pp. 161.

Balasubramonian, B.I. 1972. "Swelling of Compaction Shales", Ph.D.
Thesis, University of Alberta, Edmonton, Alberta.

Balasubramonian, B.I. 1972 a. "Chemical Tests for Soil Engineers", Internal Note No. SM 11, Dept. of Civil Engg., University of Alberta, Edmonton, Alberta.

Bishop, A.W., Green, G.E., Garga, V.K., Andresen, A., and Brown, J.D. 1971. "A New Ring Shear Apparatus and its Application to the Measurement of Residual Strength", Geotechnique, Vol. 21, pp. 273-328.

Bolt, G.H. 1955. "Analysis of the Validity of the Gouy-Chapman Theory of the Electric Double-Layer", Jour. Colloid Science, Vol. 10, pp. 206-218.

Bolt, G.H. 1956. "Physico-chemical Analysis of the Compressibility of Pure Clays", Geotechnique, Vol. 6, pp. 86-93.

Borowicka, H. 1965. "The Influence of Colloidal Content on the Shear Strength of Clay", Proc. 6th Int. Conf. Soil Mech. and Found. Eng., Montreal, Vol. 1, pp. 175-178.

Bowden, F.P., and Tabor, D. 1964. "The Friction and Lubrication of Solids", Part I and Part II, Oxford University Press, Oxford.

Bower, C.A., and Gschwend, F.B. 1952. "Ethylene Glycol Retention by Soils as a Measure of Surface Area and Interlayer Swelling", Soil Sci. Soc. Amer. Proc., Vol. 16, pp. 342-345.

Bradley, W.F. 1940. "The Structural Scheme of Attapulgite", American Mineralogist, Vol. 25, pp. 405-410.

Bragg, W.L. 1937. "Atomic Structures of Minerals", Cornell University Press, Ithaca, New York.

Braithwaite, E.R. 1964. "Solid Lubricants and Surfaces", Pergamon Press, Oxford.

Campbell, W.E. 1969. "Solid Lubricants", Boundary Lubrication: An
Appraisal of World Literature, Am. Soc. Mech. Enggs.,
pp. 197-227.

Caquot, A. 1934. "Equilibre des Massifs à Frottement Interne. Stabilité
des Terres Pulvérents et Cohérentes", Paris: Gauthier Villars.

Carlisle, D. 1965. "Sliding Friction and Overthrust Faulting",
Jour. of Geology, Vol. 73, pp. 271-292.

Chandler, R.J. 1966. "The Measurement of Residual Strength in Triaxial
Compression", Geotechnique, Vol. 16, pp. 181-186.

Crawford, C.B. 1963. "Cohesion in an Undisturbed Sensitive Clay",
Geotechnique, Vol. 13, pp. 132-146.

Cullen, R.M., and Donald, I.B. 1971. "Residual Strength Determination
in Direct Shear", Proc. 1st Aust.-N.Z. Conf. on Geomechanics,
Melbourne, Vol. 1, pp. 1-10.

Dewey, J.F. 1965. "Nature and Origin of Kink-bands", Tectonophysics,
Vol. 1, pp. 459-494.

Dreimanis, A. 1962. "Quantitative Gasometric Determination of Calcite
and Dolomite by Using Chittick Apparatus", Jour. Sed. Pet.,
Vol. 32, pp. 520-529.

Dyal, R.S., and Hendricks, S.B. 1952. "Formation of Fixed Layer Minerals
by Potassium Fixation in Montmorillonite", Soil Sci. Soc.
Amer. Proc., Vol. 16, pp. 45-48.

Eigenbrod, K.D., and Morgenstern, N.R. 1971. "A Slide in Cretaceous
Bedrock, Devon, Alberta", Second Annual Symposium on
Stability for Open Pit Mining, Vancouver,B.C., November, 1971.

Finch, G.I. 1950. "The Sliding Surface", 34th Guthrie Lecture,
Proc. Phys. Soc. (London), Section A, Vol. 63, pp. 785-803.

Gibson, R.E. 1953. "Experimental Determination of the True Cohesion
and True Angle of Internal Friction in Clays", Proc. 3rd Int.
Conf. Soil Mech. and Found. Eng., Zurich, Vol. 1, pp. 126-130.

Gillott, J.E. 1969. "Study of the Fabric of Fine-Grained Sediments with
the Scanning Electron Microscope", Jour. Sed. Pet.
Vol. 39, No. 1, pp. 90-105.

Gillott, J.E. 1970. "Fabric of Leda Clay Investigated by Optical,
Electron-optical and X-ray Diffraction Methods",
Engg. Geol., Vol. 4, No. 2, pp. 133-153.

Glasstone, S., Laidler, K., and Eyring, H. 1941. "The Theory of Rate
Processes", McGraw-Hill Book Co. Inc., New York.

Grim, R.E. 1962. "Applied Clay Mineralogy", McGraw-Hill Book Co. Inc.,
New York.

Grim, R.E. 1968. "Clay Mineralogy", 2nd Ed., McGraw-Hill Book Co. Inc.,
New York.

Haden, W.L.(Jr.), 1963. "Attapulgite : Properties and Uses",
Proc. 10th Nat. Conf. on Clays and Clay Minerals, Pergamon
Press, New York, pp. 284-290.

Heafeli, R. 1938. "Mechanische Eigenschaften von Lockergesteinen",
Schweizerische Bauzeitung, Zurich, Vol. 111, pp. 299-303,
321-325.

Horn, H.M., and Deere, D.U. 1962. "Frictional Characteristics of Minerals",
Geotechnique, Vol. 12, pp. 319-335.

Hutchinson, J.N. 1967. "The Free Degradation of London Clay Cliffs",

Proc. Geotech. Conf., Oslo, Vol. 1, pp. 113-118.

Hvorslev, M.J. 1936. "Conditions of Failure for Remoulded Cohesive Soils",

Proc. 1st Int. Conf. Soil Mech. and Found. Eng.,

Cambridge, Mass., Vol. 3, pp. 51-53.

Hvorslev, M.J. 1939. "Torsion Shear Tests and Their Place in the

Determination of the Shearing Resistance of Soils",

Proc. Am. Soc. Testing Materials, Vol. 39, pp. 999-1020.

Kay, D.H. 1965. "Techniques for Electron Microscopy", Blackwell, Oxford.

Kenney, T.C. 1967. "The Influence of Mineral Composition on the

Residual Strength of Natural Soils", Proc. Geotech. Conf.,

Oslo, Vol. 1, pp. 123-129.

Ladd, C.C. 1967. "Strength and Compressibility of Saturated Clays",

Pan American Soils Course, Universidad Catolica Andres Bello,

Caracas, Venezuela.

Ladd, C.C., and Kinner, K.B. 1967. "The Strength of Clays at Low Effective

Stresses", Phase Report No. 8, USAE Waterways Experimental

Station, Vicksburg, Miss., Contract Report No. 3-101, p.122.

La Gatta, D.P. 1970. "Residual Strength of Clays and Clay-shales by

Rotation Shear Tests", Harvard Soil Mechanics Series No. 86,

Cambridge, Mass., p. 204.

Lambe, T.W. 1951. "Soil Testing for Engineers", John Wiley and Sons,

New York.

Lambe, T.W. 1960. "A Mechanistic Picture of Shear Strength in Clays",

ASCE Res. Conf. on Shear Strength of Cohesive Soils,

Boulder, Colorado, pp. 555-580.

Lambe, T.W., and Whitman, R.V. 1969. "Soil Mechanics", John Wiley and
Sons, New York.

Lee, I.K. 1968. Editor, "Soil Mechanics: Selected Topics", Butterworths,
London.

Lincoln, B. 1953. "Elastic Deformation and the Laws of Friction",
Nature, Vol. 172, pp. 169-170.

Low, P.F. 1959. Discussion, Jour. ASCE, SM 2, Vol. 85, pp. 79-89.

Lutz, J.F., and Kemper, W.D. 1959. "Intrinsic Permeability of Clay as
Affected by Clay-Water Interaction", Soil Science, Vol. 88,
pp. 83-90.

Martin, R.T. 1960. "Adsorbed Water on Clay: A Review", Clays and Clay
Minerals, Vol. 9, pp. 28-70.

Martin, R.T. 1966. "Quantitative Fabric of Wet Kaolinite", Clays and
Clay Minerals, Proc. 14th Nat. Conf., Berkeley, Calif., pp. 271-287.

McClintock, F.A., and Argon, A.S. 1966. "Mechanical Behaviour of Materials",
Addison-Wesley Publ. Co. Inc., Mass., U.S.A.

McFarlane, J.S., and Tabor D. 1950 a. "Adhesion of Solids and the Effect
of Surface Films", Royal Soc. Proc., Series A, Vol. 202, pp. 224-243.

McFarlane, J.S., and Tabor, D. 1950 b. "Relation Between Friction and
Adhesion", Royal Soc. Proc., Series A, Vol. 202, pp. 244-253.

Mesri, G. 1969. "Engineering Properties of Montmorillonite", Ph.D. Thesis,
University of Illinois, Urbana, Illinois, p. 90.

Mitchell, J.K. 1960. "Components of Pore Water Pressure and Their
Engineering Significance", Clays and Clay Minerals,
Vol. 9, pp. 162-184.

Mitchell, J.K. 1964. "Shearing Resistance of Soils as a Rate Process",
Jour. ASCE, SM 1, Vol. 90, Proc. Paper 3773, pp. 29-61.

Mitchell, J.K., Singh, A., and Campanella, R.G. 1969. "Bonding, Effective Stress and Strength of Soils", Jour. ASCE, SM 5, Vol. 95, Proc. Paper 6786, pp. 1219-1246.

Morgan, J.R. 1967. "Shear Strength of a Kaolin", Proc. 5th Aust. - N.Z. Conf. Soil Mech. and Found. Eng., Auckland, pp. 72-78.

Morgenstern, N.R. 1967. "Shear Strength of Stiff Clay", General Report-Session 2, Proc. Geotech. Conf., Oslo, Vol. 2, pp. 59-71.

Morgenstern, N.R., and Tchalenko, J.S., 1967 a. "Microscopic Structures in Kaolin Subjected to Direct Shear", Geotechnique, Vol. 17, pp. 309-328.

Morgenstern, N.R., and Tchalenko, J.S. 1967 b. "Microstructural Observations on Shear Zones from Slips in Natural Clays", Proc. Geotech. Conf., Oslo, Vol. 1, pp. 147-152.

Newland, P.L., 1965. "A Model to Describe the Mechanical Properties of Clays", Engineering Effects of Moisture Changes in Soils, Texas A & M Press, College Station, pp. 93-107.

Norrish, K. 1954. "The Swelling of Montmorillonite", Disc. Faraday Soc., 18, pp. 120-134.

Palit, R.M. 1953. "Determination of Swelling Pressure of Black Cotton Soil: A Method", Proc. 3rd Int. Conf. Soil Mech. and Found. Eng., Zurich, Vol. 1, pp. 170-172.

Paterson, M.S., and Weiss, L.E., 1966. "Experimental Deformation and Folding in Phyllite", Geol. Soc. of America Bull., Vol. 77, pp. 343-374.

Petley, D.J. 1966. "The Shear Strength of Soils at Large Strains", Ph.D. Thesis, University of London.

P.F.R.A. 1970. "Interim Summary of Residual Direct Shear Test Results on Bearpaw Shale", Soil Mechanics and Materials Division, Saskatoon, Saskatchewan, Canada.

Preisinger, A. 1963. "Sepiolite and Related Compounds - Its stability and Application", Proc. 10th Nat. Conf. on Clays and Clay Minerals, Pergamon Press, New York, pp. 365-371.

Ringheim, A.S. 1964. "Experiences with Bearpaw Shale at the South Saskatchewan River Dam", Trans. 8th Int. Cong. Large Dams, Edinburgh, Vol. 1, pp. 529-550.

Rosenqvist, I.Th. 1959. "Physico-chemical Properties of Soils, Soil-water Systems", Jour. ASCE, SM 2, Proc. Paper 2000, pp. 31-53.

Rowe, P.W., Oates, D.B., and Skermer, N.A. 1963. "The Stress-dilatancy Performance of Two Clays", Laboratory Shear Testing of Soils, ASTM Spl. Publ. No. 361, pp. 134-146.

Rubenstein, C. 1956. "A General Theory of the Surface Friction of Solids", Proc. Phys. Soc. (London), Section B, Vol. 69, pp. 921-933.

Schmertmann, J.H. 1963. "Generalizing and Measuring the Hvorslev's Effective Components of Shear Resistance", Laboratory Shear Testing of Soils, ASTM Spl. Publ. No. 361, pp. 147-162.

Schmertmann, J.H. 1971. Lecture delivered at the University of Alberta, Edmonton, Alberta, Nov. 22, 1971.

Sembenelli, P., and Ramirez, A.L. 1969. "Measurement of Residual Strength of Clay with a Rotating Shear Machine", Proc. 7th Int. Conf. Soil Mech. and Found. Eng., Mexico City, Vol. 3, pp. 528-529.

Shouldice, J.R. 1963. "Gravity Slide Faulting on Bowes Dome, Bearpaw Mountains Area, Montana", Bull. Amer. Assoc. Pet. Geol., Vol. 47.

Skempton, A.W., and De Lory, F. 1957. "Stability of Natural Slopes in London Clay", Proc. 4th Int. Conf. Soil Mech. and Found. Eng., London, Vol. 2, pp. 378-381.

Skempton, A.W. 1964. "Long-term Stability of Clay Slopes", 4th

Rankine Lecture, Geotechnique, Vol. 14, pp. 77-101.

Smart, P. 1967. "Particle Arrangements in Kaolin", Proc. 15th Nat.

Conf. on Clays and Clay Minerals, Pergamon Press, New York.

pp. 241-254.

Soil Science Manual No. 421., Dept. of Soil Science, University of Alberta,

Edmonton, Alberta, Canada.

Spreadborough, J. 1962. "The Frictional Behaviour of Graphite",

Wear, Vol. 5, pp. 18-30.

Taylor, A.W. 1959. "Physico-chemical Properties of Soils: Ion Exchange

Phenomena", Jour. ASCE, SM 2, Vol. 85, pp. 19-30.

Taylor, D.W. 1948. "Fundamentals of Soil Mechanics", John Wiley and Sons,

New York.

Tchalenko, J.S. 1967. "The Influence of Shear and Consolidation on the

Microscopic Structure of Some Clays", Ph.D. Thesis, University

of London.

Tchalenko, J.S. 1968. "The Evolution of Kink-bands and the Development

of Compression Textures in Sheared Clays", Tectonophysics,

Vol. 6, pp. 159-174.

Tchalenko, J.S. 1970. "Similarities Between Shear Zones of Different

Magnitudes", Geol. Soc. Amer. Bull., Vol. 81, pp. 1625-1640.

Tomlinson, G.A. 1929. "A Molecular Theory of Friction", Philosophical

Mag., Vol. 7, No. 7, pp. 905-939.

Trollope, D.H. 1960. "The Fabric of Clays in Relation to Shear Strength",

Proc. 3rd Aust.-N.Z. Conf. Soil Mech. and Found. Eng.,

Sydney, pp. 197-202.

Trollope, D.H. 1961. "Effective Contact Stresses and Friction",
Nature, Vol. 191, pp. 376-377.

Trollope, D.H. 1964. "On the Shear Strength of Soils", Conf. on Soil
Stabilization, C.S.I.R.O., Melbourne, Australia.

Van Auken, F.M. 1963. "Shear Strength of Clay Shales Found in the
Southwestern U.S.A.", Proc. 2nd Panamerican Conf. Soil Mech.,
Brazil, Vol. 1, pp. 255-288.

Weeks, A.G. 1969. "The Stability of Natural Slopes in South-East
England as Affected by Periglacial Activity", Quart. Jour.
Engg. Geol., Vol. 2, pp. 49-62.

West, R. 1963. "The Characteristics of Filter Pressed Kaolinite-water
Pastes", Proc. 12th Nat. Conf. on Clays and Clay Minerals,
Pergamon Press, New York. pp. 209-22.

APPENDIX A

CHARACTERISTICS OF THE DIRECT SHEAR MACHINES

AND THE VARIOUS MEASURING SYSTEMS

A.1 <u>Characteristics of the Direct Shear Machines and Accuracies</u>

<u>of the Associated Measuring Systems</u>

i) Direct Shear Machine	Machine Friction	Negligible
	Ratio Pan Load:	
	Specimen Load	1:5 $\pm$ 0.2%
	Rates of Strain	0.0000192 to 0.05 inches/minute $\pm$ 0.5%
ii) Load Cell	Accuracy	0.3 to 0.4 lbs.
	Temperature Error	0.15 lbs./°F
	Creep	0
iii) LVDT	Accuracy	0.00002 inches of deformation

A.2 Calibration Factors for the Measuring Systems

TABLE A.1a

CALIBRATION FACTORS FOR THE MEASURING SYSTEMS USED IN THE DIRECT SHEAR MACHINES

Machine no.	Tests performed on the machine	Vertical LVDT calibration factor	Full scale displacement range (inches)	Linearity range	Horizontal LVDT* calibration factor	Full scale displacement range (inches)	Linearity range	Load cell (500 lbs.) calibration factors in compression and tension
1 (Clockhouse Engineering Limited)	K-0-1, K-0-7, K-0-13, K-2-1, K-2-5, K-35-2, K-35-4, A-0-1, A-0-8, A-2-4, A-2-10, A-41-3, A-41-9, M-1-3, M-34-4, M-L-4, M-34-8.	1mv = 0.000172" 1 volt = 0.172"	± 0.500	-2.7 volts to +1.7 volts	1mv = 0.000211" 1 v = 0.211"	± 1.000	-3.7 volts to -1.9 volts	1mv = 36.08 lbs.
2 (Clockhouse Engineering Limited)	K-0-2, K-0-8, K-0-14, K-2-2, K-2-6, K-35-1, K-35-3, A-0-3, A-2-8, A-2-9, A-41-2, A-41-10, M-1-2, M-1-4, M-34-5, M-1-5, M-34-9.	1mv = 0.000176" 1 v = 0.176"	± 0.500	-3.0 volts to +3.2 volts	1mv = 0.000172" 1 v = 0.172"	± 0.500	-1.5 volts to +1.5 volts	1mv = 37.75 lbs.
3 (Wykeham Farrance Engineering Limited)	K-0-3, K-0-5, K-0-9, K-0-12, K-2-3, K-2-7, K-2-10, K-35-6, K-35-10, A-0-5, A-2-6, A-2-7, A-41-5, A-41-6, M-1-6, M-15-1, M-15-6, M-34-1, M-1-1, M-34-6.	1mv = 0.000243" 1 v = 0.243"	± 1.000	-3.0 volts to -1.0 volts	1mv = 0.000223" 1 v = 0.223"	± 1.000	-3.0 volts to +3.0 volts	1mv = 38.05 lbs.
4 (Wykeham Farrance Engineering Limited)	K-0-4, K-0-6, K-0-10, K-0-11, K-2-4, K-2-8, K-2-9, K-35-5, K-35-8, A-0-4, A-0-6, A-2-3, A-2-5, A-41-4, A-41-8, M-1-5, M-1-7, M-15-3, M-15-5, M-34-3, M-1-3, M-34-7	1mv = 0.000227" 1 v = 0.227"	± 1.000	+3.4 volts to +4.9 volts	1mv = 0.000213" 1 v = 0.213"	± 1.000	-3.0 volts to +3.0 volts	1mv = 36.68 lbs.
5 (Wykeham Farrance Engineering Limited)	K-35-7, K-35-9, A-0-2, A-0-7, A-2-2, A-2-3, A-41-3, A-41-7, M-1-1, M-15-2, M-15-4, M-34-2, M-L-2	1mv = 0.000171" 1 v = 0.171"	± 0.500	-2.6 volts to +2.6 volts	1mv = 0.000216" 1 v = 0.216"	± 1.000	-3.0 volts to +3.0 volts	1mv = 36.97 lbs.

* Input voltage for all LVDTs = 6 volts DC

TABLE A-1 b

CALIBRATION FACTORS FOR THE LOAD CELLS

USED IN THE LEACHING TESTS

Leaching Test No.	Load Cell (500 lbs.) Calibration Factor
L-1	1 millivolt = 38.05 lbs.
L-2	1 millivolt = 27.80 lbs.
L-3	1 millivolt = 36.68 lbs.
L-4	1 millivolt = 36.08 lbs.
L-5	1 millivolt = 37.75 lbs.

A.3 Calibration of the Solu-Bridge

The solu bridge (Beckman model no. RB 3R 104) that was used for measuring the total salt contents of the decanted clear fluids during sample preparation and the effluent from the montmorillonite samples during leaching was calibrated with respect to sodium chloride. The calibration curve is presented in Fig. A.1.
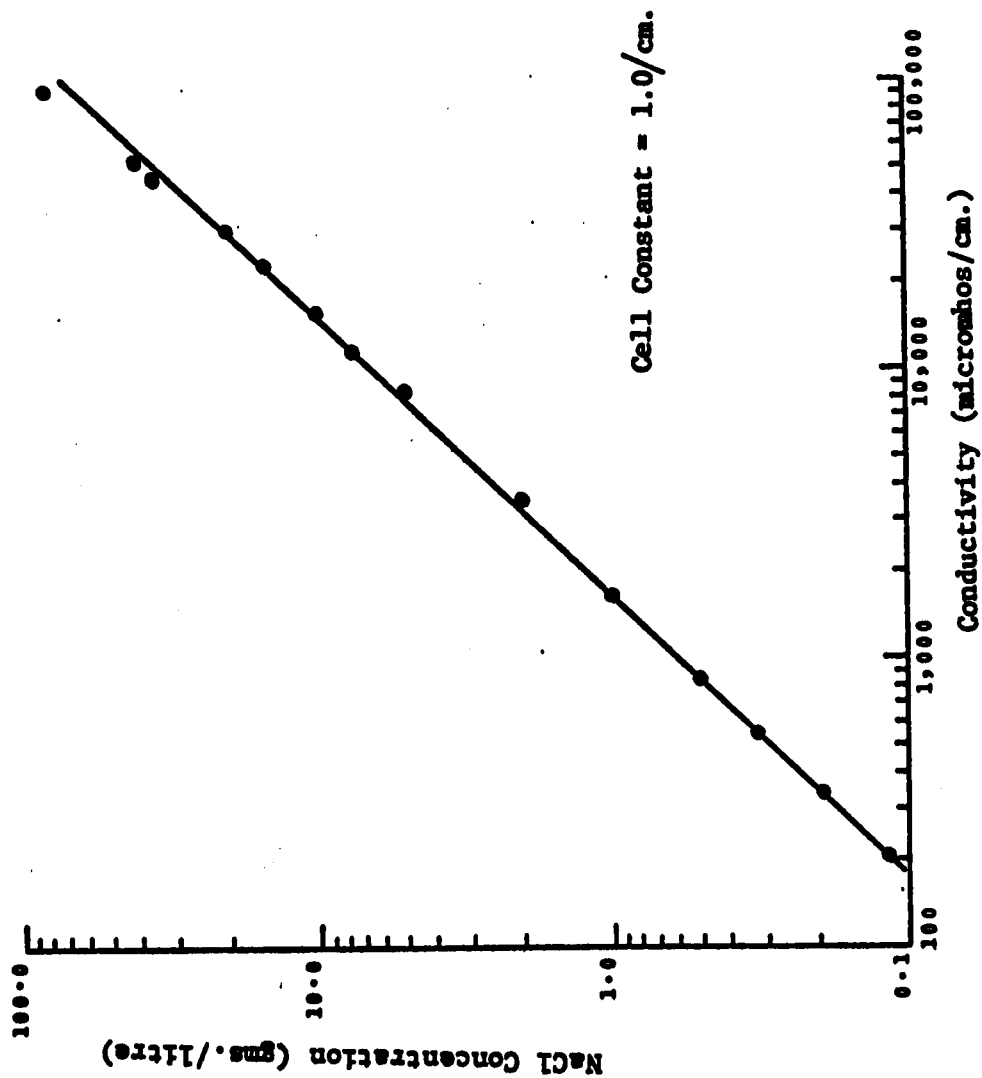
FIG. A-1 CALIBRATION CURVE FOR THE BECKMAN RB 3R 104 MODEL SOLU-BRIDGE

APPENDIX B

CONSOLIDATION AND DIRECT SHEAR TEST RESULTS

The results of the reversal direct shear tests conducted on kaolinite, attapulgite and montmorillonite along with some typical consolidation test results are compiled in this Appendix. Representative settlement versus $\sqrt{time}$ and settlement verus log (time) plots for kaolinite, attapulgite and montmorillonite obtained from the large cell consolidation tests and from the consolidation phase in the direct shear tests are presented in Figs. B-1 to B-6. The consolidation characteristics of the clay minerals obtained from these consolidation tests are summarised in Table 6.2 of Chapter VI. The settlement vs. $\sqrt{time}$ plots from the large consolidation cell tests on attapulgite and montmorillonite, presented in Figs. B-1 and B-2, clearly indicate that the large cells (11.84" ID x 10.26" high) that were primarily built for preparation of large clay mineral blocks functioned well as consolidation cells and the consolidation characteristics of the minerals obtained from the large cell tests agree favourably with the corresponding values obtained from the consolidation phase in the direct shear test (for comparison, see Table 6.2). Figs. B-5 and B-6 illustrate the inherent tendency of the attapulgite and the montmorillonite samples to undergo large secondary compressions. However, when overconsolidated samples of attapulgite were allowed to rebound in the direct shear boxes, no montmorillonite-type

B1

swelling was observed probably because of the three-dimensional structure of attapulgite.

The results of the reversal shear tests conducted on kaolinite, attapulgite and montmorillonite are presented in Figs. B-7 to B-94.
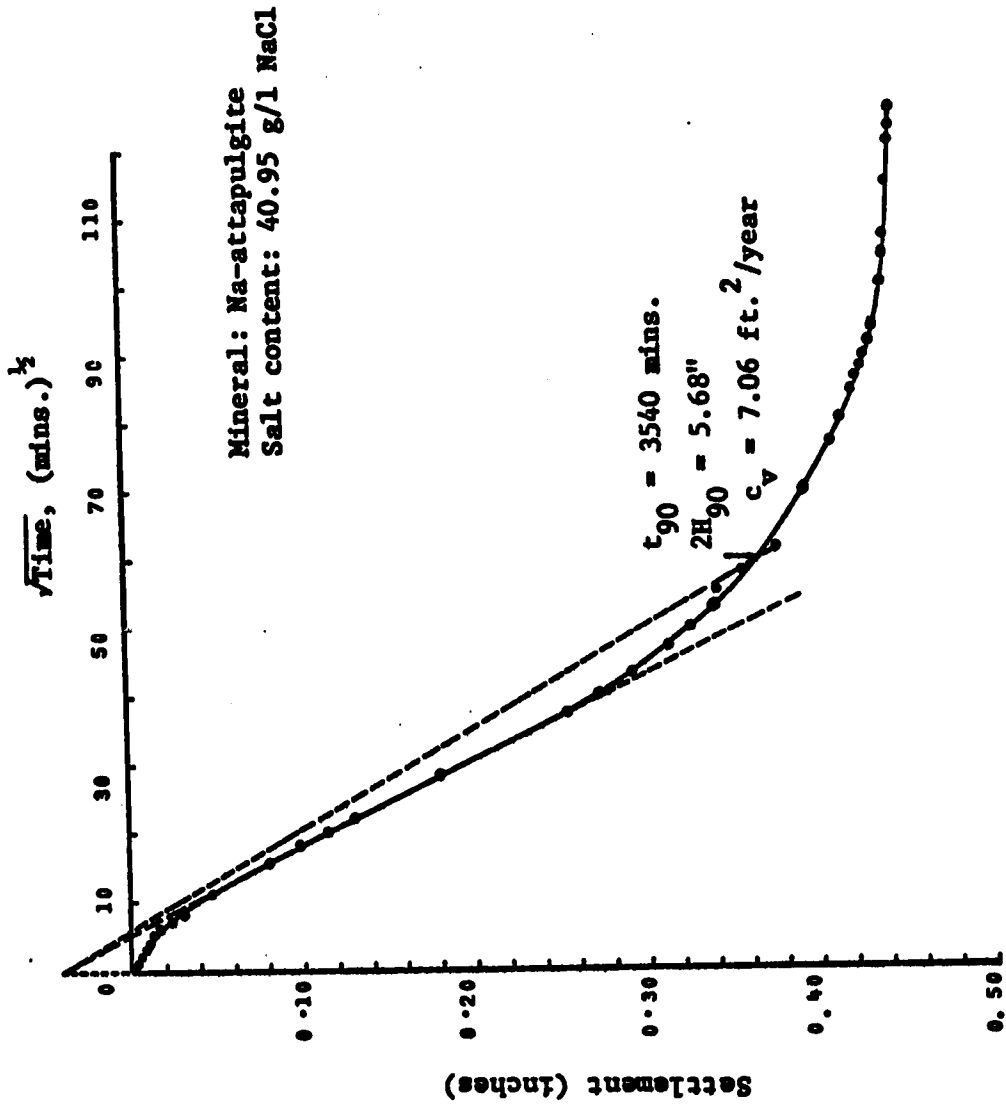
FIG. B-1   A TYPICAL SETTLEMENT - √TIME PLOT FOR CONSOLIDATION OF
Na-ATTAPULGITE IN THE LARGE CONSOLIDATION CELLS
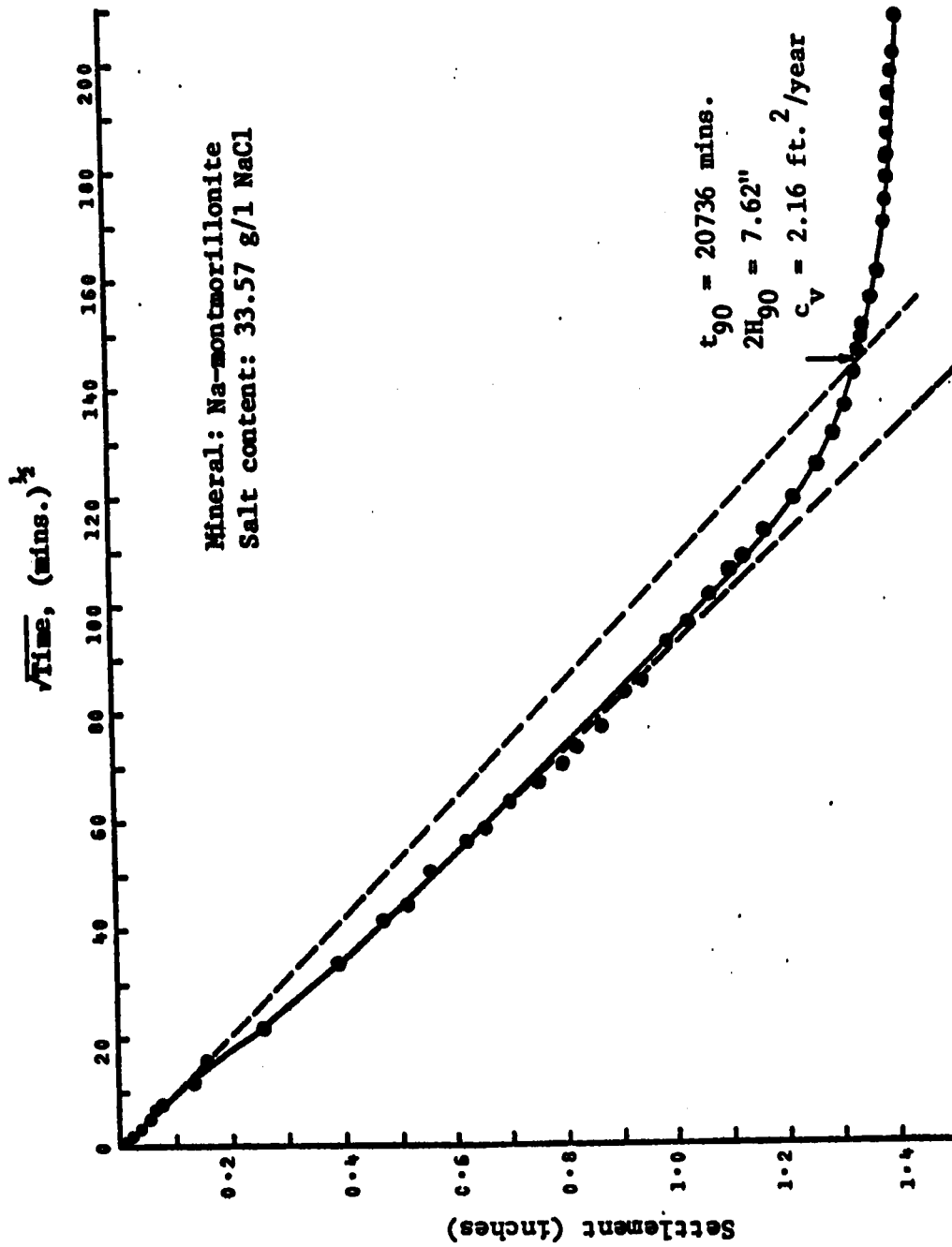
FIG. B-2   A TYPICAL SETTLEMENT – √TIME PLOT FOR CONSOLIDATION OF Na-MONTMORILLONITE
IN THE LARGE CONSOLIDATION CELLS

FIG. B-3 A TYPICAL SETTLEMENT – √TIME PLOT FOR CONSOLIDATION OF KAOLINITE IN THE DIRECT SHEAR BOX

Fig. B-4 A TYPICAL SETTLEMENT – √TIME PLOT FOR CONSOLIDATION OF Na-ATTAPULGITE IN THE DIRECT SHEAR BOX
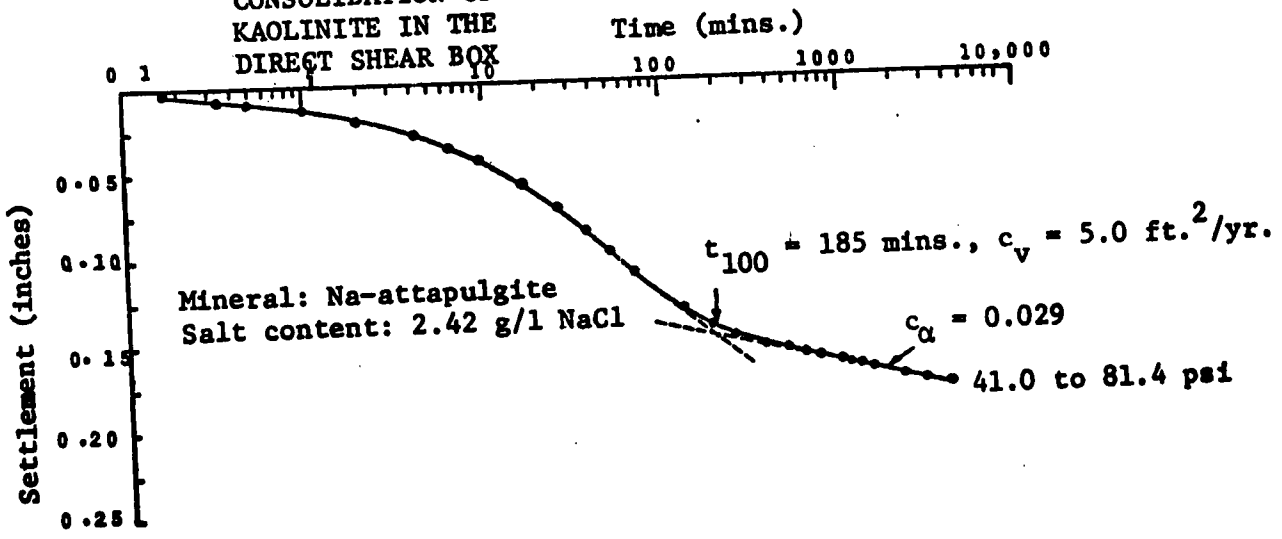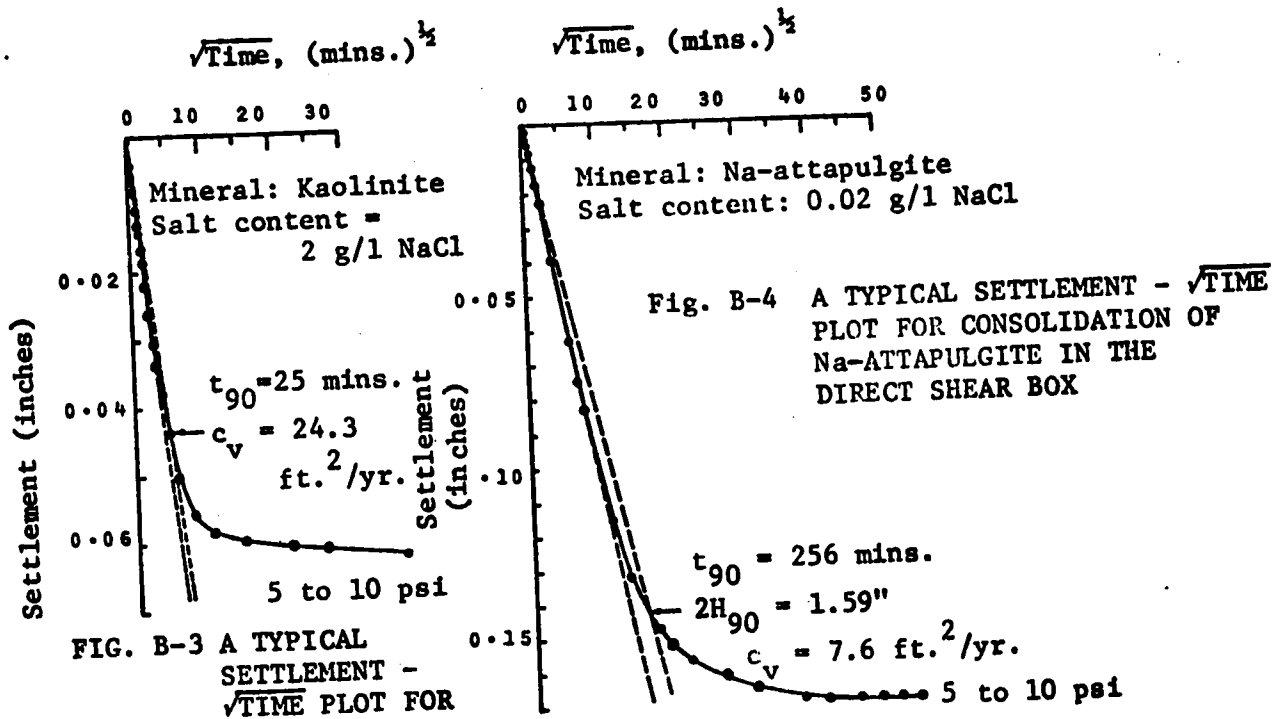
FIG. B-5 A TYPICAL SETTLEMENT – LOG (TIME) PLOT FOR CONSOLIDATION OF Na-ATTAPULGITE IN THE DIRECT SHEAR BOX

Mineral: Na-montmorillonite
Salt content: 1.15 g/l NaCl

$t_{90} = 5184$ mins., $2H_{90} = 1.59"$, $c_v = 0.38$ ft.^{2}/year

$\sqrt{Time}$, (mins.)$^{\frac{1}{2}}$
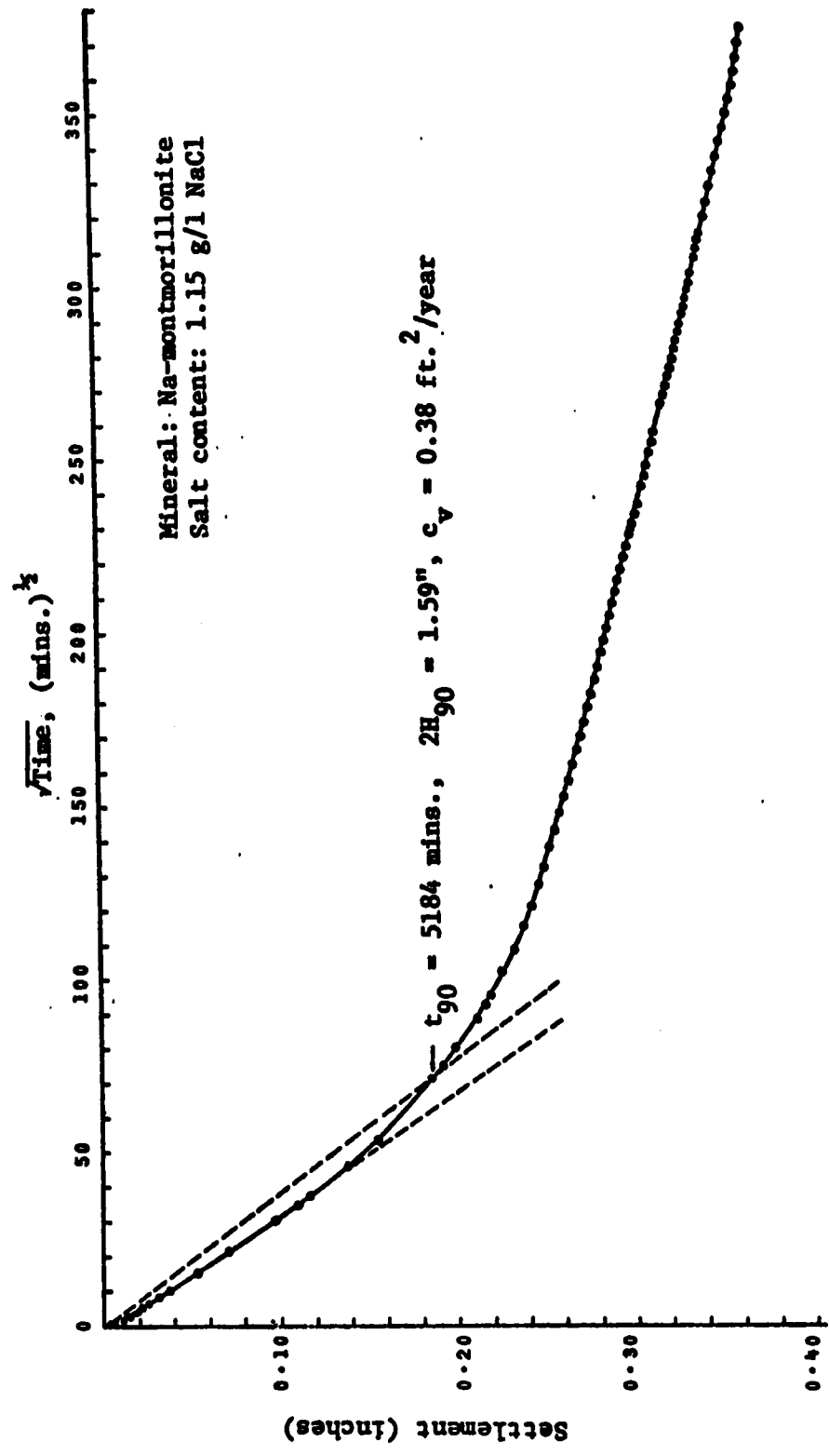
Settlement (inches)

FIG. B-6   A TYPICAL SETTLEMENT - $\sqrt{TIME}$ PLOT FOR CONSOLIDATION OF Na-MONTMORILLONITE
IN THE DIRECT SHEAR BOX

Kaolinite - 0 g/1 NaCl
Test No. K-0-1
Precut Plane Test
Rate of Displacement = 0.0024 ins./min.
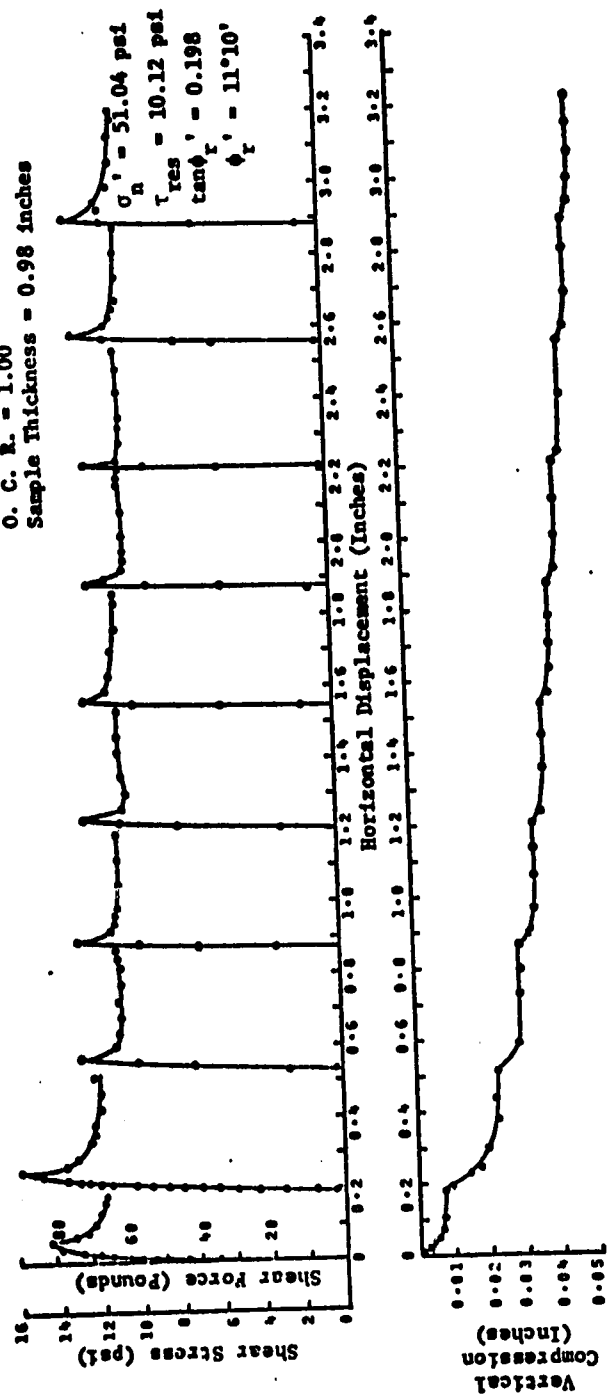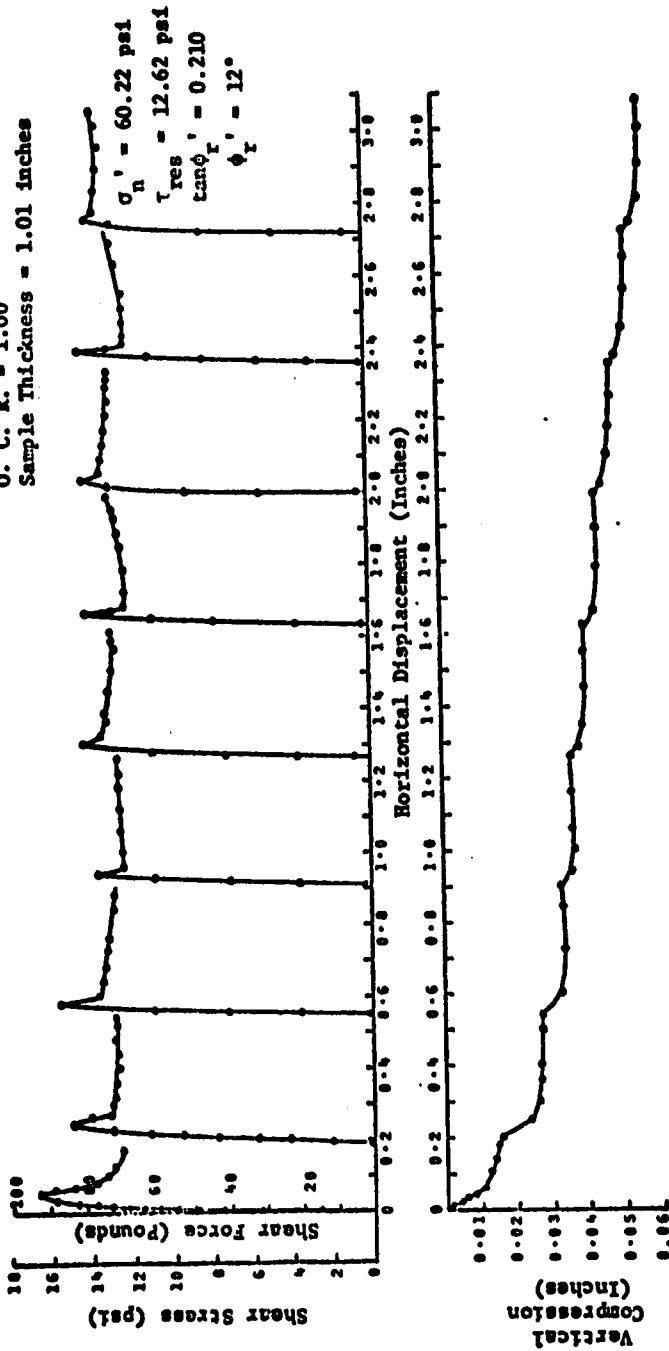O.C.R. = 1.00
Sample Thickness = 1.48 inches

$\sigma_n' = 5.00$ psi
$\tau_{res} = 2.04$ psi
$\tan\phi_r' = 0.41$
$\phi_r' = 22°20'$

Horizontal Displacement (inches)

Shear Force (Pounds)

Shear Force (Pounds)

Shear Stress (PSI)

Vertical Compression (Inches)

Horizontal Displacement (Inches)
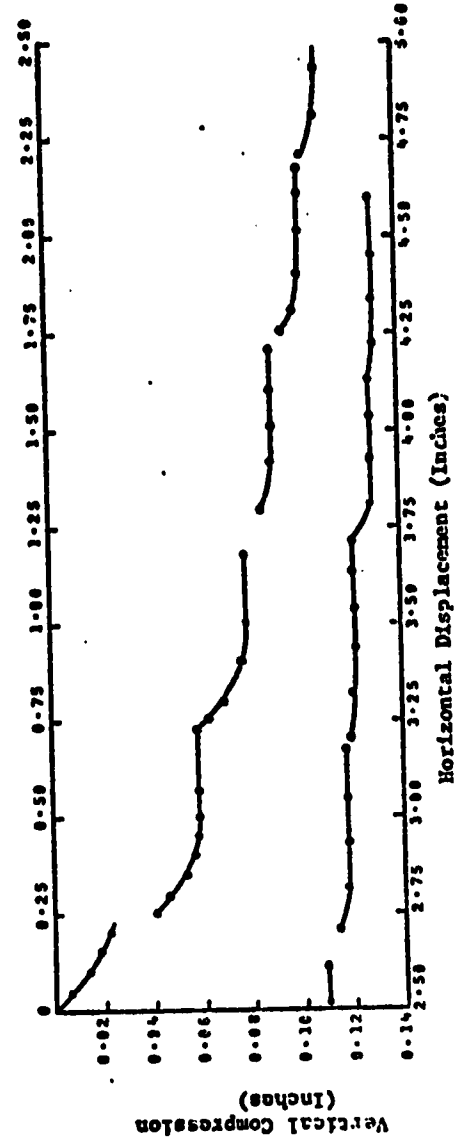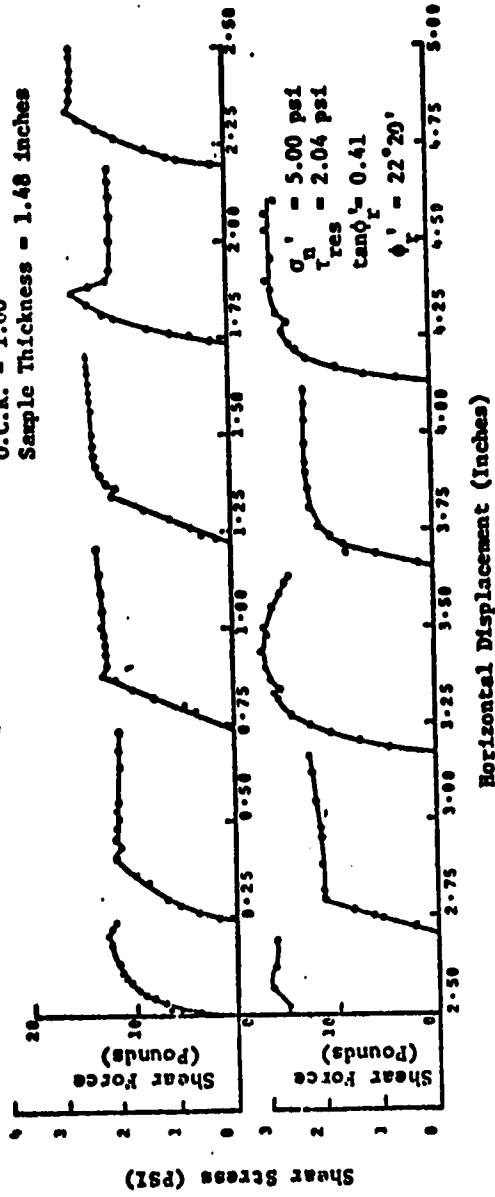
FIG. B-7 DIRECT SHEAR TEST ON KAOLINITE (K-0-1)

Kaolinite - 0 g/l NaCl
Test No. K-0-2
Precut Plane Test
Rate of Displacement = 0.0024 ins./min.
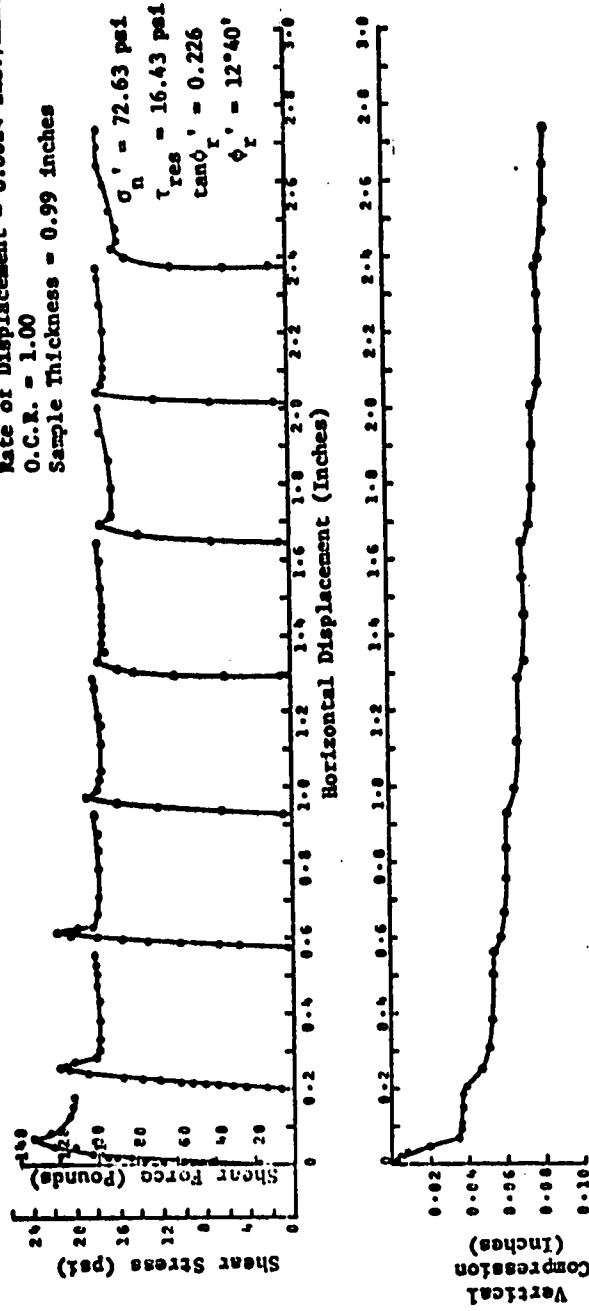O.C.R. = 1.00; Sample Thickness = 1.37 inches

σ_n' = 9.95 psi
τ_{res} = 4.35 psi
$\tan\phi_r'$ = 0.437
ϕ_r' = 23°40'

Shear Force (Pounds)

Shear Stress (psi)

Horizontal Displacement (Inches)

Vertical Compression (Inches)
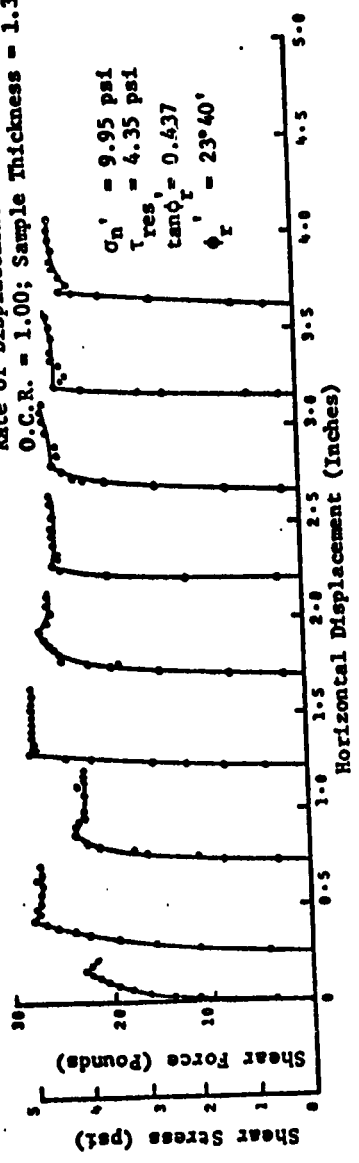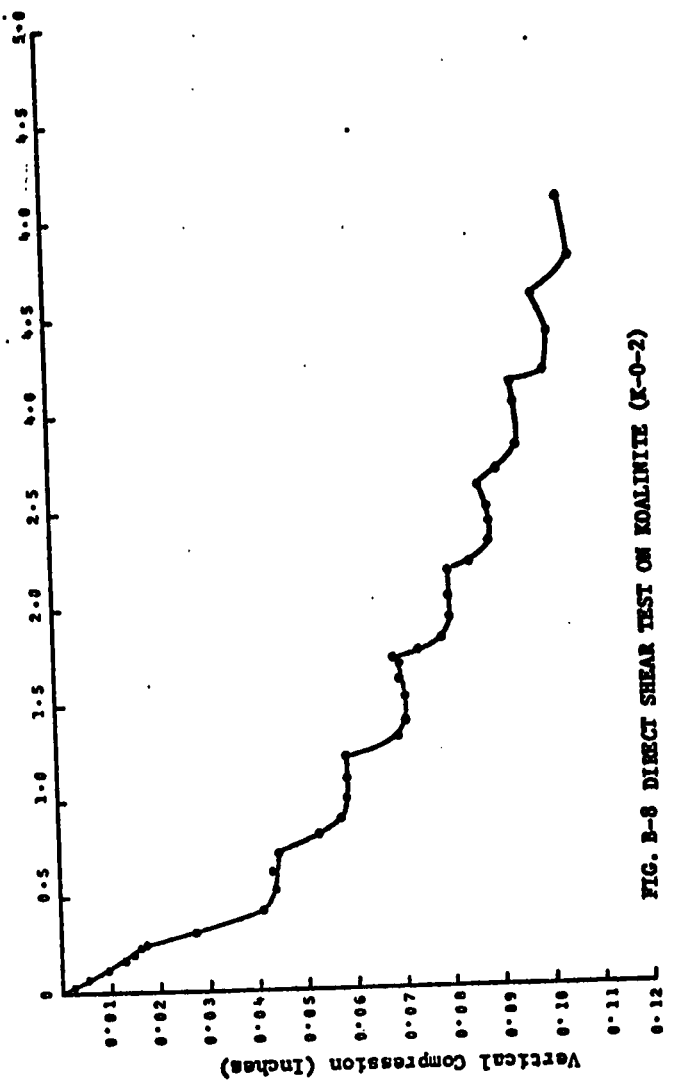
FIG. B-8 DIRECT SHEAR TEST ON KAOLINITE (K-0-2)

Kaolinite - 0 g/l NaCl
Test Nos.   K-0-3 and K-0-4
Precut Plane Tests
Rate of Displacement = 0.0019 ins./min.
O.C.R. = 1.00
Sample Thickness = 1 inch for both the tests

Test No. K-0-3

Test No. K-0-4

σ_n' = 10.25 psi
τ_{res} = 3.75 psi
$\tan\phi_r'$ = 0.366
ϕ_r' = 20°

Horizontal Displacement (Inches)
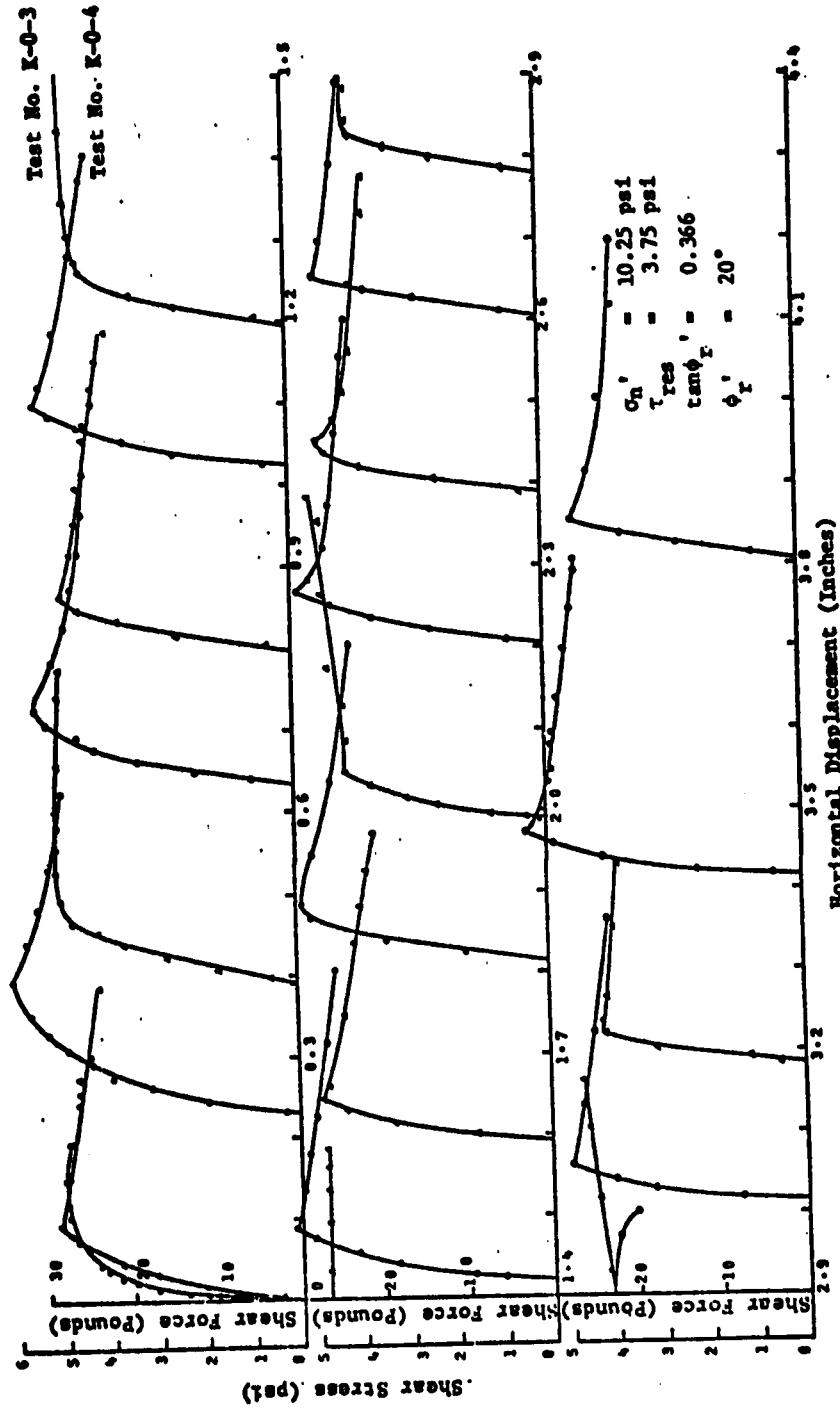
FIG. B-9a DIRECT SHEAR TESTS ON KAOLINITE (K-0-3 and K-0-4)

FIG.B-9b DIRECT SHEAR TESTS ON KAOLINITE (K-0-3 and K-0-4)

FIG.B-10a DIRECT SHEAR TESTS ON KAOLINITE (K-0-5 and K-0-6)

Kaolinite - 0 g/l NaCl
Test Nos. K-0-5 and K-0-6 (contd.)
Precut Plane Tests
Rate of Displacement = 0.0019 ins./min.
O.C.R. = 1.00
Sample Thickness = 1.27 inches for both the tests.

σ_n' = 14.97 psi
τ_{res} average = 4.28psi
$\tan\phi_r'$ = 0.286
ϕ_r' = 16°
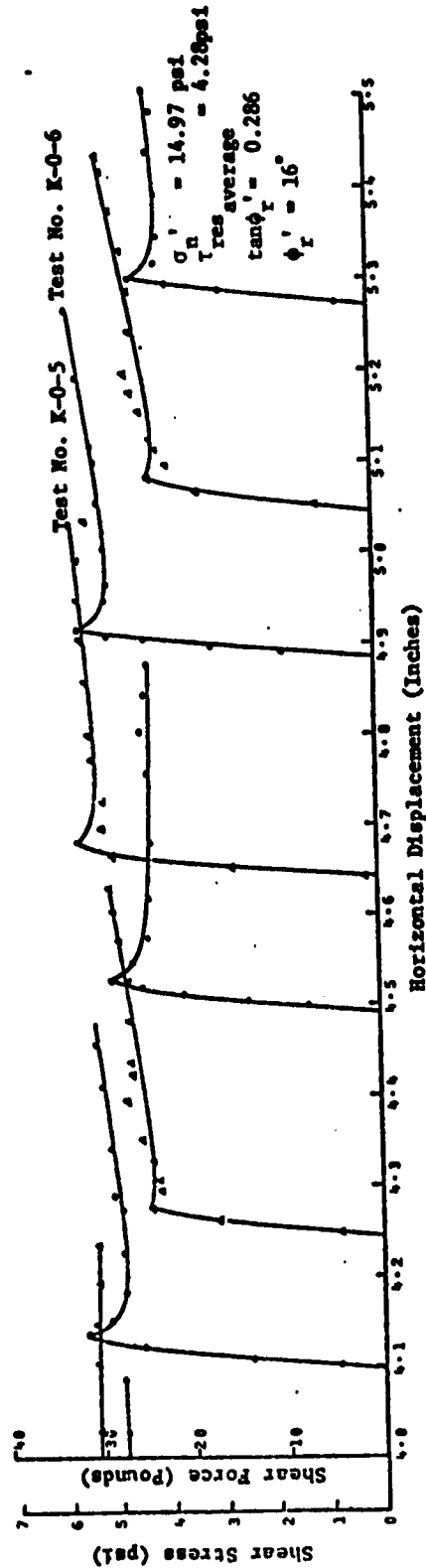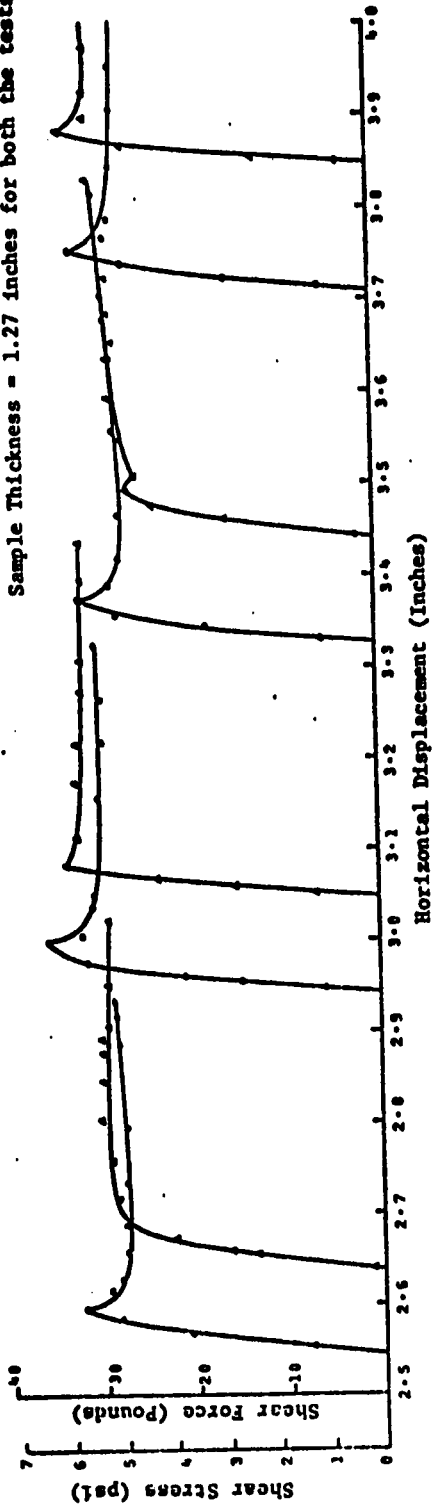
FIG. B-10b DIRECT SHEAR TESTS ON KAOLINITE (K-0-5 and K-0-6)
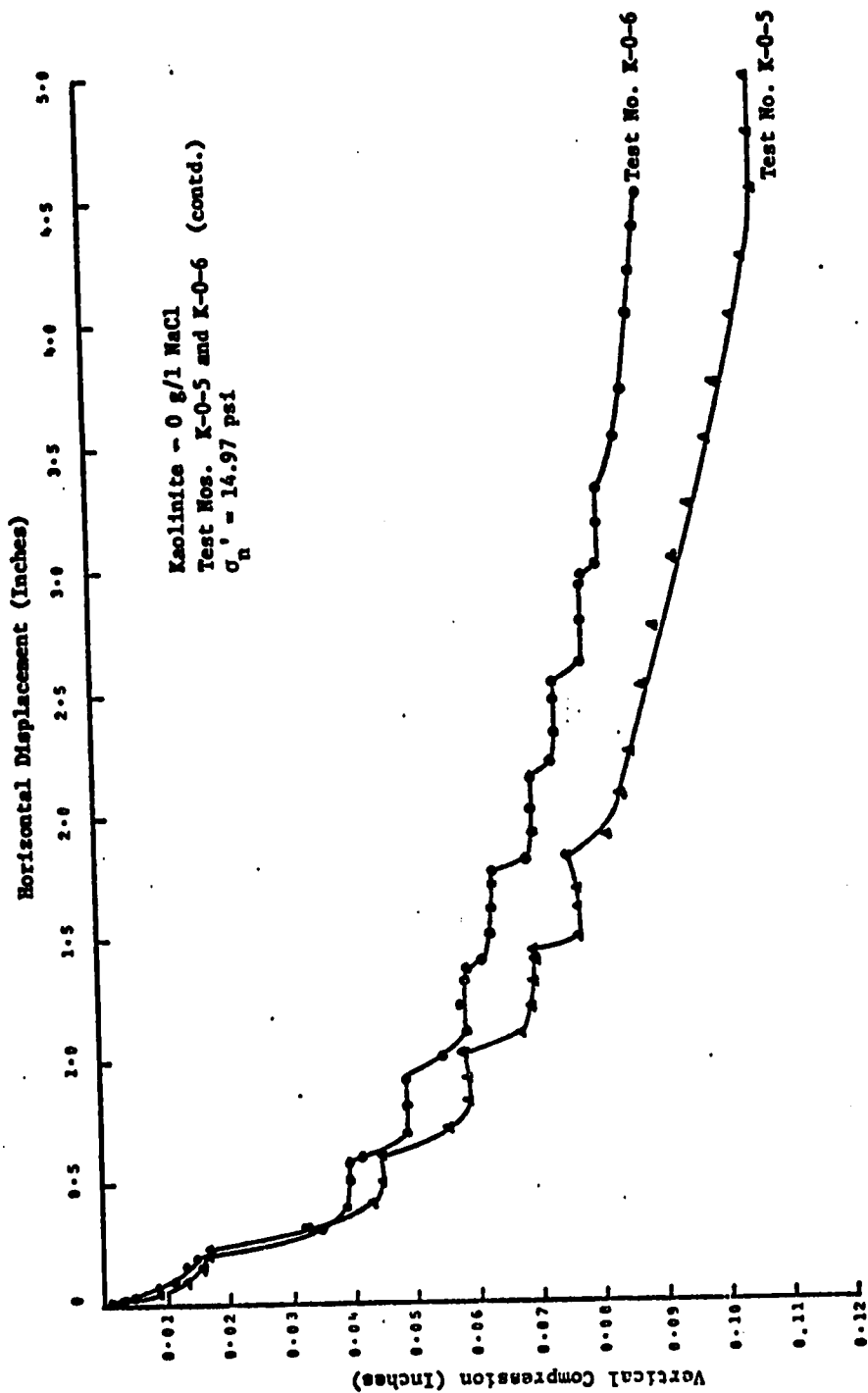
FIG. B-10c DIRECT SHEAR TESTS ON KAOLINITE (K-0-5 and K-0-6)

Kaolinite – 0 g/l NaCl
Test No. K-0-7
Precut Plane Test
Rate of Displacement = 0.0024 ins./min
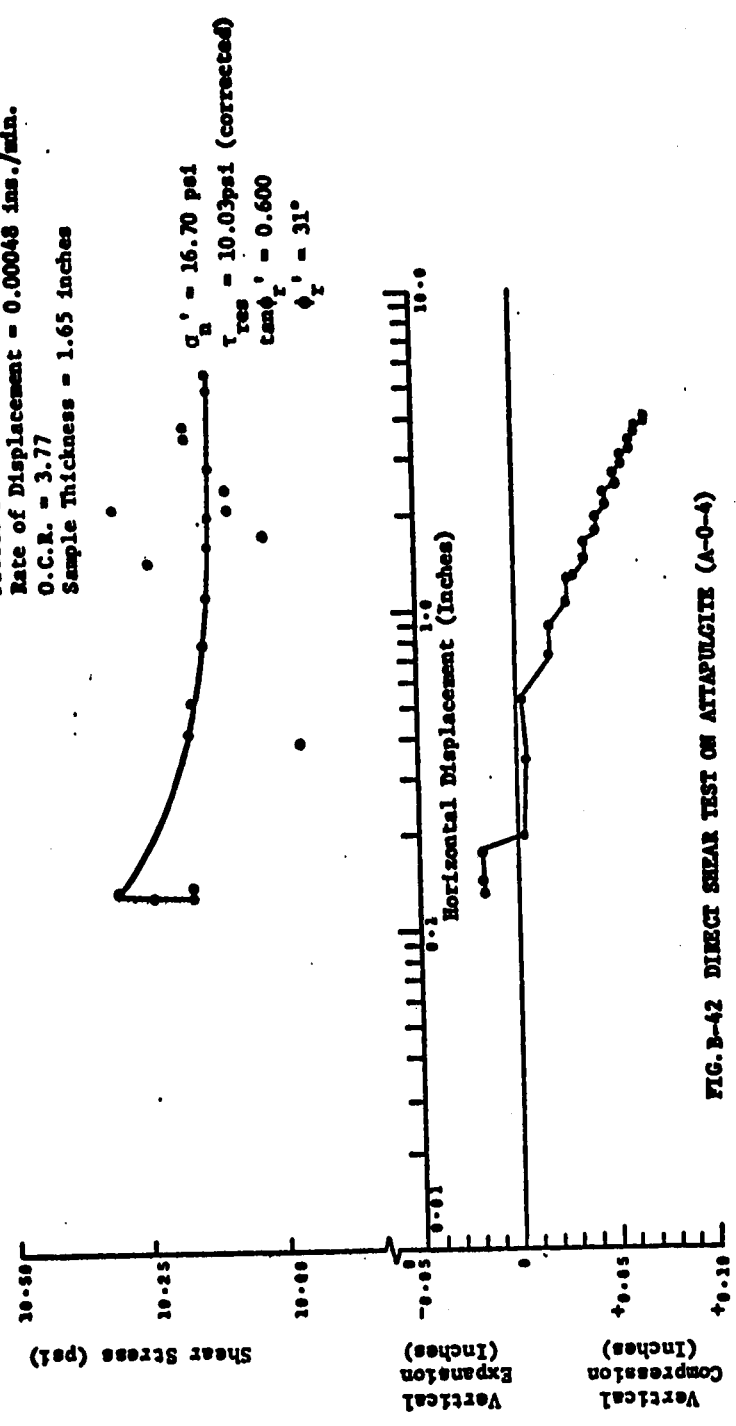O.C.R. = 1.00
Sample Thickness = 1.36 inches

σ_n' = 15.24 psi
τ_{res} = 4.48 psi
$\tan\phi_r'$ = 0.294
ϕ_r' = 16°30'
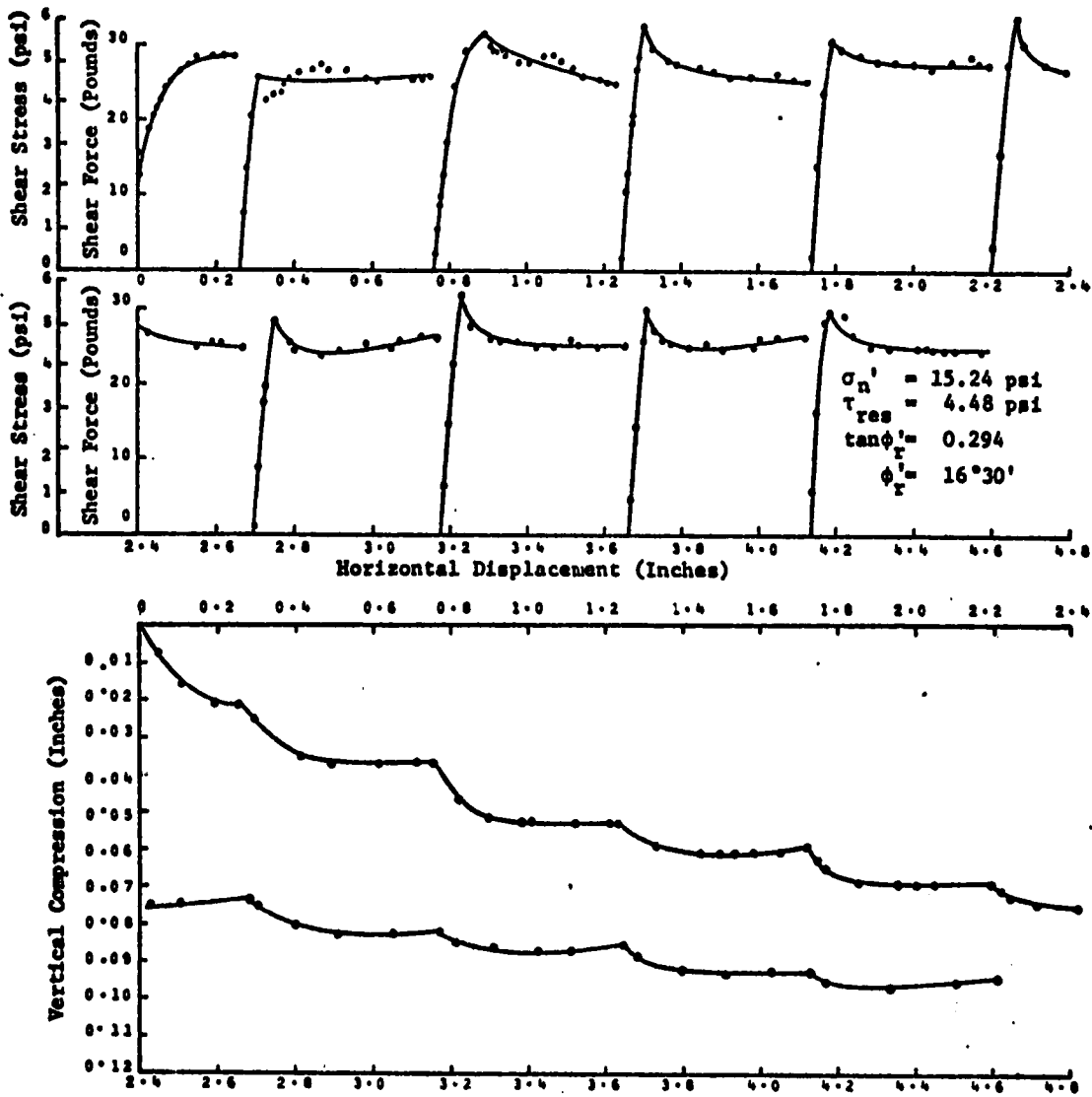
FIG. B-11 DIRECT SHEAR TEST ON KAOLINITE (K-0-7)

FIG. B-12 DIRECT SHEAR TEST ON KAOLINITE (K-0-8)
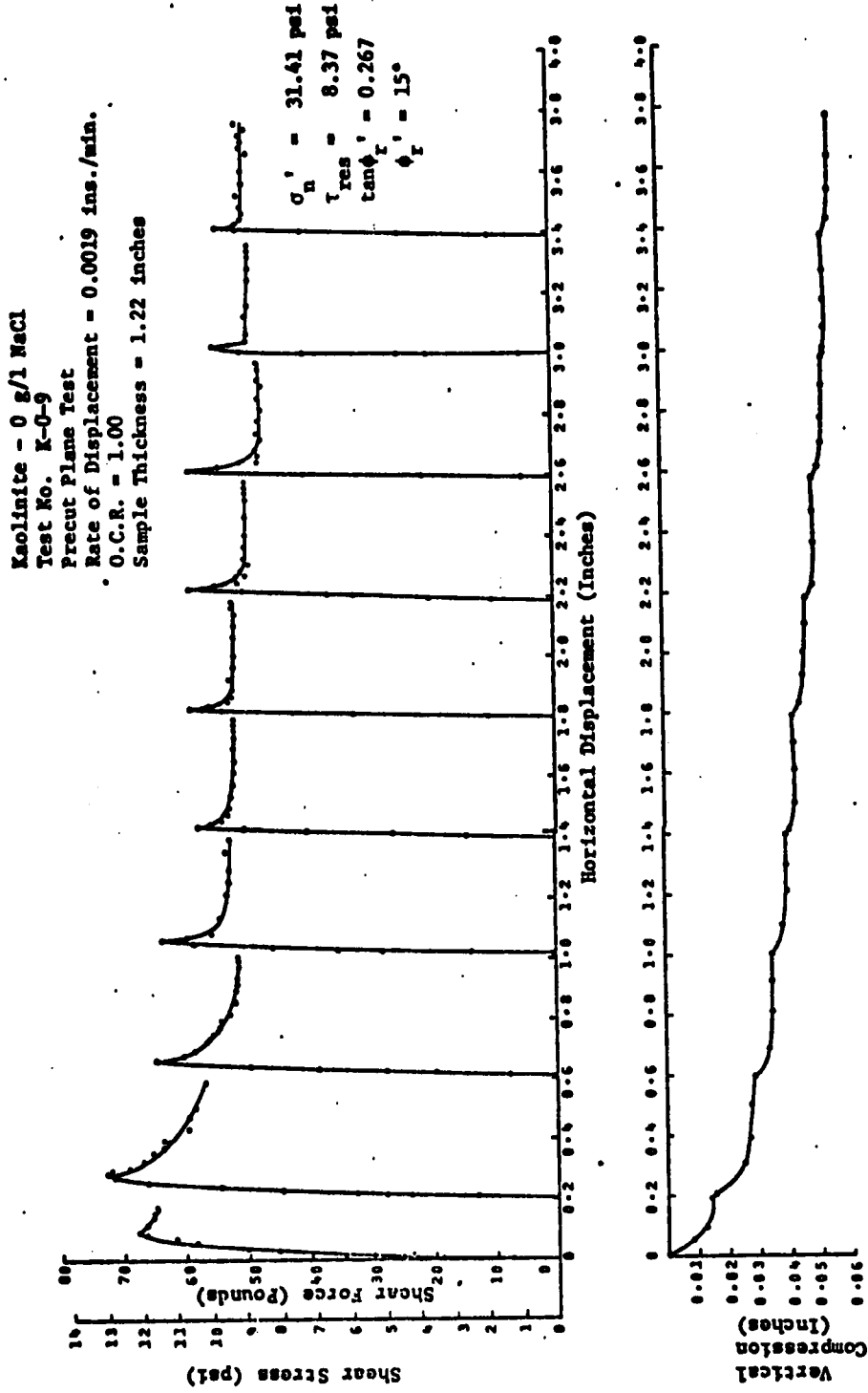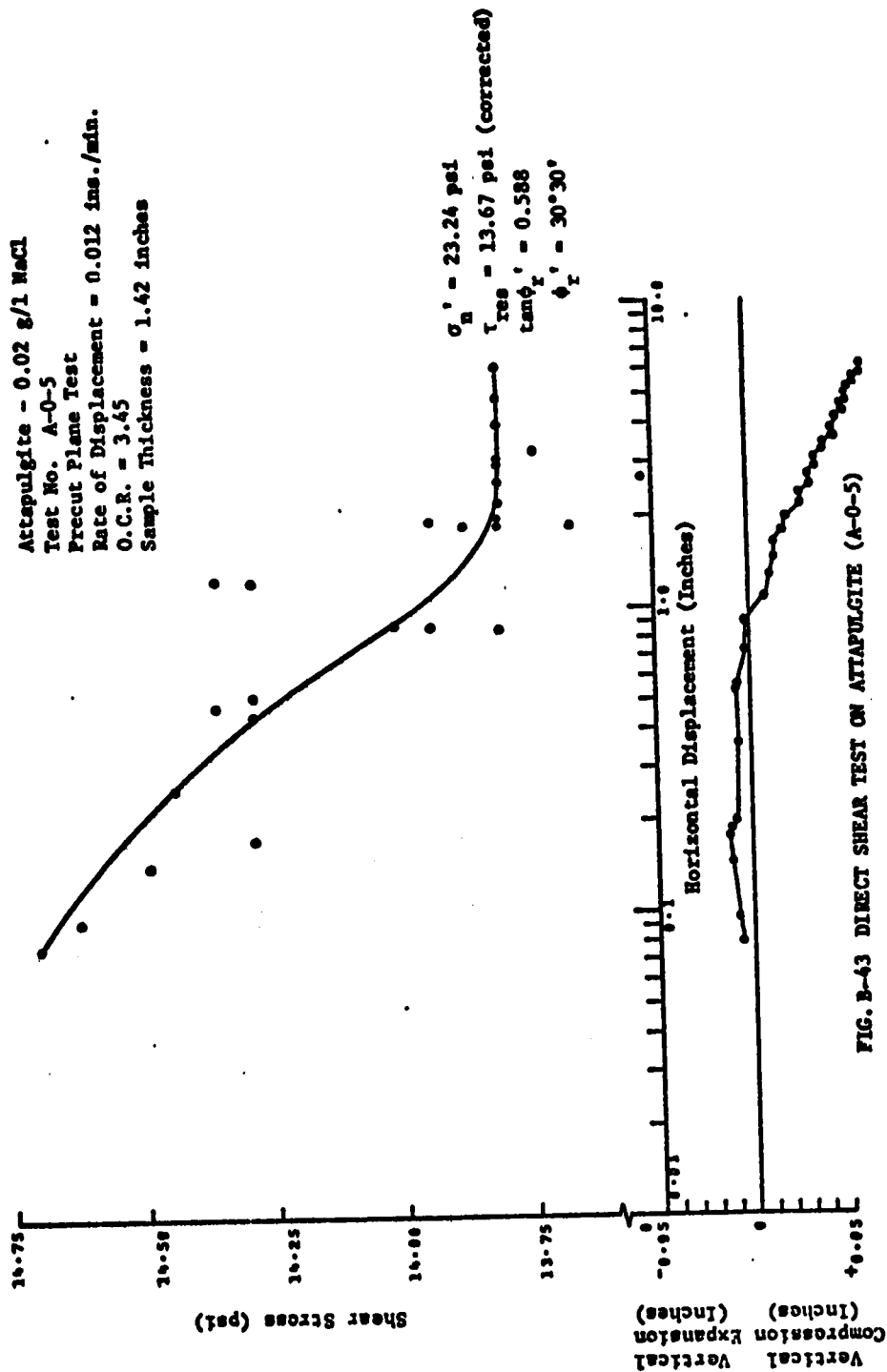
FIG. B-13   DIRECT SHEAR TEST ON KAOLINITE (K-0-9)
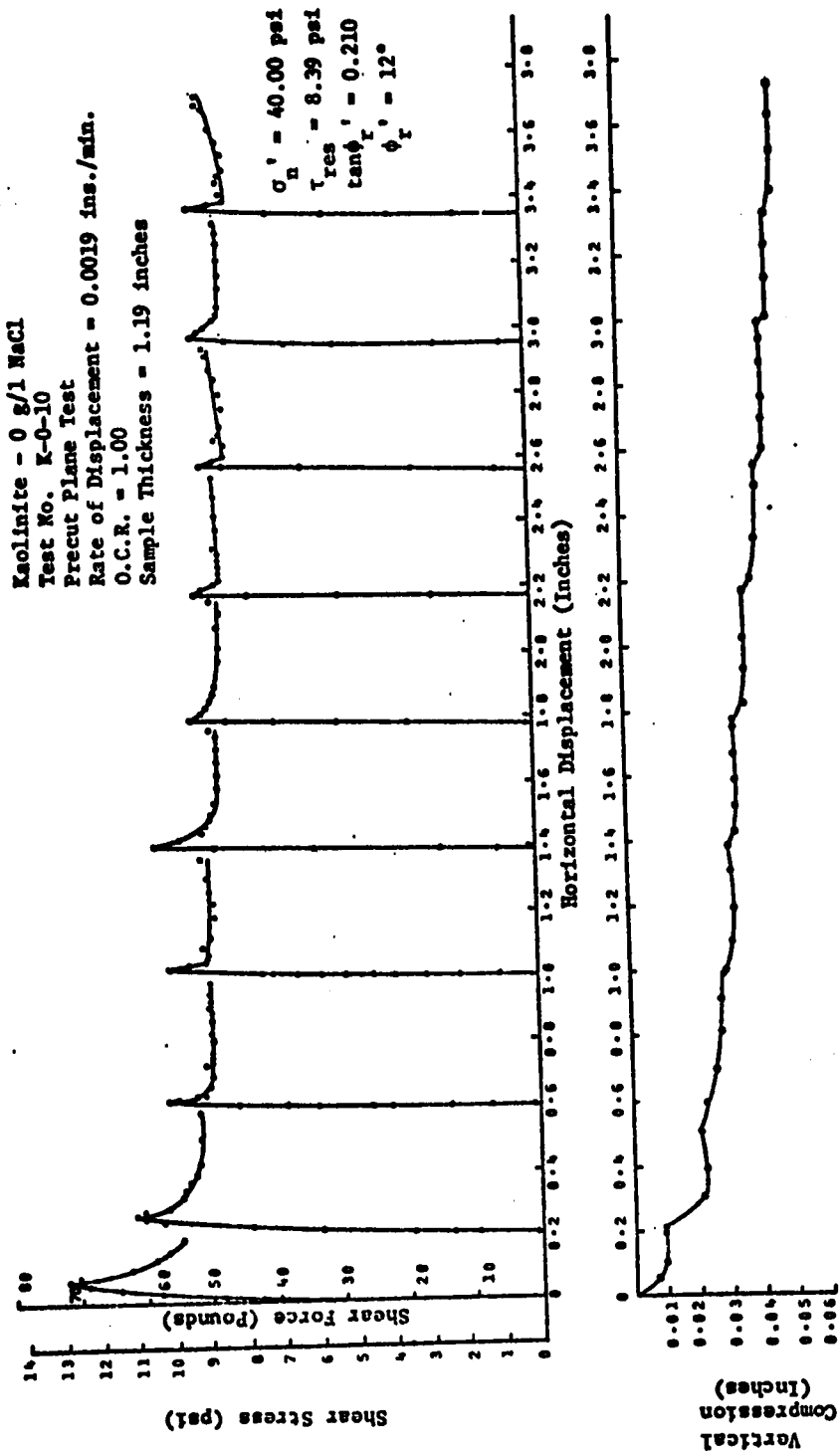
FIG. B-14 DIRECT SHEAR TEST ON KAOLINITE (K-0-10)

Kaolinite - 0 g/l NaCl
Test No. K-0-11
Precut Plane Test
Rate of Displacement = 0.0019 ins./min.
O.C.R. = 1.00
Sample Thickness = 1.21 inches

$\sigma_n' = 40.48$ psi
$\tau_{res} = 9.86$ psi
$\tan\phi_r' = 0.244$
$\phi_r' = 13°40'$

Horizontal Displacement (Inches)

Shear Force (Pounds)
Shear Stress (psi)

Vertical Compression (Inches)
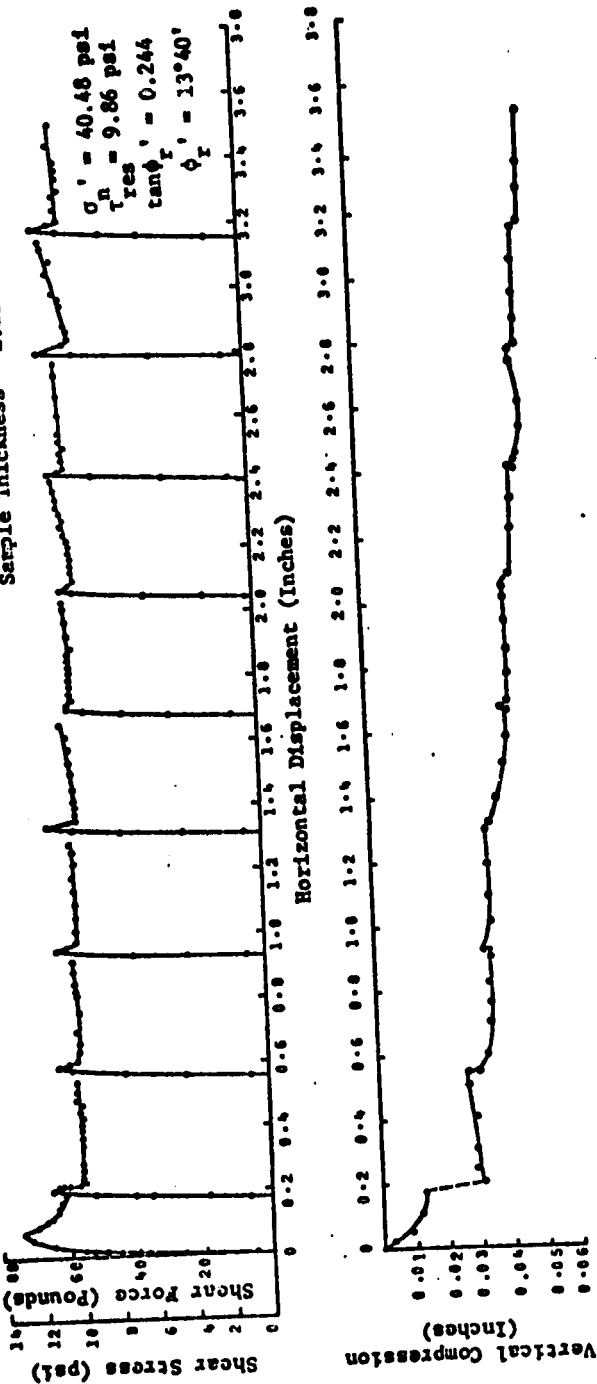
FIG. B-15   DIRECT SHEAR TEST ON KAOLINITE (K-0-11)
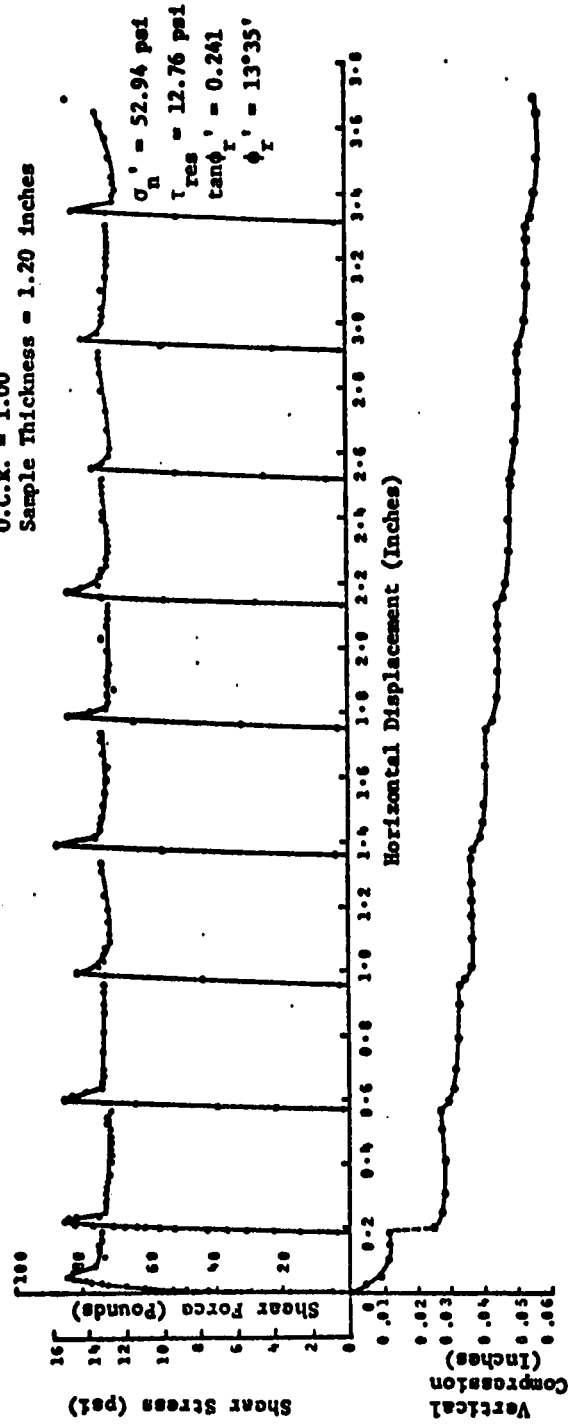
FIG. B-16 DIRECT SHEAR TEST ON KAOLINITE (K-0-12)

Kaolinite - 0 g/l NaCl
Test No. K-0-13
Precut Plane Test.
Rate of Displacement = 0.0024 ins./min.
O.C.R. = 1.00
Sample Thickness = 1.34 inches

σ_n' = 56.78 psi
τ_{res} = 12.96 psi
$\tan\phi_r'$ = 0.228
ϕ_r' = 12°50'

Horizontal Displacement (Inches)

Shear Force (Pounds)

Shear Stress (psi)

Vertical
Compression
(Inches)
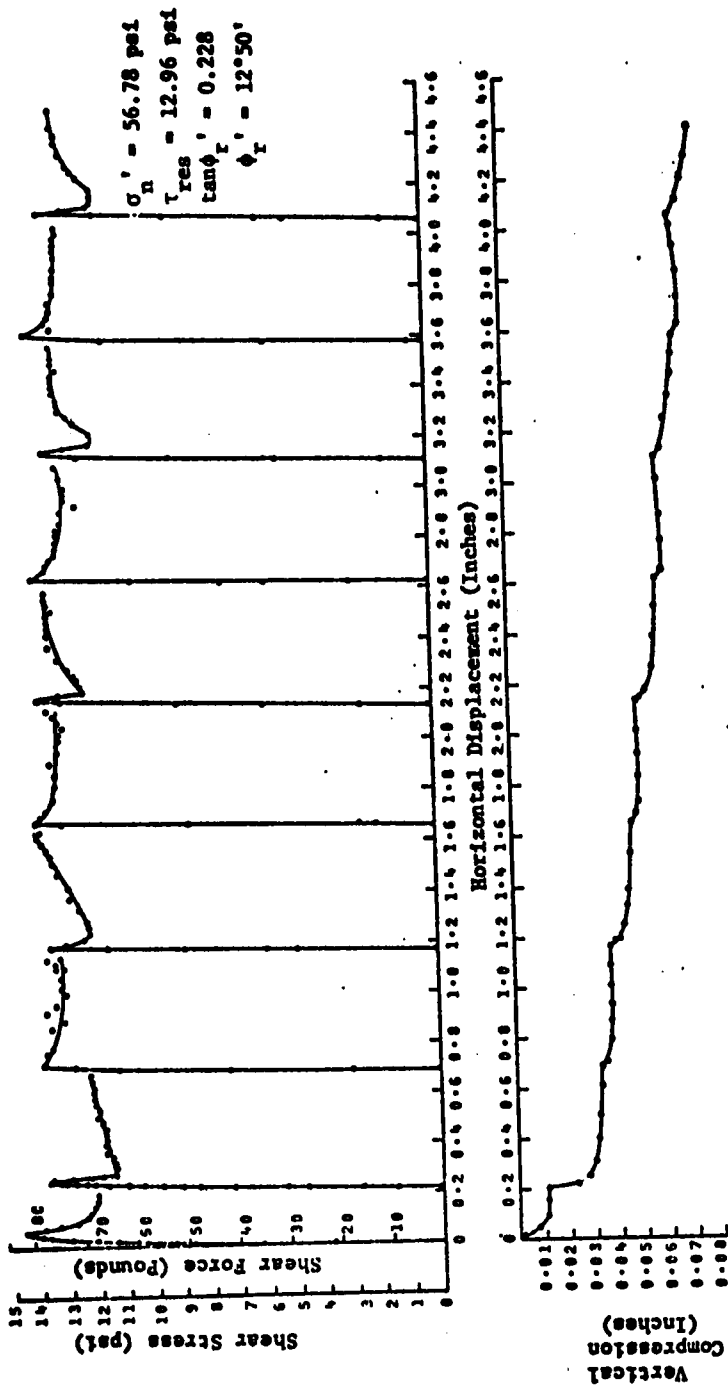
FIG. B-17 DIRECT SHEAR TEST ON KAOLINITE (K-0-13)
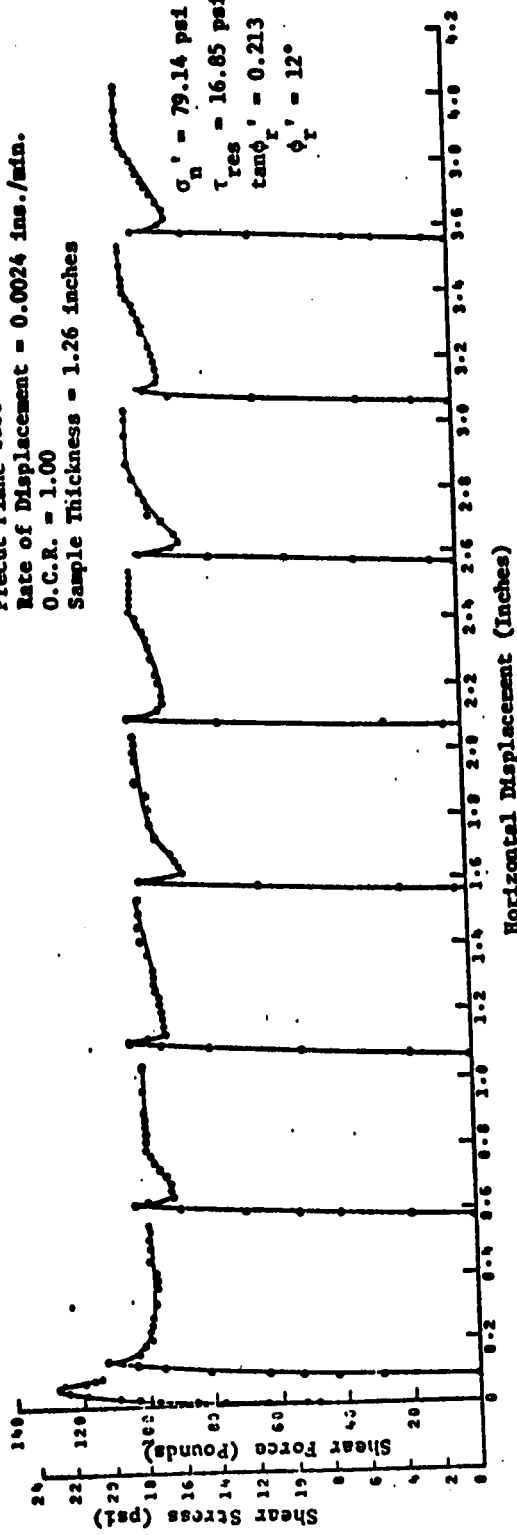
FIG. B-18 DIRECT SHEAR TEST ON KAOLINITE (K-0-14)

Kaolinite 2 g/1 NaCl
Test No. K-2-1
Precut Plane Test
Rate of Displacement = 0.0024 ins./min.
O.C.R. = 1.00
Sample Thickness = 1.36 inches
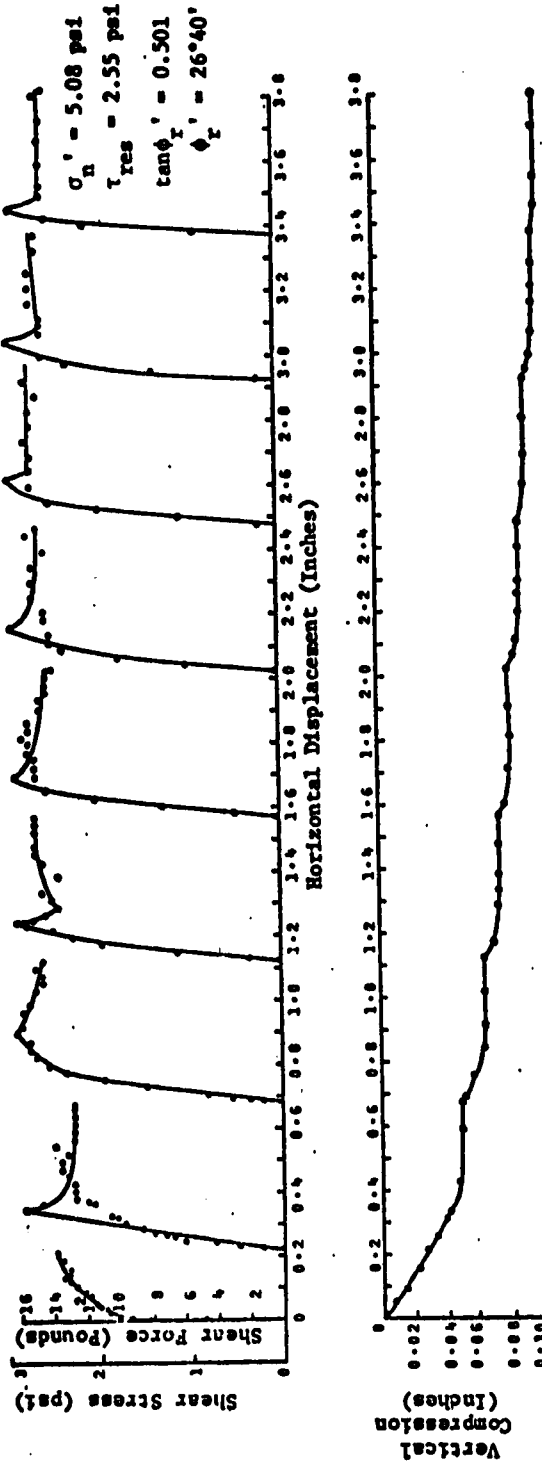
$\sigma_n' = 5.08$ psi
$\tau_{res} = 2.55$ psi
$\tan\phi_r' = 0.501$
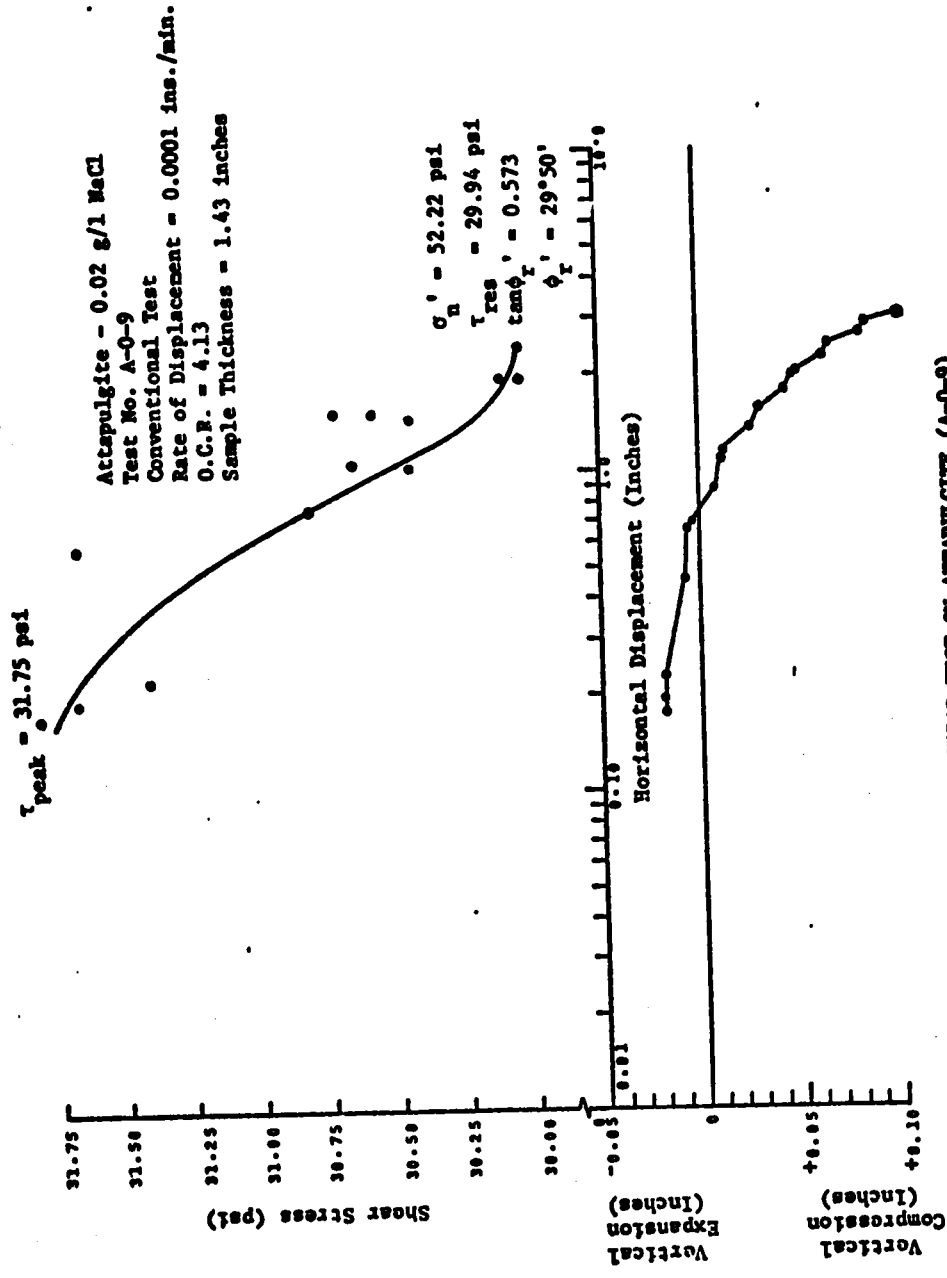$\phi_r' = 26°40'$

FIG. B-19   DIRECT SHEAR TEST ON KAOLINITE (K-2-1)
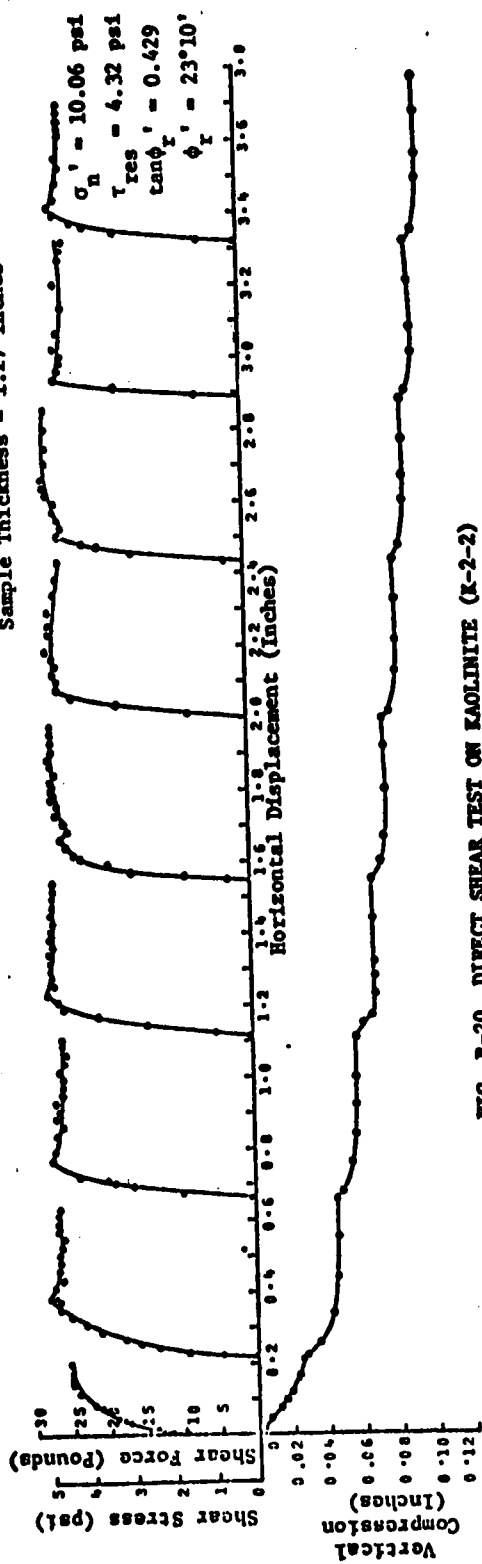
FIG. B-20   DIRECT SHEAR TEST ON KAOLINITE (K-2-2)

Kaolinite - 2 g/l NaCl
Test No. K-2-3
Precut Plane Test
Rate of Displacement = 0.0019 ins./min.
O.C.R. = 1.00
Sample Thickness = 1.27 inches

σ_n' = 14.37 psi
τ_{res} = 5.50 psi
Tanϕ_r' = 0.383
ϕ_r' = 21°
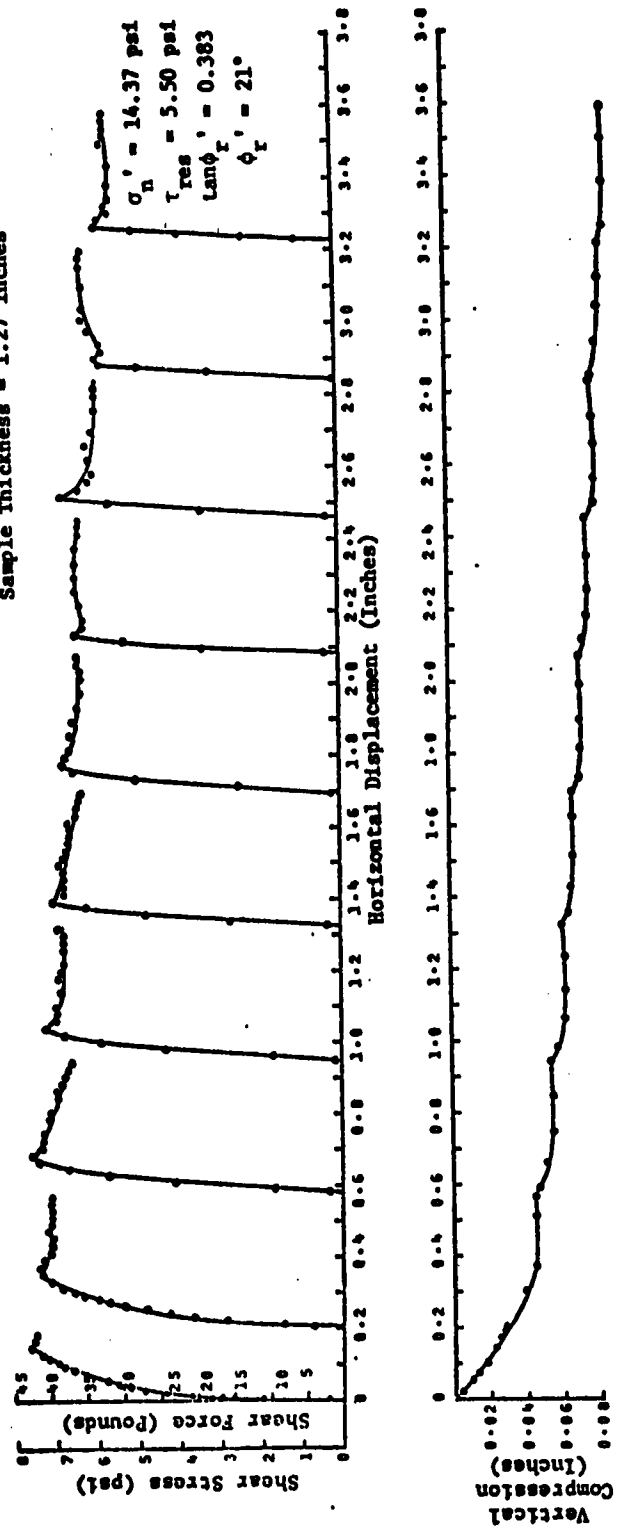
FIG. B-21 DIRECT SHEAR TEST ON KAOLINITE (K-2-3)
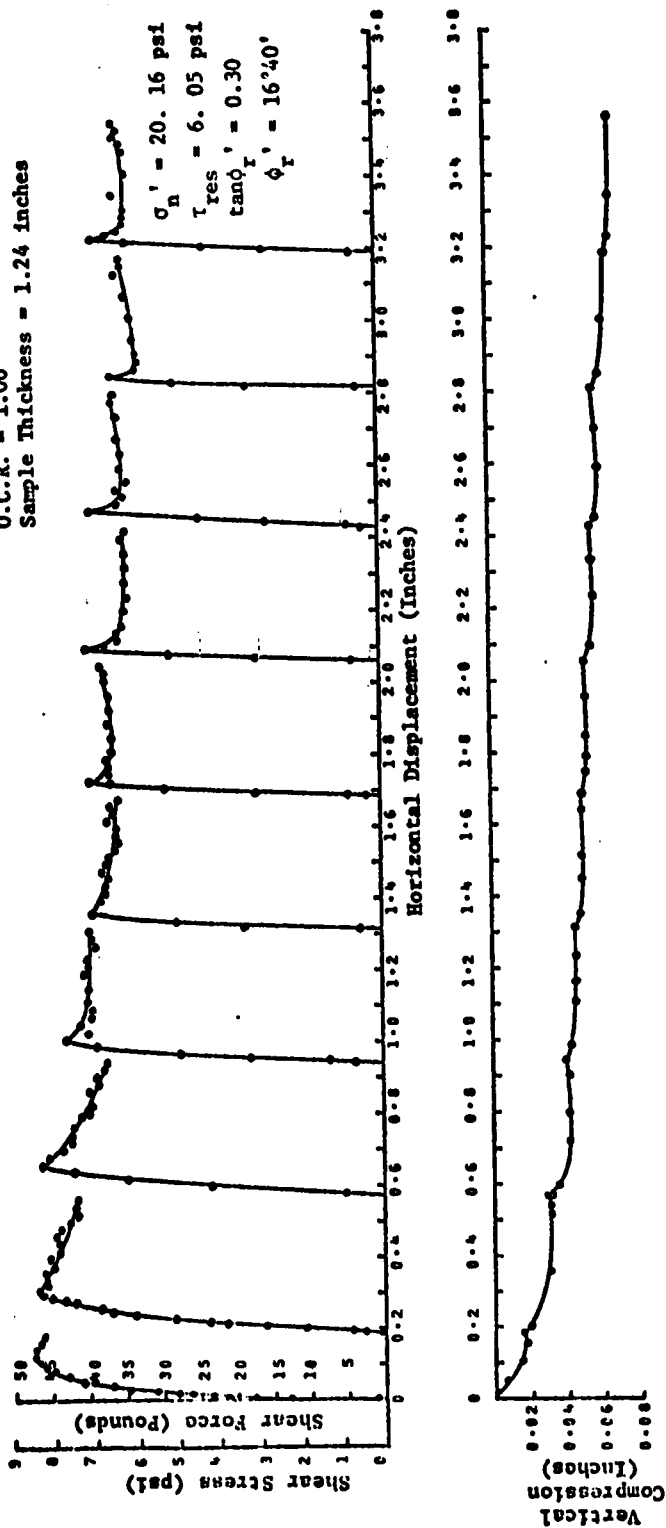
FIG. B-22 DIRECT SHEAR TEST ON KAOLINITE (K-2-4)

Kaolinite - 2 g/1 NaCl
Test No. K-2-5
Precut Plane Test
Rate of Displacement = 0.0024 ins./min.
O.C.R. = 1.00
Sample Thickness = 1.19 inches

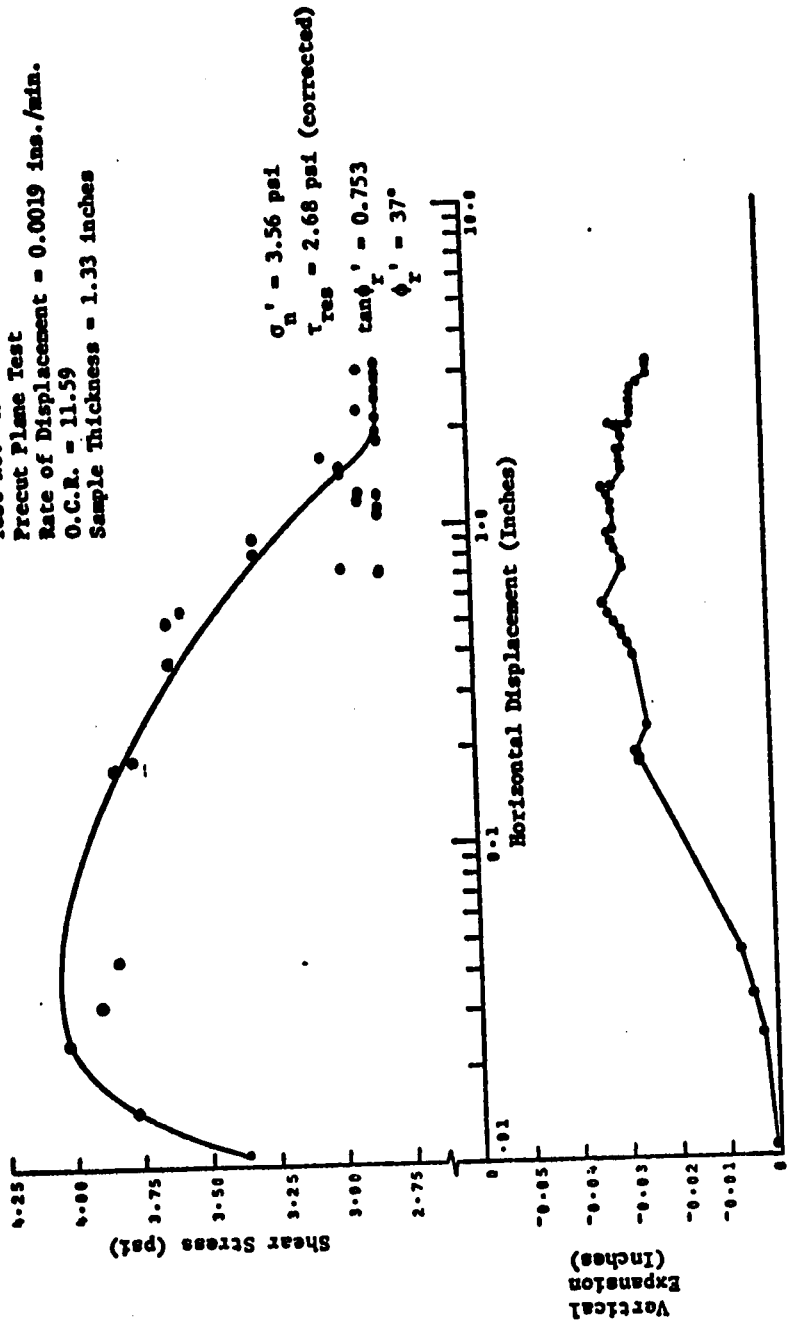σ_n' = 30.63 psi
τ_{res} = 6.21 psi
$\tan\phi_r'$ = 0.203
ϕ_r' = 11°30'
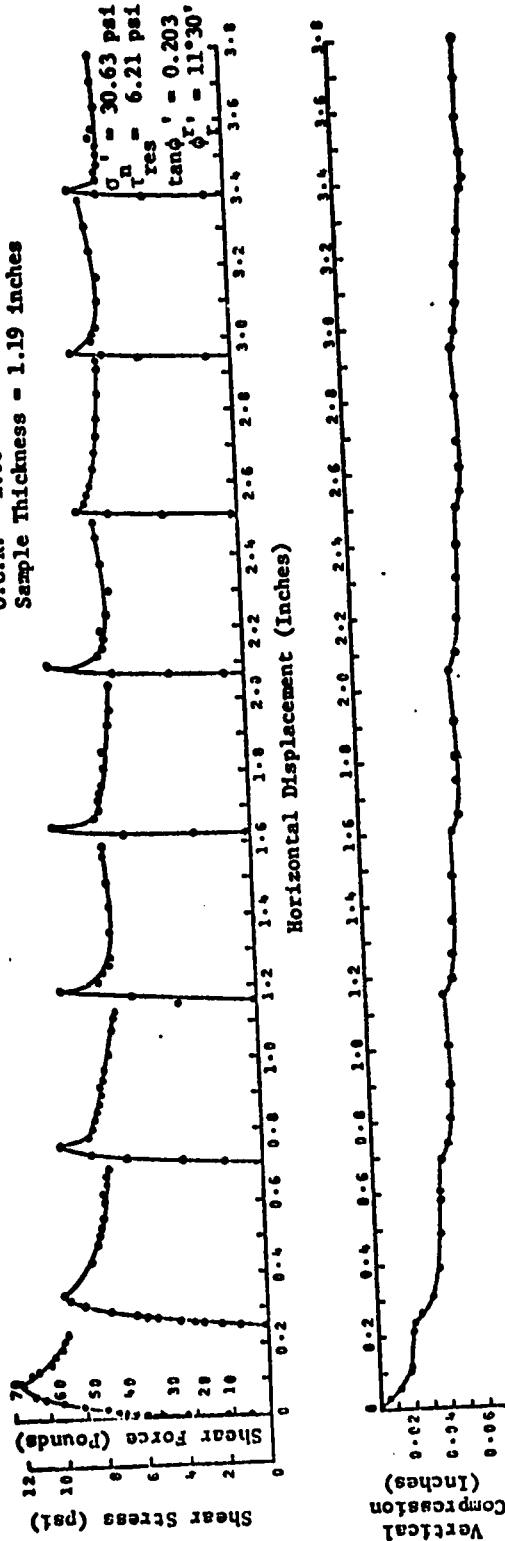
FIG. B-23 DIRECT SHEAR TEST ON KAOLINITE (K-2-5)

Kaolinite - 2 g/1 NaCl
Test No. K-2-6
Precut Plane Test
Rate of Displacement = 0.0024 ins./min.
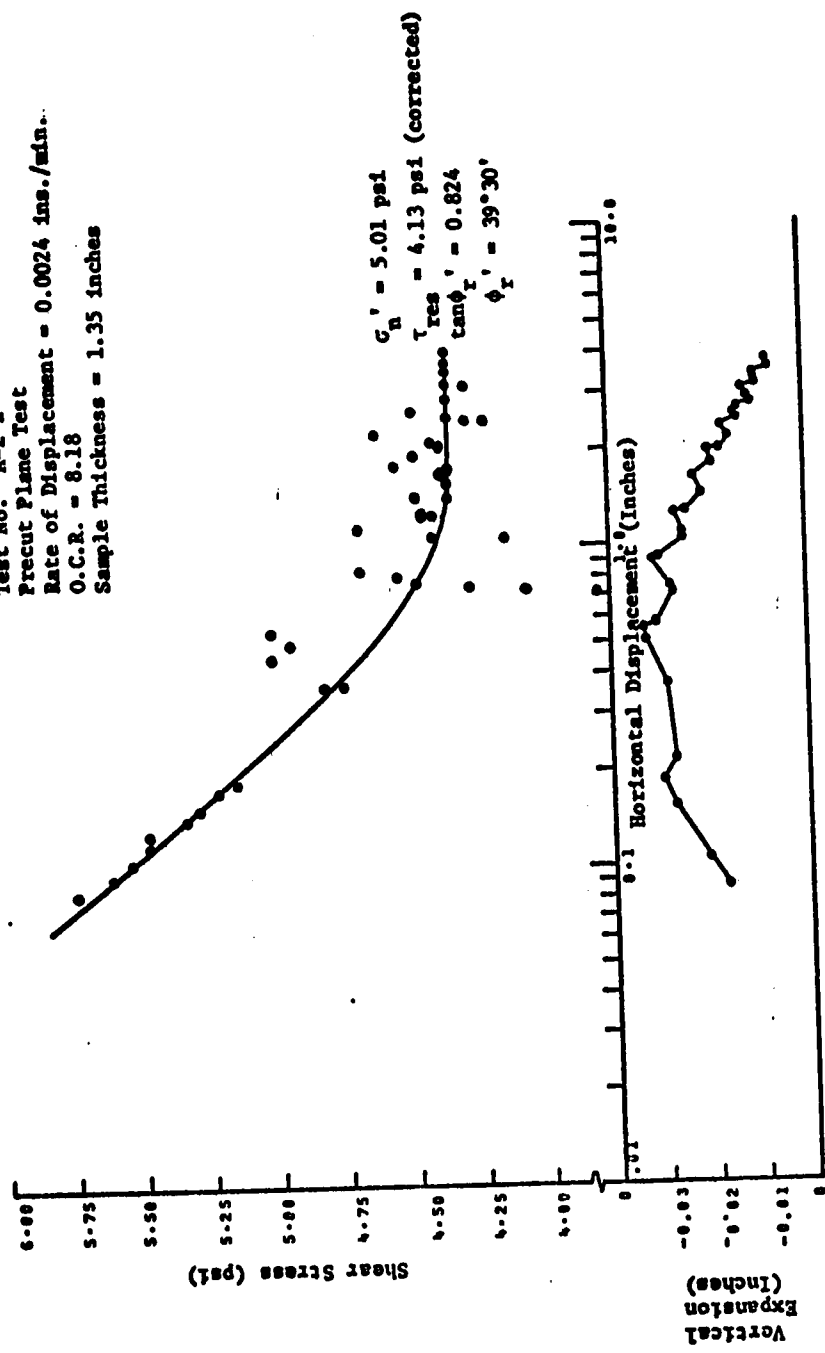O.C.R. = 1.00
Sample Thickness = 1.14 inches

σ_n' = 40.12 psi
τ_{res} = 8.53 psi
$\tan\phi_r'$ = 0.213
ϕ_r' = 12°

Horizontal Displacement (Inches)

Shear Force (Pounds)

Shear Stress (psi)

Vertical Compression (Inches)
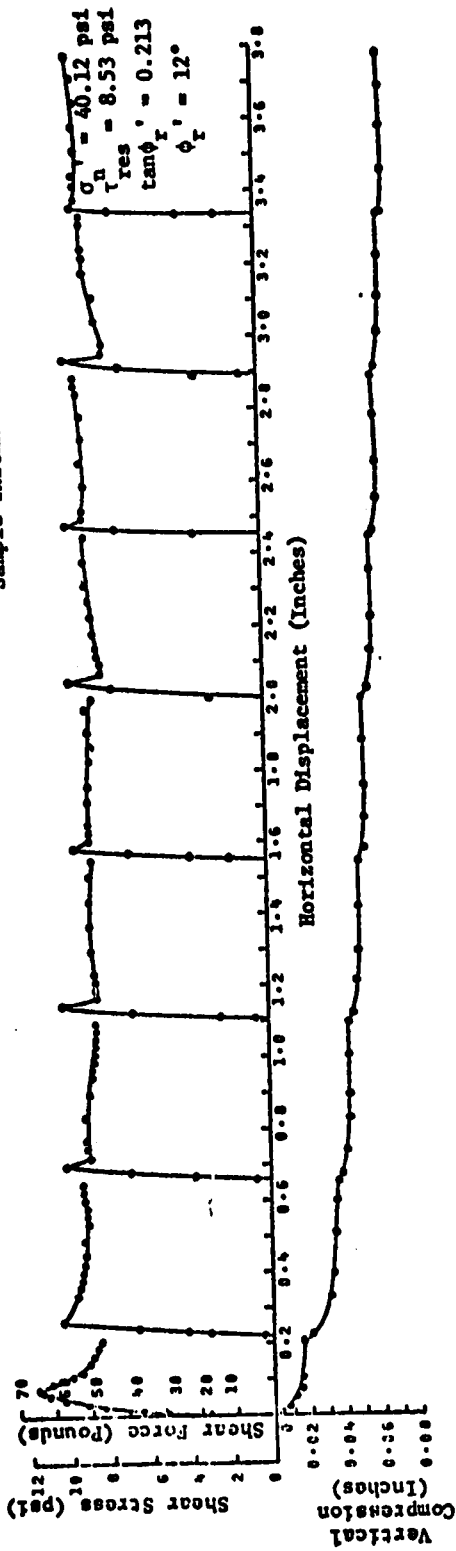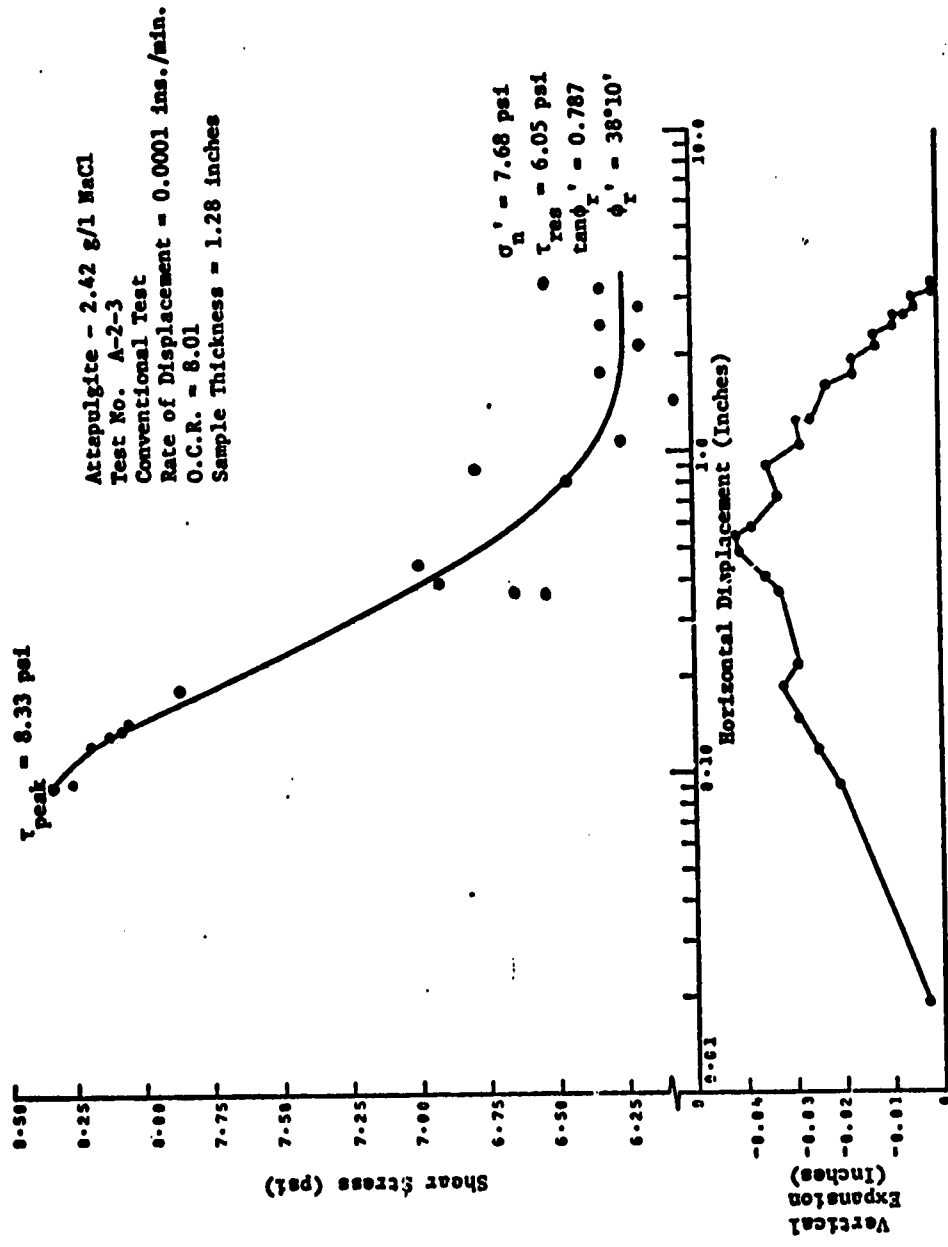
FIG. B-24 DIRECT SHEAR TEST ON KAOLINITE (K-2-6)
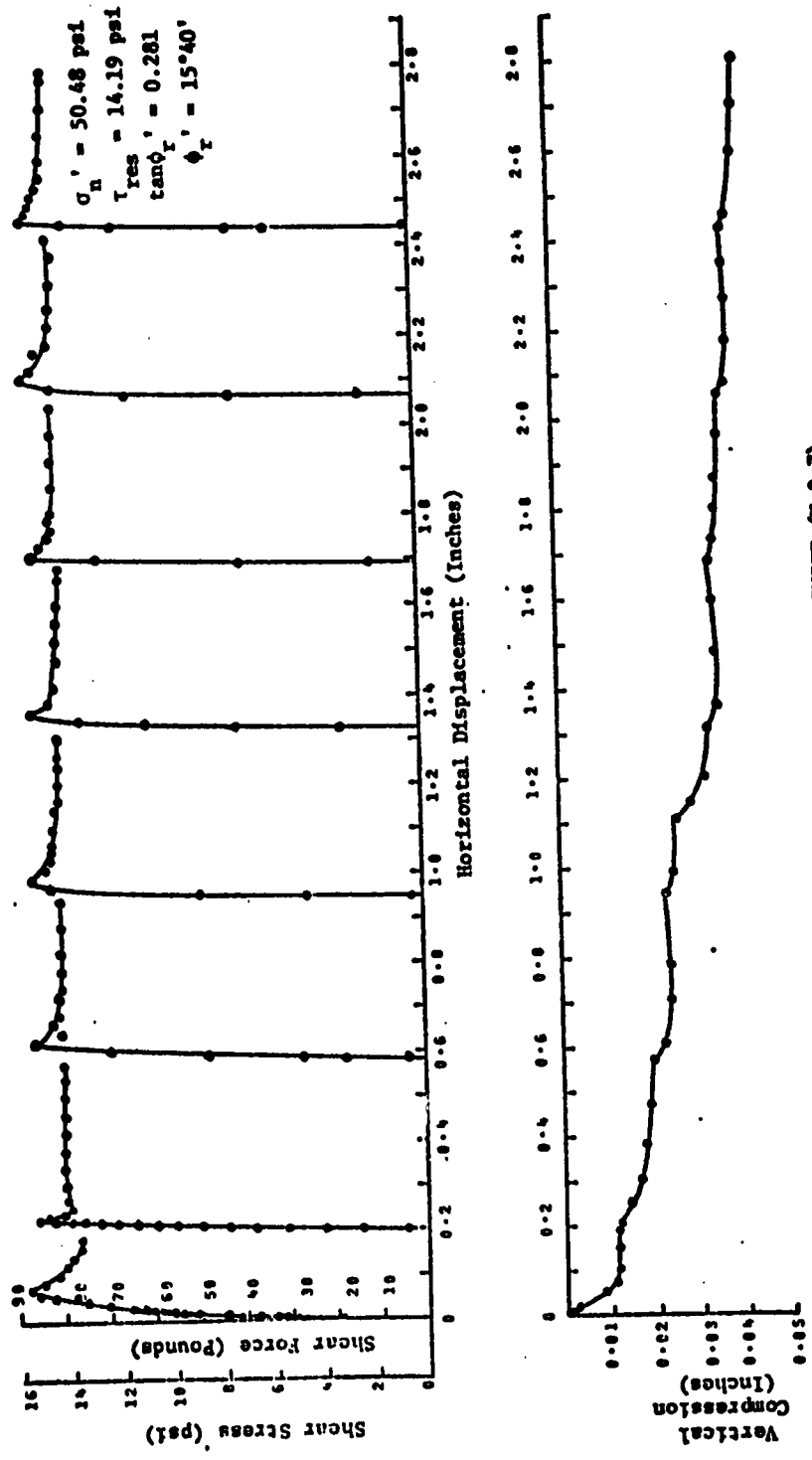
FIG. B-25   DIRECT SHEAR TEST ON KAOLINITE (K-2-7)

Kaolinite - 2 g/1 NaCl
Test No. K-2-8
Precut Plane Test
Rate of Displacement = 0.0019 ins./min.
O.C.R. = 1.00
Sample Thickness = 1.14 inches

$\sigma_n' = 60.24$ psi
$\tau_{res} = 12.62$ psi
$\tan\phi_r' = 0.210$
$\phi_r' = 12°$

Horizontal Displacement (inches)

Shear Force (pounds)

Shear Stress (psi)

Vertical Compression (inches)
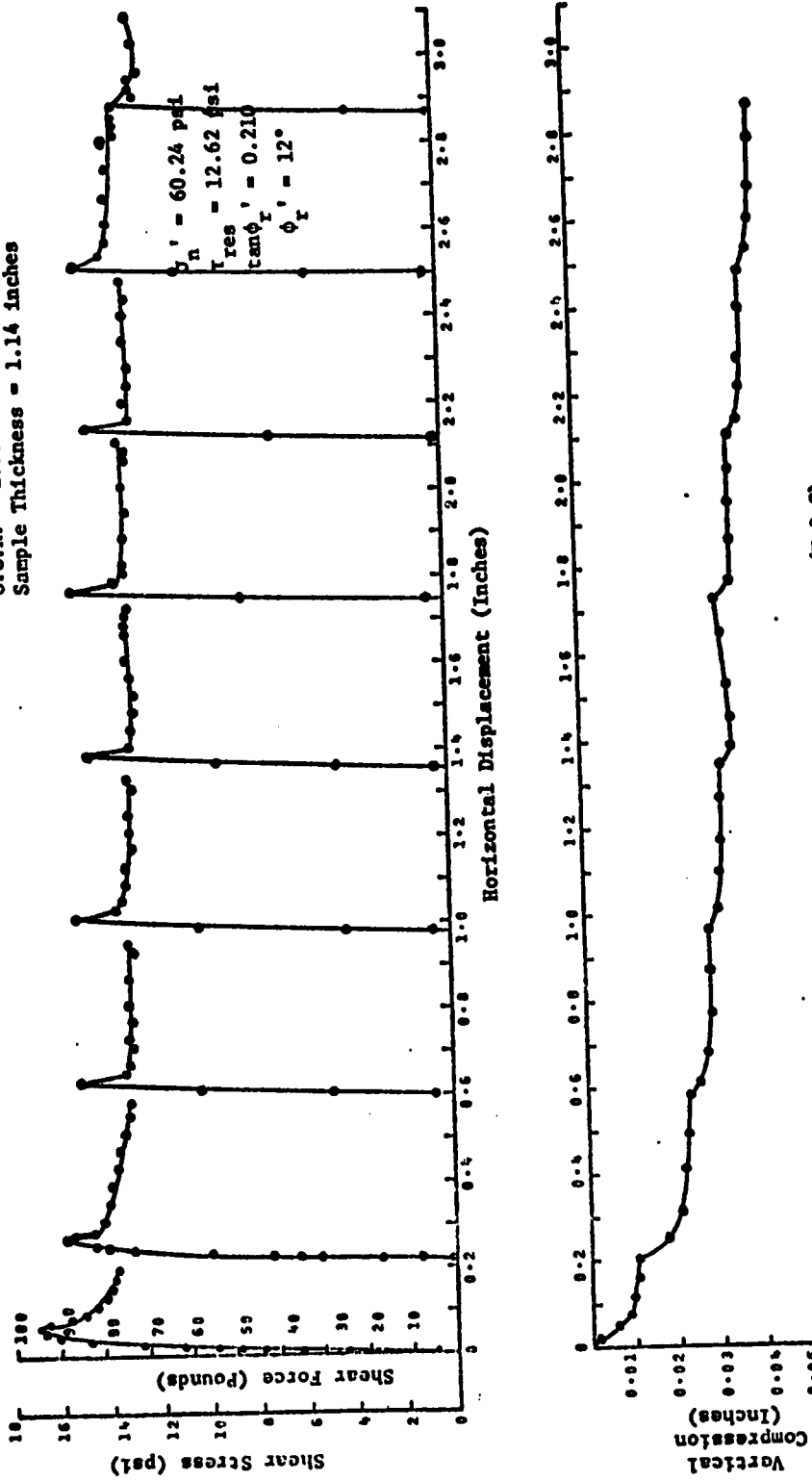
FIG. B-26 DIRECT SHEAR TEST ON KAOLINITE (K-2-8)

Kaolinite - 2 g/l NaCl
Test No. K-2-9
Precut Plane Test
Rate of Displacement = 0.0019 ins./min.
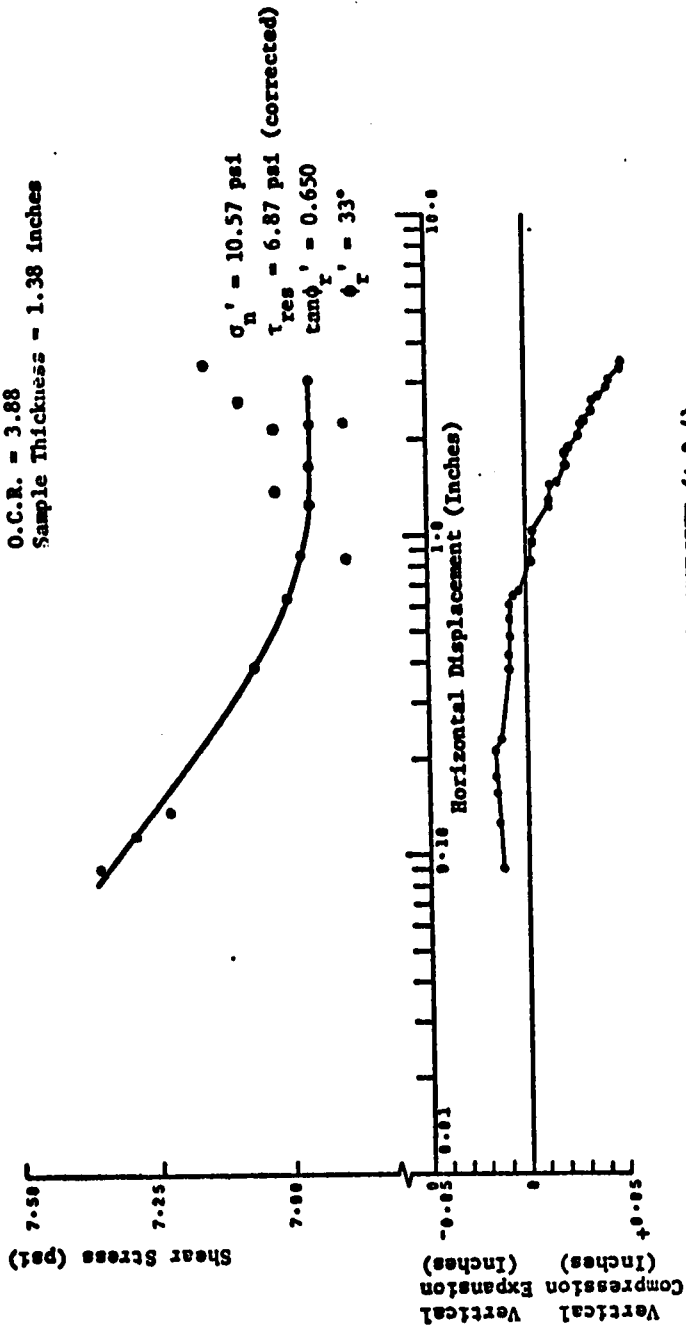O.C.R. = 1.00
Sample Thickness 1.12 inches

$\sigma_R' = 70.94$ psi
$\tau_{res} = 14.79$ psi
$\tan\phi_r' = 0.208$
$\phi_r' = 11°50'$

Horizontal Displacement (Inches)

Shear Force (Pounds)

Shear Stress (psi)

Vertical
Compression
(Inches)
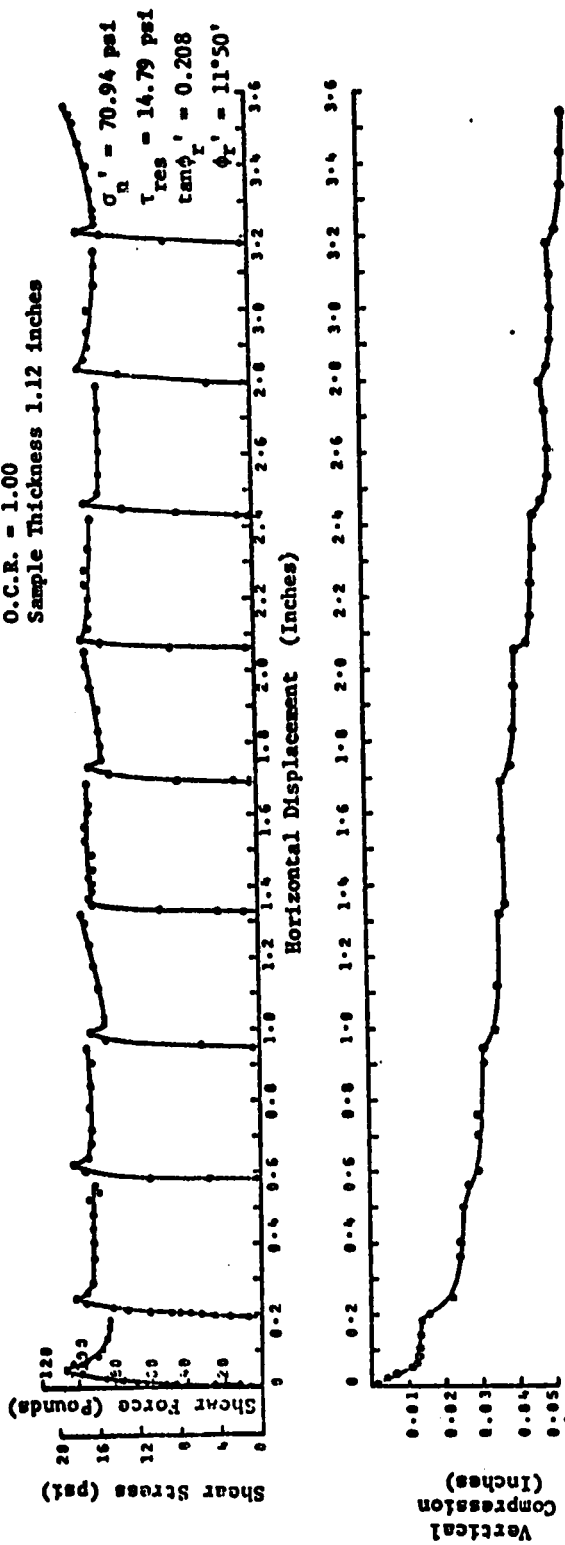
FIG. B-27 DIRECT SHEAR TEST ON KAOLINITE (K-2-9)
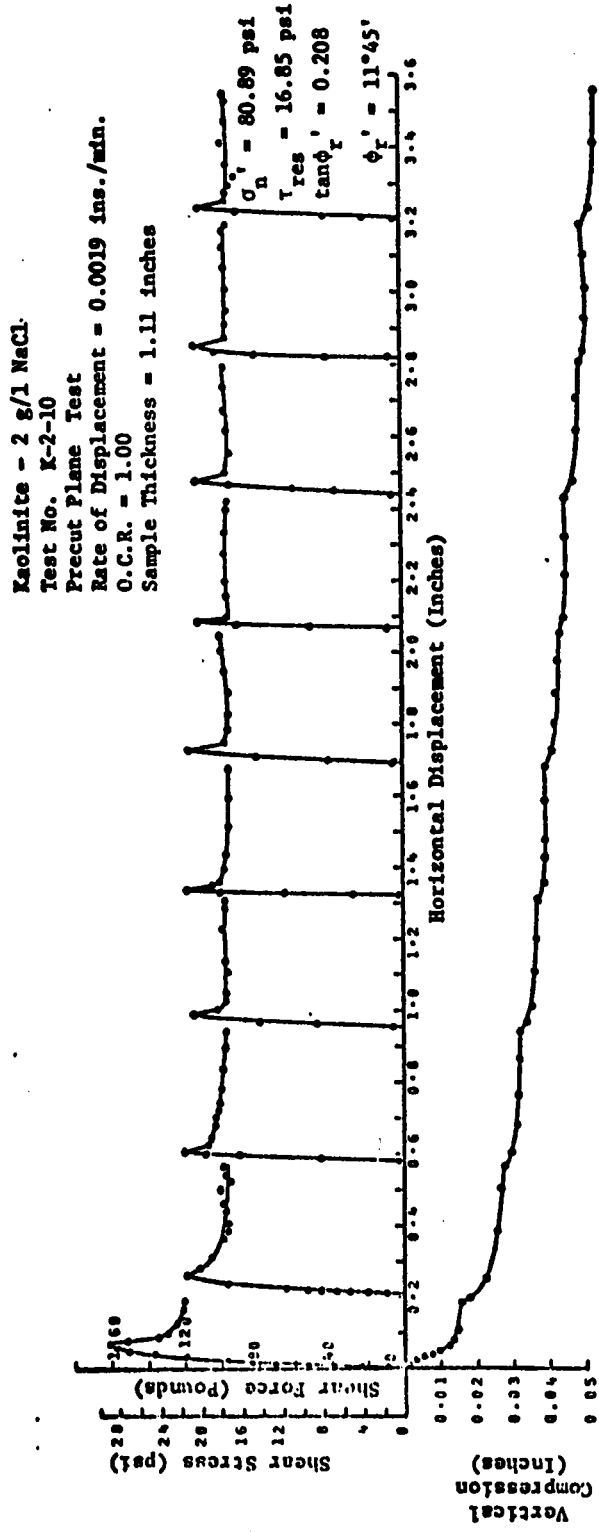
FIG. B-28   DIRECT SHEAR TEST ON KAOLINITE (K-2-10)
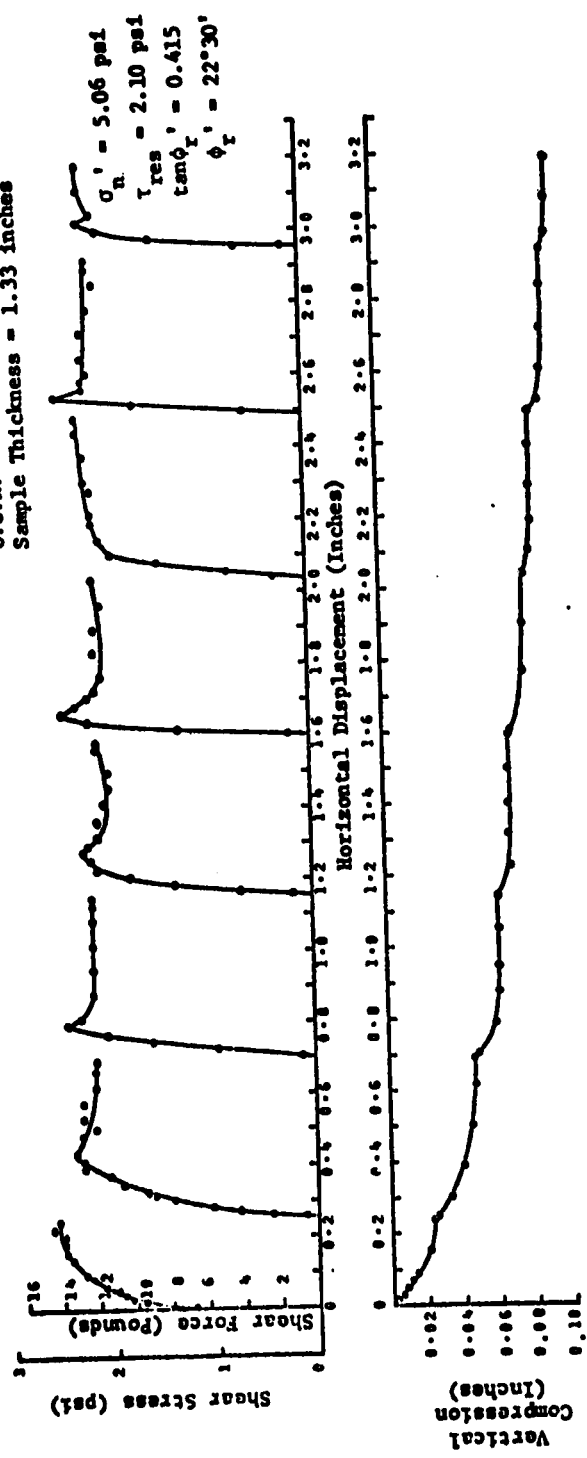
FIG. B-29 DIRECT SHEAR TEST ON KAOLINITE (K-35-1)

Kaolinite - 35 g/l NaCl
Test No. K-35-2
Precut Plane Test
Rate of Displacement = 0.0024 ins./min.
O.C.R. = 1.00
Sample Thickness = 1.28 inches

σ_n' = 10.08 psi
τ_{res} = 4.43 psi
$\tan\phi_r'$ = 0.439
ϕ_r' = 23°40'

Horizontal Displacement (Inches)

Shear Force (Pounds)

Shear Stress (psi)

Vertical Compression (Inches)
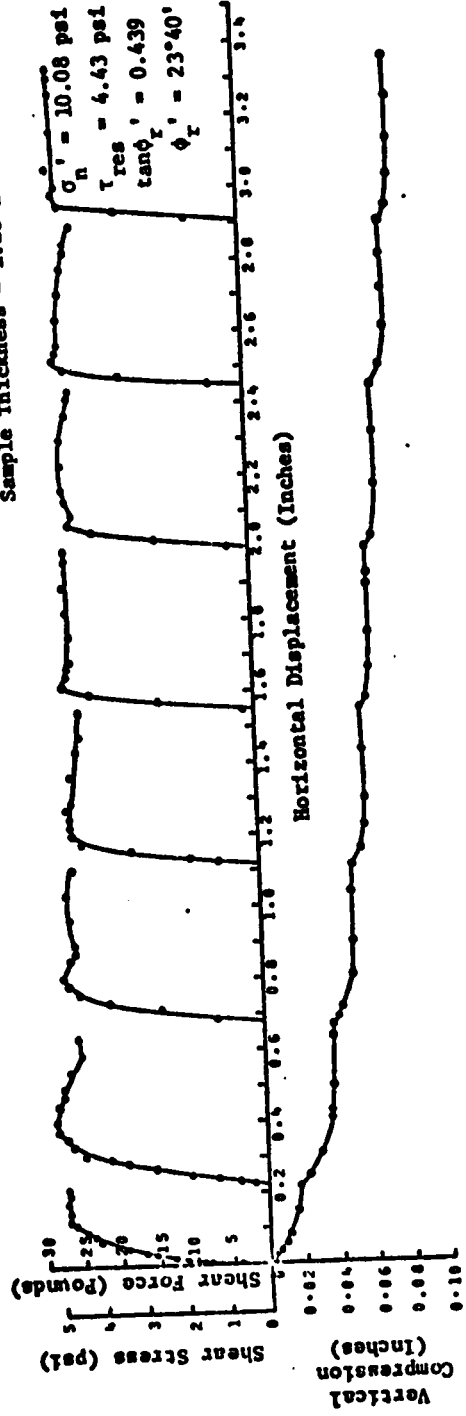
FIG. B-30 DIRECT SHEAR TEST ON KAOLINITE (K-35-2)

Kaolinite - 35 g/l NaCl
Test No. K-35-3
Precut Plane Test
Rate of Displacement = 0.0024 ins./min.
O.C.R. = 1.00
Sample Thickness = 1.28 inches

σ_n' = 15.21 psi
τ_{res} = 4.84 psi
$\tan\phi_r'$ = 0.318
ϕ_r' = 17°40'
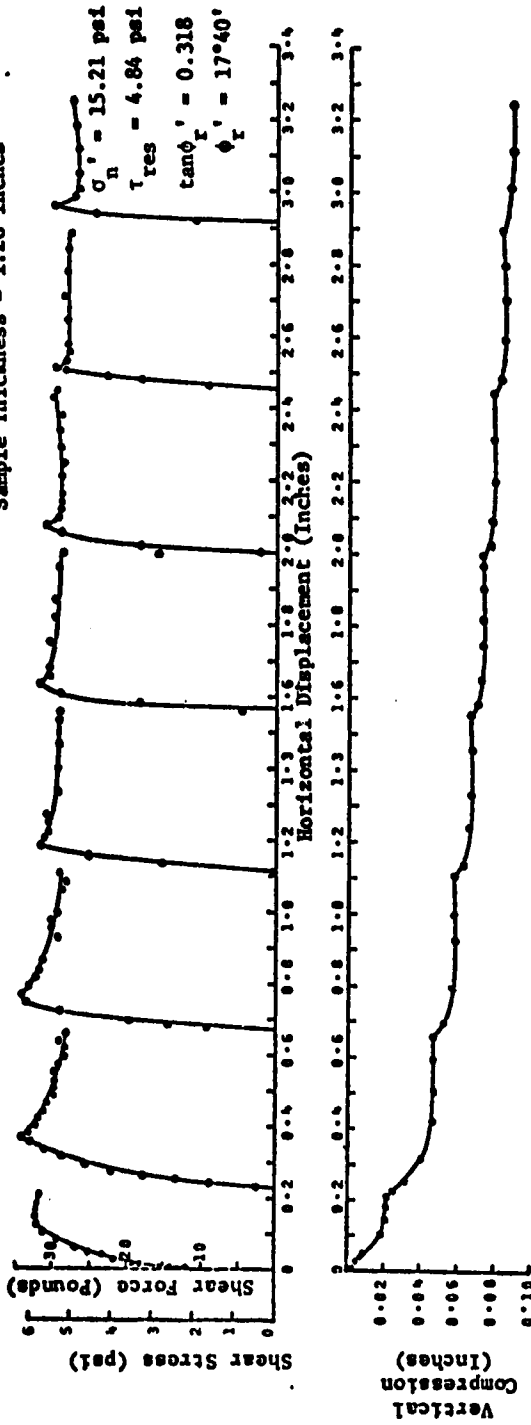
FIG. B-31 DIRECT SHEAR TEST ON KAOLINITE (K-35-3)

Kaolinite - 35 g/l NaCl
Test No. K-35-4
Precut Plane Test
Rate of Displacement = 0.0024 ins./min.
O.C.R. = 1.00
Sample Thickness = 1.13 inches

σ_n' = 20.66 psi
τ_{res} = 5.48 psi
$\tan\phi_r'$ = 0.265
ϕ_r' = 14°50'

Horizontal Displacement (Inches)

Shear Force (Pounds)

Shear Stress (psi)

Vertical Compression (Inches)
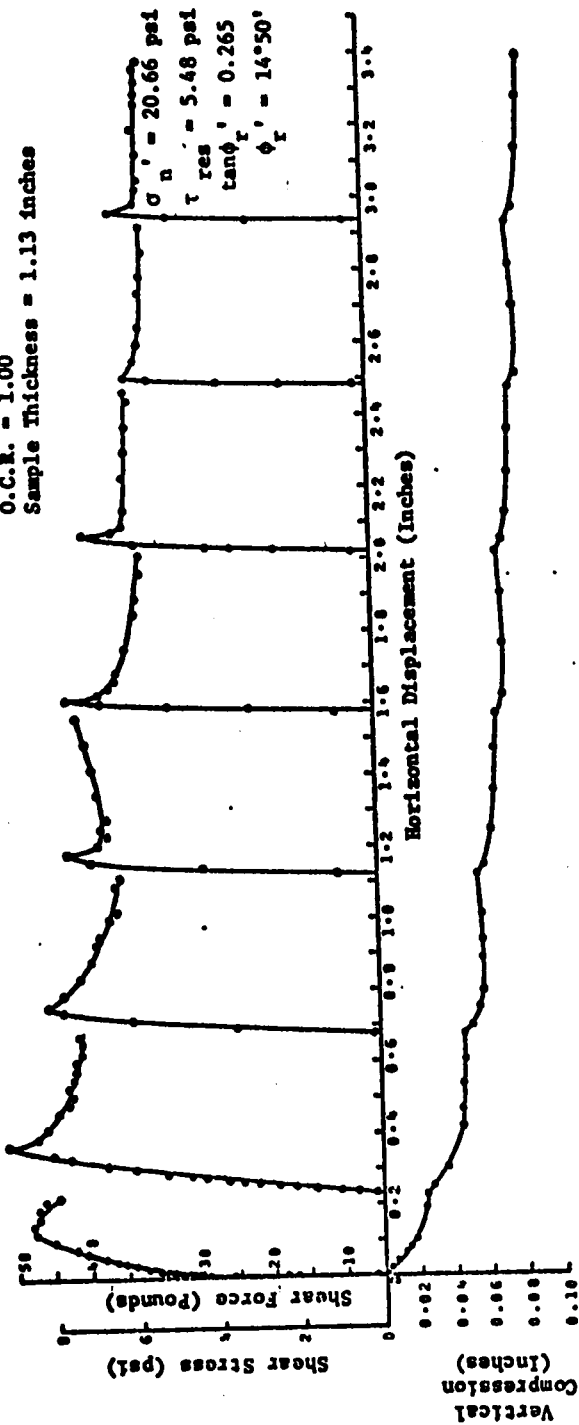
FIG. B-32   DIRECT SHEAR TEST ON KAOLINITE (K-35-4)

Kaolinite - 35 g/1 NaCl
Test No. K-35-5
Precut Plane Test
Rate of Displacement = 0.0019 ins./min.
O.C.R. = 1.00
Sample Thickness = 1.19 inches

$\sigma_n' = 30.42$ psi
$\tau_{res} = 6.81$ psi
$\tan\phi_r' = 0.224$

$\phi_r' = 12°40'$

Horizontal Displacement (Inches)

Shear Force (Pounds)

Shear Stress (psi)

Vertical Compression (Inches)
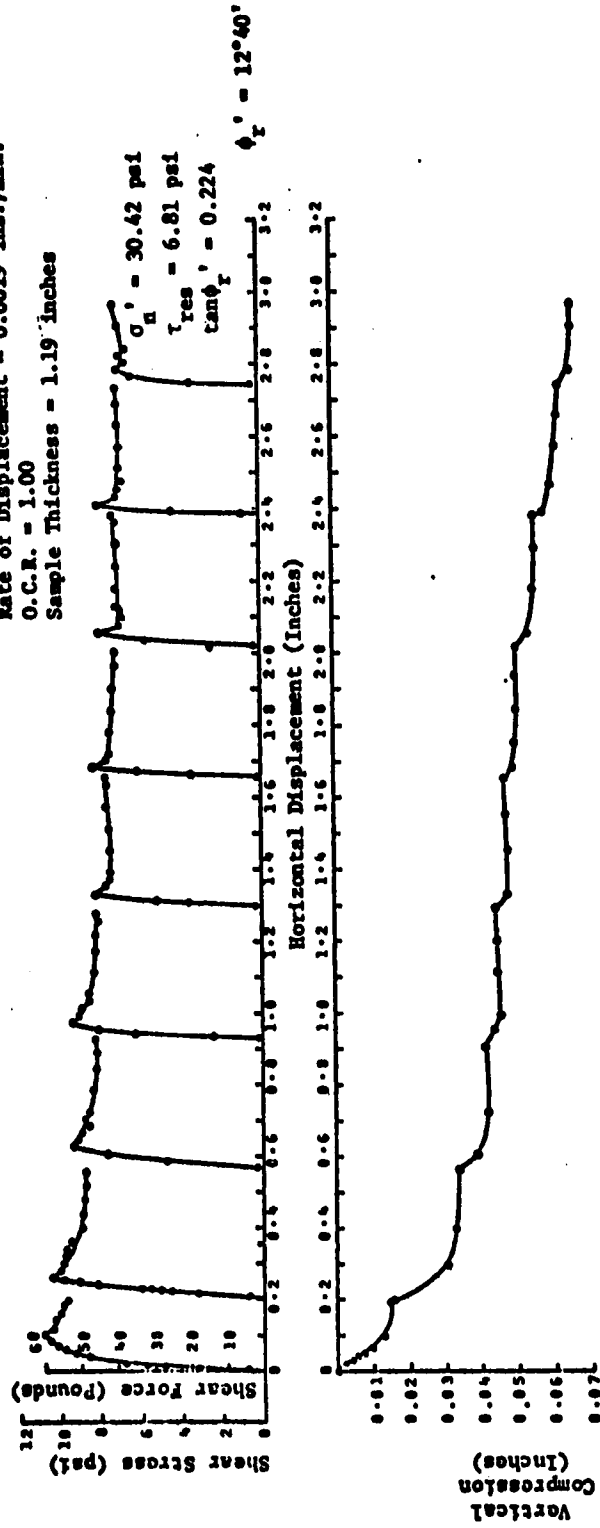
FIG. B-33. DIRECT SHEAR TEST ON KAOLINITE (K-35-5)
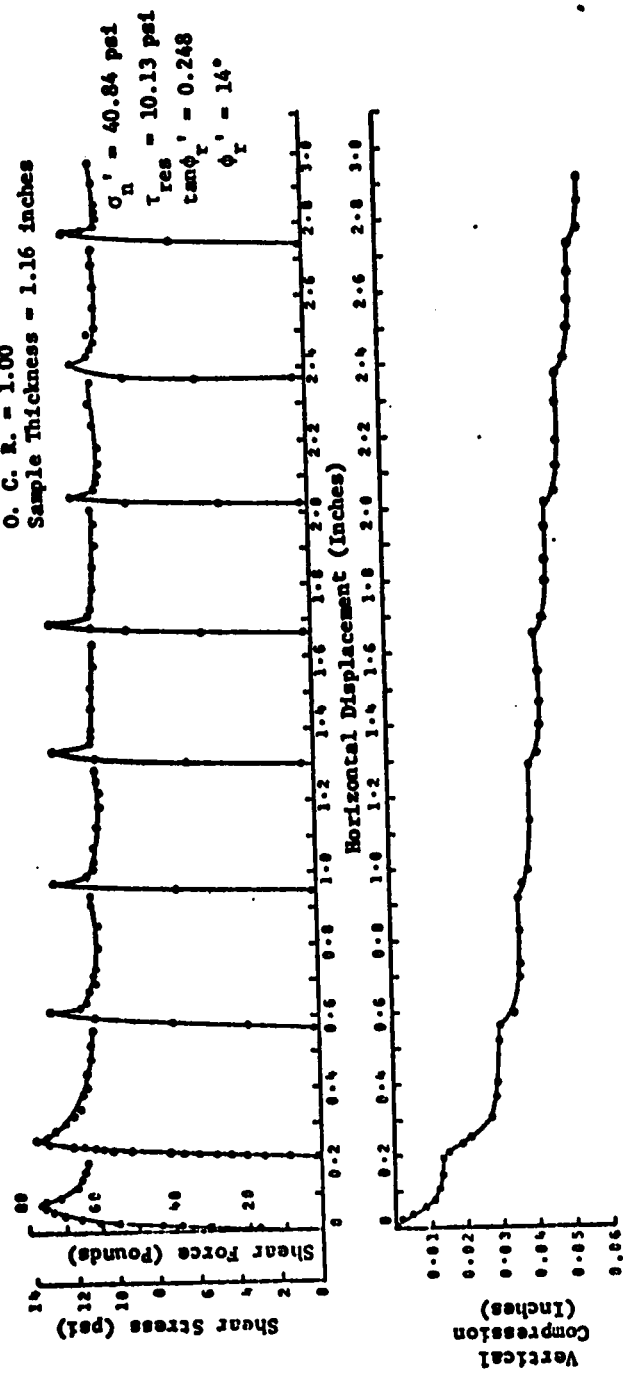
FIG. B-34 DIRECT SHEAR TEST ON KAOLINITE (K-35-6)

FIG. B-35 DIRECT SHEAR TEST ON KAOLINITE (K-35-7)

FIG. B-36 DIRECT SHEAR TEST ON KAOLINITE (K-35-8)

Kaolinite - 35 g/1 NaCl
Test No. K-35-9
Precut Plane Test
Rate of Displacement = 0.0024 ins./min.
O.C.R. = 1.00
Sample Thickness = 0.99 inches

σ_n' = 72.63 psi
τ_{res} = 16.43 psi
$\tan\phi_r'$ = 0.226
ϕ_r' = 12°40'

FIG. B-37 DIRECT SHEAR TEST ON KAOLINITE (K-35-9)
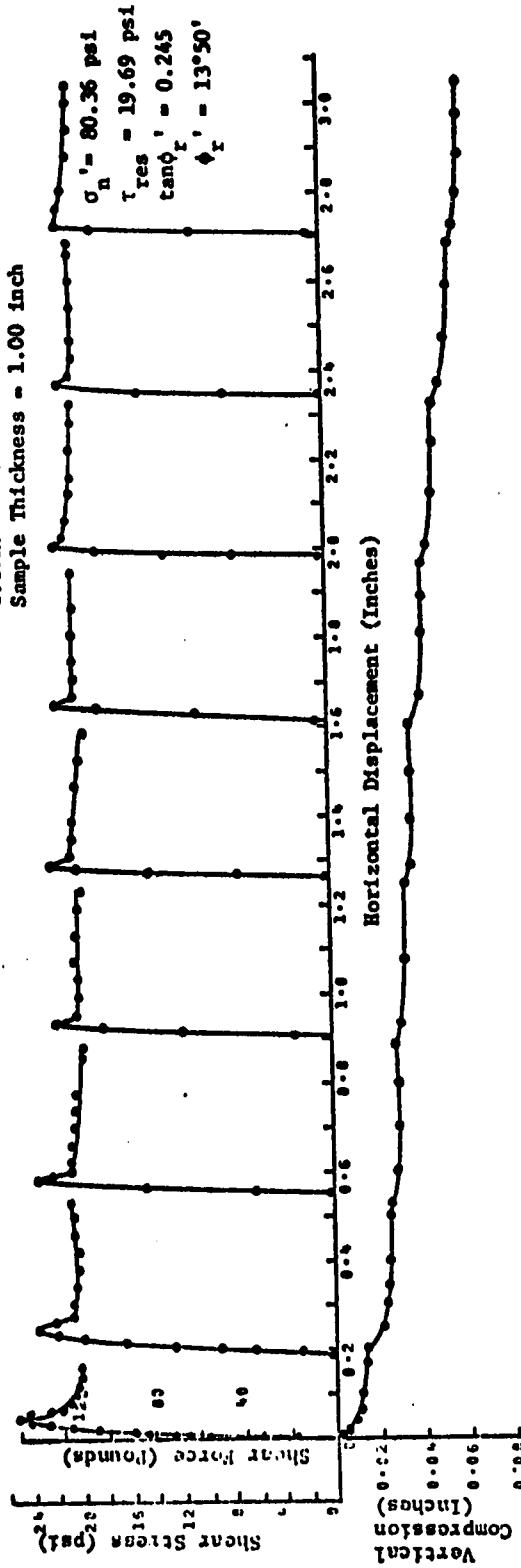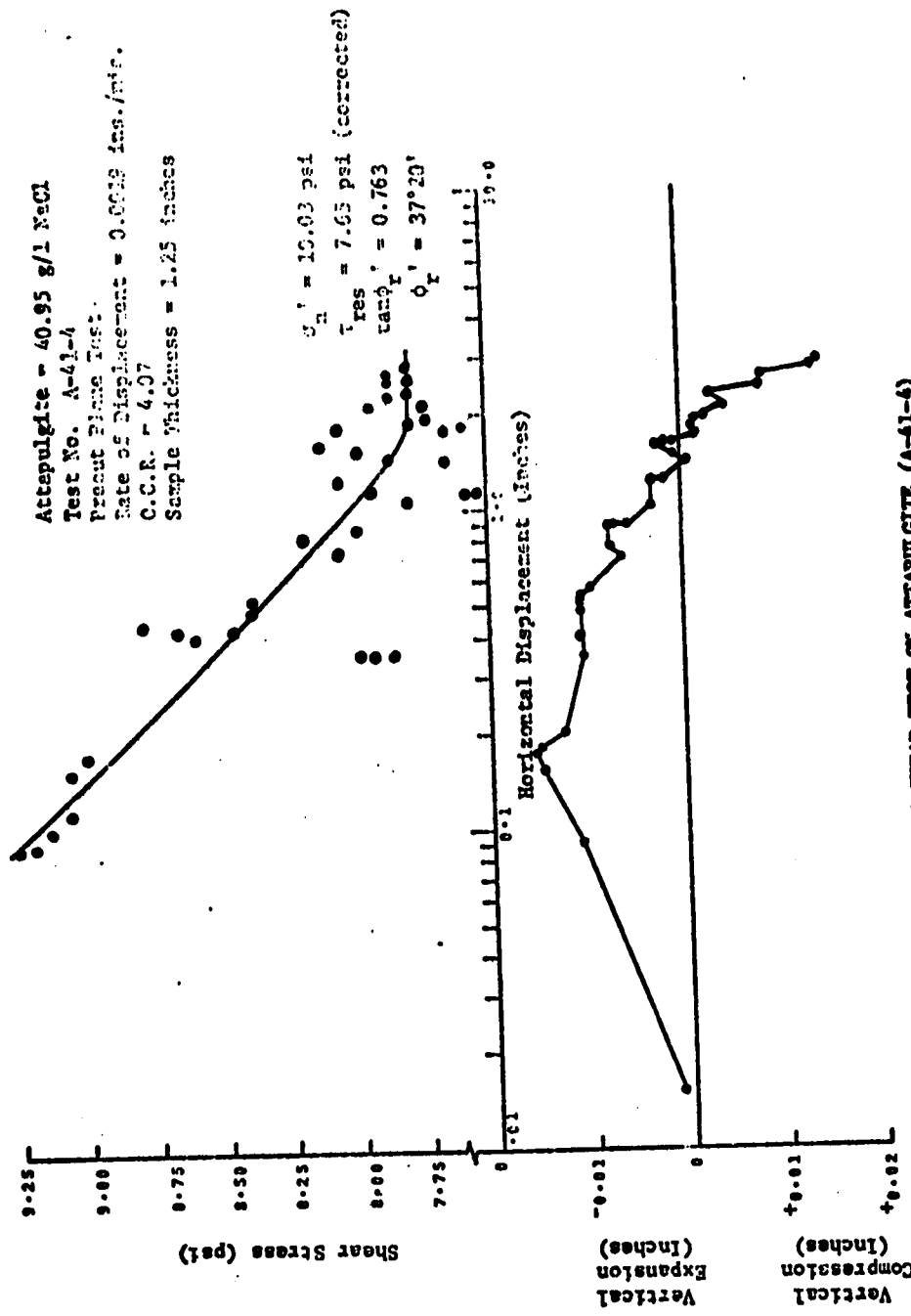
FIG. B-38 DIRECT SHEAR TEST ON KAOLINITE (K-35-10)
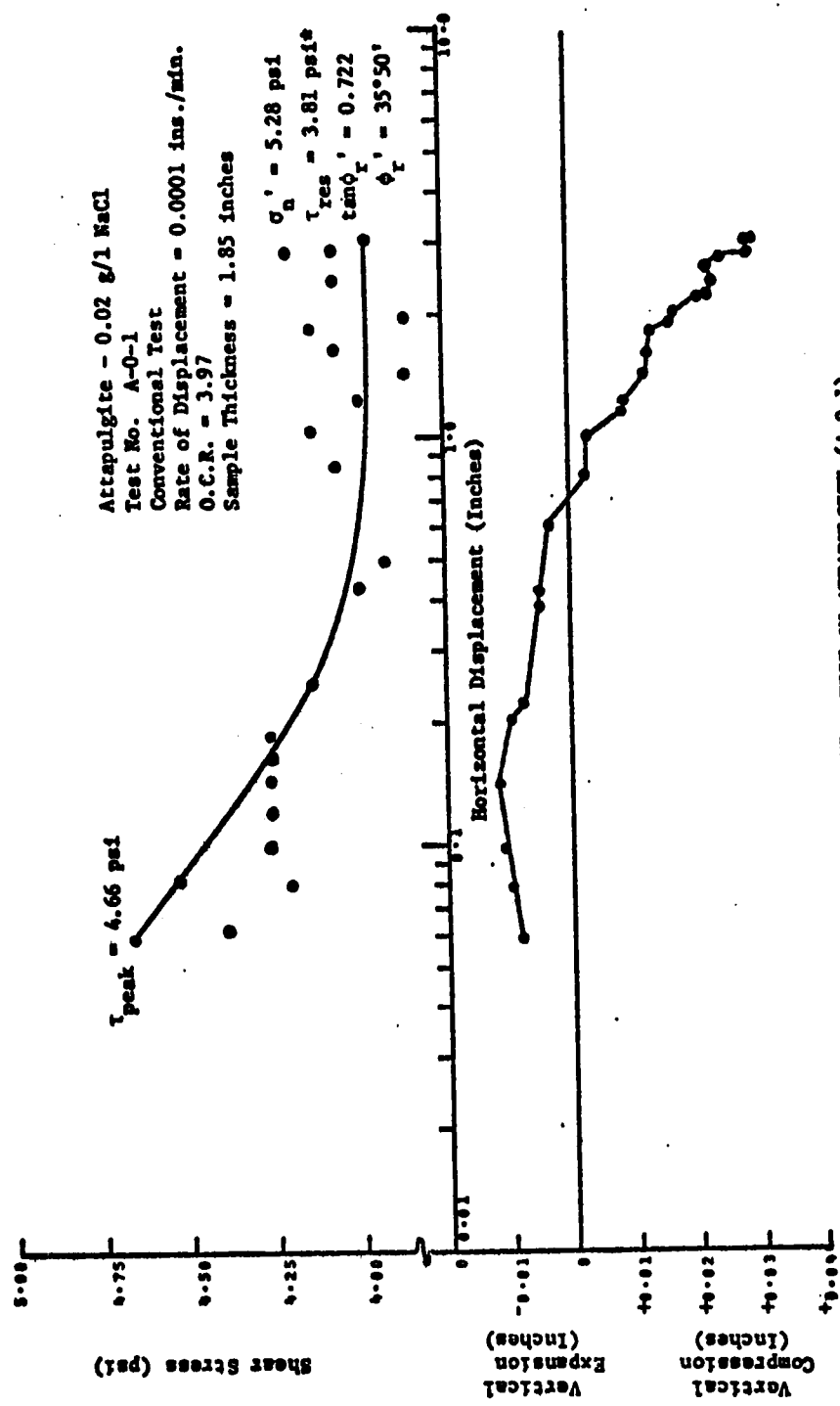
FIG.B-39 DIRECT SHEAR TEST ON ATTAPULGITE (A-0-1)

Attapulgite - 0.02 g/1 NaCl
Test No. A-0-1
Conventional Test
Rate of Displacement = 0.0001 ins./min.
O.C.R. = 3.97
Sample Thickness = 1.85 inches

$\sigma_n' = 5.28$ psi
$\tau_{res} = 3.81$ psi*
$\tan\phi_r' = 0.722$
$\phi_r' = 35°50'$

$\tau_{peak} = 4.66$ psi

Horizontal Displacement (inches)

Shear Stress (psi)

Vertical
Expansion
(Inches)

Vertical
Compression
(Inches)

* Some of the τ_{res} values are corrected for the corresponding drifts in the load cell zeros at the end of shear.

Attapulgite - 0.02 g/1 K-Cl
Test No. A-0-2
Precut Plane Test
Rate of Displacement = 0.0019 ins./min.

O.C.R. = 4.83
Sample Thickness = 1.80 inches

$\sigma_n' = 8.76$ psi
$\tau_{res} = 5.78$ psi (corrected)
$\tan\phi_r' = 0.660$
$\phi_r' = 33°30'$

Horizontal Displacement (Inches)

Shear Stress (psi)
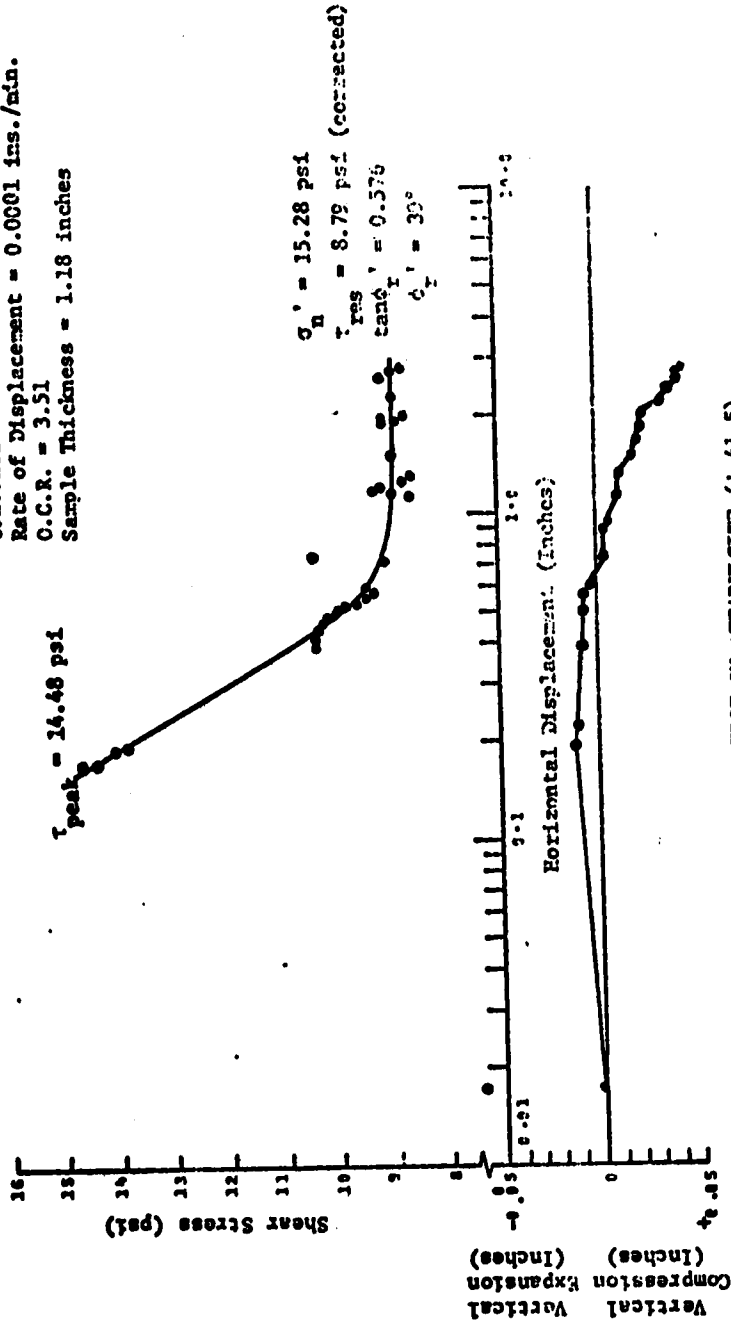
Vertical Expansion (Inches)

Vertical Compression (Inches)

FIG. B-40   DIRECT SHEAR TEST ON ATTAPULGITE (A-0-2)

Attapulgite - 0.02 g/l NaCl
Test No. A-0-3
Precut Plane Test
Rate of Displacement = 0.0024 ins./min.
O.C.R. = 4.02
Sample Thickness = 1.55 inches

$\sigma_n' = 10.55$ psi

$\tau_{res} = 6.17$ psi (corrected)

$\tan\phi_r' = 0.585$

$\phi_r' = 30°20'$

Shear Stress (psi)

Horizontal Displacement (inches)

Vertical Expansion (inches)

Vertical Compression (inches)

FIG.B-41 DIRECT SHEAR TEST ON ATTAPULGITE (A-0-3)

Attapulgite - 0.02 g/1 NaCl
Test No. A-0-4
Precut Plane Test
Rate of Displacement = 0.00048 ins./min.
O.C.R. = 3.77
Sample Thickness = 1.65 inches

$\sigma_n' = 16.70$ psi
$\tau_{res} = 10.03$ psi (corrected)
$\tan\phi_r' = 0.600$
$\phi_r' = 31°$

Shear Stress (psi)

Vertical
Expansion
(Inches)

Vertical
Compression
(Inches)

Horizontal Displacement (Inches)
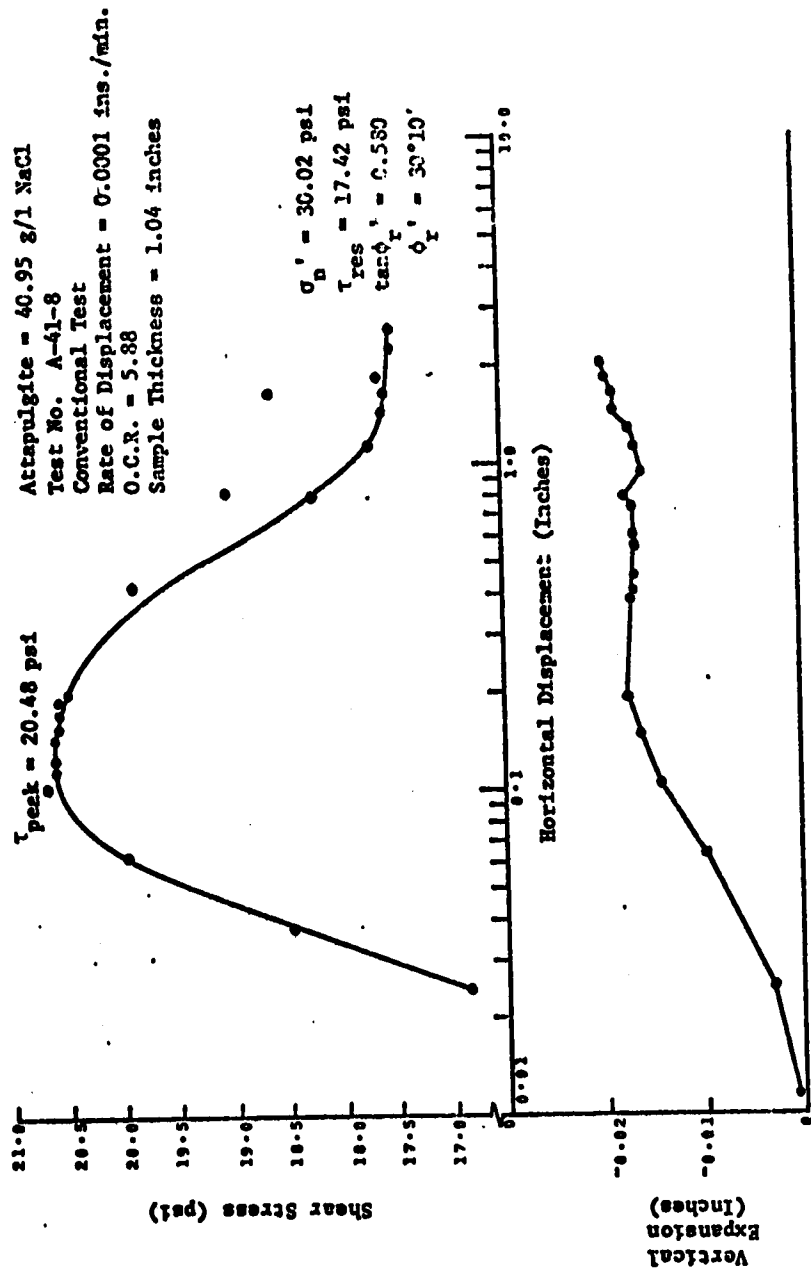
FIG.B-42 DIRECT SHEAR TEST ON ATTAPULGITE (A-0-4)

FIG. B-43 DIRECT SHEAR TEST ON ATTAPULGITE (A-0-5)
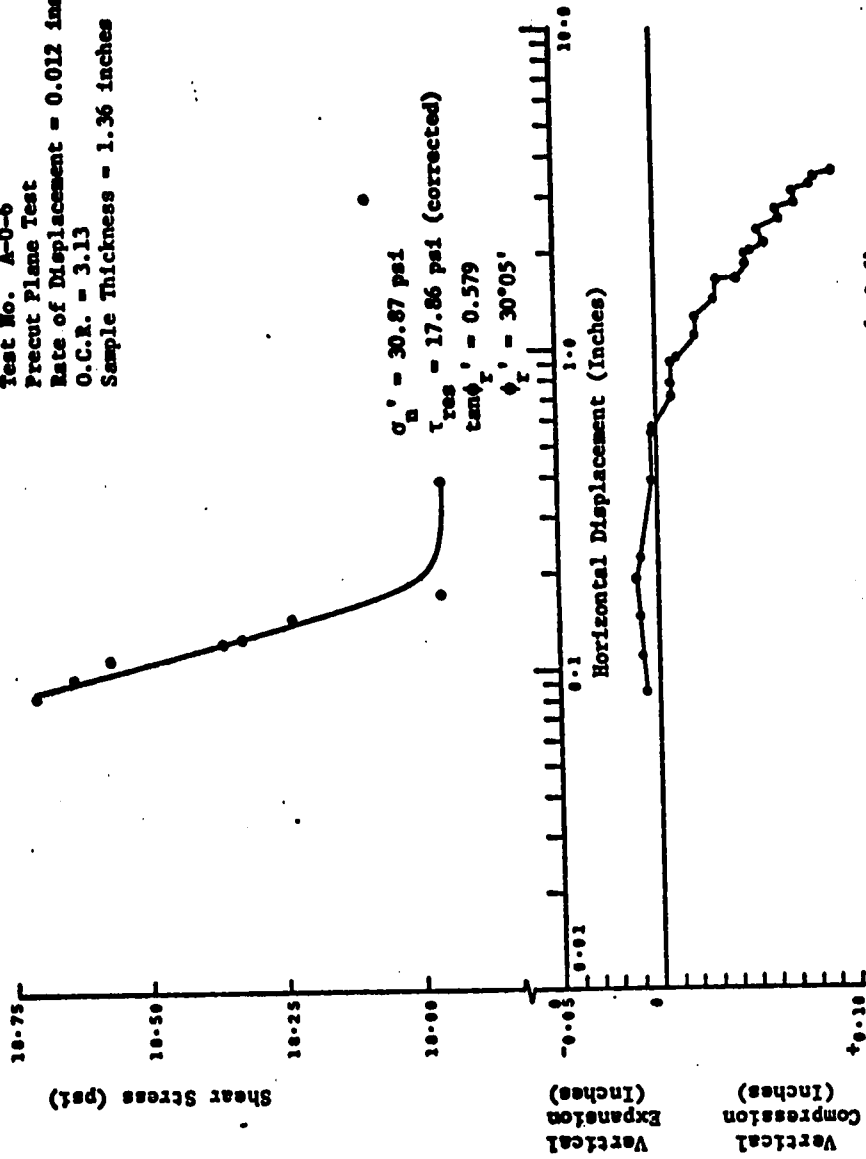
FIG. B-44 DIRECT SHEAR TEST ON ATTAPULGITE (A-0-6)

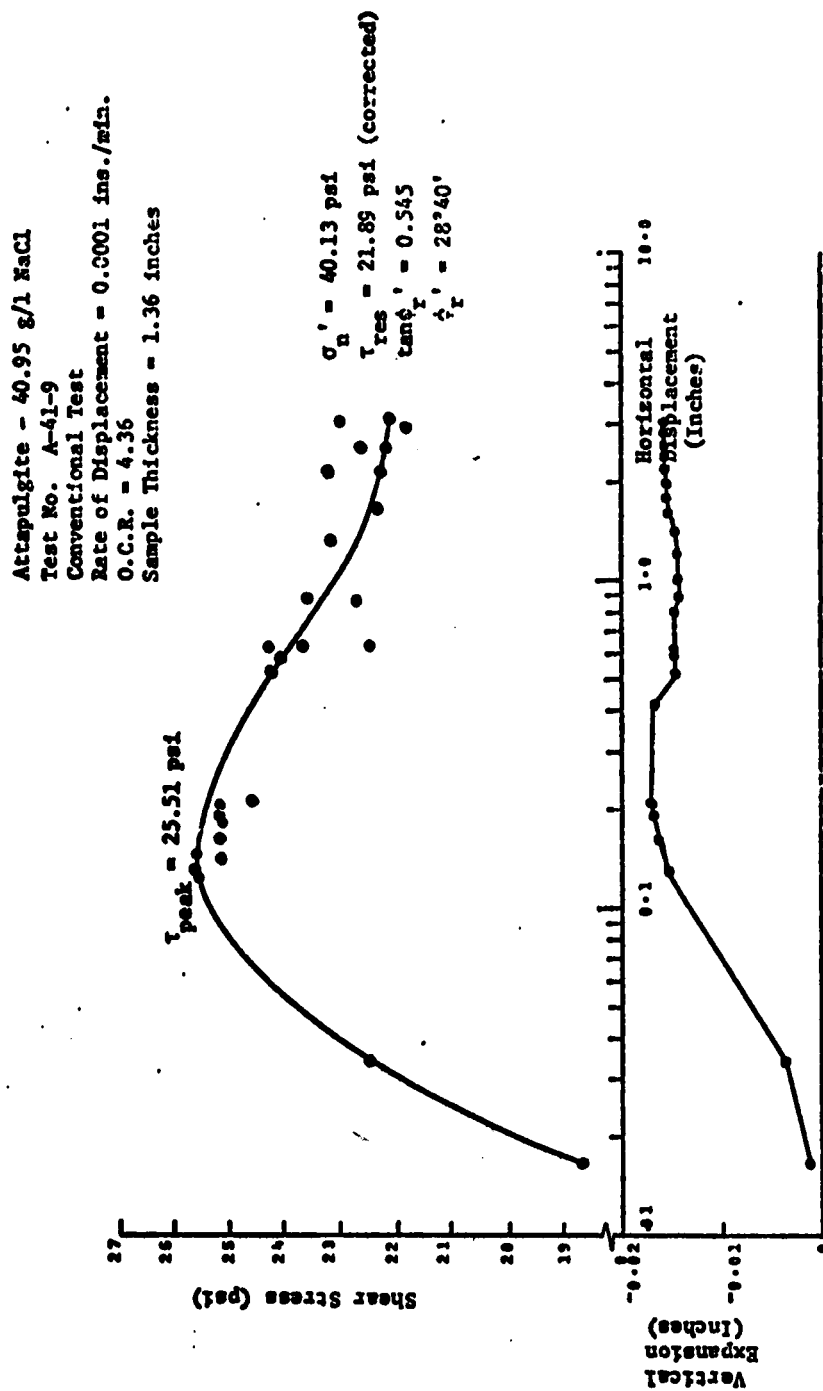Attapulgite - 0.02 g/l NaCl
Test No. A-0-7
Precut Plane Test
Rate of Displacement = 0.0096 ins./min.
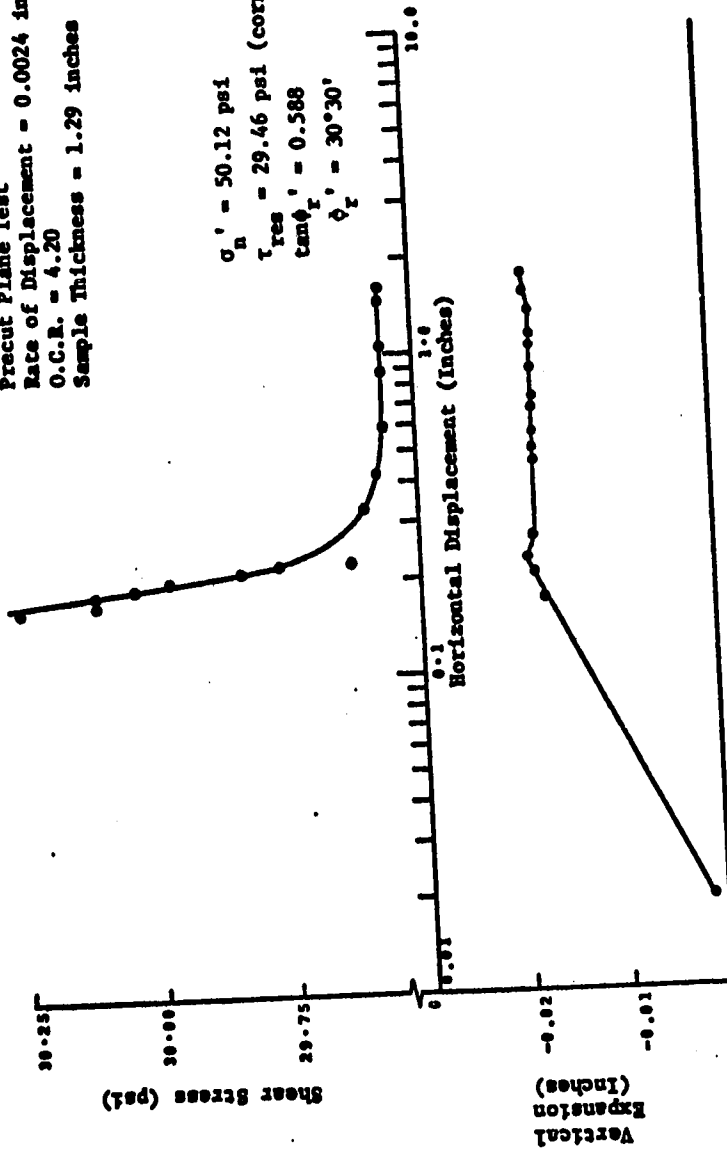O.C.R. = 2.63
Sample Thickness = 1.56 inches
$\sigma_n' = 40.97$ psi
$\tau_{res} = 23.78$ psi (corrected)
$\tan\phi_r' = 0.580$
$\phi_r' = 30°10'$
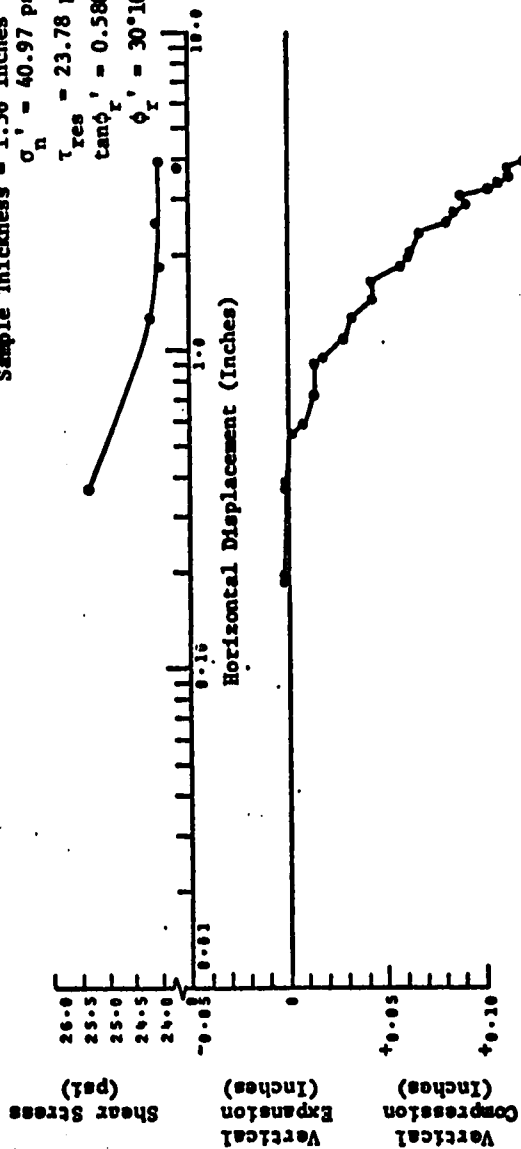
Horizontal Displacement (Inches)

Shear Stress (psi)

Vertical Expansion (Inches)

Vertical Compression (Inches)

FIG.B-45 DIRECT SHEAR TEST ON ATTAPULGITE (A-0-7)
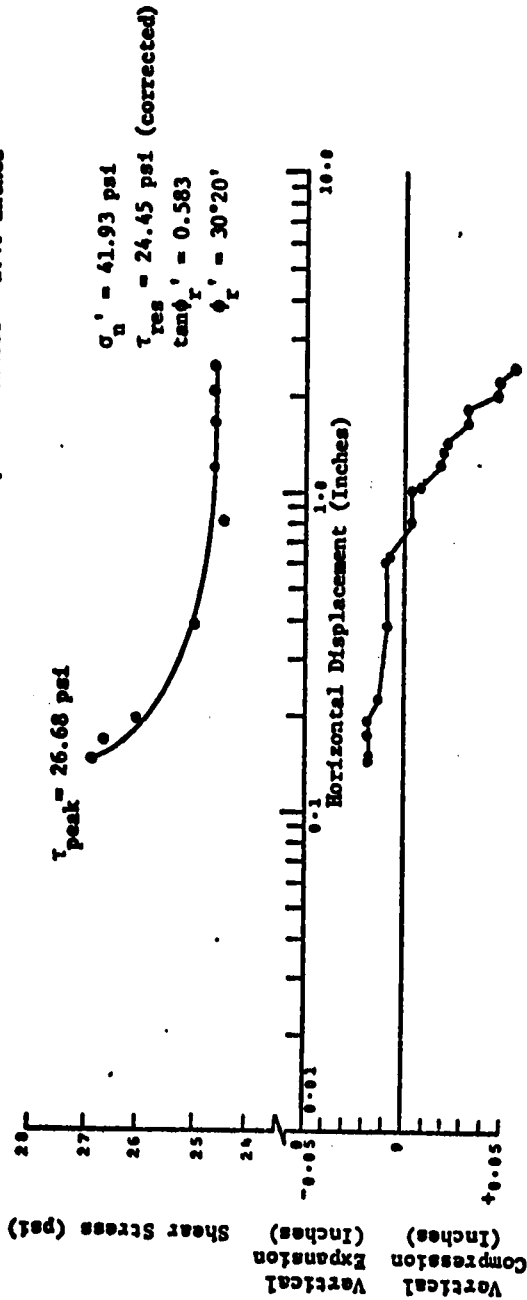
FIG.B-46 DIRECT SHEAR TEST ON ATTAPULGITE (A-0-8)

FIG. B-47 DIRECT SHEAR TEST ON ATTAPULGITE (A-0-9)

FIG. B-48 DIRECT SHEAR TEST ON ATTAPULGITE (A-2-1)

FIG. B-49 DIRECT SHEAR TEST ON ATTAPULGITE (A-2-2)

Attapulgite - 2.42 g/l NaCl
Test No. A-2-3
Conventional Test
Rate of Displacement = 0.0001 ins./min.
O.C.R. = 8.01
Sample Thickness = 1.28 inches

$\sigma_n' = 7.68$ psi
$\tau_{res} = 6.05$ psi
$\tan\phi_r' = 0.787$
$\phi_r' = 38°10'$

$\tau_{peak} = 8.33$ psi

FIG.B-50 DIRECT SHEAR TEST ON ATTAPULGITE (A-2-3)

FIG. B-51 DIRECT SHEAR TEST ON ATTAPULGITE (A-2-4)
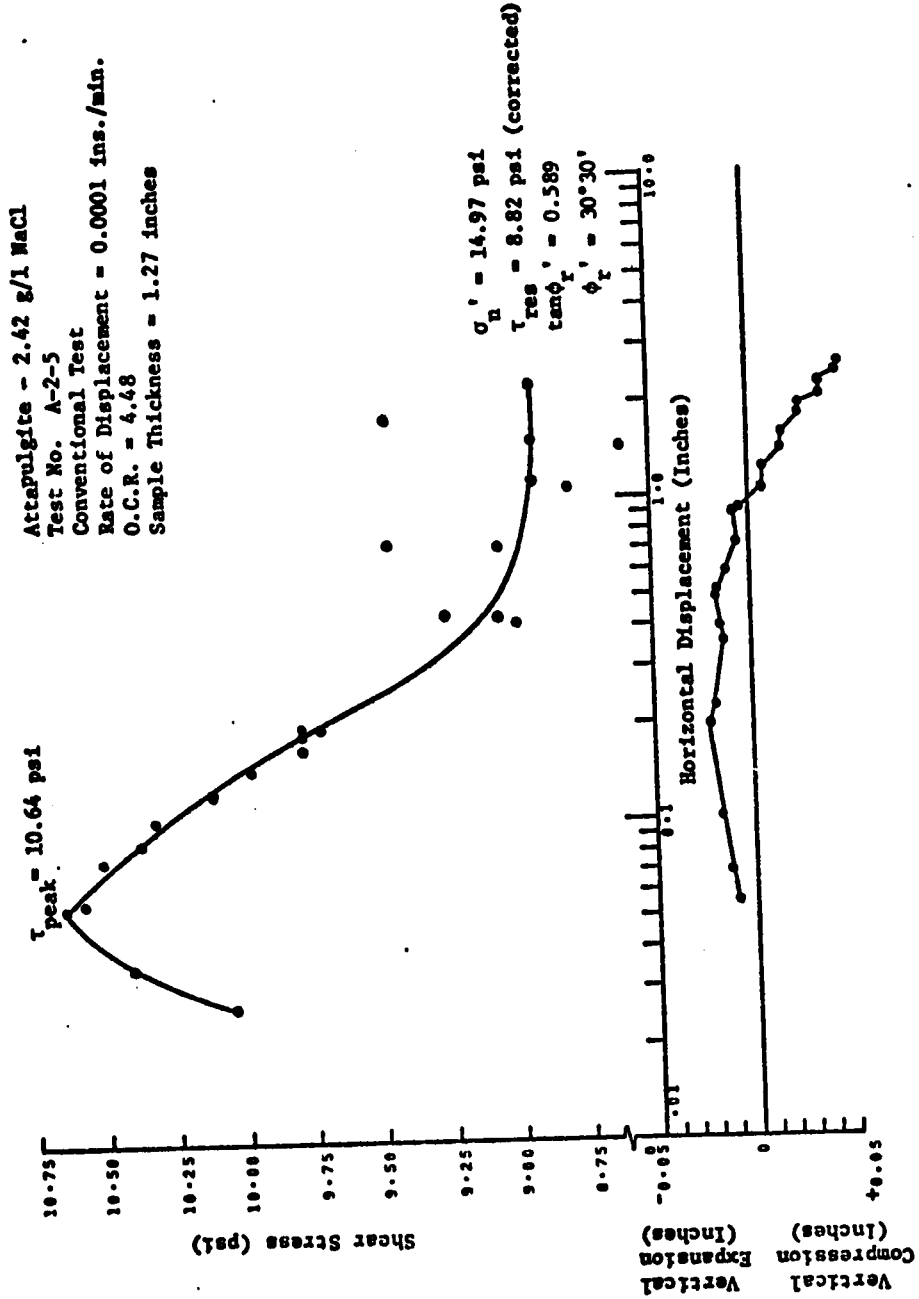
FIG.B-52 DIRECT SHEAR TEST ON ATTAPULGITE (A-2-5)
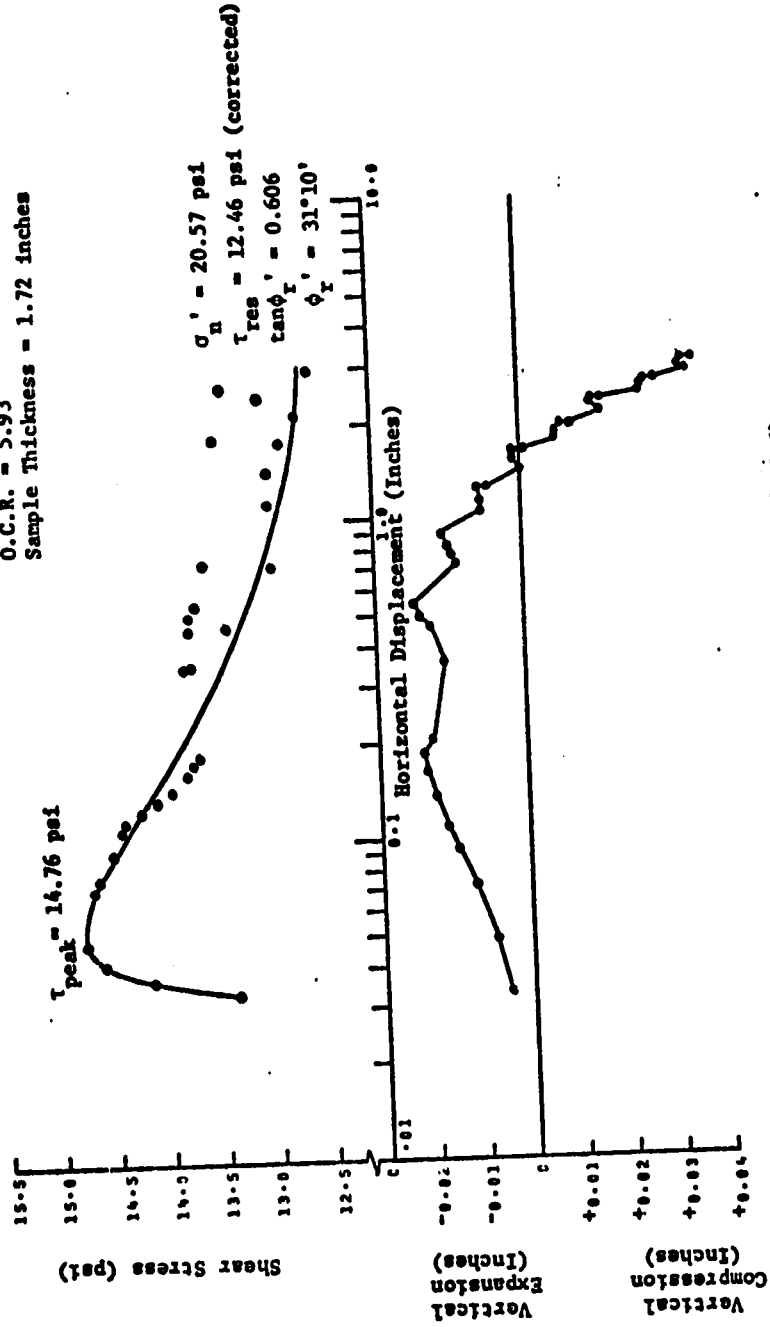
FIG. B-53 DIRECT SHEAR TEST ON ATTAPULGITE (A-2-6)
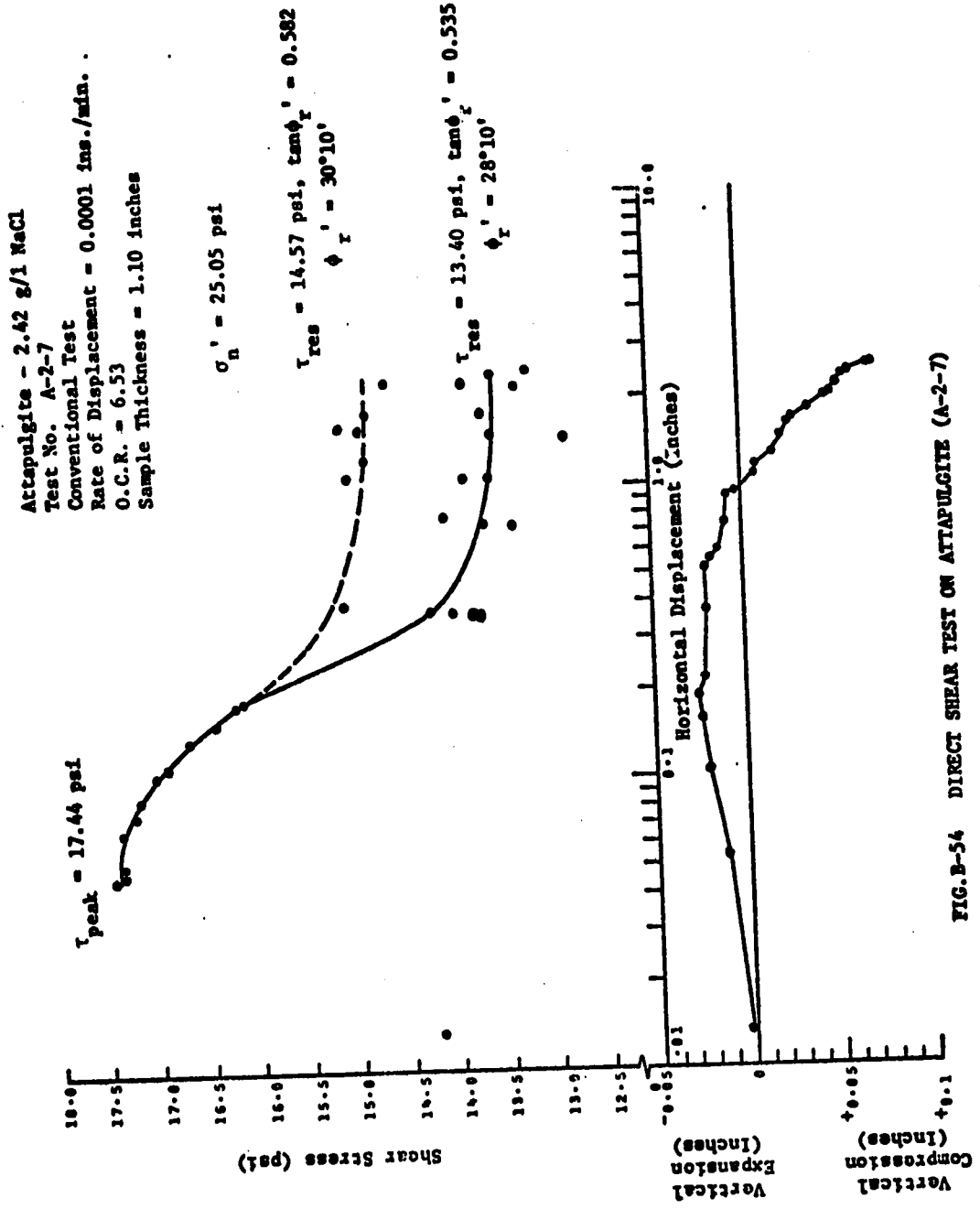
FIG.B-54   DIRECT SHEAR TEST ON ATTAPULGITE (A-2-7)

Attapulgite - 2.42 g/1 NaCl
Test No.   A-2-7
Conventional Test
Rate of Displacement = 0.0001 ins./min.
O.C.R. = 6.53
Sample Thickness = 1.10 inches

σ_n' = 25.05 psi

τ_{res} = 14.57 psi, $\tan\phi_r'$ = 0.582
ϕ_r' = 30°10'

τ_{res} = 13.40 psi, $\tan\phi_r'$ = 0.535
ϕ_r' = 28°10'

τ_{peak} = 17.44 psi

Attapulgite - 2.42 g/l NaCl
Test No. A-2-8
Precut Plane Test
Rate of Displacement = 0.0024 ins./min.
O.C.R. = 5.62
Sample Thickness = 1.11 inches

$\sigma_n' = 30.63$ psi
$\tau_{res} = 17.40$ psi (corrected)
$\tan\phi_r' = 0.568$
$\phi_r' = 29°40'$
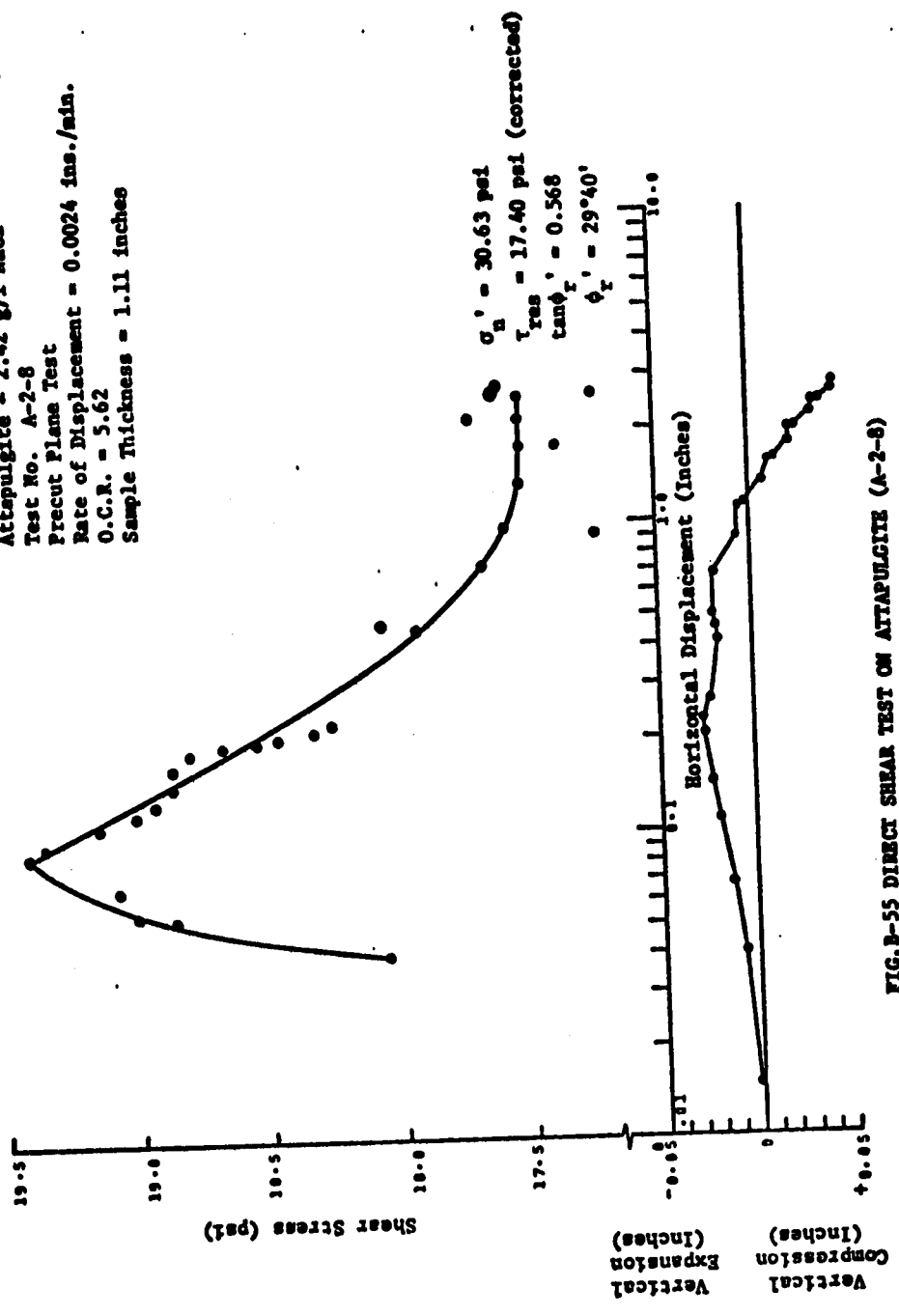
FIG.B-55 DIRECT SHEAR TEST ON ATTAPULGITE (A-2-8)
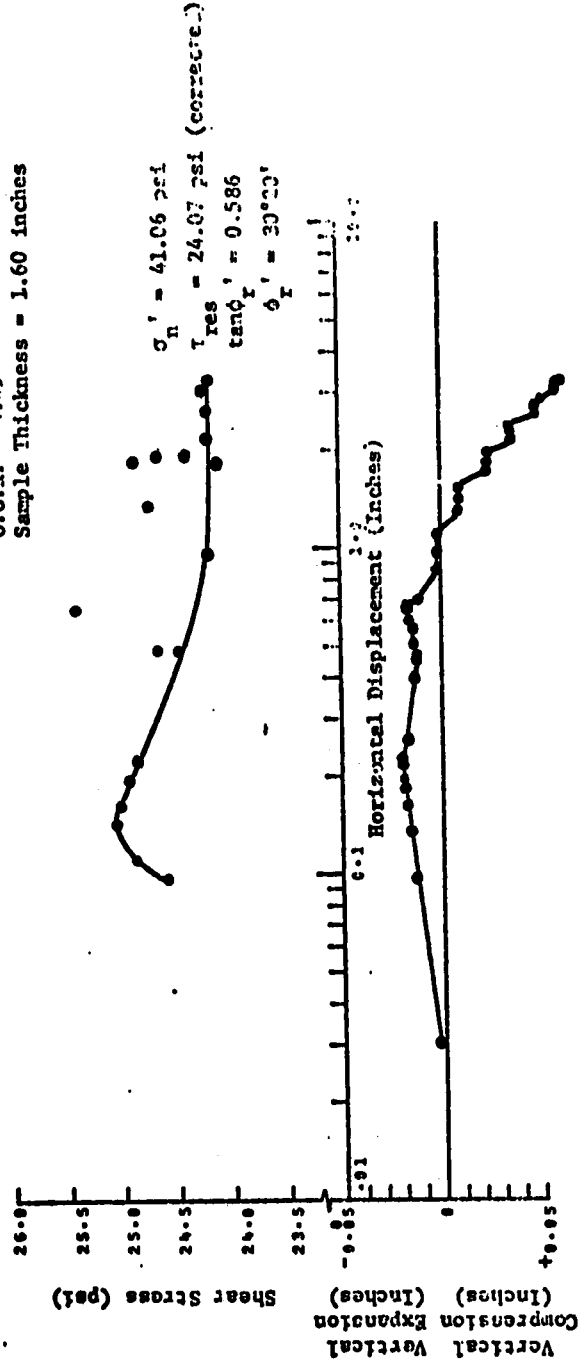
FIG. B-56 DIRECT SHEAR TEST ON ATTAPULGITE (A-2-9)

Attapulgite – 2.42 g/1 NaCl
Test No.   A-2-10
Precut Plane Test
Rate of Displacement = 0.0024 ins./min.
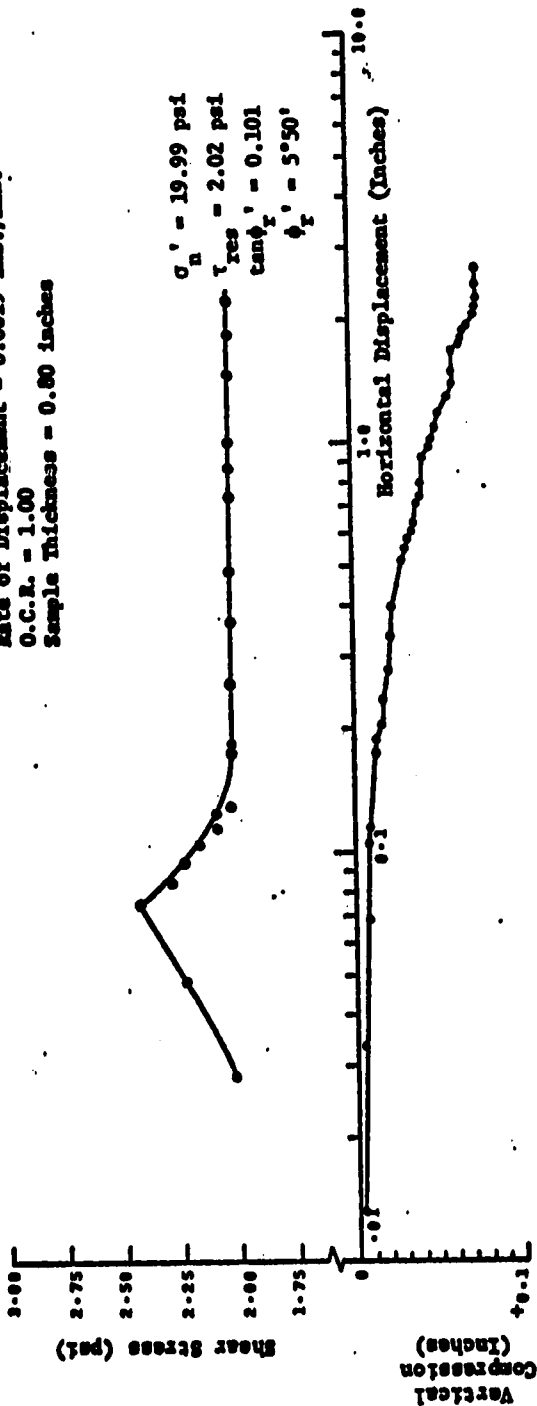O.C.R. = 4.11
Sample Thickness = 1.42 inches

σ_n' = 55.22 psi
τ_{res} = 32.31 psi (corrected)
$\tan\phi_r'$ = 0.585
ϕ_r' = 30°20'

Horizontal Displacement (Inches)

Shear Stress (psi)

Vertical
Expansion
(Inches)

Vertical
Compression
(Inches)
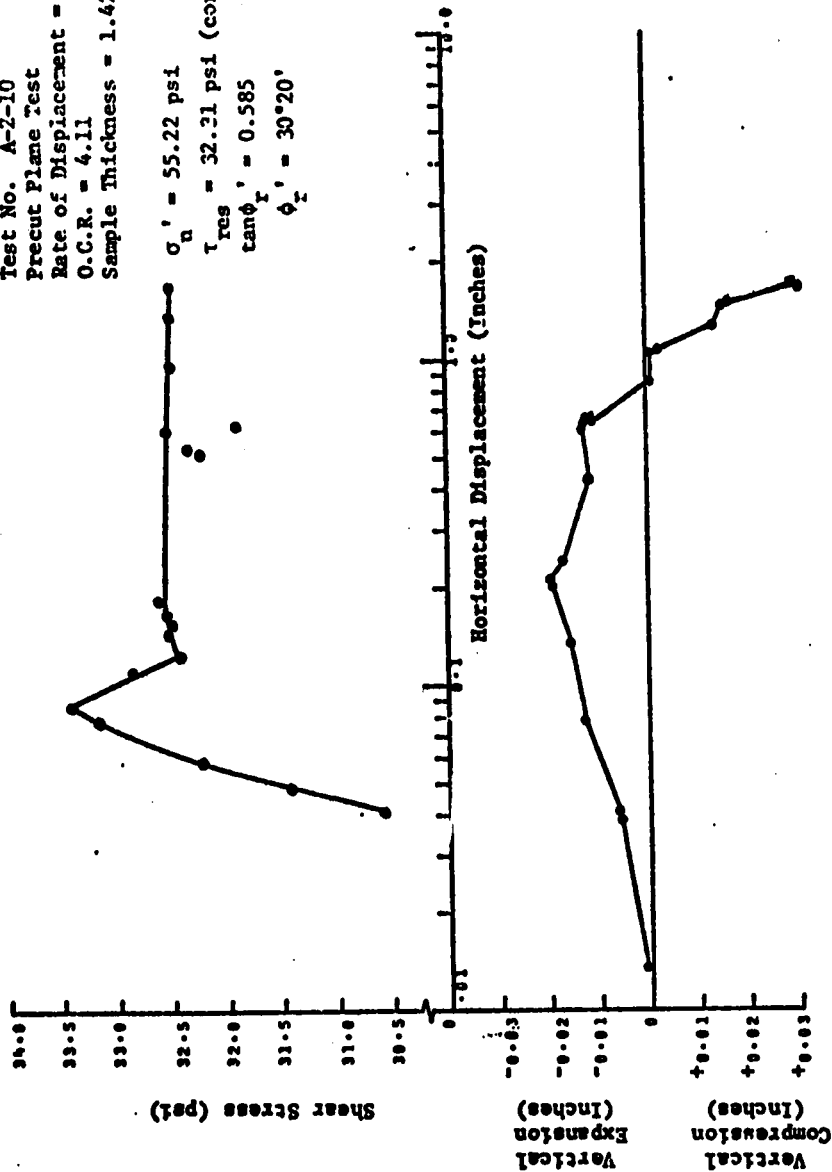
FIG. B-57 DIRECT SHEAR TEST ON ATTAPULGITE (A-2-10)

Attapulgite - 40.95 g/1 NaCl
Test No. A-41-1
Precut Plane Test
Rate of Displacement = 0.0024 ins./min.
O.C.R. = 7.88
Sample Thickness = 1.42 inches

$\sigma_n' = 2.59$ psi
$t_{res} = 1.80$ psi (corrected)
$tan\phi_r' = 0.694$
$\phi_r' = 34°50'$
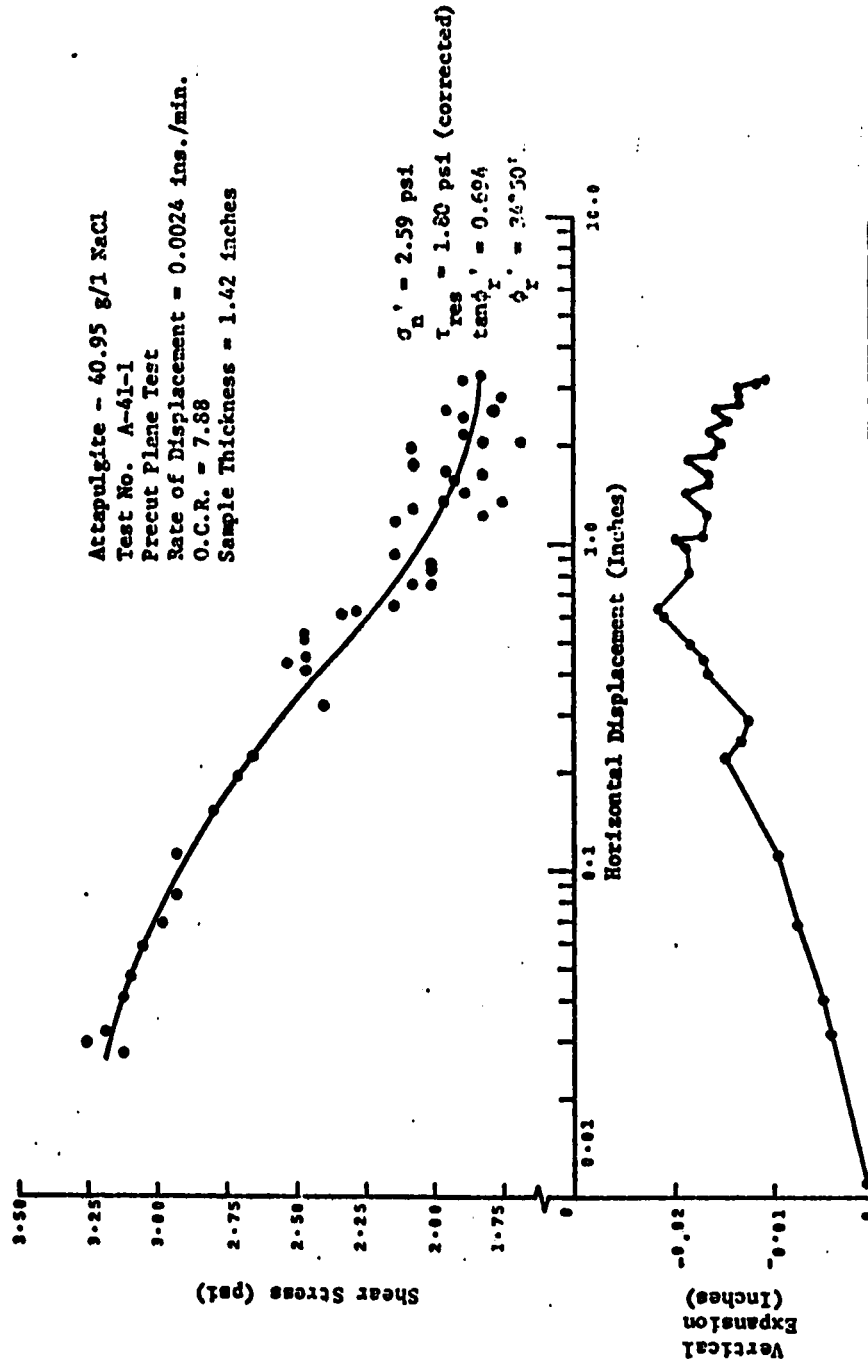
FIG. B-58   DIRECT SHEAR TEST ON ATTAPULGITE (A-41-1)
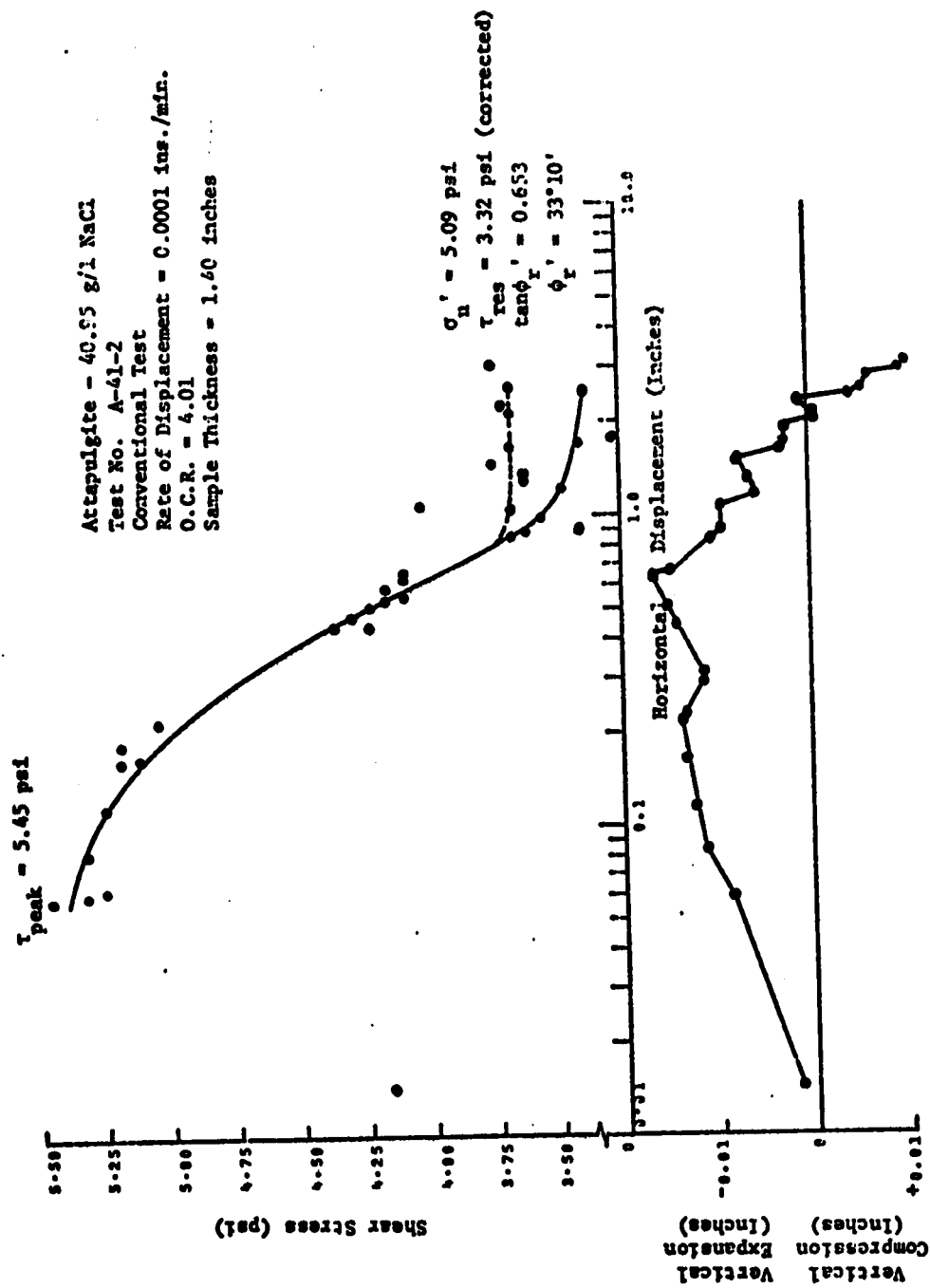
FIG.B-59 DIRECT SHEAR TEST ON ATTAPULGITE (A-41-2)

FIG. B-60 DIRECT SHEAR TEST ON ATTAPULGITE (A-41-3)

FIG. B-61 DIRECT SHEAR TEST ON ATTAPULGITE (A-41-4)

FIG. B-62 DIRECT SHEAR TEST ON ATTAPULGITE (A-41-5)

Attapulgite – 40.95 g/l NaCl
Test No. A-41-6
Precut Plane Test
Rate of Displacement = 0.0019 ins./min.
O.C.R. = 4.90
Sample Thickness = 1.08 inches

$\sigma_n' = 20.57$ psi
$\tau_{res} = 12.01$ psi (corrected)
$\tan\phi_r' = 0.584$
$\phi_r' = 30°20'$

Shear Stress (psi)

Horizontal Displacement (Inches)

Vertical   Vertical
Compression Expansion
(Inches)   (Inches)
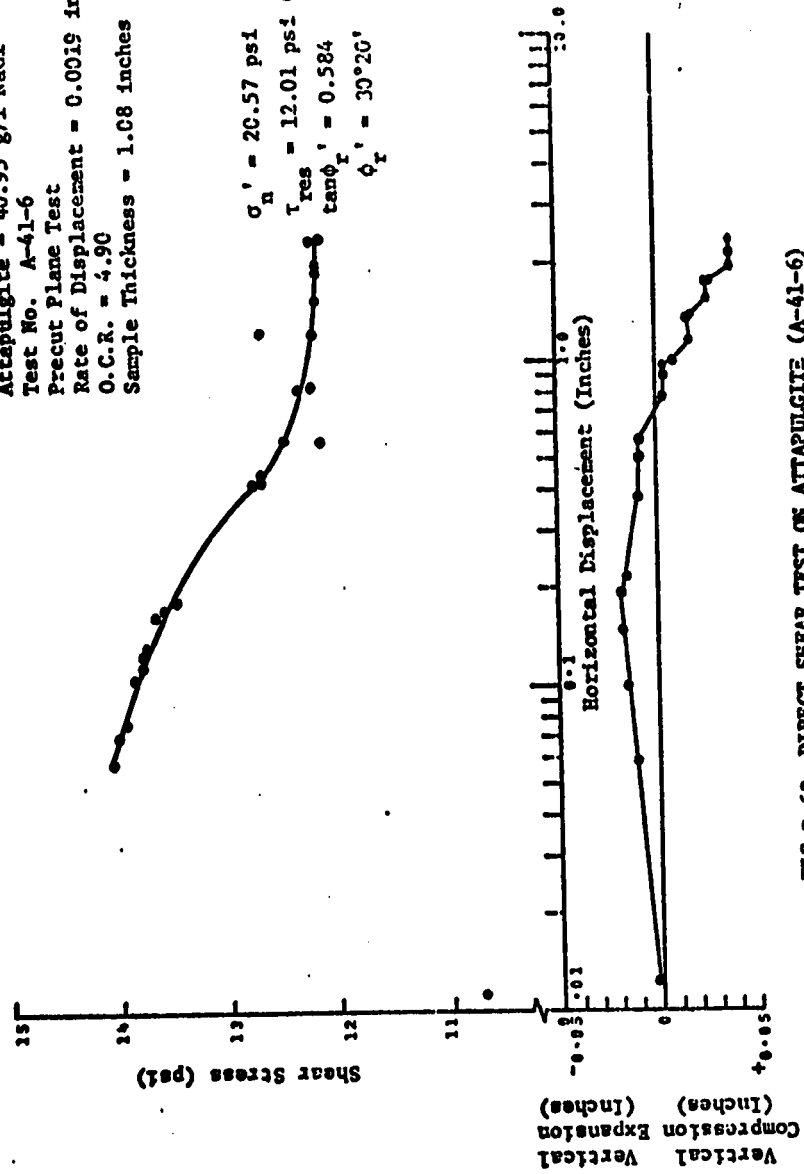
FIG. B-63   DIRECT SHEAR TEST ON ATTAPULGITE (A-41-6)
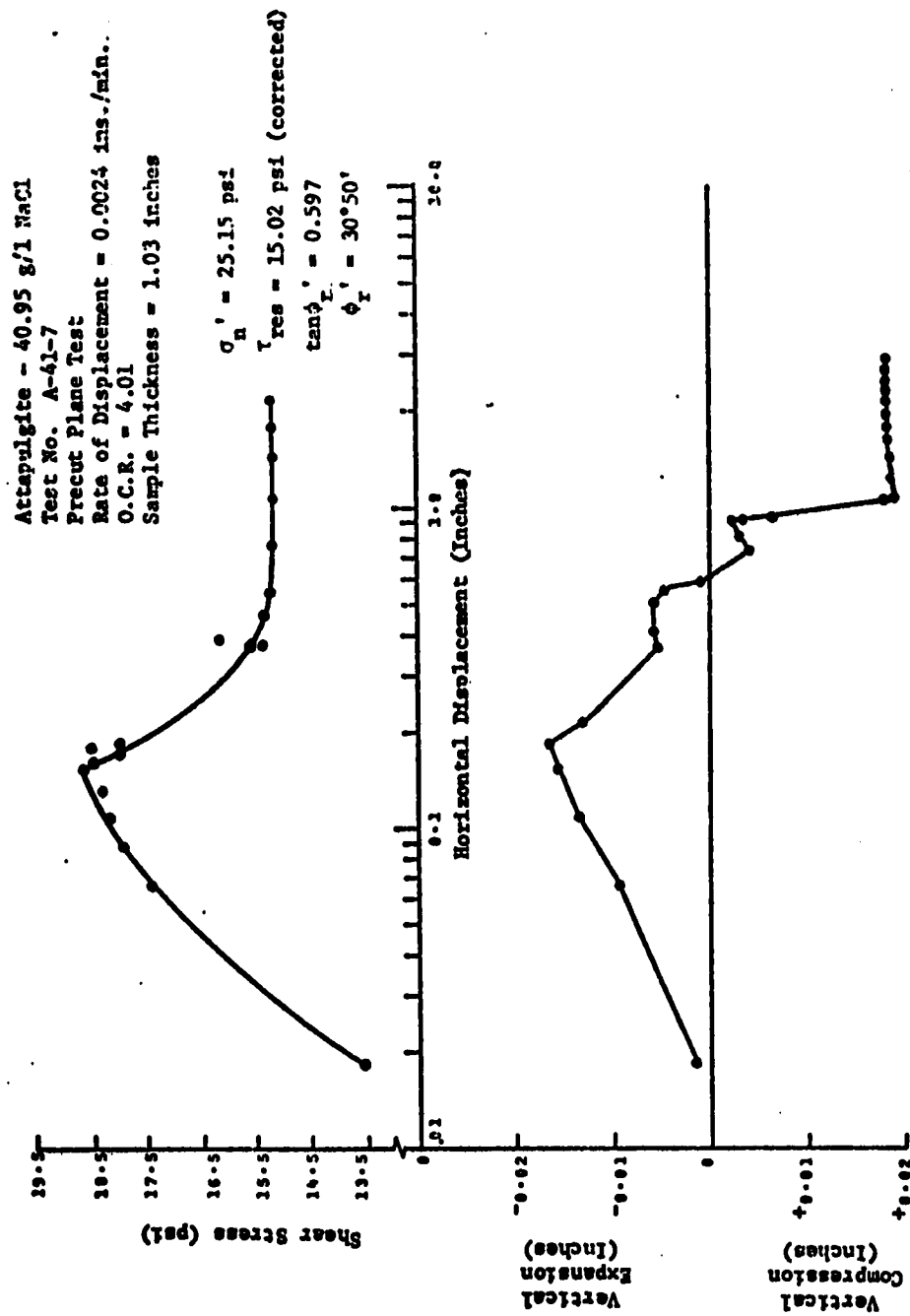
FIG. B-64 DIRECT SHEAR TEST ON ATTAPULGITE (A-41-7)

FIG.B-65 DIRECT SHEAR TEST ON ATTAPULGITE (A-41-8)

Attapulgite - 40.95 g/1 NaCl
Test No. A-41-9
Conventional Test
Rate of Displacement = 0.0001 ins./min.
O.C.R. = 4.36
Sample Thickness = 1.36 inches

σ_n' = 40.13 psi
τ_{res} = 21.89 psi (corrected)
$\tan\phi_r'$ = 0.545
$\hat{\phi}_r'$ = 28°40'

τ_{peak} = 25.51 psi

Shear Stress (psi)

Horizontal
Displacement
(inches)

Vertical
Expansion
(inches)

FIG.B-66 DIRECT SHEAR TEST ON ATTAPULGITE (A-41-9)

FIG.B-67 DIRECT SHEAR TEST ON ATTAPULGITE (A-41-10)

Montmorillonite - 1.15 g/l NaCl
Test Nos. M-1-1 and M-1-2
Precut Plane Tests
Rate of Displacement = 0.0024 ins./min.
O.C.R. = 3.94 and 1.00 respectively
Sample Thicknesses = 1.38 and 1.36 inches respectively

$\sigma_n' = 2.58$ psi
$\tau_{res} = 0.91$ psi
$\tan\phi_r' = 0.354$
$\phi_r' = 19°30'$

Horizontal Displacement (Inches)

Shear Stress (psi)
Vertical Compression Expansion (Inches)
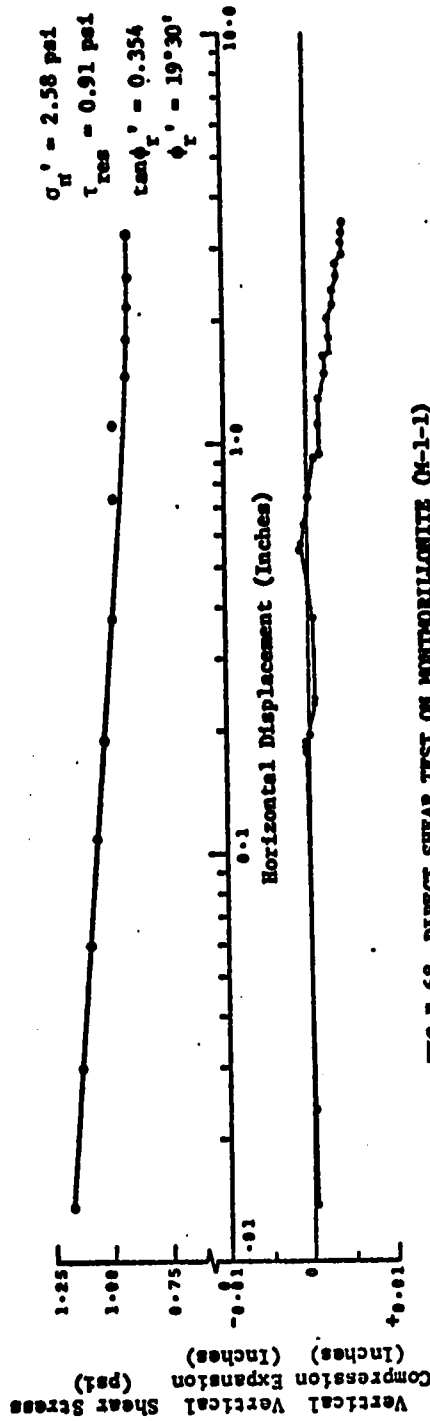
FIG.B-68 DIRECT SHEAR TEST ON MONTMORILLONITE (M-1-1)

$\sigma_n' = 4.99$ psi
$\tau_{res} = 0.82$ psi
$\tan\phi_r' = 0.164$
$\phi_r' = 9°20'$

Horizontal Displacement (Inches)

Shear Stress (psi)
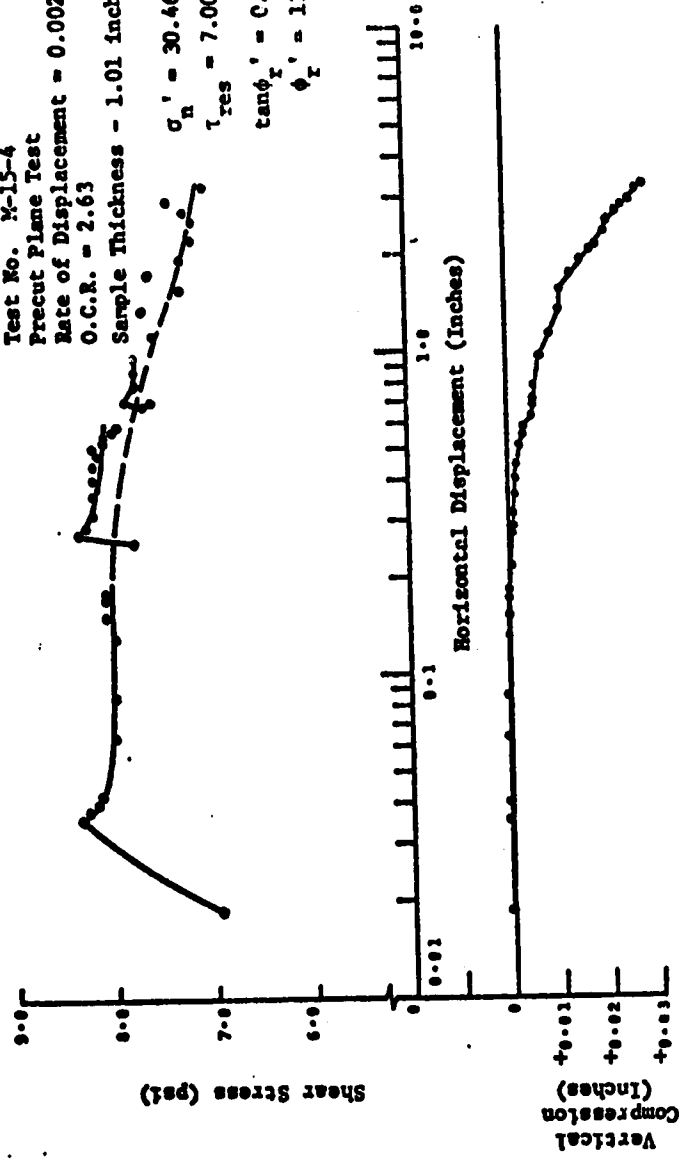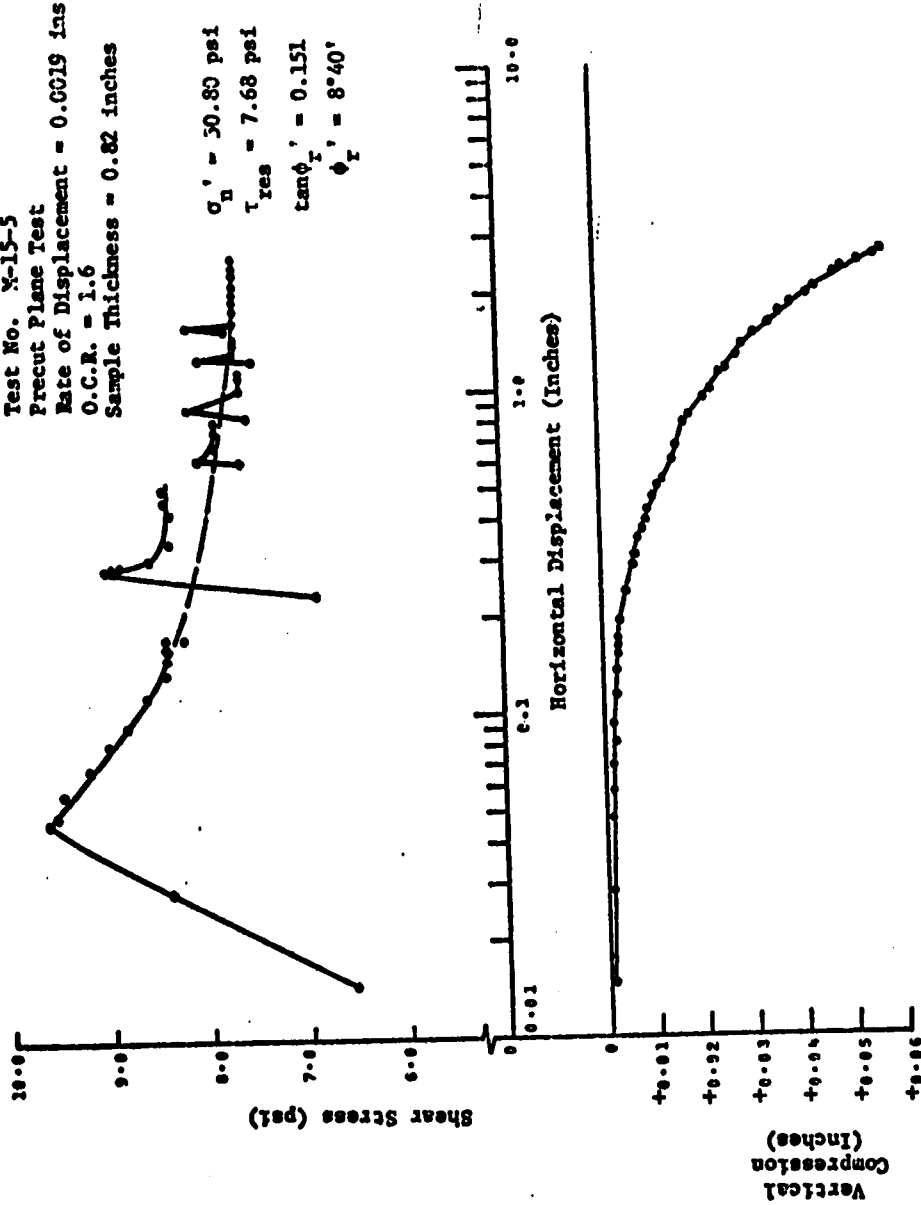Vertical Compression (Inches)
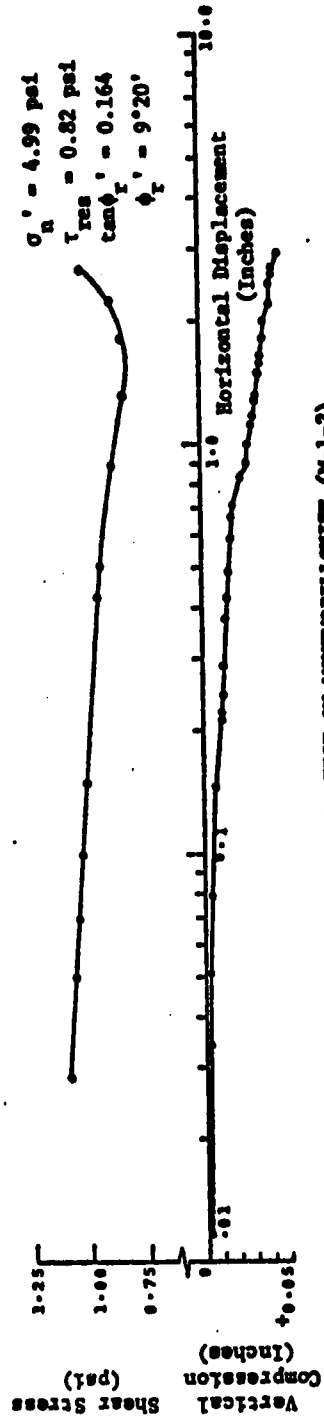
FIG.B-69 DIRECT SHEAR TEST ON MONTMORILLONITE (M-1-2)

Montmorillonite - 1.15 g/1 NaCl
Test Nos. M-1-3 and M-1-4
Precut Plane Tests
Rate of Displacement = 0.0024 ins./min.
O.C.R. = 1.00 for both the tests
Sample Thicknesses = 1.42 and 1.32 inches respectively

σ_n' = 10.12 psi
τ_{res} = 1.18 psi
$\tan\phi_r'$ = 0.117
ϕ_r' = 6°40'

Horizontal Displacement
(Inches)

Vertical
Compression
(Inches)

Shear Stress
(psi)
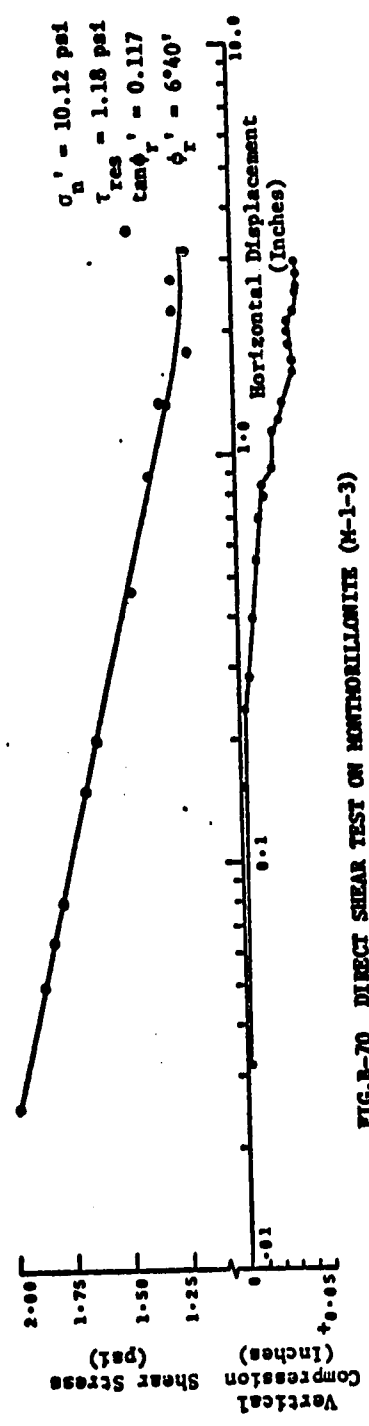
FIG.B-70 DIRECT SHEAR TEST ON MONTMORILLONITE (M-1-3)

σ_n' = 15.12 psi
τ_{res} = 1.57 psi
$\tan\phi_r'$ = 0.104
ϕ_r' = 6°

Horizontal Displacement
(Inches)

Vertical
Compression
(Inches)

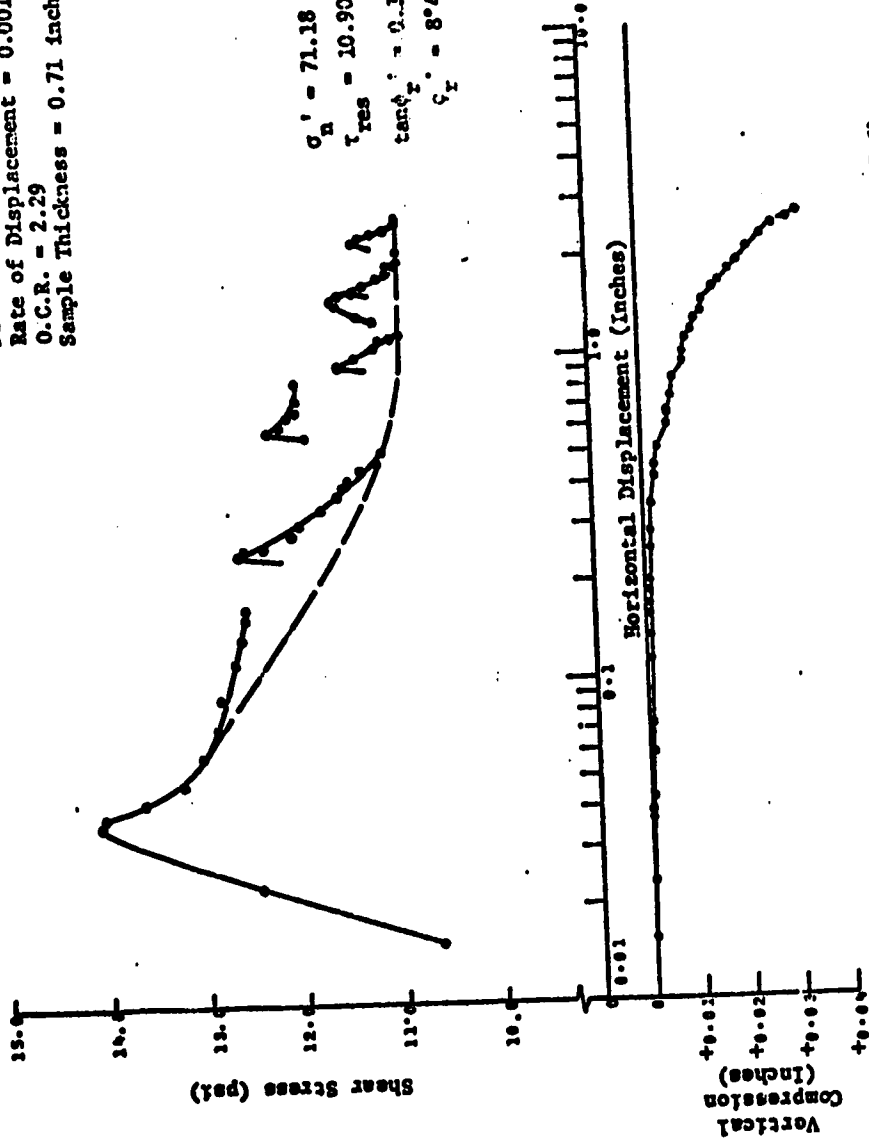Shear Stress
(psi)
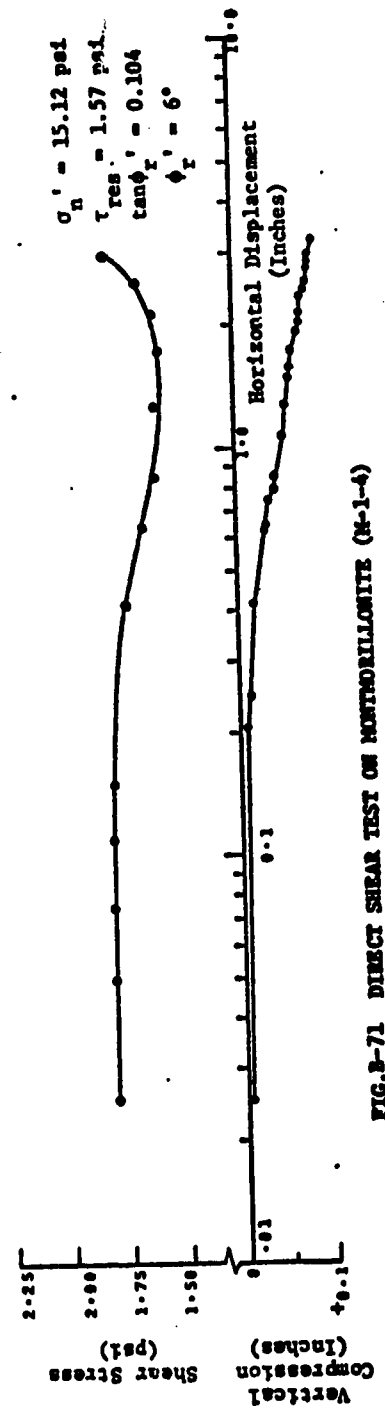
FIG.B-71 DIRECT SHEAR TEST ON MONTMORILLONITE (M-1-4)

FIG.B-72 DIRECT SHEAR TEST ON MONTMORILLONITE (M-1-5)

Montmorillonite – 1.15 g/1 NaCl
Test Nos. M-1-6 and M-1-7
Precut Plane Tests
Rate of Displacement = 0.0019 ins/min.
O.C.R. = 1.00 for both the tests.
Sample Thicknesses = 0.94 and 1.07 inches respectively.

σ_n' = 40.65 psi
τ_{res} = 3.60 psi
$\tan\phi_r'$ = 0.089
ϕ_r' = 5°05'
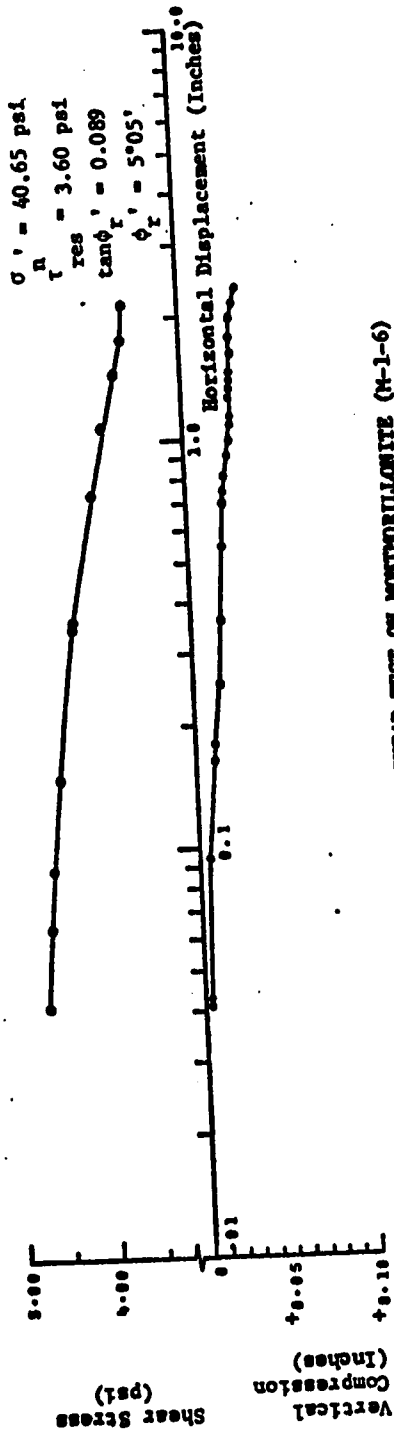
FIG.B-73 DIRECT SHEAR TEST ON MONTMORILLONITE (M-1-6)

σ_n' = 65.78 psi
τ_{res} = 5.60 psi
$\tan\phi_r'$ = 0.085
ϕ_r' = 4°50'
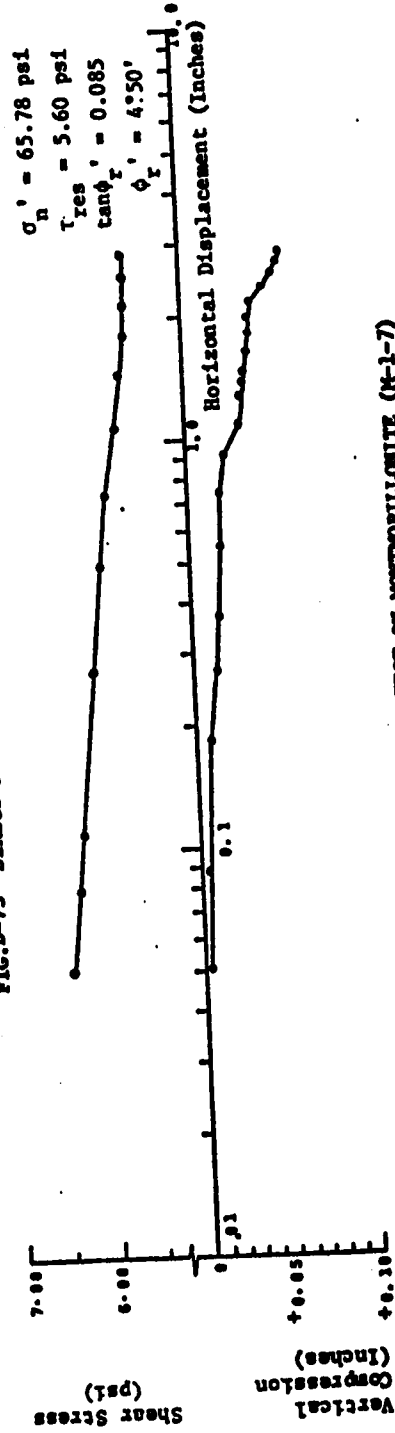
FIG.B-74 DIRECT SHEAR TEST ON MONTMORILLONITE (M-1-7)
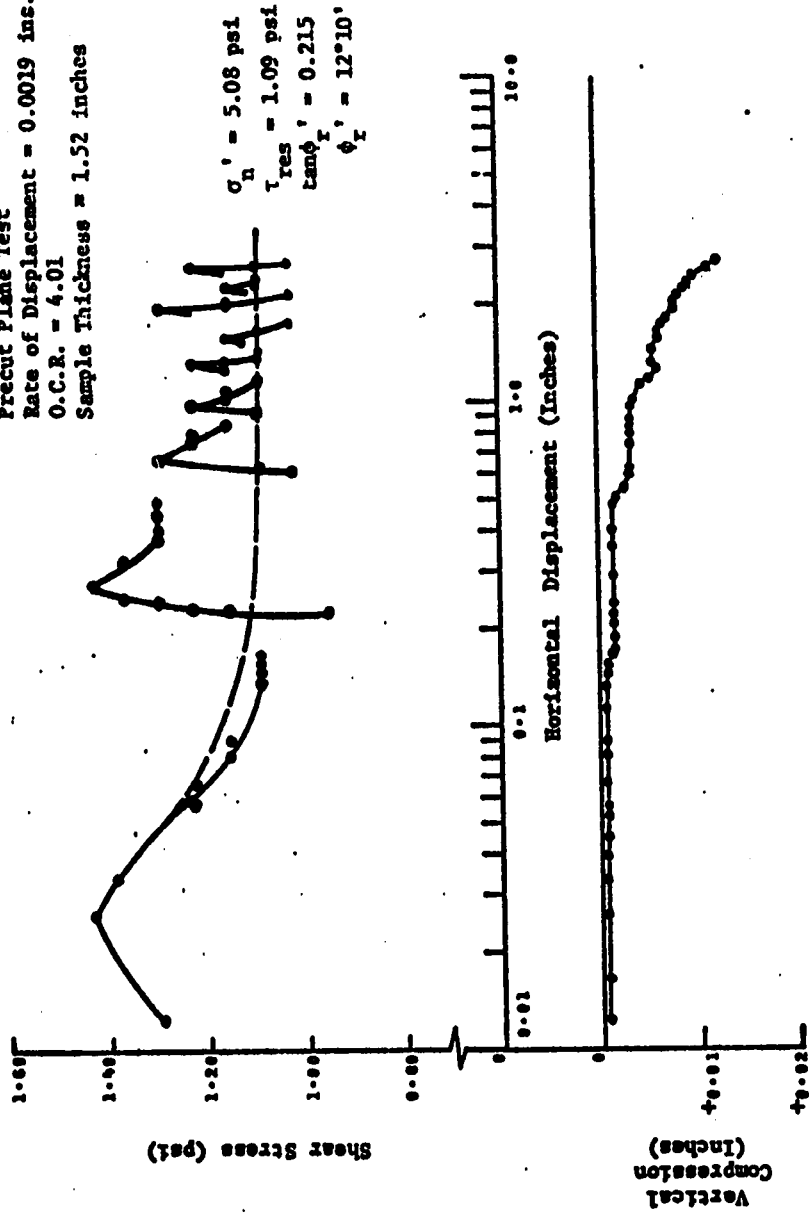
FIG.B-75 DIRECT SHEAR TEST ON MONTMORILLONITE (M-15-1)

FIG.B-76 DIRECT SHEAR TEST ON MONTMORILLONITE (M-15-2)

FIG.B-77 DIRECT SHEAR TEST ON MONTMORILLONITE (M-15-3)

FIG.B-78 DIRECT SHEAR TEST ON MONTMORILLONITE (M-15-4)

FIG.B-79 DIRECT SHEAR TEST ON MONTMORILLONITE (X-15-5)

Montmorillonite - 15.26 g/l NaCl
Test No. M-15-6
Precut Plane Test
Rate of Displacement = 0.0019 ins./min.
O.C.R. = 2.29
Sample Thickness = 0.71 inches

$\sigma_n' = 71.18$ psi
$\tau_{res} = 10.90$ psi
$\tan\phi_r' = 0.153$
$\phi_r' = 8°40'$

Horizontal Displacement (inches)

Shear Stress (psi)

Vertical Compression (inches)
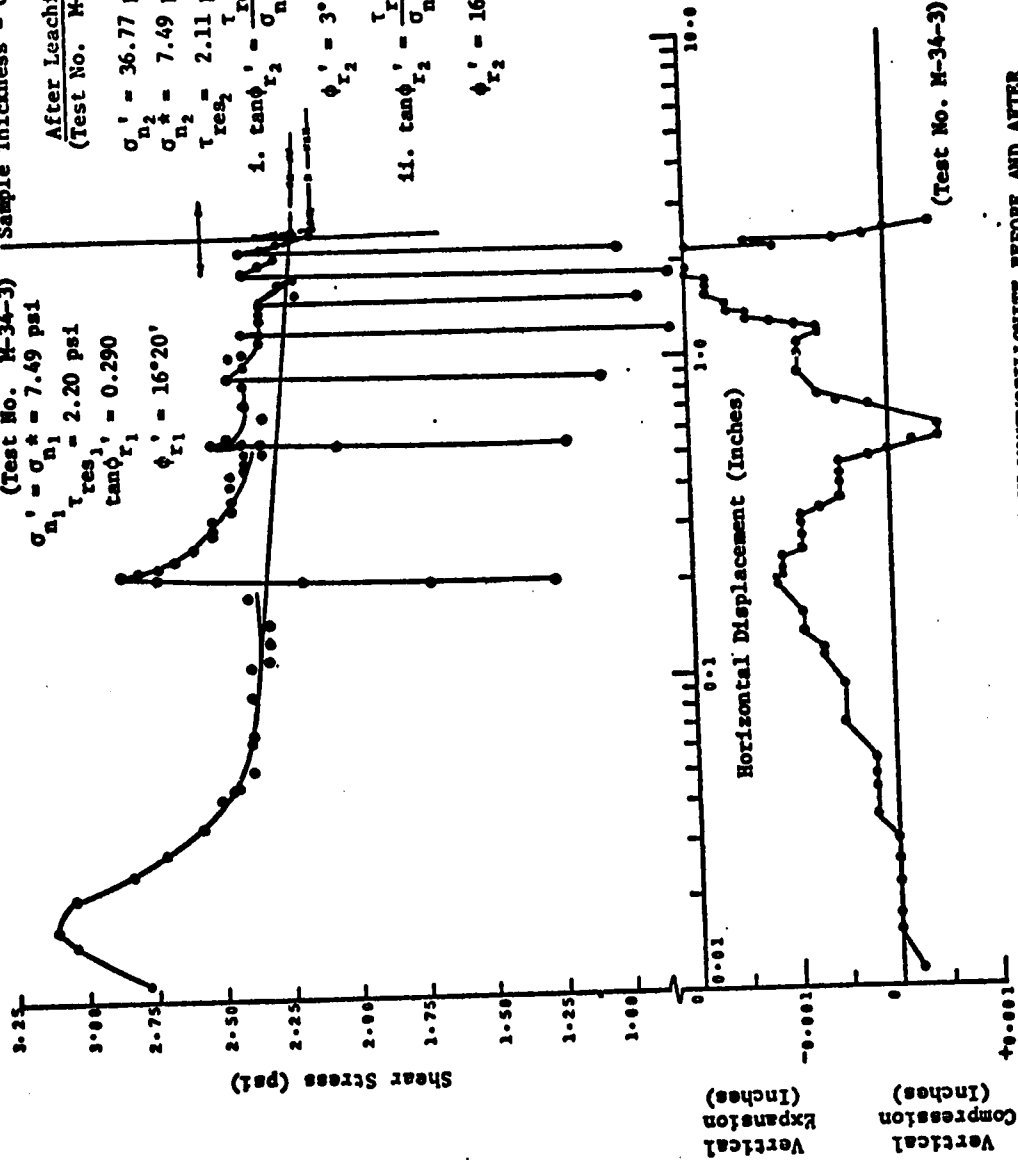
FIG.B-80 DIRECT SHEAR TEST ON MONTMORILLONITE (M-15-6)
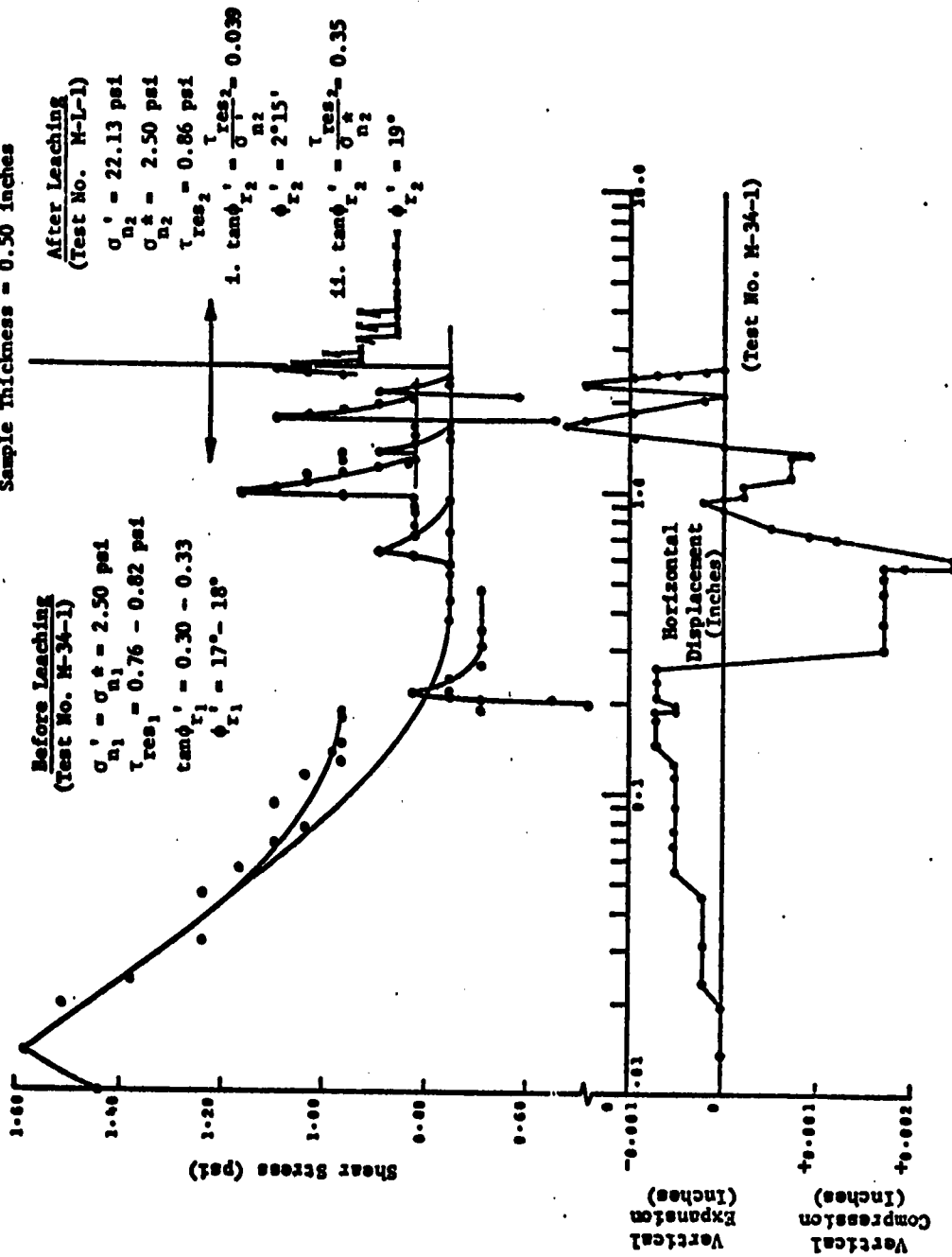
FIG.B-81 DIRECT SHEAR TEST ON MONTMORILLONITE BEFORE AND AFTER LEACHING (M-34-1 and M-L-1)

Montmorillonite - 33.57 g/l NaCl
Test Nos. M-34-2 and M-L-2
Precut Plane Tests, O.C.R. = 6.08
Rate of Displacement = 0.0024 ins./min.
Sample Thickness = 0.59 inches

Before Leaching
(Test No. M-34-2)

$\sigma_{n_1}' = \sigma_{n_1}^* = 5.00$ psi
$\tau_{res_1} = 1.60$ psi
$\tan\phi_{r_1}' = 0.320$
$\phi_{r_1}' = 17°40'$

After Leaching
(Test No. M-L-2)

$\sigma_{n_2}' = 49.94$ psi
$\sigma_{n_2}^* = 5.00$ psi
$\tau_{res_2} = 1.40 - 1.53$ psi

i. $\tan\phi_{r_2}' = \dfrac{\tau_{res_2}}{\sigma_{n_2}'} = 0.030$

$\phi_{r_2}' = 2°$

ii. $\tan\phi_{r_2}' = \dfrac{\tau_{res_2}}{\sigma_{n_2}^*} = 0.28 - 0.31$

$\phi_{r_2}' = 16° - 17°$

Shear Stress (psi)

2.50
2.25
2.00
1.75
1.50
1.25
1.00

Vertical
Expansion
(Inches)

-0.01

(Test No. M-34-2)
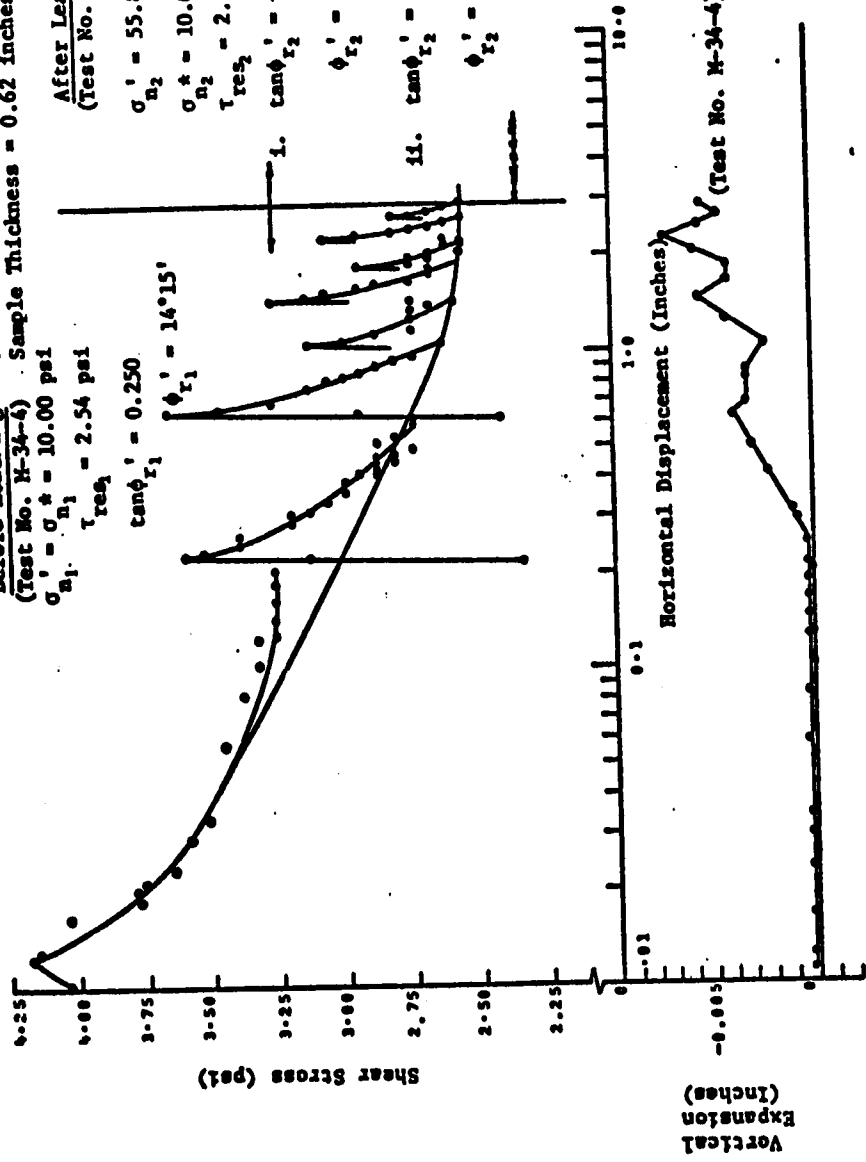
Horizontal Displacement (Inches)

0.01
0.1
1.0
10.0
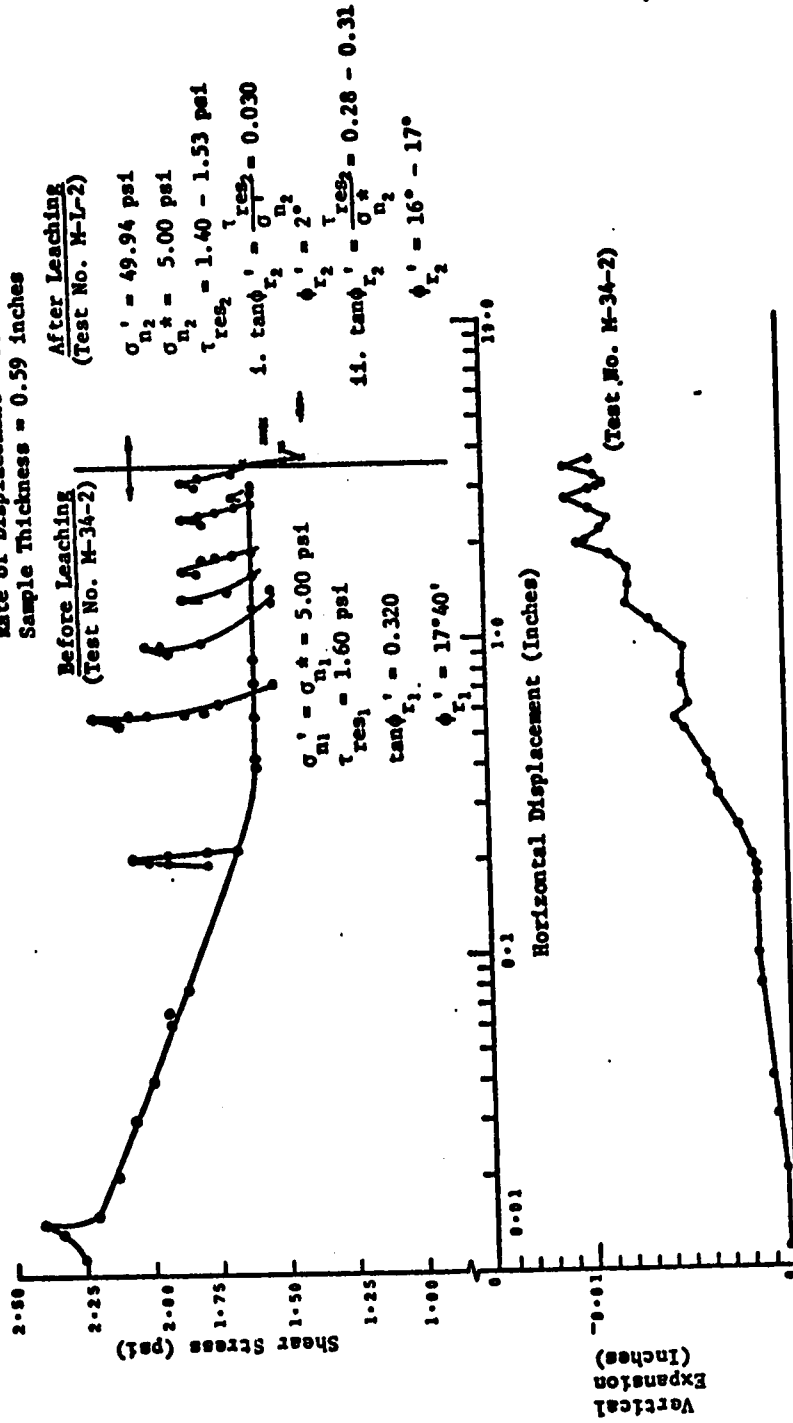
FIG.B-82 DIRECT SHEAR TEST ON MONTMORILLONITE BEFORE AND AFTER
LEACHING (M-34-2 and M-L-2)

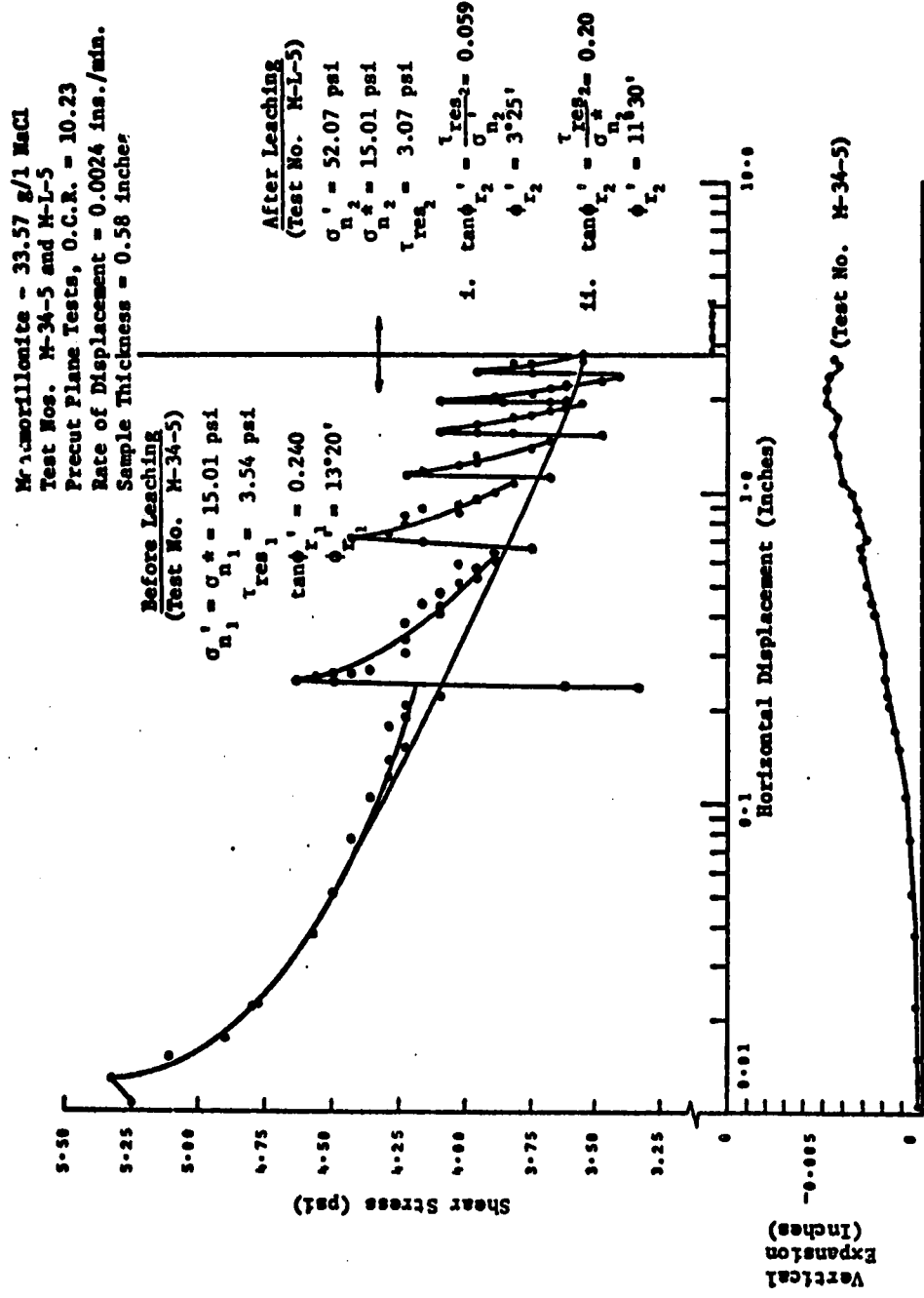FIG.B-83 DIRECT SHEAR TEST ON MONTMORILLONITE BEFORE AND AFTER LEACHING (Test Nos. M-34-3 and M-L-3)

FIG.B-84 DIRECT SHEAR TEST ON MONTMORILLONITE BEFORE AND AFTER
LEACHING (M-34-4 and M-L-4)

Montmorillonite - 33.57 g/l NaCl
Test Nos. M-34-5 and M-L-5
Precut Plane Tests, O.C.R. = 10.23
Rate of Displacement = 0.0024 ins./min.
Sample Thickness = 0.58 inches

After Leaching
(Test No. M-L-5)

σ_{n_2}' = 52.07 psi
$\sigma_{n_2}^*$ = 15.01 psi
τ_{res_2} = 3.07 psi

i. $\tan\phi_{r_2}' = \dfrac{\tau_{res_2}}{\sigma_{n_2}} = 0.059$
   ϕ_{r_2}' = 3°25'

ii. $\tan\phi_{r_2}' = \dfrac{\tau_{res_2}}{\sigma_{n_2}^*} = 0.20$
    ϕ_{r_2}' = 11°30'

Before Leaching
(Test No. M-34-5)

$\sigma_{n_1}' = \sigma_{n_1}^*$ = 15.01 psi
τ_{res_1} = 3.54 psi

$\tan\phi_{r_1}' = \dfrac{\tau_{res_1}}{\sigma_{n_1}}$ = 0.240
ϕ_{r_1}' = 13°20'

Horizontal Displacement (Inches)

Shear Stress (psi)

Vertical Expansion (Inches)

(Test No. M-34-5)

FIG. B-85 DIRECT SHEAR TEST ON MONTMORILLONITE BEFORE AND AFTER LEACHING (M-34-5 and M-L-5)

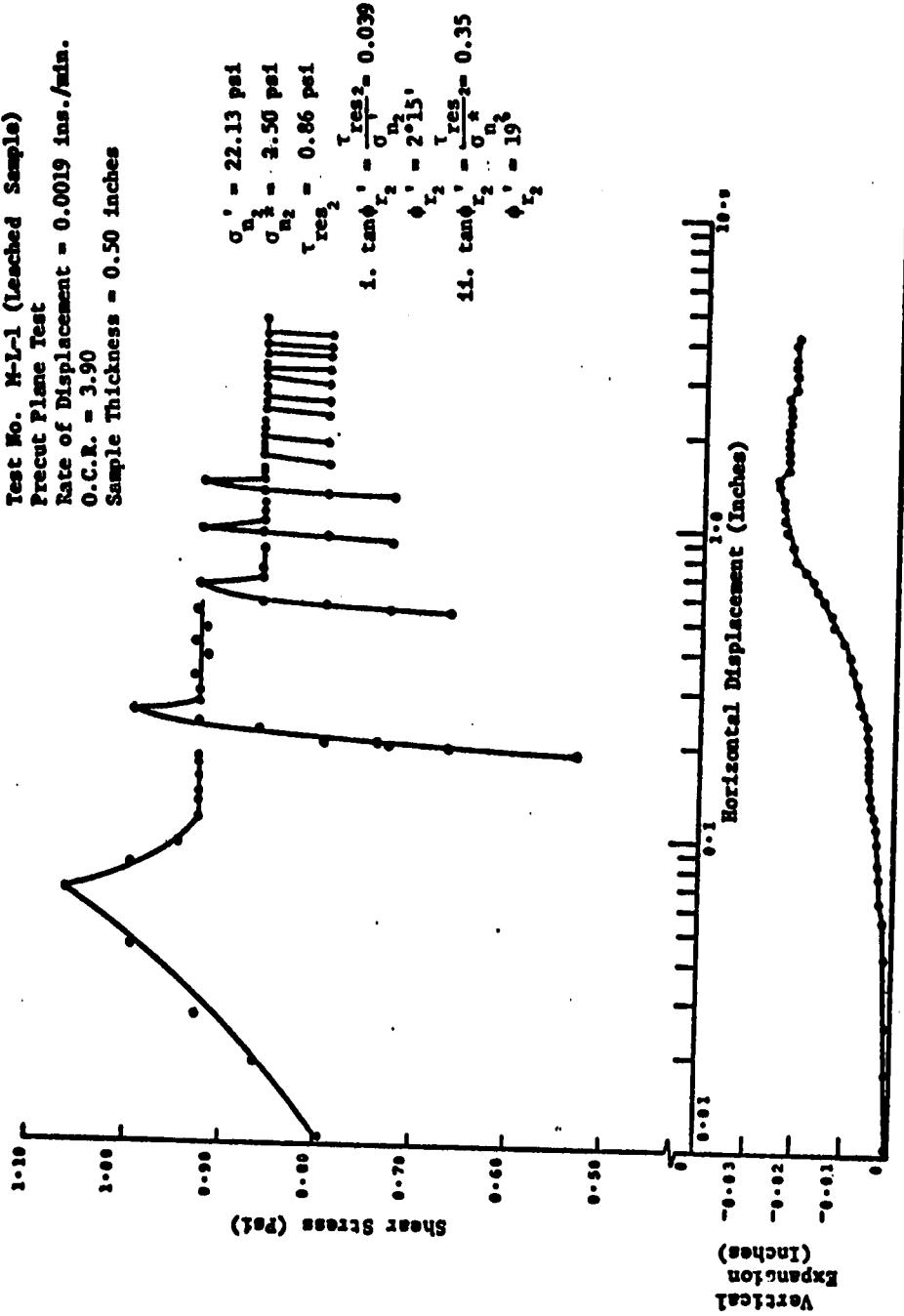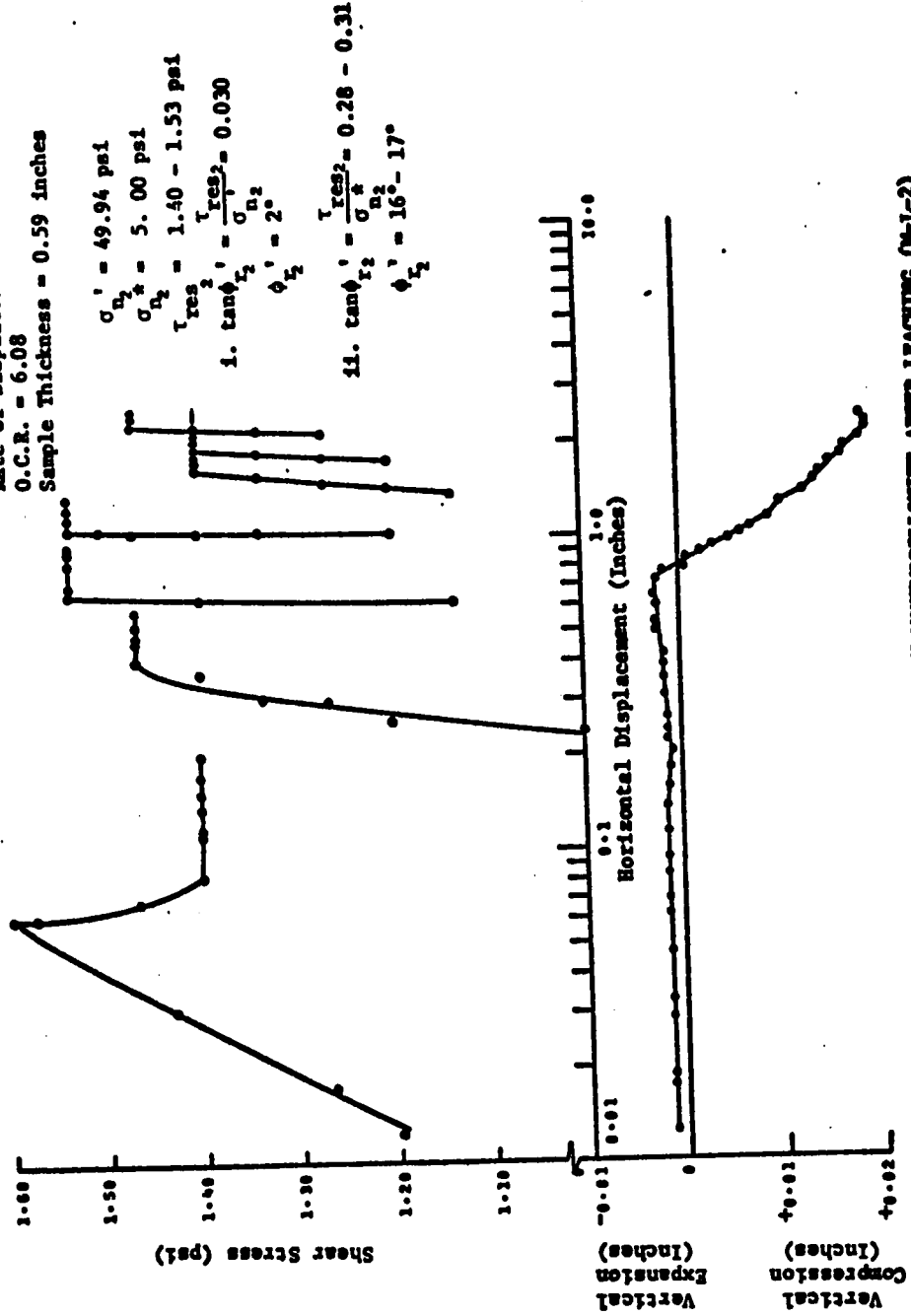FIG.B-86 DIRECT SHEAR TEST ON MONTMORILLONITE AFTER LEACHING (M-L-1)

FIG.B-87 DIRECT SHEAR TEST ON MONTMORILLONITE AFTER LEACHING (M-L-2)

Montmorillonite - 0.08 g/l NaCl
Test No. M-L-3 (Leached Sample)
Precut Plane Test
Rate of Displacement = 0.0019 ins./min.
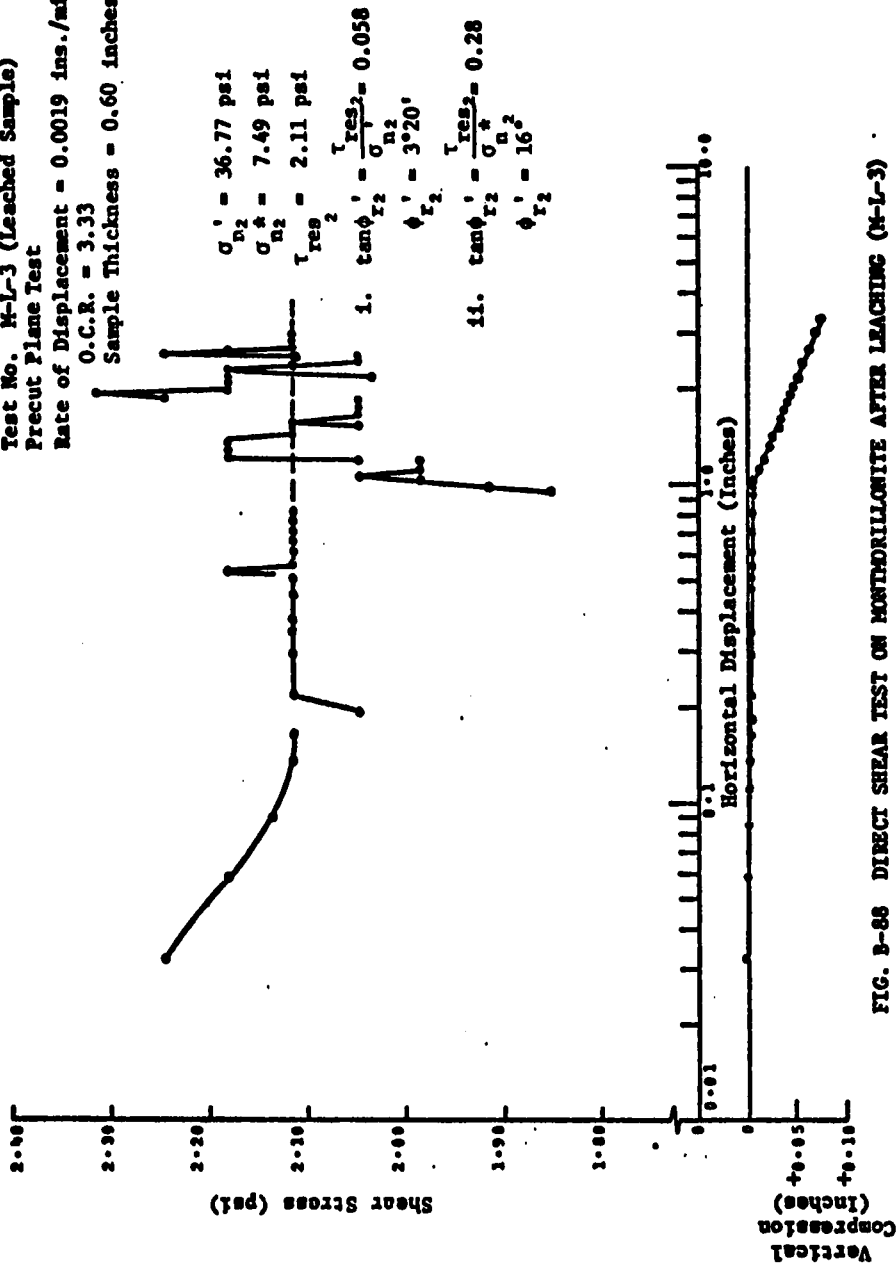O.C.R. = 3.33
Sample Thickness = 0.60 inches

$\sigma'_{n_2} = 36.77$ psi
$\sigma^*_{n_2} = 7.49$ psi
$\tau_{res_2} = 2.11$ psi

1. $\tan\phi'_{r_2} = \dfrac{\tau_{res_2}}{\sigma'_{n_2}} = 0.058$
   $\phi'_{r_2} = 3°20'$

11. $\tan\phi'_{r_2} = \dfrac{\tau_{res_2}}{\sigma^*_{n_2}} = 0.28$
    $\phi'_{r_2} = 16°2$

Shear Stress (psi)

Horizontal Displacement (inches)

Vertical Compression (inches)

FIG. B-88 DIRECT SHEAR TEST ON MONTMORILLONITE AFTER LEACHING (M-L-3)

Montmorillonite - 0.18 g/1 NaCl
Test No. M-L-4
Precut Plane Test
Rate of Displacement = 0.0024 ins./min.
O.C.R. = 9.04
Sample Thickness = 0.62 inches

σ'_{n_2} = 55.89 psi
σ'_{n_2} = 10.00 psi
τ_{res_2} = 2.34 psi

i. $\tan\phi'_{r_2} = \dfrac{\tau_{res_2}}{\sigma'_{n_2}}$ = 0.042
ϕ'_{r_2} = 2°30'

ii. $\tan\phi'_{r_2} = \dfrac{\tau_{res_2}}{\sigma'^*_{n_2}}$ = 0.23
ϕ'_{r_2} = 13°

Shear Stress (psi)
2.60
2.50
2.40
2.30
2.20
2.10
2.00

Horizontal Displacement (inches)

Vertical Compression (inches)
+0.005
+0.01
+0.015
+0.02

FIG.B-89 DIRECT SHEAR TEST ON MONTMORILLONITE AFTER LEACHING (M-L-4)

Montmorillonite – 0.08 g/1 NaCl
Test No. M-L-5 (Leached Sample)
Precut Plane Test
Rate of Displacement = 0.0024 ins./min.
O.C.R. = 10.23
Sample Thickness = 0.58 inches

$\sigma_{n_1}' = 52.07$ psi
$\sigma_{n_2}' = 15.01$ psi
$\tau_{res_2} = 3.07$ psi

i. $\tan\phi_{r_2}' = \dfrac{\tau_{res_2}}{\sigma_{n_2}} = 0.059$

$\phi_{r_2}' = 3°25'$

ii. $\tan\phi_{r_2}' = \dfrac{\tau_{res_2}}{\sigma_{n_2}^*} = 0.20$

$\phi_{r_2}' = 11°30'$

Shear Stress (psi)

3.20
3.10
3.00
2.90
2.80
2.70
2.65

Horizontal Displacement (Inches)

0.01 0.1 1.0 10.0

Extrusion

Vertical Compression (Inches)

+0.0
+0.10
+0.1

FIG. B-90 DIRECT SHEAR TEST ON MONTMORILLONITE AFTER LEACHING (M-L-5)

FIG.B-91 DIRECT SHEAR TEST ON MONTMORILLONITE (M-34-6)

FIG. B-92 DIRECT SHEAR TEST ON MONTMORILLONITE (M-34-7)

FIG. B-93 DIRECT SHEAR TEST ON MONTMORILLONITE (M-34-8)

FIG. B-94 DIRECT SHEAR TEST ON MONTMORILLONITE (M-34-9)

APPENDIX C

THE DOUBLE-LAYER REPULSIVE STRESS

In this appendix, the equations for calculating the osmotic repulsive force due to double layer interaction between two adjacent clay platelets (Bolt, 1956; Bailey, 1965) have been outlined first. The derivation of these equations is based on several assumptions which have been discussed in detail by Low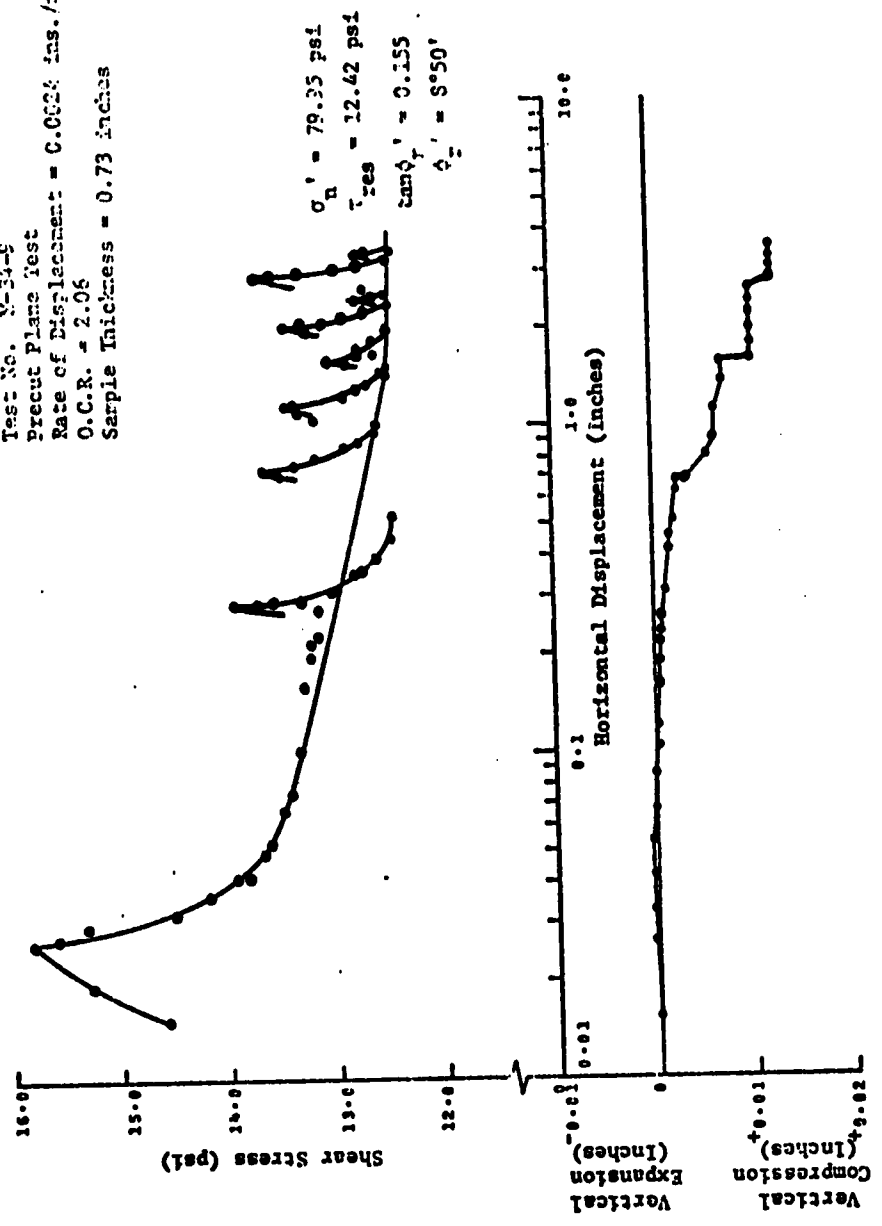 (1959). An examination of these assumptions and Low's criticisms has been included in the next section. A description of the various terms used in these equations and a sample calculation of the double-layer repulsive stress using them are presented in the next two sections.

C.1 Double-layer Repulsion Equations

$$P_y = 2 C_0 R T (\cosh y_c - 1) \tag{C.1}$$

$$y_c = 2 \ln \frac{\cosh \Delta + 1}{\cosh \Delta - 1} \qquad \text{if } y_c < 1 \tag{C.2a}$$

$$y_c = 2 \ln(\frac{\pi}{\Delta}) \qquad \text{if } y_c < 1 \tag{C.2b}$$

$$\Delta = \kappa (x_0 + d) \tag{C.3}$$

$$x_0 = \frac{4 z C_0}{\kappa^2 \sigma} \cdot 10^3 \tag{C.4}$$

$$\kappa = [\frac{8 \pi e^2 z^2 n}{\epsilon k T}]^{1/2} \tag{C.5}$$

In the above equations,

P_y = the double-layer repulsive stress in kg/cm^2

C_o = the ion concentration in the pore fluid (moles/cc). (This will be equal to the molarity of the bulk solution x 10^{-3}.)

R = the gas constant which has a value of 85 kg-cm/mole/°K.

T = the absolute temperature in °K.

z = the valency of the ions.

σ = the surface charge density of the soil in meq/cm^2.

ε = the dielectric constant of the pore fluid in esu units.

e = the electric charge on an electron having a value of 4.803 x 10^{-10} esu/charge.

n = the volume concentration of cations and anions in the bulk solution in ions/cc. (This will be equal to the molarity of the bulk solution x 10^{-3} x N_A.)

N_A = Avogadro's number having a value of 6.0232 x 10^{23} mol/gm mole

k = the Boltzmann's constant

and d = the particle half spacing in cm.

C.2 Assumptions Involved in the Double-layer Equations

Low (1959) gives the derivation of these equations and detailed discussion of the assumptions on which these equations are based.

In arriving at the above equations from the Boltzmann's

equation (which forms the basic differential equation for the double-layer repulsion equations), it is assumed that the potential energy of the ions is affected only by the electrical field of the clay particles. However, there are additional components of energy in the interparticle region, such as the polarization energy of the ions in the electric field, the energy due to ion-ion and ion-water interaction and the energy of interaction of the ions to the atoms on the surface of the particles. Bolt (1955) has made a theoretical assessment of the effect of these additional energies and he arrived at the conclusion that their net effect should be small. This, the author believes, might possibly explain why Bolt (1956), Bailey (1965) and others found good agreement between their predicted and experimental values of interparticle force (especially for Na-montmorillonites with very low molar concentrations at low pressures).

The author agrees with Low (1959) and Bailey (1965) in that the double-layer repulsive stress equations do not take care of all the forces in the particle region.* But in the absence of a complete understanding of all the forces between two adjacent clay particles, the double layer repulsive stress, as expressed by equations in section C.1, has been shown (in Chapter VI) to yield the best estimate of the net (R-A) stress between two clay particles, especially when the

---

* The presence of an interaction between the first few layers of water and the clay surface has been discussed in detail by Martin (1960).

adsorbed cations are predominantly monovalent.

C.3   Description of the Various Terms in the Double-layer Repulsion
      Equations

  i)   The dielectric constant, ε.

      The value of the dielectric constant of the double-layer
water has been taken as 80 esu units which is the dielectric constant
of free water.

  ii)   The surface charge density, σ and x_o

      The surface charge density of the soil may be estimated
from its cation exchange capacity (CEC) and the specific surface (S.S.)
as follows. If the CEC is in meq./100 gms. of dry soil and S.S. in
$m.^2/gm.$,

$$\sigma = 2.89 \times 10^5 \frac{CEC}{S.S.} \text{ esu/cm}^2 = 2.89 \times 10^5 \times \frac{CEC}{S.S.} \times (\frac{10^{-10}}{6.0232 \times 4.803}) \text{ meq/cm}^2$$

$$(C.6)$$

From the equations in Section C.1, it can be seen that σ affects only
the value of x_o directly.

      The double-layer repulsive force as given by equation (C.1)
is, in essence, an osmotic repulsive force, due to the difference in
the sum of the concentration of all the ions in the mid-plane between
the particles and the outside bulk solution. The concentration at the
mid-plane is estimated from the Boltzmann equation (Taylor, 1959),
which assumes an exponential variation for the concentration of the
ions. This assumption leads to a surface charge density of ∞ at zero

distance from the particle surface to balance a theoretical cation density of ∞ at the particle surface. This is impossible in reality. Hence a correction factor is introduced in terms of x_0, which is a distance from the imaginary surface of infinite charge density to a surface having a charge density equal to the soil under consideration. This correction thus applies only to that portion of any soil having a charge deficiency and from whose surface the double layer develops. From the known cation exchange capacity and specific surface of the clay fraction ($<2\mu$ portion) of a mineral, x_0 can be estimated. It may also be noted from equation C.4 that x_0 does not depend upon the concentration of the external solution but only on its valency.

iii) The valency, z, and κ

Since the present investigation deals with Na-homoionized minerals with NaCl as the dominant pore fluid salt, the net valency of ions in the double-layer water at the mid plane is equal to 1.0.

Substituting the appropriate values of ϵ, k, T, etc., in the equation (C.5), the expression for κ becomes

$$1/\kappa = [\frac{9.30}{N}]^{1/2} \times 10^{-8} \text{ (cms.)} \tag{C.7}$$

where   N = normality of the bulk solution.

iv) The interparticle half distance, d

The next step is the evaluation of d. From the known water content of a clay mineral sample and its specific surface, the particle half spacing may be evaluated using the following relationship (assuming

uniformly oriented infinite particles),

$$d \text{ in } \overset{\circ}{A} = \frac{\text{water content } (\%) \times 100}{\text{specific surface } (m.^2/gm.)} \qquad (C.8)$$

The assumption of uniformly oriented infinite particles is not met within most cases and for that reason the value of d calculated as above does not indicate the actual spacing between two particles. A detailed study has been made by Bailey (1965) to investigate the effects of finite particles and non-parallel orientation. However, general trends in double layer behaviour are thought to be independent of particle orientation. This statement is generally valid with respect to long range stresses since the interparticle spacings under consideration here are large enough to permit reasonably complete double-layer development. Meaningful computations for double-layer repulsion of a realistic model of non-parallel particles are difficult at the present state of knowledge of the various factors involved, such as the influence of dead volume, osmotic repulsive force between non-parallel particles and any attractive force between particles that might become important at very close spacings. Nevertheless, for the same environmental change, we should expect variations in the net (R-A) stress to be similar to those for parallel particles. Similar views have been expressed by Ladd and Kinner (1967).

The evaluation of d from eqn. (C.8) necessitates a knowledge of the specific surface of the soil. The effective surface area of a pure Na-montmorillonite system would be the total surface

area determined by the EGME technique. It was also shown in Chapter VI that the specific surface that has to be used for successful estimation of the net (R-A) stresses for a soil from the double-layer repulsive stress equation should be the specific surface of the calcium variety of the soil.

v) Evaluation of P_y

Once κ , x_0 and d have been evaluated, P_y can be calculated by direct substitution of these values in equations (C.3), (C.2) and (C.1).

C.4   Sample Evaluation of P_y

Clay mineral: Na-montmorillonite - 0 g/l NaCl (Kenney, 1967)

Effective specific surface: 800 m.^{2}/gm. (assumed)

Water content at the residual state (w_{res}): 465%

Particle half spacing (d) corresponding to the w_{res} = $\frac{465 \times 100}{800}$ = 58.13 $\overset{\circ}{A}$

Assumed normality of the bulk solution = 0.0001 N[*]

Cation exchange capacity of the <2μ portion = 115 meq./100 gm.

$$\sigma = 2.89 \times 10^5 \times \frac{115}{800} \times \left(\frac{10^{-10}}{6.0232 \times 4.803}\right)$$

$$= 0.144 \times 10^{-6} \text{ meq./cm.}^2$$

---

[*] If the ion concentration in the pore fluid is zero, the double-layer repulsive stress equation (Equation C.1) yields a value of zero for P_y. Hence a very small bulk solution concentration of 0.0001 N was chosen for evaluating P_y.

$$1/\kappa = [\frac{9.30}{N}]^{1/2} \times 10^{-8} = [\frac{9.30}{0.0001}]^{1/2} \times 10^{-8}$$

$$= 304.96 \times 10^{-8} \text{ cms.}$$

$$\therefore \kappa = 0.00328 \times 10^{8} \text{ (1/cm.)}$$

$$x_0 = \frac{4z\ C_0}{\kappa^2\ \sigma} \times 10^3$$

$$= \frac{4 \times 1 \times (0.0001 \times 10^{-3}) \times 10^3}{0.144 \times 10^{-6}} \times \frac{9.30}{0.0001} \times 10^{-16}$$

$$= 2.583 \times 10^{-8} \text{ cms.}$$

$$\Delta = \kappa(x_0 + d)$$

$$= 0.00328 \times 10^8 [2.583 \times 10^{-8} + 58.13 \times 10^{-8}]$$

$$= 0.1991$$

Now,
$$y_c = 2 \ln \frac{\cosh \Delta + 1}{\cosh \Delta - 1} \qquad \text{if } y_c < 1$$

$$= 2 \times 2.3 \log \frac{\cosh (0.1991) + 1}{\cosh (0.1991) - 1}$$

$$= 4.6 \log \frac{2.0199}{0.0199} = 9.2298$$

and if $y_c > 1$,

$$y_c = 2 \ln (\frac{\pi}{\Delta}) = 2 \times 2.3 \log (\frac{3.14159}{0.1991}) = 5.5112$$

Therefore,
$$P_y = 2 C_0 R T (\cosh y_c - 1)$$

$$= 2 \times 0.0001 \times 10^{-3} \times 85 \times 293 (\cosh 5.5112 - 1)$$

$$= 0.611 \text{ kg./cm.}^2$$

C.5 The Effect of Temperature on the Net (R-A) Stresses Measured in the Constant Volume Leaching Tests

Soon after the initiation of the development of the net (R-A) stresses in the leaching tests on Na-montmorillonite, it became apparent that the measured net (R-A) stress for each sample was affected by fluctuations in the room temperature. The double-layer repulsive stress equation given by

$$P_y = 2 C_u R T (\cosh y_c - 1) \tag{C.1}$$

indicates that the net (R-A) stress is dependent on the absolute temperature (T) and as temperature increases, the net (R-A) stress should increase. Hence, the temperature of a bath of water was continuously recorded with time during the entire leaching process and it was found that on average, the temperature of the bath fluctuated between 18.8°C and 24.1°C over a period of 24 hours. The daily maximum (R-A) stress for each leaching test was recorded when the temperature of the bath was at its daily maximum and the daily minimum (R-A) stress for each leaching test corresponded to the daily minimum temperature of the bath. The difference between the daily maximum and the daily minimum values of the net (R-A) stress varied between 0.06 and 0.08 kg./cm.^{2} for all the leaching tests. A part of this observed daily fluctuation of the measured net (R-A) stress was also due to the temperature error of the load cells (0.15 lbs./degree Farhenheit).

The change in the final net (R-A) stress for leaching test no. L-2 due to a corresponding change in the bath temperature from

18.8°C to 24.1°C is estimated from the double-layer repulsive stress equation. This estimated change in the net (R-A) stress is then added to the temperature error of the load cell corresponding to the same variation in bath temperature and the total change thus estimated is compared with the corresponding measured daily fluctuation of the net (R-A) stress in Table C.1.

From Table C.1, it is immediately seen that the agreement between the estimated and the measured fluctuation of the net (R-A) stress with temperature is excellent. This conclusively proves that the observed daily fluctuations of the net (R-A) stresses in the leaching tests were not due to any changes in volumes of the samples but they were caused by the daily fluctuation of the ambient temperature. This analysis provides further support to the fact that the leaching of the Na-montmorillonite samples was indeed carried out under constant overall volume conditions.

TABLE C.1

COMPARISON BETWEEN THE ESTIMATED AND THE MEASURED DAILY

FLUCTUATION OF THE NET (R-A) STRESS WITH TEMPERATURE

Test no.	Maximum daily bath temperature (°C)	Minimum daily bath temperature (°C)	Estimated daily change* in the net (R-A) stress due to the corresponding daily variation in the bath temperature (kg/cm^2)	Estimated contribution of the temperature error of the load cell (kg/cm^2)	Total estimated daily fluctuation of the net (R-A) stress (kg/cm^2)	Observed daily fluctuation of the net (R-A) stress (kg/cm^2)
L-2	24.1	18.8	0.05	0.02	0.07	0.06-0.08

* The estimated daily change in the net (R-A) stress with temperature reported in Table C.1 is based on the P_y values corresponding to the pore fluid salt content and the water content of the sample in Test No. L-2 after completion of leaching.